THE POTENTIAL SUSCEPTIBILITY OF URBAN HARDROCK AQUIFERS TO HYDRAULIC AND CONTAMINANT STRESSES: The case of Shah Alam, Malaysia

By

Norsyafina Roslan

A Thesis submitted to
The University of Birmingham
For the degree of
DOCTOR OF PHILOSOPHY

School of Geography, Earth & Environmental Sciences
The University of Birmingham
February 2017

ABSTRACT

Urban groundwater needs proper management since it is potentially susceptible to both hydraulic and chemical stresses. To manage an aquifer well, an understanding is needed of how the aquifer works. Much research has been done on urban aquifers but relatively little on hard-rock metasediment aquifers especially in equatorial climates such as Peninsular Malaysia. Therefore, research aim is to understand equatorial climate hard rock metasediment urban aquifers and their susceptibility to hydraulic and chemical impacts using data likely to be available to regulatory authorities. Shah Alam, a city developed over the last 50 years is investigated. Borehole log, meteorological, pumping test, and water quality data were used. The meta sandstone-shale sequence is fractured to at least 100m and covered by a weathering zone that is more clay rich where finer metasediments occur. Permeabilities ranged from 0.01 to 1 m/day. Results show that the abstraction activity has induced recharge into aquifer; which CO_2 contents indicate that it had been through a soil zone. Some weathering reactions had occurred. Water quality samples with very low salinity barely above precipitation concentrations. Many of the water samples were polluted by one or more species, and sewer influences were common. It can be concluded that aquifer very susceptible to quality stress with a very limited pollution attenuation capacity. It is quite flashy system when pumping.

ACKNOWLEDGEMENT

With the name of Allah The Most Gracious The Most Merciful

And Peace be upon Prophet Muhammad

Alhamdulillah,

I want to thank my supervisor Professor John Tellam for his generous patience and guidance. Also not to forget my modelling 'master'; Dr Alan Herbert and Professor Ray Mackay.

To Malaysian Government and People and Universiti Kebangsaan Malaysia who give their trust for me to pursue PhD.

To LUAS, JMG Selangor, DID, JPS,MACRES,JUPEM for the data.

To Ansell Sdn Bhd who gave me permission to do monitoring works in their wells

To my beloved Abah, Roslan Tiasin and Mak, Mariyam Majin and family

To my officemate; Mahmoud, Sam, Tim, Baba, and others

To my mentor Prof Abdul Ghani Rafek and Dr Azimah Hussin and other Geology UKM staff member

To my best friend Dr Syahida Che Dzulkifli

To ummah

THANK YOU.

TABLE OF CONTENTS

1 INTRODUCTION 1

1.1 Urbanization and its impact on hard rock aquifers 1

1.2 The susceptibility of urban hard rock (metasedimentary) aquifers to hydraulic and contaminant stresses 4

1.3 The usage of standard regulatory dataset to develop understanding of newly urbanised aquifers 6

1.4 Research Aims 8

1.5 Research Approach and Thesis Structure 9

1.6 Choice of Study Area 11

1.7 Shah Alam: Overview of the city 13
***1.7.1 Outline of Urban Development* 13**
***1.7.2 Climate* 16**
***1.7.3Topography & Drainage pattern* 17**
***1.7.4 Geology* 17**
***1.7.5Water and waste disposal management* 19**

2.0 AN INTERPRETATION OF THE GEOLOGY OF SHAH ALAM 20

2.1 Introduction 20

2.2 Outline Geology of Peninsular Malaysia 20
***2.2.1 Geological history of Peninsular Malaysia* 20**
***2.2.2 Geological environment* 22**

2.3 Geology of Selangor 25
2.3.1 Introduction 25
2.3.2 The stratigraphy of Selangor 25
2.3.2.1 Brief introduction 25
2.3.2.2 Lower Palaeozoic Rocks 28
2.3.2.3 Upper Palaeozoic Rocks 29
2.3.2.4 Tertiary deposits 30
2.3.2.5 Quaternary deposits 30

2.4 Geology of study area – previous research 30
***2.4.1 Introduction* 30**
***2.4.2 The age of Kenny Hill Formation* 31**
***2.4.3 Type of rocks* 33**
***2.4.4 Weathering* 37**
***2.4.5The geological structure* 39**
2.4.5.1Regional structure 39
2.4.5.2 Local geological structures 39

Folding 39
Joints 42
Faults 42
2.4.5.3 The impact of geological structures to the river pattern 44

2.4.6 Metamorphism 44

2.5 Borehole log interpretation 46
2.5.1 Introduction 46
2.5.2 Geological logs from the Ansell boreholes 49
2.5.3 Geological log from AESBI borehole and the correlation with the lithology at Ansell. 54
2.5.4 Geological logs from the MT Pictures boreholes 55
2.5.5 Geological logs from the Carlsberg boreholes 57
2.5.6 Geological logs from Mitsui High Tech and the correlation with the lithology at Carlsberg 58
2.5.7 Geological logs from Good Year 61
2.5.8 Geological logs from Scientex Polymer and the correlation with lithology at Ansell and MT Pictures 62
2.5.9 Geological logs from Gaya Color Lab boreholes and the correlation with lithology at Scientex Polymer. 63
2.5.10 Geological logs from Universal Nutri Beverages and correlation with Mitsui High Tech and Carlsberg. 65
2.5.11 Geological logs from the CCM Fertilizer boreholes and the correlation with the lithology at Universal Nutri Beverages and Gaya Color Lab. 65
2.5.12 Geological logs from the PROTON boreholes and the correlation with lithology at AESBI 67
2.5.13 Geological logs from the Canon Opto boreholes 69
2.5.14 Geological logs for the Aquarium Express and Aquatic International boreholes 71

2.6 Fieldwork observations 73
2.6.1 Introduction 73
2.6.2 Observation at Outcrop A 73
2.6.3 Observation at Outcrop B 77
Discontinuity Survey 89
2.6.4 Observation at Outcrop C 96
2.6.5 The interpretation of Shah Alam's river pattern 100

2.7 The Geological Summary of Shah Alam 110
2.7.1 Introduction 110
2.7.2 The central part of Shah Alam 114
2.7.3 The eastern part of Shah Alam 121
2.7.4 The western part of Shah Alam 125

2.7.5 The northern part of Shah Alam 128

2.8 Conclusion 131

3.0 HYDROGEOLOGY OF SHAH ALAM 135

3.1 Introduction 135

3.2 Preliminary Aquifer Assessment 135
3.2.1 Introduction 135
3.2.2 Well yield & specific capacity of the wells 138

3.3 Implications of Geological Data 148
3.3.1 Introduction 148
3.3.2 Porosity and permeability of the Kenny Hill Formation 149
3.3.2.1 Rock mass 149
3.3.2.2 Fractures; some general considerations 153
Bedding and other joints 156
Faults 160
Folds 164
3.3.3.2Weathered rock 164
3.3.3Hydrogeological conclusions from geological studies of the Shah Alam area 176

3.4 Implications of Groundwater Head Data 178
3.4.1 Introduction 178
3.4.2 The factors that might influence the groundwater level during measurement 179
3.4.3 Groundwater abstraction 183
3.4.4 River flows 187
3.4.5 Groundwater head distribution 190
3.5 Conclusion 192

4.0 GROUNDWATER RESOURCES IN SHAH ALAM. 196

4. 1 Introduction 196
4.2 Meteorological background 196
4.2.1 Introduction 196
4.2.2 Precipitation 198
4.2.3 Temperature 208
4.2.4 Air Humidity 209
4.2.5 Wind speed 212
4.2.6 Solar radiation 213
4.2.7 Pan evaporation 215
4.2.8 Evapotranspiration 218

4.3 Recharge in the urban aquifer 226

4.3.1 Introduction 226
4.3.2 Rainfall as main recharge sources 226
4.3.3 Leakage from the pipe utilities 229

4.4 Recharge estimation 229
4.5 Conclusion 234

5.0 PUMPING TEST ANALYSIS: DEVELOPING THE CONCEPTUAL MODEL AND ESTIMATION OF AQUIFER CHARACTERISTICS 235

5.1 Introduction 235

5.2 The selection of pumping test analysis method 237
5.2.1 Single well test with well bore storage and well loss effect 237
5.2.2 Diagnostic plot 238
5.2.3 Step test drawdown 238
5.2.3.1 Introduction 238
5.2.3.2 Bierschenk & Wilson method 240
5.2.3.3Eden- Hazel method 242
5.2.4 Constant Yield Tests 244
5.2.5 Recovery Analysis 247

5.3 Results and interpretation -Preliminary Aquifer Characterization Using Diagnostic Plots 249
5.3.1 Introduction 249
5.3.2 Class A pumping test responses 253
5.3.3 Class B pumping test responses 257
5.3.4 Class C pumping test responses 261
5.3.5 Class D pumping test responses 263
5.3.6 Class E pumping test responses 267
5.3.7 Conclusions 270

5.4 Aquifer and Well Characterization Using Step Drawdown Test Analysis 277
5.4.1 Introduction 277
5.4.2 Bierschenk & Wilson method 277
5.4.3 Eden & Hazel method 282
5.4.4 Comparison between two methods 284
5.4.5 The causes of non-linear and negative s_w/Q v. Q relationships 286
5.4.5.1 Introduction 286
5.4.5.2 Presence of hydraulic boundaries 287
5.4.5.3 Well bore storage 289
5.4.5.4 Seepage face 289
5.4.5.5 Low or high K layers 291
5.4.5.6 Hydraulic conductivity changes near to the well 291

5.4.5.7 Turbulent conditions in fractures 291
5.4.5.8 The change of aquifer condition 292
5.4.6 Conclusion 292

5.5 Aquifer Characterization Using Constant Yield Test Analysis 293
5.5.1 Introduction 293
5.5.2 Results and interpretation 296
5.5.3 Discussion and Conclusion 298

5.6 Aquifer Characterization Using Analysis of Water-Level Recovery Data 304
5.6.1 Introduction 304
5.6.2 Results and interpretation 310
5.6.3 Conclusion 312

5.7 Aquifer Characterization Using Water Level Measurement in Selected Areas 313
5.7.1Introduction 313
5.7.2 Monitoring work in Ansell compound 314
5.7.3 Results and interpretation 316

5.8 Aquifer Characterization Using Numerical Model 322
5.8.1 Introduction 322
5.8.2 The flow model 324
5.8.2.1 Model Representation 324
5.8.2.2 Aquifer scenarios 325
5.8.2.3 Calibration procedure 326
5.8.3 Modelling the aquifer in the fractured shale (Mitsui High Tech, Class E) 326
5.8.4 Modelling a well in an individual compartment (AESBI, Class D) 329
5.8.5 Modelling the confined-semi confined aquifer (Scientex Polymer, Class B) 332
5.8.6 Conclusion 335

5.9 A revised hydrogeological conceptual using pumping test data analysis 336

6.0 WELLWATER CHEMISTRY ANALYSIS 340
6.1 Introduction 340

6.2 Water sampling method and sample analysis 341
6.2.1 Introduction 341
6.2.2 Sampling method 342
6.2.3 Sample analysis 344
6.2.4 Checking the analyses 345
6.2.5 Phreeqc 349

6.3 The wellwater chemistry of the Shah Alam aquifer 351
***6.3.1 Introduction* 351**
***6.3.2 Classification in Water Types* 352**
***6.3.3 Water Type 1* 358**
***6.3.3.1 The introduction* 358**
***6.3.3.2 The chemistry of Type 1 wellwaters* 360**
***6.3.4 Water Type 2* 368**
***6.3.5Water Type 3* 372**

6.4 Pollution 375
***6.4.1 Introduction* 375**
***6.4.2 Rivers as sources of pollution* 376**
***6.4.3 Correlation between wellwater chemistry and industrial landuse* 378**
***6.4.4 Determinands of anthropogenic origin* 379**
***6.4.5Nitrogen Species* 383**
***6.4.6Synthetic Organics* 386**
***6.4.7 Bacteria* 388**
***6.4.8 Aluminium* 390**
***6.4.9 Heavy Metals, Metalloids and CN and F* 392**

6.5 Discussion of Wellwater Chemistry Findings 397

7.0 SUMMARY, CONCLUSIONS AND RECOMMENDATIONS. 399

7.1 Introduction 399

7.2 The Development of A Conceptual Understanding of The Hydrogeology Of An Urban Hardrock Aquifer In An Equatorial Climate 399

7.3 Potential Susceptibility Of the Shah Alam Urban Hardrock Aquifer to Hydraulic And Contaminant Stresses 402

7.4 Research approach and its limitations 403

7.5 Research contribution and its wider implications. 404

7.6 Recommendations for future research 405
7.7 Recommendations for local authority to improve the quality of pumping test data 407

REFERENCES 409

APPENDIXES A –Semi log and log-log plots 429

APPENDIXES B- Eden & Hazel plots 439

APPENDIXES C- Cooper Jacob plots **444**

APPENDIXES D-Theis recovery plots **464**

APPENDIXES E-Monitoring data plots **471**

LIST OF TABLES

Table 2.1 The tectonic division of Peninsular Malaysia which is based on the characteristics of the granite intrusions (Hutchison 1977). 24

Table 2.2 The stratigraphic sequence of Selangor (? indicates uncertain; T indicates major tectonic event / unconformity) 27

Table 2.3 The rock description as observed by Musbah (1980) at Bukit Pantai, Kuala Lumpur. 35

Table 2.4 The description of each lithology of Kenny Hill Formation (modified from Rosly 1979) 38

Table 2.5 The comparison of quartz grains size in sandstone (BP) with different weathering grade from Grade 2 (less) to 5 (more) (Zainab et al. 2007) 39

Table 2.6 The compression directions observed at few localities in the Kenny Hill Formation by Tjia (1976). 41

Table 2.7 The chemical composition of Kenny Hill formation and Dinding schist (Hamzah et al. 1986) 46

Table 2.8 The drilling companies and the wells that they constructed 49

Table 2.9 The thickness of sandstone layer as observed at Ansell. 53

Table 2.10 The comparison of sandstone layer thickness at Ansell, Mt Pictures and Scientex Polymer. 63

Table 2.11a) Discontinuity survey data at Location 1 90

Table 2.11b) Discontinuity survey data at Location 2 90

Table 2.11c) Discontinuity survey data at Location 3 91

Table 2.12 The range of depth and thickness of carbonaceous shale in study area 116

Table 2.13 The thickness of the weathered layer in central area 118

Table 2.14 The type of lithology with fractures with range of depth in central area 120

Table 2.15 The type of lithology with fractures with range of depth in eastern area 124

Table 2.16 The thickness of the weathered layer in eastern area 124

Table 2.17 The thickness of the weathered layer in western area 127

Table 2.18 The type of lithology with fractures with range of depth in western area 127

Table 2.19 The type of lithology with fractures with range of depth in northern area 130

Table 2.20 The thickness of the weathered layer in northern area 131

Table 3.1 The properties of each class of aquifer in Malaysia (JICA 1981) 136

Table 3.2 The depth of water is encountered during drilling 138

Table 3.3 The porosity values of quartzite in Malaysia 150

Table 3.4 The porosity values of weathered shale in Malaysia by Ibrahim (1986) 152

Table 3.5 The permeability of sandstone and shale 153

Table 3.6 Hydraulic parameters in fractured bedrock 155

Table 3.7 Weathering classification for metasedimentary rock (Ibrahim & Mogana 1988) 168

Table 3.8 Engineering properties classification for metasedimentary rock (Ibrahim & Jasni 1990) 169

Table 3.9 The physical properties of quartzite and phyllite of Kenny Hill Formation in Shah Alam at various location 170

Table 3.10 The soil (granite origin) properties at disturbed and undisturbed area (Kamaruzaman, 1989) 174

Table 3.11 The water levels recorded at Ansell in 2005 and 2007 180

Table 3.12 The annual abstraction rate record for wells in Shah Alam 185

Table 3.13 The daily abstraction record and duration of pumping for wells in Shah Alam 186

Table 4.1 The differences in climatic elements of Klang Valley area compared with nearby rural areas (from Sham 1980) 198

Table 4.2 Years with less than 2000mm/yr of rainfall (data from Malaysian Meteorological Department and Department of Irrigation and Drainage Malaysia) 206

Table 4.3 The monthly average temperature recorded at Subang station From 2004 to 2008 (data from Malaysian Meteorological Department and Department of Irrigation and Drainage Malaysia) 209

Table 4.4 The monthly average humidity observed at Subang station from 2004 to 2008 (data from Malaysian Meteorological Department and Department of Irrigation and Drainage Malaysia) 210

Table 4.5 The monthly average wind speed recorded at Subang station (data from Malaysian Meteorological Department and Department of Irrigation and Drainage Malaysia) 213

Table 4.6 The monthly average radiation recorded at Subang station (data From Malaysian Meteorological Department and Department of Irrigation and Drainage Malaysia) 214

Table 4.7 The climatic parameters calculated for estimating reference evapotranspiration,ET_o 223

Table 4.8 The 'impermeablity factor' of Shah Alam based on Butler & Davies (2000) 228

Table 5.1 Well response classes 251

Table 5.2 The properties of wells in Class A 256

Table 5.3 The properties of wells in Class B. The wells with (*) mark show the gradual changes of time-drawdown plots. 259

Table 5.4 The properties of well in Class C 262

Table 5.5 The properties of wells in Class D 265

Table 5.6 The Properties of wells in Class E 268

Table 5.7 The hydraulic properties interpreted using the Bierschenk & Wilson method for wells in Class 1 279

Table 5.8 The hydraulic properties for wells in Class 2 interpreted using the Bierschenk & Wilson method 280

Table 5.9 Comparison of hydraulic property values obtained from the Bierschenk & Wilson / Logan (B & W) and Eden & Hazel (E & H) methods 286

Table 5.10 Drawdown of each steps in step drawdown test for wells in C 289

Table 5.11 The depth of the casing and the pumping water level of each of the wells. 290

Table 5.12 Processes that could possibly have affected the step drawdown tests in particular wells where responses were not as expected from theory (CM is conceptual model; Rushton & Rathod ,1988) 292

Table 5.13Well losses (observed-calculated drawdown) for wells in Class 1 (C>0) 295

Table 5.14 Water table information during the constant yield test recovery Period 306

Table 5.15 Hydraulic properties obtained from Cooper Jacob and Theis recovery method. 312

Table 5.16 The pumping rate, Q for wells in Ansell area. 316

Table 5.17 The period of measurement for each cycle. 317

Table 5.18. Hydraulic properties obtained from numerical modelling 335

Table 6.1 The type of industries in Shah Alam which are using groundwater 342

Table 6.2 The ionic balance error for each of the tubewell (with major ion analysis) 347

Table 6.3 The calculated TDS values (TDS_c) obtained from Electrical conductivity values with measured TDS (TDS_m). 350

Table 6.4 Major ion analyses (mg/l) of wells in Shah Alam. 353

Table 6.5. Wellwaters with no indication of pollution or have only one of the possible determinands indicative of pollution listed in Table 6.10. Concentrations in mg/L. Bold is for outlier concentrations including local pollutants. 361

Table 6.6 Saturation indices for carbonate mineral 362

Table 6.7. Saturation indices for feldspars and clays for the 'unpolluted' waters. 365

Table 6.8. Saturation indices for silica and simple aluminium minerals for the'unpolluted' wellwaters. Calculated using Phreeqc. 367

Table 6.9. Saturation indices for Fe and Mn minerals assuming pe = 4. Using Phreeqc 367

Table 6.10. The parameters evaluated Water Quality Index. Source : LUAS (2008) and Zaki (2010) 377

Table 6.11. Pollution indicating determinands (PIR – a pollution indicating ratio, that is number of the determinands listed with positive recorded concentrations as a fraction of the total number of determinands listed expressed as a %) 382

Table 6.12. The wells with E.coli and coliform (N.M-not measured;
N.D-not detected; MPN – most probable number) 389

LIST OF FIGURES

Figure 1.1 Shah Alam location (Director of National Mapping, Malaysia, 1970) 12

Figure 1.2. The urban aquifer development model of Morris et al. (1997) 13

Figure 1.3 Shah Alam with other cities in Selangor. The river networks comprise of Klang river, Damansara river and other river tributaries only in study area (Director of National Mapping, Malaysia, 1970). 14

Figure 1.4 Most of the tubewells in Shah Alam are in the Central area from Section 1-24 (Director of National Mapping, Malaysia, 1970). 15

Figure 1.5 The type of land use in Shah Alam (MBSA Shah Alam City Council Report 2020) 16

Figure 1.6 The geological map of study area.The tubewells are located in Kenny Hill Formation (Director General , Geological Survey Malaysia 1976). 18

Figure 2.1 Major faults in Peninsular Malaysia by Gobbett & Tjia (1973). 1) Bok Bak Fault, 2) Lebir Fault zone, 3) Kuala Lumpur – Endau fault zone, 4) Bukit Tinggi fault, 5) Chegar Perah-Benta fault, 6) Kledang fault. See the orientation of fault (3) to the regional pattern of faults in Peninsular Malaysia 23

Figure 2.2 The geological map of Selangor produced by Mineral & Geosciences Department Malaysia (1985). The study area is marked by the circle. 26

Figure 2.3 Locations of previous studies conducted in Kenny Hill Formation which is mainly in Kuala Lumpur and a few areas in Shah Alam. 32

Figure 2.4 The geological cross section through Kuala Lumpur presented by Yeap (1986). The line of section is shown in Figure 2.3. 34

Figure 2.5 The ground profile of the Kenny Hill Formation at Jalan Shaw, Kuala Lumpur by Lim (1995). 34

Figure 2.6 The stratigraphic sequence of Kenny Hill Formation at Bukit Pantai,Kuala Lumpur by Musbah (1980) 36

Figure 2.7 The lineaments mapped by Gobbett & Tjia (1973) in the Kuala Lumpur area which have been classified as the Kuala Lumpur - Bukit Tinggi fault zone,Ampang fault and Klang Gate Quartz dyke. 43

Figure 2.8 The borehole log distribution in Shah Alam. The topographic

contour is 50m interval. 48

Figure 2.9 The tubewells in Ansell compound (Google Earth). 50

Figure 2.10 The ground profile of Ansell TW2,TW3, TW4 and TW5 51

Figure 2.11 The ground profile of Ansell TW1,TW6 and TW7 53

Figure 2.12 The correlation between lithology at AESBI and Ansell 55

Figure 2.13 The ground profile of MT Pictures 57

Figure 2.14 The ground profile at Carlsberg 59

Figure 2.15 The correlation between Carlsberg and Mitsui High Tech 60

Figure 2.16 The correlation of lithology at Scientex Polymer with Gaya Color Lab 64

Figure 2.17 The correlation of rock at Universal Nutri Beverages with rock at Mitsui High tech and Carlsberg and Gaya Color Lab. 66

Figure 2.18 The rock correlation at CCM Fertilizer, Universal Nutri Beverages and Gaya Color Lab 67

Figure 2.19 The rock correlation at PROTON with AESBI 69

Figure 2.20 The ground profile at Canon Opto 70

Figure 2.21 The ground profile at Aquarium Express and Aquatic International 72

Figure 2.22 Outcrop A. It is located in front of Scientex Polymer area. The outcrop is oriented in a northwest / southeast direction. 75

Figure 2.23 Interbedded sandstone and shale at the southeast of the outcrop 76

Figure 2.24 The massive sandstone on the northwest 76

Figure 2.25 The rock sequence at Outcrop B. The yellow dashed line shows the antiform structure. 78

Figure 2.26 The sandstone with thin bed of shale (between yellow lines) at Outcrop B.The rock sequence is dipping to the southwest at an angle of 12º. The GPS device is 10 cm in length. 78

Figure 2.27 Joint is perpendicular to the bedding 79

Figure 2.28 Quartzite with thin layer of shale (white colour) 79

Figure 2.29 Quartz vein / lenses in sandstone at further east-southeast side. The diameter of the coin is 2.3cm 80

Figure 2.30. The thin layer of shale interbedded with quartzite 80

Figure 2.31 Faults observed in quartzite at Outcrop B 82

Figure 2.32The quartzite in fault zone is hard which is possibly due to the presence of quartz lenses. The size of the compass is 7cm. 83

Figure 2.33 The sheared quartzite 83

Figure 2.34 Fault is observed in massive quartzite outcrop 84

Figure 2.35 The sheared quartzite with quartz lenses 85

Figure 2.36 Fine fractures in mottled sandstone. The fractures are filled with iron oxide. The diameter of the coin is 2.3cm. 86

Figure 2.37 The quartz veins are displaced by fault 86

Figure 2.38 Phyllite which is dipping to the southeast at steep angle. The size of the compass is 20cm 87

Figure 2.39 The fault plane is almost vertical 88

Figure 2.40 Fold in quartzite 88

Figure 2.41 Joint in quartzite ranges from 0.5 to 1 metres length. The size of the GPS device is 10cm. The yellow dashed lines are the main joint set observed at Location 1 91

Figure 2.42 a) The joint spacing is smaller in weathered quartzite outcrop which located at the east-southeast of the outcrop ‘B’ (Location 2). 92

Figure 2.42 b) The wider joint spacing in massive quartzite at outcrop B (Location 2). 93

Figure 2.43 Location 3 of discontinuity survey at Outcrop B. 94

Figure 2.44 The lower hemisphere pole plots of the joints observed at Outcrop ‘B. The mean direction of each of the defined sets is indicated by the great circles, as labelled. The bedding dip poles are indicated by squares, with the great circles labelled ‘Bedding’. 94

Figure 2.45a) The lower hemisphere pole plots for faults observed at Outcrop B with faults from previous research 95

Figure 2.45b) The plots for fault set observed at Outcrop B. There are three sets of fault observed at Outcrop B. 95

Figure 2.45c) The plots of all the discontinuities observed at Outcrop B 96

Figure 2.46 The rock sequence at Outcrop C comprises sandstone overlying hard grey shale 97

Figure 2.47 The joint sets in the hard grey shale at Outcrop C. 97

Figure 2.48 This outcrop is located around 300 m north of Outcrop C. It is oriented in a north / south direction. The outcrop has an antiformal structure which plunges towards the north. The rock on the south side of outcrop is folded and a fault is present in the middle part (as shown by the yellow line). The arrows show the displacement. The rock sequence is dipping towards the northwest 99

Figure 2.49 The river alignment as observed in topographic map of Shah Alam published by Director of National Mapping Malaysia 1974 101

Figure 2.50 The plots for river lineaments 102

Figure 2.51 a) The distance of the well to Damansara river. The wells with → are those where quartz veins were recorded in their borehole cores. 102

Figure 2.51b) The distance of the well to Renggam river. The wells with → are those where quartz veins were recorded in the borehole cores. 103

Figure 2.51c) The distance of the well to Klang river. The wells with → are with quartz vein 103

Figure 2.52 The approximate distance of the well to granite (east of Shah Alam). No quartz veins for wells with → 104

Figure 2.53 Wells which quartz veins were observed 105

Figure 2.54 The wells with fractures observed in borehole. 106

Figure 2.55 The plots of faults of the Bukit Tinggi fault zone and the river lineaments. 108

Figure 2.56 The bedding and lineaments 109

Figure 2.57 The lineaments and fault from previous research and fault in phyllite;two sets of faults, one associated with the event that gave rise to the Bukit Tinggi fault zone with quartz vein fills, and one that is parallel with the extensional system seen at the Klang Gates dam area. The first is oriented in the NW/SE direction and is probably low K, and the other in the NE/SW direction and is probably of higher K 110

Figure 2.58 The geological map of study area. 113

Figure 2.59 The summary of the rock sequence in the central of Shah

Alam. 115

Figure 2.60 The weathering depth in central area of Shah Alam. 117

Figure 2.61 Depth of fractures encountered in central area of Shah Alam 119

Figure 2.62 The summary of the rock sequence in the eastern part of Shah Alam and its correlation with the rock sequence in the central part. 122

Figure 2.63 Depth of fractures encountered in eastern area of Shah Alam 123

Figure 2.64 The thickness of weathered layer in central and eastern area of Shah Alam 125

Figure 2.65 The rock sequence at western part of Shah Alam 126

Figure 2.66 Depth of fractures encountered in western area of Shah Alam 128

Figure 2.67 The rock sequence at the northern part of Shah Alam. 129

Figure 2.68 Depth of fractures encountered in western area of Shah Alam 130

Figure 2.69 The geological cross section of Shah Alam (see Figure 2.58) 132

Figure 2.70 The thickness of weathering layer observed in Shah Alam. 133

Figure 2.71 Depth of fractures encountered in Shah Alam 134

Figure 3.1 The abstraction rate, Q in m^3/day for wells in study area, with the classification system of JICA (1984) indicated. 137

Figure 3.2 A plot of drawdown for wells in study area, with the classification system of JICA (1984) indicated. 137

Figure 3.3 Depth of wells drilled in Shah Alam 140

Figure 3.4 Wells with depth less than 100m 141

Figure 3.5 Wells with depth deeper than 100m 142

Figure 3.6 The well yield showing no significant relationship with well depth 143

Figure 3.7 The relationship of log (specific capacity) with depth of well 143

Figure 3.8 The distribution plot for specific capacity for wells in study area, with the classification system of JICA (1984) indicated. 144

Figure 3.9 The wells with higher specific capacity that coincide with lineaments in the NE-SW direction. 145

Figure 3.10 a**)** Fracture distribution (black bars) with well screen location In the central part of the study area (note that some wells have multiple entries) 146

Figure 3.10b) Fracture distribution (black bars) with well screen location in the eastern part of the study area 147

Figure 3.10 c) Fracture distribution (black bars) with well screen location in the western part of the study area 147

Figure 3.10 d) Fracture distribution (black bars) with well screen location in the northern part of the study area 148

Figure 3.11 A summary of literature values for hardrock terrains split according to rock type (from Sam, 2014). 156

Figure 3.12 Water movement in quartzite in Shah Alam. In this case, water is assumed to flow along approximately vertical joints that are perpendicular to the bedding and then along the approximately horizontal bedding plane joints. 159

Figure 3.13 Bedding plane joints in Shah Alam, possibly developed somewhat due to weathering in shale layer 159

Figure 3.14 The tree roots are along the bedding and joint 160

Figure 3.15 Shale in fault zone 162

Figure 3.16 Iron oxide-hard crust in a fault zone in Shah Alam. 163

Figure 3.17 Interbedded quartzite and shale in fault zone 163

Figure 3.18Weathering profile for quartzite in Shah Alam (Ibrahim & Mogana 1988) with porosity and permeability plot with depth 166

Figure 3.19 A plot of percentage of clay against percentage of moisture in soil from quartzite and phyllite in Shah Alam. Data are from Tan & Ezdiani (2005) 171

Figure 3.20 Saturated hydraulic conductivity trends at OR,NR & NS with depth (Noguchi et al., 1997) 173

Figure 3.21 The infiltration rate in a sandstone slope at Sepang (grade III-V) (Bujang et al., 2005) 175

Figure 3.22 The bedding and joint in sandstone is heavily coated with iron oxide 176

Figure 3.23 Horizontal conductivity,Kh is possibly bigger than vertical hydraulic conductivity,Kv 177

Figure 3.24 Water level measured at Ansell's wells in 2005, 2007, 2008 and 2010. 180

Figure 3.25 The response of water level with rainfall. The measurement was carried out at Ansell in 2005. 181

Figure 3.26 The response of water level to rainfall. The measurement was carried out at Mitsui High tech and Good Year in 2006. 182

Figure 3.27 The water level responses to the rainfall as observed at Ansell TW7 183

Figure 3.28 The abstraction record in Shah Alam from 2005 to 2010 184

Figure 3.29a)The relationship between rainfall and Damansara river stage (TTDI station). 188

Figure 3.29b) The relationship between rainfall and Damansara river stage (Batu Tiga Station).Data in 2005 is missing. 188

Figure 3.30 Klang river hydrograph from 1973 until 2009. 189

Figure 3.31 Hydrograph of Klang river and corresponding rainfall records. 189

Figure 3.32 The groundwater head distribution of the study area 192

Figure 3.34 A hydrogeological conceptual model of Shah Alam under no pumping condition 195

Figure 4.1 The pattern of air streams in the southeast Asia region (Sham 1980) 197

Figure 4.2 The rainfall stations outside (Ladang Harpendent, Ladang North Hummock and Pusat Penyelidikan Getah Sg.Buloh), and inside the study area 200

Figure 4.3 Double mass plot for rainfall at TTDI and Subang station 201

Figure 4.4 Double mass plot for rainfall at UiTM and Pusat Penyelidikan Getah Sg.Buloh station 201

Figure 4.5 The rainfall stations outside Shah Alam area (data from Malaysian Meteorological Department and Department of Irrigation and Drainage Malaysia) 203

Figure 4.6 The annual rainfall recorded at three stations outside Shah

Alam area (data from Malaysian Meteorological Department and Department of Irrigation and Drainage Malaysia) 204

Figure 4.7 The monthly rainfall pattern for three rainfall stations outside Shah Alam area (data from Malaysian Meteorological Department and Department of Irrigation and Drainage Malaysia) 204

Figure 4.8 The annual rainfall for stations in Shah Alam area (data from Malaysian Meteorological Department and Department of Irrigation and Drainage Malaysia). 207

Figure 4.9 The average monthly rainfall distribution in Shah Alam area (data from Malaysian Meteorological Department and Department of Irrigation and Drainage Malaysia). 207

Figure 4.10 The average temperature recorded at Subang station from 2004 to 2008 (data from Malaysian Meteorological Department and Department of Irrigation and Drainage Malaysia). 208

Figure 4.11 Monthly average humidity level from Subang station (data from Malaysian Meteorological Department and Department of Irrigation and Drainage Malaysia) 209

Figure 4.12 The monthly average humidity saturation level and average temperature (data from Malaysian Meteorological Department and Department of Irrigation and Drainage Malaysia) 211

Figure 4.13 The relationship between mean annual temperature and humidity at Subang Station from 2004 to 2008 (data from Malaysian Meteorological Department and Department of Irrigation and Drainage Malaysia). 211

Figure 4.14 The relationship between annual average temperature and humidity for the Subang station (data from Malaysian Meteorological Department and Department of Irrigation and Drainage Malaysia). 212

Figure 4.15 The monthly average wind speed (data from Malaysian Meteorological Department and Department of Irrigation and Drainage Malaysia) 213

Figure 4.16 The monthly average radiation record (data from Malaysian Meteorological Department and Department of Irrigation and Drainage Malaysia). 214

Figure 4.17 The radiation and relative humidity (data from Malaysian Meteorological Department and Department of Irrigation and Drainage Malaysia). 215

Figure 4.18 The average evaporation pan recorded at Subang station (data from Malaysian Meteorological Department and Department of Irrigation 216

and Drainage Malaysia)

Figure 4.19 The monthly precipitation and evaporation pan in 2006 (data from Malaysian Meteorological Department and Department of Irrigation and Drainage Malaysia). 216

Figure 4.20 The relationship between evaporation and solar radiation (data from Malaysian Meteorological Department and Department of Irrigation and Drainage Malaysia) 217

Figure 4.21 The relationship between evaporation and temperature (data from Malaysian Meteorological Department and Department of Irrigation and Drainage Malaysia). 217

Figure 4.22 The relationship between evaporation and wind speed (data from Malaysian Meteorological Department and Department of Irrigation and Drainage Malaysia) 218

Figure 4.23 The precipitation and calculated reference evapotranspiration, ET_o, measured at Subang Station 223

Figure 4.24 The precipitation with reference evapotranspiration,ET_o (both evaporation methods) and pan measured at Subang Station. All units are mm d^{-1}. 225

Figure 4.25 The land use of Shah Alam area (Rancangan Tempatan Majlis Bandaraya Shah Alam MBSA 2020 (2003) 228

Figure 5.1 The specific drawdown (s_w /Q) plot with discharge rate, Q 243

Figure 5.2. The residual drawdown plot against ratio t/t' for one of the wells in the study area 248

Figure 5.3. The residual drawdown is s'. The drawdown curve, s is extended to obtain the calculated recovery value (s –s'). The calculated recovery then is plotted against time after pumping stopped. 249

Figure 5.4 The wells in study area is grouped into 5 classes (A to E) based on diagnostic plots. 252

Figure 5.5 An example of a drawdown curve representing Class A. The red box on both plots represents the zone where well bore storage effects should be negligible. The red line on double log plot represents slope of 1, expected where well bore storage dominates the water level decline. 255

Figure 5.6 An example of a Class B where the drawdown increase becomes gradually shallower with time. 258

Figure 5.7 An example of a Class B well where there is a sudden shallowing of slope part way through the test. 258

Figure 5.8 Example wells with Class C responses. 261

Figure 5.9 An example of a well in Class D where the flattening drawdown curve indicates strong, sudden recharge. 263

Figure 5.10 Wells in Class D which are near to the rivers. 264

Figure 5.11. An example of a well in Class E, wells in homogeneous confined aquifer 267

Figure 5.12 The transmissivity values for Class A and B. T values for Class B are higher (>10m^2/day) along the lineament. 273

Figure 5.13 Transmissivity values for wells in Class C & D. T values in these two classes are higher than 10m^2/day except for AESBI and Gaya Color Lab. 274

Figure 5.14 K values distribution for Class A and B. 275

Figure 5.15 K values distribution for Class C and D. 276

Figure 5.16 Wells in Class 1 with positive slopes 278

Figure 5.17 Wells in Class 2 with no variation of specific discharge (zero slopes) 280

Figure 5.18 Wells in Class 3 with negative slopes. Group E and Group B respectively 281

Figure 5.19 Efficiency of wells from Class 1 (C > 0). 282

Figure 5.20 An example of well where the Eden & Hazel method was attempted (Mitsui High Tech) 283

Figure 5.21 The example of well with negative C (Universal Nutri Beverages). 284

Figure 5.22 An example of a test which can be approximately fitted by the Theis curve Mitsui High Tech -Class E). 297

Figure 5.23. An example of a well in Class E (Mitsui Hightech) where the Cooper Jacob plot has been applied. Well bore storage effects are negligible when t > about 3.5 minutes. 297

Figure 5.24 An example of a well in Group B (Ansell TW7) where the slope of straight line changes with time. The change of slope is interpreted as recharge where the drawdown encountered the water source at t=50min. 298

Figure 5.25. The linear relationship of specific capacity with Transmissivity obtained by Cooper Jacob method. 300

Figure 5.26. The frequency distribution plot of log transmissivity for wells in study area 300

Figure 5.27 Wells with higher T values (T>10m^2/day) 301

Figure 5.28 A plot of log hydraulic conductivity frequency for wells in study area 302

Figure 5.29. K value increases with decreasing depth of well. 303

Figure 5.30.Step drawdown test analysis using Bierschenk & Wilson method 303

Figure 5.31. Step drawdown test analysis using Eden & Hazel method 304

Figure 5.32.The duration of recovery for each well and by how much the water level at the end of the test is short of recovery 308

Figure 5.33. The pumping rate for each well and how much water level needs to be recovered 309

Figure 5.34 The relationship of pumping rate with short of recovery of water level 309

Figure 5.35 Theis recovery plot for one of the wells in Class E (Mitsui High Tech) 311

Figure 5.36. Theis recovery plot for one of the wells with high deviation t/t'. 311

Figure 5.37. The T values obtained using Cooper Jacob and Theis Recovery shows good agreement. 313

Figure 5.38. Tubewells in the Ansell compound. 315

Figure 5.39.The static water level recorded in Ansell TW7 316

Figure 5.40. The water level measurement at Ansell TW7. 317

Figure 5.41. The duration of pumping and recovery in Ansell TW7. 318

Figure 5.42. The response of water level at Ansell TW7 when pump was ON and OFF 319
OFF.

Figure 5.43. The example of semi log and double log plots for Ansell

TW7 (Cycle 1) 320

Figure 5.44. An example of a recovery plot for Ansell TW7 (Cycle 1) 320

Figure 5.45. The water level dropped in Cycle 27 and 30 during recovery period before the water level becomes approximately static 321

Figure 5.46. Drawdown curves for the constant yield pumping test and from a typical cycle. The monitoring data are obtained at minute intervals whereas the pumping test data are obtained at increasing minute intervals. 322

Figure 5.47 The conceptual model of Mitsui High Tech 328

Figure 5.48 The modelled value fits the observed value with error -0.46 which is obtained from MODFLOW mass balance error. 328

Figure 5.49 The conceptual model of AESBI 330

Figure 5.50. Location of well at AESBI and the river 330

Figure 5.51. The modelled value fits the observed value except at the early of pumping and at recovery stage with error -0.13 which is obtained from MODFLOW mass balance error. 332

Figure 5.52. The conceptual model for Scientex Polymer 334

Figure 5.53. The modelled value fits the observed value with error -0.61 which is obtained from MODFLOW mass balance error. 334

Figure 6.1 Water sample is taken directly from the well through sampling tap. 344

Figure 6.2. Plot of measured TDS against EC (top) and a plot of TDS calculated by summing the analysed major ions plotted against EC (bottom). Also included in the latter plot is the best fit straight line from the upper plot (in red). Only samples with full major ion analysis are included. 348

Figure 6.3. Plot of Na concentrations against Cl concentrations. 354

Figure 6.4. Plot of NO_3 concentrations against Cl concentrations. 355

Figure 6.5. Plot of Ca concentrations against Cl concentrations. 355

Figure 6.6. Plot of SO_4 concentrations against Cl concentrations. 356

Figure 6.7. Plot of K concentrations against Cl concentrations. 356

Figure 6.8. Plot of Mg concentrations against Cl concentrations. 357

Figure 6.9. Plot of HCO_3 concentrations against Cl concentrations. 357

Figure 6.10. Plot of TDS against Cl concentrations. 358

Figure 6.11. The distribution of Type 1 wellwaters. 359

Figure 6.12. A plot of pH against log[HCO3-] for all samples where data are available. Lines are for pPCO2 ~ 1, 2 and 3. 363

Figure 6.13. Fe relationships. Upper plot: a plot of turbidity against Fe concentrations for Type 1 waters. Middle plot: a plot of NO_3 concentrations for Type 1 waters. Lower plot: a plot of Fe against NO_3 concentrations for all water types 366

Figure 6.14. Wellwater samples (Type 2) in study area. 369

Figure 6.15. A plot of turbidity against Fe concentrations for Type 2 waters. 371

Figure 6.16. Plot of Fe against Mn concentrations (mg/l) for Type 2. 372

Figure 6.17. Type 3 waters are at Ansell and Panasonic only. 373

Figure 6.18. Relationship between Ca and HCO_3. The almost zero Ca concentrations in Type 2 water may be in error. 374

Figure 6.19. The wellwater samples have a low background of NH_3-N and Cl^-.The sample with highest values of NH_3-N is Proton 1. 378

Figure 6.20 Wells with higher total dissolved solids (>100mg/l) and the industries with which they are associated. 379

Figure 6.21. TDS is used as a pollutant indicator. 381

Figure 6.22 The wellwater samples have a low background of NO_2^- and Cl^-. The sample with highest values of NO_2^- is Proton 1 and Proton 2. 384

Figure 6.23. The relationship of Fe with NO_3 for Wellwater Type 1 384

Figure 6.24 The organic matter in water samples (mg/l). 385

Figure 6.25. Detergent as MBAS in the wellwaters. The anionic detergent at three other wells are 0.05ppm (Proton 1 and 2 in 2006)) and 0.001ppm (Ueda Plating1 also in 2006). 387

Figure 6.26. The relationship between P and Cl concentrations. 388

Figure 6.27. The wellwater samples have a low background of $Al^{3+}$and Cl^{-}. 390

Figure 6.28 The relationship between Al and pH. 391

Figure 6.29. The relationship between Al^{3+} and $Si^{4+.}$ 391

Figure 6.30. The wellwater samples have a low background of $Zn^{2+}$and Cl^{-}. 393

Figure 6.31. The wellwater samples have a low background of $Pb^{2+}$and Cl^{-}. 394

Figure 6.32. The wellwater samples have a low background of $CN^{-}$and Cl^{-}. 394

Figure 6.33. The wellwater samples have a low background of $Cl^{-}$and F^{-}. 395

Figure 6.34 The relationship between Cu and Zn. 395

Figure 6.35. The relationship between Pb and Cd. 396

Figure 6.36. The relationship of heavy metals with pH (all but Zn on secondary axis). 396

1.0 INTRODUCTION

1.1 Urbanization and its impact on hard rock aquifers

In the last few years the world's proportion of urban dwellers has exceeded 50% (2850 million)(UN, 2009), with most of the most rapid expansions in urban populations taking place in developing nations. Most urban areas in developing countries are located on the coast or on major rivers as in Malaysia (Noorazuan et al. 2003) such as Madras, India (Somasundaram et al. 1993), Bangladesh (Abdullah 1982), Bangkok, Jakarta and Metro Manilla (Murakami et al.2005).

When population is increasing, there will be more water demand, water consumption and waste production causing much greater pressures on urban water management (Hellström et al.2000). The uncontrolled urbanization leads to urban water problem especially pollution (e.g Sim & Balamurugam 1991) and also encourages flooding to occur by reducing direct infiltration (Hara et al.2005; Khan 2005; Huong & Pathirana 2013).

Malaysia is an example of a country that is currently experiencing such urban water problems especially in Selangor. Selangor is the most developed state in Malaysia and Klang Valley is located in central Selangor (Figure 1.1). Disruptions to water supply in the Klang Valley area occur frequently. The history of water supply disruption can be traced to as early as 1998 (Aini et al.2001; Ibrahim & Fakhru'l-Razi 2006). For example, there were at least four water disruption events reported last year (Anonymous 2014, Bernama 2014a, 2014b & 2014c) and at least four cases until end of September in 2015 (Anonymous 2015,Bernama 2015a & 2015b). The water disruption is either due

to the dry weather especially in February and in June, or due to pollution occurring at the reservoir or due to maintenance operations.

Groundwater is chosen as an alternative water source due to the growing demand for water. This demand comes from rapid population growth, industrial or agricultural expansion, deterioration in quality of surface water and reduced flow of surface sources during prolonged droughts (Chu 2004). Groundwater is widely used in Kelantan for domestic purposes while in Selangor, the groundwater is mainly used for industrial purposes. The groundwater in Kelantan is at shallow depth (alluvium aquifer) therefore it is easier and cheaper to tap the water compared to aquifer in Selangor area which is at deeper depth (in fractured rock).

Groundwater study in Malaysia has been driven by the growing demand for water. The first groundwater exploration in Peninsular Malaysia was started in 1935 in the Kota Bharu area, Kelantan by the Geological Survey Department of Malaysia (GSM) which is now known as the Minerals and Geosciences Department Malaysia. A detailed study of the Kelantan Basin later was carried out by Ismail (1979) on the alluvial deposits as a potential aquifer. A regional groundwater potential study in Malaysia was carried out by JICA (1984). Kelantan Basin becomes the most studied regarding variety issues related groundwater and surface water ever since (Nur Hayati et al.2013, Fauzie et al. 2014).

The groundwater potential in fractured rock aquifer is further explored by Ismail (1981) by carried out first hydrogeology study on the Klang Valley area and

followed by Saim (1991) on Kuala Lumpur Limestone as a potential aquifer. The potential for fractured hard rock as aquifer was further explored by Raja Zainariah (1997), Umar et al. (2006), Mohammed Thamer & Abdul Halim (2009), Nasiman et al. (2011, 2012). These researches in general discussed the potential and well yield in fractured aquifer. The research which is focused on the hard rock aquifer especially in urban area is relatively new and only focused on Langat Basin (Ahmad Fariz et al. 2009, Manap et al.2013). Lack of urban groundwater study in Malaysia shows that there is a need to conduct urban groundwater research.

Urbanization affects the groundwater quantity and quality (e.g. Lerner & Barrett 1996, Foster et al.1998; Foster et al.1999; Foster 2001; Howard & Israfilov 2002; Foster et al 2011). To tackle these problems, it is necessary to understand the impacts of urbanization on groundwater systems if they are to be properly managed. Much work has been completed on urbanization and its effects on aquifers in many parts of the world, e.g. Chilton et al. (1999), Schirmer et al. (2013), such as: in shallow alluvial aquifers for cities in Asia (e.g. Somasundaram et al. 1993; Ahmed et al.1999; Ramnarong 1999; Nickson et al. 2000; Umezawa et al. 2008; Hayashi et al. 2009); in sedimentary rock aquifers in the United Kingdom (e.g. Rivett et al. 1990; Burston et al. 1993; Ford et al.1992; Ford & Tellam 1994; Tellam & Thomas 2002; Shepherd et al. 2006, Rivett et al. 2011). There has been some research on urban hardrock aquifers, but it is very much biased towards crystalline basement settings, particularly in semi-arid settings (e.g. Cronin et al. 2007; Naik et al. 2008; Courtois et al. 2010; Kale et al. 2010; Pauwels et al. 2010; Prasad et al. 2011). However, there is a relative

lack of international studies on hard rock fractured metasedimentary urban aquifers especially in climates relevant to many parts of Malaysia. Indeed there has been much less research on the hydrogeology of regionally metamorphosed sedimentary rocks of greenschist facies in general, the literature tending to concentrate on plutonic igneous and highly metamorphosed basement complexes (e.g. Lloyd, 1999);

Thus there is little international evidence to use in assessing likely vulnerability of fractured metasedimentary aquifers in the rapidly developing industrial abstraction areas such as those of the Klang Valley. Thus the research described in this thesis has been undertaken in order to help fill this research gap. As metamorphosed sedimentary sequences are relatively common internationally, research on their behaviour and vulnerability as aquifers would be relevant in many countries.

1.2 The susceptibility of urban hard rock (metasedimentary) aquifers to hydraulic and contaminant stresses

Here and throughout the thesis the word ‘susceptibility’ will be used in place of the more usual used word ‘vulnerability’ as ‘vulnerability’ has been used very extensively in the context of development of vulnerability maps and the application of such methods as DRASTIC, neither which will be used in the present research.

The susceptibility of an aquifer to chemical stress is determined by the potential of pollutant from the surface to reach the aquifer (Palmer et al. 1995) which is dependent upon the recharge mechanisms (Robins 1998). In urban aquifers, the

recharge mechanisms are altered due to city development e.g. less rain water infiltrates the ground and additional sources of recharge coming from leakage of water supply pipes (Lerner 1990) and wastewater sewers and drainage systems (Foster & Chilton 2004). The variety sources of recharge provides a variety sources of pollutants. The permeability of the unsaturated zone layer is an important factor in the study of the susceptibility of aquifers (e.g. Adams & Foster 1992; Swartz et al. 2003) as low permeability material like clay acts a barrier, providing a natural protection / natural attenuation, protecting the aquifer from pollution (e.g. Fretwell et al. 2000). Unsaturated zones with higher permeability like sandy material and presence of fractures will increase the permeability of the layer hence increasing the susceptibility of the aquifer to chemical stress (e.g. Foster 1998; Jones & Cooper 1998).

Crystalline hard rock aquifers have been found to be susceptible to chemical stresses, often having small solute residence times, water rapidly travelling through fractures with limited filtering or reactive interactions (Taylor & Howard 2000; Marechal et al. 2004; Wyns et al. 2004; Dewandel et al.2006). Is this also the case for metasedimentary aquifers or do the weathering characteristics and different mineralogy mean that there is greater protection from contamination?

Urban hard rock aquifers would also be expected to be susceptible to hydraulic (quantity) stresses, as they often have small aquifer response ($\sim = Sx^2/T$) times, and thus stresses such as pumping or change in recharge will be seen to be rapidly transmitted through the system from the point of stress. Again a

complicating issue in the case of metasedimentary hardrock aquifers is the presence of the often clay-rich weathered zone which may damp the responses in the underlying aquifer to impacts at ground surface and the other way around. For example, change in recharge may not be entirely passed onto the aquifer if the weathered zone still drains during a period of low rainfall, or the weathered zone acts as a source of leakage when pumping stresses are applied.

Though all of these suggestions are feasible, the important issue in assessing a newly urbanised aquifer is to what degree is each susceptibility present. For example, does the weathered zone really protect the aquifer to a useful extent from pollution, does it really provide an extent of buffering when pumping is heavy (i.e. does leakage provide a useful added amount of recharge?).

1.3 The usage of standard regulatory dataset to develop understanding of newly urbanised aquifers

A fundamental problem in Malaysia where urbanization is occurring in hard rock areas, and a number of other geographically and geologically similar countries, is circumventing the problem of limited data availability.

This is central in two ways. Firstly when new cities are developed or existing cities expand into rural areas there is usually very few data available and no pre-urbanisation monitoring available. And secondly, in many countries there is a problem with funding sufficiently detailed monitoring in the longer term and data therefore will always be limited.

The research in this project is concerned with trying to determine the hydraulic and chemical susceptibility of a Malaysian urban hard rock aquifer using only existing and very cheaply gathered data. Existing methods based on vulnerability mapping will not be used as these are well established in the literature and the standard methods have yet to be fully tested on metasedimentary fractured aquifers. Instead the work will concentrate on the detailed study and interpretation of available data collected to satisfy national regulatory legislation. This addresses a second research gap in that there has been very little assessment as to whether the data required of licenced abstractors is adequate for aquifer susceptibility evaluations.

The area chosen for investigation is the newly urbanised area of Shah Alam on the southwestern side of Kuala Lumpur. The data available for Shah Alam consist of:

1. The results of previous geological and hydrogeological investigations. As summarised above, these are very limited.
2. Data collected for licensing purposes, specifically borehole drilling records, pumping test results of borehole completion, water level on completion and water quality analysis on completion.
3. Additional data obtained by the industries owning the boreholes.
4. Site investigation engineering data.
5. Meteorological data.
6. Water supply data.
7. Topography maps.
8. Annual water level measurement and water quality analysis.

The borehole specific data are for industrial sites only, and are located in a non-ideal distribution across only one part of the city .

There is no real possibility from these data of obtaining regional maps of the entire aquifer, or of setting up a constrained water balance for the city as there are no data for most of the aquifer and not enough water level data to construct a piezometric surface map for any date, especially given the numerous closely located surface water features that will cause there to be local variations in head. Can the basic regulatory authority data and the other data listed above be used to produce an understanding that though lacking a spatial element in general might be used to assess probability of susceptibility at any one site?

1.4 Research Aims

The basic aim of the research project is to develop a conceptual understanding of the hydrogeology of an urban hardrock aquifer in an equatorial climate, to use the understanding gained to determine the susceptibility of the aquifer to hydraulic and chemical impacts and to do all this using only information available from regulatory authorities and simple cheap additional observations (e.g. basic geological observations on outcrops and water level data logging of abstraction wells).

In doing this, ancillary aims are:

- to build an understanding of the Shah Alam aquifer that would be of use for local water resource development;
- to use the understanding to further knowledge in general of hard rock urban aquifers in equatorial climates;

- to suggest ways that the approach used might be improved and to identify limitations of it.

The methods used are seen as complementary to more traditional vulnerability mapping.

1.5 Research Approach and Thesis Structure

The data existing in Shah Alam are mostly submitted by industrial companies when seeking licences for abstraction wells but there are also climate data and some data from engineering site investigation. All these data are commonly found in cities like Shah Alam in Malaysia. The research described here uses these data and very limited fieldwork to develop a conceptual model which is then used to evaluate the likely general qualitative susceptibility of the aquifer to hydraulic and chemical stresses.

The geology of study area is interpreted using geological information which is obtained from borehole log interpretations, fieldwork and very limited previous research (Chapter 2). In Chapter 3, the initial hydrogeological conceptual model of the study area is built using very limited previous aquifer assessment data, the geology interpretation from Chapter 2, the river - aquifer relationship, water level records, topography and abstraction data. The hydrogeological conceptual model then is integrated with meteorological (e.g. precipitation, evapotranspiration) to propose the recharge mechanisms of aquifer in the study area (Chapter 4).

In Chapter 5, the initial conceptual hydrogeological model is tested and developed using constant yield and step test pumping test data obtained from

licence files for 38 wells in the study area. The interpretation of aquifer system is carried further using numerical modelling for better understanding of the aquifer behaviour. The emphasis here is not on obtaining aquifer properties (though this is done) but on using the tests as experiments that can provide information about aquifer processes. The conceptual model is then further developed using groundwater chemistry data in Chapter 6. In Chapter 7, all the study findings will summarized and with recommendations for further research are proposed.

Though the approach used here is a standard one in the sense of developing a conceptual model using geological and meteorological and pumping test and chemical data, it differs from previous major research investigations of urban aquifers in the following ways: it relies entirely on licence file data supplemented by simple and cheap fieldwork (geological observations and water level logging); no regional groundwater flow modelling is attempted as no observation well data exist for the aquifer, and instead of using a numerical model to predict future impacts it concentrates on using the understanding developed to evaluate qualitatively the susceptibility of the aquifer to both quantity and quality impacts. It is hoped that the results will provide an assessment of the Shah Alam system that is very urgently required before irreparable damage is done to the system whilst also indicating what can be done with limited data. It is also hoped that it will provide an almost uniquely early evaluation of the hydrogeological behaviour of a new city.

1.6 Choice of Study Area

Shah Alam, a recent urban development close to Kuala Lumpur (Figure 1.1), has been chosen as the study area because:

1. the Shah Alam aquifer is a hard rock aquifer apparently typical of many in Malaysia and elsewhere in the world;
2. the aquifer is used actively for groundwater supply and the regulatory authorities are willing to supply all the data for the research;
3. no interpretation of the aquifer as a whole has previously been attempted, or even of its geology other than in very broad terms, and hence Shah Alam would be a good test of whether standard data collected by regulatory authorities, supplemented by engineering studies that would be available almost all cities, are adequate to develop a good understanding of the system behaviour;
4. the city has been recently (1970 onwards) developed from agricultural land, a common occurrence in many rapidly expanding cities in Asia and elsewhere.

It is noted that the investigation of such a newly urbanised area is almost unique in the literature, and is important in from the point of view of being able to see how quickly impacts occur and also to see differences in modern city design from older city design.

From a local point of view, there is also much interest in studying the Shah Alam aquifer as the sustainability of the groundwater supply is unknown, and much industrial activity depends on good water supply. In addition, there are many

parts of Malaysia with similar rocks (including the states of Kedah, Selangor, Johor, Sabah and Sarawak) and any specific hydrogeological conclusions from studying Shah Alam might be transferable to these areas too, in addituion to methodological conclusions being transferable to other cities worldwide. Shah Alam has both flooding and drought problems and any added understanding about the city's groundwater would be important.

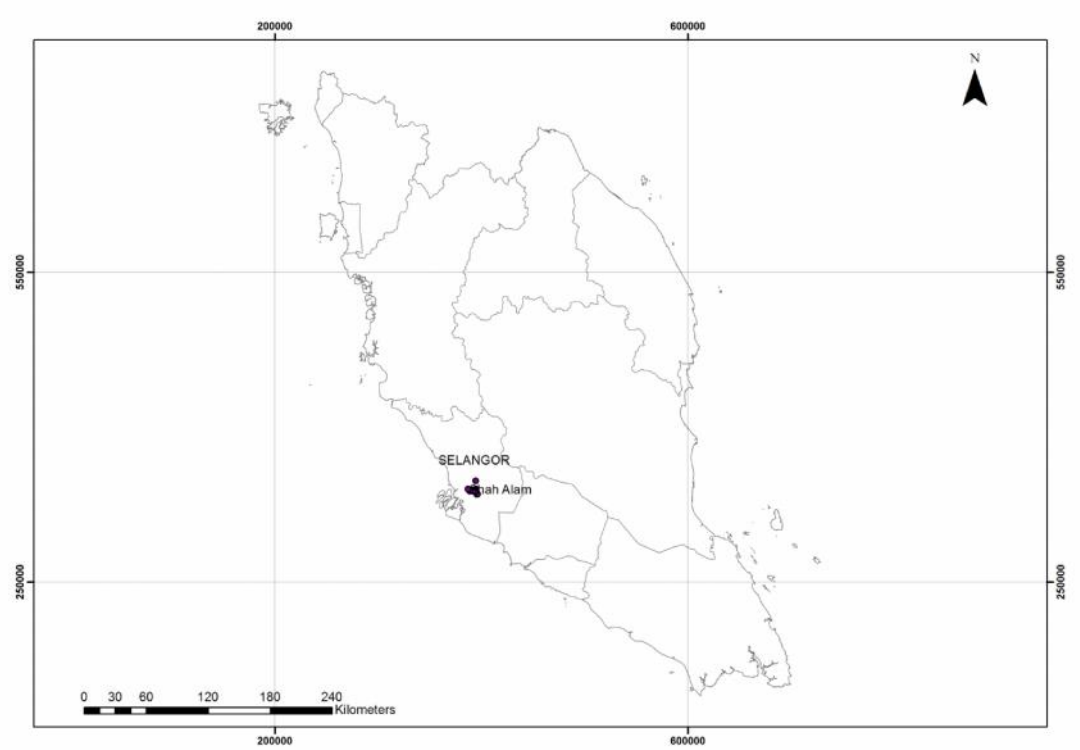

Figure 1.1 Shah Alam location (Director of National Mapping, Malaysia, 1970)

Shah Alam is in the early stages of the general development model of Morris et al. (1997) (Figure 1.2), a big difference with many cities that have been studied for example in Europe (e.g. Birmingham; Shepherd et al., 2006; Tellam, 2007). The newness of the city may make the interpretation of its behaviour simpler than in the case of an older city as there is little complex history of land use and abstraction. This may mean that depending on existing data for most of the study

may be more appropriate than for an older city. Infrastructure may be in a better state of repair than older cities and hence recharge contributions from water pipes and sewers may be less extensive than in older cities (Foster et al. 1999). In addition, depending on the results of the study, modifying management practice in Shah Alam may be easier than in older more established urban aquifers.

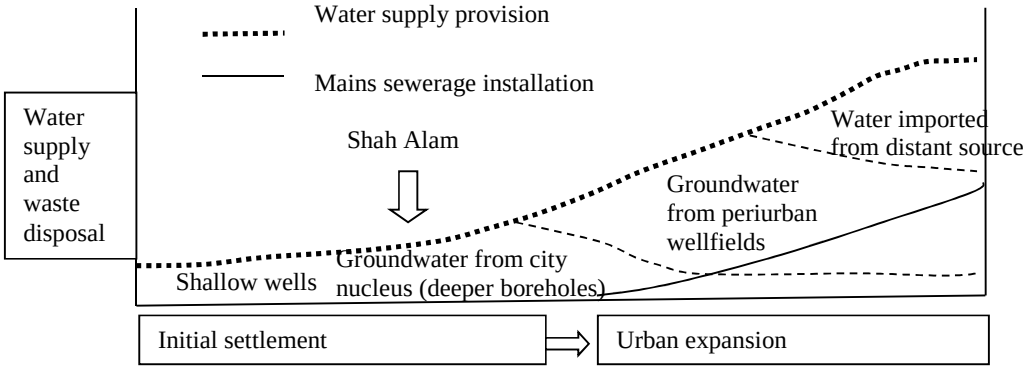

Figure 1.2. The urban aquifer development model of Morris et al. (1997)

1.7 Shah Alam: Overview of the city

1.7.1 Outline of Urban Development

Shah Alam was once a palm oil estate which was known as Sg Renggam. It started its development in 1963 in a way to replace Kuala Lumpur as the administrative centre of Selangor. Shah Alam then became a Federal Territory on 1st February 1974. On 7th December 1978, it was declared as the new state capital of Selangor and bestowed with city status on 10th October 2000.

Shah Alam covered an area of 41.69km^2 in 1979 but since then has expanded rapidly to cover an area of 290.3km^2 with population of 475,260 people as

recorded in 2005 (MBSA Shah Alam City Council Report 2020). It is situated 25 km from Kuala Lumpur and 16 km from Klang. It is surrounded by big cities such as Subang Jaya, Klang and Putrajaya (Figure 1.3). It is managed by Shah Alam City Council (SACC) and is divided into 56 sections (Figure 1.4) which are North Area (Section U1-U20), Central Area (Section 1-24) and South Area (Section 25-36).

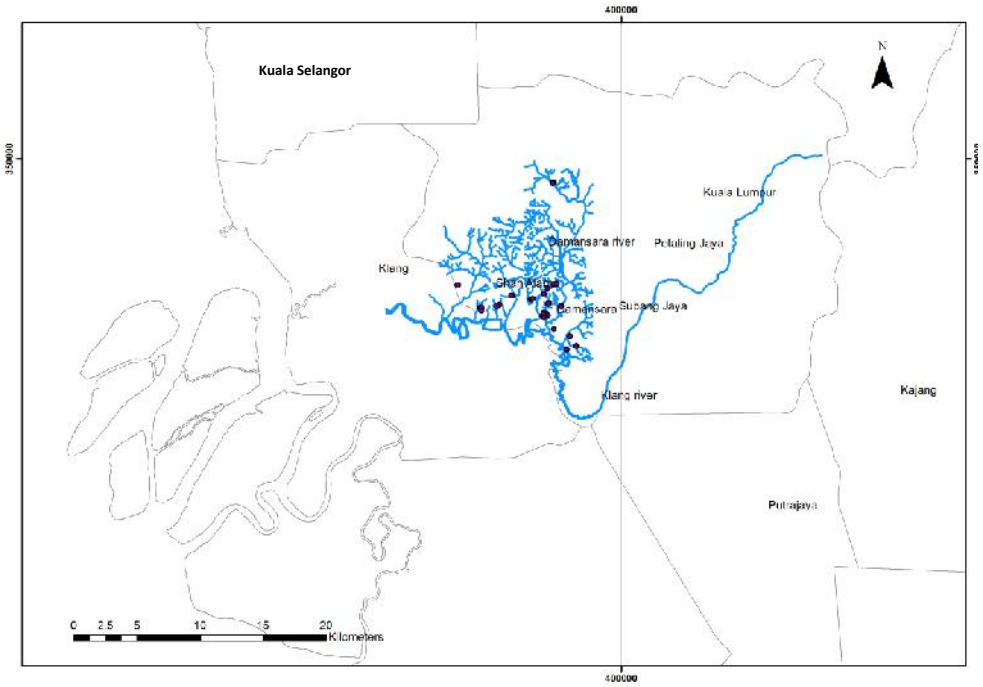

Figure 1.3 Shah Alam with other cities in Selangor. The river networks comprise of Klang river, Damansara river and other river tributaries only in study area (Director of National Mapping, Malaysia, 1970).

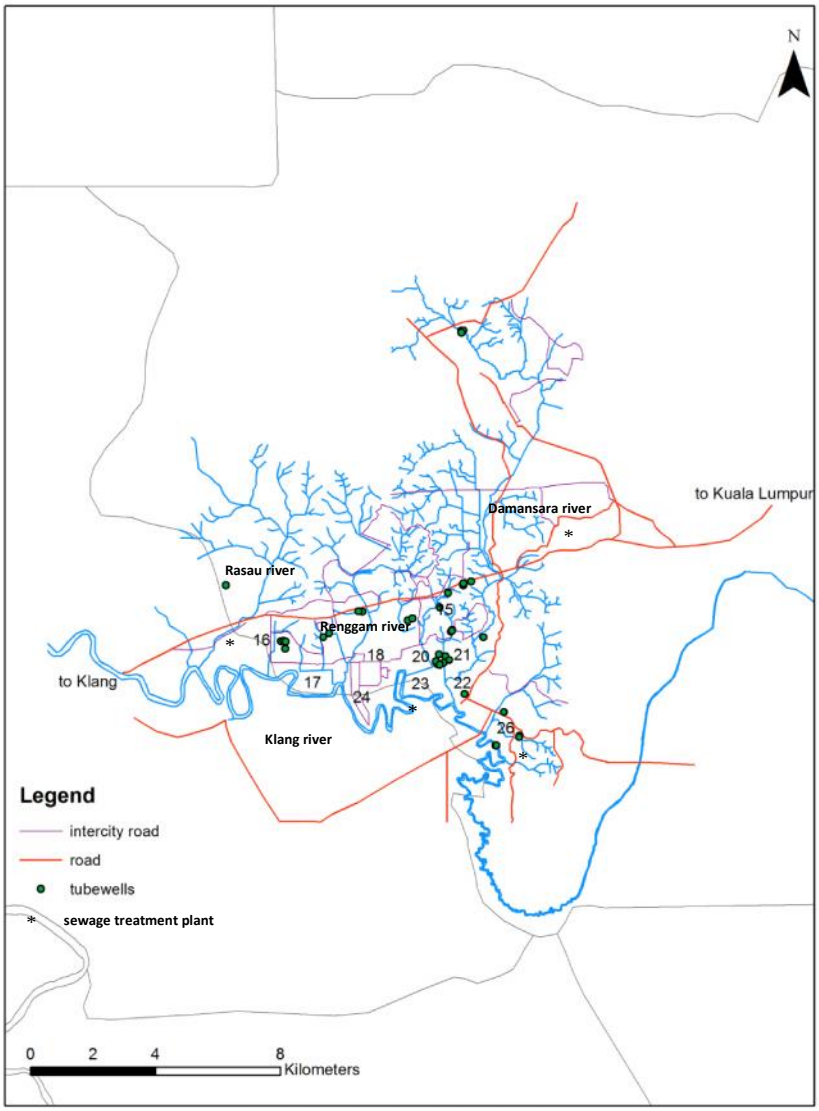

Figure 1.4 Most of the tubewells in Shah Alam are in the Central area from Section 1-24 (Director of National Mapping, Malaysia, 1970).

Figure 1.5 shows the type of land use in Shah Alam (MBSA Shah Alam City Council Report 2020). 24% of the Shah Alam area is covered with shrubs. 16% is for accommodation and housing area. 12% of the area is occupied each for

road as there are six highways connecting Shah Alam with major cities and for agriculture. 8% of the area is used for institution and public amenities and 8% for industry. 3% of the area is used each for industry and infrastructure. 9% of the area is still forested. 6% is for recreational area and parks. Only 2% of Shah Alam area is covered with water bodies and for infrastructure and utilities. 1% of Shah Alam area is for business and service activities. The variety type of land use in Shah Alam makes this area an interesting one in which to conduct a groundwater study. Besides, the tubewells in Shah Alam are located in highest populated area (central part) with 30.8 people per hectare.

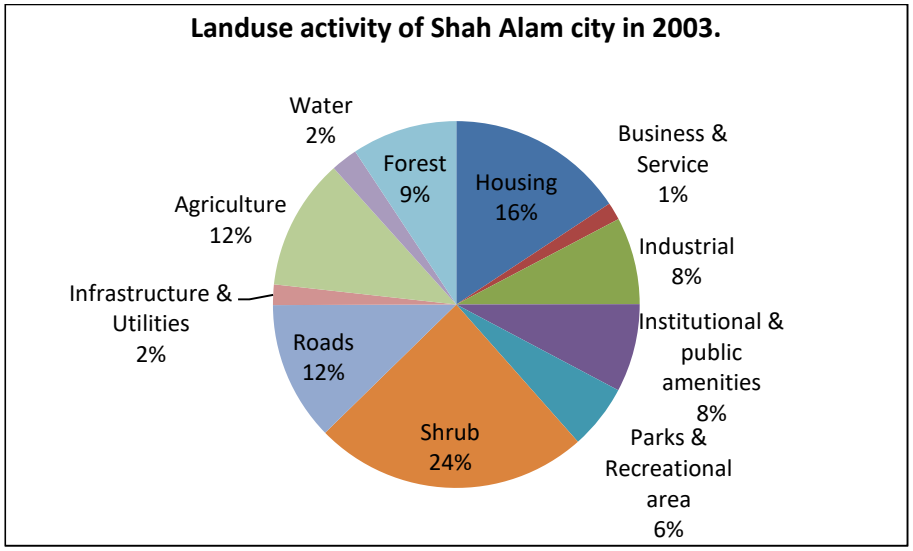

Figure 1.5 The type of land use in Shah Alam (MBSA Shah Alam City Council Report 2020)

1.7.2 Climate

The average temperature is 25-33 celcius. There is no distinct season except for the interchanging warm tropical season and rainy monsoon throughout the year with average rainfall of 2300mm/year.

1.7.3 Topography & Drainage

The central Shah Alam area lies in a low topographical area which is less than 25 m above sea level. The topography is higher to the northwest of Shah Alam, with Sapu Tangan Hill as the highest peak (210 m a.s.l).

The Klang river is the main river flowing across this area. It starts from the Mountain Range of Titiwangsa and flows in a southwest direction towards the Straits of Malacca. The Klang river is fed by seven main tributaries including Damansara river and Renggam river that run across the Shah Alam area (Figure 1.4). The total area of this basin is approximately 1290km^2.

1.7.4 Geology

Shah Alam area is poorly known as underlain with alluvium on the top of Kenny Hill Formation and overlying the limestone (Figure 1.6). Kenny Hill Formation comprises a sequence of metamorphosed clastic sedimentary rocks (Gobbett & Hutchinson 1973). The age of this formation is Upper Silurian to Devonian. This formation occurs as a broad synclinal belt comprising a monotonous sequence of interbedded shales, mudstone and sandstone, and conglomerate**.** Both are very much weathered but sandstone beds are more resistant. Shale and mudstone are sometimes phyllitic.

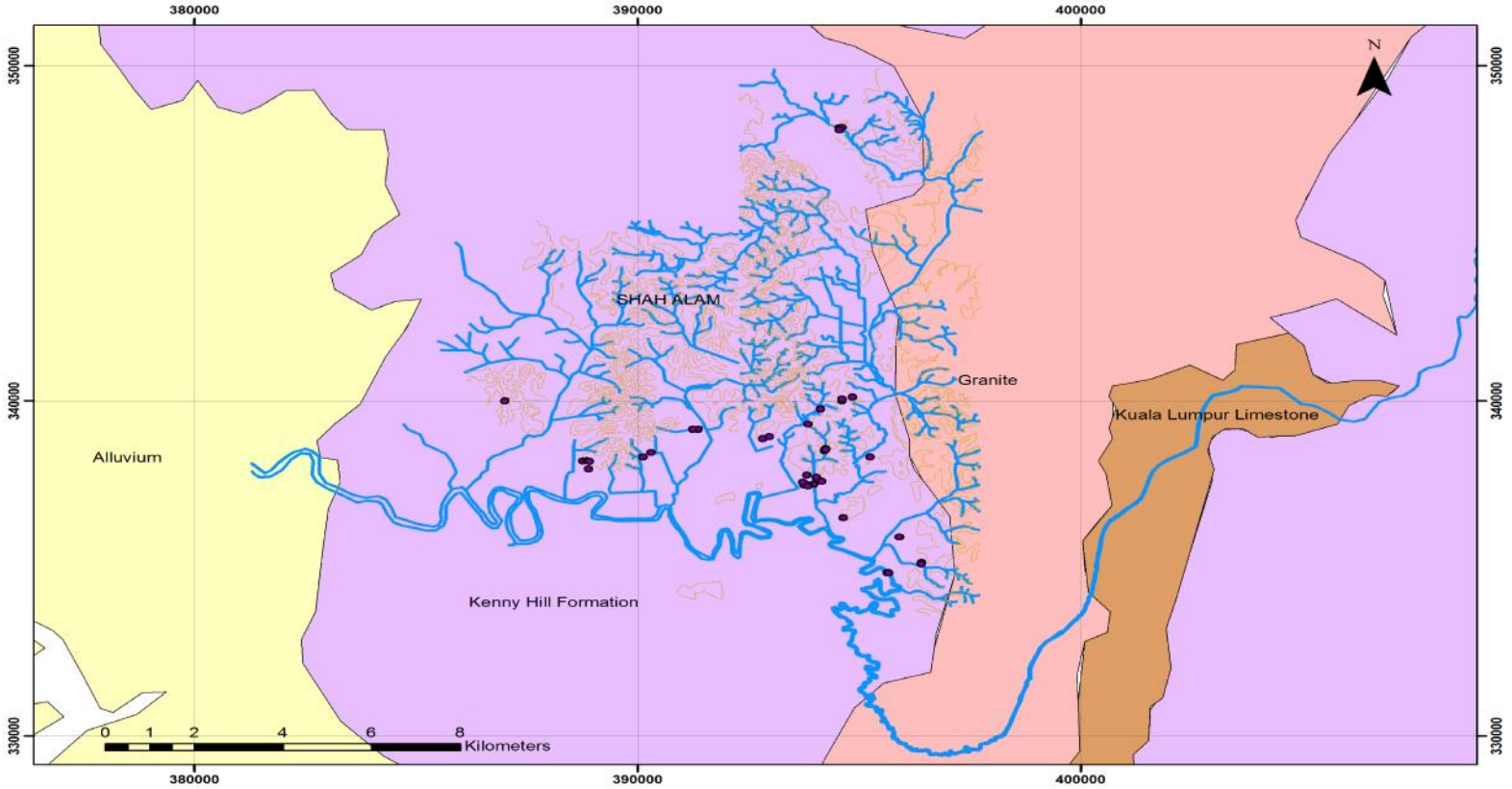

Figure 1.6 The geological map of study area.The tubewells are located in Kenny Hill Formation (Director General, Geological Survey Malaysia1976).

1.7.5 Water and waste disposal management

All the surface and subsurface water sources in Selangor including Shah Alam are managed by Selangor Waters Management Authority or LUAS since 1997. From 1 January 2005, SYABAS has been awarded a contract to manage water supply and distribution for a period of 30 years. Treated water for Shah Alam area is supplied from Selangor River Treatment Plant Phase 3 (SSP3) which is located at Kuala Selangor (Figure 1.3). The maximum capacity for this plant is 800 million litres per day (MLD) and in average supplies 582 MLD to Shah Alam area for domestic and industrial purpose.

The sewerage service in Malaysia is provided by Indah Water Konsortium (IWK) including in the Shah Alam area. There are two types of sewerage system which are either connected to public sewage treatment plants or to individual septic tanks. There are five sewage treatment plants in Shah Alam (Figure 1.4). The industrial waste is treated separately before being discharged to the river.

All the stormwater will be flow into the drain and will be transferred to main culvert/open drain through underground pipe.

2.0 AN INTERPRETATION OF THE GEOLOGY OF SHAH ALAM

2.1 Introduction

In this chapter the geology of the study area will be discussed. The geology of the area has only previously been described in a general way, and this chapter combines the previous limited work with data obtained from borehole logs from water wells to produce a more detailed interpretation of the area underlying the urban area. The national geological setting will be discussed first in Section 2.2 and the regional geological setting in Section 2.3. Section 2.4 summarizes the previous geological work undertaken in the study area. Section 2.5 then presents and interprets the geological information collected as part of the current study (mainly borehole logs). Finally, Section 2.6 summarizes the geological conceptual model that later (Chapter 3) will be used to develop the hydrogeological conceptual model of study area.

2.2 Outline Geology of Peninsular Malaysia

2.2.1 Geological history of Peninsular Malaysia

The geological history of Peninsular Malaysia as summarized by Gobbett (1973) began in Late Cambrian time. It started with marine geosynclinal sedimentation. This geosyncline was divided into two parts by a geoanticlinal ridge; a "miogeosyncline" (shallower water deposits) occurred to the west and a "eugeosyncline" (deeper water deposits) to the east.

The sedimentation phase was terminated by major orogenic phase where massive uplift occurred in Triassic times until Early Cretaceous (Burton 1973). Metcalfe (1991) suggested the uplift was caused by the collision between Sibumasu and mainland Asia that occurred in the Early Triassic. Sibumasu is the elongate continental block comprising Peninsular Malaysia, western Thailand and Burma. Harbury et al. (1990) stated that there were two compressional events that affected Peninsular Malaysia. One was in Late Permian times while the other was in mid - late Cretaceous times.The latter event was confined to the central basin only. The compressional event was accompanied by plutonic and diastrophism activity.

Later, there was a long period of erosion, and repeated uplift and granite intrusion during Cenozoic time which caused molasse type sedimentation in the continental basin. This event was linked with normal faulting and local volcanism. Peninsular Malaysia was tectonically stable by the end of Mesozoic or in early Tertiary time except for some uplift, tilting and fault movements. During the Neogene, major sinistral strike-slip faults developed in an east – southeasterly direction correspond to the formation of the Sunda Arc and large scale earth movements in Indonesia. This event has set up an arcuate form to the regional strike and the axis of the Main Range Granite in the western side of the Peninsula.

No Lower Tertiary sediments have been recorded. Coal was developed in small sedimentary basins in the Late Tertiary and some in depressions aligned with the

major faults. Alluvial deposits were deposited in coastal and also in presently offshore areas (due to the sea level changes) in the Quaternary.

2.2.2 Geological environment

The tectonic events played an important role in creating the Peninsular Malaysia geological environment. Peninsular Malaysia is elongated in N-NW direction which is parallel to its main structural trend, a trend that was developed during Late Triassic-Early Jurassic. In 1985, Tjia & Zaiton have divided Peninsular Malaysia based on lineaments developed from the tectonic events. There are four geologic domains which are northwest, west and central and east .The East and Central domain is separated by Lebir Lineament. Bentong Lineament separates the Central and the West domain. The Krian – Bentong Line separates Northwest and West domain. They suggested that the geologic transport is to the west except in central domain.

The Palaeozoic rock sequences have been faulted and folded with the effects of the two series of compressional events. Figure 2.1 shows the major faults in Peninsular Malaysia. In 1989, more faults were identified using remote sensing technique by Tjia. They are striking to north, north-northwest, northwest and west-northwest. The majority of large faults, which are striking between NNW and WNW, show a left slip displacement with 55km to probably 200km offset. The faults that strike north show a right slip displacement. Large faults that are parallel or normal to regional strike are normal faults.

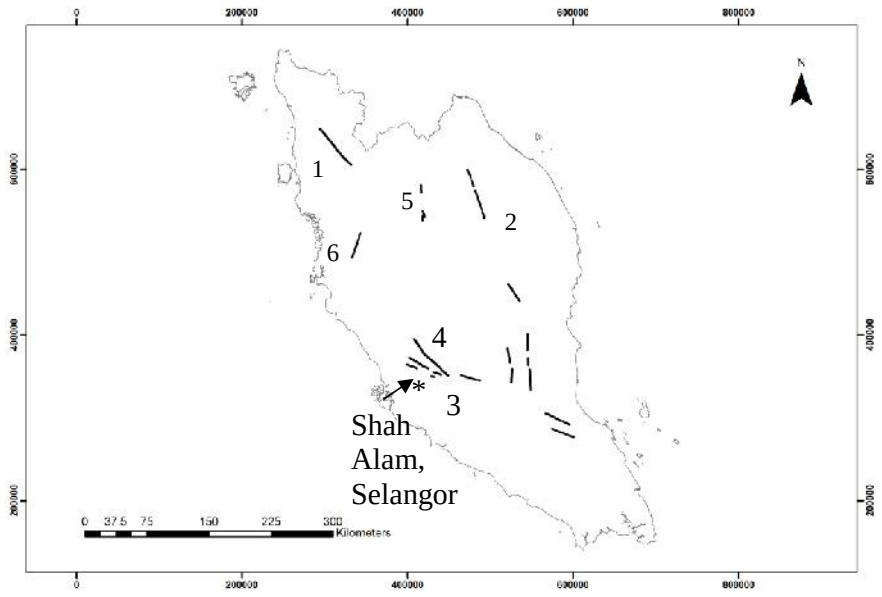

Figure 2.1 Major faults in Peninsular Malaysia by Gobbett & Tjia (1973). 1) Bok Bak Fault, 2) Lebir Fault zone, 3) Kuala Lumpur – Endau fault zone, 4) Bukit Tinggi fault, 5) Chegar Perah-Benta fault, 6) Kledang fault. See the orientation of fault (3) to the regional pattern of faults in Peninsular Malaysia

The Palaeozoic rocks experienced metamorphism from the plutonic activity that associated with the compressional events. Peninsular Malaysia can be divided into four regions based on granite emplacements (Hutchison 1977). They are Western stable shelf, Main Range Belt, Central Graben and Eastern Belt. Shah Alam is in Main Range Belt region. Table 2.1 shows the characteristics of each region.

Table 2.1 The tectonic division of Peninsular Malaysia which is based on the characteristics of the granite intrusions (Hutchison 1977).

	Western Stable Shelf	Main Range Belt	Central Graben	Eastern Belt
Granite characteristics	Intermediate microcline	Batholiths. Coarsely porphyritic, alkali feldspar-microcline	Highly sodic fine grained which found only along a narrow line of Gunung Benom and Gunung Stong.	Equigranular-weakly porphyritic. Alkali feldspar-orthoclase to intermediate microcline
Country rock	the oldest rock (the Lower & Upper Paleozoic miogeoscline deposits At Langkawi, the contact aureoles is observed.	Phyllitic and isoclinally folded of Lower Paleozoic metasediments. Upper Paleozoic formations is less folded	A complex belt; the sedimentary environment changes from marine to continental. (Triassic / Mesozoic formations are gently folded & underlain by strongly folded Permian rocks).	Gently deformed sedimentary, volcanic and pyroclastic formations.well developed contact aureoles
Radiometric evidence		Rb:Sr and K:Ar dates are discordant shows that Main Range Granite has been uplifted since Triassic with 5-11 km of emplacement depth.		Rb:Sr and K:Ar are concordant shows that the granite were epizonally emplaced (from near surface to 5km depth).
Age		Were emplaced from Late Carboniferous to Late Triassic. In deep seated environment – continental collision (Mitchell 1977)		Has been stable since the Triassic.

2.3 Geology of Selangor

2.3.1 Introduction

Selangor lies in the Western Domain (see Figure 2.1). It is the most developed state in Malaysia. The first geological studies of Selangor area were carried out by Roe in 1951 which covered Fraser's Hill, Perak and Pahang (see Figure 2.3). In 1953, he wrote another memoir covering Kuala Selangor and Rasa (see Figure 2.3). In 1973, Gobbett & Hutchinson (1973) compiled all the geological information available including for the Selangor area. In 1986, Yin prepared a draft of geology and mineral resources of Kuala Lumpur to Klang area. There are limited previous geological studies in the region; therefore the geology of Selangor is mainly based on these reports especially from Yin 2011 and Gobbett & Hutchinson (1973). However, the urbanization has exposed outcrops and resulted in borehole drilling, both of which provide useful information on which to base the geological interpretation needed for the present study.

2.3.2 The stratigraphy of Selangor

2.3.2.1 Brief introduction

Figure 2.2 shows a geological map of Selangor (Department Mineral & Geosciences 1985). Table 2.2 shows the stratigraphic column of Selangor. The Lower Palaeozoic sequence in Selangor comprises the Dinding Schist, the Hawthornden Schist and the Kuala Lumpur Limestone. The Upper Palaeozoic sequence in Selangor comprises the Kajang Formation and the Kenny Hill Formation. The Kajang Formation is still not completely defined and accepted in the literature due to lack of information. There were two tectonic events that have

occurred in this area. The first event occurred after the Kajang Formation was deposited causing the Lower Palaeozoic rocks and Kajang

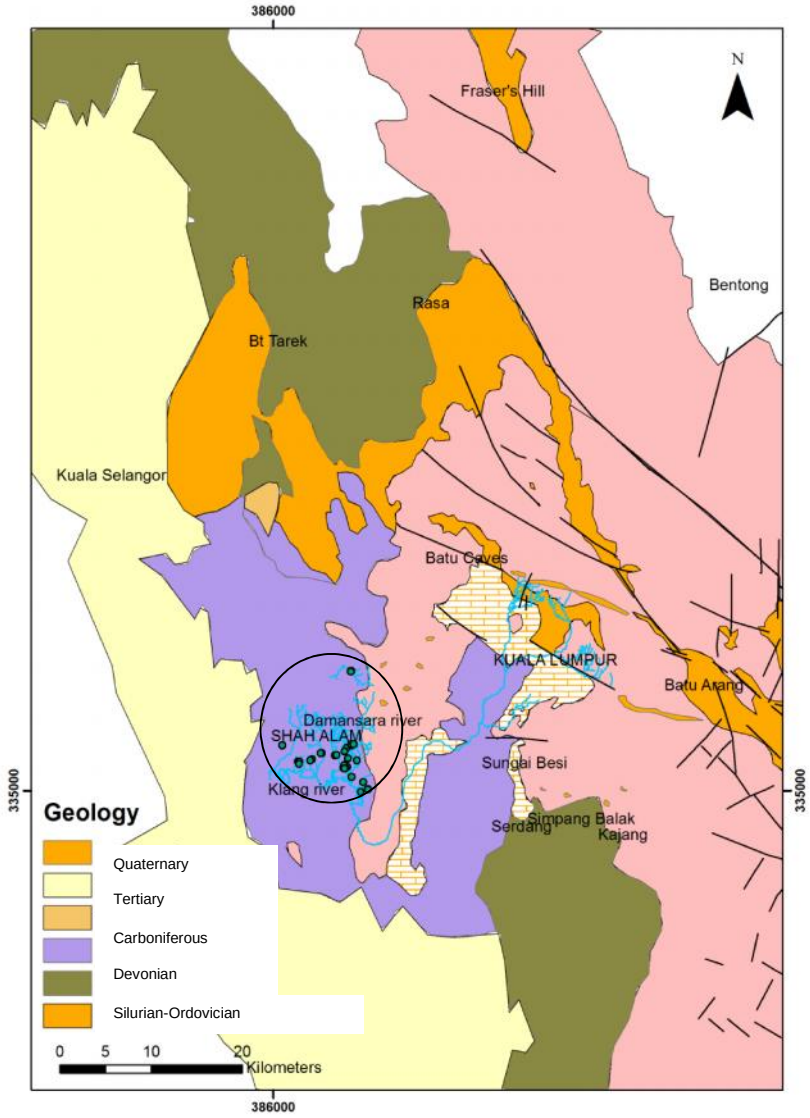

Figure 2.2 The geological map of Selangor produced by Mineral & Geosciences Department Malaysia (1985). The study area is marked by the circle.

Table 2.2 The stratigraphic sequence of Selangor (? indicates uncertain; T indicates major tectonic event / unconformity)

Cenozoic		Quaternary	Alluvium
		Tertiary	Batu Arang Beds
Mesozoic		Cretaceous	T T T T T
		Jurassic	Granite
		Triassic	T T T T T
Palaeozoic	Upper	Permian	Kenny Hill Formation
		Carboniferous	T T T T
		Devonian	Kajang Formation?
	Lower	Silurian	Kuala Lumpur Limestone
		Ordovician	Hawthornden Schist
		Cambrian	Dinding Schist

sediments to be folded and metamorphosed, and subsequently uplifted and eroded. Then, the Kenny Hill Formation was deposited uncomformably. Another tectonic event occurred in mid Mesozoic, probably in Triassic/Jurassic, causing both Upper and Lower Palaeozoic sequences to be folded but differently from the earlier folding event. The granite emplacement (Table 2.2) has slightly metamorphosed Kenny Hill Formation. Later, in Cenozoic times, the rock sequence was overlain by the Batu Arang Beds which are a Tertiary deposit. Except for Quaternary alluvium, no younger deposits are preserved in the region.

2.3.2.2 Lower Palaeozoic Rocks

Dinding Schist

Dinding Schist is the oldest rock in the sequence (Cambrian – Ordovician). It consists of 3400 metres of quartz- mica schist with a variable amount of mica and microcline. It was classified as Lower Palaeozoic and a “eugeosynclinal” sequence.

Hawthornden Schist

This unit overlies the Dinding Schist Formation. It is been described as unfossiliferous carbonaceous schist and phyllite. It is 900 metres thick. The age of this Formation is at least Ordovician to Middle Silurian. It is basin deposits.

Kuala Lumpur Limestone

This unit outcrops only at Batu Caves, north of Kuala Lumpur (Figure 2.2). It was described as a thickly bedded marble with a finely crystalline grey to cream

composition. It is 1830 metres thick. Its age is Middle – Upper Silurian. Kuala Lumpur Limestone is a shelf deposit.

2.3.2.3Upper Palaeozoic Rocks

Kajang Formation

This formation comprises quartz schist with lenses of limestone and shale. The thickness of this unit is unknown. It is overlain by the Kenny Hill Formation. With limited exposures, the detailed stratigraphy of this formation is uncertain. Rosly (1979) has observed limestone, graphitic schist, sandstone and shale at Simpang Balak which is 2km north of Kajang (Figure 2.2). The beds dip 25^{o} towards 200^{o}. He classified these rock sequences as facies changes rather than a formation. It is interpreted as a sequence representing a reducing environment.

This formation was observed near Sungai Besi Town and limited to south of Kajang town by Yin 2011(Figure 2.2). It is absent at North of Serdang where Kenny Hill Formation lies directly on top of the Kuala Lumpur Limestone.

Kenny Hill Formation

Stauffer (1973) described the Kenny Hill Formation as a monotonous sequence of interbedded shales, mudstones and sandstones. Yin (2011) described Kenny Hill Formation as series of interbedded quartzites and shales with occasional phyllite near the base of the formation. It is 1200 – 1500 metres thick. This formation is deposited near a slope or unstable shelf of moderate depth, near a delta or a shelf edge (Stauffer 1973). The Kenny Hill Formation will be discussed in detail in Section 2.4.

2.3.2.4 Tertiary deposits

Batu Arang Beds

This coal-bearing sequence consists of clay, carbonaceous shale and fine-grained sandstone (Stauffer 1973) which only can be found at Batu Arang, Selangor (Figure 2.2). The age of this sequence is Late Tertiary or younger.

2.3.2.4 Quaternary deposits

Quaternary deposits are mainly alluvium which fluvial origin. The deposits are derived from erosion of the sedimentary hills nearby. These deposits are sandy but often with clay beds interstratified with the sands: at the base there is a boulder unit (Yin 2011).The thickness of alluvium that covers the non-calcareous rocks is around 15 metres but can exceed 30 metres in the limestone area. Alluvium is mainly found in the river valley covering the Kuala Lumpur Limestone.

2.4 Geology of study area – previous research

2.4.1 Introduction

Shah Alam lies mainly on the Kenny Hill Formation. Therefore, this Formation will be discussed in detail. Not much geological study was carried out in the study area. However, the Kuala Lumpur area, which is located ~30 km to the northeast of Shah Alam is well studied area due to the development. Therefore, the geological information of the study area together with the geological information of Kuala Lumpur will be used to interpret the geology of the study area due to the similarity of the two areas. Figure 2.3 shows the geological map of Kuala Lumpur area and study area. This section, highlighting the findings

from previous research, begins with the age of formation (Section 2.4.2), the type of rock (Section 2.4.3), weathering (Section 2.4.4), the geological structures (Section 2.4.5) and the metamorphic grade (Section 2.4.6). All the locations of the previous studies are shown in Figure 2.4. Later, all this geological information will be used in interpreting the borehole logs collected as part of the present study (Section 2.5). In Section 2.6, the observation from the fieldwork undertaken during the present study will be discussed. In Section 2.7 all the findings will be summarized and a geological model of the study area will be proposed.

2.4.2 The age of Kenny Hill Formation

The Kenny Hill Formation is poorly fossiliferous. The only fossil found until recently is *Agathiceras* which is an ammonite, dated as Lower Permian (Abdullah 1985). Stauffer (1973) claimed that the age of Kenny Hill Formation ranges from Silurian to Mid Mesozoic. The age of the formation then has been identified using the structural geology evidence. The contact of Kenny Hill Formation with Kuala Lumpur Limestone was observed at Salak South by Rosly (1979) as shown in Figure 2.2. It dips greater than 50^{o} towards 330 ^{o} and less steep (30^{o}) approaching Kuala Lumpur Limestone. He suggested that the contact between these two formations is faulted based on the material observed near the contact zone which is highly silicified, iron cemented and fractured. It is interpreted as younger than the Kuala Lumpur Limestone and older than the granitic rocks.

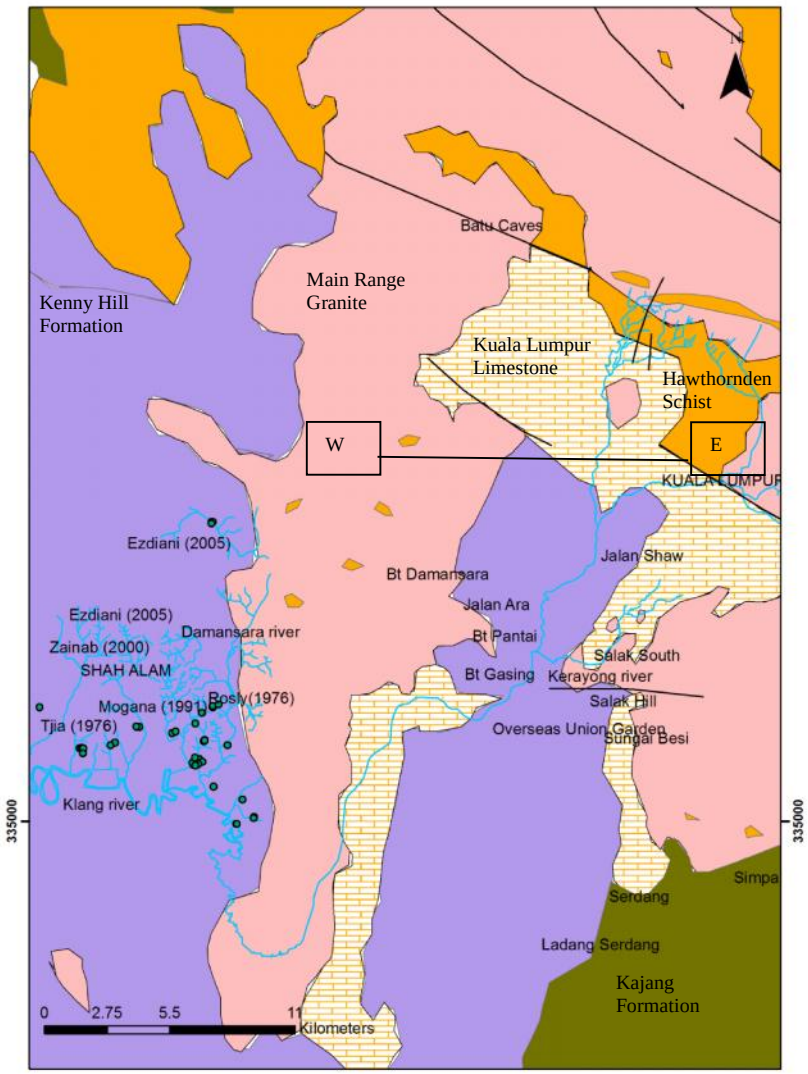

Figure 2.3 Locations of previous studies conducted in Kenny Hill Formation which is mainly in Kuala Lumpur and a few areas in Shah Alam.

Yin (2011) agreed that this Formation is younger than the Kajang Formation and probably the age is Carboniferous to Permian or possibly Triassic. Later, Chen et al. (2002) identified several species of spores which indicate either

Carboniferous or Permian age. It is concluded that the Kenny Hill Formation is therefore Carboniferous to Permian in age.

2.4.3 Type of rocks

The rock sequence of the Kenny Hill Formation as observed at Shah Alam and Kuala Lumpur area is similar. It comprises interbedded sandstone and shale which has been metamorphosed to quartzite and phyllite by the granite intrusion. The rock sequence is folded, jointed and faulted. The tension cracks are filled with quartz veins and lenses. The occurrence of quartz vein changed the sandstone to quartzite through silicification processes (Yeap 1970).

Figure 2.4 shows the schematic geological cross section through the Kuala Lumpur area presented by Yeap (1986). The cross section area is shown in Figure 2.3. The rock sequence comprises Kenny Hill Formation sitting uncomformably on Lower Paleozoic rock that comprises marble and schist. The Kuala Lumpur Limestone occurrence is suggested as large lenses in the schist. The Kenny Hill Formation as observed at Jalan Shaw, Kuala Lumpur (see Figure 2.3) is dipping to the southeast (Lim 1995). He constructed a subsurface profile using borehole logs as shown in Figure 2.5. The rock sequence comprises interbedded sandstone, mudstone and phyllite. Usually the sequence has a weathered top.

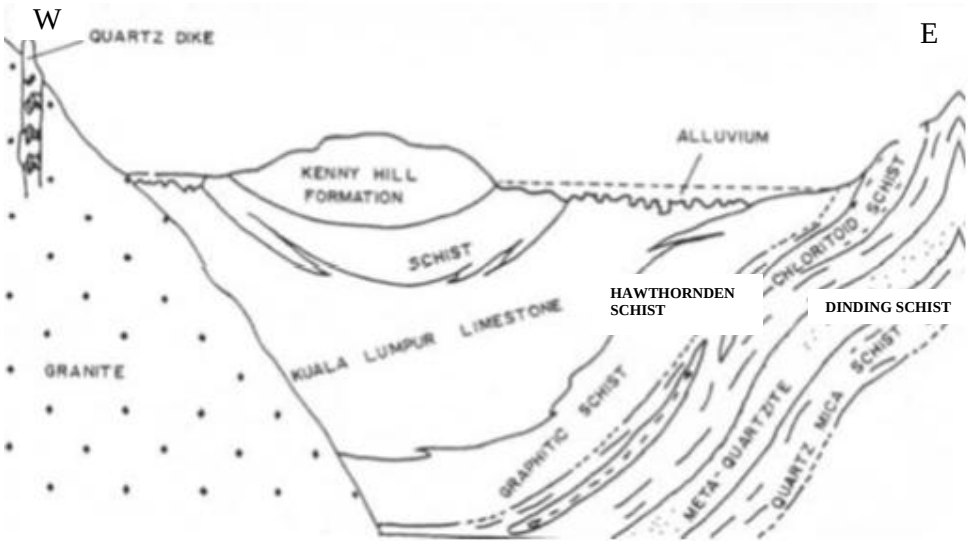

Figure 2.4 The geological cross section through Kuala Lumpur presented by Yeap (1986). The cross section area is shown in Figure 2.3.

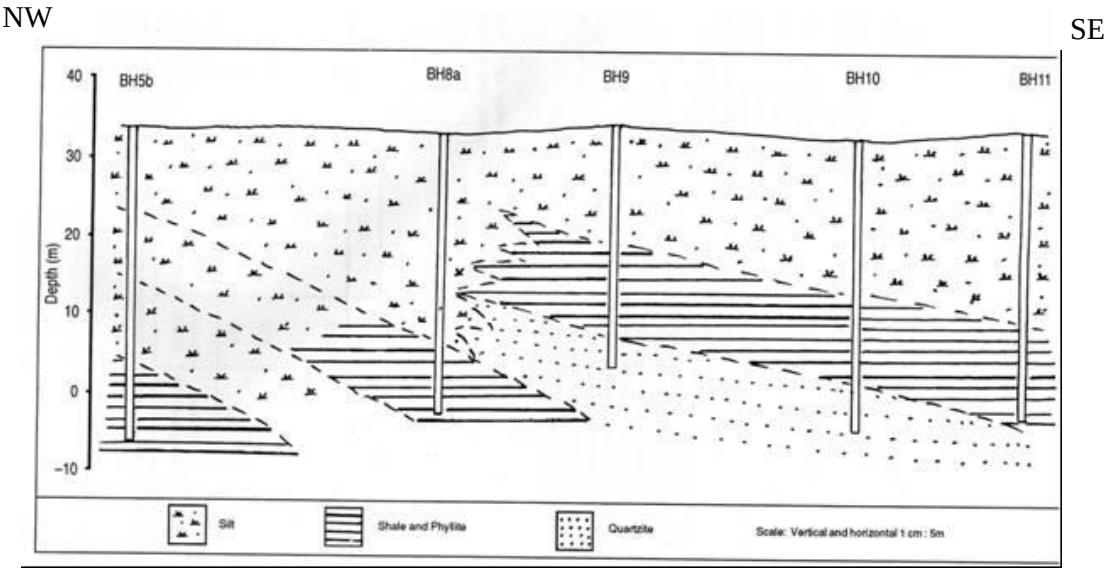

Figure 2.5 The ground profile of the Kenny Hill Formation at Jalan Shaw, Kuala Lumpur by Lim (1995).

One of the outcrops in Kuala Lumpur which has been well studied by the previous researchers was Bukit Pantai which is located in the northeast of Shah Alam area (see Figure 2.3). Tjia (1979) described a sequence of recumbent folds that he observed as two foliated metasandstone units, 8 – 10 metres thick, interstratified with two or more series of alternating foliated metasandstones and slates/phyllites (10-40cm thick) and black and dark grey phyllites. Musbah (1980) identified the rock sequence at Bukit Pantai as interbedded sandstone and phyllite. He classified the sandstone at Bukit Pantai into three types: massive, foliated and banded. Table 2.3 shows the detailed description of each rock. Due to the granite intrusion, veins and quartz lenses can be found in the rock sequence. Figure 2.6 shows stratigraphic sequence of Bukit Pantai.

Table 2.3 The rock description as observed by Musbah (1980) at Bukit Pantai, Kuala Lumpur.

Location	Sandstone (Metasandstone/quartzite)			Phyllite
	Massive	Foliated	Banded	Dark grey and reddish purple Foliated and folded.
Bukit Pantai	>1.5m thick beds Yellowish grey, with quartz lenses	0.2-0.6m thick Interbedded with phyllite Whitish grey with iron oxide bands	Thin layers (4-10cm) with thicker layers of phyllite Light-dark grey.	

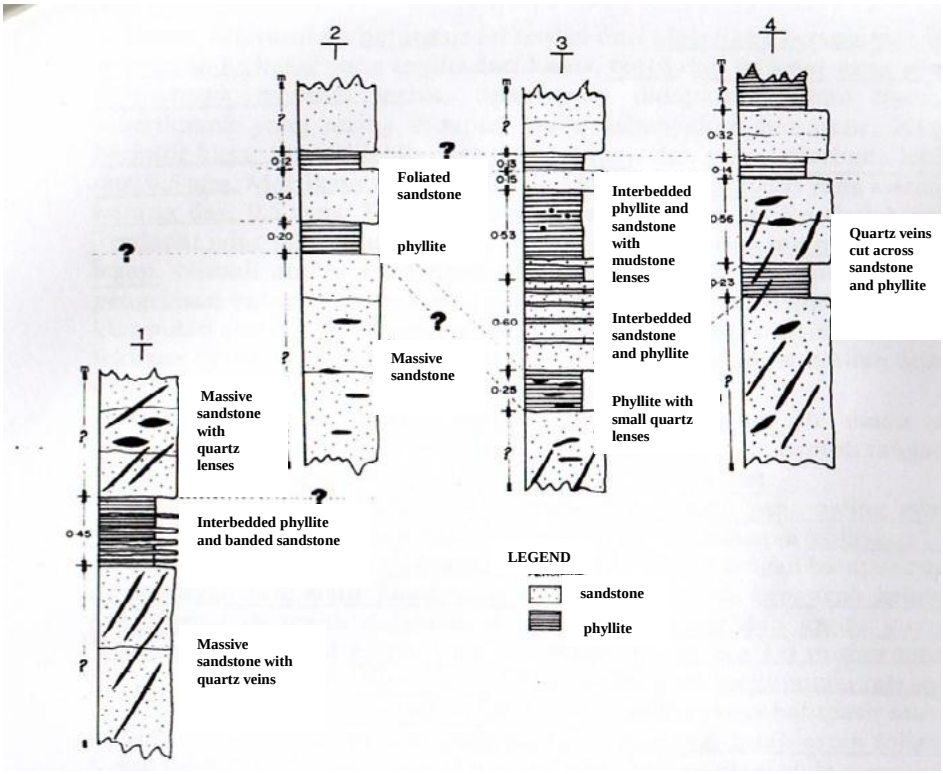

Figure 2.6 The stratigraphic sequence of Kenny Hill Formation at Bukit Pantai, Kuala Lumpur by Musbah (1980)

Rosly (1979) identified schist, chert and graphitic schist in the Shah Alam area (see Figure 2.3). He interpreted these rocks as the lower sequence of the Kenny Hill Formation. The schist consists of mica and quartz. It is greyish to greenish black in colour. The chert layer is 2-4 cm thick and yellowish to reddish in colour. The graphitic schist is black in colour, strongly foliated and banded with quartz layers which could have affinity with the Hawthorndern schist. Table 2.4 shows the rock descriptions of lithology of Kenny Hill Formation.

Mogana (1991) in his observation at two localities (see Figure 2.3) described the rock sequence as interbedded quartzite and phyllite which graded into schist to the northwest. Ezdiani (2005) described the rock sequence at Taman Pertanian

Bukit Cahaya Seri Alam, Shah Alam (see Figure 2.3) as interbedded phyllite and quartzite. Quartzite is dominant and is up to 10 metres thick and the sequence is quartz veined. The phyllite units are 0.5 – 1.5 metres thick.

2.4.4 Weathering

The fresh sandstone outcrop of Kenny Hill Formation becomes friable in 5-6 months due to intense weathering (Yeap 1970). According to Yin (2011), quartzites are weathered to a sandy soil and the soil cover is thin. Zainab et al. (2007) described the rock sequence observed on a cut slope at Jalan 8/22 in Shah Alam (see Figure 2.3) as interbedded thick sandstone and shale with a thin layer of siltstone. The weathering grades of the sandstone and shale were investigated using a technique based on thin section analysis. The quartz size reduces with increasing weathering grade. However, no obvious changes were recorded in shale except that mica has changed to sericite. The shape of the quartz grains in the sandstones were found to be subrounded or subangular. Three sizes of quartz grains were observed: >0.25mm (medium grain size); <0.25mm (fine grain size); and < 0.125mm for (very fine grain size, comprising the matrix). Table 2.5 summarizes the quartz grain sizes for the sandstone with different weathering grades. The percentage of quartz grains in the sandstone increases with higher weathering grade, while the percentage of the largest quartz grains decreases with higher weathering grade.

Table 2.4 The description of each lithology of Kenny Hill Formation (modified from Rosly 1979)

Types of lithology	Description
Sandstone	It is interbedded with shale,slate and phyllite It is stained with iron oxide It is greyish to whitish in colour
Metaquartzite	It is mainly quartz with traces of chlorite, mica and iron oxide
Quartzite	It is very hard rock with preferred orientation It is greyish to whitish in colour
Shale	It is associated with slate and sandstone It contains high proportion of carbonaceous material, clay and sericite.
Slate	It is light grey to blackish in colour It is rock with cleavage. It comprises of mica, fine grain quartz, opaque minerals with traces of clay and iron oxide.
Phyllite	It is light grey to greenish-black in colour; with shiny and flaky appearance It comprises of fine grain quartz, mica, carbonaceous material, sericite and iron oxide
Schist	It is greyish to greenish black in colour It consists of elongated mica and quartz It is rock with cleavage (preferred orientation)
Chert	It is yellowish to reddish in colour The thickness is 2-4 cm.
Graphitic schist	It is blackish, compact, strongly foliated banded with quartz layer and with trace of pyrite.
Siltstone/mudstone	It is whittish, yellowish to brownish It consists of fine grained quartz, mica and clay The trace fossils have been found in siliceous cherty siltstone/mudstone

Table 2.5 The comparison of quartz grains size in sandstone (BP) with different weathering grade from Grade 2 (less) to 5 (more) (Zainab et al. 2007)

Sample	Quartz size >0.25mm (%)	Quartz size <0.25mm (%)	Quartz (%)
BP2	10.1 – 32.6	30.6 – 47.5	22.8 - 59
BP3	2 – 5.3	50 - 62	37 - 48
BP4	0.9 – 3.0	38 - 44	53 - 61
BP5	0.6 – 1.4	27 - 43	56 - 70

2.4.5 The geological structure

2.4.5.1 Regional structure

Stauffer (1973) described the Kenny Hill Formation in Kuala Lumpur area as a broad synclinal belt of 7 to 10km wide (see Figure 2.3). The dips of the Kenny Hill Formation beds are less than 30º and steeper at western limb. According to Yin (2011), the beds strike north-south and dip 10 to 20 degrees near the axis and on the eastern limb. The beds dip more steeply (45 to 70 degrees) in the western limb. Therefore it is an asymmetrical syncline.

2.4.5.2 Local geological structures

Folding

The rock was described as gently folded compared to the Lower Palaeozoic rock until in 1974, Tjia proposed the idea that the Kenny Hill Formation is often overturned with the major structure being a recumbent fold or isoclinal folding. This is based on his observations of sedimentary structures at Bukit Pantai, Kuala Lumpur. The sedimentary structures he observed such as aligned bulbous ridges

with ‘internal twisting’ and subparallel ridges with regular inter-ridge spacing are projected from sandstone into overlying finer grained clastic rocks. These structures are interpreted as load casted ripples. The beds are moderately tilted (25 - 27^{o}), overturned, and represent isoclinals or possibly recumbent zig-zag folds.

Later, in 1976, Tjia found further evidence to support his theory. He discovered small to medium scale isoclinal to recumbent folds (10metres across), low angle to ordinary reverse faults and an overturned sequence of beds over distances of 300 metres or more. The observations were carried out at a few localities in Selangor including Shah Alam (later situated at the east of administration building of UiTM). The outcrop is in a north-south direction . A major low angle thrust fault has been traced over 60 metres along its strike. The foliation in the phyllite host rock strikes 270^{o}±10^{o}. The outcrop inclines 40 degrees to the north over a distance of more than 250 metres. Isoclinal folds of amplitude 3m were observed. He suggested that the sequence is overturned from the observation on the boundary of a tuffaceous arenite and overlying shale-slate. The laminae in the arenite are comformable with this boundary. He concluded that all these structures are caused by north-south and NE-SW horizontal compression. He added that the ENE – WSW and SE –NW directions are also common as observed at other localities. Table 2.6 shows the compression direction for all localities in Shah Alam and Kuala Lumpur that he investigated.

Tjia’s idea was disputed by Tan and Yeap (1977). Their main argument is that there were no tectonic features in the Kenny Hill Formation that would suggest

such a structure. They claimed that the faulting affects the rock dips locally as they observed at the Happy Garden housing estate off Old Kuchai Road, Kuala Lumpur (see Figure 2.3). The recumbent folds observed at Overseas Union Garden and Shah Alam were interpreted as sedimentary slumps. Other observations at Salak South found that the sedimentary structures such as graded bedding and cross bedding are the right way up.

Table 2.6 The compression directions observed at few localities in the Kenny Hill Formation by Tjia (1976).

Locality	Compression direction	Thrusting towards (or inclination of axial plane
Shah Alam	1) north-south 2) NE-SW	south SW
Bukit Gasing	1) north-south 2) 60^o-240^o	north none
Overseas Union Garden	Between east and SE	west and NW
Bukit Pantai	60^o-240^o	WSW
Bukit Damansara	1) east-west 2) 68^o-248^o	west none

Through his observation of the Kenny Hill rocks at Bukit Pantai in 1979, Tjia proved that recumbent folds are present in the Kenny Hill Formation in Kuala Lumpur area. The folds are interpreted as tectonic origin, with transport towards the west.

In 1984, Tjia observed phyllite and foliated metaquartzite of the Kenny Hill Formation at Salak Hill, which is located near the southern border of Kuala Lumpur(see Figure 2.3). They are striking to N and NNE and dip uniformly at approximately 30 degrees towards the west. He interpreted the rock structure as a cross folding consisting of an isoclinally refolded syncline and anticline which

was possibly caused by movement on the Kuala Lumpur Fault. Another cross folding is striking E-W which Tija (1984) suggests is a result of movement on a normal fault that strikes 100 degrees and with an almost vertical dip.

Joints

There are two sets of near vertical joints striking north-northeast to south-southwest and east-west direction observed in Kuala Lumpur area. This is similar to the sets of joints that have been observed by Mogana (1991) at two localities in Shah Alam area (see Figure 2.3). The northeast joints are open fractures as observed at Klang Gates Dam area (near Klang Gate Quartz Dyke) and classified as extension joints (Gobbett & Tjia 1973). While north-south and east-southeast joints are the second order of shear joints with left and right lateral displacement.

Faults

From the observations in Kuala Lumpur area, the Kenny Hill Formation is cut by numerous small and some larger faults. Vertical faulting is prominent with an orientation of 100-110º, 135º and 65º. The major fault observed in Kenny Hill Formation is the Kuala Lumpur-Endau fault zone as shown in Figure 2.7. The fault zone is striking southeast and east-southeast, and often filled with quartz veins e.g Klang Gates Quartz Dyke. This fault was active after the late Triassic-early Jurassic granite intrusion and stopped by late Cretaceous or early Tertiary. Another fault is observed in the Kuala Lumpur area which is striking north-northeast; this is parallel to lineaments observed in sedimentary rocks at Bentong. This lineament is interpreted as having left lateral displacement by

Gobbett & Tjia (1973). Tjia (1976) and Mogana (1991) have observed faults at 3 different locations in Shah Alam which strike parallel to these two faults.

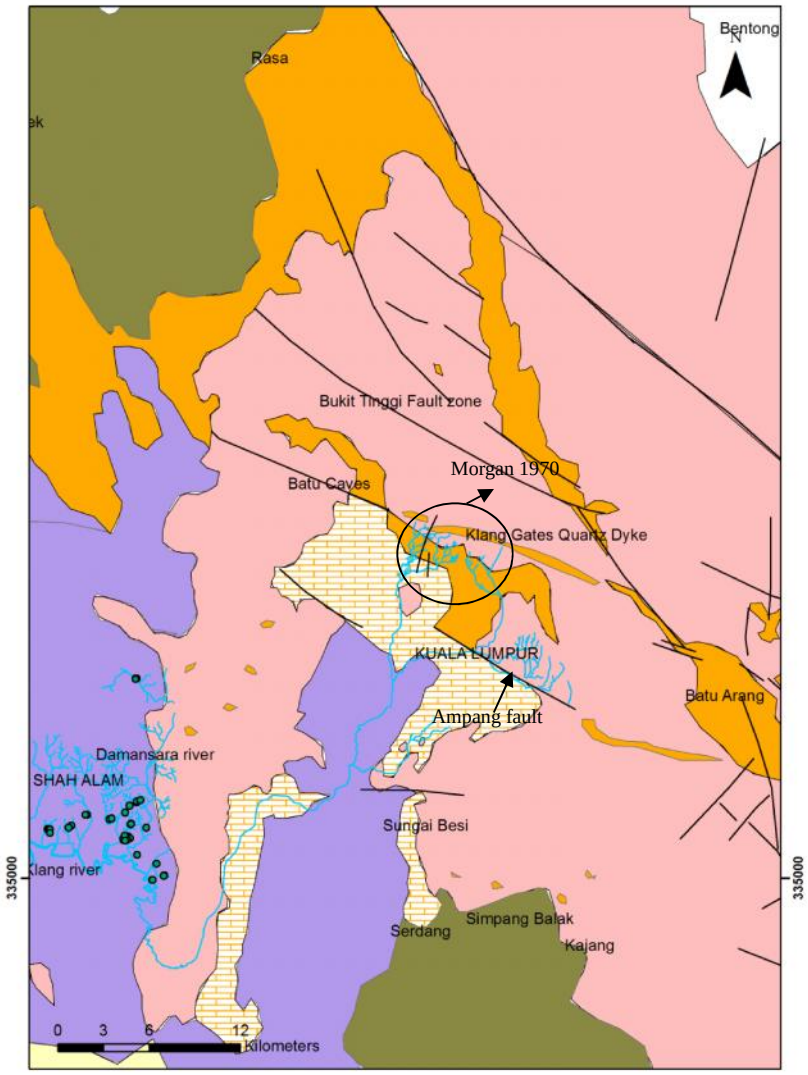

Figure 2.7 The lineaments mapped by Gobbett & Tjia (1973) in the Kuala Lumpur area which have been classified as the Kuala Lumpur - Bukit Tinggi fault zone, Ampang fault and Klang Gate Quartz dyke.

2.4.5.3 The impact of geological structures on the river pattern

River patterns provide some ideas in understanding the regional structure of the study area. Shah Alam lies in the Klang River Basin. The drainage pattern of the Klang river tributaries is dendritic with the main stream is joint and fault controlled (Morgan, 1970). Yeap (1970) interpreted Kerayong river as fault controlled (see Figure 2.2). This strikes west- north- west which is similar to Kuala Lumpur-Endau fault zone.

Morgan (1970) has classified some of fourth order basins of Upper Klang River Basin (lying on granitic rocks) as asymmetric basins (see Figure 2.7). The asymmetry is interpreted to be due to structural control with the maximum being along the preferred alignment at 30^o, 105^o and 140^o. The 105^o alignment corresponds to lithological boundaries and faults within Kuala Lumpur area (e.g. Klang Gates Quartz Dyke), and the 30^o alignment is often found in granitic rock as observed by Alexander (1968) at Bentong. Holmes (1965) said that the 140^o alignment corresponded to a conjugate system of joints or shear planes.

2.4.6 Metamorphism

Roe (1953) suggested that most of the metamorphism results from both regional and temperature. However, this Formation has suffered low grade metamorphism due to both Mesozoic folding and granite emplacement. The metamorphic grade in Selangor ranges from epizone to mesozone. Epizone is characterized by a low grade of metamorphism, from surface temperature to 250-350 ^{o}C. Mesozone belongs to greenschist facies with temperature 250 -500^{o}C.

Hamzah et al. (1986) suggested that the Kenny Hill Formation has been metamorphosed up to greenschist facies by using biotite as the mineral indicator. They compared the Kenny Hill Formation with the metapelites of the Dinding Schist. These two formations have different ages and different geological structures. The Dinding Schist is much older than Kenny Hill Formation.

The Dinding Schist comprises chlorite + phengite (hydro-muscovite) + microcline, biotite + phengite + microcline and chlorite + phengite + biotite. The Kenny Hill Formation contains chlorite and phengite. With biotite in Dinding schist, it has been suggested as metamorphosed to a slightly higher grade than the Kenny Hill Formation. However, the absence of biotite in the Kenny Hill Formation may be because the schist and phyllite contain more aluminium (Table 2.7); more aluminous rocks need higher grades of metamorphism to allow the formation of biotite. It is concluded that the whole sequence, including the Kenny Hill Formation, has undergone greenschist metamorphism.

Table 2.7 The chemical composition of Kenny Hill formation and Dinding schist (Hamzah et al. 1986)

	1	2	3	4
SiO_2	64.79	68.84	71.36	75.48
Al_2O_3	18.26	14.48	12.90	13.35
TiO_2	0.81	0.82	0.39	0.38
Fe_2O_3	1.06	3.51	2.61	2.39
FeO	0.04	0.03	0.41	0.39
MgO	0.85	1.91	0.98	1.03
MnO	0.01	0.02	0.02	0.03
CaO	0.10	–	0.36	0.50
Na_2O	3.55	2.23	2.71	2.80
K_2O	3.96	4.76	5.53	3.89
L.O.I.	6.24	4.80	3.70	0.44
	99.70	101.40	100.97	100.68

1 Ladang Serdang, Selangor } Kenny Hill Formation
2 Bukit Pantai, Kuala Lumpur }
3 & 4 Taman Melawati, Hulu Kelang, Selangor. } Dinding Schist

2.5 Borehole Log Interpretation

2.5.1 Introduction

Borehole geological logs have been collated and examined to improve the understanding of the geological sequence. The interpretation is aided by the previous geological studies in Shah Alam and Kuala Lumpur described above. Thirty seven borehole logs from 18 factories are available and have been studied. However, four of these logs were found to contain less useable information. Figure 2.8 shows the borehole log distribution in Shah Alam. Any correlations suggested will necessarily be quite uncertain.

First, the borehole logs from each factory will be interpreted individually. Later, the correlation between the factory sites will be made. The geological information obtained, together with the ideas and findings from the previous researchers will be used to build a geological model of study area. A limited amount of fieldwork has also been carried out to confirm the nature of the rock types and structures (Section 2.6).

The boreholes were drilled by different drilling companies as shown in Table 2.8. In all cases, the drilling method that has been used is mud rotary or down-the-hole hammer (DTHH) drilling. Some of the borehole logs were made by geologists and some of them were not, and therefore the quality of the identifications of rock types is probably variable, and descriptions of the same rock may vary from log to log.

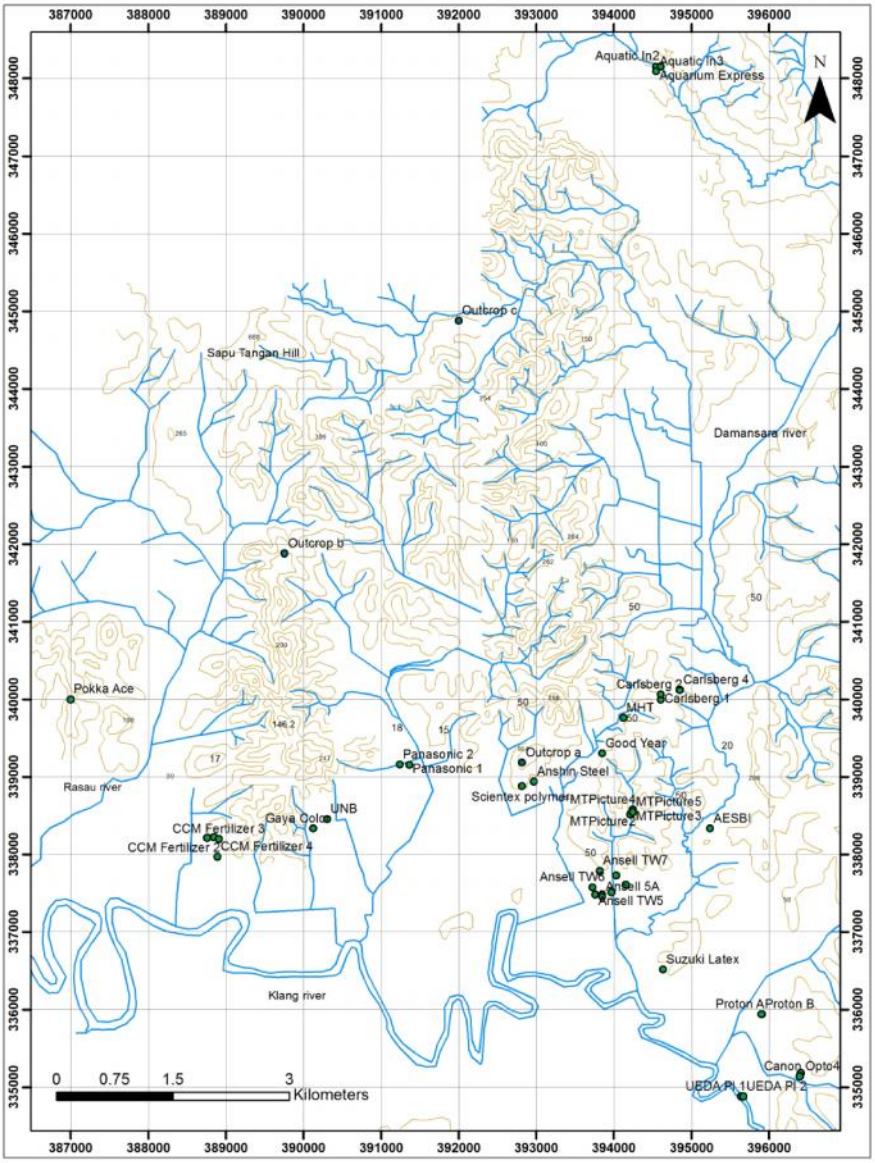

Figure 2.8 The borehole log distribution in Shah Alam. The topographic contour is 50m interval.

Table 2.8 The drilling companies and the wells that they constructed.

Drilling company	**Tubewell**
Drilco Technologies (M) Sdn Bhd	Ansell Panasonic Manufacturing CCM Fertilizers 1,2,3 MT Picture Display (M) Sdn Bhd Mitsui High Tech (M) Sdn Bhd
Geo Pacific Sdn Bhd	AESBI Carlsberg PROTON Scientex Polymer Sdn Bhd Gaya Color Laboratory Sdn Bhd
Korekan Instantflow Sdn Bhd	Aquarium Express Aquatic International
Elite Drilling Technology Sdn Bhd	Canon Opto
Mecserve Engineering	Good Year Malaysia Berhad Anshin Steel Industries Sdn bhd
Kagawa Engineering Sdn Bhd	Pokka Ace Universal Nutri Beverages CCM Fertilizer TW4
Conseal Sdn Bhd	Ueda Plating

All the depths refer to measurement from ground level. The ground elevation varies from 6 metres to 23 metres above national datum (sea level). The ground level is estimated from the topographic map of the Shah Alam.

2.5.2 Geological logs from the Ansell boreholes

From December 2004 until June 2005, Drilco Technologies (M) Sdn Bhd carried out the drilling and construction works for five production wells at the Ansell site. These production wells have been labelled TW1 to TW5. From February until March 2007, another two wells (TW6 and TW7) were constructed. In 2011, TW5 was closed. All wells were drilled using the mud rotary method except for TW1. There is no information regarding how samples were obtained and who

described the sample in detail, though it is likely that the interpretations were undertaken by the drillers based on the mud returns. Figure 2.9 shows the location of each tubewell in Ansell compound.

Figure 2.9 The tubewells in Ansell compound (Google Earth).

These tubewells have been divided to two sections for the purpose of borehole interpretation. The rock sequence for tubewells TW2 to TW5 is compared to each other since they are located within 100 metres of each other. Figure 2.10 shows the geological logs for TW2, TW3, TW4 and TW5. The lithology in this area as indicated by the borehole logs comprises interbedded sandstone and shale, sandstone, shale, interbedded shale with quartzite and interbedded quartzite with phyllite at deeper depth. A carbonaceous shale unit with quartzite is present in boreholes TW3 and TW5. The same unit is also possibly present at deeper levels in TW4 and TW2. This interpretation is based on the occurrence of

carbonaceous shale which is mainly found in the east part of Shah Alam and will be discussed in the next section. The rock sequence is interpreted as striking north-northwest with an apparent dip somewhere to the northeast.

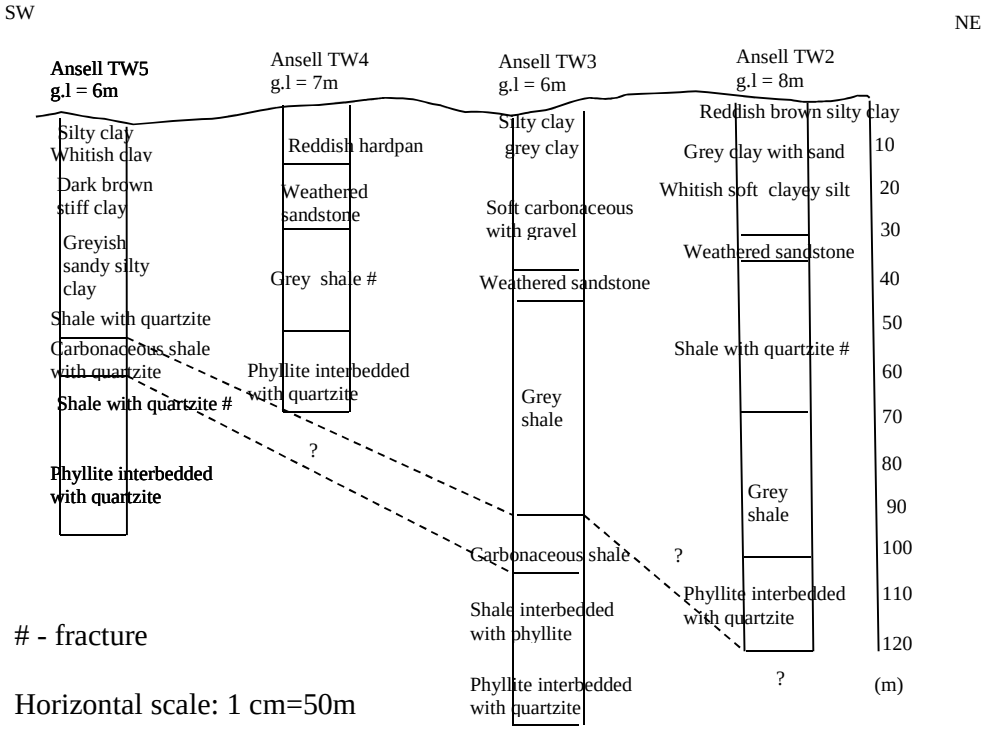

- fracture

Horizontal scale: 1 cm=50m

Figure 2.10 The ground profile of Ansell TW2, TW3, TW4 and TW5

The weathered layer thickness varies from 27 m to 42 m, being thickest at TW5 (up to 42 m). It comprises reddish brown silty clay on the top (3 m thick), followed by grey clay which is up to 10 m thick. The weathering material at the latter depth is a bit different in TW5 varying from clayey to sandy material. The weathering material of this area is interpreted as weathered interbedded shale and sandstone with weathered carbonaceous shale at Ansell TW3 at 18 to 36 metres depth.

Fractures have been noted in three of the four logs at depths between 40 and 60 m, within units marked as being interbedded shale-quartzite and grey shale.

Figure 2.11 shows the ground profile of TW1, TW7 and TW6. The rock sequence is similar to rock sequence for the borehole logs shown in Figure 2.10. The thickness of weathered layer is up to 30 m and the material is interpreted as weathered interbedded sandstone-shale. The sandstone unit in TW1 and 7 is up to 20m thick, but no sandstone unit is observed at TW6. Fractures have been observed within weathered interbedded phyllite-quartzite at depth 40 to 100 m for TW6 and TW7 and at deeper depths (100 to 115 m) for TW1.

Table 2.9 shows the thickness of sandstone observed in Ansell. The sandstone layer is thicker (up to 15 metres) in the middle part of Ansell as shown by borehole TW4 and TW7. The occurrence of sandstone at Ansell TW1, TW2 and TW3 at deeper depth than Ansell TW4 and TW7 supports the earlier interpretation; the rock sequence strikes north to northeast with apparent dip to the northeast.

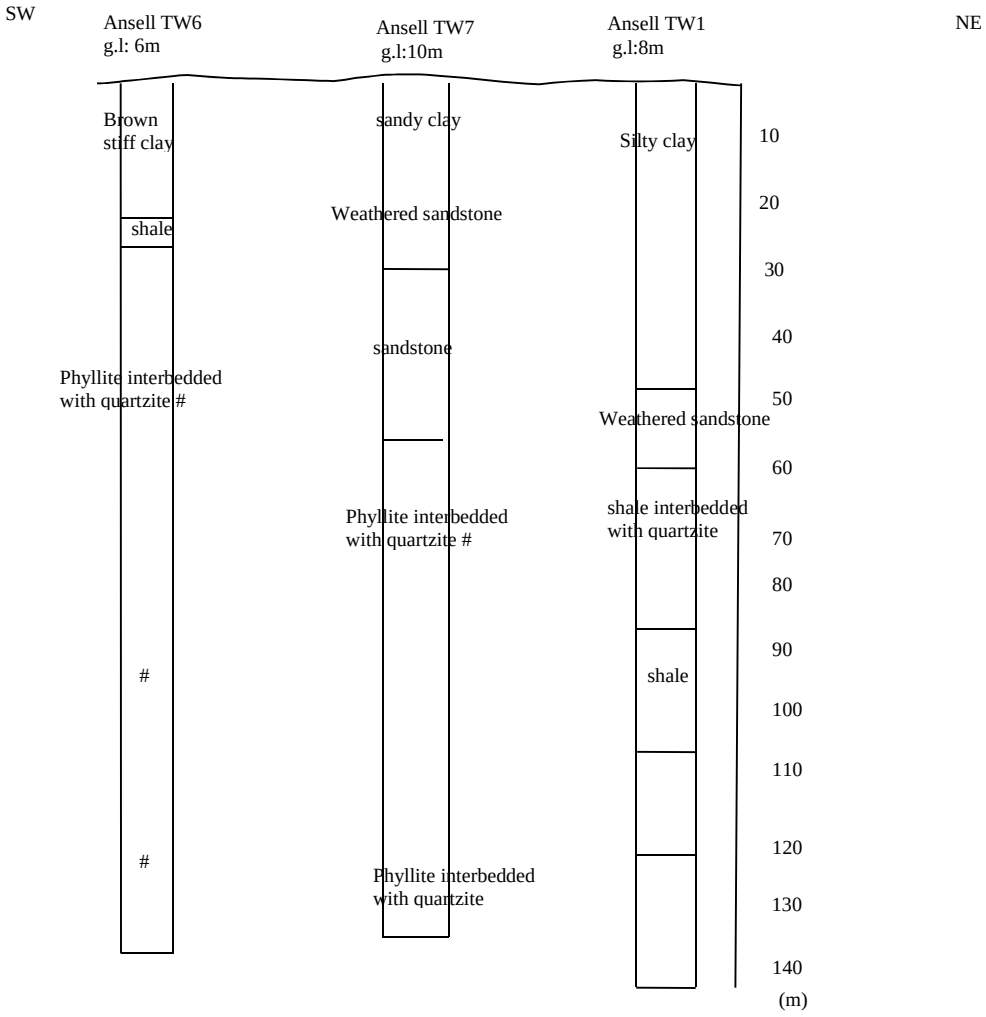

Figure 2.11 The ground profile of Ansell TW1,TW6 and TW7

Table 2.9 The thickness of sandstone layer as observed at Ansell.

Tubewell	Thickness of sandstone layer (m)	Range of depth from ground level (m)
Ansell TW1	9	45 - 54
Ansell TW2	6	30 - 36
Ansell TW3	6	36 - 42
Ansell TW4	15	12 - 27
Ansell TW7	14	14 - 28

2.5.3 *Geological log from AESBI borehole and the correlation with the lithology at Ansell.*

The AESBI borehole was drilled in June 2004 by Geo Pacific Sdn Bhd. They used a roller bit and a DTHH technique. There is no detail regarding on how the rock description was carried out.

The AESBI site is located on the further northeast side of the Ansell site as shown in Figure 2.8 and Figure 2.9. It comprises 39 metres of weathered shale with 20 metres of weathered shale with sandstone beds. The next sequence is carbonaceous shale layer. The first 3 metres of carbonaceous shale is with sandstone. It is possible that this layer is similar to the one that was observed at Ansell TW3 and TW5. Figure 2.12 shows a possible correlation of the lithology at these two areas. There is probably a fault between these sites due to the sudden change of lithology; from interbedded sandstone and shale (Ansell) to carbonaceous shale (AESBI). The Damansara river flows between the sites which could lie along the line of a fault.

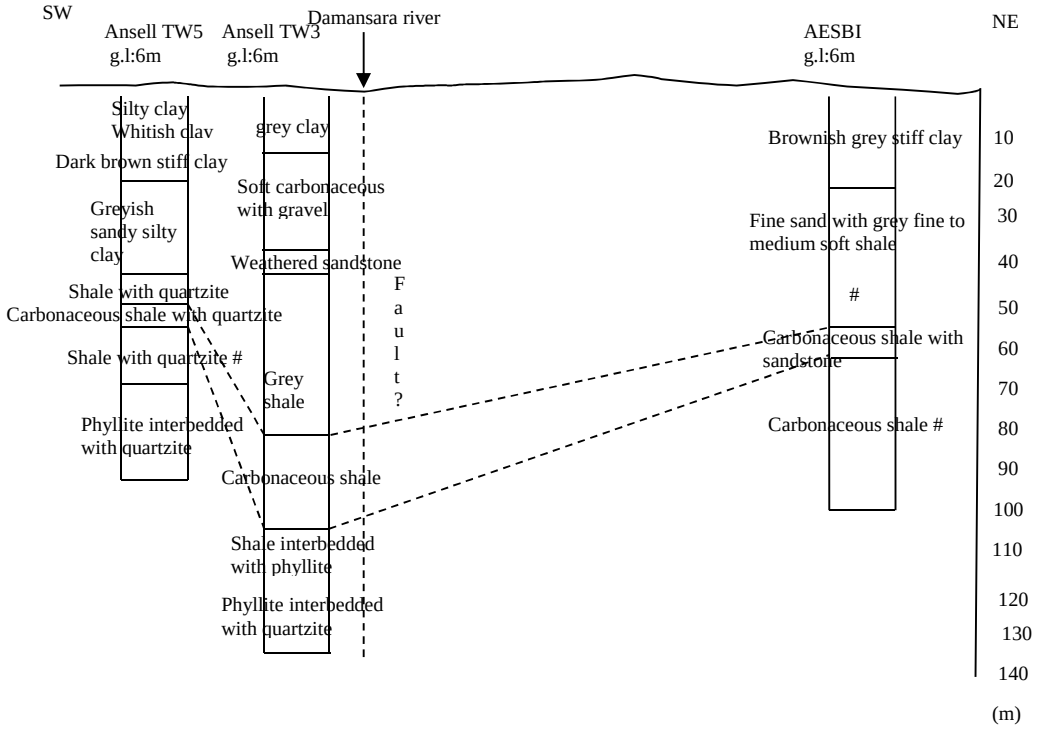

Figure 2.12 The correlation between lithology at AESBI and Ansell

2.5.4 Geological logs from the MT Pictures boreholes

MT Pictures is situated to the north-northeast of Ansell (see Figure 2.8 and Figure 2.9). There are 5 borehole logs in this area. Since the exact location of the boreholes cannot be confirmed, the information obtained from this area cannot be used in geological correlation. However, it can be used in understanding the sequence of the area.

The wells construction started in August 2005 and finished in December 2005. It was the same driller as Ansell. They drilled using a DTHH technique.

Figure 2.13 shows the geological logs from MT Pictures. The lithology in this area is mainly interbedded sandstone and shale. The weathered layer is up to 40 m thick. The layer is interpreted as originally interbedded sandstone and shale. It lies on thin weathered sandstone (2 to 5 m thick). The next unit in the sequence is interbedded sandstone and shale (up to 20 m), followed by interbedded grey shale and quartzite (up to 24 m). The next unit is grey shale (up to 30 m thick) on top of interbedded grey shale and quartzite. Fractures are observed around 60 to 80 m and 90 to 120 m in interbedded shale and quartzite bed/sequence. The rock sequence at TW5 is less fractured compared to TW4 and also other boreholes.

The rock sequence in MT Pictures is quite similar to the rock sequence in the Ansell area which comprises interbedded sandstone and shale. Lack of phyllite occurrence has lead to the interpretation that this rock sequence sits on top of the rock sequence at Ansell. This interpretation is made based on previous research by Yin (2011) saying that the phyllite occurrence is at the base of Kenny Hill Formation.

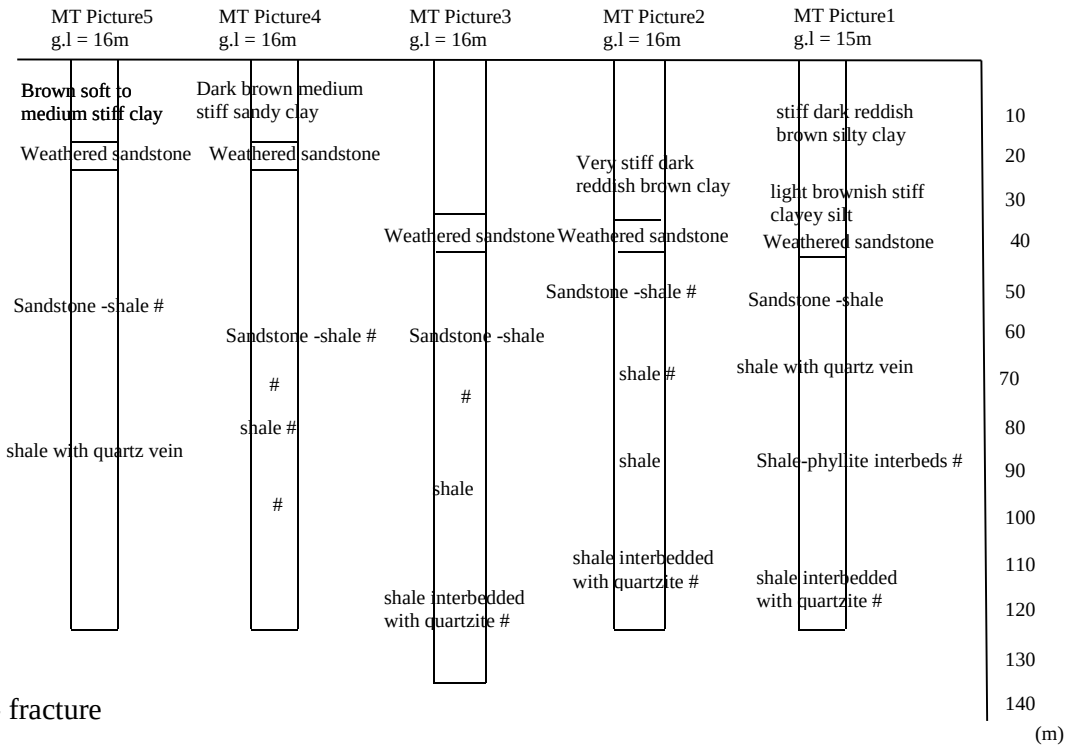

- fracture

Figure 2.13 The ground profile of MT Pictures

2.5.5 Geological logs from the Carlsberg boreholes

Wells have been constructed in different years by Geo Pacific Sdn Bhd. They drilled using roller cone bit and DTHH. Well No.1 was drilled in October 1985, Well No. 2 in November 1985 and Well No. 4 in December 2003. The Carlsberg site is situated north of AESBI and MT Pictures (Figure 2.8).

Figure 2.14 shows the ground profile of Carlsberg. The lithology of Carlsberg W1 and 2 is similar. It comprises weathered shale (up to 20 m thick), followed by weathered shale with sandstone (up to 10 m thick) and then shale. The lithology in Carlsberg W4 comprises weathered shale with sandstone which is up

to 30 m thick. It lies on carbonaceous shale (80 m thick) and then shale. This carbonaceous shale is possibly similar to the carbonaceous shale that was observed at AESBI and Ansell.

Fractures have been observed in Carlsberg W1 and W2 from 40 to 150 metres depth in shale and at 90 to 100 metres in carbonaceous shale and at 150 metres in shale for Carlsberg W4.

2.5.6 Geological logs from Mitsui High Tech and the correlation with the lithology at Carlsberg.

The ground investigation at Mitsui High Tech was carried out by Drilco Technologies Sdn Bhd in June 2009. They drilled using drag bit and tricone bit until 18 m depth and then changed to DTHH.

Figure 2.8 shows the location of Mitsui High Tech which is situated to the southwest of Carlsberg. Figure 2.15 shows a ground profile of the Mitsui High Tech and Carlsberg area.

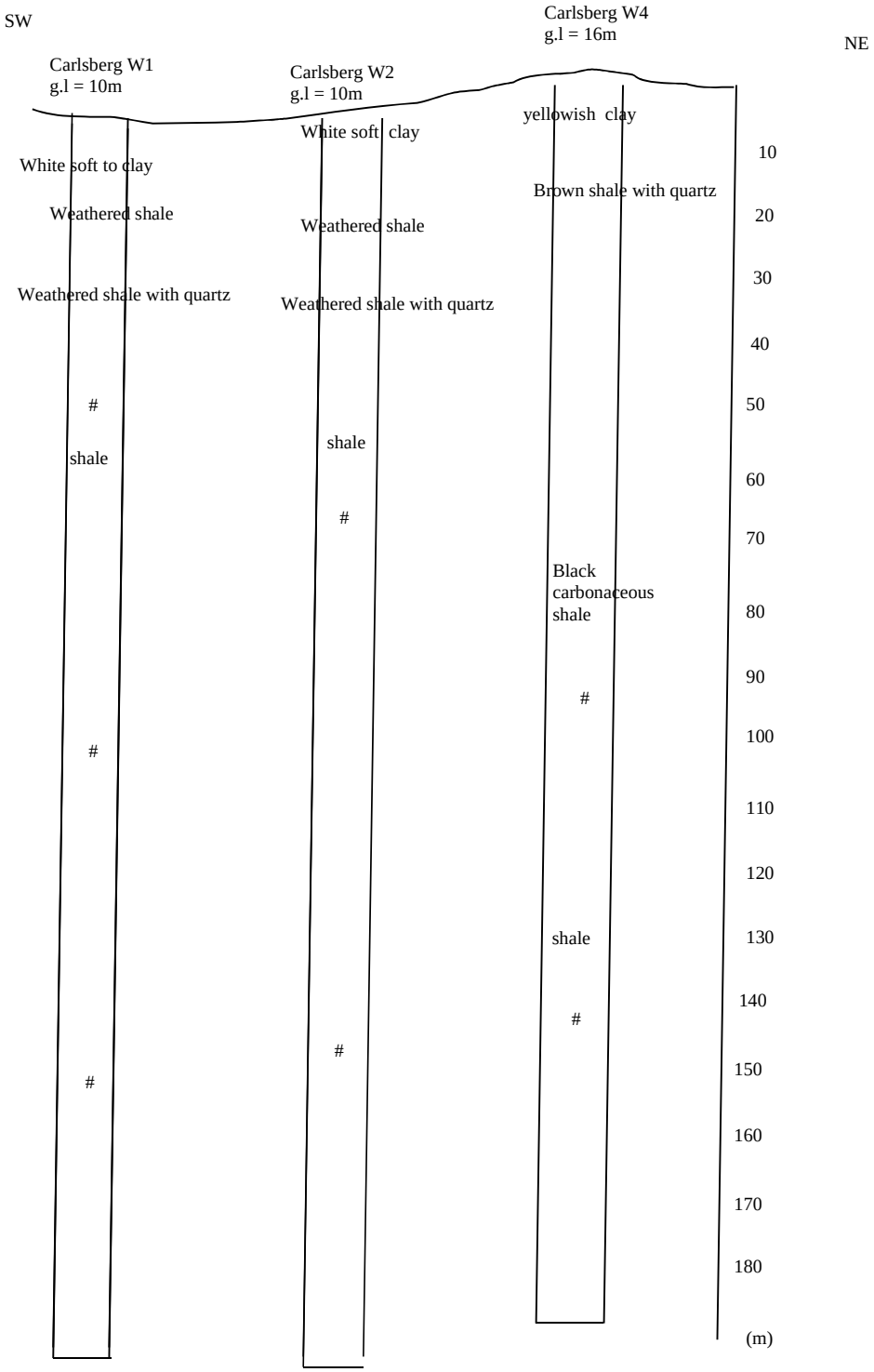

- fracture

Figure 2.14 The ground profile at Carlsberg

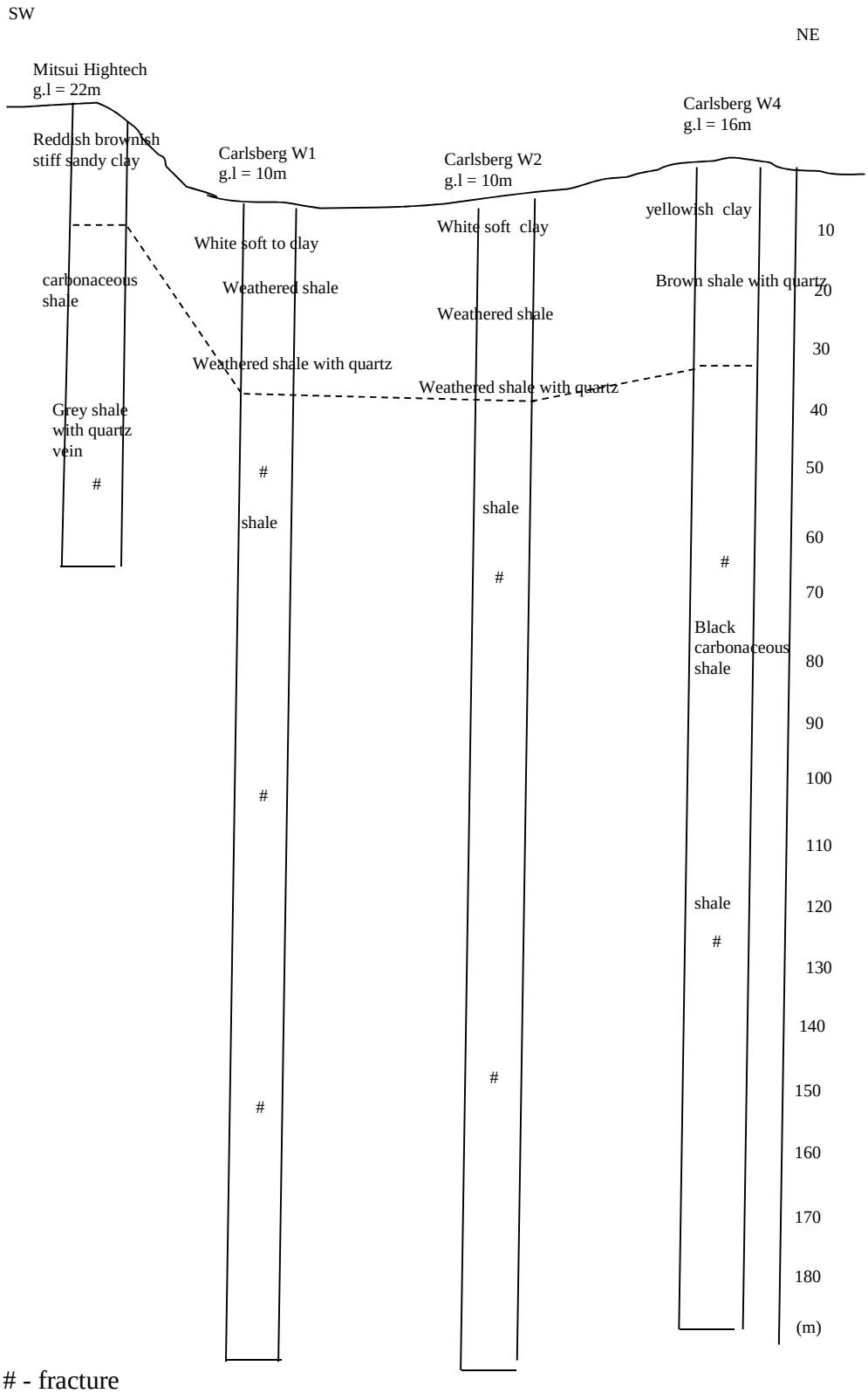

- fracture

Figure 2.15 The correlation between Carlsberg and Mitsui High Tech

The weathered layer comprises reddish and brownish stiff and sandy clay which is interpreted as originally shale with sandstone. It is 10.5 m thick and lies on 7 metres of weathered carbonaceous shale and phyllite. The carbonaceous shale layer observed in this area is probably similar to the carbonaceous shale layer observed at Ansell and AESBI.

Carbonaceous shale was observed at 18 to 32 m depth. This carbonaceous unit is possibly similar to the one observed at Carlsberg W4. Fractured slate with quartz veins are reported at 32 metres to the end of the borehole (100m). The occurrence of quartz veins in the slate unit in the lower part of the Mitsui High Tech borehole possibly represents a metamorphosed shale / slate sequence. This is also an indicator that the lithology is near to the granite. The granite contact with Kenny Hill Formation is approximately 1200 metres to the east of Shah Alam (see Figure 2.3).

2.5.7 Geological logs from Good Year

The ground investigation at Good Year was carried out by Mecserve Engineering. No detailed information was given and the lithology at Good Year is not well described. Therefore not much information can be used to correlate the rock sequence with other boreholes nearby.

Good Year is situated to the north of MT Pictures and to the southwest of Mitsui High Tech as shown in Figure 2.9. The first 18 m observed in the borehole is a weathered sequence which interpreted as originally being shale. This weathered

sequence lies on shale/phyllite. No fractures have been reported in within the rock sequence but it is quite possible that they are present but just not recorded.

2.5.8 Geological logs from Scientex Polymer and the correlation with lithology at Ansell and MT Pictures

In May 1985, borehole drilling was carried out at Scientex Polymer by Geo Pacific Sdn Bhd. The drilling method used was rotary drilling with roller bit and DTHH.

The rock sequence at Scientex Polymer is mainly sandstone. The first 3 metres comprises yellowish brown silty clay, which is probably decomposed interbedded sandstone with shale, lying on 12 metres of fine grained greyish brown material which is interpreted as decomposed sandstone. The weathered sequence lies on a sandstone sequence. No fracture zones are indicated, but it is uncertain whether this is because of lack of record or because they do not exist.

Sandstone observed in Scientex Polymer is possibly similar to the sandstone at MT Pictures and Ansell. There is phyllite in the rock sequence and the shale occurs as a thin layer. Table 2.10 shows the thickness of the sandstone at Scientex Polymer compared to Ansell and MT Pictures. The sandstone layer is thicker to the northwest of Ansell and thinner to the northeast. The rock sequence in Scientex Polymer is interpreted as sittings in between the rock sequences at Ansell and MT Pictures.

Table 2.10 The comparison of sandstone layer thickness at Ansell, Mt Pictures and Scientex Polymer.

Tubewell	Thickness of sandstone layer (m)	Range of depth from ground level (m)
Ansell TW1	9	45 - 54
Ansell TW2	6	30 - 36
Ansell TW3	6	36 - 42
Ansell TW4	15	12 - 27
Ansell TW7	14	14 - 28
MTPictures TW1	1.1	41.8-42.9
MTPictures TW2	5.9	36.1-42
MTPictures TW3	6.9	35.2-42.1
MTPictures TW4	5.5	18-23.5
MTPictures TW5	5.9	17.8-23.7
Scientex Polymer	23	12 - 35

2.5.9 Geological logs from Gaya Color Lab boreholes and the correlation with lithology at Scientex Polymer.

The drilling at Gaya Color Lab was carried out by Geo Pacific Sdn Bhd in May 2001. The drilling work was carried out using the rotary drilling method with a roller bit and DTHH. This borehole is situated on the west bank of Sungai Renggam (Figure 2.8).

The first 30 m is weathered material which is interpreted here as weathered sandstone. Deeper, the rock sequence comprises an alternating sequence of sandstones and quartzites.

No fractures are observed. It is uncertain whether they do not exist or are present but not recorded. Quartz veins are observed at 122 to137 metres.

Figure 2.16 shows the correlation with the rock sequence at Scientex Polymer. The rock sequence is similar up to 73 m depth. The rock sequence at Scientex Polymer possibly sits on top of the rock sequence at Gaya Color Lab.

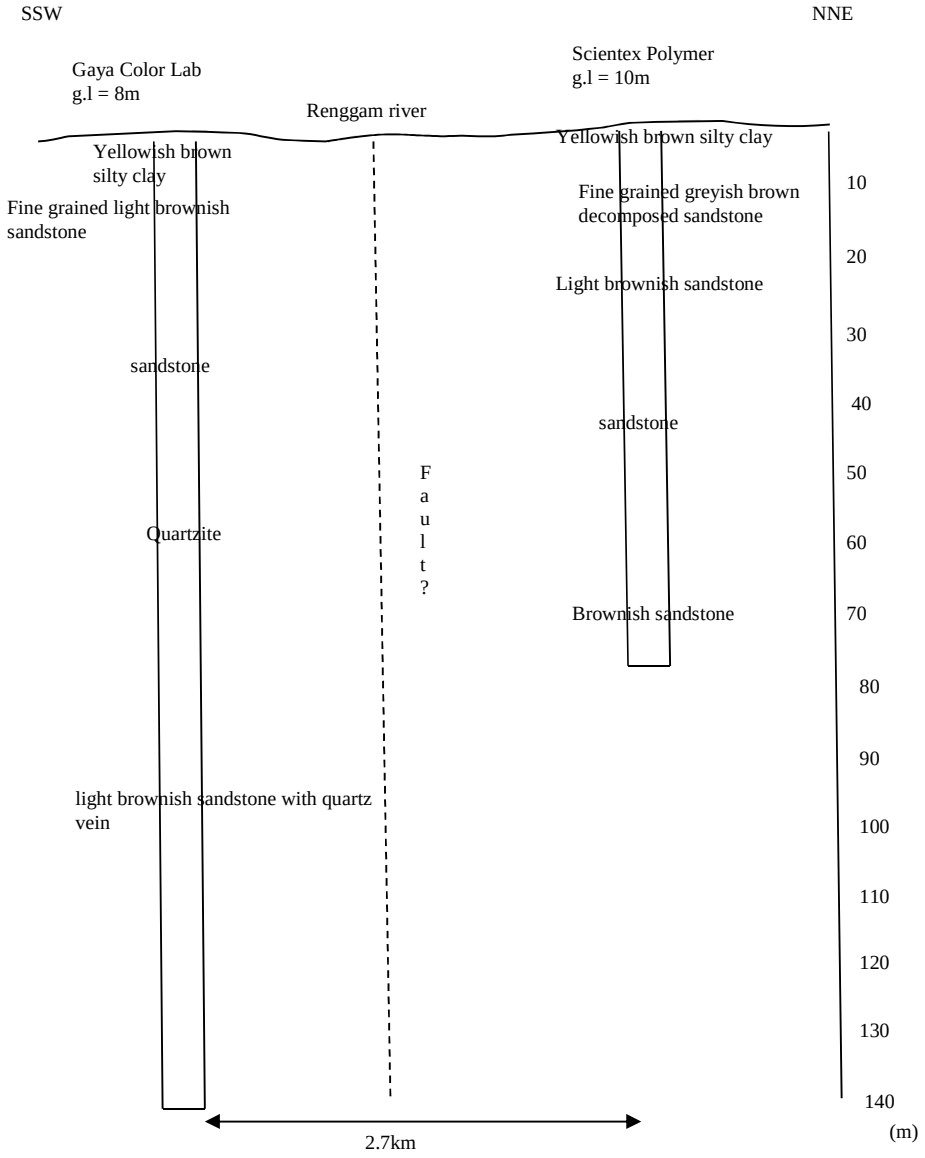

Figure 2.16 The correlation of lithology at Scientex Polymer with Gaya Color Lab

2.5.10 Geological logs from Universal Nutri Beverages and correlation with Mitsui High Tech and Carlsberg and Gaya Color Lab.

The drilling at Universal Nutri Beverages was carried out in December 2006 by Kagawa Drilling Sdn Bhd. There is no information regarding the drilling method that was used. The Universal Nutri Beverages well is located on the west bank of Sungai Renggam and to the northeast of Gaya Color Lab (Figure 2.8).

The upper part of the sequence at Universal Nutri Beverages consists of silty clay material which is interpreted as weathered shale. It lies on black shale. The rock sequence observed at Universal Nutri Beverages is possibly similar to those at Mitsui High Tech and Carlsberg. The boreholes all lie in a predominantly shale sequence.

The lithology here is not similar to the lithology at Gaya Color Lab. It is possible that the rock sequence here sits on top of rock sequence at Gaya Color Lab. Figure 2.17 shows the rock sequence at Universal Nutri Beverages and its correlation with the lithology at Mitsui High Tech and Carlsberg and Gaya Color Lab.

2.5.11 Geological logs from the CCM Fertilizer boreholes and the correlation with the lithology at Universal Nutri Beverages and Gaya Color Lab.

From June to July 2004, drilling at CCM Fertilizers was carried out by Drilco Technologies Sdn Bhd. They drilled using mud rotary drilling and air percussion methods. There are 4 boreholes in this area, but lithological data only exist for 3 of the boreholes.

CCM Fertilizer boreholes are located to the west of Gaya Color Lab and south-southwest of Universal Nutri Beverages (Figure 2.8). They are drilled into sandstone, quartzite and mudstone interbedded sequences. There is possibility

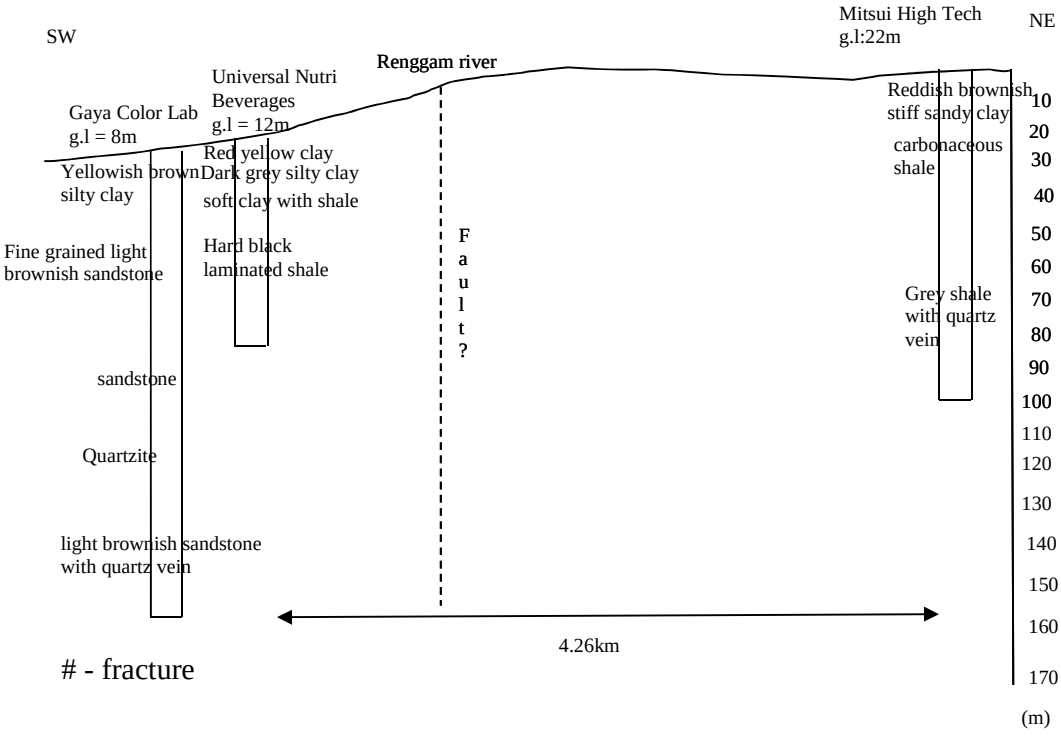

Figure 2.17 the correlation of rock at Universal Nutri Beverages with rock at Misui High tech and Carlsberg and Gaya Color Lab.

that the shale is mistakenly identified as mudstone since this is the first time mudstone is reported. The weathered layer is clay to sandy clay material which is interpreted as weathered interbedded shale sandstone layer. The thickness of weathered layer is up to 50 metres. "Laterite" is observed from 38 to 50 m for CCM Fertilizer 1, 80 to 97 m for CCM Fertilizer 2 and 54 to 72 m for CCM Fertilizer 3. This is interpreted as weathered rock heavily coated with iron oxide. Fractures have been observed in quartzite units between 70 and 140 m depth.

The rock sequence at CCM Fertilizer is possibly sits at the bottom of the rock sequence of Universal Nutri Beverages and Gaya Color Lab (Figure 2.18). This interpretation is based on the presence of quartz veins at different depths in all boreholes at CCM Fertilizer. Quartz vein material is present in some of the rock sequence and becomes dominant at deeper depths and decreases to the southeast. However, the nearest granite body is located far away from this area, approximately 7.4 km to the east.

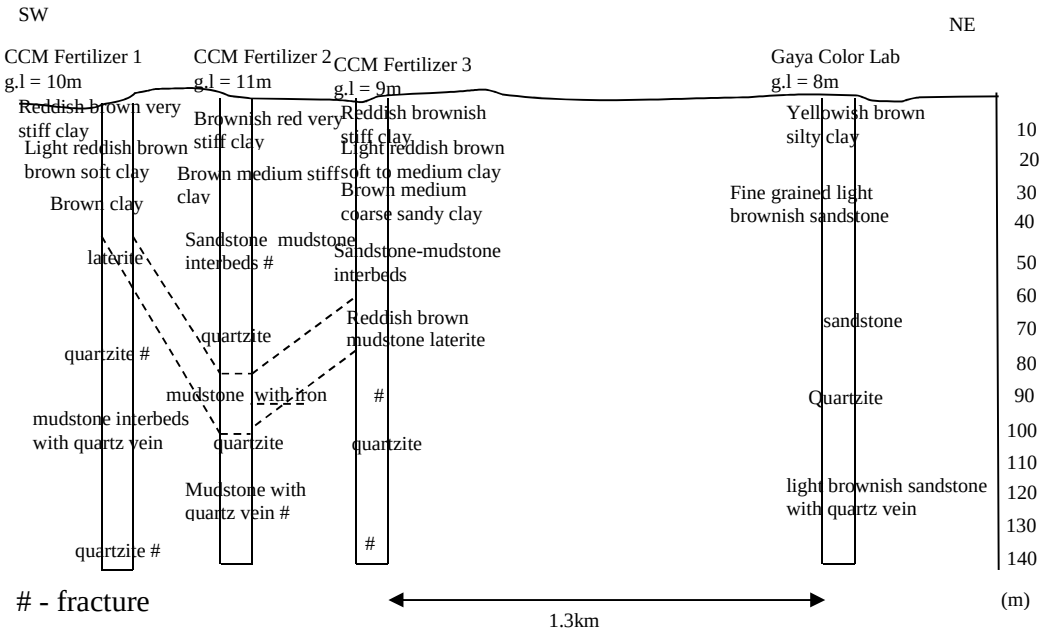

Figure 2.18 The rock correlation at CCM Fertilizer, Universal Nutri Beverages and Gaya Color Lab

2.5.12 Geological logs from the PROTON boreholes and the correlation with lithology at AESBI

The drilling of the boreholes at PROTON was carried out by Geo Pacific Sdn Bhd in April 1997 (Well A) and August 1997 (Well B). The drilling was carried out using the rotary drilling method with a roller bit. The rock description was obtained by analysing the sludge material.

Figure 2.8 shows the location of PROTON boreholes which are situated southeast of AESBI. They are drilled into grey carbonaceous schist. The rock sequence was well described for Well A but briefly described for Well B. Quartz veins can be found in fractured zones which are located between 57 and 75 m and between 90 and 100 m in Well A. Pyrite also been noted at Well A at 90 to 94 m depth.

The first 18 metres comprises weathered carbonaceous shale with sandstone which sits on top of weathered carbonaceous schist (22 metres thick). The carbonaceous schist rock is observed from 40 to 122m. The lithology here can be compared with the lithology at AESBI as the nearest location at which a carbonaceous shale unit exists (Figure 2.19). The carbonaceous shale sequence is thicker to the south. The rock sequence at AESBI is interpreted as sitting on top of the rock sequence here. There is a greater quartz vein presence in this rock sequence compared to the rock sequence at AESBI. More fractures and quartz veins in the rock sequence shows the location of the borehole is near to granite body which is approximately 1.4km to the east.

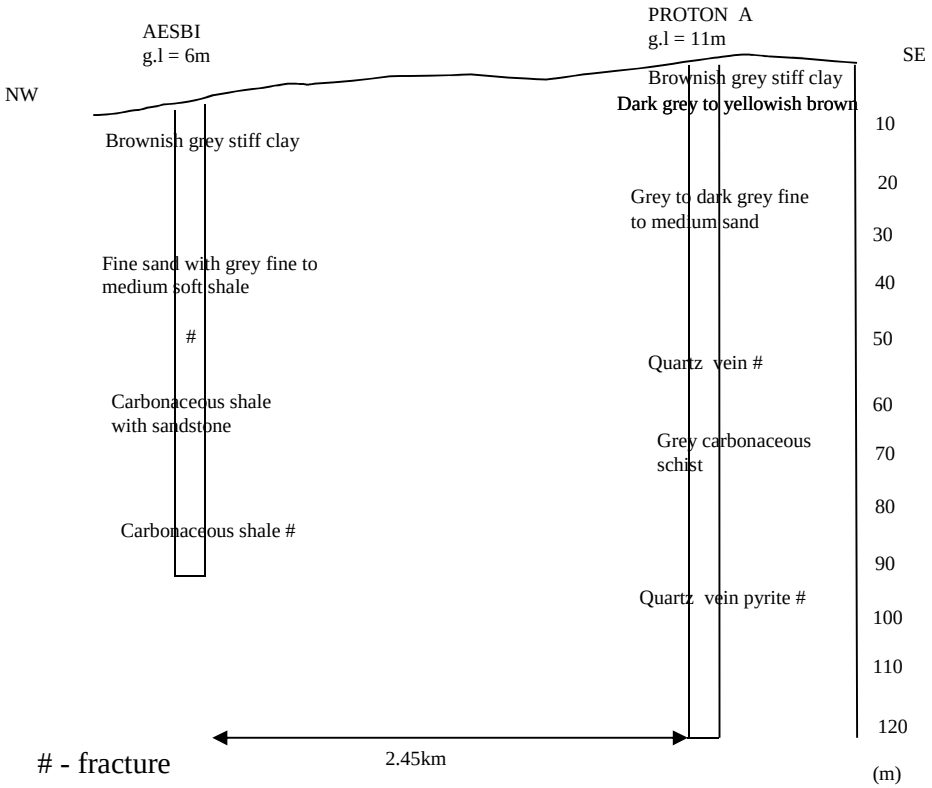

Figure 2.19 The rock correlation between lithology at AESBI and PROTON

2.5.13 Geological logs from the Canon Opto boreholes

The drilling works at Canon Opto were carried out by Elite Drilling Technology Sdn Bhd in June 2006 using the DTHH method. There are 4 boreholes in this area.

Figure 2.8 shows the location of Canon Opto. It is situated to the southeast of the Proton compound. Figure 2.20 shows the ground profile in the Canon Opto boreholes. Canon Opto TW1 and TW2 wells lie in granite while granite is observed at 46 metres depth at Canon Opto TW4. Canon Opto TW3 is embedded in shale of the Kenny Hill Formation. The weathered layer of granite is reddish brown sandy clay with up to 20 metres thick. The weathered layer of shale is covered with brown sandy clay material which is up to 25 m thick. It is

interpreted as weathered interbedded sandstone and siltstone. There is a possibility that shale is mistaken with siltstone since this is the first time the siltstone is reported. The granite is present in all boreholes except at Canon Opto TW3. The elevation of granite observed in the boreholes decreases to the southwest.

The borehole evidence in this area agrees with the interpretations regarding the existence of the granite body in study area. It can be concluded that the granite intrusion occurs at the east side of Shah Alam.

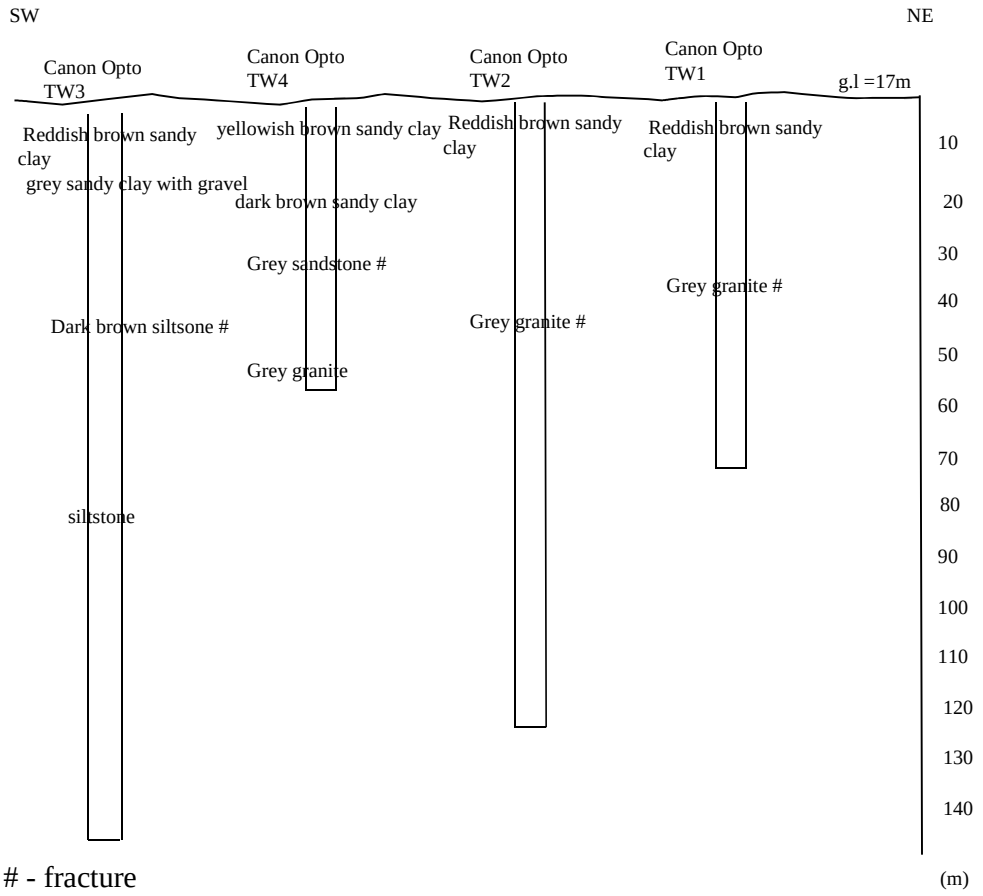

- fracture

Figure 2.20 The ground profile at Canon Opto

2.5.14 Geological logs for the Aquarium Express and Aquatic International boreholes

The drilling of the boreholes at Aquarium Express and Aquatic International was carried out by Korekan Instantflow Sdn Bhd. The Aquatic International TW2 and TW3 boreholes were drilled in December 2003 while borehole TW1 at

Aquarium Express was drilled in September 2005. The rotary air percussion method has been used with a drag bit and DTHH.

This area is situated further north than the other tubewells. Figure 2.8 shows the location of Aquarium Express and Aquatic International TW2 and TW3.

Figure 2.21 shows the borehole log for Aquarium Express. The weathered layer consists of brownish fine to medium grained sand with clay material. It is interpreted as a weathered interbedded sandstone and shale sequence. The thickness of the layer is up to 25.6 m. Limestone was found from 25.6 m depth. Fractures are observed at 25.6 to 41.75m in the limestone. This limestone is possibly part of the Kuala Lumpur Limestone. The only Kuala Lumpur Limestone outcrop is located at Batu Caves, Selangor which is around 19 km to the northeast of this site.

The other two boreholes (Aquatic International TW2 and TW3) comprise brownish to greyish fine to medium grained sand with clay material (24 and 15 metres thick respectively) which is interpreted as weathered interbedded sandstone and shale sequence. It sits on top of dark grey schist (22 and 36 metres

thick respectively). Fractures are observed in grey schist at 26 metres at Aquatic International TW2 and at 50 metres in Aquatic International TW3.

There is a possibility that limestone occurs at depths below the base of these boreholes. This interpretation fits with the observation by Rosly (1976) where he observed a fault as the contact between Kenny Hill Formation and Kuala Lumpur Limestone at Salak South. Salak South is located approximately 18km to the southeast of this area (see Figure 2.3).

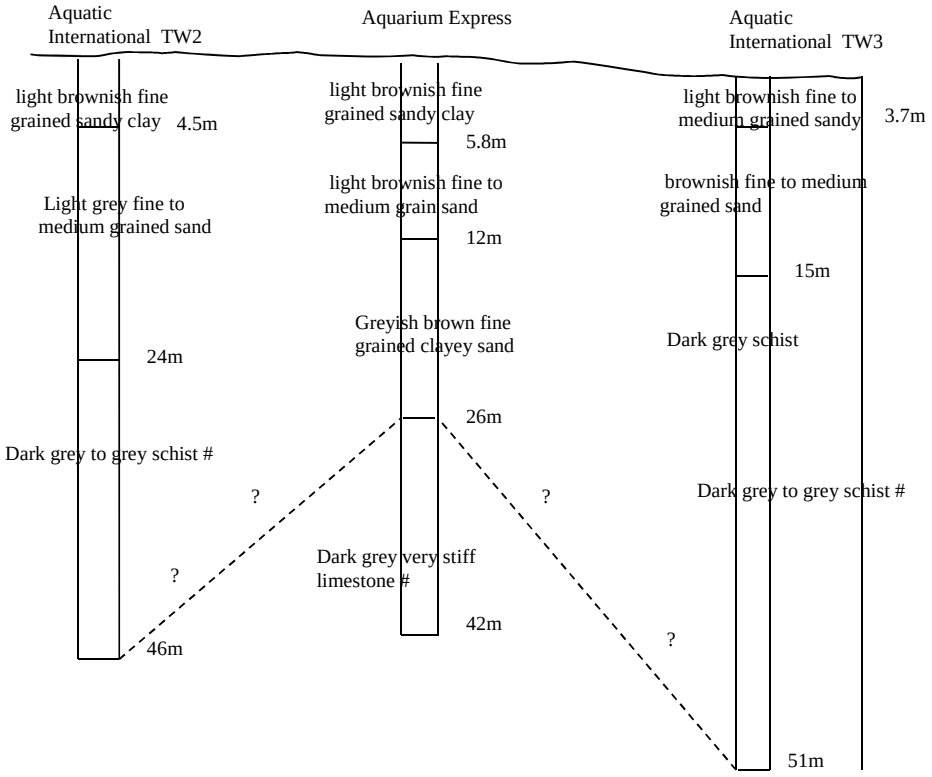

Figure 2.21 The ground profile at Aquarium Express and Aquatic International

2.6 Fieldwork Observations

2.6.1 Introduction

Brief reconnaissance fieldwork has been carried out with the purpose of observing at first hand the outcrop of the bedrock in the Shah Alam area. This is one way, for example, of determining whether matrix flow is possible. Three exposures were found (Figure 2.8). The outcrops are labelled ‘A’ to ‘C’ respectively.

2.6.2 Observation at Outcrop A

Outcrop ‘A’ is situated around 350 m to the northeast of Scientex Polymer (see Figure 2.8). The outcrop is approximately 25 metres high and 130 metres wide. The outcrop is oriented in a northwest / southeast direction. Observations were made from distance since the outcrop is in privately owned area to which it was not possible to gain entrance. This site has probably existed since 2004 or earlier.

The outcrop comprises of massive sandstone at the northwest which changes to interbedded sandstone and shale to the southeast (Figure 2.22). The sandstone and shale are distinguished by their colour; sandstone is dark brown in colour which is darker. The shale is denoted by the white stripe on the outcrop and it is whitish in colour (Figure 2.23). Besides, the sandstone is more resistant to the weathering as indicated by the effect of erosion on the outcrop by rainfall (Figure 2.24). Massive sandstone is less eroded than interbedded sandstone and shale. The bedding planes are still preserved in sandstone and they appear to dip to the northeast.

This outcrop agrees with the information obtained from the borehole log from Scientex Polymer.

Figure 2.22 Outcrop A. It is located in front of Scientex Polymer area. The outcrop is oriented in a northwest / southeast direction.

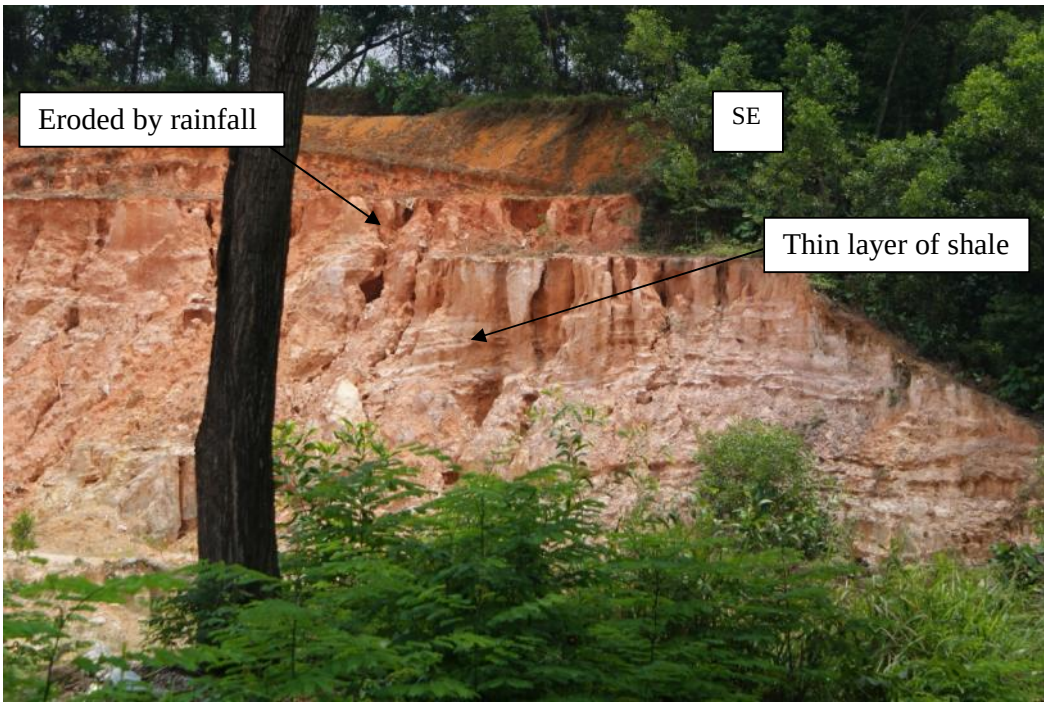

Figure 2.23 Interbedded sandstone and shale at the southeast of the outcrop

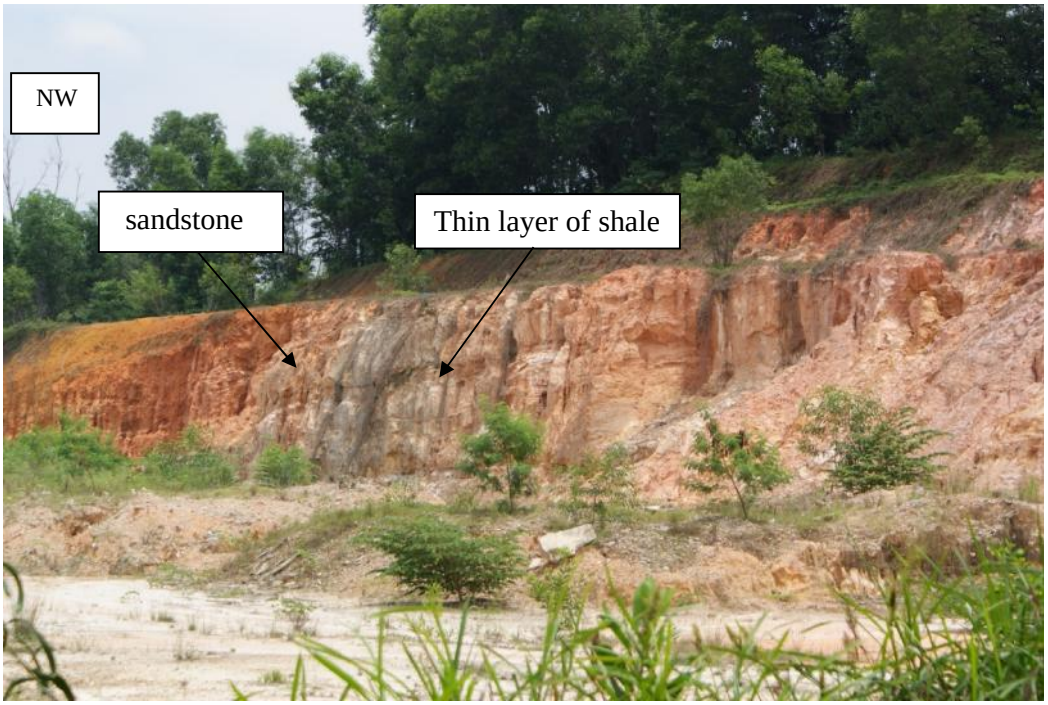

Figure 2.24 The massive sandstone on the northwest

2.6.3 Observation at Outcrop B

Outcrop B is located around 4 km to the northwest of outcrop 'A' (Figure 2.8). Figure 2.25 shows outcrop B. The outcrop is 2 metres high and 54 metres wide. It comprises of an interbedded sequence of quartzite with variable thickness of shale (Figure 2.26). The rock sequence on the west-northwest is dipping to the southwest at an angle of 12º which is quite similar to the outcrop at Scientex Polymer, while the rock sequence on the east-southeast side is dipping to the southeast at angle 28 º. The rock sequence is folded, forming an antiform structure.

The quartzite is grey in colour. However most of the quartzite appears as brown in colour on the surface, presumably because of oxidation of a reducing component in the unweathered quartzite. It is a medium-grained quartzite. The size of quartz grains is 1-2mm in a finer matrix (silt and clay). The framework grain size is uniform with subangular to subrounded shapes. The joints in quartzite are persistent and perpendicular to the bedding (Figure 2.27). The quartzite on west-northwest of the outcrop is interbedded with thin units of shale as shown in Figure 2.28. It is 2 metres high and 16 metres wide. This outcrop is dipping to southwest at an angle of 8º. It can be concluded that the shale layer at Outcrop B is thinner to west-northwest.

Quartz veins are observed at two spots in this area, to the further east-southeast and further northwest of the outcrop (Figure 2.29). The shale that is near the quartz veins is whiter and harder possibly due to silicification (Figure 2.30).

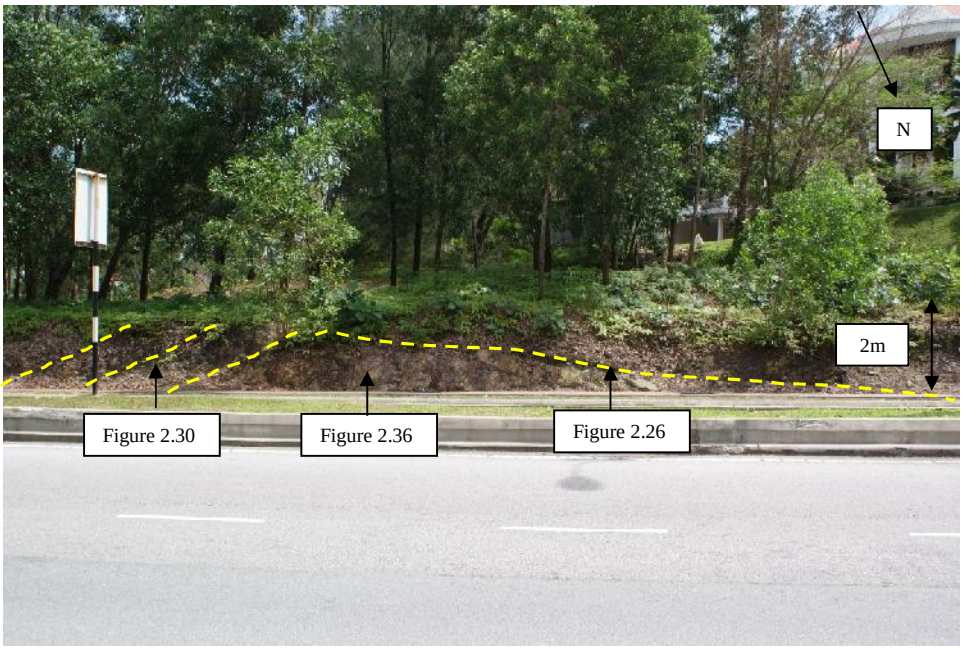

Figure 2.25 The rock sequence at Outcrop B. The yellow dashed line shows the antiform structure.

Figure 2.26 The sandstone with thin bed of shale (between yellow lines) at Outcrop B. The rock sequence is dipping to the southwest at an angle of 12º The GPS device is 10 cm in length.

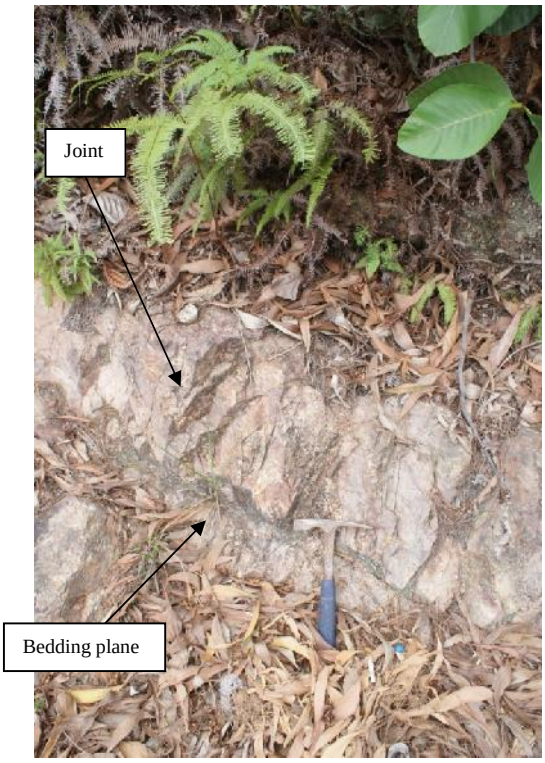

Figure 2.27 Joint is perpendicular to the bedding

Figure 2.28 Quartzite with thin layer of shale (white colour)

Figure 2.29 Quartz vein / lenses in sandstone at further east-southeast side. The diameter of the coin is 2.3cm

Figure 2.30. The thin layer of shale interbedded with quartzite

From the fieldwork observation carried out at Outcrop B, there are evidences that the rock sequence experienced a series of faulting events. There are at least 2 sets of fault have been observed (Figure 2.31). The quartzite which is adjacent to the fault is very strong compared to quartzite nearby (Figure 2.32 and Figure 2.33). It is massive with fine fractures and very hard which is believed to be caused by silicification with the presence of quartz lenses (Figure 2.32 and Figure 2.33). The fine fractures in this rock are coated with iron oxide (Figure 2.34). Iron is commonly observed coating the rock surface in Kenny Hill Formation. Other minerals such as pink zircon and tourmaline were not found anywhere at outcrop. The quartz veins are also faulted as observed at further northwest of the outcrop (Figure 2.35).

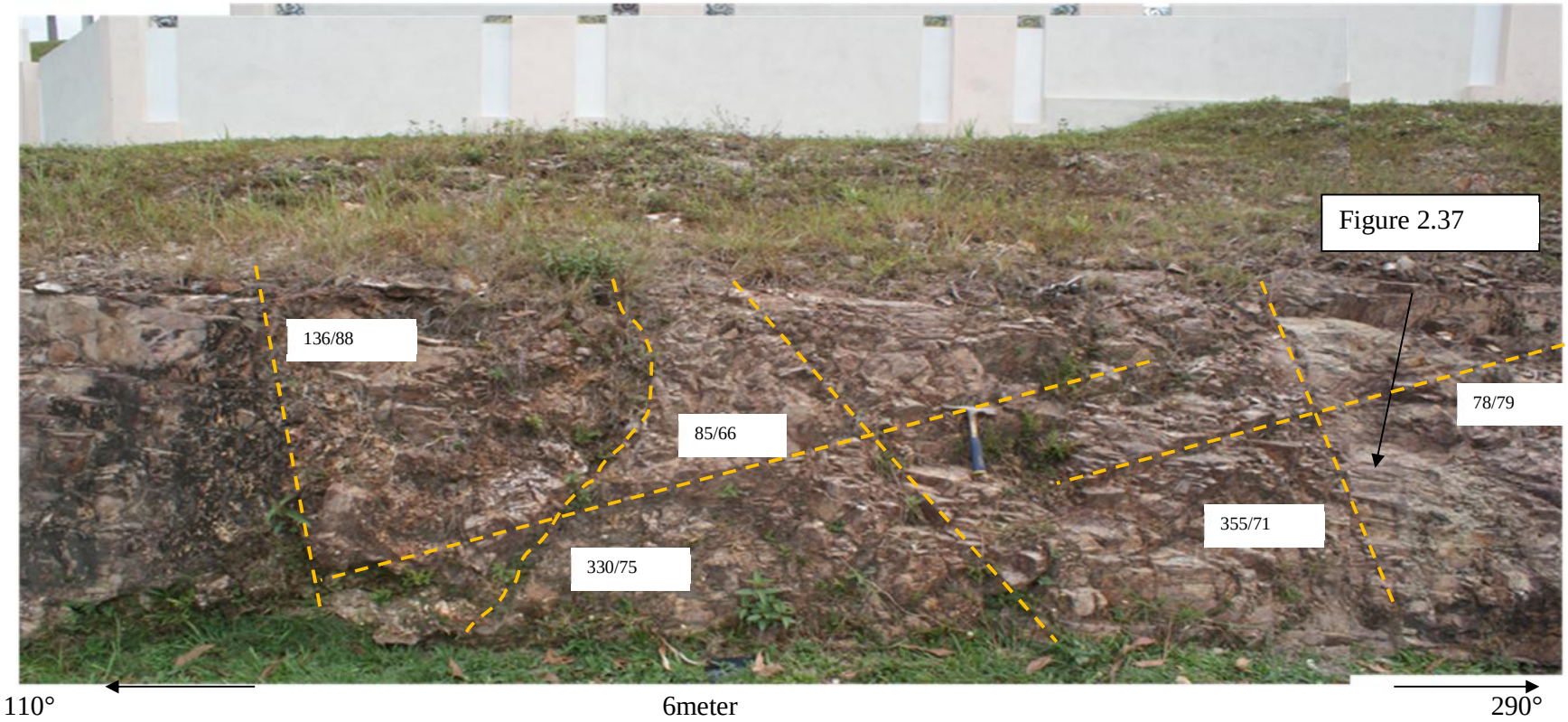

Figure 2.31 Faults observed in quartzite at Outcrop B

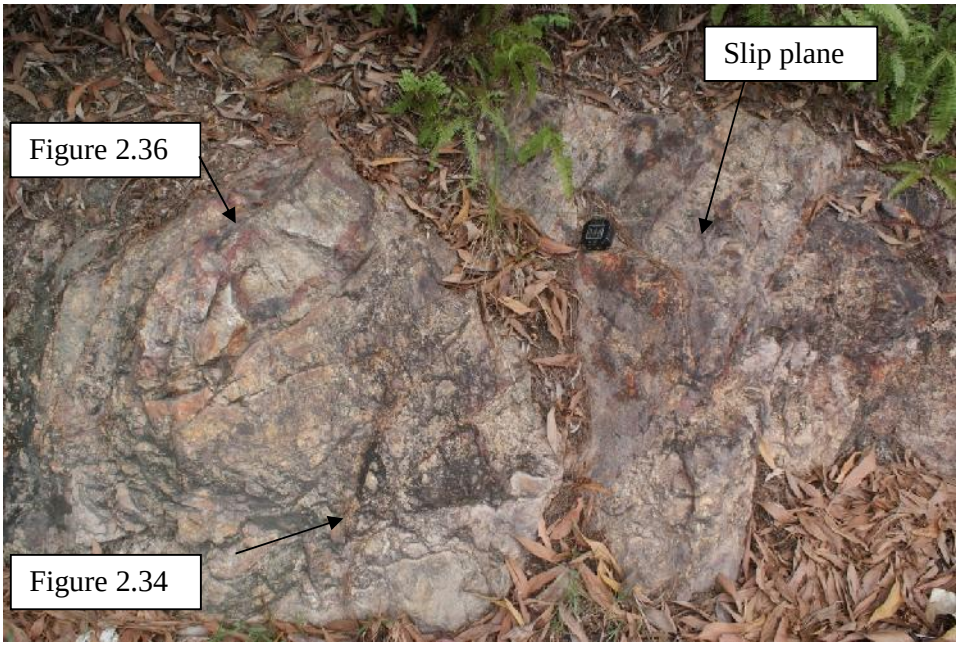

Figure 2.32The quartzite in fault zone is hard which is possibly due to the presence of quartz lenses. The size of the compass is 7cm.

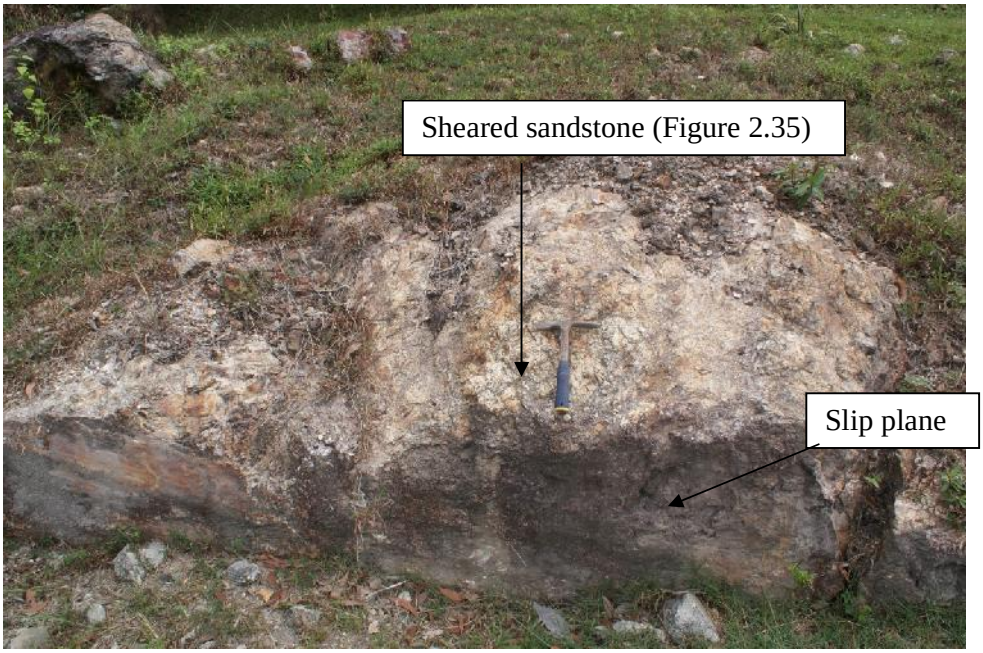

Figure 2.33 The sheared quartzite

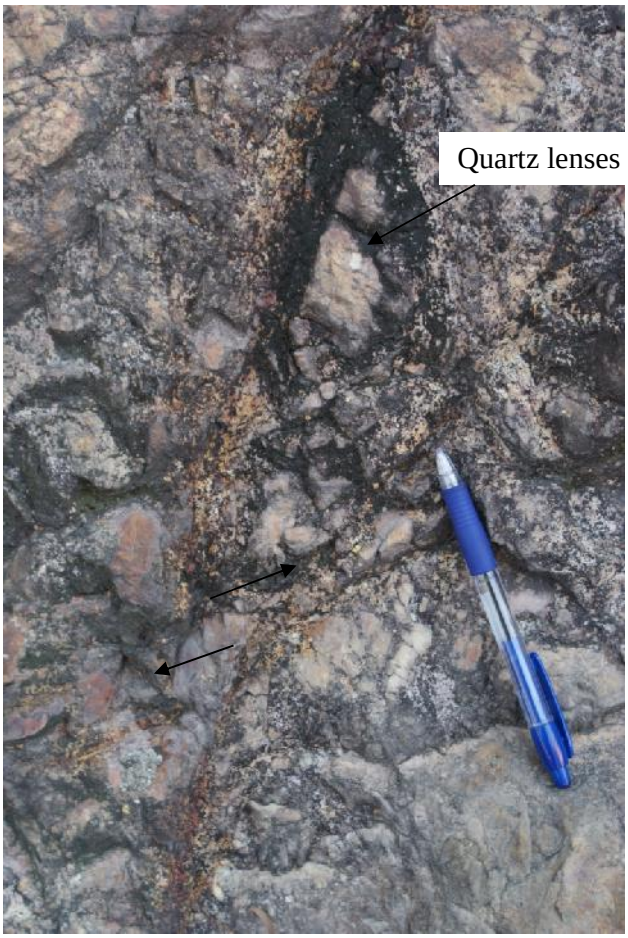

Figure 2.34 Fault is observed in massive quartzite outcrop

Figure 2.35 The sheared quartzite with quartz lenses

Figure 2.36 Fine fractures in mottled sandstone. The fractures are filled with iron oxide. The diameter of the coin is 2.3cm.

Figure 2.37 The quartz veins are displaced by fault

Phyllite is also observed at the east-southeast of outcrop ‘B’ (see Figure 2.25) as shown in Figure 2.38. The contact between quartzite and phyllite is fault as shown in Figure 2.39. The fault plane is almost vertical and dipping to the south-southeast. Phyllite in the fault zone is fractured and easily fall off. The foliation is 80/72 which is almost parallel to the fault plane. The rock sequence on the east-southeast of outcrop ‘B’ dips steeply after the fault; with strike direction has changed to the northeast which is parallel to the fault plane as shown in Figure 2.25.

Fold with smaller scale is also observed at Outcrop B (Figure 2.40). It was observed in quartzite near the sheared quartzite. The axis of the fold plunges towards the northwest.

Figure 2.38 Phyllite which is dipping to the southeast at steep angle. The size of the compass is 20cm

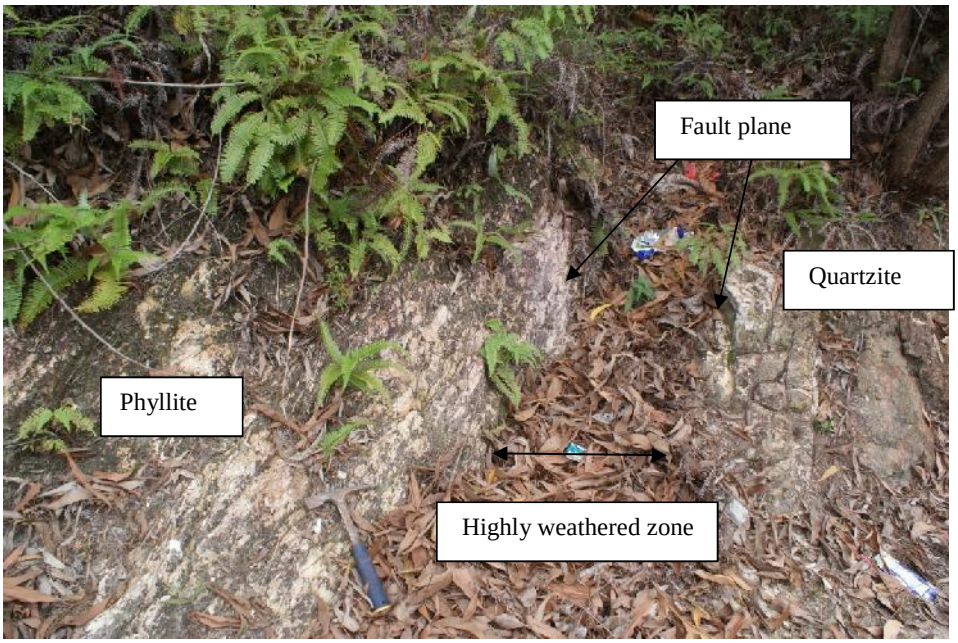

Figure 2.39 The fault plane is almost vertical

Figure 2.40 Fold in quartzite

Discontinuity survey

Table 2.11 shows the discontinuity data survey which has been carried out at Outcrop B. 33 readings have been taken. Each location of the discontinuity survey is shown in Figures 2.41 to 2.43. Figure 2.44 is a stereonet showing the lower hemisphere pole plots for the joints observed. Three sets of joints have been observed: the great circles in this figure were obtained using the averaged joint orientations within each joint set. The main joint sets appear to be the ones that dip toward the south and southeast (J1-J2) and northeast (J3) with angles of almost 70^{o}. The joints in sandstone are more persistent compared to the joints in phyllite as shown in Figure 2.41. The joint spacing is smaller (up to 5cm) in the weathered quartzite compared to the less weathered outcrop, the latter being up to 1 m as shown in Figure 2.42. The aperture of the joints observed is 1 mm which is classified as gapped features (Brown et al., 1981). The joints with soil infill are 2-3mm wide. The joint surfaces are rough and planar.

Figure 2.45a) shows the plot for faults observed at Outcrop B. There are three sets of faults, one dipping steeply to the SSW, one dipping steeply to the ENE, and the other with shallow dip. The major set is the faults which strike to the north and east as shown in Figure 2.45b), and these seem to correspond with the orientations of joint sets J1 and J3. Figure 2.45c) shows all the discontinuities for Outcrop B.

Table 2.11a) Discontinuity survey data at Location 1

spacing(cm)	strike/dip	length (m)	aperture (mm)	surface
16	78/60		3	
40	79/88	1 - 2		
70	88/60	1	1	wavy
133	222/64	0.43	1	planar
158	245/58	0.46	1	wavy
194	340/54	0.56		planar,smooth
204	8/42	0.45		planar,smooth
208	45/70	across the slope		
272	305/56	0.2		planar
	62/65	across the slope		

Table 2.11b) Discontinuity survey data at Location 2

spacingcm)	strike/dip	length (m)
9	35/69	45
19	25/76	across the slope
27	20/74	
46	34/64	
70	140/65	
89	335/72	
100	76/86	
120	56/88	
134	38/70,318/63	0.15/0.18
138	25/75	
180	306/82,94/78	
	45/85	

Table 2.11c) Discontinuity survey data at Location 3

spacing(cm)	strike/dip	length (m)	aperture (mm)	surface
30	344/65	1		
	96/84	1		
50	50/67	0.44	<1mm	
	97/88			
74	331/59	0.3		smooth
	280/80	0.28		
107	325/74			
140	105/79			
226	24/77	1.37		

Figure 2.41 Joint in quartzite ranges from 0.5 to 1 metres length. The size of the GPS device is 10cm. The yellow dashed lines are the main joint set observed at Location 1

Figure 2.42 a) The joint spacing is smaller in weathered quartzite outcrop which located at the east-southeast of the outcrop ‘B’ (Location 2).

Figure 2.42 b) The wider joint spacing in massive quartzite at outcrop B (Location 2).

Figure 2.43 Location 3 of discontinuity survey at Outcrop B.

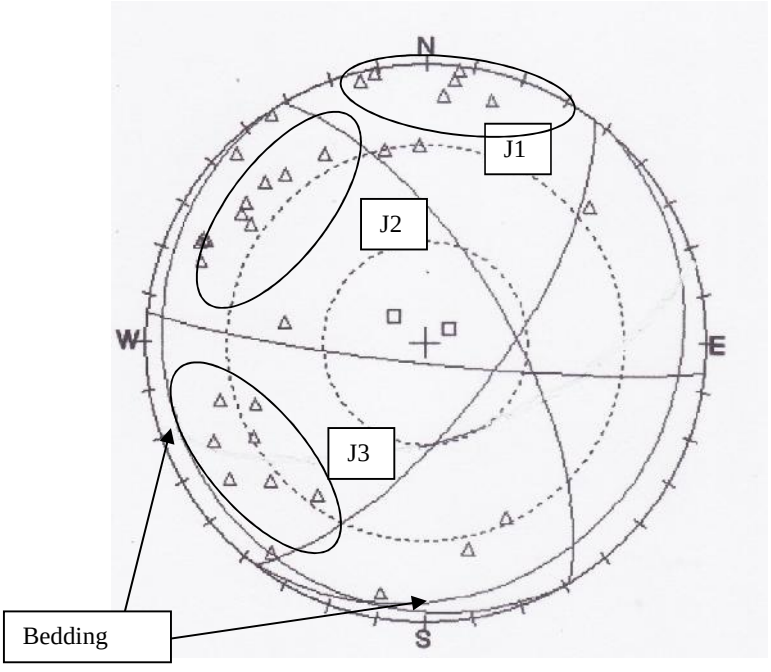

Figure 2.44 The lower hemisphere pole plots of the joints observed at Outcrop ‘B’. The mean direction of each of the defined sets is indicated by the great circles, as labelled. The bedding dip poles are indicated by squares, with the great circles labelled ‘Bedding’.

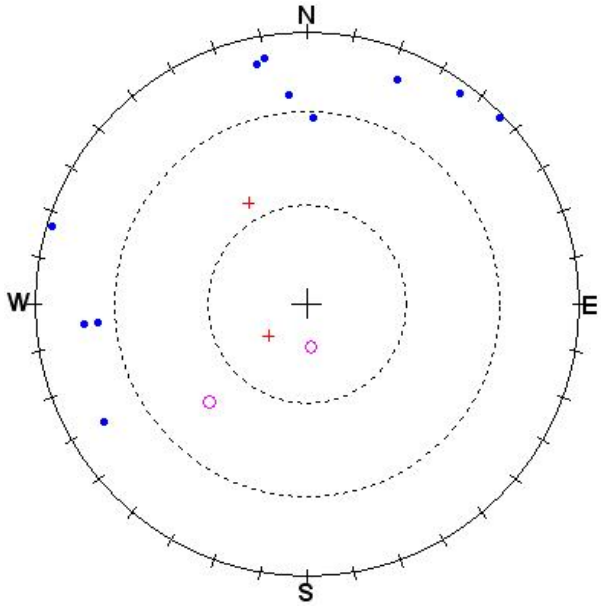

● Fault observed at Outcrop B

° Fault (Tjia 1976)

+ Fault (Mogana 1991)

Figure 2.45a) The lower hemisphere pole plots for faults observed at Outcrop B with faults from previous research

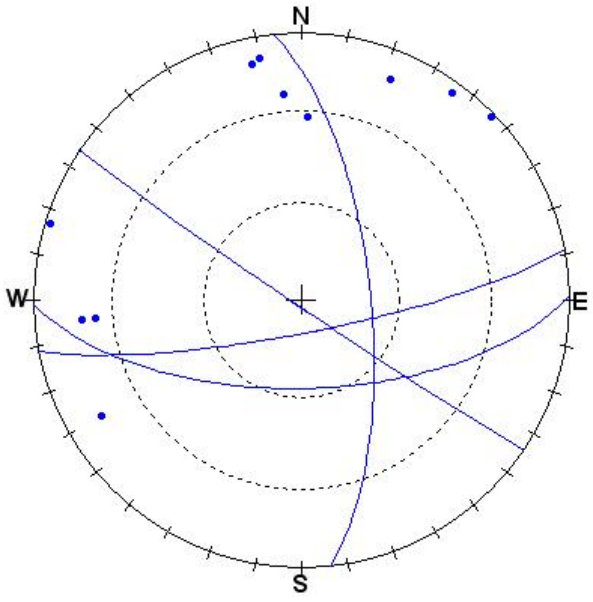

Figure 2.45b) The plots for fault set observed at Outcrop B. There are three sets of fault observed at Outcrop B.

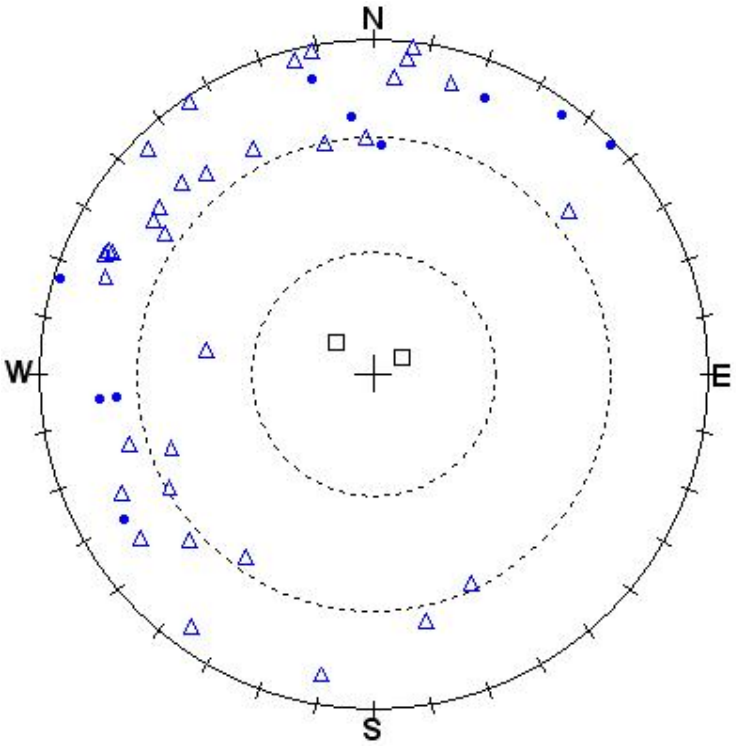

● Fault observed at Outcrop B

□ Bedding

Δ Joint

Figure 2.45c) The plots of all the discontinuities observed at Outcrop B

2.6.4 Observation at Outcrop C

Outcrop 'C' is located around 4 km to the northeast of Outcrop B (see Figure 2.8). The rock sequence comprises weathered sandstone, denoted by its brownish colour. It lies on top of greenish grey shale (Figure 2.46) which is a hard rock. It is stained with iron oxide on the surface. The rock sequence is dipping towards south-southeast at an angle of 4^{o}. It is foliated and jointed, with at least three sets of joints. The length of the joints is up to 5cm (Figure 2.47). The surfaces of the joints are smooth and planar.

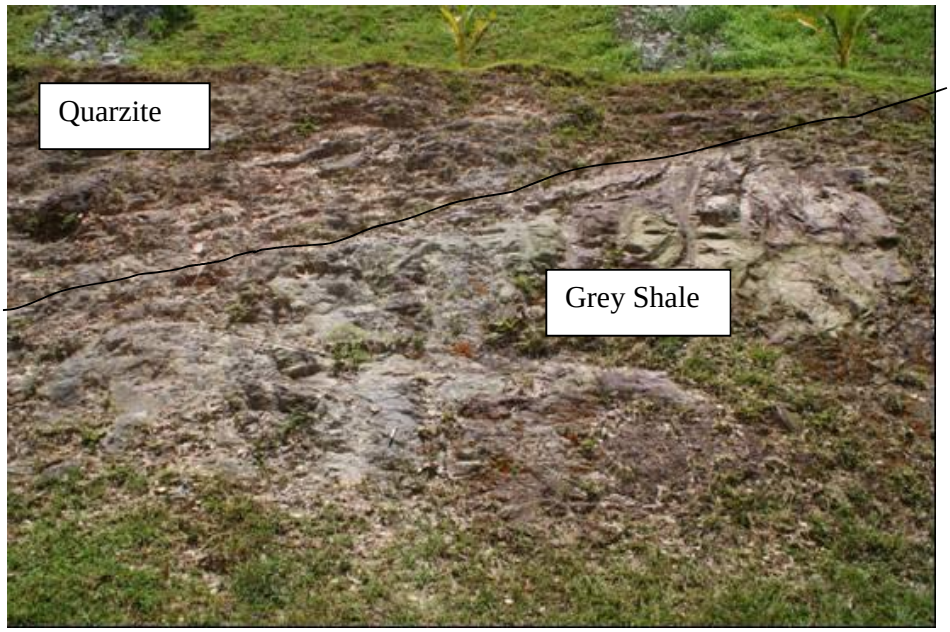

Figure 2.46 The rock sequence at Outcrop C comprises sandstone overlying hard grey shale.

Figure 2.47 The joint sets in the hard grey shale at Outcrop C.

There is a big slope which is located around 310 m north of Outcrop C as shown in Figure 2.48. Due to reasons of safety, it was observed only from distance. It is around 15 m high and 110 m wide, in north to south direction. The weathered brown material on the right (north) side of the picture is possibly of sandstone origin while the rest of the outcrop comprises shale. The beds dip towards the northwest. The outcrop has an antiform structure with the axis visible on the right side of the outcrop. There is a fault cutting through the centre of the outcrop as indicated on the figure. Probable drag folds are seen on the south side of the fault.

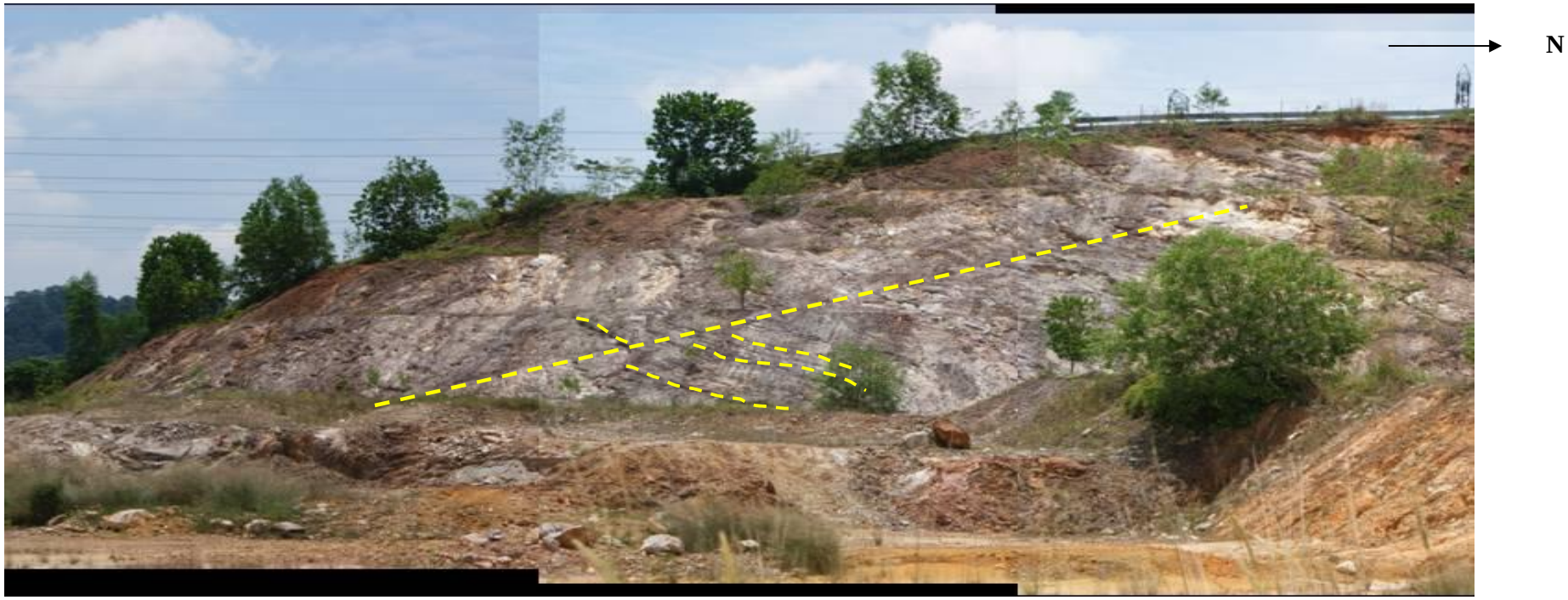

Figure 2.48 This outcrop is located around 300 m north of Outcrop C. It is oriented in a north / south direction. The outcrop has an antiformal structure which plunges towards the north. The rock on the south side of outcrop is folded and a fault is present in the middle part (as shown by the yellow line). The arrows show the displacement. The rock sequence is dipping towards the northwest

2.6.5 The interpretation of Shah Alam's river pattern

The river patterns in Shah Alam are analysed to see if there is any significant relationship with the geology, and therefore allow further mapping of fault or other fracture patterns. The topographic maps of Kuala Lumpur and Pelabuhan Kelang & Kelang with scale 1:63630 are used together with Google Earth images to analyse the rivers pattern. First, the river patterns were identified using Google Earth images. Each of the lineaments have then been checked with the topographic maps to make sure that the features are not man-made structures (e.g affected by drainage engineering). Figure 2.49 shows the lineaments that have been chosen. There are three rivers that flow through the Shah Alam area. The Damansara river (on the east side of Shah Alam) and the Renggam river (on the west side of Shah Alam) flow into the Klang river in a southwest direction in general. The Klang river flows to the west into the sea.

After the river patterns have been recognized, the lineaments have been plotted on a stereonet diagram as strikes with assumed dip directions of almost vertical (Figure 2.50). As Figure 2.50 shows, the river patterns in Shah Alam can be divided into two directions, southeast-northwest and northeast-southwest. Figures 2.51 and 2.52 were plotted to see if there is any relationship between distance from main rivers and presence of quartz veining, as veining is often associated with fracturing (Section 2.6.3, Outcrop B) and may be also associated with granite intrusion. Figure 2.51 indicates no clear relationship between proximity to main rivers and quartz veining, and Figure 2.52 also indicates no clear relationship with distance to granite. However, quartz veins occur in wells

that coincide or near to river tributaries as shown in Figure 2.53. The fracture occurence in wells are associated with granite intrusion as shown in Figure 2.54. The fractures were observed in wells near to granite intrusion in the east side of study area.

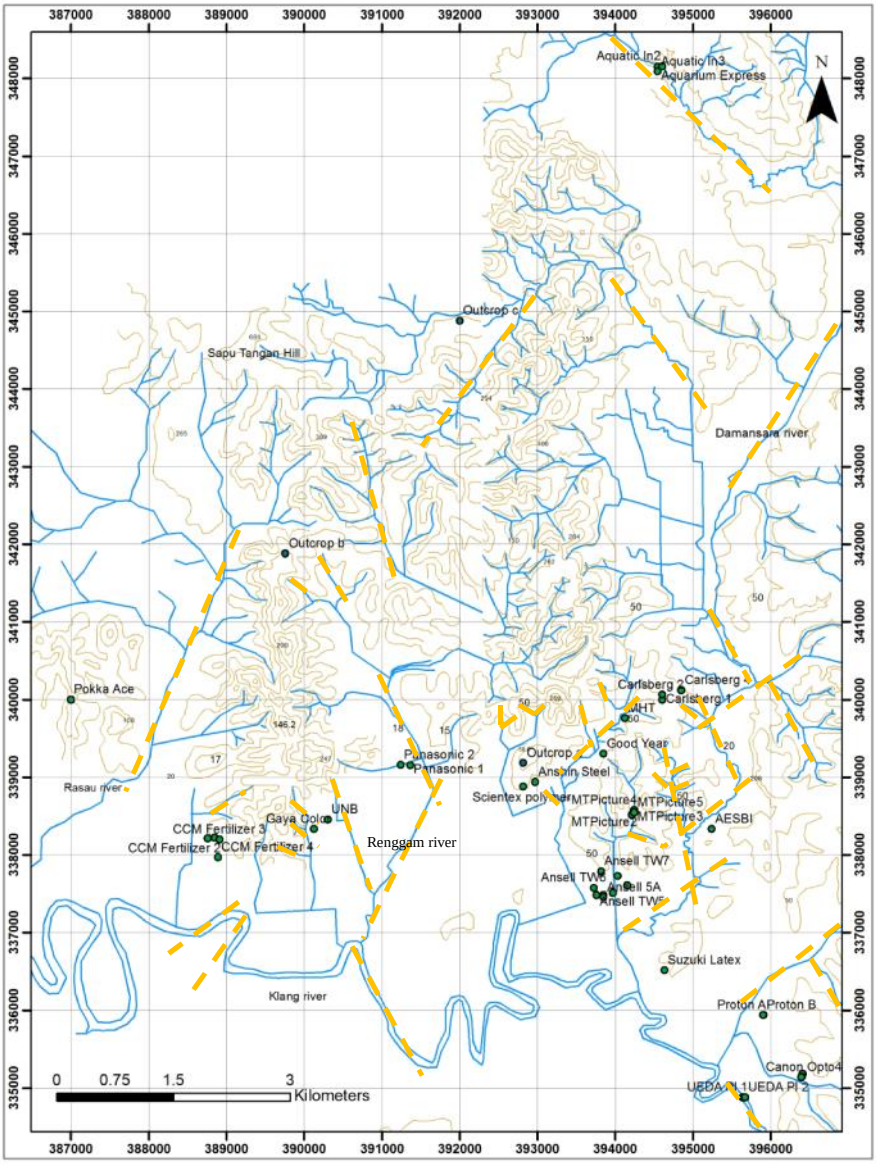

Figure 2.49.The river alignment as observed in topographic map of Shah Alam published by Director of National Mapping Malaysia 1966&1970

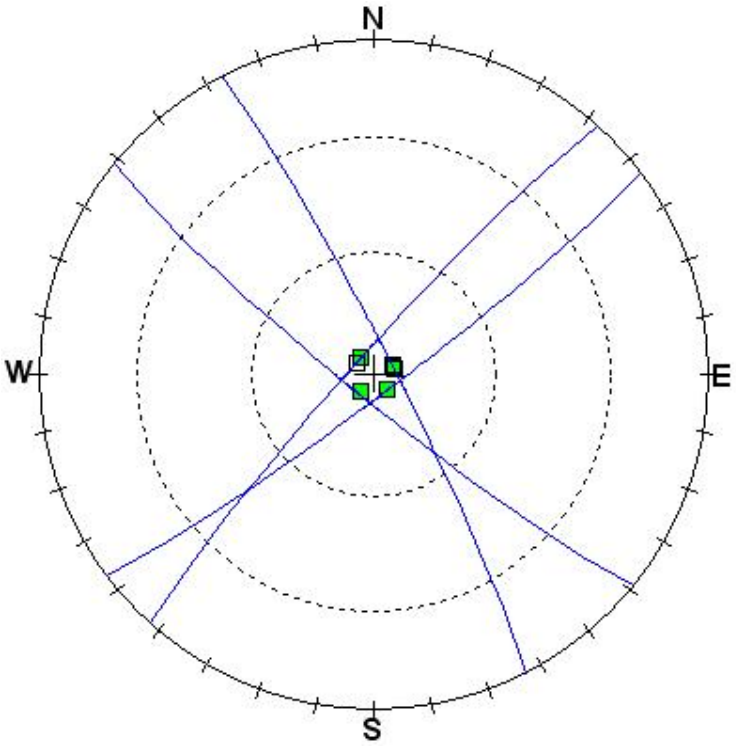

Figure 2.50 The plots for river lineaments

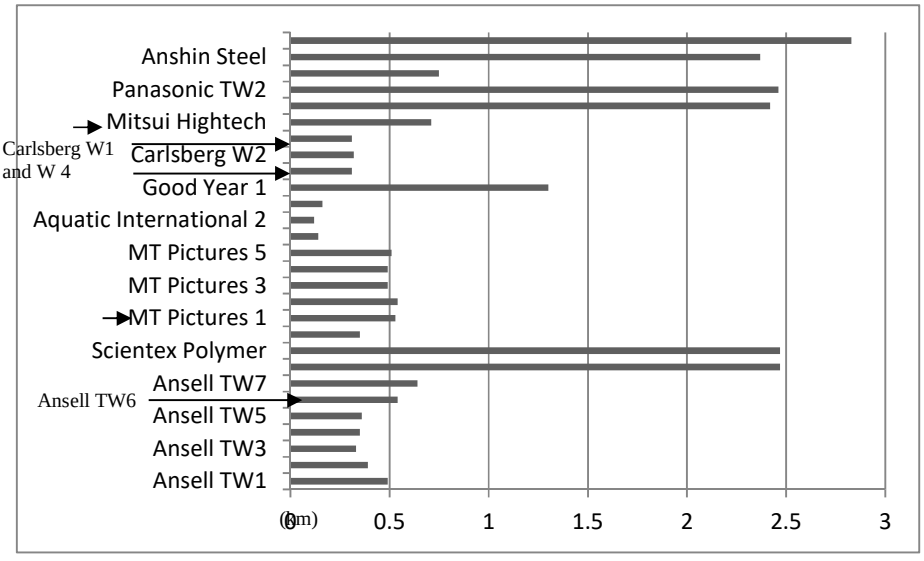

Figure 2.51 a) The distance of the well to Damansara river. The wells with ► are those where quartz veins were recorded in their borehole cores.

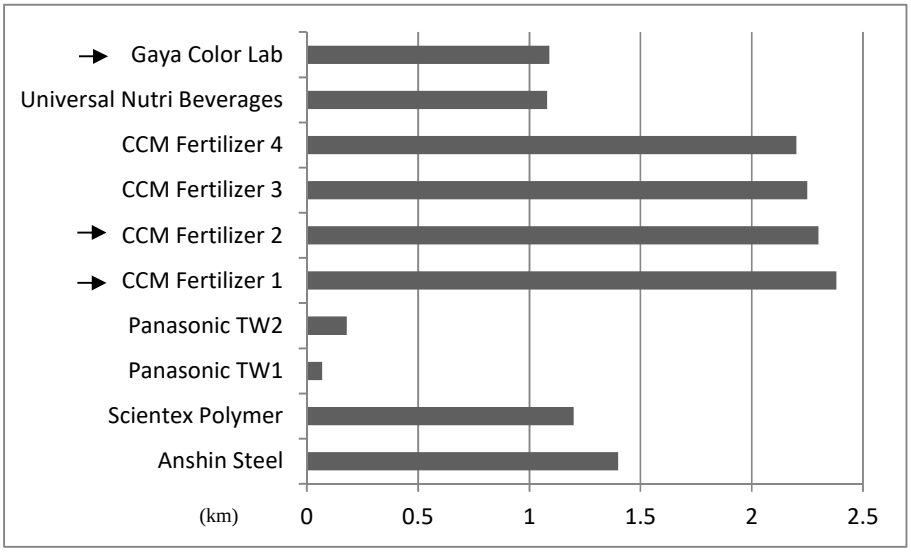

Figure 2.51b) The distance of the well to Renggam river. The → wells with → are those where quartz veins were recorded in the borehole cores.

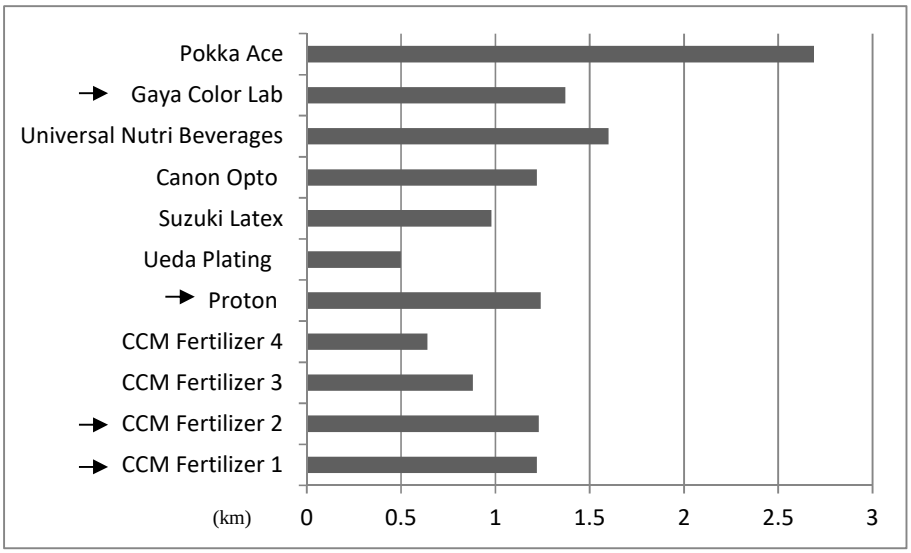

Figure 2.51c) The distance of the well to Klang river. The wells with → are with quartz vein

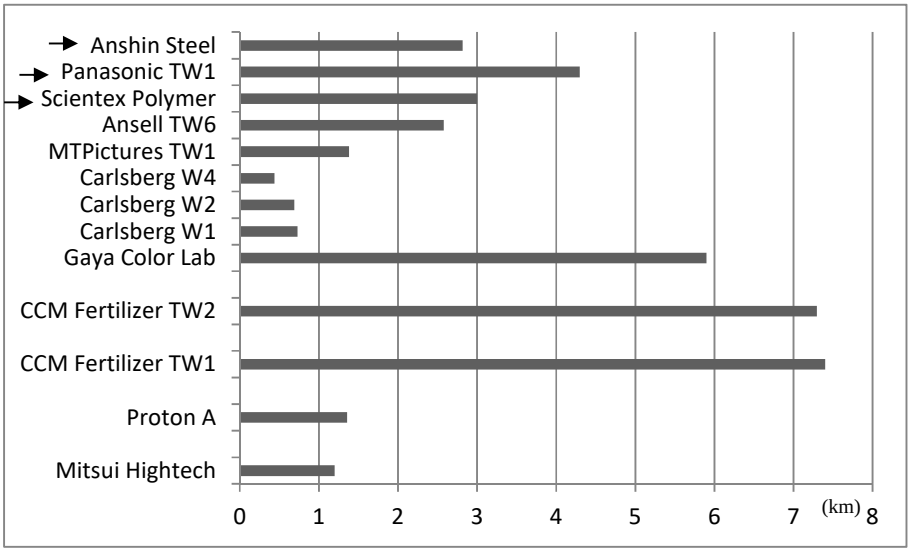

Figure 2.52 The approximate distance of the well to granite (east of Shah Alam). No quartz veins for wells with →.

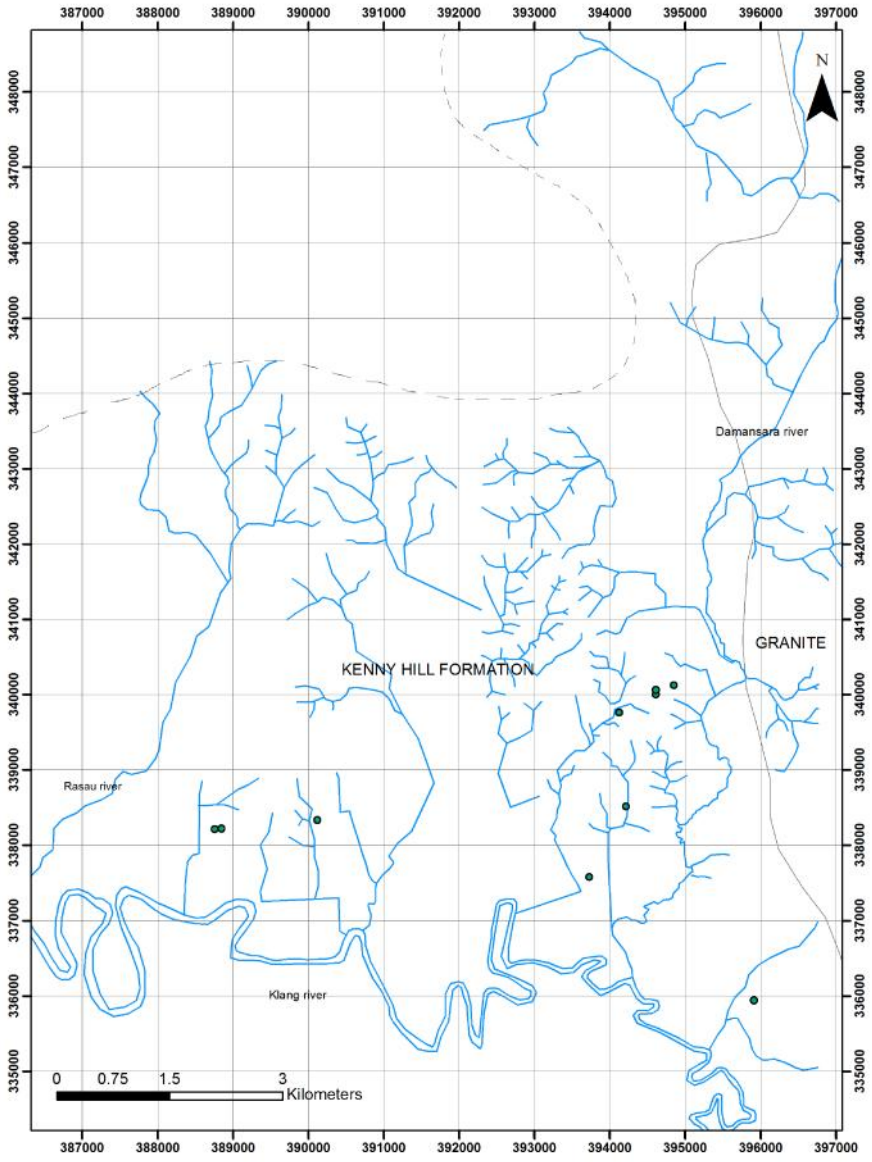

Figure 2.53 Wells which quartz veins were observed

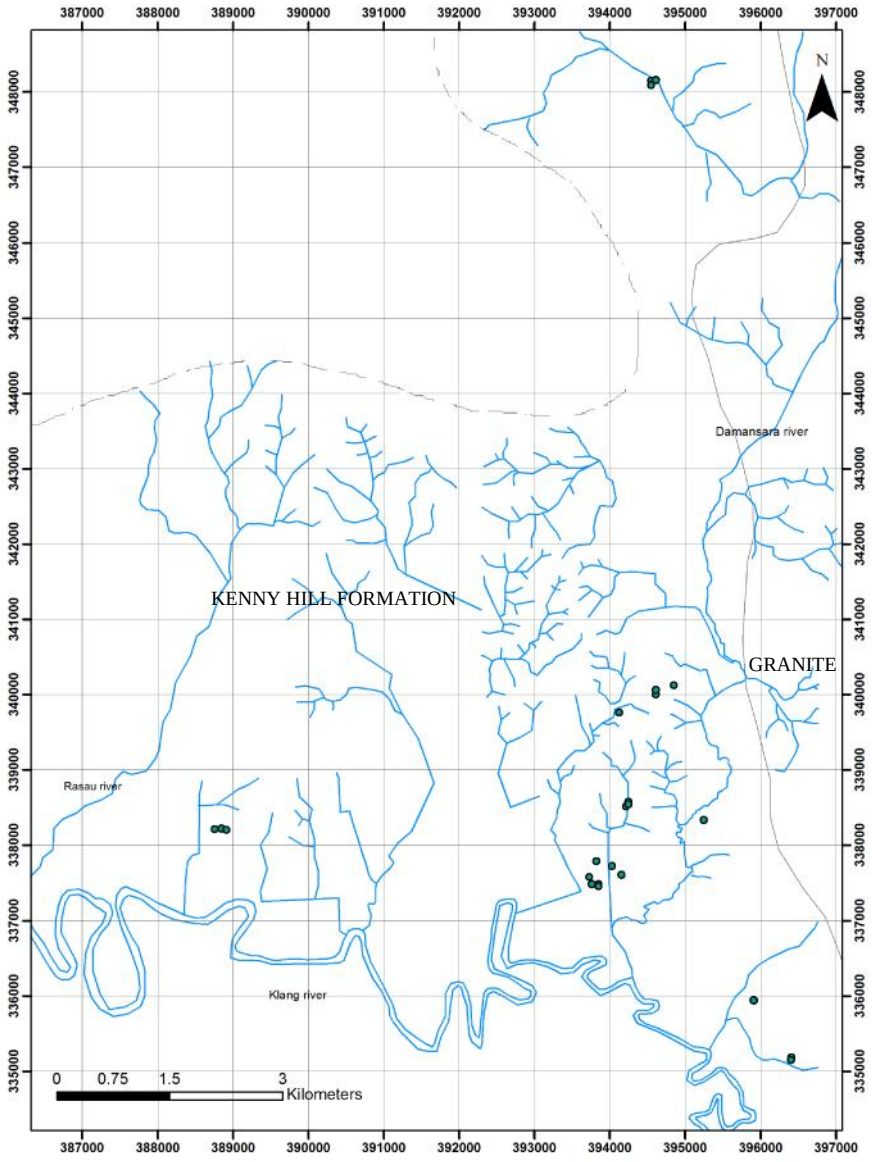

Figure 2.54 The wells with fractures observed in borehole.

The river lineaments in the southeast-northwest direction are consistent with one of the sets of joints (J3) at Outcrop B (see Figure 2.44). They are also consistent with the faults of the Bukit Tinggi fault zone (see Figure 2.7 and Figure 2.55), and also consistent with the strike direction of the Kenny Hill Formation (Figure

2.56; bedding interpretation based on the occurrence of the carbonaceous shale as discussed in Section 2.5 (see also Figure 2.10) and also from information at Outcrop A). The regional structure of Peninsular Malaysia (see Figure 2.1) is also oriented in a southeast-northwest direction.

Faulting in the direction of the Bukit Tinggi fault zone (southeast-northwest) in particular is associated with quartz veining (see Figure 2.7). For example, the Klang Gates quartz dyke was described by Gobbett & Tjia (1973), Toh et al. (1987) described the fault that they found in Kuala Lumpur area to have been filled with a quartz vein which is up to 0.3m thick, and Outcrop B has much quartz veining. It is therefore possible that some of the fracturing in this southeast-northwest direction is infilled by quartz veining.

The river lineaments in the southwest-northeast direction are consistent with joint set J2 at Outcrop B (Figure 2.44), the orientation of the fault at Outcrop 'B' (Figure 2.39) and with the fault of Mogana (1991) as shown in Figure 2.57. The fault at Outcrop B is interpreted as a slip along the foliation plane of phyllite. All the joint sets at Outcrop B are interpreted to be from one fracture system based on the interpretation by Gobbett & Tjia (1973) who studied fractures in the Klang Gates dam area (near Klang Gates Quartz Dyke). The joints that strike southwest-northeast are interpreted as extension joints by Gobbett & Tjia (1973), and are therefore tentatively assumed to be extensional joints in the study area too.

Though relatively few, the river lineaments suggest that the outcrop structures are regionally important orientations that are important also over much bigger lateral distances than can be seen in the outcrops.

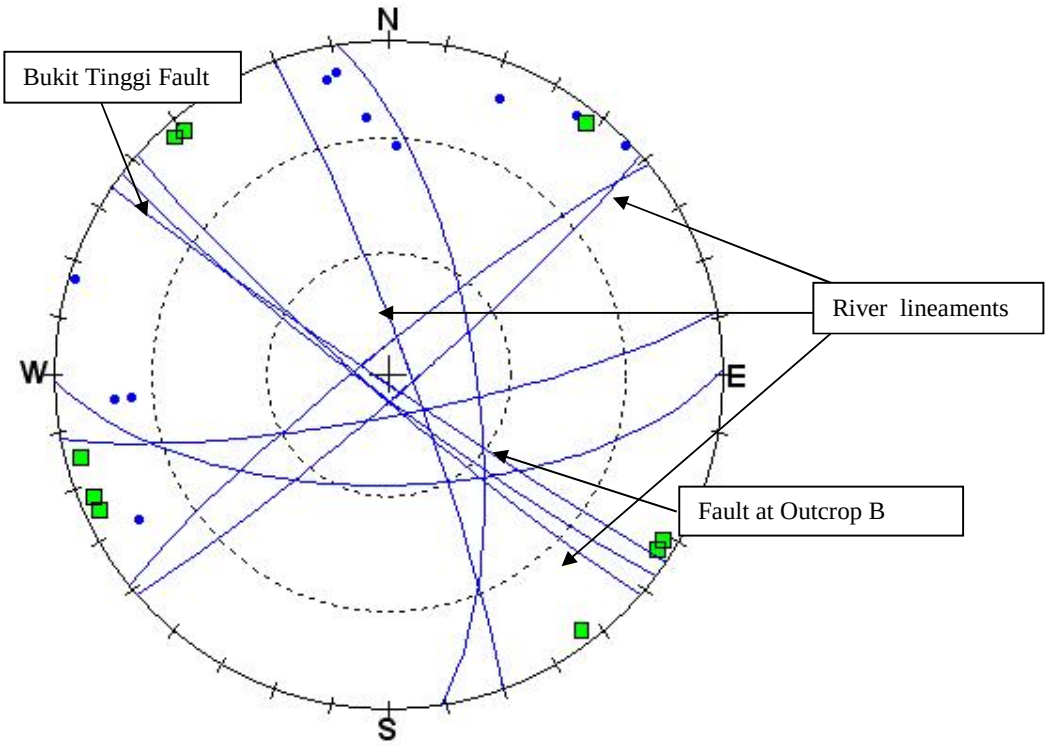

Figure 2.55 The plots of faults of the Bukit Tinggi fault zone and the river lineaments.

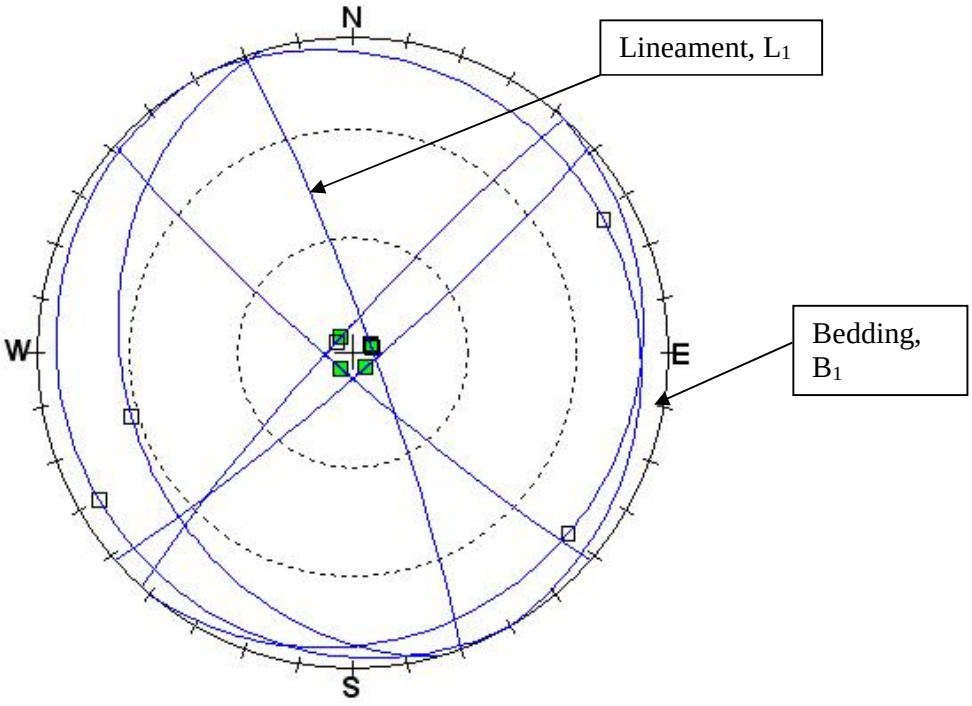

Figure 2.56 The bedding and lineaments

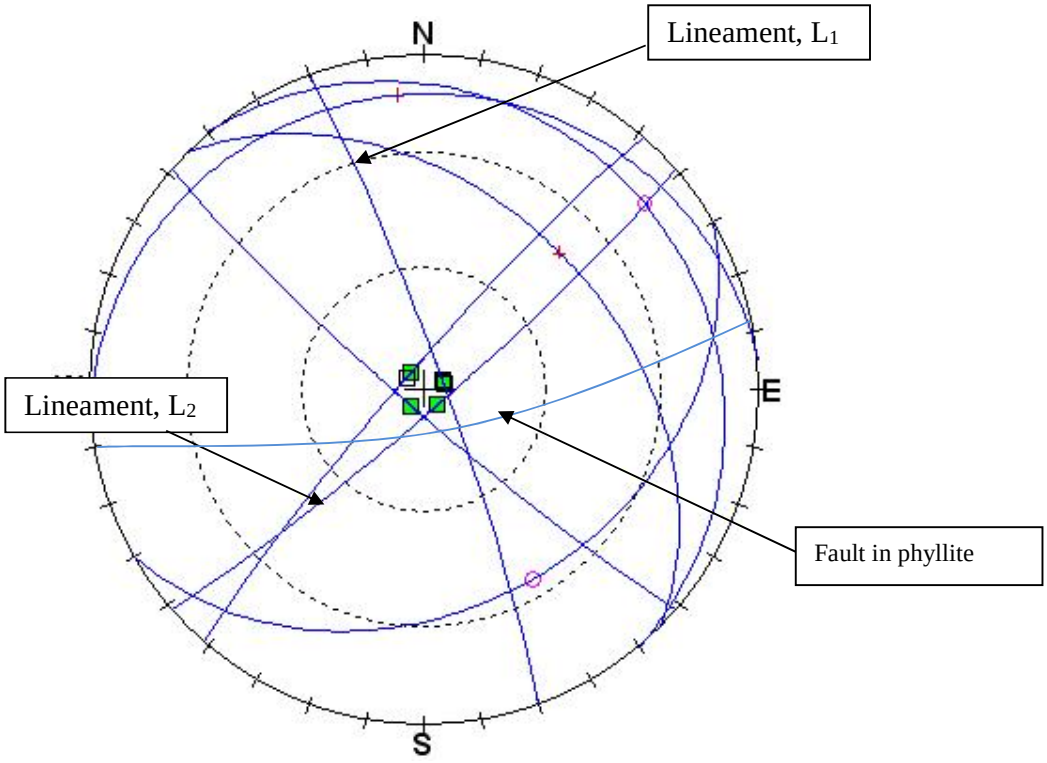

° Fault (Tjia 1976)

+ Fault (Mogana 1991)

Lineament 1

Figure 2.57 The lineaments and fault from previous research and fault in phyllite; two sets of faults, one associated with the event that gave rise to the Bukit Tinggi fault zone with quartz vein fills, and one that is parallel with the extensional system seen at the Klang Gates dam area. The first is oriented in the NW/SE direction and is probably low K, and the other in the NE/SW direction and is probably of higher K.

2.7 The Geological Summary Of Shah Alam

2.7.1 Introduction

Shah Alam lies on the Kenny Hill Formation. The Kenny Hill Formation is a sequence of marine sedimentary clastics deposited in Carboniferous to Permian times in shelf environment. The clastic deposits range from clay to sand, showing

the alternating energy during the deposition. The formation is assumed to sit uncomformably on the Kajang Formation and Lower Palaeozoic rocks. However, even the existence of the Kajang Formation is disputed by some authors. The contact between Kenny Hill Formation and Kuala Lumpur Limestone is faulted in the only location where it has been directly observed.

The rock sequence is jointed, folded and faulted due to the tectonic activity which occurred in the Triassic/Jurassic. This event was accompanied by granite intrusion activity which has metamorphosed the sandstone and shale to quartzite and phyllite. The fresh rock is covered by a weathering layer which varies in thickness depending on the type of the parent rock. Sandstone is weathered to sandy soil and its thickness is usually less compared to soil with shale origin. Some areas especially along the river valleys, e.g. in Kuala Lumpur, are covered by alluvium. No alluvium is observed in Shah Alam.

From literature reviews, borehole interpretation and fieldwork observation, local rock correlation is possible especially in the central and west part of Shah Alam. There are uncertainties in interpretation; the geological setting is complex, with extensive faulting and folding and there are only limited numbers of boreholes and available outcrops. The rivers valley patterns are thought to reflect the main geological structural features of the area, but since the rock types are varying rapidly, it is probable that many faults are unmapped.

To summarize the geology of Shah Alam, the study area has been divided to four sections which are: the central part; the eastern part; the western part; and the

northern part. These sections are based on the rivers in the study area as shown in Figure 2.58. The central part is situated between the Damansara river and Renggam river. The eastern part is located on the east bank of the Damansara river while the western part is on the west bank of the Renggam river. The northern part is located to the north of central area.

In the next chapter, all these geological information will be used and developed to build the hydrogeological conceptual model of the study area.

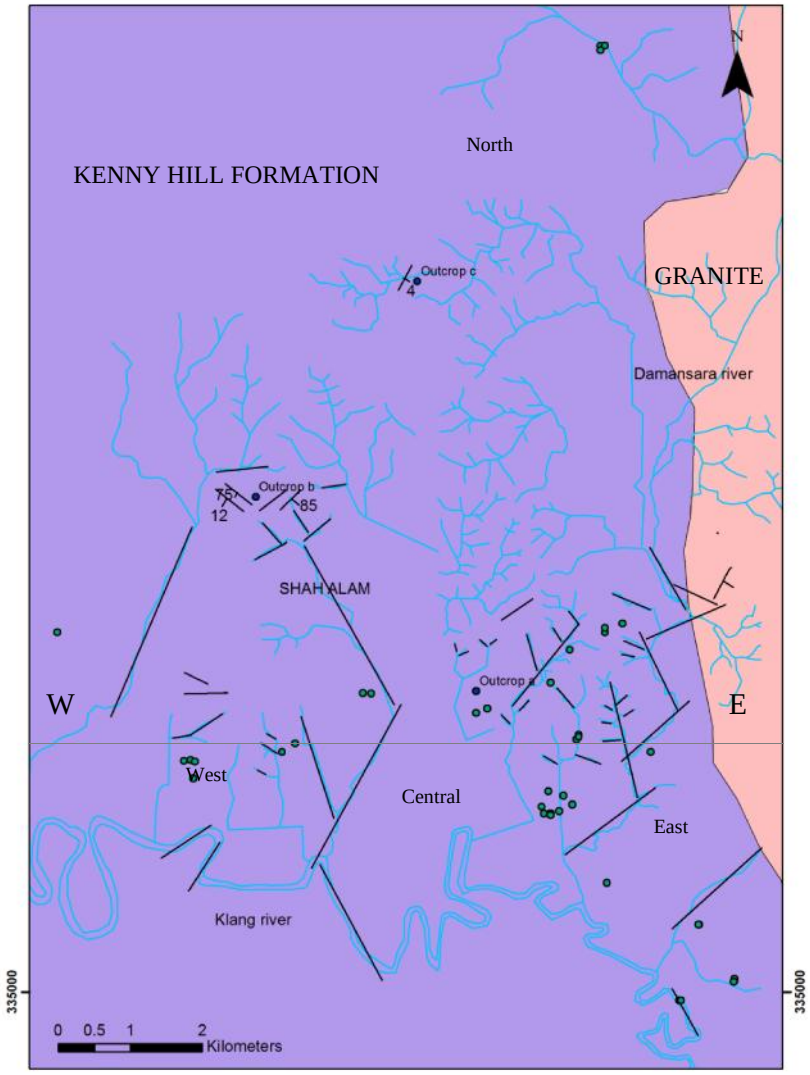

Figure 2.58 The geological map of study area

2.7.2 The central part of Shah Alam

Figure 2.59 shows the rock sequence in the central part of Shah Alam. The lithology observed in this area is interbedded phyllite and quartzite, interbedded grey shale and quartzite, carbonaceous shale, shale, sandstone and interbedded sandstone and shale. The sandstone appears to be dominant to the northwest of this area while shale becomes dominant to the northeast. The carbonaceous shale is interpreted as a variation in the shale sequence. The estimated thickness of the rock sequence is approximately 300m.

The rock sequence is interpreted striking north to northwest and dipping to northeast. This interpretation is based on the carbonaceous shale sequence that is observed at Ansell TW3 & TW5 (see Figure 2.10). The carbonaceous layer is observed in Shah Alam only at a few areas near Damansara river on both side of the river. The details are shown in Table 2.12. The sudden change of the rock sequence leads to conclusion that there is a fault between Ansell and AESBI as discussed in Section 2.5.3, probably along the line of the Damansara river.

Central area

Scientex Polymer	Ansell & Mt Pictures	MHT	Carlsberg W1 & W2	Carlsberg W4
		Sh-Sst	Sh-Sst	Sh-Sst
Sst - Sh		Cs-Phy + Qv	Sh+Qv	Cs
Sst	Sst-Sh	Cs		Sh
	Sst	Sl +Qv		
	Sh			
	Cs			
	Sh-Qt			
	Phy-Qt			

Sst –sandstone **Phy**-phyllite

Sh –shale **Sh-sst** –interbedded sequence

Cs-carbonaceous shale **Qv**- quartz vein

Qt-quartzite **Sl** -slate

Figure 2.59 The summary of the rock sequence in the central of Shah Alam.

Table 2.12 The range of depth and thickness of carbonaceous shale in study area

Tubewell	Depth (b.g.l,m)	Thickness of carbonaceous shale layer (m)
Ansell TW3	13 – 36 90 - 102	23 (weathered carbonaceous shale layer) 12 (carbonaceous shale)
Ansell TW5	49 - 56	7 (fractured carbonaceous shale with quartzite)
Mitsui High Tech	10-18 18 - 32	8 (weathered carbonaceous shale and phyllite) 14 (Carbonaceous shale and slate with quartz vein)
Carlsberg	30 - 110	80 (fractured carbonaceous shale)
AESBI	59 – 62 62 - 98	3 (carbonaceous shale with sandstone) 36 (fractured carbonaceous shale)
PROTON A	18 - 122	Carbonaceous schist

The rock sequence at Ansell is suggested to be at the base of formation as Yin (2011) suggests phyllite occurs in the lower part of the sequence. Phyllite is observed both at depth (Ansell, MT Pictures) and at shallower depths at few localities such as at Mitsui High Tech at 10 to 18 metres (b.g.l), at Outcrop 'B', and also as observed by Tjia (1976) and Mogana (1991) at outcrop. Therefore, if this is the lower part of the sequence, phyllite (thrust) fault movement is probably involved with distributing the rock vertically.

The fractured rock is covered with various thicknesses of weathering material which depends on its parent rock as shown in Table 2.13. The material is silty and sandy clay except in Carlsberg where the weathered material is clay. The weathered layer is thicker in interbedded sandstone and shale (e.g at Ansell and

MT Picture) and in shale (e.g Carlsberg) compared to sandstone (Scientex Polymer) as shown in Figure 2.60. There is no alluvium reported by previous studies. The soil cover is thin since it was washed away by runoff down the slope as observed by Yin (2011). He described the weathering layer of quartzite as loosely compacted yellowish red to brown sandy soil and less sandy for soil

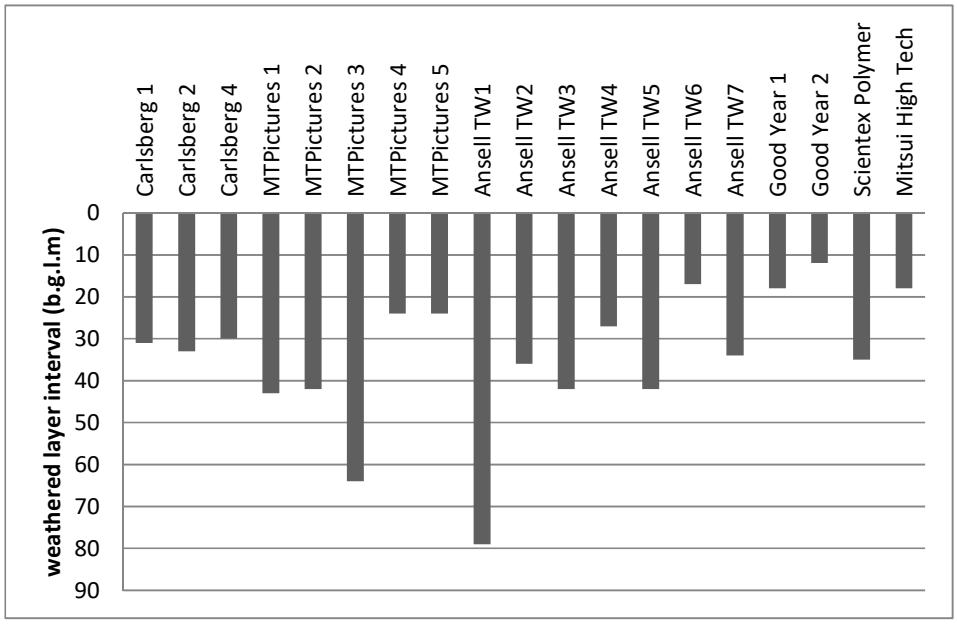

Figure 2.60 The weathering depth in central area of Shah Alam.

derived from shale. From the observation at outcrop 'A' (see Figure 2.26), the soil cover of sandstone fits the description given by Yin (2011) and also with the bedding structure that still preserved.

The fractures occur at variable depths and in different rock types. Fractures are observed from 28 – 183 metres as shown in Figure 2.61. The upper limit is due to the presence of weathered material, and the lower limit due to the base of the wells. Hence fracturing occurs throughout the depth penetrated by the wells. Fractures are observed occur frequently at depth less than 100 metres. Many of

the fractures are reported in interbedded quartzite and shale/phyllite (see Table 2.14), but fractures occur in all rock types penetrated. It is observed that fractures are mainly distributed near the river and this is interpreted as the fracturing is associated with river pattern as discussed in Section 2.6.5.

Quartz vein material is observed only to the northeast side of the area which is suggesting that the granite contact with Kenny Hill Formation is getting close on the east side of Shah Alam (see Figure 2.53).

Table 2.13 The thickness of the weathered layer in central area

Tubewell	The origin of weathered layer	Thickness of weathered layer (m)
Ansell TW 2,3, 4,5 Ansell TW 1,6,7	Interbedded sandstone and shale	27-42 30
MT Pictures	Interbedded sandstone and shale	40
Mitsui High Tech	Interbedded sandstone and shale, carbonaceous shale	18
Carlsberg	Interbedded sandstone and shale, shale	30
Scientex Polymer	Sandstone with shale	15
Good Year	shale	18

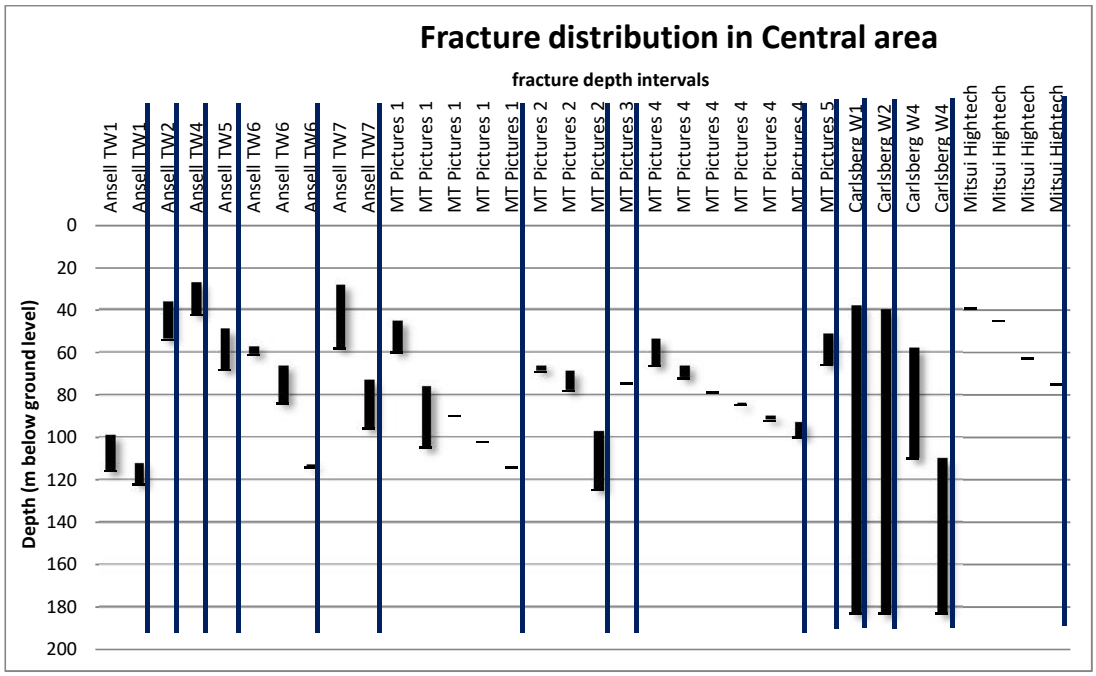

Figure 2.61Depth of fractures encountered in central area of Shah Alam

Table 2.14 The type of lithology with fractures with range of depth.

Tubewell	Type of the lithology with fractures	Range of depth (m) from ground level
	interbedded quartzite-phyllite	99 - 116
Ansell TW1	shale	112-122
Ansell TW2	interbedded grey shale- quartzite	36-54
Ansell TW4	grey shale	27 - 42
Ansell TW5	interbedded grey shale- quartzite	49 - 68
Ansell TW6	interbedded quartzite-phyllite	57 – 61 66 – 84 113 - 114
	sandstone	28 - 58
Ansell TW7	interbedded quartzite-phyllite	73 - 96
	sandstone-shale	45 - 60
	Interbedded shale - phyllite	76 - 105
MT Pictures 1	Interbedded shale - quartzite	90 102 114
	grey shale	66-69
MT Pictures 2	Interbedded grey shale-quartzite	69 – 78 97-125
	Interbedded shale - quartzite	54 - 66.2
MT Pictures 4	shale	66 - 72 79 84 - 85 90 - 92 93 - 100
MT Pictures 5	Interbedded sandstone-shale	51 - 66
Carlsberg W1	shale	38 - 183
Carlsberg W2	shale	40 - 183
Carlsberg W4	carbonaceous shale	58 - 110
	shale	110 - 183
Mitsui Hightech	grey slate with quartz vein	39 45 63 75

2.7.3 The eastern part of Shah Alam

Figure 2.62 shows the rock sequence for eastern part of Shah Alam and its correlation with the rock sequence in central part of Shah Alam. The rock sequence in this part comprises a thick shale sequence with interbedded sandstone and shale in between, the carbonaceous shale, and interbedded sandstone and shale which is intruded by granite. The rock sequence at eastern part is interpreted as faulted by fault movement along the Damansara river as previously discussed in Section 2.5.3.

Carbonaceous shale is observed mainly in the boreholes located in the east side of Shah Alam. Grey carbonaceous schist is observed at PROTON, but whether this is different from the carbonaceous shale is not certain, but seems likely not. The rock sequence of Kenny Hill Formation (comprising interbedded sandstone and shale on a shale sequence) at Canon Opto is intruded with granite. Granite is observed at three of the boreholes of Canon Opto. The granite is becoming dominant to the northeast. Therefore, the granite body is interpreted as occurring at the far eastern side of Shah Alam as shown in Figure 2.53.

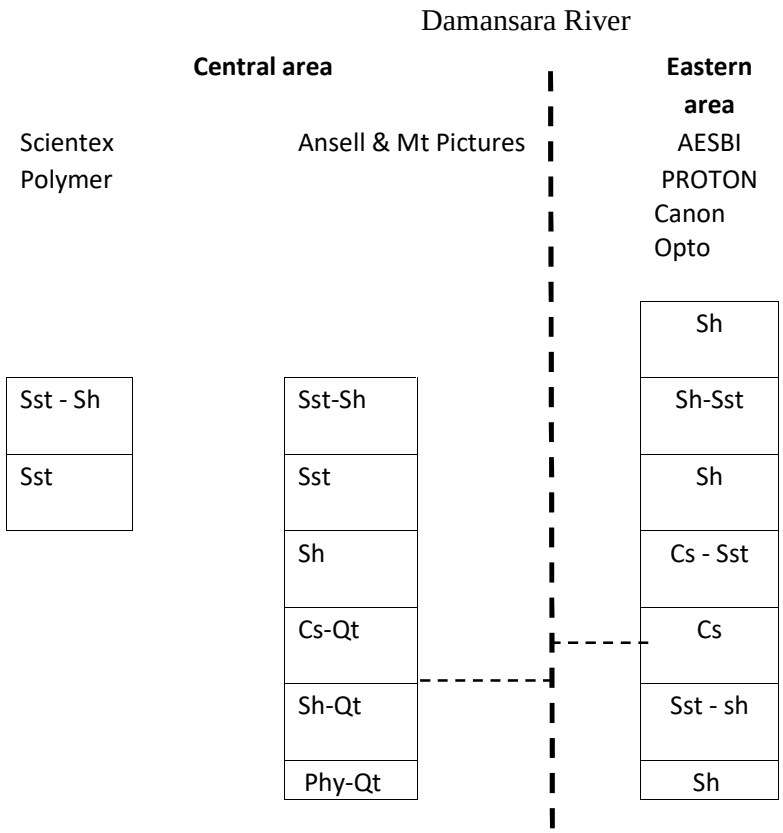

Sst –sandstone **Phy**-phyllite

Sh –shale **Sh-sst** –interbedded sequence

Cs-carbonaceous shale **Qv-** quartz vein

Qt-quartzite

Figure 2.62 The summary of the rock sequence in the eastern part of Shah Alam and its correlation with the rock sequence in the central part.

The fractures in the rock sequence are at variable depth with mostly at shallower depth (less than 100m) at Canon Opto and at deeper depth at AESBI and Proton as shown in Figure 2.63. Fractures occur in both metasedimentary rocks and the granites as shown in Table 2.15.

The weathering layer thickness in this area is not much different compared to the weathered layer in the central area as shown in Figure 2.64. The material of weathered layer is clay except in Canon Opto. Table 2.16 shows the parent rock of the weathered layer.

The borehole logs in this area are fewer than in the central part. Therefore it is difficult to determine the orientation of the bedding.

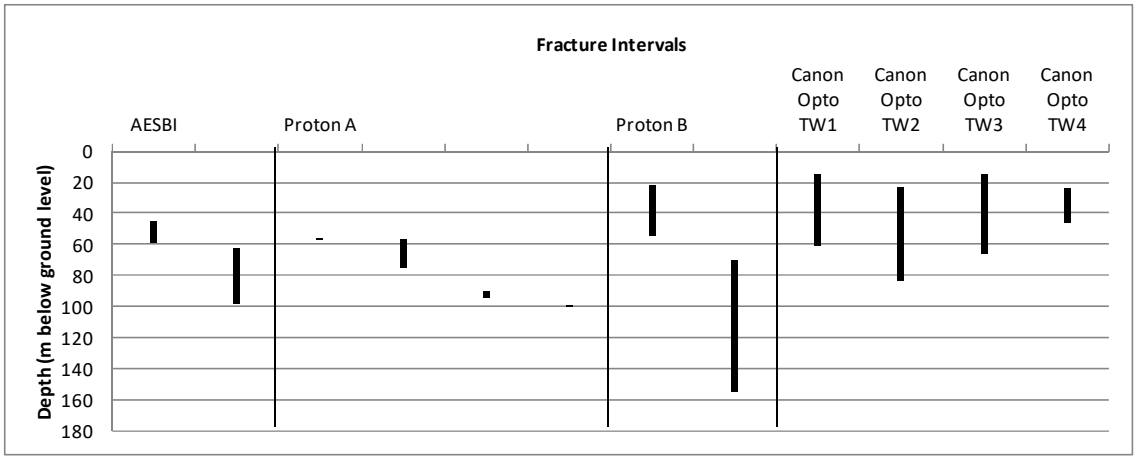

Figure 2.63 Depth of fractures encountered in eastern area of Shah Alam

Table 2.15 The type of lithology with fractures with range of depth in eastern area

Tubewell	Type of the lithology with fractures	Range of depth (m) from ground level
AESBI	carbonaceous shale	45-59 62-98
Proton A	grey carbonaceous schist	56 – 57 57 -75 90 – 94 99 - 100
Proton B	grey carbonaceous schist	22 – 54 70 - 155
Canon Opto TW1	grey granite	15 - 61
Canon Opto TW2	grey granite	23 - 83
Canon Opto TW3	dark brown shale	15- 66
Canon Opto TW4	sandstone	24- 46

Table 2.16 The thickness of the weathered layer in eastern area

Tubewell	The origin of weathered layer	Thickness of weathered layer (m)
AESBI	shale shale with sandstone shale	25 20 14
Proton A	Carbonaceous shale with sandstone Carbonaceous shale	18 22
Canon Opto TW1 Canon Opto TW2 Canon Opto TW3 Canon Opto TW4	granite granite shale interbedded shale-sandstone	20 20 25 25

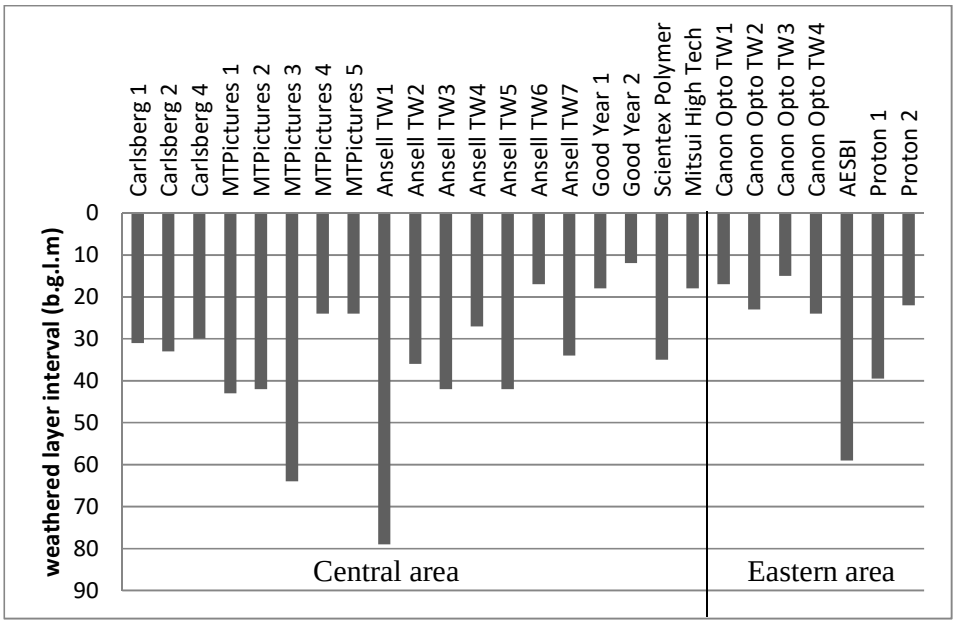

Figure 2.64 The thickness of weathered layer in central and eastern area of Shah Alam

2.7.4 The western part of Shah Alam

Figure 2.65 shows the rock sequence at the western part of Shah Alam. The rock sequence comprises interbedded quartzite and shale, sandstone and shale. This is similar to the rock sequence at the central area. No phyllite is observed in this area. It is dipping to the northeast following the rock sequence at the central part.

The thickness of weathered layer varies up to 50 metres as shown in Table 2.17. The material of weathered layer is clay to silty clay except in CCM Fertilizer TW3 where 10 m sandy clay material also present. The fractures are observed mainly in quartzite (see Table 2.18) at deeper depth (>80 m) as shown in Figure 2.66. No quartz vein is observed except at to the southwest of the area which is in CCM Fertilizer compound. Here quartz vein is observed in the quartzite layer at

CCM Fertilizer at greater depths in great amounts. It is possible that the rock sequence is near to granite intrusive body at depth.

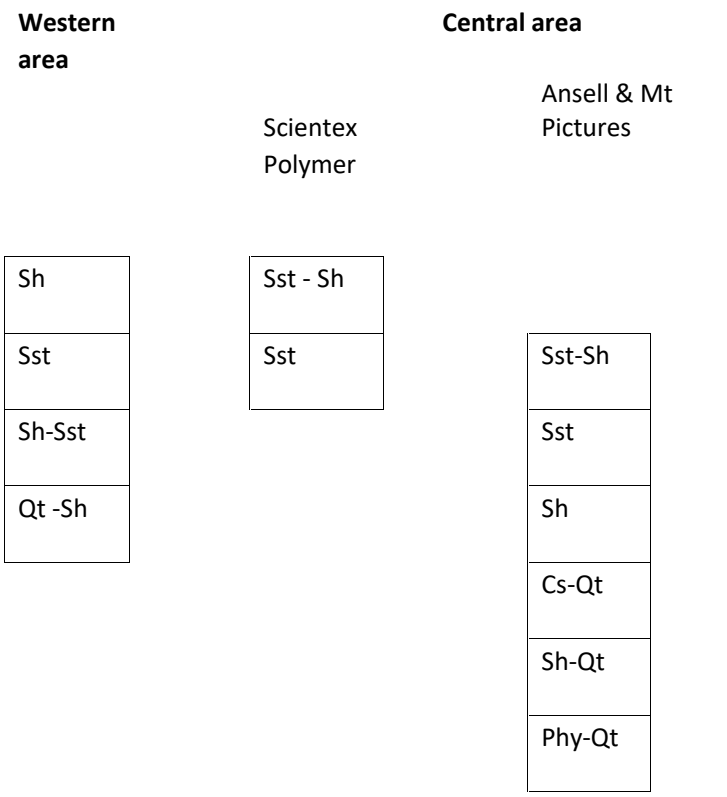

Sst –sandstone **Phy**-phyllite

Sh –shale **Sh-sst** –interbedded sequence

Cs-carbonaceous shale **Qv-** quartz vein

Qt-quartzite

Figure 2.65 The rock sequence at western part of Shah Alam

Table 2.17 The thickness of the weathered layer in western area

Tubewell	The origin of weathered layer	Thickness of weathered layer (m)
Universal Nutri Beverages	shale	17
Gaya Color Lab	sandstone	30
CCM Fertilizer TW1 CCM Fertilizer TW2 CCM Fertilizer TW4	shale	50 30 38

Table 2.18 The type of lithology with fractures with range of depth in western area

Tubewell	**Type of the lithology with fractures**	**Range of depth (m) from ground level**
CCM Fertilizer 1	Interbedded quartzite-shale	75 84 - 85 121 - 122
	quartzite	140-142
CCM Fertilizer 2	sandstone-shale	54
	quartzite	122 – 128 154 - 155
CCM Fertilizer 3	quartzite	84- 85 87 91
	sandstone	111
	quartzite	134

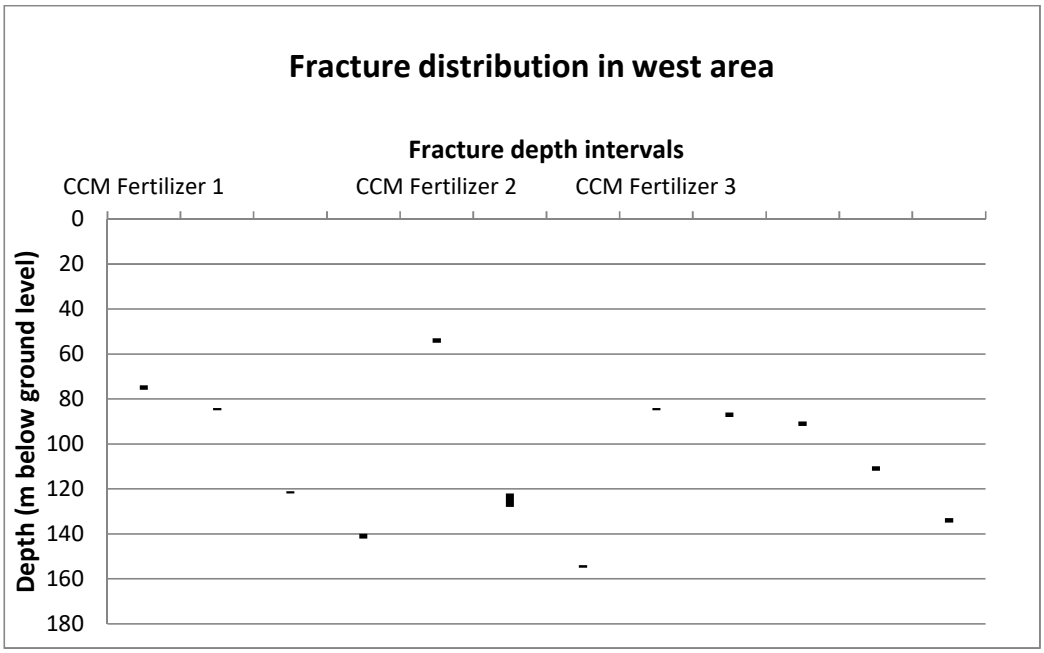

Figure 2.66 Depth of fractures encountered in western area of Shah Alam

2.7.5 The northern part of Shah Alam

Figure 2.67 shows the rock sequence at the northern part of Shah Alam. Since the rock sequence in this area is further north from other wells in Shah Alam, it is difficult to make any correlation. Therefore, the correlation is just made between the wells in same compound.

The rock sequence in this area comprises grey schist as observed at Aquatic International, with limestone observed in Aquarium Express compound. The limestone is covered with 26 metres of weathered interbedded sandstone and shale which is interpreted as belonging to the Kenny Hill Formation. The rock in this area is possibly the contact zone between Kenny Hill Formation and Lower Palaeozoic rock (schist, limestone). The only limestone outcrop is exposed at

Batu Caves, Selangor. This limestone is interpreted as belonging to the Kuala Lumpur Limestone.

The occurrence of schist indicates possibly that the rock sequence is folded and faulted. There is a possibility that limestone occurs at depths below the base of these boreholes. This interpretation fits with the observation by Rosly (1976) where he observed fault as the contact between Kenny Hill Formation and Kuala Lumpur Limestone at Salak South. Salak South is located approximately 18km to the southeast of this area (see Figure 2.3). Yeap (1986) suggested that Kuala Lumpur Limestone occurs as a large lens in schist.

Northern Area

Sst – Sh (KHF)
Sch
KL Ls

Sst –sandstone

Sh –shale

Sch-schist

KL Ls- Kuala Lumpur limestone

Figure 2.67 The rock sequence at the northern part of Shah Alam.

The depth of wells in northern part is at shallow depth which is less than 50m. Fractures are observed in both limestone and schist as shown in Table 2.19 with range from 15 to 50m (Figure 2.68).The material of weathered layer is sandy clay. The thickness of the weathered layer is up 15 to 26 m.

Table 2.19 The type of lithology with fractures with range of depth in northern area

Tubewell	**Type of the lithology with fractures**	**Range of depth (m) from ground level**
Aquarium Express	dark grey limestone	26 - 42
Aquatic International 2	dark grey schist	24 - 46
Aquatic International 3	dark grey schist	15 - 51

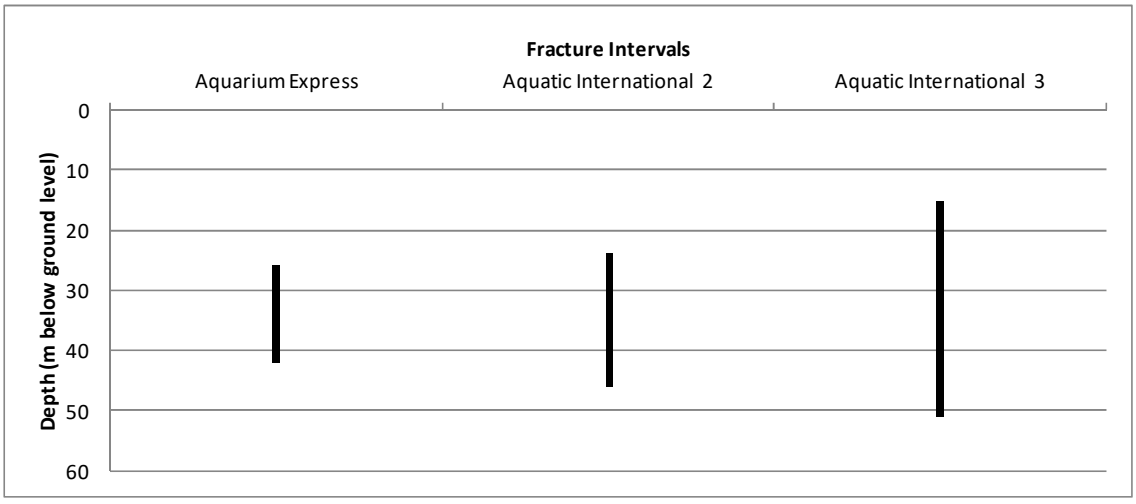

Figure 2.68 Depth of fractures encountered in western area of Shah Alam

Table 2.20 The thickness of the weathered layer in northern area

Tubewell	The origin of weathered layer	Thickness of weathered layer (m)
Aquarium Express	Interbedded sandstone-shale	26
Aquatic International 2		24
Aquatic International 3		15

2.8 Conclusion

Figure 2.69 shows the geological cross section for Shah Alam area which summarizes the geology of the study area. From all the geological evidence, it can be concluded that Shah Alam is in a geological environment that has been subject to tectonic activity with thrusting and probably isoclinals folding and a travel direction to the north. In this the geology of Shah Alam is typical of many parts of the world such as in countries in Southeast Asia and also other continents such as Europe (e.g. SW England).

The rock sequence in Shah Alam is mainly interbedded sandstone and shale which is metamorphosed to quartzite and phyllite due to regional metamorphism and associated granite intrusion which are in turn associated with the folding and faulting events. The sequence is difficult to determine, partly because of the lack of data but also because of the complexities of the probable folding and faulting. However there are some patterns in the occurrence of the rock types. For example, phyllite appears to be deeper and to the east. And the carbonaceous

shale sequence occurs mainly on the east and west bank of the Damansara river. This rock is interpreted as part of the main shale sequence but appears to occur in this specific zone. To the west sandstones start to occur more frequently. This change in lithology is consistent with the dips recorded in outcrop and also with the structural travel direction of the rocks.

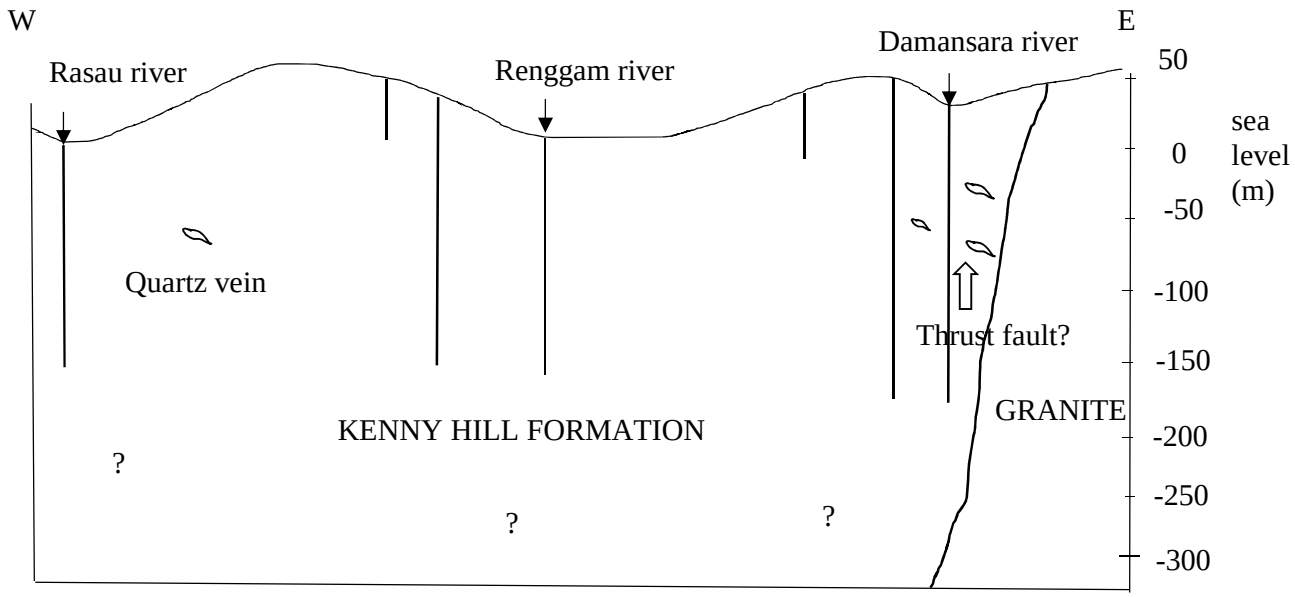

Figure 2.69 The geological cross section of Shah Alam (see Figure 2.58)

Figure 2.70 shows the thickness of weathering layer as observed in Kenny Hill Formation in Shah Alam. The thickness varies from 15 to 50 metres, being thicker at two wells (up to 80 metres). The weathering layer is thicker in Central part of Shah Alam where the interbedded shale and sandstone is more dominant compared to other parts.The weathering material is more sandy and thinner in sandstone areas and more clayey and thicker in shale areas.

The rock sequence is fractured. The fractures are found at all depths below the weathered zone as shown Figure 2.71. The deepest fractures occur at the deepest levels of the wells, up to 183m below ground surface. The joint set which is striking northeast is interpreted as extensional joint. This joint set is, however, possibly filled with quartz near the rivers which follow the line of major faults. The joint set that is striking northwest is parallel to the regional structure of Peninsular Malaysia; this also coincides with the alignment of other parts of the river system.

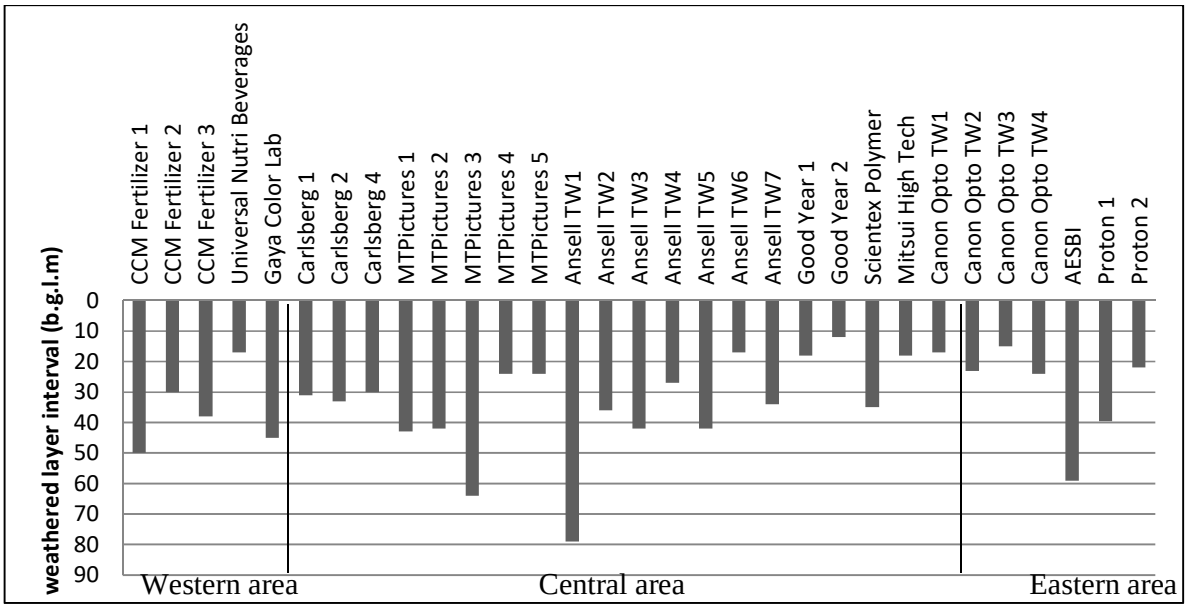

Figure 2.70 The thickness of weathering layer observed in Shah Alam.

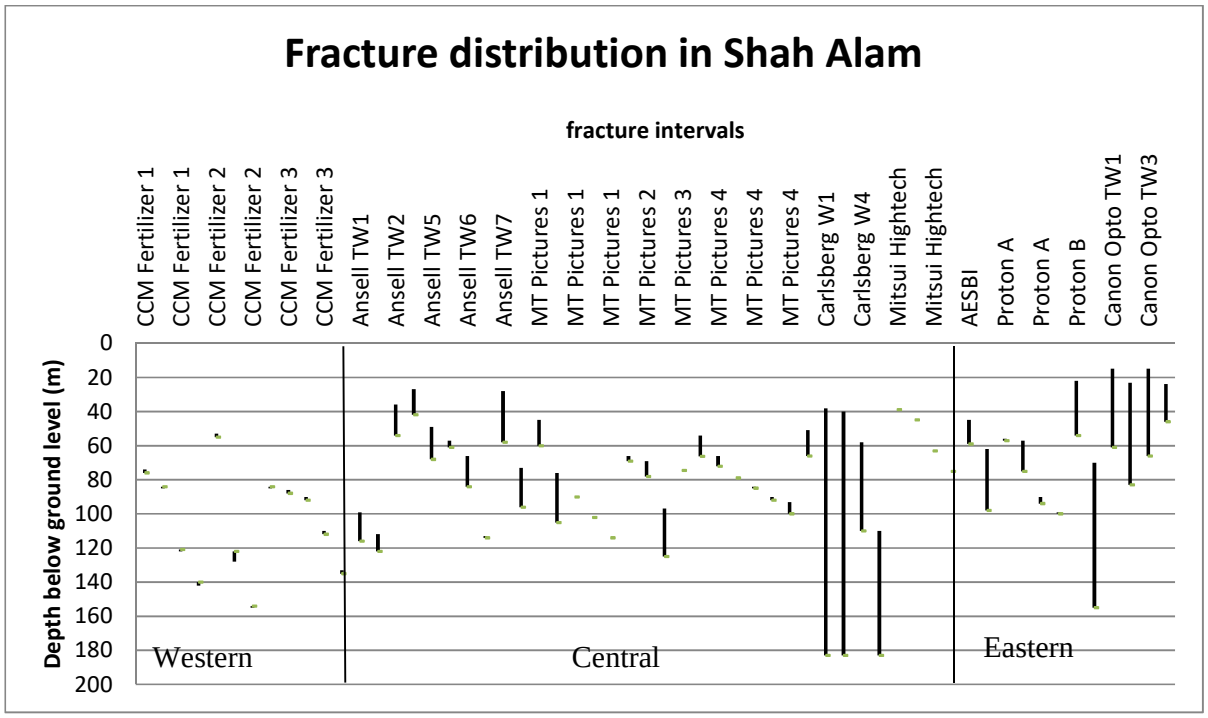

Figure 2.71 Depth of fractures encountered in Shah Alam

3.0 HYDROGEOLOGY OF SHAH ALAM

3.1 Introduction

The main aim of this chapter is to build an initial hydrogeological conceptual model for the Shah Alam area. This is very important as a starting point to understand the aquifer behaviour which will be further discussed in the following chapters. In the previous chapter, the geology of study area has been discussed. In this chapter, how geology plays a role in defining the hydrogeology of Shah Alam will be discussed.

The discussion will start with a preliminary aquifer assessment in Section 3.2. In the next section (Section 3.3), the role of the weathered layer and fractured rock in groundwater storage will be discussed. In the final section (Section 3.4), water table information is analysed to determine the correlation with topographic variation, drainage type information, climate pattern and groundwater usage to produce an indication of how groundwater heads might be expected to vary across the area. The hydrogeological conceptual models later will be updated with recharge processes in Chapter 4 including the climate pattern of the study area and its role as main groundwater recharge source.

3.2 Preliminary Aquifer Assessment

3.2.1 Introduction

JICA (1984), in a detailed hydrogeological study of Peninsular Malaysia, recognized the potential of hard rock with fissures as aquifers. Most of the aquifers were thought to be located in fault and fractured zones. The hard rock

aquifer was divided by JICA (1984) into three classes. Limestone was classified an excellent aquifer (Class I), sandstone as good to fair (Class II) and other rocks as Class III (fair to poor aquifer). Table 3.1 shows the properties assumed by JICA (1984) for each class.

Table 3.1 The properties of each class of aquifer in Malaysia (JICA 1984)

Class	I (excellent aquifer)	II (good – fair aquifer)	III (fair – poor aquifer)
Thickness of aquifer (m)	10-25	5-15	5-15
S_y (%)	5-10	2-8	2-5
Abstraction, Q m^3/day [l/s]	300-1500 [3.5 – 17.4]	100-300 [1.2 – 3.5]	0-100 [0 – 3.5]
Transmissivity, T m^2/day	50-500	10-50	0-15
Drawdown, s (m)	1-10	5-10	10-25
Specific capacity (Q/s,m^3/day/m)	30-1500	10-30	0-10
Rock units	Limestone	Sandstone	Other rocks

However, the values estimated differ from those observed in the study area. The fractured rock aquifer in Shah Alam is estimated to be possibly over 100m thick based on the depth of fractures zone (as previously discussed in Chapter 2).The inflows to boreholes also have been observed to 66m as shown in Table 3.2 and fractures to at least 180m. There are 12 wells with pumping rate below 200m^3/day [2.3 l/s], 16wells with pumping rate 200-300 m^3/day [2.3 – 3.5 l/s] and 12 wells with pumping rate over 300m^3/day [3.5 l/s] (up to 600 m3/day [6.9 l/s]) (Figure 3.1). Fifty eight percent of the wells in study area have drawdowns of over 30m (Figure 3.2). Thus the classification of JICA (1984) does not fit the local conditions observed very well in that the most appropriate classification is Good-Fair aquifer from the point of view of specific capacity (Q/s), but the wells

with these properties are in a wide range of rock types, certainly not just sandstone, and the thickness of the aquifer is greater suggesting a lower permeability than JICA (1984) imply.

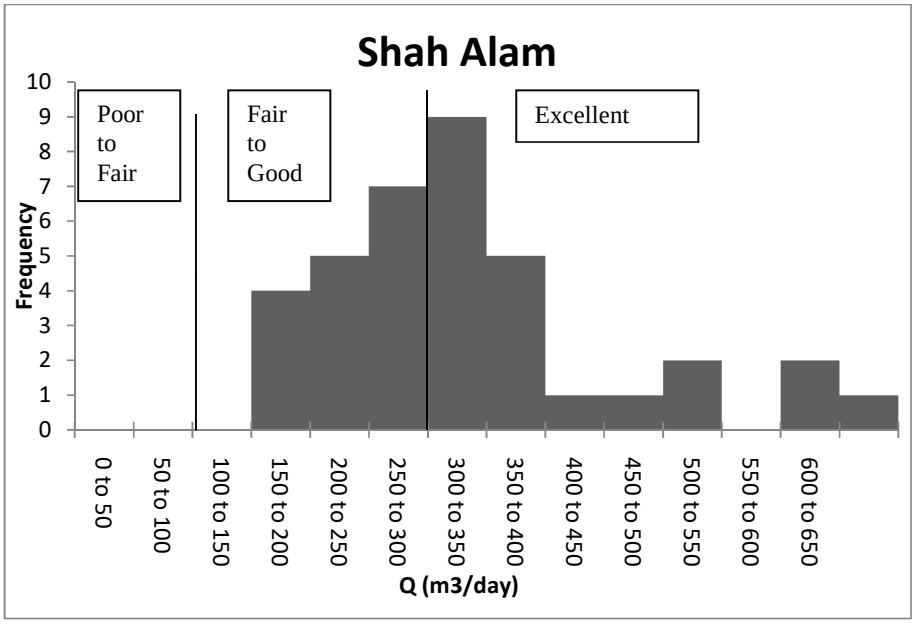

Figure 3.1 The abstraction rate, Q in m^3/day for wells in study area, with the classification system of JICA (1984) indicated.

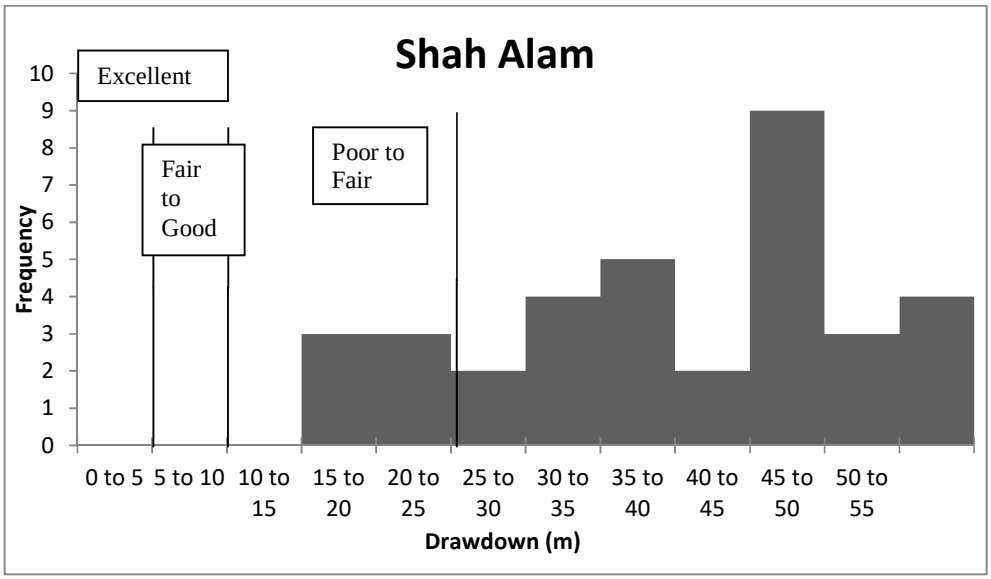

Figure 3.2 A plot of drawdown for wells in study area, with the classification system of JICA (1984) indicated.

Table 3.2 The depth of water is encountered during drilling

Tubewell	Depth of well screen (m)	Depth of encountered water (m)	Type of the lithology
Ansell TW1	102 - 129.5	48.2	Weathered interbedded sandstone-shale
Ansell TW2	42 - 122.5	35.5	Weathered sandstone
Ansell TW3	54 - 136.3	49.5	Interbedded grey shale-quartzite
Ansell TW4	20 - 67.55	9.6	Weathered sandstone
Ansell TW5	30 - 92.35	23.5	Weathered shale
Ansell TW6	36 - 66 70 - 114	30	Interbedded quartzite-phyllite
Ansell TW7	42 - 99	30	Weathered sandstone
MT Pictures 1	60 - 120	47.4	Interbedded sandstone-shale
MT Pictures 2	66 - 120	66	Grey shale
MT Pictures 3	66 - 130	66	Interbedded grey shale-quartzite
MT Pictures 4	48 – 69 76 - 96	48	Interbedded shale - quartzite
MT Pictures 5	52 – 72 78 - 108	52	Interbedded sandstone-shale
AESBI	45-59 62-98	60	Carbonaceous shale
CCM Fertilizer 1	54 - 143.3	49.5	Laterite (shale)
CCM Fertilizer 2	34 - 178.4	54	Interbedded sandstone-shale
CCM Fertilizer 3	42 - 141.8	55.2	Weathered interbedded sandstone-shale
Panasonic	60-100	60	Interbedded sandstone- shale

3.2.2 Well yield & specific capacity of the wells

The average well yield for study area is 268m^3/day (3.1 l/s). The well yield for Figure 3.3 shows the depth of wells drilled in Shah Alam. There are 12 wells with depth less than 100m while the rest are deeper than 100m. The wells that lie close to the lineaments oriented in a NE-SW direction and also intersecting with other sets of fractures e.g. Mitsui High Tech and Good Year are less than 100 m in depth (see Figure 3.4). On the other hand, wells that lie close to the lineaments with a NW-SE strike direction and intersecting less fractures are 100 to 150 metres in depth (e.g. Ansell and MT Pictures) as shown in Figure 3.5. This

suggests that design depth is controlled by yield obtained, but there is no information if this is a common approach when drilling.

Well yield is also affected by interference from other wells (Misstear & Beeson 2000). As in Shah Alam, there are more than 8 factories that have more than one pumping well. For example, wells in Ansell are 200m distant from each other. This will affect the drawdowns reported in Figure 3.2.

The well yield shows no significant increase with depth of well (Figure 3.6). The specific capacity also shows no significant relationship with depth of the well as shown in Figure 3.7. The specific capacity for most of the well ranges from 1 to 10 m^3/day/m which is low as shown in Figure 3.8. Some of the wells with higher specific capacity values (>10m^3/m/day) lie close to the NE-SW lineaments as shown in Figure 3.9. The highest value is 130m^3/day/m. This well is embedded in limestone which is located further north in the study area (see Figure 2.2).

Some records exist on the depth of where water is encountered during drilling (Table 3.2). Only 17 wells provided this information. Water is encountered in both the weathered layer (e.g. weathered quartzite) and in the rock. Most of the well screens are located in rock as shown in Figure 3.10 with seven wells which are also screened in the weathered layer (see Table 3.2). Fractures are found to intersect with the well screen. The significance of the fractures and weathered rock layer to the hydrogeology of study area will be further discussed in the next section.

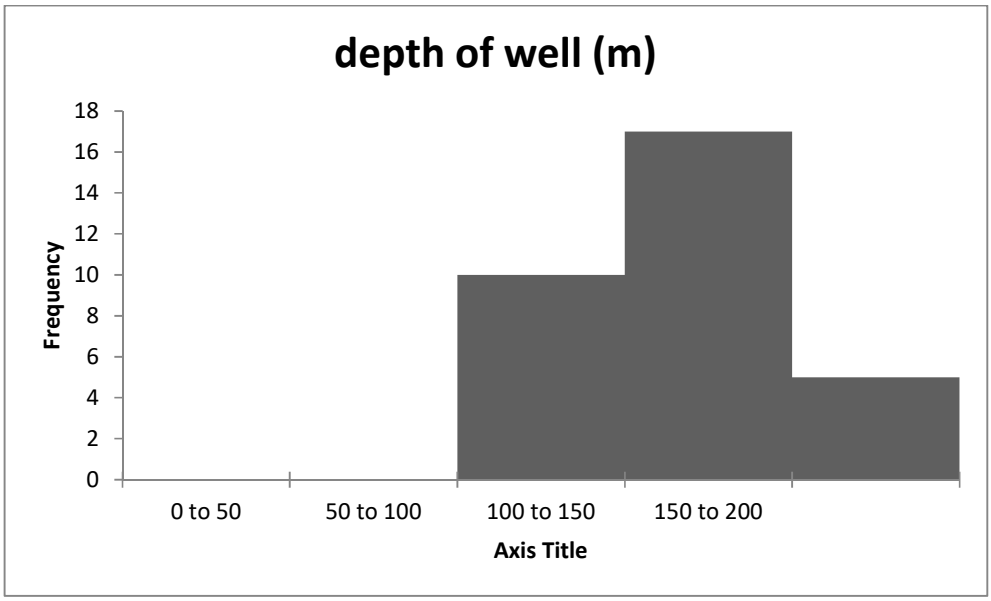

Figure 3.3 Depth of wells drilled in Shah Alam

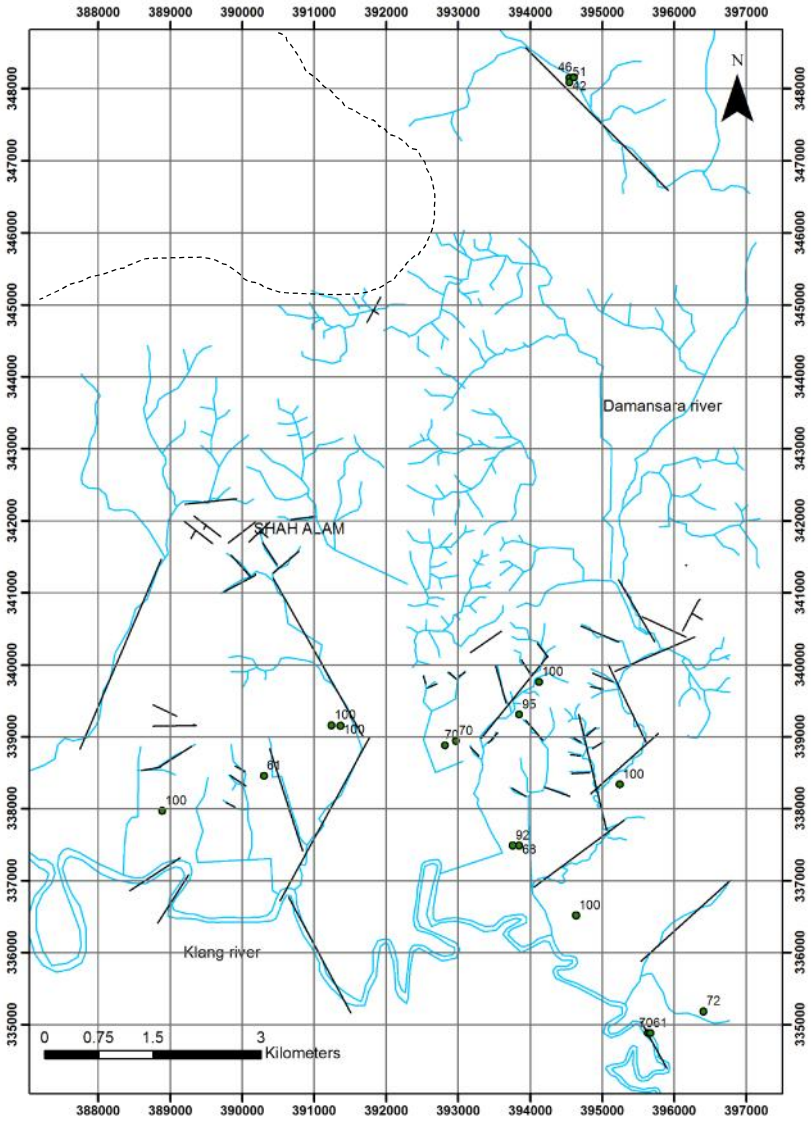

Figure 3.4 Wells with depth less than 100m

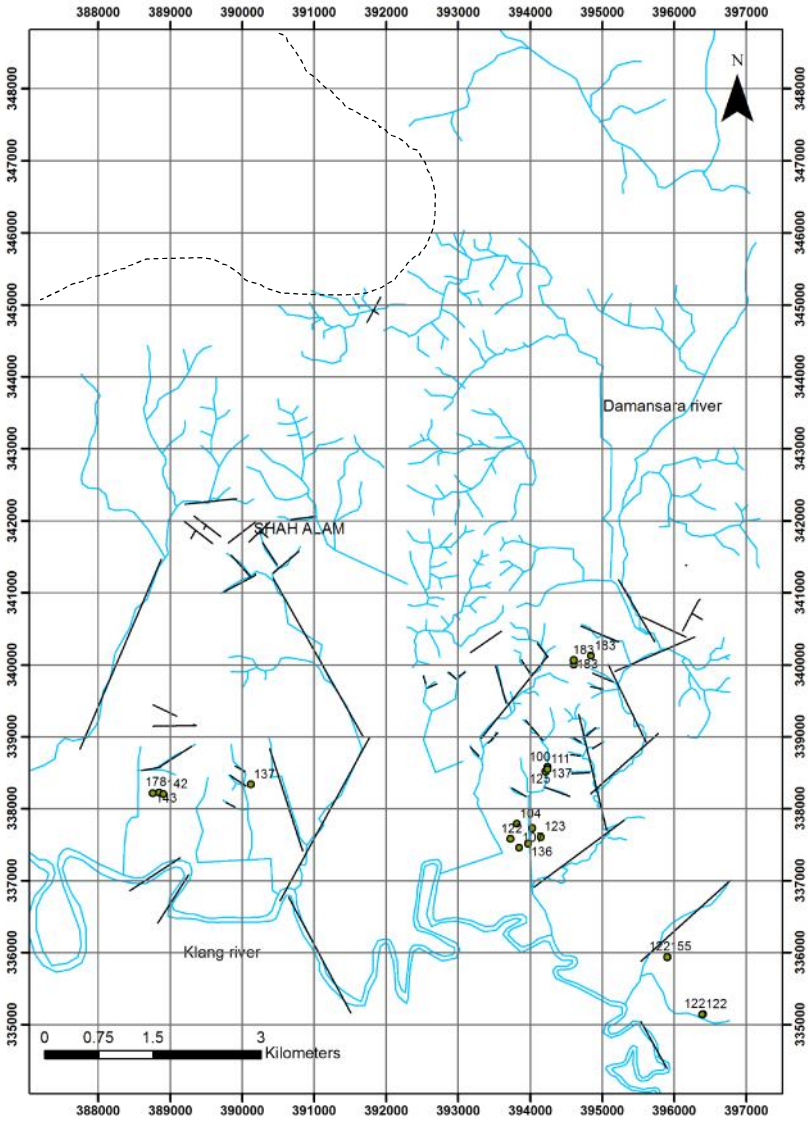

Figure 3.5 Wells with depth deeper than 100m

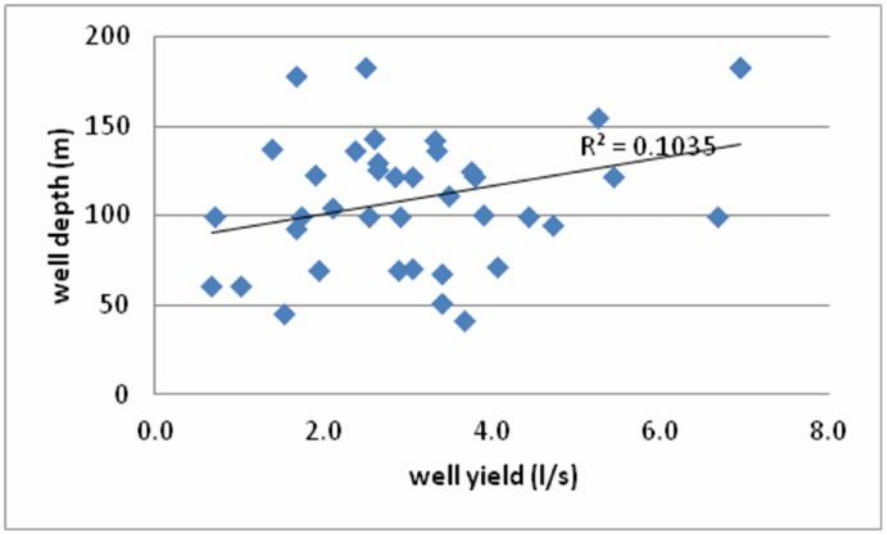

Figure 3.6 The well yield showing no significant relationship with well depth

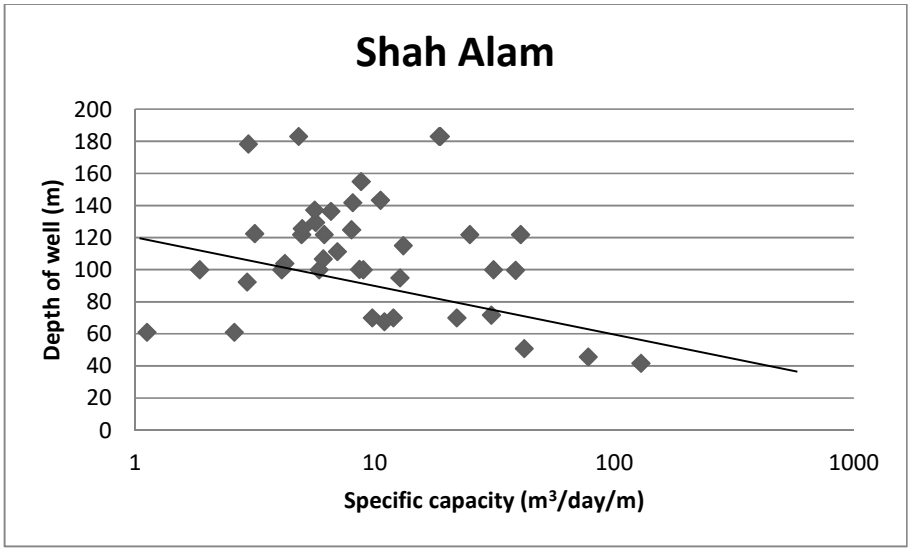

Figure 3.7 The relationship of log (specific capacity) with depth of well

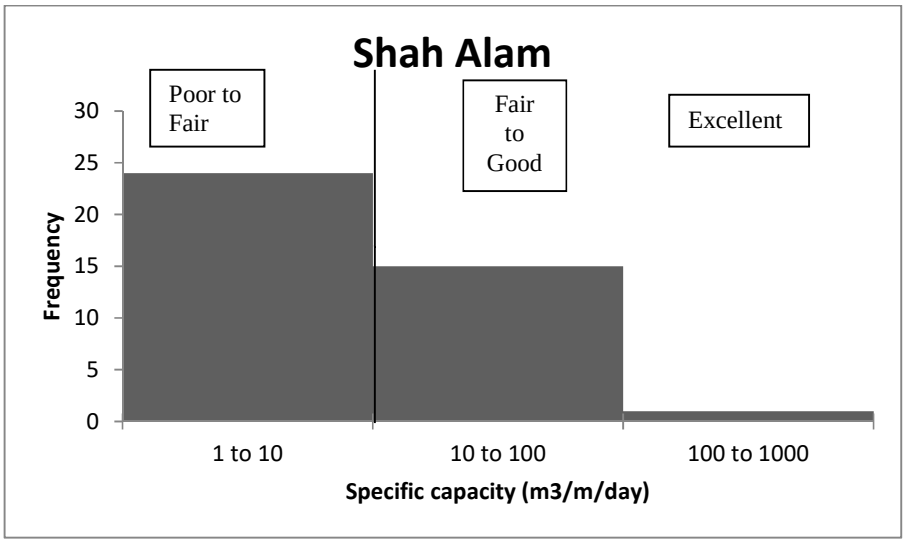

Figure 3.8 The distribution plot for specific capacity for wells in study area, with the classification system of JICA (1984) indicated.

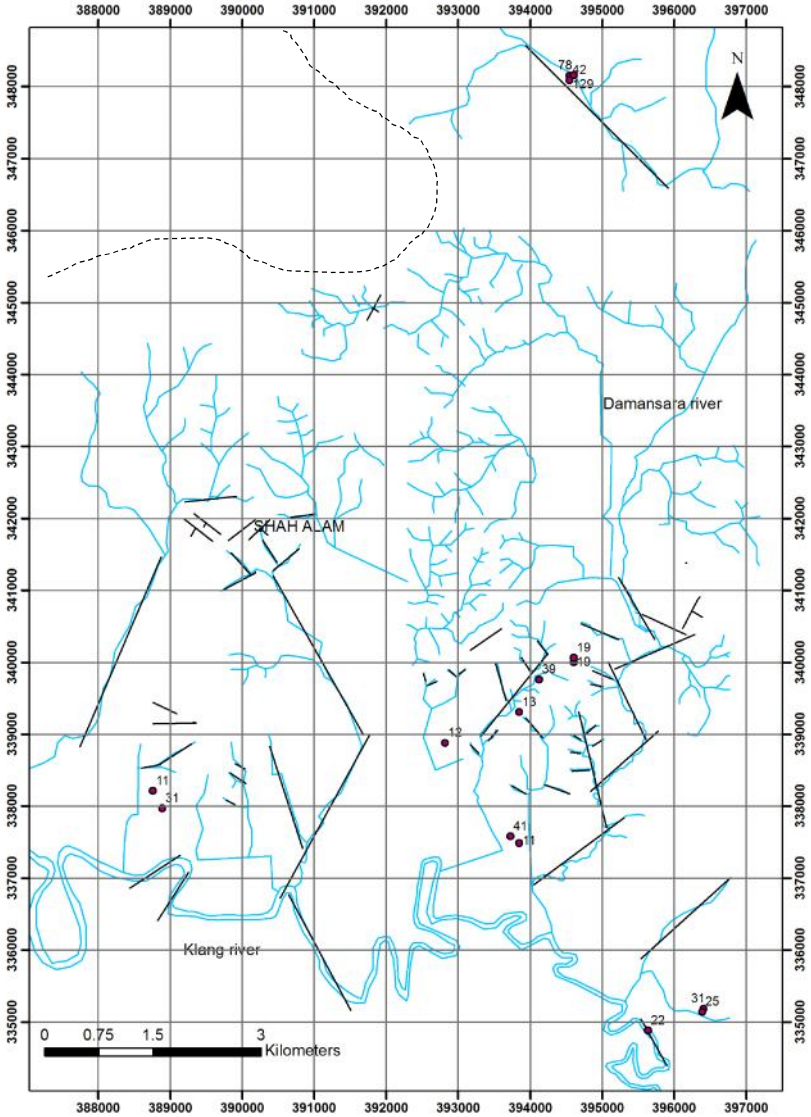

Figure 3.9 The wells with higher specific capacity that coincide with lineaments in the NE-SW direction.

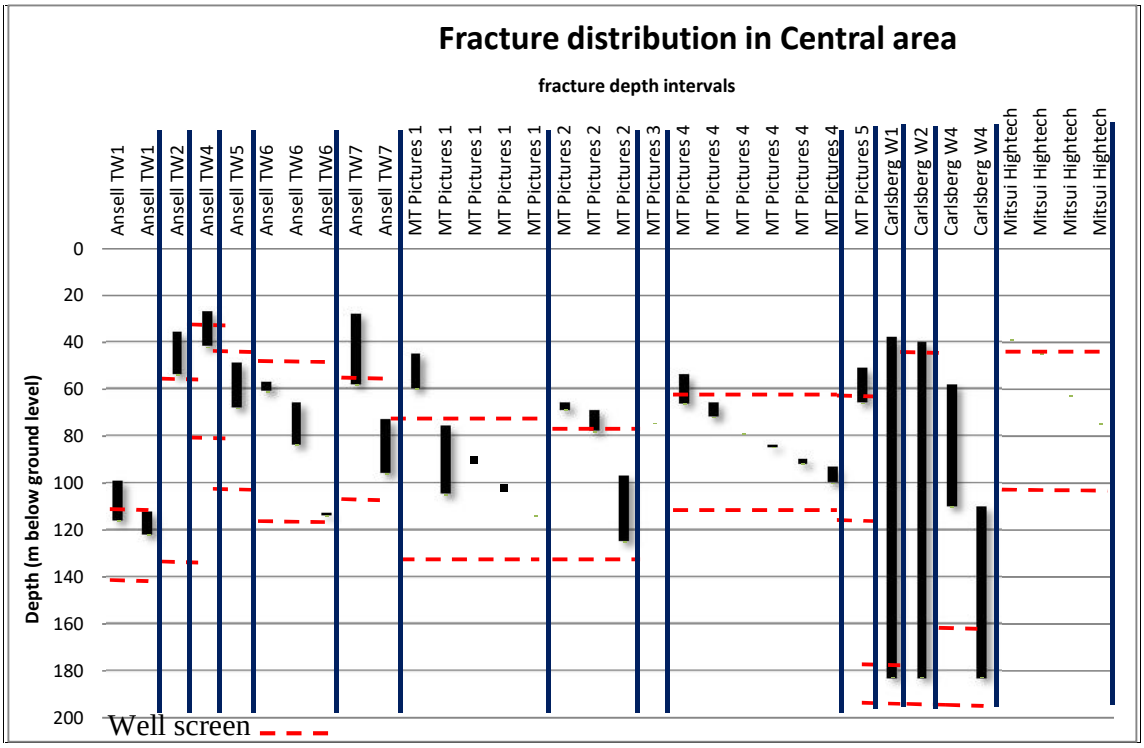

Figure 3.10 a**)** Fracture distribution (black bars) with well screen location in the central part of the study area (note that some wells have multiple entries)

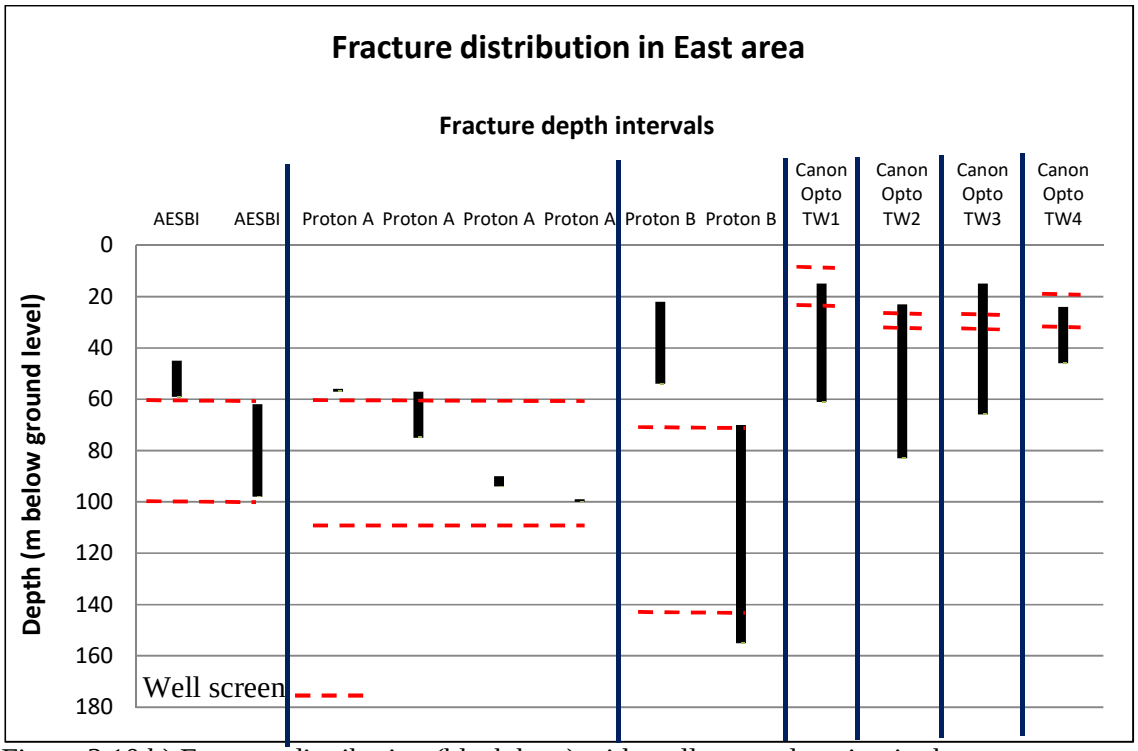

Figure 3.10 b) Fracture distribution (black bars) with well screen location in the eastern part of the study area

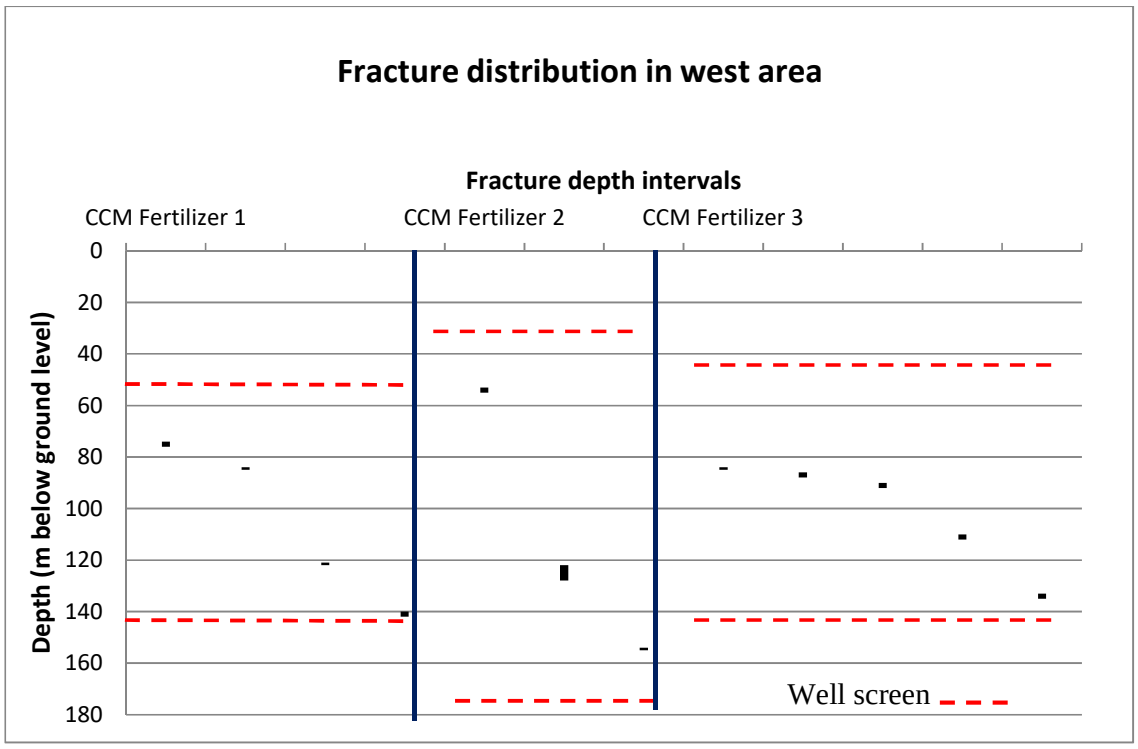

Figure 3.10 c) Fracture distribution (black bars) with well screen location in the western part of the study area

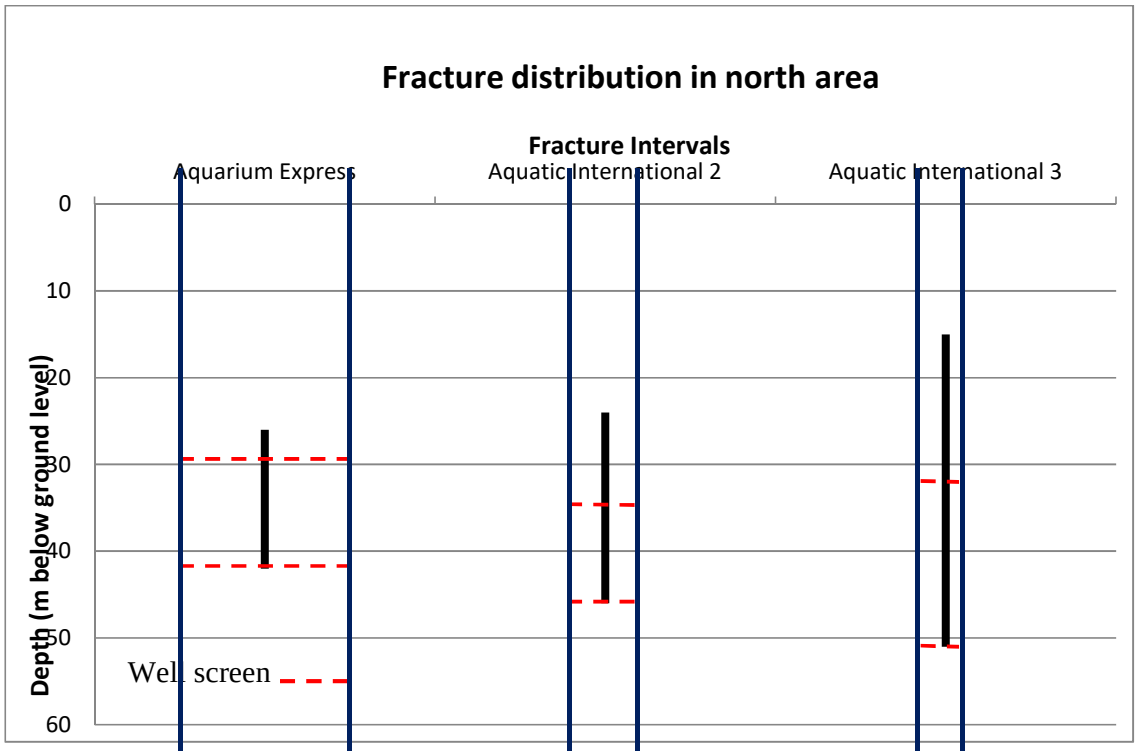

Figure 3.10 d) Fracture distribution (black bars) with well screen location in the northern part of the study area

3.3 Implications of Geological Data

3.3.1 Introduction

In Chapter 2, the detailed geological setting of Shah Alam has been discussed. The lithology in Shah Alam comprises interbedded sandstone and shale. The rock sequence is metamorphosed at a low grade due to tectonic activities and granite intrusion. All the wells available are drilled into this 'hard rock'. The unweathered metamorphic rock is likely to be of very low permeability (Clark 1985). To manage an aquifer system, it is necessary to understand its behaviour and the factors that control the groundwater flow. This can be particularly challenging in a hardrock aquifer because of the presence of much heterogeneity in aquifer properties brought about by variable weathering, fracturing, and complex rock type geometries, as are clearly present in the Shah Alam area.

In this section, the effect of the geology of the area (including the physical and chemical properties of rock, the geological structure, and the weathering processes) on porosity and permeability, which control the groundwater occurrence and movement, is investigated. All the previous research available on the Kenny Hill Formation and much research on similar metasedimentary rock is gathered and analysed in an attempt to estimate the hydraulic properties of the rock.

3.3.2 Porosity and permeability of the Kenny Hill Formation

3.3.2.1 Rock mass

It is very important to understand the lithification process of the rock formation to be able to estimate its porosity and permeability. Porosity and permeability are the most important hydraulic properties that govern groundwater distribution .

Diagenesis plays an important role in controlling the porosity and permeability of sandstone. The porosity of sandstone is usually reduced linearly with depth while the porosity of ‘shale’ is reduced exponential with depth (Magara 1980). The porosity of rock is often seen to reduce with increasing age as hardening is usually greater in older rocks (Goodman 1989, Singhal & Gupta 1999).

The permeability of sandstone and shale is also reduced with reduction in porosity. For example, in some cases the permeability of sandstone can increase tenfold with 3% increase of porosity (Archie 1950). The orientation and the packing of sandstone grains have strong influence on the permeability of the rock, including in a direction perpendicular to the bedding (Mast & Potter 1963). Permeability anisotropy in sandstone can be caused by sedimentary structures.

Stratified sandstone can show a very clear permeability variation (Hurst & Rosvoll 1991).

The quartzite of the Kenny Hill Formation comprises mainly quartz. The grain size is uniform with subangular to subrounded shapes. The size of quartz framework grains is 1-2mm with a finer matrix of silt and clay**.** The matrix of the unweathered quartzite in hand specimen is estimated by Yeap (1970) to be between 5 and 25% by volume, with a porosity of less than 1%. Examination in the field suggests that very low porosities and permeabilities are to be expected. It is composed predominantly of quartz (Zainab et al. 2007). Table 3.3 shows the porosity value given by different authors for the quartzite of the Kenny Hill Formation and also for other units in different parts of Malaysia. The porosity of sandstone in the Klang Valley area as measured by Saim (1991) ranges from 3.33 to 10.82%. These values are higher than estimated by Yeap (1970). The porosity of quartzite collected around Malaysia by Jasni (1989) ranges from 5-12%.

Table 3.3 The porosity values of quartzite in Malaysia

	Type of rock	Weathering grade	Porosity %	Location	Sample description
Jasni (1989)	Quartzite	IV III II	12 7 5	Various places in Malaysia	Not available
Saim (1991)	Quartzite	II	8.43	Klang	closed fissures
		II	3.33	Kuang	
		II	5.8	Kuang	with stained fissures,2mm width
		I I	7.03 10.82	Brickfield, Kuala Lumpur	with quartz vein 2-3mm thick

The porosity of unweathered quartzite is lower due to its texture which is cemented and recrystallized. The cement, i.e. silica, may have originated from dewatering of the shales during diagenesis. During the burial process, the water in the shale will be squeezed out and flow vertically into sandstone units (Magara 1976, Hayes 1979). Water acts as an agent carrying dissolved minerals. The cementing fluid also migrates horizontally within formations (Levadowski et al 1973). The cementation is often found, for example, along shale-sandstone contacts in interbedded sequences (McBride 1989). The quartz grains will be pressured upon burial until quartz is dissolved. The dissolved quartz will migrate and precipitate in the pores (Hayes 1979).

The quartz grains of quartzite in Shah Alam show the interlocking structure (Zainab et al. 2007). The interlocking texture of the quartz grains indicate that the quartz grains went through a recrystallization process (Levadowski et al. 1973, Pettijohn 1987). Sandstone and shale of the Kenny Hill Formation is metamorphosed to quartzite and sometimes phyllite due to the granite intrusion and metamorphism associated with tectonic activity. The depth of the granite body beneath the Kenny Hill Formation is unknown. A maximum estimation of the minimum distance to the granite can be made based on the distance to the granite outcrop that is exposed in the Damansara river, in the Subang and Puchong areas. The granite is also observed in the borehole at Canon Opto, southeast of central Shah Alam.

Relatively, the porosity value of shale is lower than sandstone in cases where deep burial has occurred (Davis 1969), so the porosity of the shale would be expected to be perhaps less than 10%. There is no porosity value for the unweathered shale of the Kenny Hill Formation available. However, Ibrahim (1986) measured the porosity value of weathered "shale" from the Kenny Hill Formation located in Bangi (30km to the southeast of study area), and the data from this paper are given in Table 3.4: note that most of the grain size analyses suggest that the material has not been derived from weathering of pure shale.

Table 3.4 The porosity values of weathered "shale" in Malaysia by Ibrahim (1986)

Depth of sampling (m)	Weathering grade	Moisture content %	Porosity %	Dry density g cm^{-3}	Grain size (%)			
					Gravel	Sand	Silt	Clay
0.5	VI	12.5	32	1.75	40	26.5	19	14.5
2.5		12.2	31	1.84	27.5	29.5	26	17
4.0		11	26	1.89	3.5	22.5	46.0	28.0
5.5	V	20.4	36	1.69	0.5	23.0	62.5	14
6.5		17.1	38	1.62	3.0	33.0	61.0	3.0
8.0		18.5	38	1.67	3.5	39.0	57.0	0.5

There are no data on the matrix permeability of the Kenny Hill Formation. Therefore the data of other places with similar lithology and age as Kenny Hill of other areas have been assessed to estimate the K value of sandstone in study area. The intrinsic permeability ranges for shale matrices given by Brace (1980) and Neuzil (1994) are 10^{-20} to 10^{-18} m^2 and 10^{-23} to 10^{-17} m^2 (with porosity of 0.12), corresponding to approximate hydraulic conductivity ranges of 10^{-8} to 10^{-6} and 10^{-17} to 10^{-5} m/d at ~ 25 ^oC. Table 3.5 shows K values for sandstone and shale which were obtained by careful laboratory measurement, confirming the older

reviews. From these studies, K matrix values for sandstone and shale in study area are estimated to be as low as 10^{-8} m/d to 10^{-5}m/d.

Table 3.5 The permeability of sandstone and shale

Sandstone,Yangzhuang colliery,China (Wang & Park 2002)	Fine sandstone	(0.05 - 6.57) x 10^{-7} Darcy (approx. 4 x 10^{-9} to 5 x 10^{-7} m/d at 25 ^{o}C)
	Mudstone	(0.0146 - 1.16) x 10^{-7} Darcy (approx. 1 x 10^{-9} to 1 x 10^{-7} m/d at 25 ^{o}C)
The Passaic Formation, New Jersey (Morin et al.1997)	Sequence of mudstone, siltstone and fine-grained sandstone (minor)	2.59 x 10^{-8} m/d with n = 3-5%
Shale (Eaton et al., 2007)		10^{-7} to 10^{-9} m/d

3.3.2.2 Fractures

Some general considerations

Since the primary porosity of rock sequences in the study area is low, secondary porosity plays an important role in enhancing the permeability of the rock. The storage capacity of aquifer in hard rock system is governed by discontinuities such as joints, bedding plane, joints, faults and foliation (Larsson 1984, Greenbaum 1992) and also by the weathered zone (Clark 1985, Jones 1985). The permeability of fractures is governed by their fill material and apertures, the latter being affected in the field by the fracture orientation and by the stress field (Gale 1982). The permeability of a rock mass is also governed by the frequency (spacing) of the fractures and their connectivity.

When sedimentary rock is deeply buried and/or uplifted, secondary porosity will usually be developed (Hayes 1979). The development of secondary porosity in sandstone is due to rock and grain fracturing and dissolution of grains and cements (Schmidt & McDonald 1979). Fractures developed in interbedded sandstone and shale is due to the release of high pressure in shale (which is developed upon loading) due to uplift and erosion activity (Magara 1981). In metamorphic rock, fractures develop after the main compressions associated with tectonic activity occurred (Price 1966). The degree of metamorphism affects the strength of rock; rock with a low grade of metamorphism is often heavily fractured (Larsson 1984).

Brittle rocks like sandstones and quartzites are often considered to have greater fractured rock aquifer potential (Lloyds 1999). However, there are studies that show the potential of argillaceous formation as aquifers (Michalski 1990, Michalski & Britton 1997, Morin et al. 1997 & Eaton & Bradbury 2007). Field inspection of the Kenny Hill Formation (Chapter 2) indicates that fracturing in both rock types seen is common.

The permeability of fractured formations is best estimated using pumping tests (Megahan & Clayton 1986, Black 1987, Wright 1992), though fracture analysis can also be used (Hitchmough et al. 2007). As Table 3.6 indicates, the rock mass permeability is often much greater than the matrix permeability (Table 3.5). Sam (2014) undertook a detailed international review of published field permeability values in hard-rock systems, and the results he presented classified according to rock type are given in Figure 3.11. The most relevant rock types are grouped

under B, C, D, and K, and have median field permeabilities in the range 10^{-7} to 10^{-6} m/d, i.e. 10^{-2} to 10^{-1} m/d. The permeability in certain fracture sets, e.g. that associated with bedding planes, is often greater than that in other directions (e.g. Pettijohn et al 1987), so fractured sequences often have anisotropic permeability.

Table 3.6 Hydraulic parameters in fractured bedrock

Type of rock	Method of measurement	Apparent permeability value m /day
Crystalline bedrock; gneiss, granite, Africa (Wright 1992)	Pumping test	0.01 to 3m/day
Shale (Eaton et al. 2007)	Pumping test	0.01 to 1m/d

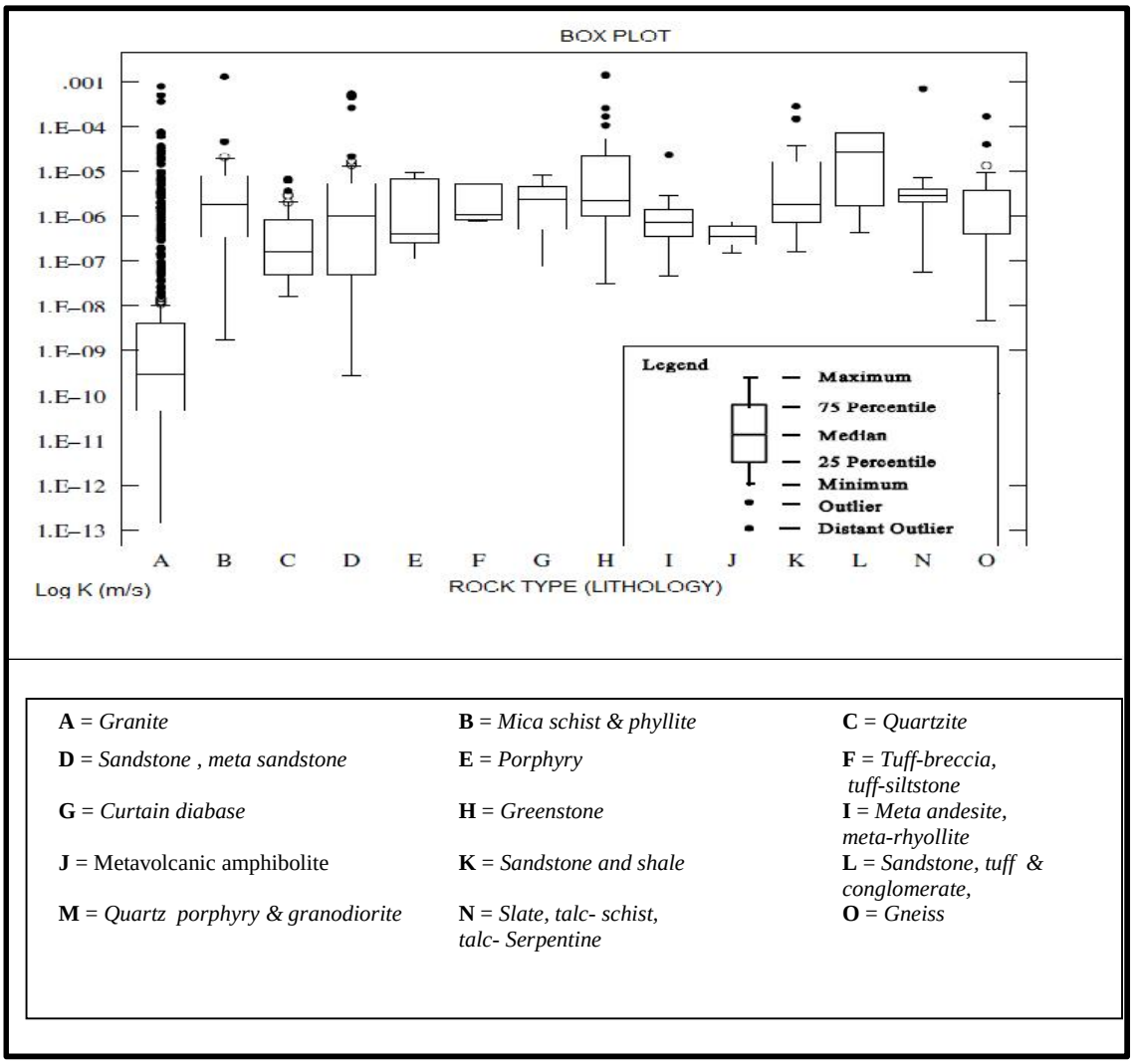

Figure 3.11 A summary of literature values for hardrock terrains split according to rock type (from Sam, 2014).

Bedding and other joints

Discontinuities such as joints and bedding plane joints can provide the paths for the water to flow. Bedding plane joints are often suggested as the primary pathway for water flow in interbedded sequences in sedimentary rock (Novakowski & Lapcevic 1988, Michalski 1990, Michalski & Britton 1997& Hitchmough et al. 2007). In systems where the bedding planes have low dips,

the transmissivity value of bedding plane joints decreases with increasing depth suggesting that the fluid flow near surface is controlled by bedding plane joints while increasing stress at depth closes such joints up resulting in fluid flow at depth being controlled more by high dip fractures (Morin et al.1997). This argument could be extended to systems where the bedding plane joints are not the lowest dipping fractures by replacing bedding planes by the fracture set that does have the lowest angle dip: the implication is that the anisotropy as well as bulk permeability can change significantly with depth.

There are two types of joint: dilational fractures (open fractures) and shear fractures (Holmes 1964). Shear fractures are often tightly closed and with smooth surfaces while dilational fractures are open, rough and have irregular surfaces. The hydraulic conductivity of dilational fractures is higher than shear fractures (Singhal & Gupta 2010). Tensional (dilational) joints can be a pathway for water. This can lead to reactions, and minerals will be deposited coating the joint surface and thus reducing the permeability. Fracture with clay infill such as smectite will decrease the permeability (Banks et al. 1992).

The fractures that are observed in boreholes in study area will probably often be associated with bedding planes, except where dips are significant. Other joints in sandstone with lower angle dips (e.g. Outcrop B) might not be often seen in boreholes due to their orientation, though nevertheless still be of importance for regional flow (or even by connections through bedding plane joints, to the wells).

Joints were observed at outcrop as perpendicular to the bedding. Fractures are persistent in sandstone/quartzite compared to shale/phyllite. Foliation plane can be observed clearly in phyllite.

Bedding planes and other joints are interpreted as the main paths for water to flow (Figure 3.12). Shale is less resistant to weathering than sandstone. The contact between shale and quartzite (a bedding plane), provided it is associated with a joint and has not been smeared by differential movement, provides a pathway for water to flow causing the chemical interaction between water and shale material (Figure 3.13), and this can result in deposits that can reduce the permeability. The roots of trees often follow the bedding plane and other joints when the bedrock is shallow, thus opening them up further for water flow and weathering (Figure 3.14).

In Chapter 2 (Section 2.6.3), it was proposed that quartz veins were associated mainly with the faulting aligned parallel with the Bukit Tinggi fault zone (NW/SE), and that the other main fracture trend, NE/SW, was mainly associated with extensional stresses. It seems reasonable therefore to conclude that the fractures oriented in the NW/SE direction are likely to have lower permeability than those oriented in the NE/SW direction.

Figure 3.12 Water movement in quartzite in Shah Alam. In this case, water is assumed to flow along approximately vertical joints that are perpendicular to the bedding and then along the approximately horizontal bedding plane joints.

Figure 3.13 Bedding plane joints in Shah Alam, possibly developed somewhat due to weathering in shale layer

Figure 3.14 The tree roots are along the bedding and joint

Faults

The morphology of faults can be divided into zones with variable permeability which are protolith (unfaulted zone), damage zone (fractured zone, with veins) and core zone (breccias/gouge/cataclasite) (Caine et al.1996). The damage zone has the highest permeability and Caine et al. (1996) suggests a range of 10^{-16} – 10^{-14} m^2 (approx. 10^{-4} to 10^{-2} m/d at 25 ^oC) though the permeability for shallow systems can be much greater than this (e.g. Sam, 2013). The lowest permeability is at the core of fault which can have values lower than 10^{-20} m^2 (less than 10^{-8} m/d at 25 ^oC) (Evans et al. 1997).

The fault behaviour can be divided into four types: a transmitting fault; a sealing fault; a fault that is vertically transmitting but sealing horizontally; and a fault that transmits and seals intermittently (Aydin 2000; Jolley et al. 2010).

When sandstone is faulted against shale, a sealing fault will often be created (Smith 1980). Faults in siliciclastic sequences will often produce a clay smear (Fisher & Knipe 1998, 2001, Sperrevik et al.2000 , Clausen & Gabrielsen 2002, Koledoye et al. 2003, Takahashi 2003 and Van Der Zee & Urai 2005).

Groundwater flow can therefore be influenced in different ways by faults (Bense & Balen 2004; Seymour et al. 2006). Faults can act as groundwater flow barriers due to clay smearing along the fault zone. Some faults, with high permeability, allow most groundwater flow to occur along them. Faults with hydraulic anisotropy of two to three orders of magnitude can act as conduit and also as a barrier for horizontal flow in siliciclastic sequences (Bense & Person 2006). Faults with low permeability can divide the aquifer into individual compartments (Seymour et al., 2006; Mohamed & Worden 2006). The compartmentalisation by faults is widely discussed in petroleum industry (Jolley et al. 2010, Gill et al. 2010).

The aquifer in Shah Alam, especially near the Damansara River where quartz veining is most common in the northwest-southeast aligned faults, may occur in individual compartments due to the faulting. Faulting in the study area is interpreted as aligned with rivers in Shah Alam especially Damansara river (see Figure 2.49). The size of compartments is suggested to be in the range 500 m to 1000m based on the distance of the lineaments observed.

The nature of faults is different based on the lithology of host rock. The fault zones in shale or phyllite are identified by the occurrence of highly weathered to

completely weathered material (grade IV-V) as shown in Figure 3.15. The fault zone in quartzite is recognized by the presence of a highly fractured zone and also with quartz veins. The presence of iron oxide in the fractured zone and along the fractures shows the active water movement, though when is not possible to say (see Figure 3.16). The faults in quartzite are interpreted as relatively higher permeability than the faults in shale. Faults in the shale/phyllite area act possibly as groundwater flow barriers. The fault zones in quartzite have potential as water conduits. The faults in interbedded sequences are possibly of low permeability due to clay smear from the shale (Figure 3.17)

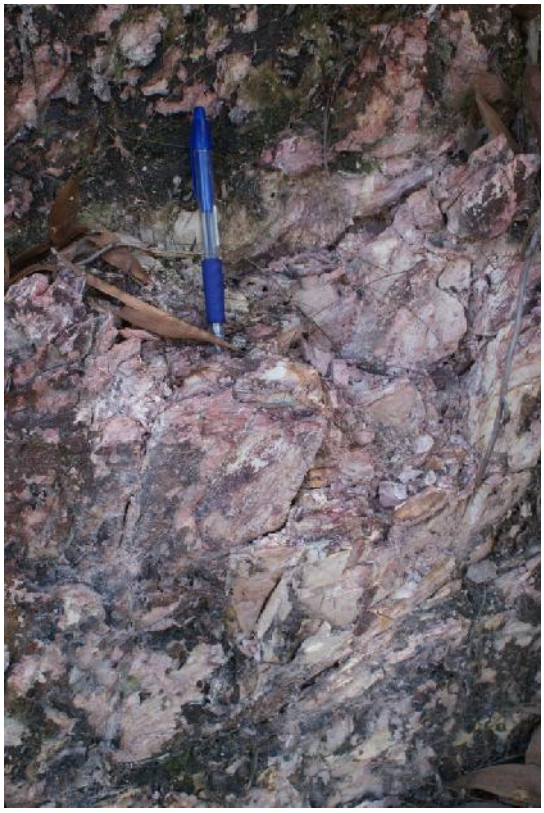

Figure 3.15 Shale in fault zone

Figure 3.16 Iron oxide-hard crust in a fault zone in Shah Alam.

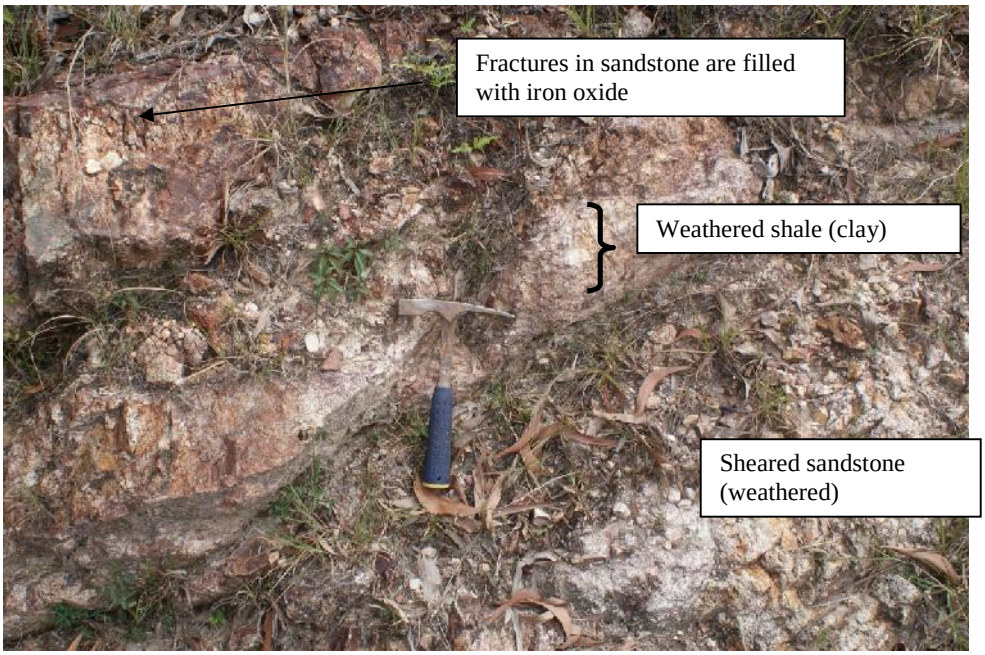

Figure 3.17 Interbedded quartzite and shale in fault zone

Folds

Fracture patterns often are affected by folding, either because the fractures developed as part of the tectonic activity occurring with folding, or because pre-existing fractures were subsequently folded (Van Golf Racht 1982). Often fractures in units on the outside of folds are extensional and more likely to be open whereas fractures in the cores of folds may well be compression and shear fractures and hence lower permeability. Thus anisotropy and zones of greater flow can be strongly affected by the presence of folding.

In study area, the bedding orientation changes direction, from gentle to steep and from southwest to southeast, due to folding events (see Figure 2.25). This may have an effect on permeability anisotropy, flow directions and heads.

3.3.2.3 Weathered rock

Weathering processes play a significant role in hardrock aquifer systems. It changes the permeability and the porosity of the rock, often reducing the permeability of fractures, eventually destroying them, and often increasing the permeability of the matrix. The thick weathered layer on top of fractured rock is an aquifer material in its own right (Jones 1985). It can also sustain the yield of a well drilled to greater depths by increasing the storage capacity of the fractured rock aquifer (Clark 1985; Acworth 1987). Therefore, it is important to understand the role of weathering in affecting the hydraulic properties and behaviour of a hardrock aquifer system.

Malaysia lies in the equatorial climate region. With hot and wet conditions all year, chemical weathering processes play a greater role than mechanical weathering process producing a thick weathered layer. The weathered layer also tends to be thicker in areas with low relief such as Shah Alam (Acworth, 1987). The hydraulic properties of weathered layers depend on the parent rock, the climate, the tectonic activity and the topography (Wright & Burgess 1992). The weathering is concentrated along the fractures causing a deep weathering profile which can go deeper than 90m (Jones 1985). The density and pattern of fractures and lineaments reflect the weathering activity; the weathering in highly fractured areas is more intense than the area with less fracture (Greenbaum 1992).

The weathering profile developed on a hardrock sequence is similar despite different climates (Larsson 1984). In very general terms the weathered layer can be divided into four zones (a-d). Zone (a), immediately below ground level, is up to a few metres thick with sands, sandy clays or clay with sand. The material in zone (b) is up to 30 metres thick. It is enriched with secondary minerals (clay), with high porosity but low permeability. The material in zone (c) is degraded rock, up to 30 metres. The material in zone (d) is fresh fractured rock with low porosity but with moderate permeability. This weathering profile is compared with the weathering profile of metasedimentary rock in Malaysia proposed by Ibrahim & Mogana (1988) in the subsequent discussion. This information will help to estimate the hydraulic properties of the weathered layer in the study area.

Table 3.7 and Table 3.8 show the weathering classification (Ibrahim & Mogana 1988) and the engineering properties for metasedimentary rock in Malaysia

(Ibrahim & Jasni 1990). The classification used is broadly the same as that proposed by Larsson (1984) described above, but is more detailed and adapted for metasedimentary sequences. Quartzite is more resist to the weathering than shale. Fractures intensity increases with weathering grade as observed in both quartzite and shale as discussed in Section 2.6.3. The quartzite is weathered to sand or sandy clay while the weathered material for shale is clay to silty clay. Figure 3.18 shows the weathering profile of quartzite area according to Ibrahim & Mogana (1988). The porosity increases with depth initially. Weathered zone is often with iron oxide crust (see Figure 2.36) hindering water to infiltrate deeper. A perched aquifer might develop in this area.

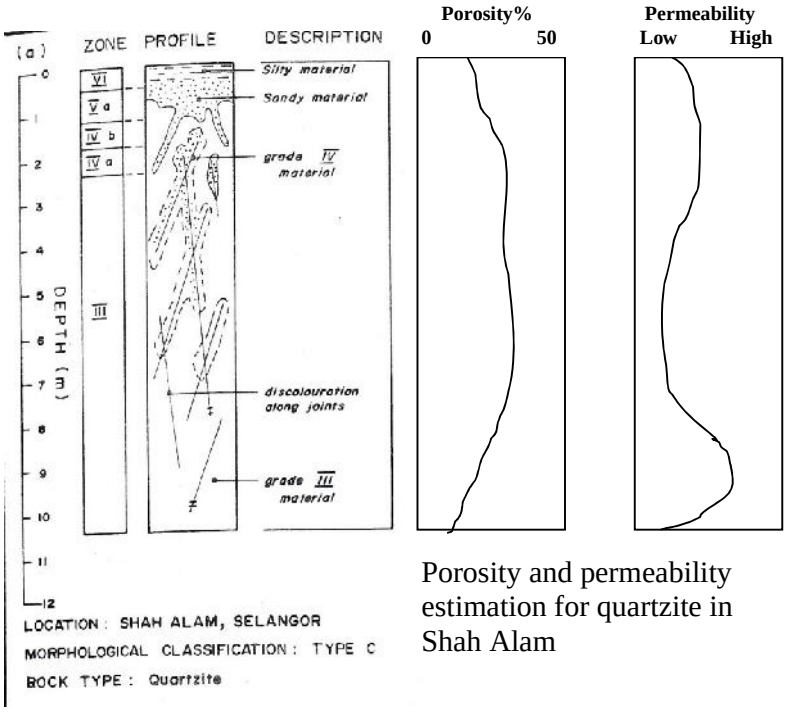

Porosity and permeability estimation for quartzite in Shah Alam

Figure 3.18 Weathering profile for quartzite in Shah Alam (Ibrahim& Mogana 1988) with porosity and permeability plot with depth

In the following paragraphs, the physical properties of weathered material of the Kenny Hill Formation rocks from previous studies are assessed to estimate the hydraulic conductivity of the weathered layer with the information from these tables being used as a guideline.

Table 3.9 shows the physical properties of the Kenny Hill Formation obtained by other studies. The moisture content of weathered meta-argillite at Bangi increases with depth (Ibrahim 1986). The water content of the weathered phyllite is higher than that of the weathered quartzite as shown in Figure 3.19, and this presumably reflects the greater porosity and smaller pore size of the weathered phyllite. These differences will affect recharge rates, the weathered phyllite requiring more water to reach saturation and a greater head difference to move the water at the same rate, but perhaps drying out less. The plasticities are higher for phyllite soils as a result of higher average clay content which is 36% compared with quartzite which is 21%.

Table 3.7 Weathering classification for metasedimentary rock (Ibrahim & Mogana 1988)

Weathering classification		Description
Term	Zone	
Residual soil	VI	All rock material is concerted to soil. The mass structure and material table (texture) are destroyed. The material shows homogeneous colour and has not been significantly transported
Completely weathered	V	All rock material is decomposed to soil. The mass structure and material texture are partially preserved. The material is friable if soak in water or squeeze by hand. The material commonly contain iron- rich concretions and non homogeneous or mottled in colour
Highly weathered	IV	The rock material is in the transitional stage to form soil. More than 50% mass structure and total material texture are preserved. The material formed smaller fragments or blocks if soak in water or squeeze by hand
Moderately weathered	III	Discolouration indicates some of rock material is affected by weathering. The mass structure and material structure are preserved. Material fragment or block corners can be chipped by hand. Discontinuity commonly filled by iron-rich material
Slightly weathered	II	Discolouration along discontinuity and may be part of rock material. The mass structure and material texture are preserved. Material is generally weaker but fragment or block corners cannot be chipped by hand
Fresh rock	I	No visible sign of rock material weathering. Some discolouration on major discontinuity surfaces

Table 3.8 Engineering properties for metasedimentary rock (Ibrahim & Jasni 1990)

Weathering classification		Dry density (g/cm-3)	Porosity x(%)	Slake durability 1d2 (%)	Brinell hardness index (N/mm)	Point Load Index (MPa)	UCS (MPa)
Term	Grade						
Completely weathered	V	<2	N.D	0-20	<1	<0.1	<5
Highly weathered	IV	2.00-2.25	>0.12	IVb 0-30 IVa30-80	IVb 1-6 IVa6-40	0.1-0.5	5-20
Moderately weathered	III	2.25-2.45	0.06-0.12	80-95	>40	0.5-3.0	20-80
Slightly weathered	II	2.45-2.55	0.02-0.06	95-100	N.D	3.0-6.0	80-140
Fresh rock	I	>2.55	<0.02	N.D	N.D	>6.0	>140

Table 3.9 The physical properties of quartzite and phyllite of the Kenny Hill Formation in Shah Alam at various locations

	Depth of sampling (m)	Water content W_o %	porosity %	Liquid limit %	Plastic limit %	Plasticity index %	Sand %	Silt %	Clay %	Parent rock	Location
West & Dumbleton (1970)	0.6			41	20	21				Interbedded sandstone - shale	Batu Tiga
	1.8			46	23	23					
	3.4			50	22	28					
Ibrahim (1986)	0.5	12.5	32				40	26.5	19		
	2.5	12.2	31				27.5	29.5	26		
	4	11	26				3.5	22.5	46	Meta-argilite	Bangi
Tan & Ezdiani (2005)	shallow depth	35.49		73	56	17	31	28	41	Phyllite	
		31.63		45	33	12	39	20	41		
		29.92		59	47	12	29	27	44		
		27.3		50	34	16	24	60	20		
		26.48		42	26	16	45	42	21		
		26.01		72	47	25	44	20	36	Quartzite	
		21.77		30	19	11	37	20	43		
		20.76		24	18	6	52	32	16		
		17.26		45	30	15	48	36	16		
		16.26		48	32	16	67	27	6		
		13.66		42	32	10	66	28	6		
		12.91		26	21	5	39	37	24		
		11.36		28	15	14	43	39	18		
		10.34		52	17	15	57	20	23		

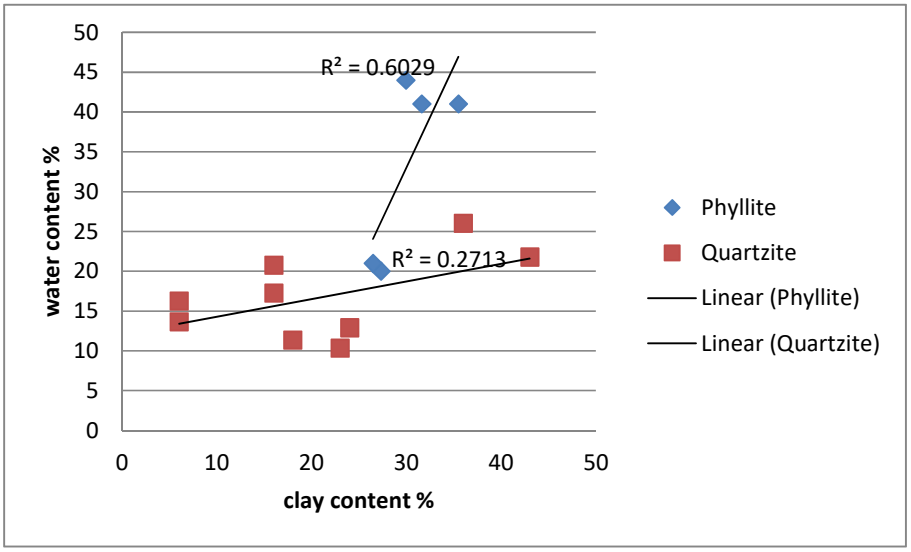

Figure 3.19 A plot of percentage of clay against percentage of moisture in soil from quartzite and phyllite in Shah Alam. Data are from Tan & Ezdiani (2005)

From the physical properties obtained by others, the permeability of weathered phyllite in study area is estimated. The coefficient of permeability of clay, *K*, in the weathered phyllite is estimated using the method proposed by Nishida & Nakizawa (1969) where void ratio, *e* and plasticity index value, PI is used. The relationship of hydraulic conductivity with the void ratio and plasticity index is as shown below.

$e = \{0.01\ (PI) + 0.05\}\ (10 + \log_{10} K)$

where e = void ratio

PI plasticity index in percent

K coefficient of permeability (in cm/sec)

Using this relationship, a *K* value is estimated for the Grade VI (residual soil) of the meta-argillite/phyllite of the Kenny Hill Formation. The *n* value used was the average value measured by Ibrahim (1986) and PI average value represents by values provided by Tan & Ezdiani (2005).

For the phyllite residual soil:

$e = \{0.01\ (PI) + 0.05\}\ (10 + \log_{10} K)$

where $e = n / (1-n) = 0.504$
PI % = 13
Therefore, $0.504 = \{0.01\ (13) + 0.05\}\ (10 + \log_{10} K)$
$K = 6.3 \times 10^{-8}$ cm/sec
$= 5.4 \times 10^{-5}$ m/d

According to this calculation, the *K* value of the residual soil of phyllite origin is low. The *K* value obtained can be compared with the *K* values obtained by Noguchi et al (1997) who investigated the physical and water flow properties of soils at Bukit Tarek Experimental Watershed. This tropical rain forest is located 45 km to the north of study area (see Figure 2.2). The lithology in this area comprises quartzite, quartz schist mica, graphitic schist and phyllite. The sampling was carried out at the ridge (OR), upper slope (NR, DP) and lower slope (NS) of selected slopes in the basin. Vertical undisturbed soil cores ($100cm^2$ in area and $400cm^3$ in volume) were taken at depths of 10, 20, 40 and 80cm. The saturated hydraulic conductivity, *K* was measured using a constant head permeameter.

The *K* values decrease with depth as shown in Figure 3.20. *K* is higher in the area with decayed roots. The mean *K* value decreases with depth as shown by the results that range from 4×10^{-4} m s^{-1} at 10 cm depth to 5×10^{-5} m s^{-1} at 80cm depth. Noguchi et al. (1996) suggested that runoff may not be dominant in this area, as the *K* values are larger than the rainfall intensity and they stressed the importance of subsurface flow for generating stormflow. These values are very high for soils that have a great deal of clay in them and, comparing with the value estimated from Atterberg limits above, there must be other pathways, perhaps root holes or shrinkage cracks. This suggests that there may be some penetration of even clayey soils by water, though it is not clear if this would result in recharge.

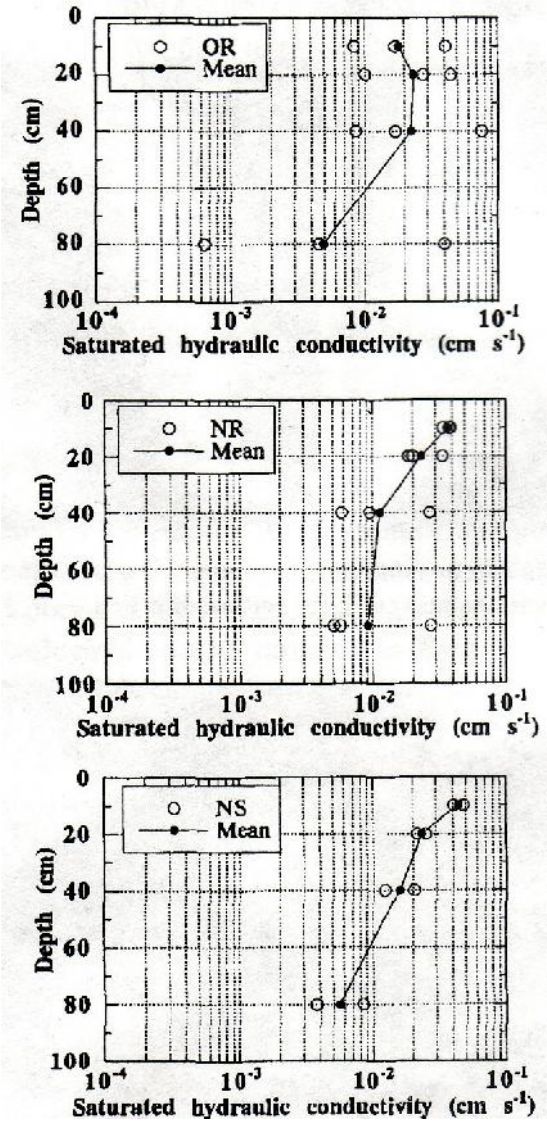

Figure 3.20 Saturated hydraulic conductivity trends at OR, NR & NS with depth (Noguchi et al., 1997)

Table 3.10 shows the soil properties from granite or siliceous rock at Kanching Forest Reserve which is situated around 26 km from Kuala Lumpur (Kamaruzaman, 1989). The saturated hydraulic conductivity, *K* value is 4 $x10^{-5}$ ms^{-1} (disturbed area) and $7x10^{-5}$ ms^{-1} (undisturbed area). The *K* value is close to the *K* value measured at Bukit Tarek. Samples were collected using metal core rings with 7.6cm diameter and 4.0 cm high, and any soil

organic layer was removed. The soil is dominated by coarse and fine sand which produced a high saturated hydraulic conductivity value though interestingly similar to that obtained for the clayey soils.

Table 3.10 The soil (granite origin) properties at disturbed and undisturbed area (Kamaruzaman, 1989)

	Disturbed area	**Undisturbed area**
Bulk density (g/cm3)	1.28 ± 0.16	0.99 ± 0.18
Total porosity (%)	51.6 ± 6.05	62.6 ± 6.66
Saturated hydraulic Conductivity (m/s)	0.0000416 ± 1.42	0.00007 ± 1.13
Coarse sand %	46.35 ± 8.21	42.31 ± 5.62
Fine sand %	16.15 ± 3.67	13.62 ± 3.86
Silt %	8.24 ± 4.69	7.65 ± 3.80
Clay %	25.91 ± 8.38	32.30 ± 7.34

Bujang et al. (2005) measured the infiltration rate of sandstone at a sandstone outcrop located along a link road near Kuala Lumpur International Airport, Sepang. There are no physical properties of sandstone supplied in the paper. However the outcrop is believed to belong to the Kenny Hill Formation. Figure 3.21 shows the infiltration rate increases with increasing weathering grade. If it is assumed that a head gradient of 1 was established, then the infiltration rates approximate to permeability values and appear to be an order of magnitude lower than the values reported for the soils above.

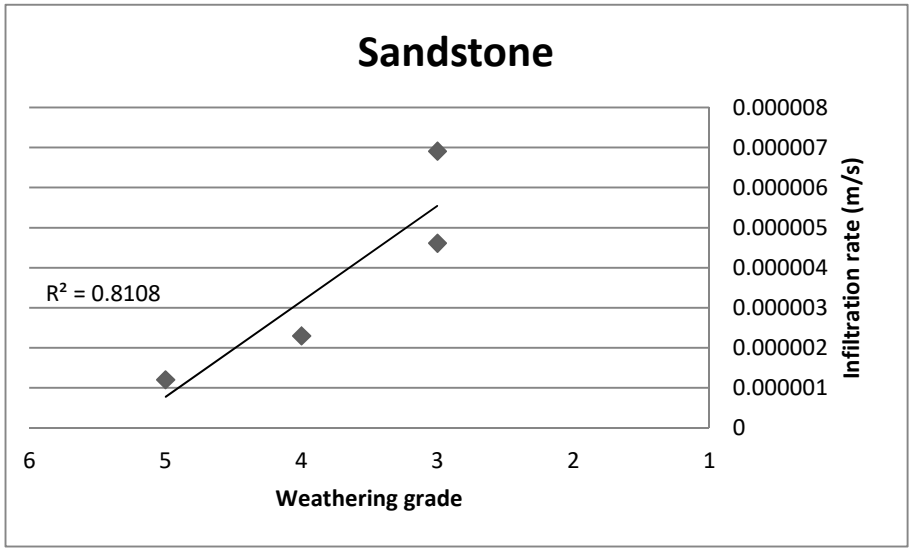

Figure 3.21 The infiltration rate in a sandstone slope at Sepang (grade III-V)(Bujang et al., 2005)

From the *K* values obtained, the physical properties of weathered material appear to be really important. The hydraulic conductivity of the coarser material, i.e. the quartzite residual soil, is higher than the shale/phyllite residual soil, and this will affect recharge and vertical leakage. For areas in which is quartzite is dominant, infiltration may be dominant whereas for areas dominated by shale, surface runoff may be dominant.

The common clay minerals that exist in soil layers in Malaysia are kaolinite and illite (Tan & Tai 1999, Zulhaimi 2000 & Tan & Yew 2002). Montmorillonite is normally found in lower rainfall regions (Appelo & Postma 2005). From x-ray diffraction analysis on soil samples overlying the Kenny Hill Formation at Batu Tiga Shah Alam, quartz, kaolinite and some goethite were found (West & Dumbleton 1970).

In addition to clay, iron oxide is also product of the weathering. The iron oxide heavily coats the bedding planes and joints in the sandstone (Figure 3.22) and also the fault zone (see Figure 3.16).

Figure 3.22 Bedding planes and joints in sandstone heavily coated with iron oxide in Shah Alam

3.3.3 Hydrogeological conclusions from geological studies of the Shah Alam area

By understanding the role of fractures and the weathered layer as discussed by previous researchers and from the geological information from the study area, an initial conceptual model of the hydraulic properties of the Shah Alam aquifer is proposed.

- The groundwater flow in Shah Alam aquifer is assumed to be governed by fracture rather than matrix flow
- The hydraulic conductivity can be anisotropic as shown in Figure 3.23.

- The quartzite of the Kenny Hill Formation is interpreted as the main aquifer. However, the wells in Shah Alam are also tapping from fractured shale (cf. Table 3.2). Since shale is argillaceous rock, with low permeability, fractures play an important role in making such rocks permeable.
- The quartzite remote from the Damansara River area possibly has less metamorphism and therefore is possibly more porous and permeable.

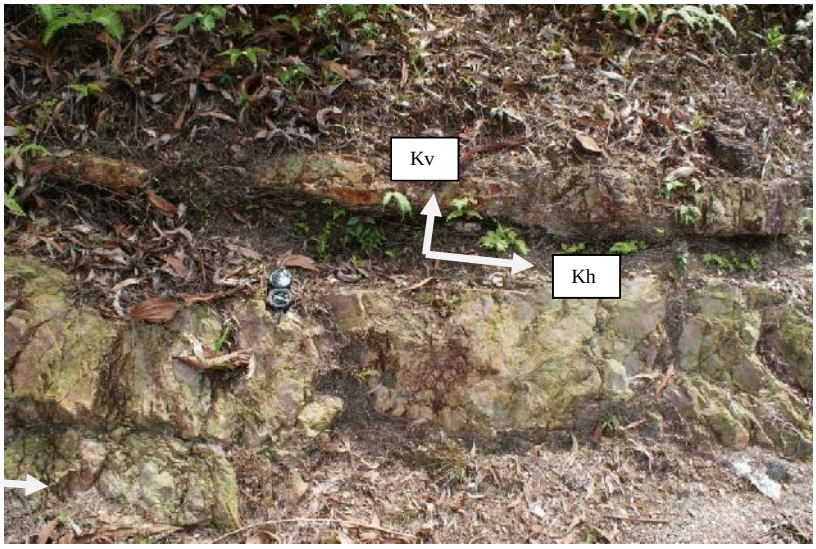

Figure 3.23 Horizontal conductivity,Kh is interpreted as bigger than vertical hydraulic conductivity,Kv

- As there is a fault system along which the Damansara river has aligned itself, there is a potential connection between the river and an important aquifer fracture network. There is possibility that the river can recharge the groundwater, or vice versa.
- The weathered layer will affect recharge rates, and also act as a leakage unit – an aquitard – for the fractured aquifer below.

- The K value for the sandy clay is higher than that of the silty clay or clay. Therefore, for the area with silty clay material (weathered shale), overland flow is possibly more dominant than subsurface flow and infiltration is dominant in the quartzite area.
- The weathered sandstone increases the storage capacity of the aquifer in fractured quartzite and in interbedded sequence areas.
- The weathering also can be viewed as dividing the aquifer into ~horizontal 'compartments' (weathered layer – fissured layer- deep fractured zone) (Ayraud et al., 2008)
- The fractured shale will be capped by a clay layer (weathered shale) and may be effectively classified as a confined aquifer
- The fractured interbedded sequence and the quartzite with a thick weathered layer may be expected to behave as a confined to leaky aquifer.
- The fractured quartzite which is overlain with weathered quartzite may be expected to behave as a leaky to unconfined aquifer depending on the thickness of the capping layer.
- The average abstraction rate is low (268m^3/day)

3.4 Implications of Groundwater Head Data

3.4.1 Introduction

The aim of this section is to identify the groundwater flow patterns as far as possible in the Shah Alam aquifer using the limited water level information available. Though water levels in the Shah Alam wells have not been monitored, data exist for the initial water levels in all 42 of the wells that have been pumping tested. The measurements were taken before the pumping test was carried out in each well. The water levels were recorded at different times and by different companies. Therefore, although the data are not perfect, if they are examined

with care they may give an indication of possible groundwater flow. The only periodic data that are available are from Ansell. The rest of the wells have no water level records other than during the time when the pumping tests were carried out. Because of the limitation of the data set a groundwater contour map will be at best indicative and will not cover more than a small proportion of the aquifer.

3.4.2 The factors that might influence the groundwater level during measurement

There are a few factors that might affect the accuracy of the water level measurement that need to be considered. First, most of the factories have more than one pumping well. In Ansell for example, the location of each well is approximately 200 m from the others yet the water level varies. There is a possibility that other wells are pumping while the initial water level measurement is carried out. There would be greater confidence in the data if all the wells at same site had similar water levels, especially if they have similar depths. Therefore, for groundwater head contour construction, only the earliest water level record will be used. Each of the factory compounds will be represented by one well except Ansell. This assumes that the fracture network is connected throughout a site.

Figure 3.24 shows the water level at the Ansell compound. The water level measurements are for 2005, 2007, 2008 and 2010. The water level was recorded at different times only in 2005 and 2007 as shown in Table 3.11 and was measured at the same day in 2008 and 2010. The water level at Ansell TW1 and TW7 do not change very much with time. The water levels at wells Ansell TW3 and Ansell TW4 show significant change in 2008 and 2010, but in general all except TW1 show some drop in head from 2005 to 2008/10.

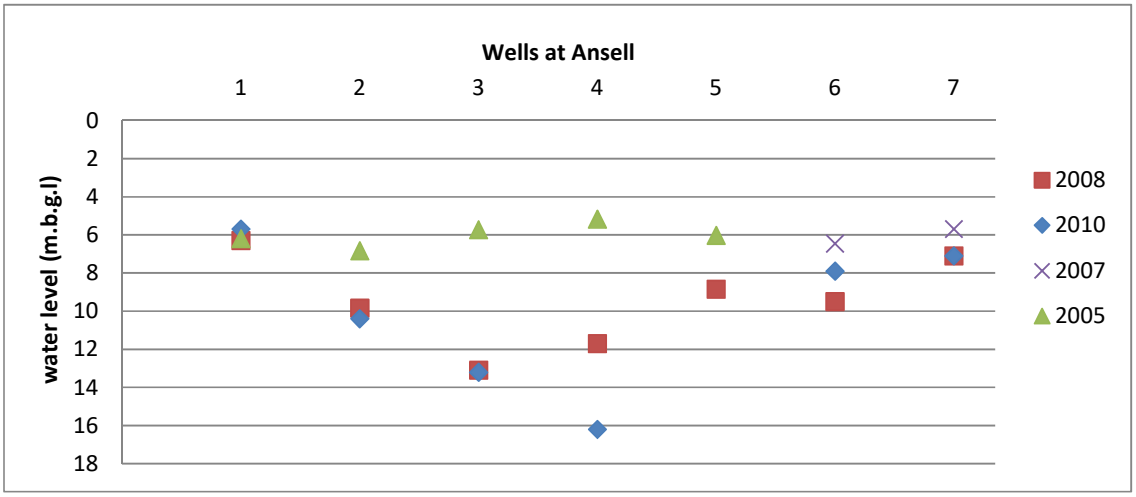

Figure 3.24 Water level measured at Ansell's wells in 2005, 2007, 2008 and 2010.

Table 3.11 The water levels recorded at Ansell in 2005 and 2007

Tubewell	Water level from ground surface (m)	Date of measurement
Ansell TW1	6.20	2 Feb 2005
Ansell TW2	6.83	3 Feb 2005
Ansell TW3	5.33	18 April 2005
Ansell TW4	5.17	18 April 2005
Ansell TW5	6.0	30 June 2005
Ansell TW6	6.45	21 March 2007
Ansell TW7	5.69	13April 2007

It is worth considering if the water levels vary with monsoon season, even though rainfall is fairly evenly distributed through the year. Table 3.11 and Figure 3.25 indicate that the water level is higher in April than February or June 2005. The monsoons are from late November to March and June to October so highest water levels would be expected to occur in

March/April and October/November. It is possible therefore that higher April water levels are due to monsoon effects but more data are needed to justify this.

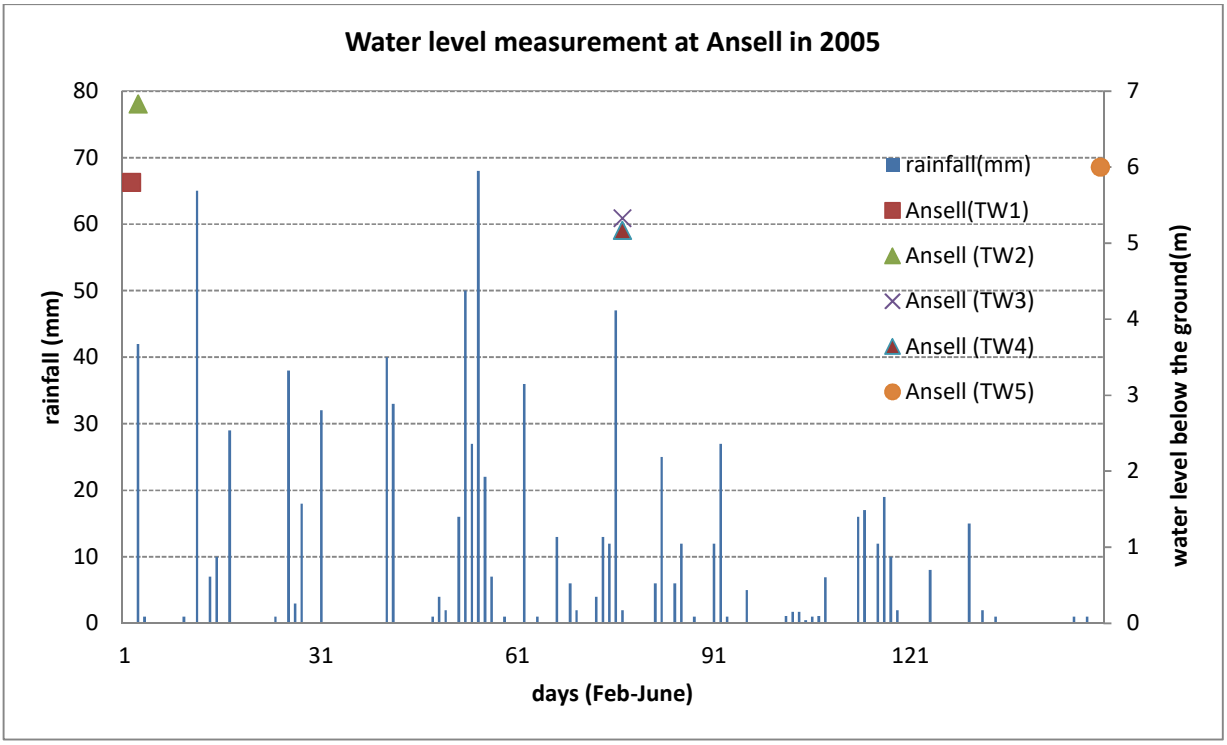

Figure 3.25 The response of water level with rainfall. The measurement was carried out at Ansell in 2005.

Another case is shown in Figure 3.26 (the water levels at Mitsui Hightech and Good Year). Both wells lie in shale areas and are located 540m from each other. The water levels for these wells were measured at different times but in the same year. The Mitsui Hightech water level was measured in a drier period (July, southeast monsoon) compared to Good Year where the measurement was taken in December (northeast monsoon), a wetter period. It is clear that the level in the wetter period is deeper than the level in the drier period, the reverse of what might be expected unless there was a long lag time. A long lag time might be due to low permeability of weathered layer which covers the fractured rock, but the difference in water

levels might just as easily be caused by a number of other processes. Unlike Mitsui High Tech and Good Year, Ansell lies in interbedded sandstone and shale where the fractured rock is covered with a sandy silt weathered layer which is more permeable compared to the clayey weathered material at the Mitsui High tech and Good Year compounds.

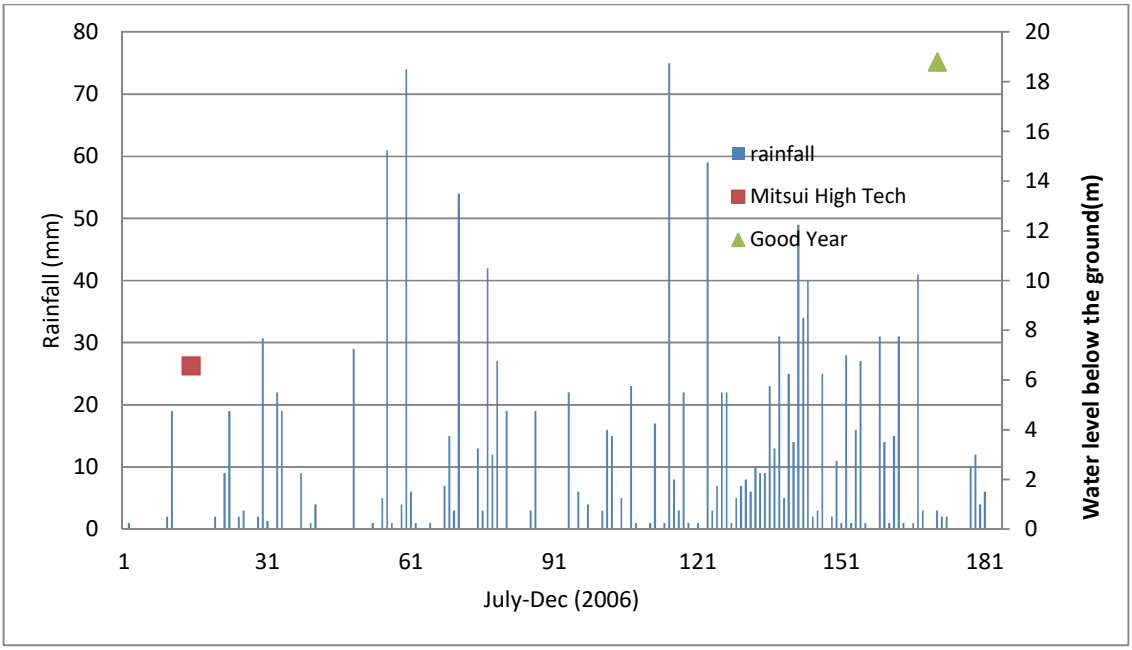

Figure 3.26 The response of water level to rainfall. The measurement was carried out at Mitsui High tech and Good Year in 2006.

It is concluded that there are not enough data to determine the impacts of rainfall using the regulatory authority datasets with any certainty though possibly the data that are available indicate that responses to rainfall can be both significant (Ansell in Figure 3.25) and insignificant or at least lagged (Figure 3.26). Therefore to investigate further the response of water level to rainfall, water level monitoring work was carried out at the Ansell TW7 well. The details on this monitoring work will be given in Section 5.7. Figure 3.27 shows the water level data which were measured from 18 February 2011 until 2 March 2011. Water level data in this plot represents series of water level data when well is not pumping (during recovery period). It shows that water level responded almost a day after the heavy rainfall event on

27th February (from 12960 to 14400 minutes). The water level above the Diver increased to 40m starting 15120 minute. This shows that the weathered layer here is permeable enough to let the rain water infiltrate through and recharge the aquifer, or at least the recharge occurred somewhere close by and the increase in head was transmitted through the aquifer to this site quickly.

In conclusion, the very limited data available are consistent with the idea that the aquifer is fracture-flow dominated and/or largely confined (quick response) though protected by a differing cover of weathered zone (slow response).

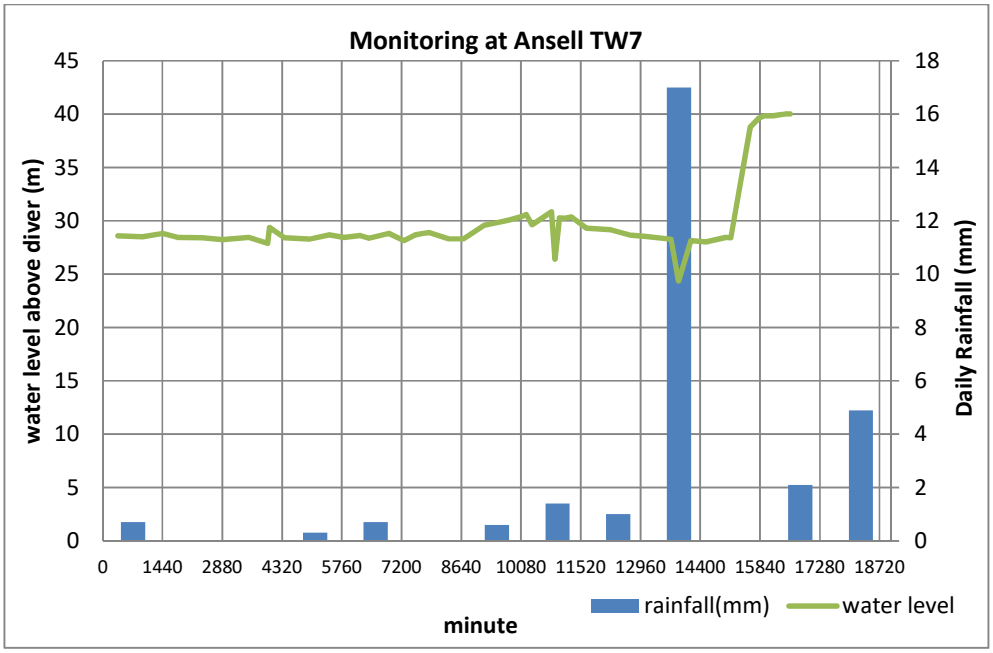

Figure 3.27 The water level responses to the rainfall as observed at Ansell TW7.

3.4.3 Groundwater abstraction

The total abstraction from the Shah Alam aquifer is 1.25 Mm^3/year, a relatively limited amount of water, about 0.5% of the total rainfall (latter taken to be across a square area from

the most southern well to the most northern outcrop examined (Outcrop C); but much rainfall runsoff). There may also be illegal abstraction but there is no information on this. Figure 3.28 shows the abstraction in Shah Alam decreasing slightly over the last few years of data. Table 3.12 shows the abstraction records of wells in Shah Alam. Proper records were started in 2005 by LUAS (Lembaga Urus Air Selangor) a government body which manage all the water sources in Selangor. Therefore, the abstraction records earlier than 2005 are not available. Wells in MT Pictures were closed after 2005 because the factory‘s operation was stopped while Carlsberg No. 3 and Ansell TW5 were closed in 2008 and 2011 due to the wells’ poor conditions. The duration of pumping varies. Some of the wells are used continuously such as Ansell, Carlsberg 1, Scientex Polymer and Suzuki Latex. The minimum period of pumping is 4 hours by the well in Gaya Color Lab. The record shows the wells are daily used at constant pumping rate until present, with well ages up to about 30 years e.g. Panasonic, Carlsberg (see Table 3.13).

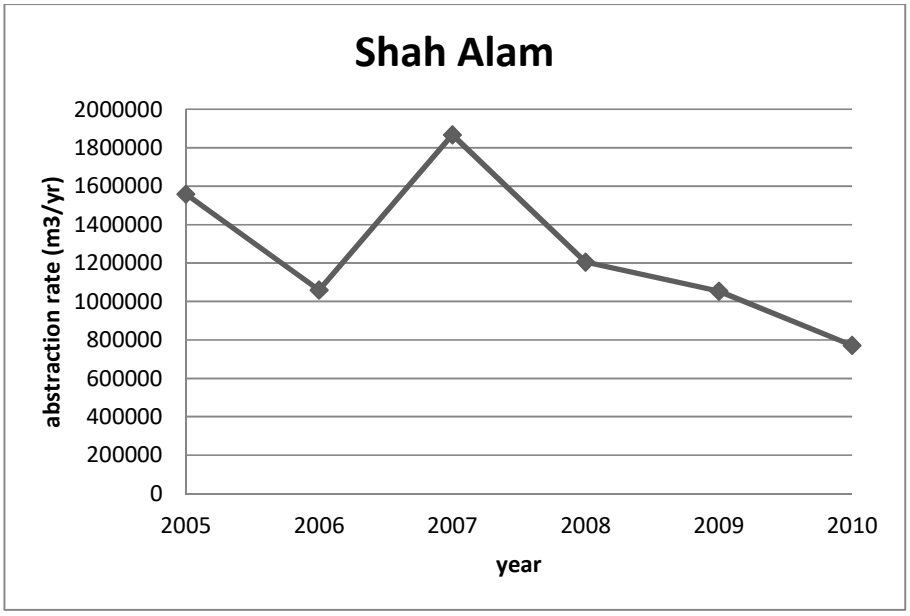

Figure 3.28 The abstraction record in Shah Alam from 2005 to 2010

Table 3.12 The annual abstraction rate record for wells in Shah Alam

	Abstraction record (m^3/yr)					
	2005	**2006**	**2007**	**2008**	**2009**	**2010**
Aquatic International 3		600	600	600	600	600
Aquarium Express		600	600	600		600
Aquatic International 2		300	300	300	300	300
Scientex Polymer			72708	72708	72708	72708
Anshin Steel	16912	16912	16912	17472	17472	17472
Ansell TW1	76380	76380	76380	52682.4	29404.8	29404.8
Ansell TW 7			58692	44481.6	41727.6	41727.6
Canon Opto TW2		71832	71832	70080	59940	30660
Good Year 1	36135	36135	22770			
Proton A	19200	19200	19200	19200	19200	
MT Pictures TW1	76285					
MT Pictures TW2	108405					
MT Pictures TW3	68255					
MT Pictures TW4	112420					
MT Pictures 5	100375					
Panasonic TW2	21080	21080	24800	20160	20160	16200
Suzuki Latex	16500	16500	16500	16500	16500	16500
Ansell TW5	44220	44220	44220	34261.2	33487.2	33487.2
Canon Opto 4		162936	162936	162936	87600	39420
Ansell TW6			119136	80658	102578.4	102578.4
Canon Opto TW1		127720.8	127720.8	127720.8	74460	56940
AESBI	21900	21900	21900	21900		12539.23
Carlsberg No 2	219000		216000	11826	31528.7	
Gaya Color Lab	4800	4800	4800	4800	4800	4800
Proton B	38400	38400	38400	38400	38400	
Carlsberg No. 1	219000		216000	168849	160143.8	131400
Carlsberg No. 3			77760			
Universal Nutri Beverages	7300	7300	7300	7300	7300	7300
Panasonic 1	21080	21080	24800	23040	19800	16200
Ueda Plating 1	74460	91104	91104	2828.8	2828.8	3029.25
Mitsui High Tech		2000	2000	2000	2000	2000
Pokka Ace	56160	56160	56160	56160	55555.2	68766
CCM Fertilizers 1			54208	54208	54208	
Ansell TW2	44220	44220	44220	36154.8	17715.6	17715.6
Ansell TW3	96480	96480	96480	27727.2	49762.8	49762.8
Ansell TW4	60300	60300	60300	34056	31341.6	31341.6
Ueda Plating 2		21204	21204	1305.6	1533.25	
TOTAL	**1,559,267**	**1,059,184**	**1,867,763**	**1,204,959**	**1,052,828**	**771,499**

Table 3.13 The daily abstraction record and duration of pumping for wells in Shah Alam

	Duration of pumping (hour)	Pumping days
Aquatic International 3	10	12
Aquarium Express	10	12
Aquatic International 2	5	12
Scientex Polymer	24	365
Anshin Steel	16	302 (2005-2007) 312 (2008-2010)
Ansell TW1	24	335
Ansell TW 7	24	365
Canon Opto TW2	24	365
Good Year 1	11	365
Proton A	8	240
MT Pictures TW1	24	365
MT Pictures TW2	24	365
MT Pictures TW3	24	365
MT Pictures TW4	24	365
MT Pictures 5	24	365
Panasonic TW2	10	248
Suzuki Latex	24	275
Ansell TW5	24	335
Canon Opto 4	24	365
Ansell TW6	24	365
Canon Opto TW1	24	365
AESBI	8	365
Carlsberg No 2	24	365
Gaya Color Lab	4	240
Proton B	8	365
Carlsberg No. 1	24	360
Carlsberg No 3	24	360
Universal Nutri Beverages	24	365
Panasonic 1	24	248
Ueda Plating 1	24	365
Mitsui High Tech	24	365
Pokka Ace	24	312 (2005-2007)
	24	365 (2008-2010)
CCM Fertilizers 1	24	308
Ansell TW2	24	335
Ansell TW3	24	335
Ansell TW4	24	335
Ueda Plating 2	24	365

3.4.4 River flows

River flows can be investigating by analysing hydrographs and their relationships with rainfall. For the Damansara river, only river stage data are available. Figure 3.29 shows the response of river stage to rainfall. River stage increases with rainfall in the beginning and at the end of each year due to the monsoon season.

River stage increases gradually as observed at both stations since 2002. The significant increases started in August 2008 as observed at the TTDI station and in November 2009 as observed at the Batu Tiga station. However, river stage measured at the TTDI station stays at ~3.7m even though it received less rainfall starting in May 2009. This might be because the groundwater inflow to the river increases and this might possibly be related to decreases of groundwater abstraction as discussed in previous section. However, the rates of abstraction are small (change in abstraction ~ 10^6 m^3/y, discharge of Klang ~ $20m^3/s$ (Figure 3.30), i.e. < 0.2%) and other causes are more likely (e.g. change in rainfall intensity, change in urban drainage measures).

Figure 3.30 shows the hydrograph of the Klang river from 1973 to 2009. Figure 3.31 shows the relationship of the Klang river hydrograph with rainfall. River flow increases with rainfall as expected. Lower river flows are observed in 1982, 1983, and 2001 to 2005. The low river flows in 1982 and 1983 were related to El Nino events which will be explained further in the next chapter.

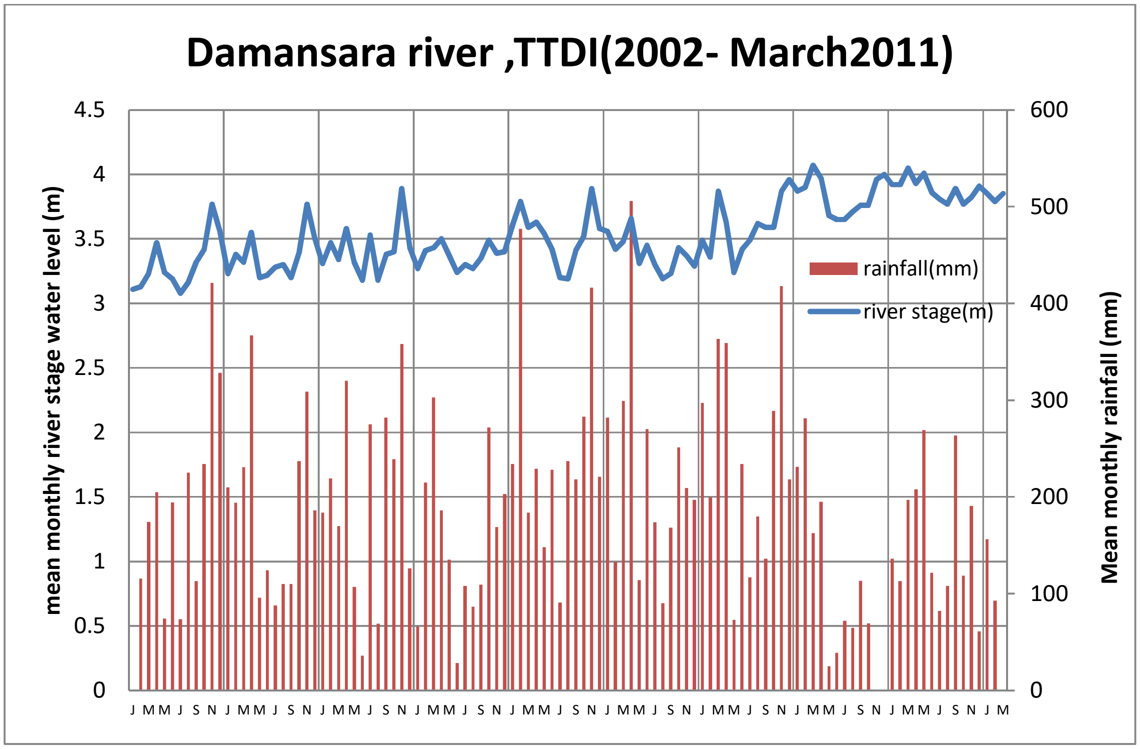

Figure 3.29a)The relationship between rainfall and Damansara river stage (TTDI station).

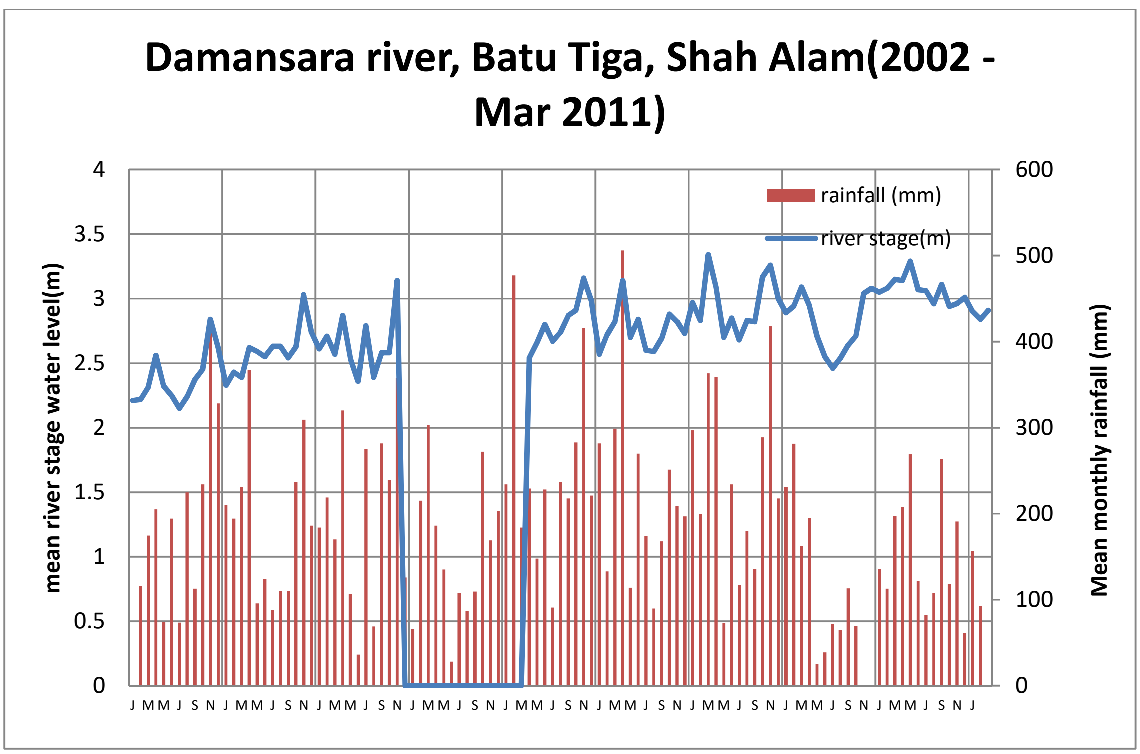

Figure 3.29b) The relationship between rainfall and Damansara river stage (Batu Tiga Station).Data in 2005 is missing.

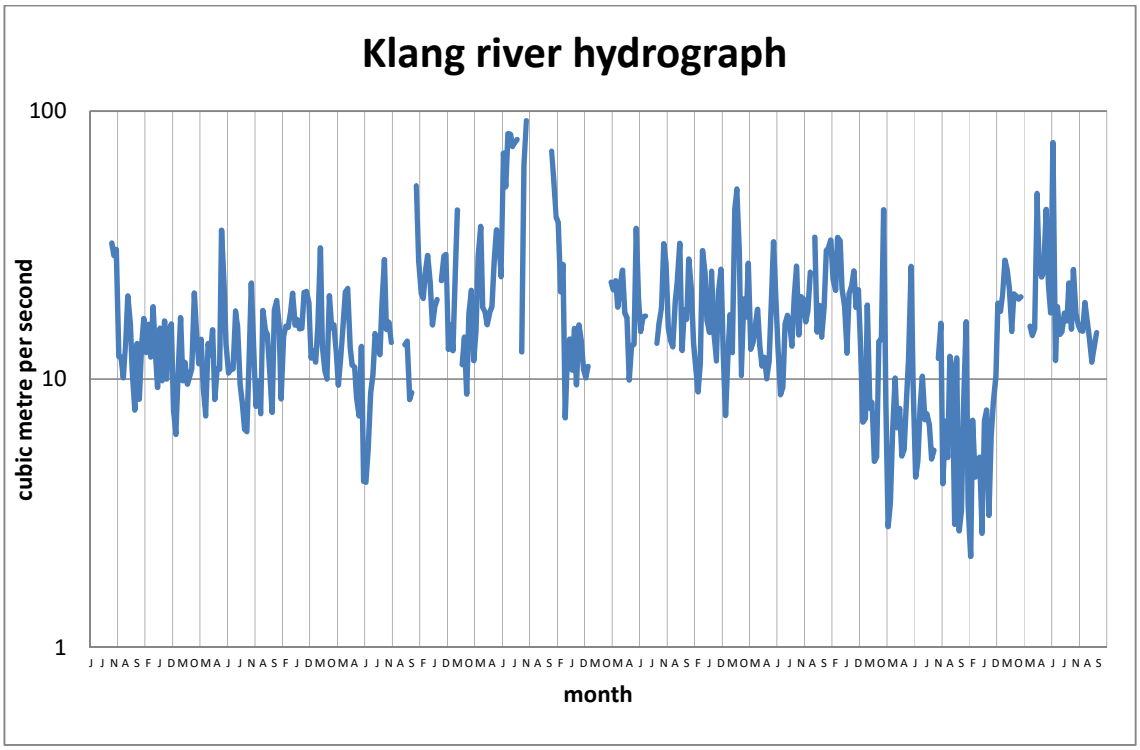

Figure 3.30 Klang river hydrograph from 1973 until 2009.

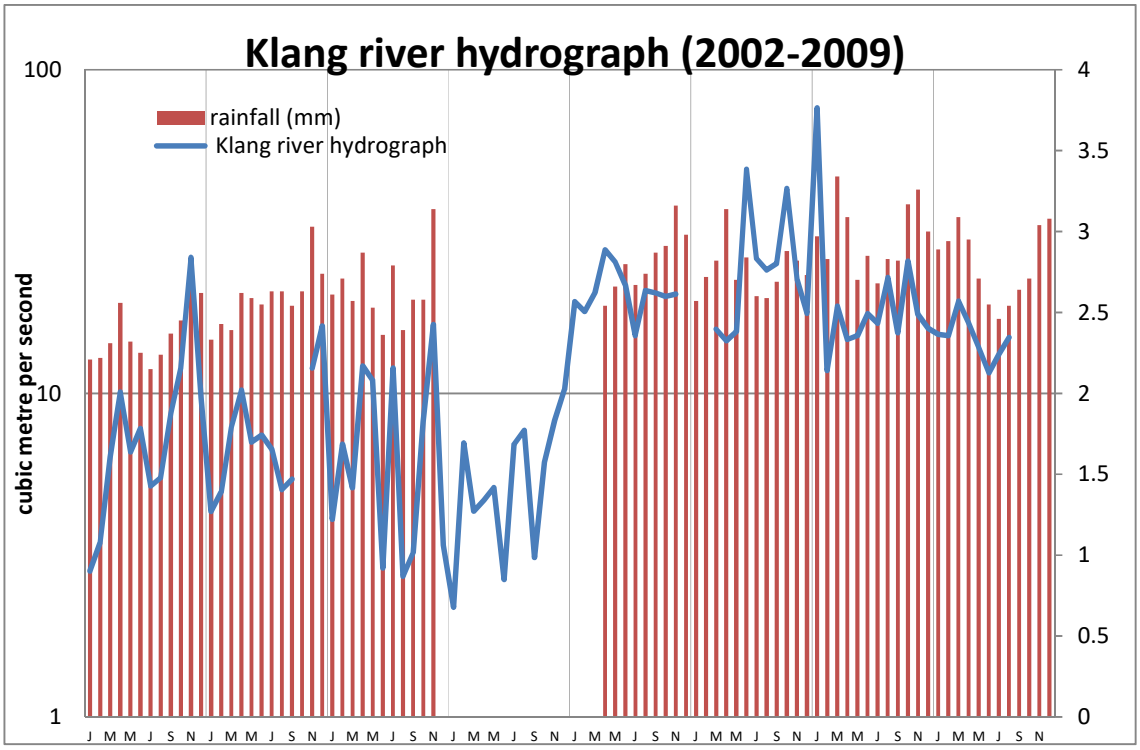

Figure 3.31 Hydrograph of Klang river and corresponding rainfall records.

3.4.5 Groundwater head distribution

The landscape and the drainage pattern of the study area have been studied by assessing information from topographic maps, geological maps and satellite images. The information obtained is useful to identify the sub areas of possible groundwater recharge and the possible discharge locations for groundwater flow. Most of the tubewells in the aquifer are near to the rivers.

Despite the very limited and poorly distributed data and the numerous water bodies an attempt will be made to construct a partial, indicative piezometric surface map for Shah Alam. Groundwater in Shah Alam will be assumed to following the topography. There are two major identified groundwater divides: the granite outcrop at the east of the study area; and to the west of the Renggam river. Using this as the basis, and taking the earliest head data available for each well (assumed to have the minimum impact from pumping – see above), the possible groundwater head distribution in Shah Alam is as shown in Figure 3.32. The areas without groundwater head contours are due to lack of water level information. In the Shah Alam area the heads in the rivers are close to sea level, i.e. approximately at 0 m b.s.l suggesting that either permeability is high or flow is low. Flow may be low on the river flood plains if there is up-flow spring discharge. However, it appears that the groundwater in Shah Alam is discharging towards the rivers since the groundwater heads are higher than the water levels in the river. In all but one case the heads close to the river are close to the heads in the river and lower than the heads at the sites between the rivers. The groundwater head is high to the north and to the east of Shah Alam.

Taking the contour map of Figure 3.32 it is clear that there are relatively steep gradients especially in the direction parallel with northwest-southeast (though much less so to the

southeast of the Damansara) and much shallower gradients in the northeast-southwest direction. A simple 1D model has been applied to this contour map to see what might cause these different gradients and also to see if the map is broadly consistent with what is known of the transmissivity and recharge so far. The model was obtained by integrating the general steady-state 1D groundwater flow equation ($d^2h/dx^2 = - q/T$; h = head, x = distance, q = recharge rate, T = transmissivity) with the following boundary conditions: $dh/dx = 0$ at $x = 0$ (the water divide); $h = H$ at $x = L$ (the river). The equation is

$h = -qx^2/(2T) + H + qL^2/(2T)$.

Applying this simple model to the lines on Figure 3.32 marked A to D indicates that for example with a recharge of 200 mm/y, T would have to vary in the order 50, 500, 35, and 150 m^2/d. These values are within the range estimated in Chapter 5. If R is increased to 400 mm/y, section A and C could be represented using T values of around 150 and 80 m^2/d. These calculations are very approximate but they indicate that the contours may be reasonable and may suggest some anisotropy.

As over 60% of the wells in Shah Alam have drawdowns of greater than 30m (Section 3.2.1) it means that the water levels are a lot below the river levels and that there is an opportunity for water to flow into the aquifer from the rivers particularly given that they flow along faults in many cases. The data are not enough to determine a pumped water level map for the whole Shah Alam area to support this idea; since the periodic water level data are only available for the Ansell area.

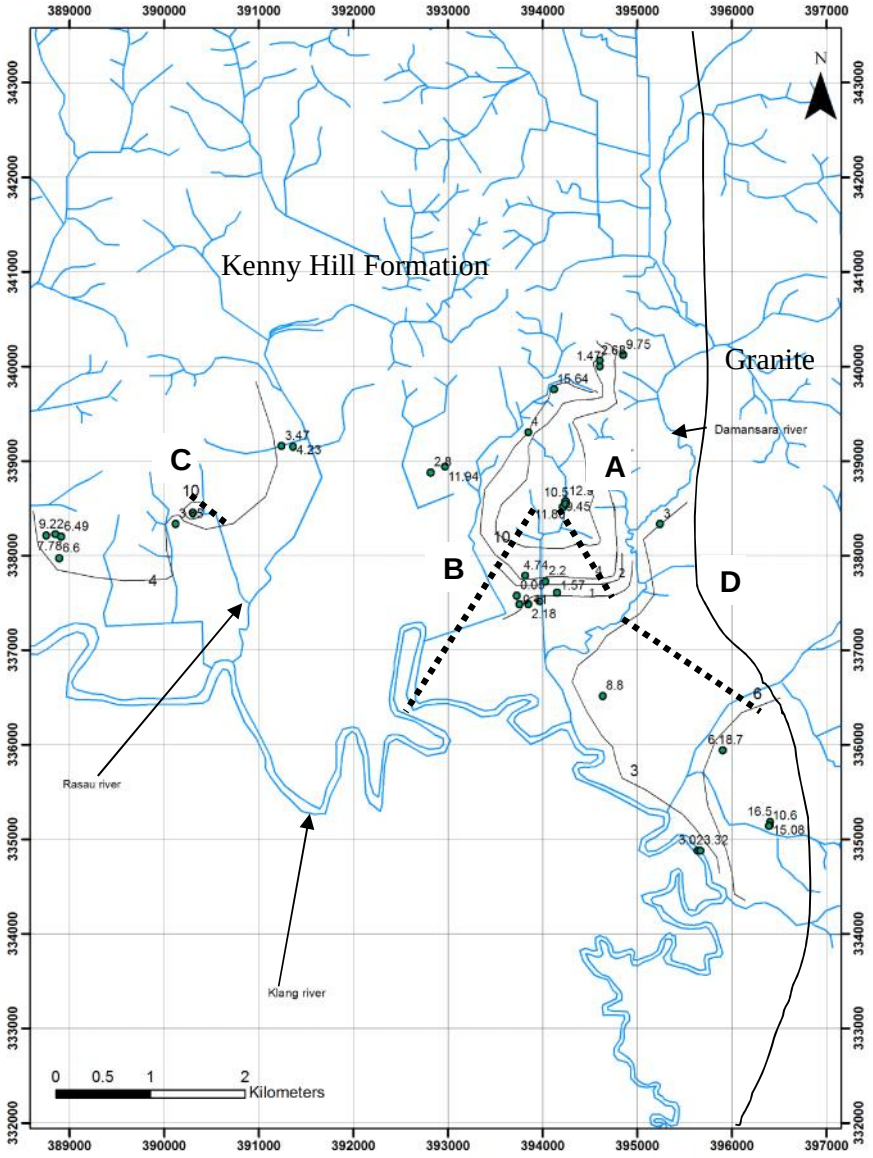

Figure 3.32 The groundwater head distribution of the study area

3.5 Conclusion

This section summaries the discussions of the chapter. The aquifer is a hardrock one consisting of fractured indurated arenaceous slightly metamorphosed rocks (quartzite, sandstone) and argillaceous rocks (‘shale’, phyllite). It is permeable to at least 180 m below ground level, the rock permeability coming almost entirely from fracturing. The permeability

is not high with median drawdowns being over 30m for median abstractions of 300 m^3/d. It is covered by a weathering zone up to 60m thick which is clayey and of low permeability where the argillaceous sediments are dominant and more sandy where the arenaceous rocks are dominant. Faulting has two dominant directions northwest-southeast and northeast-southwest. The former is associated with quartz veining more commonly than the latter and the latter is extensional. So the northwest-southeast faults are likely to be lower permeability and may at least partly compartmentalise the aquifer. The rivers also have reaches whose directions seem to be controlled by the faulting and this may help connect rivers and aquifer. The heads in the aquifer are usually a few metres below ground level and reflect the limited topographic relief, with flow to the rivers from the interfluves areas. Limited number of water level measurements indicate a range of response types from quick to slow probably dependent on the sorts of weathering layers.

Figure 3.34 summaries some of the main points of the initial conceptual model. The section is for northwest-southeast as shown in Figure 2.3. To the southeast the granite rises close to groundlevel and the metasediments are mainly argillaceous with a clayey weathering layer. To the northwest the granite is much deeper always below the base of the wells and arenaceous deposits dominate with more sandy and permeable weathering layer. The weathering layer in the southeast is almost always saturated and probably much of that to the northwest is also nearly saturated a lot of the time. Flow occurs towards the rivers (Klang, Damansara and Renggam) under no pumping conditions shown. Pumping boreholes often have drawdowns greater than 30m and this means that locally the piezometric surface and hence flows will be very much different. This reduction in head will induce more recharge through the weathering layer and will cause the wells to become locally unconfined (or semi-confined).

The hydrogeological conceptual model developed in this chapter will be tested/ investigated further using numerical modelling in the next Chapter where the recharge processes occur in study area will be discussed.

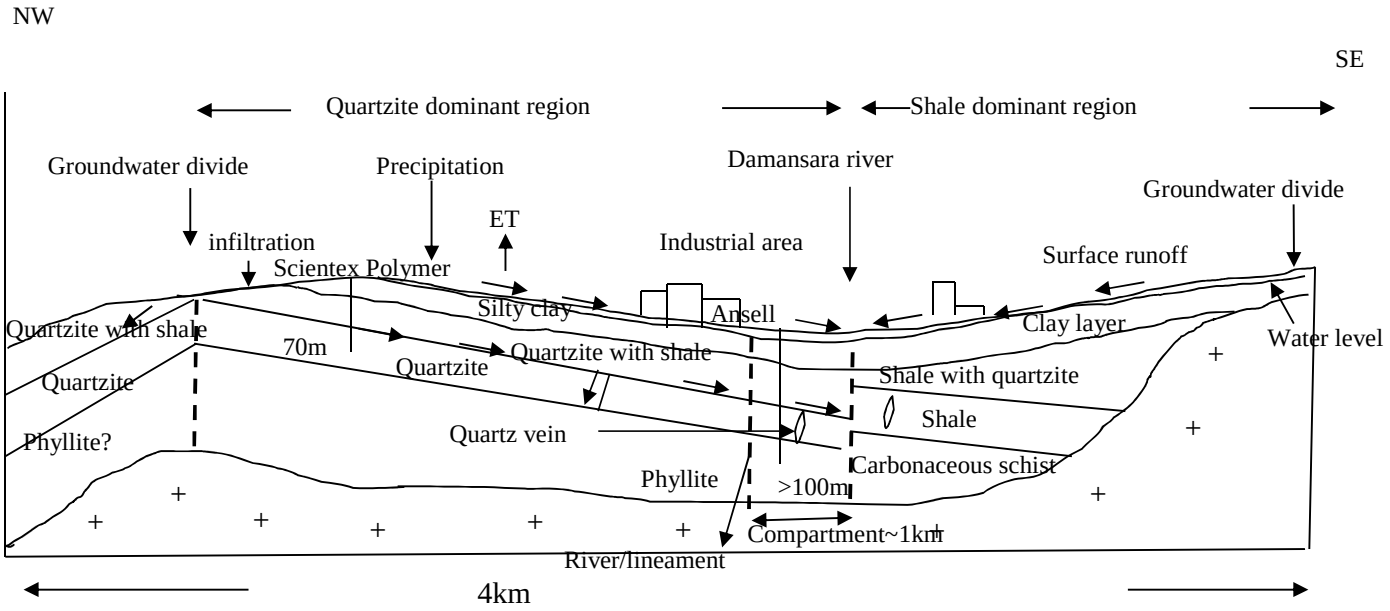

Figure 3.34 A hydrogeological conceptual model of Shah Alam under no pumping condition

4.0 GROUNDWATER RESOURCES IN SHAH ALAM.

4. 1 Introduction

In this chapter, all the possible potential recharge in Shah Alam will be discussed. As an equatorial climate country, Malaysia is blessed with hot and rain all year. Therefore, the main recharge source is rainfall which will be discussed in next section (Section 4.2). In Section 4.3, all the potential sources of recharge such as leakage from pipe utilities in urban area like Shah Alam will be discussed. The issues regarding the changes of hydrological processes such as the reduction of water infiltrates the ground and the increment of surface runoff due to development also will be in this section. Recharge estimation will be discussed in Section 4.4 and the conclusion will be in Section 4.5.

4.2 Meteorological background

4.2.1 Introduction

The climate of southeast Asia region is influenced by the pattern of the air stream (Figure 4.1). The Northeast Monsoon dominates from late November until early March while the Southeast Monsoon dominates from June to October. The months in between, April to May and late October to early November, are the transitional periods. Heavier rainfall is expected during the monsoons and also during April and October in the transitional periods.

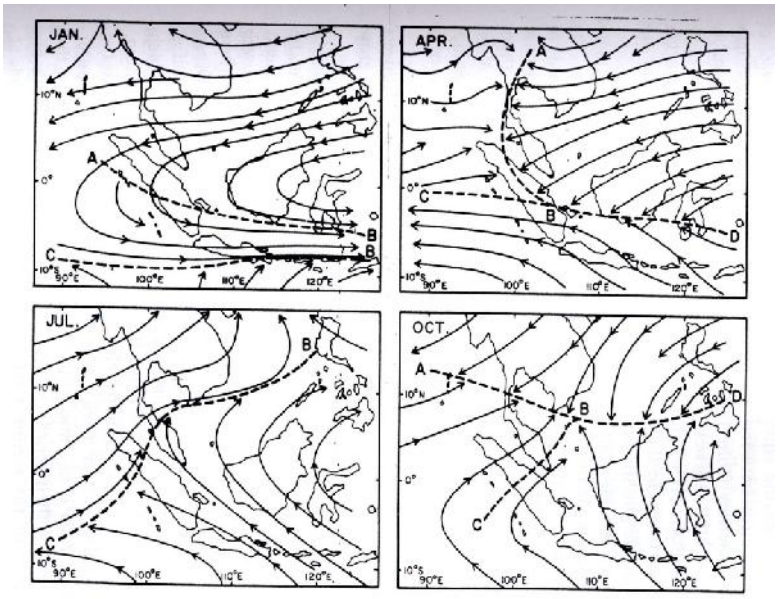

Figure 4.1 The pattern of air streams in the southeast Asia region (Sham 1980)

The climate of the Klang Valley area has been well-studied, especially in Kuala Lumpur and associated cities such as Petaling Jaya, Shah Alam and Klang, by Sham (1973, 1980, 1990). He discovered that the temperature in Kuala Lumpur-Petaling Jaya area is higher than rural areas nearby – an urban heat island effect. Sham (1980) summarizes the differences in other climatic elements between the urban and rural areas in Table 4.1.

Table 4.1 The differences in climatic elements of Klang Valley area compared with nearby rural areas (from Sham 1980)

Elements	Comparison with rural environment
Global radiation	Evidence of low values for urban location was unclear. Perhaps due to microclimatic factors of instrument sites
Sunshine duration	9-10% less
Temperature Annual mean Nightime	 1-2 ^{o}C more 6-7 ^{o}C more
Wind speeds With light winds <1.5ms^{-1} With winds >1.5ms^{-1}	 40-50% more 9-10% less
Precipitation	Slight increase in the downwind areas but statistically not significant
Relative humidity Annual Nighttime	 2-4% less 10-15% less

The meteorological data for Shah Alam will next be analysed to see the climate pattern of study area. The climate pattern of the study area is examined using sets of meteorological data and precipitation records. These data have been provided by the Malaysian Meteorological Department and Department of Irrigation and Drainage Malaysia. The meteorology data available is air temperature, wind speed, air humidity, solar radiation and pan evaporation data. The meteorology data is measured at Subang Airport. The data available for this study are from 2004 to 2008 and are at a daily interval.

4.2.2 Precipitation

Dale (1960) described the daily rainfall pattern of Malaysia as similar throughout the year. There are three types of diurnal rainfall pattern in Malaysia; the west coast type, the east coast type and the inland type. The daily rainfall pattern for

the Kuala Lumpur – Petaling Jaya area is the inland type where it rains in the afternoon. The heavy and high intensity rainfall is in October, November and December (October is heaviest) for north of the Kuala Lumpur area and in March and April for south of the Kuala Lumpur area. The maximum rainfall is in April. The driest months are February and July. The driest month is July.

Figure 4.2 shows the rainfall stations outside and inside study area. The rainfall stations outside Shah Alam have data back to 1942 (Pusat Penyelidikan Getah Sg.Buloh station). The historical rainfall data are useful to see how the rainfall pattern changes with time. The historical rainfall pattern later will be compared with recent rainfall data recorded at five stations in the Shah Alam area.

The period of study interest is mainly over the last ~10 years, as this is the date of the installation of the first wells in Shah Alam (2001). There are four rainfall stations in Shah Alam area but only two stations provide data within the required period.

The rainfall data for these stations have been checked using the double mass technique (Allen et al., 1998). The cumulative data from rainfall stations will be plotted against cumulative data from another rainfall station which is considered homogeneous. The time length and elevation for both rainfall stations must be the same. The rainfall data from station TTDI are checked against rainfall data from the Subang station as shown in Figure 4.3 while rainfall data from UiTM are checked against rainfall data from the Pusat Penyelidikan Getah Sungai Buloh station (Figure 4.4). The data error is identified when the data deviate

from a straight line correlation as may be the case in Figure 4.4. After checking the rainfall data from UiTM station, less rainfall was recorded during the identified period which is possibly due to instrumentation error.

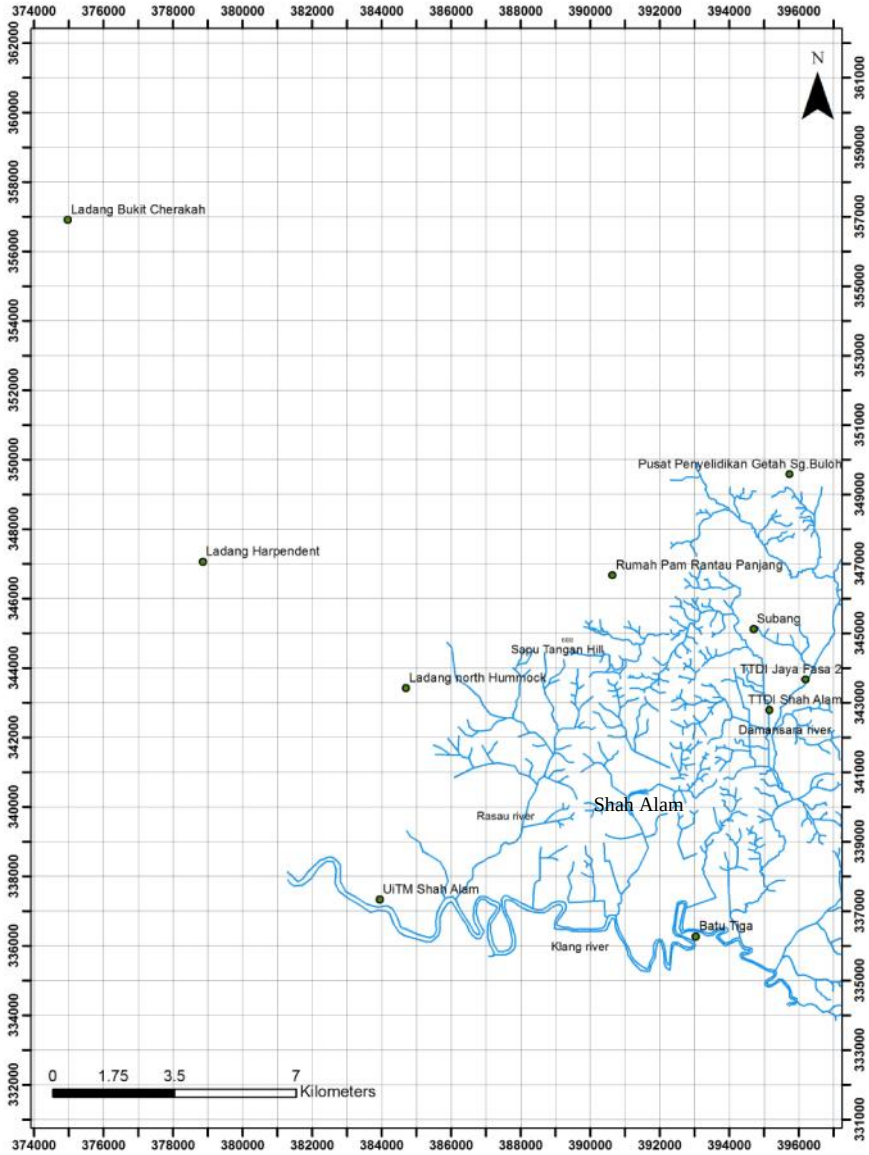

Figure 4.2 The rainfall stations outside (Ladang Harpendent, Ladang North Hummock and Pusat Penyelidikan Getah Sg.Buloh), and inside the study area

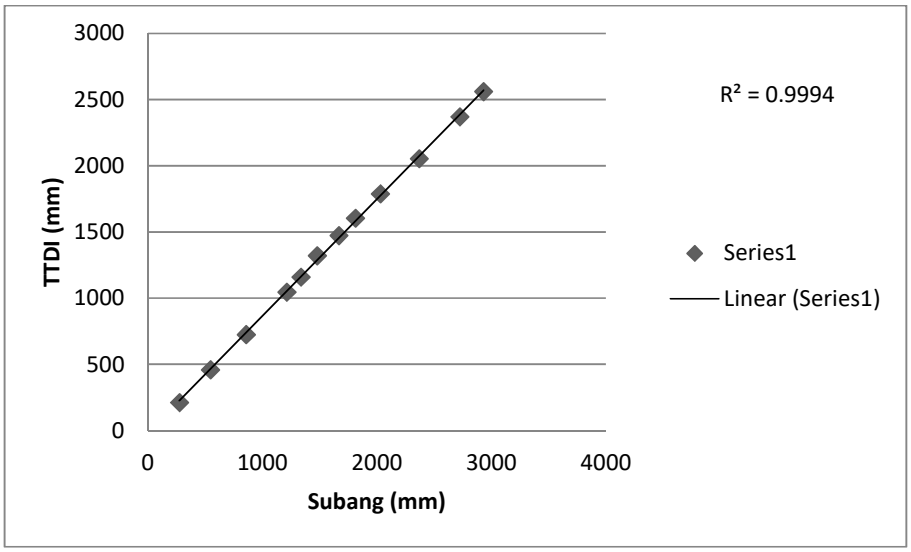

Figure 4.3 Double mass plot for rainfall at TTDI and Subang station

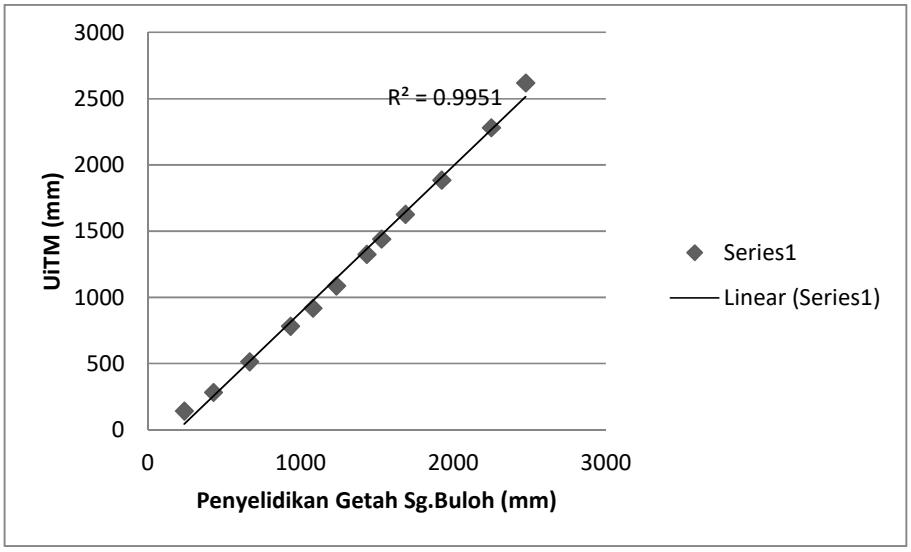

Figure 4.4 Double mass plot for rainfall at UiTM and Pusat Penyelidikan Getah Sg.Buloh station

Figure 4.5 shows the annual rainfall for each of the stations outside Shah Alam area. The mean annual rainfall is 2183mm/year (Ladang North Hummock), 1886mm/year (Ladang Harpenden) and 2393mm/year (Pusat Penyelidikan Getah Sg.Buloh). This variation is possibly due to the different elevations for each station. Pusat Penyelidikan Getah Sg Buloh is at 45m above sea level while Ladang Harpenden is at 4m a.s.l.

The rainfall ranges from 2000 to 2500mm until 1970. The rainfall totals vary more widely after 1970, from 1200 to 2500mm (Figure 4.6). The highest rainfall recorded, over 3000 mm/year, was recorded at Ladang North Hummock in 1959 and at Pusat Penyelidikan Getah Sg. Buloh in 2006. Figure 4.7 shows the seasonal rainfall for all three stations. The driest month is June and the wettest month is November. This pattern will next be compared with the annual rainfall pattern observed at rainfall stations in Shah Alam.

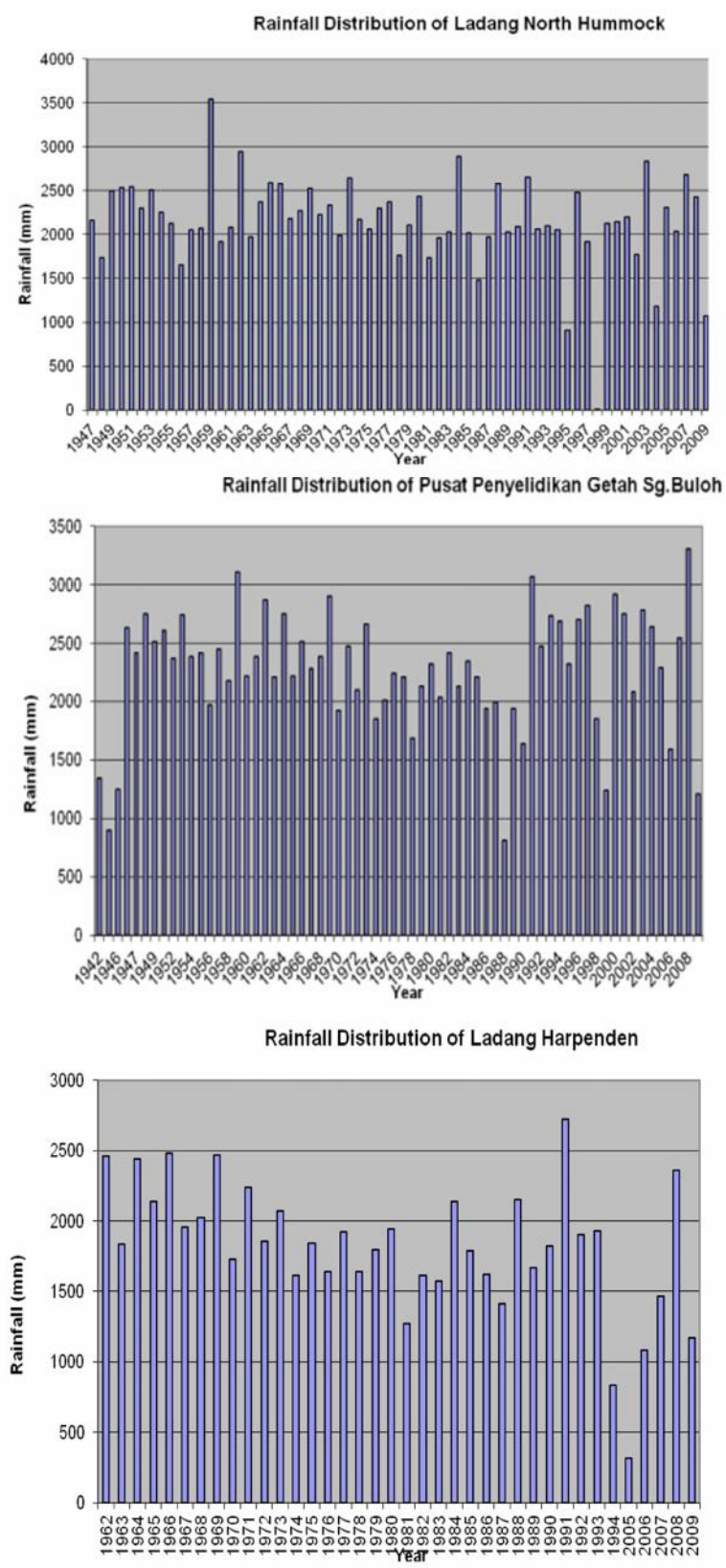

Figure 4.5 The rainfall stations outside Shah Alam area (data from Malaysian Meteorological Department and Department of Irrigation and Drainage Malaysia).

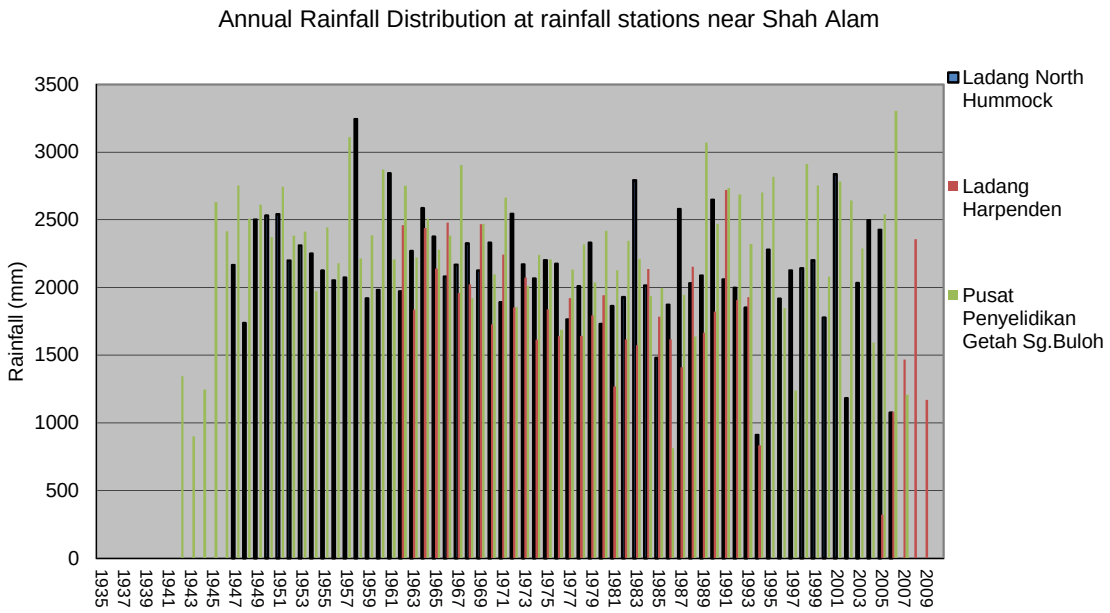

Figure 4.6 The annual rainfall recorded at three stations outside Shah Alam area (data from Malaysian Meteorological Department and Department of Irrigation and Drainage Malaysia)

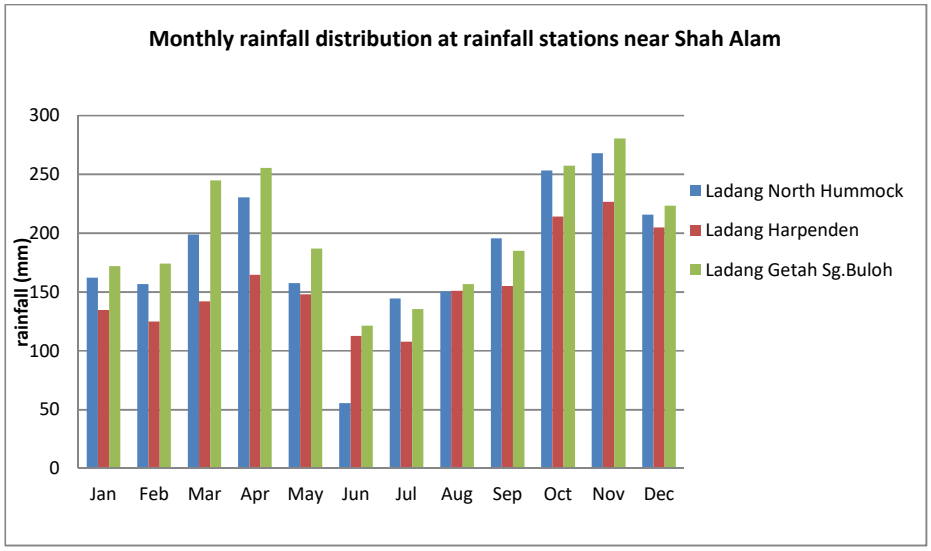

Figure 4.7 The monthly rainfall pattern for three rainfall stations outside Shah Alam area (data from Malaysian Meteorological Department and Department of Irrigation and Drainage Malaysia)

Table 4.2 shows the years which received less than 2000mm/year of rainfall. All stations received less than 2000mm/year of rainfall in 1963, 1967, 1970, 1972, 1974, 1977-1979, 1981-1983, 1986-1987 and 1997. Heavy rainfall over 3000mm/year was recorded in 2006 and 2008 and this caused a series of flash floods in Shah Alam.

The extreme weather which caused droughts and floods in Malaysia is linked with El Nino and La Nina phenomena. El Nina is warm phase and La Nina is a cold phase. This phenomenon oscillates at intervals of 2-7 years. The El Nino has caused drought (hot weather) conditions triggering forest fires and haze in Southeast Asia in the past (Lim & Azizan 2004). There have been 12 major El Nino events recorded since 1950. The strongest events are recorded in 1982-83 and 1997-98. La Nina brought floods in 2006 and 2008 due to heavy rainfall.

Table 4.2 Years with less than 2000mm/yr of rainfall (data from Malaysian Meteorological Department and Department of Irrigation and Drainage Malaysia)

Station	Elevation above mean sea level (m)	Period with no measurement	Year which receive less than 2000mm/year of rainfall
Ladang North Hummock	NA	1946,1956, 1995(Feb-Sept), 1998,2004(Aug-Dec),2005,2009 (Nov-Dec)	1948,1960,1961,**1963, 1967**,**1970**,**1972**,**1977, 1978,1979,1981,1982, 1983,1986,1987**,1997 **1993**-1994,2002
Ladang Harpenden	4	1961,1995, 2004(Aug-Dec), 2005(Jan-Sept), 2009(Nov-Dec)	**1963**,**1967**,**1970**,**1972**, **1974**,**1975-1983**, **1985-1987**, 1989-1990,1992-1993,2007
Pusat Penyelidikan Getah Sg.Buloh	45	1942 (Jan-Jul), 1943 (Jun-Dec), 1944-1945, 1946(Jan-Jul), 1988(Apr-Nov), 1999(Jun-Nov), 2009(Okt-Dec)	1956,**1970, 1974,1978,** 1986,1987, 1989,1990, 1995-**1997**

Shah Alam has received heavy rainfall every year except in 2009 (Figure 4.8). The heaviest rainfall recorded is in the La Nina years 2006 and 2008 (>3000mm/year). Figure 4.9 shows the average monthly rainfall distribution. The wettest month is in April and November with >250 mm rainfall per month. The driest period of the year is in May. The rainfall patterns outside and inside study area are similar.

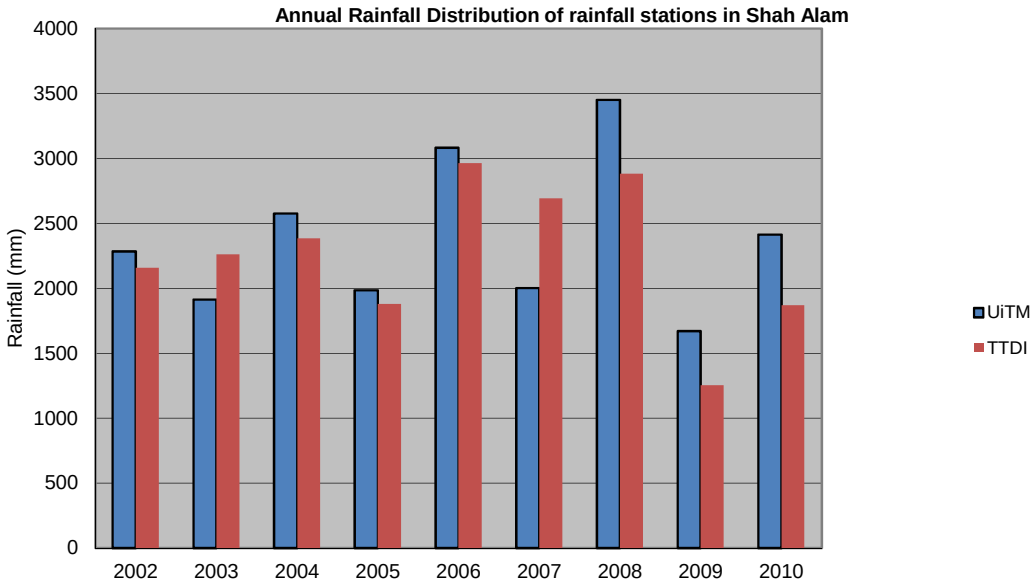

Figure 4.8 The annual rainfall for stations in Shah Alam area (data from Malaysian Meteorological Department and Department of Irrigation and Drainage Malaysia).

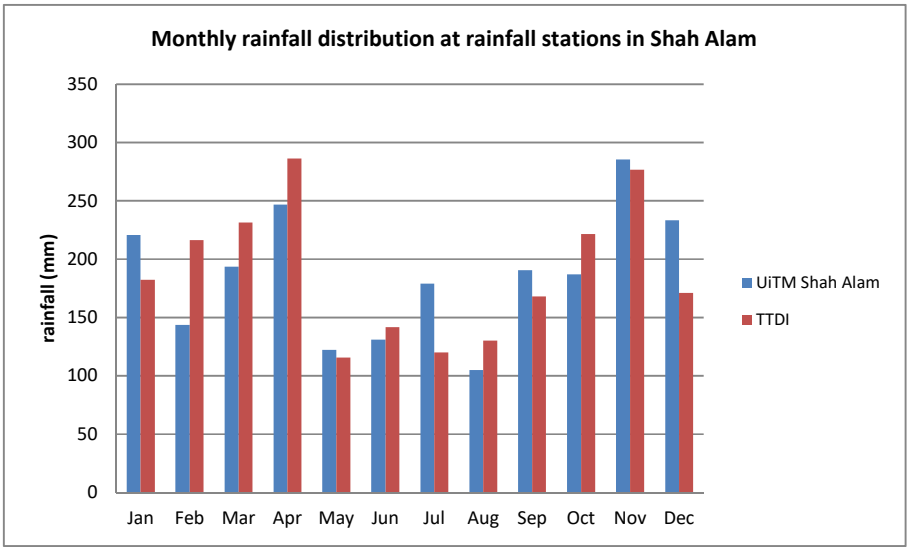

Figure 4.9 The average monthly rainfall distribution in Shah Alam area (data from Malaysian Meteorological Department and Department of Irrigation and Drainage Malaysia).

4.2.3 Temperature

The temperature of Malaysia is high and with limited change through the year (Dale 1960). Figure 4.10 shows the average temperatures recorded at Subang station from 2004 to 2008. The temperatures recorded every month and the average value is shown in Table 4.3. The highest mean monthly temperature was recorded in May 2005 (28.7 ^{o}C) and the lowest was recorded in November 2006 (25.4 ^{o}C). The temperature is highest in the middle of the year with the peak of temperature in March, May and July. The temperature then decreases until December. This pattern repeats every year except in 2005. In 2005, the temperatures are higher and constant at 28 ^{o}C from January until June. The temperature drops in July and increases until September. The temperature decreased to the lowest point in December.

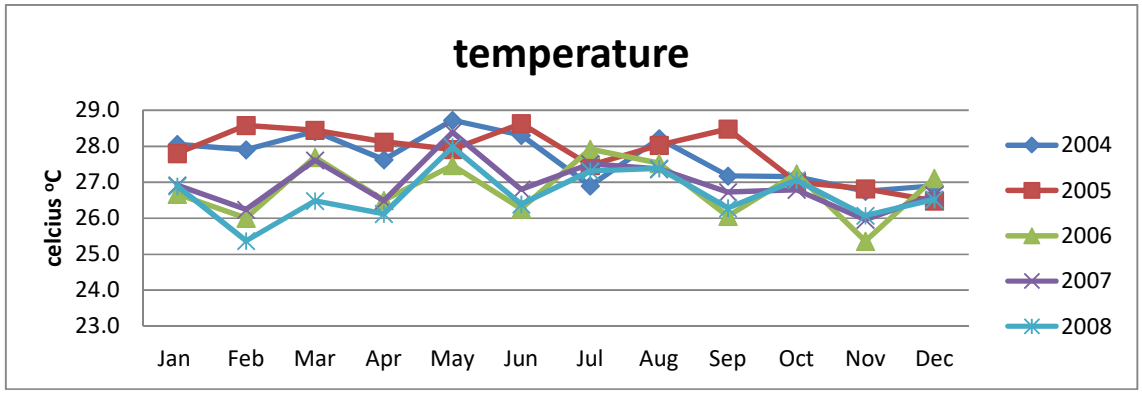

Figure 4.10 The average temperature recorded at Subang station from 2004 to 2008 (data from Malaysian Meteorological Department and Department of Irrigation and Drainage Malaysia).

Table 4.3 The monthly average temperature recorded at Subang station from 2004 to 2008 (data from Malaysian Meteorological Department and Department of Irrigation and Drainage Malaysia)

Year	Jan	Feb	Mar	Apr	May	Jun	Jul	Aug	Sep	Oct	Nov	Dec	Average
2004	28.1	27.9	28.4	27.6	28.7	28.3	26.9	28.2	27.2	27.2	26.8	26.9	27.68
2005	27.8	28.6	28.4	28.1	27.9	28.6	27.5	28.0	28.5	27.0	26.8	26.5	27.82
2006	26.7	26.0	27.7	26.5	27.5	26.3	27.9	27.5	26.1	27.2	25.4	27.1	26.82
2007	26.9	26.2	27.6	26.5	28.4	26.8	27.5	27.4	26.7	26.8	26.0	26.6	26.96
2008	26.9	25.4	26.5	26.1	28.0	26.4	27.3	27.4	26.3	27.1	26.1	26.5	26.66
Average	**27.3**	**26.8**	**27.7**	**27.0**	**28.1**	**27.3**	**27.4**	**27.7**	**26.9**	**27.0**	**26.2**	**26.7**	

4.2.4 Air Humidity

The humidity is measured at Subang Airport station as relative humidity. Figure 4.11 shows the monthly average humidity as observed at the station from 2004 to 2008. Table 4.4 shows the humidity average values. Most of the monthly average humidity values range between 75 and 80%. The highest annual average humidity value is recorded in 2004 (79.8%) and the lowest is 75% in 2008. It is relatively more humid in April and also at the end of the year (from October to December).

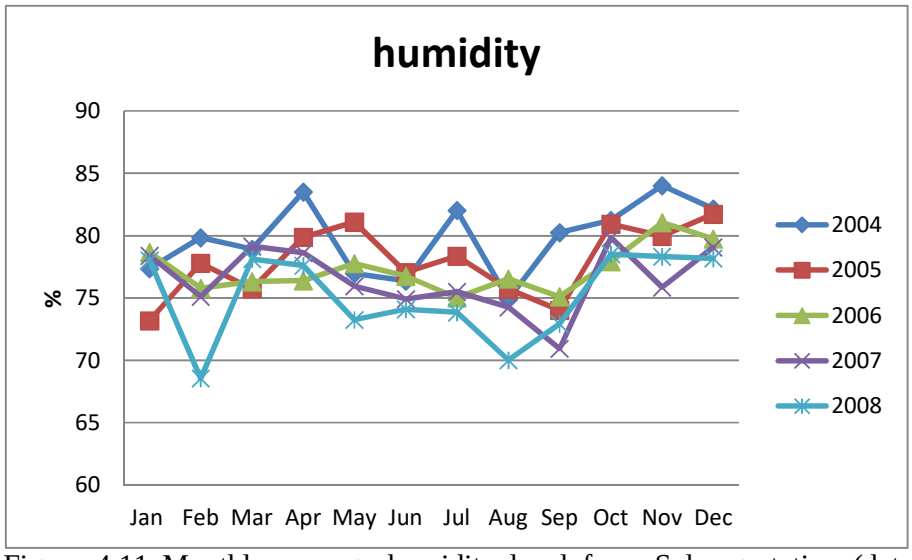

Figure 4.11 Monthly average humidity level from Subang station (data from

Malaysian Meteorological Department and Department of Irrigation and Drainage Malaysia)

Table 4.4 The monthly average humidity observed at Subang station from 2004 to 2008 (data from Malaysian Meteorological Department and Department of Irrigation and Drainage Malaysia)

Year	Jan	Feb	Mar	Apr	May	Jun	Jul	Aug	Sep	Oct	Nov	Dec	Av
2004	77	80	79	84	77	76	82	75	80	81	84	82	80
2005	73	78	76	80	81	77	78	76	74	81	80	82	78
2006	79	76	76	76	78	77	75	77	75	78	81	80	77
2007	78	75	79	79	76	75	75	74	71	80	76	79	76
2008	78	69	78	78	73	74	74	70	73	79	78	78	75
average	77	75	78	79	77	76	77	74	75	80	80	80	

Figure 4.12 shows the relationship between monthly average temperature and humidity. Temperature and humidity possibly show some general correlation though not at the end of the year. Figure 4.13 shows the relationship between annual average temperature and humidity. In general, the humidity and temperature show a decreasing trend. Figure 4.14 shows that there is an approximate positive linear relationship between annual average humidity and temperature (R^2=0.67).

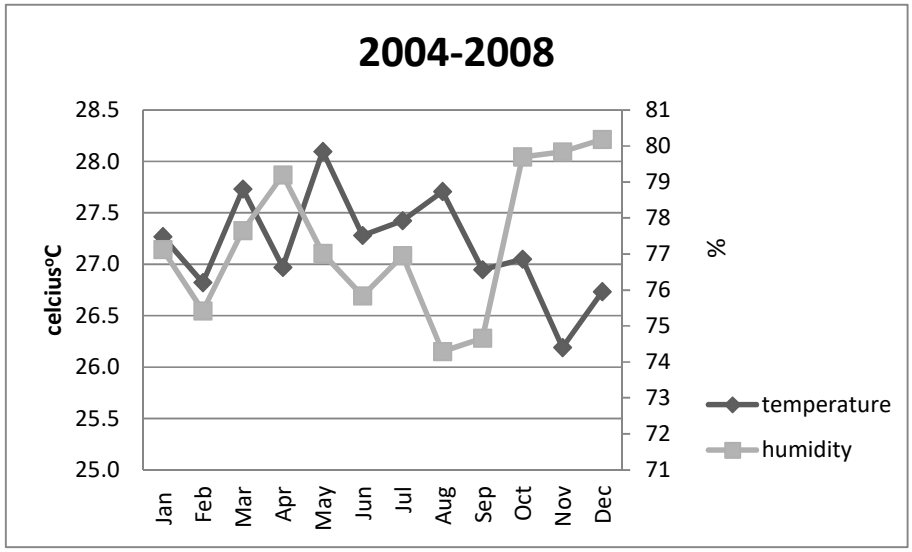

Figure 4.12 The monthly average humidity saturation level and average temperature (data from Malaysian Meteorological Department and Department of Irrigation and Drainage Malaysia)

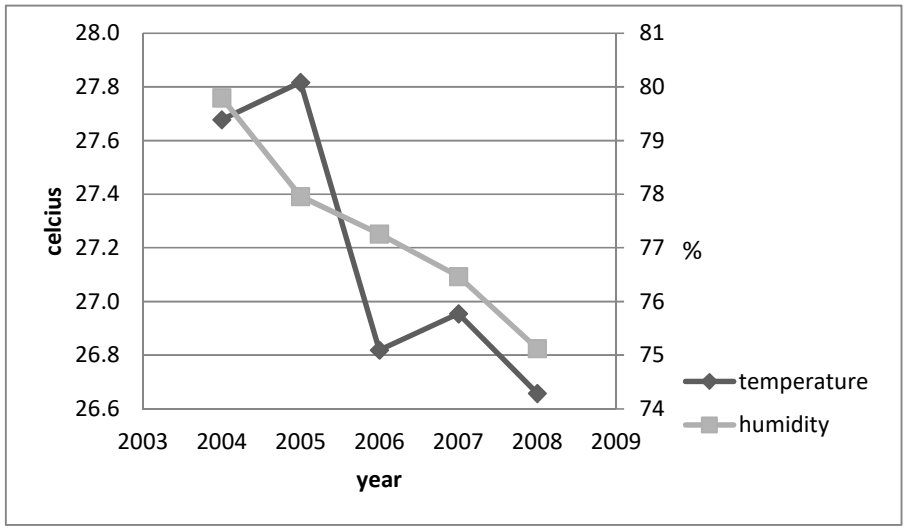

Figure 4.13. The relationship between mean annual temperature and humidity at Subang Station from 2004 to 2008 (data from Malaysian Meteorological Department and Department of Irrigation and Drainage Malaysia).

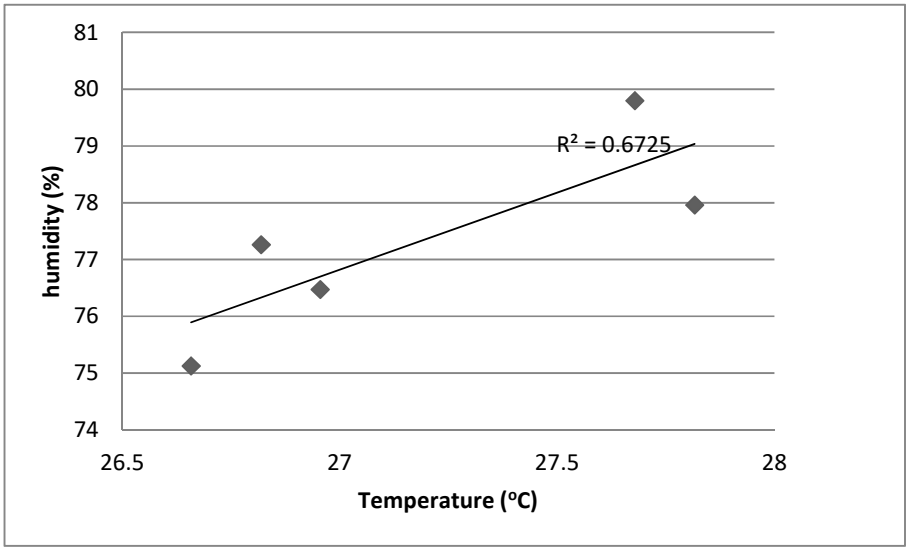

Figure 4.14. The relationship between annual average temperature and humidity for the Subang station (data from Malaysian Meteorological Department and Department of Irrigation and Drainage Malaysia).

4.2.5 Wind speed

The climate pattern in Malaysia is influenced by the direction and speed of wind (Dale 1960). Figure 4.15 shows the average monthly wind speed from 2004 to 2008. The range of the average monthly wind speed is from 1.0 to 1.5m/s (Table 4.5). The highest wind speed is in August 2004 (over 2 m/s) while the lowest wind speed is recorded in April 2005 (1 m/s).

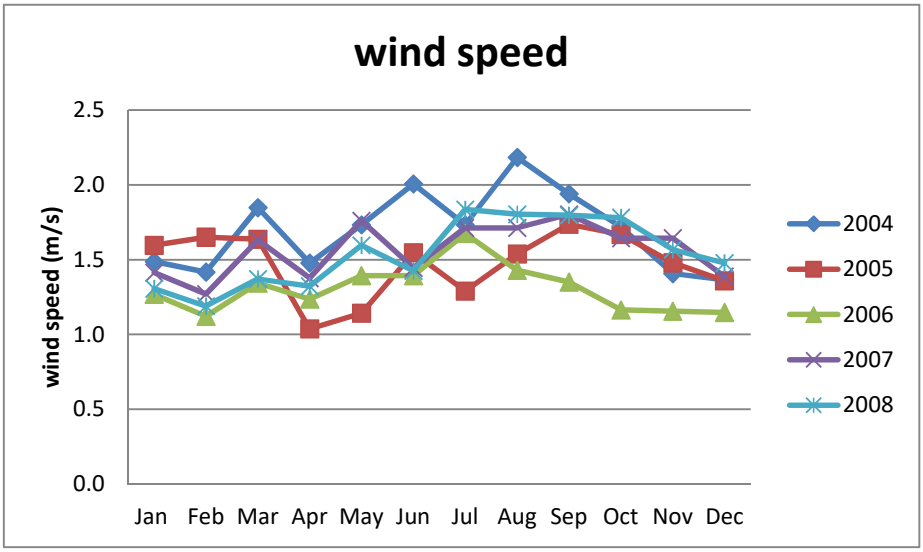

Figure 4.15 The monthly average wind speed (data from Malaysian Meteorological Department and Department of Irrigation and Drainage Malaysia)

Table 4.5 The monthly average wind speed recorded at Subang station (data from Malaysian Meteorological Department and Department of Irrigation and Drainage Malaysia)

	Jan	Feb	Mar	Apr	May	Jun	Jul	Aug	Sep	Oct	Nov	Dec	Year
2004	1.5	1.4	1.8	1.5	1.7	2	1.7	2.2	1.9	1.7	1.4	1.4	1.7
2005	1.6	1.7	1.6	1	1.1	1.5	1.3	1.5	1.7	1.7	1.5	1.4	1.5
2006	1.3	1.1	1.3	1.2	1.4	1.4	1.7	1.4	1.4	1.2	1.2	1.1	1.3
2007	1.4	1.3	1.6	1.4	1.8	1.4	1.7	1.7	1.8	1.6	1.6	1.4	1.6
2008	1.3	1.2	1.4	1.3	1.6	1.4	1.8	1.8	1.8	1.8	1.6	1.5	1.5
av	1.4	1.3	1.6	1.3	1.5	1.6	1.6	1.7	1.7	1.6	1.5	1.3	

4.2.6 Solar radiation

Solar radiation is measured by Casella bimetallic actinograph by the Malaysian Meteorological Department. Figure 4.16 shows the average radiation recorded at the Subang station. The radiation values range from 15 to 20 MJm^{-2} (Table 4.6).

The highest radiation is recorded in May 2007 (20 MJm^{-2}). Figure 4.17 shows the inverse relationship of radiation and humidity.

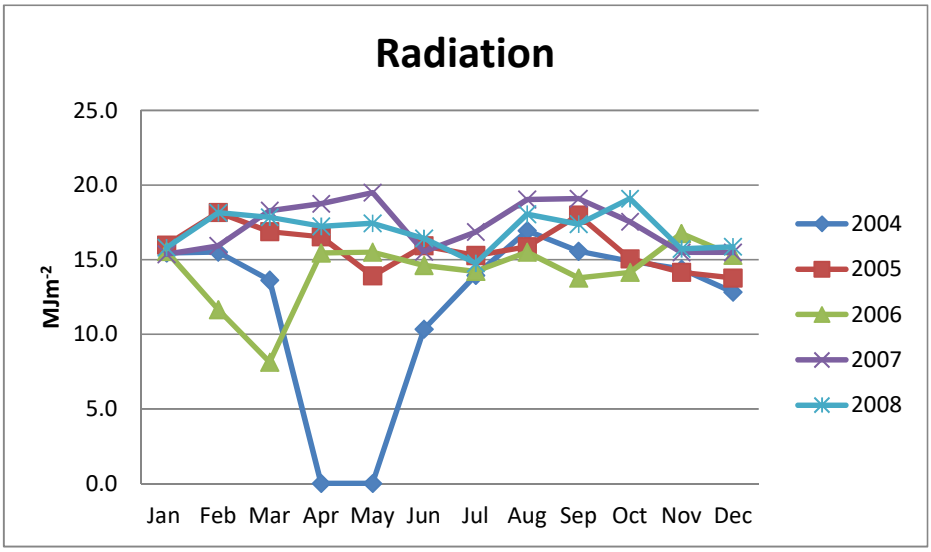

Figure 4.16 The monthly average radiation record (data from Malaysian Meteorological Department and Department of Irrigation and Drainage Malaysia).

Table 4.6 The monthly average radiation recorded at Subang station (data from Malaysian Meteorological Department and Department of Irrigation and Drainage Malaysia)

	Jan	Feb	Mar	Apr	May	Jun	Jul	Aug	Sep	Oct	Nov	Dec	Year
2004	15.5	16	14	0	0	10	14	17	16	15	14	13	12
2005	16	18	17	17	14	16	15	16	18	15	14	14	16
2006	16	12	8	15	16	15	14	16	14	14	17	15	14
2007	15	16	18	19	20	16	17	19	19	18	15	15	17
2008	16	18	18	17	17	16	15	18	17	19	16	16	17
Av	15.6	15.9	15	13.6	13.3	14.6	15	17.1	16.8	16.2	15.3	14.6	

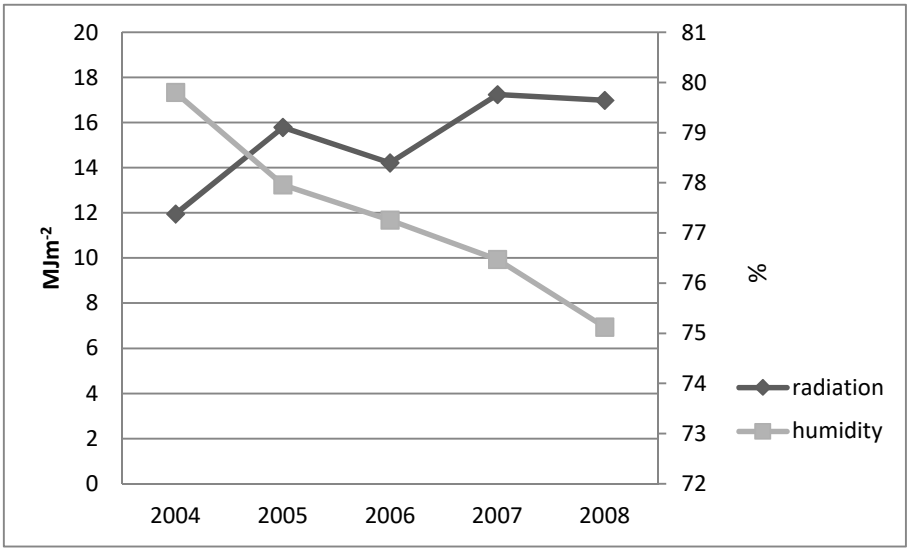

Figure 4.17. The radiation and relative humidity (data from Malaysian Meteorological Department and Department of Irrigation and Drainage Malaysia).

4.2.7 Pan evaporation

Figure 4.18 shows the average pan evaporation recorded at Subang station. The evaporation rate is measured using a US Class A evaporation pan. The evaporation value ranges from 100 to 150mm per month. However, the evaporation measured in Feb 2006 is 236 mm which is extremely high, and may be in error. Figure 4.19 shows the evaporation plotted with the precipitation for year 2006.

Figure 4.20, Figure 4.21 and Figure 4.22 show evaporation plotted with solar radiation, temperature and wind speed. All parameters appear to be related to evaporation rate, as expected.

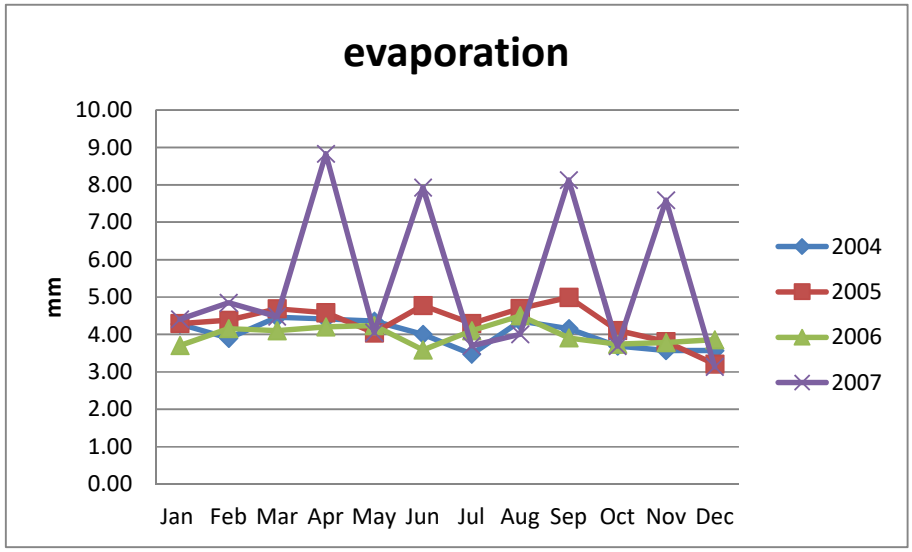

Figure 4.18 The average evaporation pan recorded at Subang station (data from Malaysian Meteorological Department and Department of Irrigation and Drainage Malaysia)

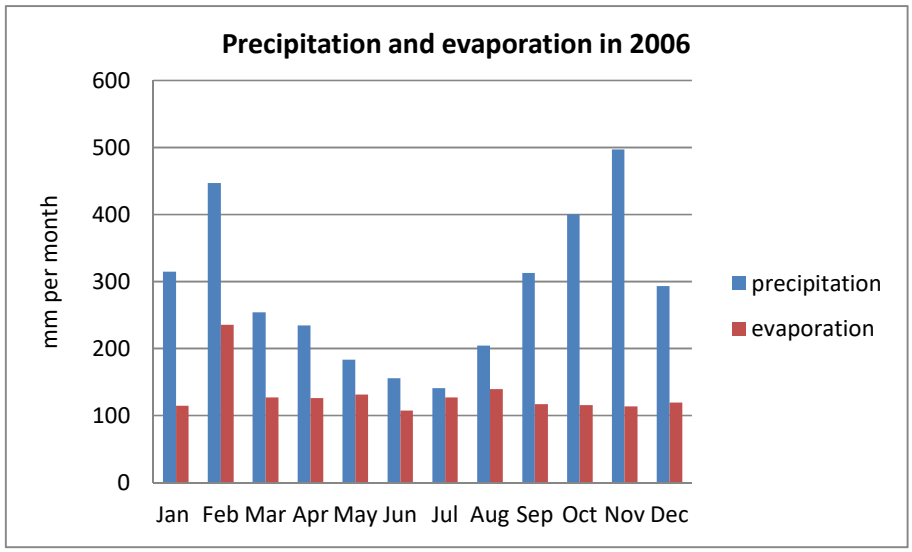

Figure 4.19 The monthly precipitation and evaporation pan in 2006 (data from Malaysian Meteorological Department and Department of Irrigation and Drainage Malaysia).

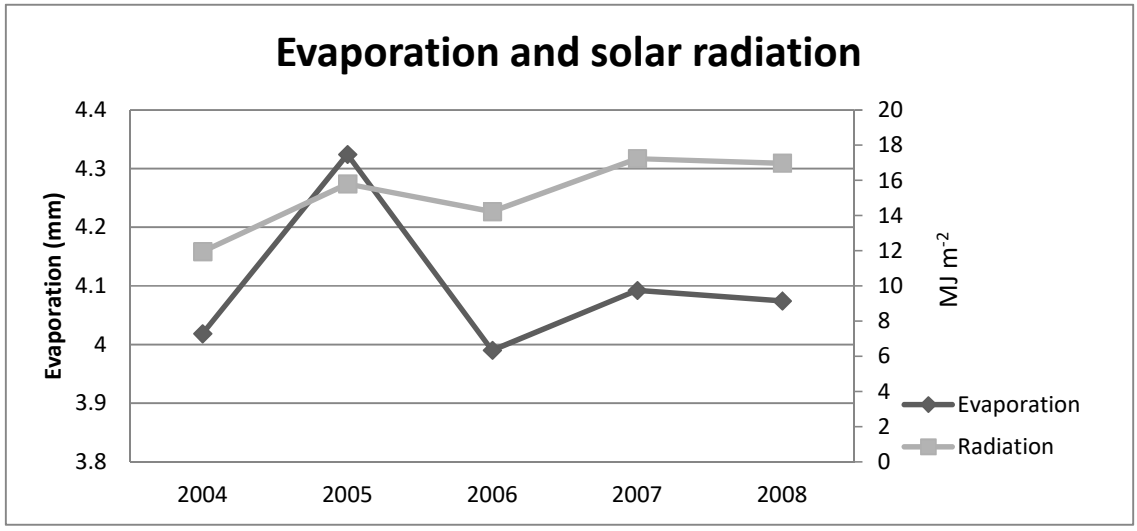

Figure 4.20 The relationship between evaporation and solar radiation (data from Malaysian Meteorological Department and Department of Irrigation and Drainage Malaysia)

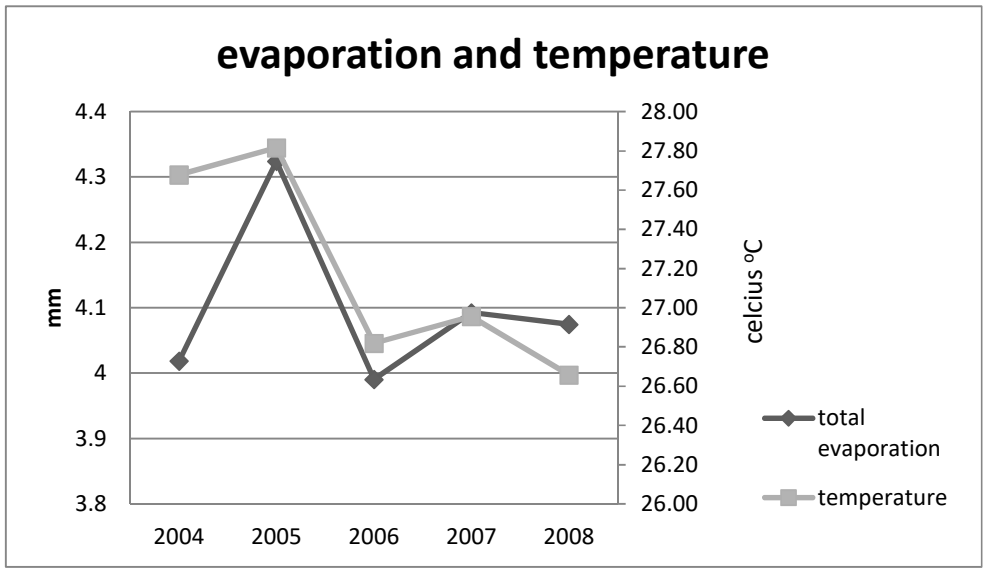

Figure 4.21 The relationship between evaporation and temperature (data from Malaysian Meteorological Department and Department of Irrigation and Drainage Malaysia).

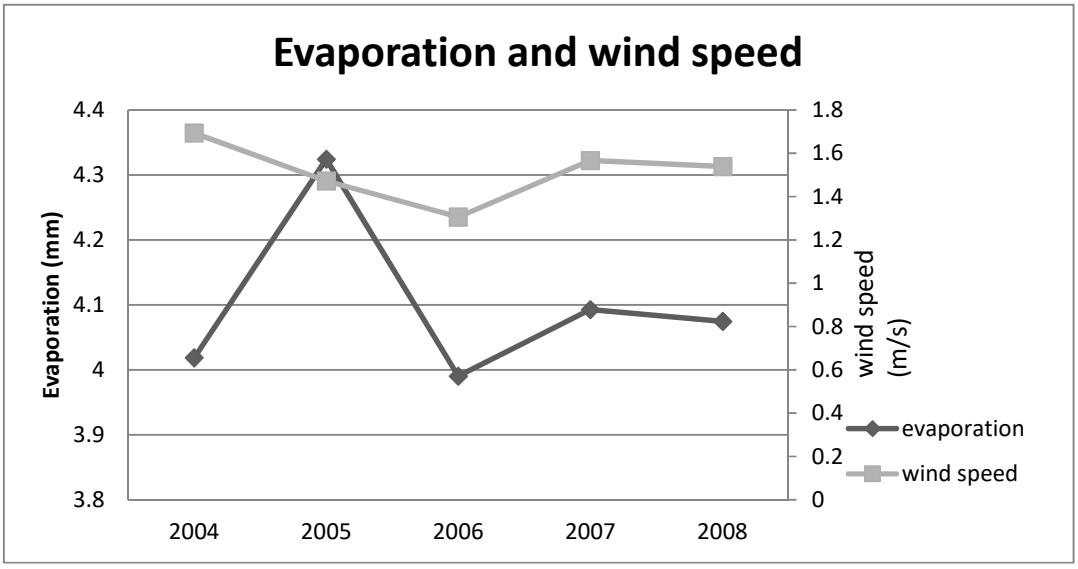

Figure 4.22 The relationship between evaporation and wind speed (data from Malaysian Meteorological Department and Department of Irrigation and Drainage Malaysia)

4.2.8 Evapotranspiration

Reference evapotranspiration, ET_o has been calculated using the FAO Penman-Monteith method which later will be compared with ET_o value using the pan evaporation data. The monthly temperature, air humidity, wind speed and solar radiation data which are measured at Subang station will be used. All the calculation procedures are adopted from Allen et al., (1998). Table 4.7 shows the step by step results for estimating for evapotranspiration, ET^o. Each of the parameters will be used to calculate ET_o using formula below.

$$ET_o = \frac{0.408\Delta (R_n - G) + \gamma \frac{900}{T + 273} U_2 (e_s - e_a)}{\Delta + \gamma (1 + 0.34U_2)}$$

ET_o is the reference evapotranspiration (mm day^{-1})

R_n is the net radiation at the crop surface {$=R_{ns} - R_{nl}$, both of which are defined below}(MJ m^{-2} day^{-1})

G is the soil heat flux density (MJ m^{-2} day^{-1})

T is the air temperature at 2m height (^oC)

U_2 is the wind speed at 2m height (ms^{-1})

e_s is the mean saturation vapour pressure (kPa)

e_a is the actual vapour pressure (kPa)

$(e_s - e_a)$ is the saturation vapour pressure deficit (kPa)

Δ is the slope vapour pressure curve (kPa $^oC^{-1}$)

γ is the psychrometric constant (kPa $^oC^{-1}$)

1) To calculate mean saturation vapour pressure (e_s), the saturation vapour pressure function e^o (T) was obtained from Table 2.3, Annex 2 of Allen et al., (1998) which is based on the following relationship:

$$e^o(T) = 0.611 \exp\left(\frac{17.27T}{T + 237.3}\right)$$

The mean saturation vapour pressure was estimated using the e^o values from the table corresponding to the maximum and minimum temperatures using the following expression:

$$e_s = \frac{e^o(T_{max}) + e^o(T_{min})}{2}$$

2) The actual vapour pressure (e_a) value was obtained from:

$$e_a = e^{\circ}(T_{min}) = 0.611 \exp\left[\frac{17.27 T_{min}}{T_{min} + 237.3}\right]$$

where T_{min} is taken as an approximation of the dew point temperature.

3) The slope of saturation vapour pressure curve, Δ, is obtained from Table 2.4, Annex 2 of Allen et al., (1998) where average temperature is approximated as $(T_{min} + T_{max})/2$.

4) The extraterrestrial radiation (R_a) values were obtained from Table 2.6 of Annex 2 of Allen et al., (1998) using degrees for Subang station which were then converted to radians.

5) The clear sky solar radiation (R_{so}) was calculated using:

$$R_{so} = (0.75 + 2\ 10^{-5} z) R_a$$

where z is the station elevation above sea level [m].

6) The net solar radiation (R_{ns})was estimated using:

$$R_{ns} = (1-\alpha) R_s$$

where

R_{ns} is the net solar or shortwave radiation [MJ m^{-2} day^{-1}],

α is the albedo or canopy reflection coefficient, which is 0.23 for the grass reference crop [1], R_s is the incoming solar radiation [MJ m^{-2} day^{-1}].

7) To estimate the net longwave radiation (R_{nl}), the following formula was used:

$$R_{nl} = s[T_{max,K} + T_{min,K}]/2(0.34-0.14\sqrt{e_a})(1.35R_s/R_{so} - 0.35)$$

where

R_{nl} is the net outgoing longwave radiation [MJ m^{-2} day^{-1}]

σ is the Stefan-Boltzmann constant [4.903 10^{-9} MJ K^{-4} m^{-2} day^{-1}]

$T_{max, K}$ is the maximum absolute daily temperature [K]

$T_{min, K}$ is the minimum absolute daily temperature [K]

e_a is the actual vapour pressure [kPa]

R_s/R_{so} is the relative shortwave radiation (constrained to ≤ 1.0)

R_s is the measured solar radiation [MJ m^{-2} day^{-1}]

R_{so} is the calculated clear-sky radiation [MJ m^{-2} day^{-1}].

The σ Stefan-Boltzmann constant value was obtained from Table 2.8, Annex 2 of Allen et al., (1998) using T_{max} and T_{min} values.

8) To estimate the soil heat flux (G) for monthly period (MJ m^{-2} d^{-1}), the following relationship was used.

$G_{month, i} = 0.07 (T_{month, i+1} - T_{month, i-1})$

or, if $T_{month, i+1}$ is unknown:

$G_{month, i} = 0.14 (T_{month, i} - T_{month, i-1})$

where

$T_{month, i}$ is the mean air temperature of month i [°C],
$T_{month, i-1}$ is the mean air temperature of previous month [°C],
$T_{month, i+1}$ is the mean air temperature of next month [°C].
G is positive when the soil is warming and negative when it is cooling.

9) Wind speed measured at 10m height (aviation station) needs to be corrected because the data are required at 2m height

$$u_2 = u_z \frac{4.87}{\ln(67.8z - 5.42)}$$

where

u_2 is the wind speed at 2 m above ground surface [m s^{-1}]

u_z is the measured wind speed at z m above ground surface [m s^{-1}]

z is the height of measurement above ground surface [m].

10) To calculate ET_o using evaporation pan data, Case A of Allen et al., (1998) is adopted. The pan is located in a short green cropped area. The wind speed is assumed to be less than 2 ms^{-1} with the distance of green crop to the windward side being 1000m. Relative humidity is > 70%. The pan coefficient, K_p is assumed to be 0.85. The reference evapotranspiration, ET^o, from evaporation data, E_{pan}, was then calculated using:

$$ET_o = K_p E_{pan}$$

The ET_o values calculated in this way are given in Table 4.7. Figure 4.23 shows that the Penman-Monteith ET_o values vary little with month and are about 3mm/d (average = 2.86mm/d). This is less than half the precipitation rate. Figure 4.24 compares both ET estimates with the precipitation rates. The pan ET values are greater than the Penman-Moneith values by just over 20% (average = 3.48 mm/d). This discrepancy is within the uncertainty of the K_p value estimate (FAO 1998).

Table 4.7 The climatic parameters calculated for estimating reference evapotranspiration,ET_o

Parameter	Jan	Feb	Mar	Apr	May	Jun	Jul	Aug	Sep	Oct	Nov	Dec
Tmax ^oC	28.1	28.6	28.4	28.1	28.7	28.6	27.9	28.2	28.5	27.2	26.8	27.1
Tmin ^oC	26.9	25.4	26.5	26.1	27.5	26.3	26.9	27.4	26.1	26.8	25.4	26.5
Tmean ^oC	27.5	27.0	27.4	27.1	28.1	27.5	27.4	27.8	27.3	27.0	26.1	26.8
$e^o(T_{max})$,kPa	3.78	3.891	3.891	3.78	3.891	3.891	3.78	3.78	3.891	3.565	3.565	3.565
$e^o(T_{min})$,kPa	3.565	3.263	3.462	3.361	3.671	3.462	3.565	3.671	3.361	3.565	3.263	3.462
e_s,kPa	3.673	3.577	3.677	3.571	3.781	3.677	3.673	3.726	3.626	3.565	3.414	3.514
Δ, kPa $^oC^{-1}$	0.215	0.209	0.215	0.209	0.220	0.215	0.215	0.220	0.215	0.209	0.199	0.209
e_a,kPa	3.549	3.239	3.459	3.387	3.664	3.416	3.546	3.646	3.374	3.523	3.237	3.468
e_s-e_a,kPa	0.123	0.338	0.218	0.184	0.117	0.261	0.127	0.079	0.252	0.042	0.177	0.045
R_a, MJ m^{-2} day^{-1}	36.200	37.500	37.900	36.800	34.800	33.400	33.900	35.700	37.200	37.400	36.300	35.600
R_s, MJ m^{-2} day^{-1}	15.637	15.884	14.953	13.594	13.277	14.580	15.016	17.085	16.759	16.151	15.304	14.649
R_{so},MJ m^{-2} day^{-1}	27.162	28.137	28.438	27.612	26.111	25.061	25.436	26.787	27.912	28.062	27.237	26.712
R_{ns},MJ m^{-2} day^{-1}	12.040	12.230	11.514	10.467	10.224	11.227	11.562	13.155	12.905	12.436	11.784	11.280
σT_{maxK4}, MJ m^{-2} d^{-1}	40.330	40.600	40.600	40.330	40.600	40.600	40.330	40.330	40.600	39.800	39.800	39.800
σT_{minK4},MJ m^{-2} d^{-1}	39.800	39.010	39.530	39.270	40.060	39.530	39.800	40.060	39.270	39.800	39.010	39.530
R_{nl},MJ m^{-2} day^{-1}	1.567	1.858	1.411	1.289	1.133	1.760	1.644	1.741	1.910	1.587	1.826	1.506
R_n,MJ m^{-2} day^{-1}	10.473	10.373	10.103	9.178	9.091	9.467	9.918	11.414	10.995	10.849	9.958	9.774
G,MJ m^{-2} day^{-1}	3.848	-0.003	0.010	0.045	0.023	-0.048	0.024	-0.010	-0.058	-0.085	-0.011	0.107
U_z, ms^{-1}	1.414	1.330	1.566	1.290	1.525	1.564	1.649	1.734	1.726	1.595	1.451	1.347
U_2,ms^{-1}	1.058	0.995	1.171	0.965	1.141	1.169	1.233	1.297	1.291	1.193	1.085	1.008
$0.408\Delta(R_n - G)$	0.581	0.885	0.885	0.779	0.814	0.835	0.868	1.025	0.970	0.932	0.809	0.824
$\gamma(900/T+273)U_2(e_s-e_a)$	0.026	0.068	0.051	0.036	0.027	0.061	0.031	0.021	0.065	0.010	0.039	0.009

$\Delta+\gamma(1+0.34u_2)$	0.306	0.299	0.309	0.298	0.313	0.309	0.310	0.317	0.311	0.303	0.291	0.299
ET_o calculated,mm d^{-1}	1.984	3.189	3.034	2.733	2.686	2.902	2.900	3.304	3.323	3.109	2.918	2.788
E_{Pan}, mm d^{-1}	4.057	4.320	4.345	4.344	4.112	4.106	3.843	4.330	4.309	3.965	3.886	3.585
ET_o from pan,mm d^{-1}	3.449	3.672	3.693	3.692	3.495	3.490	3.267	3.680	3.663	3.370	3.303	3.047

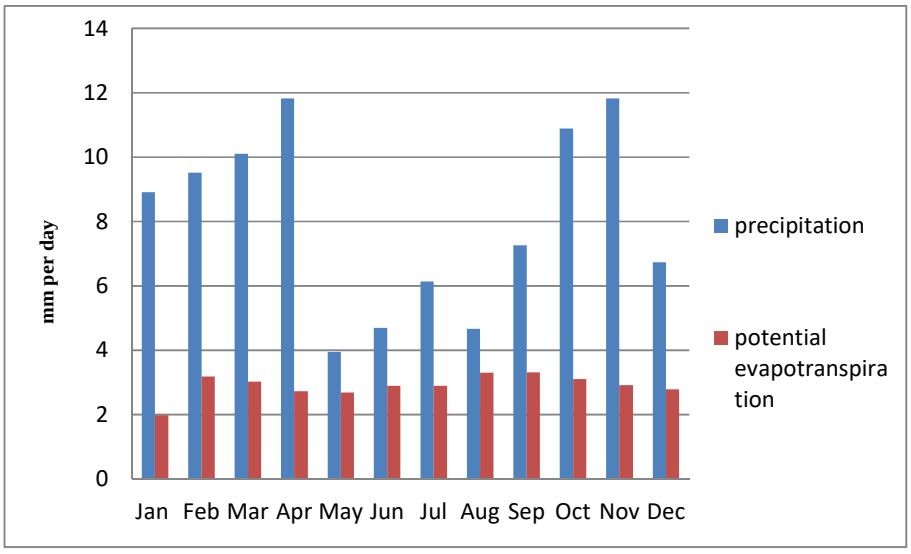

Figure 4.23 The precipitation and calculated reference evapotranspiration,ET_o, measured at Subang Station

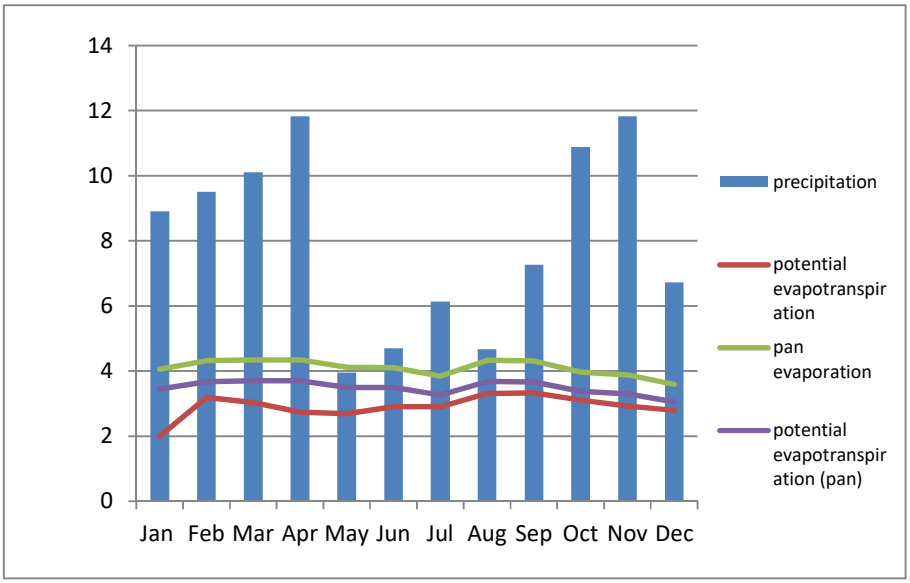

Figure 4.24 The precipitation with reference evapotranspiration,ET_o (both methods) and pan evaporation measured at Subang Station. All units are mm d^{-1}.

4.3 Recharge in the urban aquifer

4.3.1 Introduction

The aim of this section is to make a preliminary estimate the likely possible recharge rate for the Shah Alam aquifer. Urban groundwater can be recharged by natural sources such as precipitation, river infiltration, and lake infiltration, and also from human activities connected with urbanisation (Lerner et al. 1990, De Vries & Simmers 2002). In the natural hydrologic cycle, rainfall will run as surface runoff or recharge the groundwater or evaporate to the atmosphere or be transpired by plants. However, in an urban area, the system is altered by reducing the direct infiltration and evaporation, increasing the surface runoff, and importing water into the city which then leaks through the water supply and sewage network systems (Foster 1988, Lerner et al. 1990, Foster et al.1994, Chilton 1999). The vegetation is cleared and the area is covered with low permeability ground/pavement (e.g. Lerner, 2002). Full analysis of this is complex, and often uncertain (Thomas and Tellam, 2006; Schirmer et al., 2013), especially without a regional numerical model to constrain the values obtained. In the current work, no regional model will be produced, and the main requirement is to determine approximate ranges of potential recharge rates that can be used in local modelling work undertaken on pumping tests.

4.3.2 Rainfall as main recharge sources

The main source of recharge of the aquifer in Shah Alam is the rainfall since it receives over 2000 mm of rainfall per year. For equatorial climates and low

topographic areas which receives precipitation more than 1000 mm/year, 20-30% of rainwater will infiltrate the soil layer according to Larsson (1984).

However, the actual amount of recharge to the Shah Alam aquifer is probably much less. First, the area is mainly covered by 20-40 m of silty and sandy clay. The recharge rate is therefore likely to be relatively slow due to low K value of this layer. Perched water table can be developed due to this less permeable layer at shallow depth, causing greater runoff (Foster, Morris & Lawrence 1994).

Since the study area is an urban area, the impact of land cover and of leaking pipeworks must also be considered (Lerner et al. 1990; 2002). Figure 4.25 shows the land use for central Shah Alam. It is estimated 76.8% of study area has reduced permeability. Using the 'impermeability factors' listed in Table 4.8, based on those given by Butler & Davies (2000), the total area of 'impermeability' is 58%, very close to the estimate of 61% given by Abustan et al. (2008) for the Sg Kayu Ara catchment which is the upper part of Damansara catchment . Therefore, much of the rainfall on the ground will runoff or be collected as stormwater. It travels quicker to the river through sewers compared to the natural ground (Butler & Davies 2000). Most of the rainfall water runs on low permeability surfaces and discharges through drain systems to local water courses. Therefore, it is assumed that much of the rainfall discharges to the river as surface runoff rather than discharging to the aquifer. There will be some leakage from the waterways / sewers, but as Shah Alam is so young a city, it is assumed that the repair of the drainage network will be better than in many other cities.

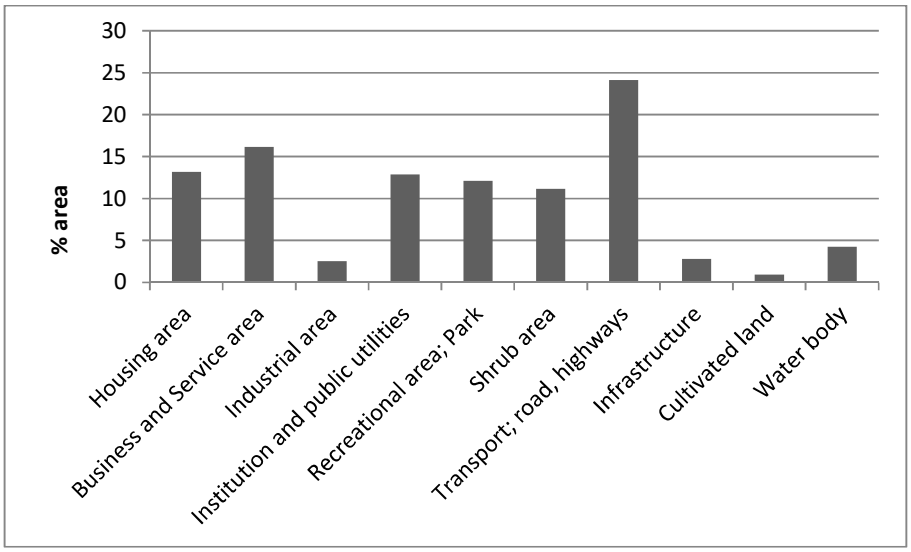

Figure 4.25 The land use of Shah Alam area (Rancangan Tempatan Majlis Bandaraya Shah Alam MBSA 2020 (2003)

Table 4.8 The 'impermeablity factor' of Shah Alam based on Butler & Davies (2000)

	Proportion of Land Covered	Proportion Impermeable (based on Butler & Davies (2000)
Housing	0.13	0.5
Business & Service	0.16	0.9
Industrial	0.025	0.9
Institutional	0.13	0.9
Parks	0.12	0.05
Shrub	0.11	0
Roads	0.24	0.9
Infrastructure	0.025	0.5
Cultivated	0.01	0.05
Water	0.045	0
Total	0.995	

4.3.3 Leakage from the pipe utilities

The other potential source of recharge to the aquifer is water supply and sewer pipe leakage. From the information given by SYABAS, the average water supply for Shah Alam area is 582 million litres per day. The size of water distributing pipes is 100 – 1200mm. In 2007 there were around 385 cases of water supply pipe leakage reported in Shah Alam and 335 cases in 2008. Unfortunately, there is no direct estimate of leakage available, but again given the youngness of the city, the losses would be expected to be much less than that seen in more mature cities (often up to around 25% of water supplied in Europe; Lerner, 2002). In addition, all the pipes which are older than 30 years have been replaced in Shah Alam.

The design criterion for one of the sewage treatment plant in Shah Alam is 85500 m^3/d of daily average sewage flow. The industrial waste is treated separately before being discharged to the river. The pipe network for sewers is located along the road. Again, these sewers may leak, but are relatively young and therefore presumably in relatively good repair. Because sewers are not pressurised, in general sewer leakage is less than water supply leakage (e.g. Yang et al., 1999). In some cases, sewers are likely to discharge groundwater rather than recharge it especially if water availability is greater than recharge rates so that the shallow subsurface remains saturated.

4.4 Recharge estimation

There are various methods for estimating recharge (e.g. Scanlon et al. 2002), including by using soil water balances (Grindley, 1967, 1969; Lloyd et al., 1966),

using water table fluctuations (e.g. Healy & Cook 2002) and by using porewater concentrations (e.g. Lerner et al., 1990). Here the focus will be on determining likely maximum potential recharge rates for later use. Potential recharge is the recharge before interflow or recharge rejection (i.e. aquifer full conditions) are taken into account.

The recharge to Shah Alam will be estimated using the following equation:

$$R = P - AE - RO$$

where

R is the recharge (mm/d)

P is the precipitation (mm/d)

AE is the actual evapotranspiration (mm/d)

RO is the runoff (mm/d).

Often recharge is calculated using small timesteps. Daily ones are recommended by Howard and Lloyd (1978) in temperate areas. This is very important because often evapotranspiration will be greater than precipitation on average through a year but recharge occurs when for short periods precipitation rate is bigger than evapotranspiration rate.

In the study area the climate is equatorial. In the Section 4.2. it has been shown that there is little seasonality in precipitation and reference evapotranspiration and that reference evapotranspiration is less than precipitation (because precipitation rates are so high and because humidity is high). Hence the need for short time steps for recharge calculations is not so important. In this assessment hence recharge will be calculated on an annual basis. This is viewed as sufficient

for the purpose for which the recharge rate is needed (Chapter 5 pumping test interpretations in particular). Any recharge calculated here is potential recharge and will be reduced by the low permeability weathering zone deposits in many cases (cases where the bedrock is clay rich – shales and shale and sandstone sequences).

ET_o values have been estimated using the Penman-Monteith method (Section 4.2.8) and represent potential evapotranspiration rates, i.e. rates that are appropriate for short grass crops, probably suitable for much of the vegetated surface in Shah Alam. They are also appropriate as an estimate of actual evapotranspiration for when there is no moisture limitation. In Shah Alam rainfall is high (average >2000 mm/y) and much greater than the estimated and pan potential evapotranspiration, and water will also exist from runoff from paved areas and from pipe leakage and other waste water discharges. It is suggested that water is unlikely to be limiting in this environment, and as a result actual evapotranspiration is likely to be similar as potential evapotranspiration. Hence in the recharge estimates the ET_o value will be used.

Runoff rates for the Sg Kayu Ara catchment (upper part of Damansara catchment) have been studied by Abustan et al., (2008). They found a relationship between runoff rates (mm/d) and precipitation (mm/d) for individual storms as follows

$$RO = 0.612P - 2.94$$

For their area they estimated an “impermeable” proportion of 61%, very close to that estimated for the study area (58% see above). Their discussion implies that

they think that the runoff is largely controlled by land cover not low permeability soils. The 2.94mm intercept represents “initial losses” that is detention storage and interception storage. It seems reasonable to take the relationship proposed by Abustan et al. (2008) for the current work. To change this relationship to an annual calculation rather than a storm calculation the following is proposed

$$RO = \sum_{i=1}^{n}\{0.612P_i - 2.94) = 0.612P - 2.94n$$

where P_i is the precipitation for an individual storm and n is the number of storms per year. Dan’azumi et al. (2010) indicate that there are between 100 and 200 storms per year in peninsular Malaysia. For calculation of recharge the ‘interception’ term must be considered as it includes water that fills up available soil storage and is then possibly available for recharge. The proportion that remains on paved surfaces and evaporates and the proportion that wets up the soil is difficult to estimate. It will be assumed that 58% of the water is lost to evaporation and the rest reaches the soil.

Hence a first estimate for the potential recharge for the whole study area is

$$R = P - ET_o(1-F_{paved}) - 0.612P - 2.94n\ F_{paved}$$

where F_{paved} is the fraction of the study area that is paved. For average P and ET_o values (~2200 mm/y, 1060 mm/y) and 150 storms per year (see above) and F_{paved} = 0.58,

$$R = 2200 - 1060(1-0.58) - 0.612(2200) - 2.94 \times 150 \times 0.58 = 153 \text{ mm/y}.$$

This calculation assumes no evapotranspiration from the paved areas, which is an underestimate. But it also assumes that no runoff infiltrates and completely

ignores supply leakage and intentional discharges. It is therefore an underestimate of the true value.

In the vegetated areas of the city the potential recharge rate will high. For these areas if RO = 0 then R = 1140 mm/y.

The equation for RO used is based on measured runoff rates (Abustan et al., 2008) and so includes the effect of low permeability soils. But Abustan et al. (2008) claim that the relationship is dominated by the proportion of low permeability land cover so it is assumed that the soils were quite permeable. If this is the case, should consider the effect of low permeability soils in Shah Alam. Section 3.3.2.3 reviews the permeability values got by previous research and also calculates a new value based on a relationship between K and porosity and plasticity index. The values obtained are:

1. $K = 5 \times 10^{-5}$ to 4×10^{-4} m/s for probably quartzite soils by Noguchi et al. (1997)
2. $K = 4\text{-}7 \times 10^{-5}$ m/s for granite soils
3. infiltration rate of $1 - 7 \times 10^{-6}$ m/s for sandstone soils probably from the Kenny Hill Formation by Bujang et al. (2005)
4. $K = 5 \times 10^{-10}$ m/s for clay soils from the Kenny Hill phyllites using the PI correlation method using data from Ibrahim (1986) and Tan & Ezdiani (2005)

The K values for the shallowest quartzite and granite soils are so high that they will not restrict recharge if the recharge was infiltrating downwards through a uniform soil (so head gradient is 1). The infiltration rates measured by Bujang et

al. (2005) are also higher than the recharge rates. But the PI estimated values from the clay soils of Kenny Hill Formation phyllites indicate that the maximum recharge rate (head gradient =1) would be about 16 mm/y and so would make actual recharge much less than potential recharge.

4.5 Conclusion

It concluded that the potential recharge rate will be greater than 150 mm/y and that leakage from water supply pipes and sewers and also discharges from industrial sites will increase this rate further. It is also concluded that the sandy soils on the Kenny Hill Formation (sandstone quartzite areas) will not slow down the recharge rate but that in clayey weathered zones (phyllite, schist) the soils would limit the recharge to much less than the potential recharge rate. The rainfall rate is high but much of the water is likely to runoff because of the urban cover. As a result the potential rainfall recharge rate is relatively low in comparison to what it might otherwise have been, and may be lowered still further by the low permeability of the deposits on the argillaceous metasediments. In addition there will be leakage from water supply pipes and sewers (also may be some discharge to sewers) and some industrial discharges to the ground to add to the possible recharge. The recharge to runoff ratio in the southeast is lower than in the northwest because the weathered deposits are finer grained.

5.0 PUMPING TEST ANALYSIS: DEVELOPING THE CONCEPTUAL MODEL AND ESTIMATION OF AQUIFER CHARACTERISTICS

5.1 Introduction

Pumping test data provide a valuable source of evidence on aquifer behaviour, and could in principle provide not only estimates of aquifer hydraulic properties but also indications of degree of confining, layering, heterogeneity of properties, anisotropy of properties, recharge mechanisms, and lateral boundary conditions including evidence of fault barriers and connections with surface water bodies.

In the previous chapter, the aquifer in Shah Alam is interpreted as a confined or semi-confined aquifer (at least under unpumped conditions) of fractured metasedimentary rock which is capped with various thicknesses of weathered material, the confining unit. The sandstone of the Kenny Hill Formation (which is metamorphosed to quartzite) has a very low matrix hydraulic conductivity and a low storage capacity. The quartzite is interbedded with slightly metamorphosed argillaceous rocks (‘shale’) of various thicknesses, also with nearly zero matrix permeability. The permeability of the rock mass, both quartzite and ‘shale’ is greatly enhanced by fractures. The fractures are bedding plane fractures, other joints (often approximately perpendicular to the bedding planes), foliations and faults. Some fault planes are probably of low permeability, especially those that are oriented northwest-southeast, but others may be of high permeability both parallel and perpendicular to the fault plane. The low permeability faults may provide barriers and even compartments in the aquifer.

The main aim of this chapter is to characterize the aquifer system and also interpreting the aquifer behaviour in study area by analysing the pumping test data. The hydrogeological conceptual model which developed in previous chapter is useful in interpreting the pumping test data in a way to understand the aquifer system of Shah Alam. There are 42 pumping wells in the Shah Alam area (see Figure 2.8) and at the time of drilling many were test pumped using a step test and a constant yield approach or both. The hydraulic properties values obtained from pumping test analysis are for the area near the pumping well. The results may provide evidence corroborating, or otherwise, the initial hydrogeological conceptual model developed in Chapter 3 and 4, and extending this model**.**

The basic approach is to analyse the pumping tests using ordinary analytical methods initially and then to study various issues that arise using a numerical modelling approach.

In the next section, Section 5.2, the pumping test analysis method will be reviewed. Then, the aquifer system will be identified by plotting diagnostic and specific plots (Section 5.3). After the initial classification, the aquifer system is interpreted further by analysis of the available step test drawdown data (Section 5.4). Constant yield pumping test data are interpreted in Section 5.5 and recovery data in Section 5.6. Section 5.7 shortly discusses water level monitoring as a means of confirming the pumping test data. Section 5.8 then uses numerical modelling to study various issues that have not been properly explained by using the analytical methods.

In all cases the emphasis is on deducing aquifer behaviour rather than interpreting aquifer properties, though the latter are also of considerable interest in the present context too.

5.2 The selection of pumping test analysis method

5.2.1 Single well test with well bore storage and well loss effect

The pumping test is carried out in the well itself. Therefore, it is called 'single test well analysis' which is influenced by well bore storage and well loss. Well bore storage effects in confined aquifers are negligible when $t<25r_c^2/KD$ where r_c is the radius of the well where water level changes and (Papadopulos & Cooper 1967). Another method to determine the well bore storage effect by using Schafer (1978) method where 1:1 slope is plotted on log-log time drawdown plot. Well loss effects will be examined by analysing step drawdown test data which will be discussed in Section 5.4.

In the area, the companies Ansell, Proton, Panasonic, MT Pictures, Aquarium & Aquatic International, CCM Fertilizers, Canon Opto and Carlsberg all have more than one abstraction well in their compounds. There is therefore a possibility that the cone of drawdown of each well overlaps with others. In the case of interfering wells, effects can be seen even beyond 1km (Rushton 2003). Also the pumping tests have not been done for scientific purposes and there is not much information as to how well they were done. Drawdown can be affected quite a lot at early times by, for example, changes in pumping rate as the testers adjust the rate or as the pump responds to the greater lift.

To get around these problems is not easy but one way is to perhaps avoid the problems with early data (well bore storage and changes in rate) is to estimate the time when well bore storage effects may be important. Well bore storage will result in a log(s)-log(t) slope of one and will be important at times less than $25r_c^2/T$.

5.2.2 Diagnostic plot

The pumping test analysis begins with diagnostic plots. The diagnostic plot approach is useful in choosing the best analytical method to analyze the pumping test data (Kruseman & de Ridder 1994, Lloyd 1999 & Singhal & Gupta 2010) and therefore also in recognizing significant hydrogeological processes. The diagnostic plot is usually simply a drawdown versus time plot using either double log scales or semi log scales. Semi log scales is useful in analysing the drawdown effect away from the well while the double log plot is focusing on near well (Butler 1990).The plots then are compared with the theoretical model plots and from this various aquifer conditions may be recognisable like leaky, recharge boundaries, delayed recharge. There can, however, be significant ambiguity.

5.2.3 Step test drawdown

5.2.3.1 Introduction

The step drawdown test data is used to characterise the aquifer, to see if the step tests can confirm or extend the interpretation from diagnostic plots and to determine well losses before interpreting the constant yield tests.

During a step test, a single well is pumped with increasing discharge rate in a series of steps. Each discharge rate is kept constant ideally until the drawdown reaches steady-state. The procedure is repeated with higher discharge rates in at least two more steps. The duration of each step is usually designed to be equal to each other. If no well losses occur (see below), the drawdown will be linear with increasing pumping rate.

Jacob (1947) suggested that when pumping a well there are aquifer losses due to flow through the aquifer and both linear and non-linear well losses as water enters the well. The relationship of these components he suggested as stated below:

$$s_w = B(r_{ew}, t)Q + CQ^2, \quad (1)$$

s_w = drawdown in the pumping well,
Q = discharge rate
$B(r_{ew}, t) = B_{1(rw, t)} + B_2$
$B_{1\,(rw, t)}$ = linear aquifer –loss coefficient
B_2 = linear well - loss coefficient
C = non linear well-loss coefficient
r_{ew} = effective radius of the well,
r_w = actual radius of the well
t = pumping time.

Jacob combined the different linear well losses and dealt with them by defining an effective well radius at which the theoretical head matches the measured head. Unfortunately this cannot be uniquely defined using single well tests and hence there is some uncertainty. Other authors have modified the relationships recognising that well losses are more complex than Jacob's equation suggests. For example, Equation (1) was rewritten by Rorabaugh (1953) as:

$_{Sw} = BQ + CQ^P$ with P > 2; average value is 2.5 (2)

Step tests are usually used to calculate the well efficiency [using BQ/(BQ + CQ^2)] and well losses. Walton (1962) used the C value obtained from step drawdown test for well development assessment. Mogg (1969) in his review shows how the interpretation using well efficiency can be misleading. Other authors have suggested ways around the problems (e.g. Kawecki 1995).

Step drawdown test analysis also can be used to understand the aquifer behaviour. For example, Rushton & Rathod (1988) listed causes of responses not conforming to Equation (1) obtained from step drawdown tests and these include issues concerned with aquifer layering. Likewise Karami & Younger (2002) used step tests to determine something about aquifer heterogeneity. Quinn et al. (2011) used step tests to get the hydraulic aperture values of a fractured rock aquifer.

There are a few papers that review the analysis of step drawdown test data, e.g. Clark (1977) and Kruseman & De Ridder (1994). The methods that have been chosen to analyse the step drawdown test data of the study area are those of Bierschenk & Wilson and Eden-Hazel (Kruseman & De Ridder 1994). Bierschenk & Wilson has the advantage of simplicity and allows the validity of Equation (1) to be determined. Eden & Hazel is useful in that it allows aquifer properties to be determined.

5.2.3.2 Bierschenk & Wilson method

This method is chosen because of its simplicity and suitability for all types of the aquifer for the purposes of predicting pumped well drawdown (though not

necessarily for determining aquifer properties). The Biershenk & Wilson (1961) method is based on the Jacob equation (Equation(1)). Dividing Equation (1) by Q:

$$\frac{s_w}{Q} = B + CQ \qquad (3)$$

The value of specific drawdown (s_w /Q) is plotted against the discharge rate (Q) as shown in Figure 5.1. The slope of the line is therefore the C value and the intercept of the line is the B value. The transmissivity, T of the aquifer can be estimated using Logan's approximation T = 1.22 / B.

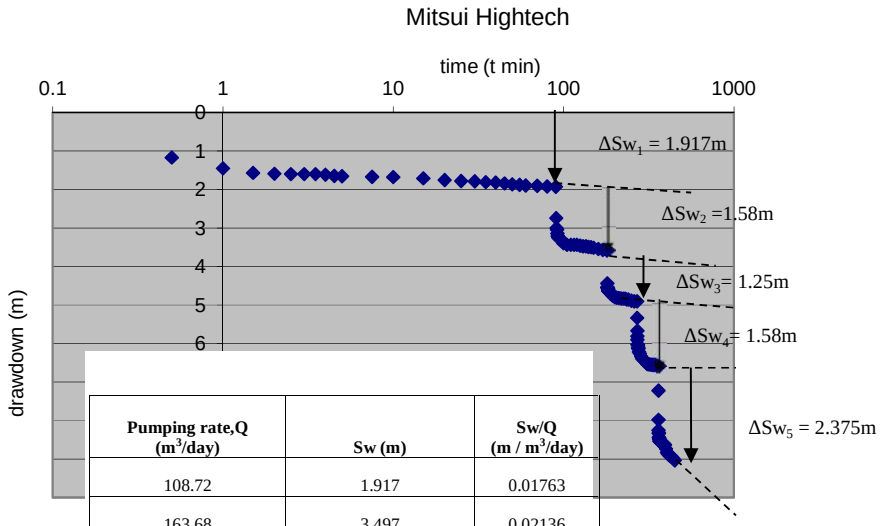

Pumping rate,Q (m^3/day)	Sw (m)	Sw/Q (m / m^3/day)
108.72	1.917	0.01763
163.68	3.497	0.02136
218.88	4.747	0.02169
272.64	6.327	0.02321
382.32	8.702	0.02276

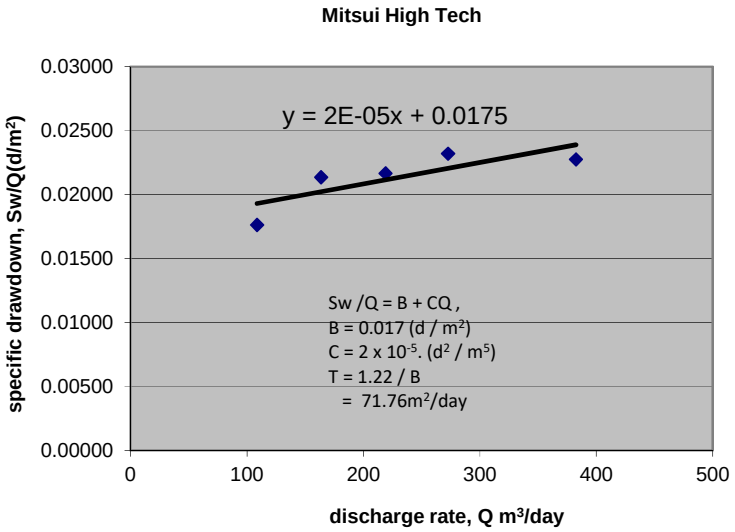

Figure 5.1 The specific drawdown (s_w /Q) plot with discharge rate, Q

5.2.3.3 Eden- Hazel method

This method is based on Jacob's approximation of the Theis equation which is shown in Equation (4).

$$s_w = \frac{2.3Q}{4\pi T} \log \frac{2.25Tt}{r_w^2 S} \quad (4)$$

where S is storage coefficient and T is transmissivity and r_w is well radius. Equation (4) can be rewritten:

$$s_w = (a + b \log t)\, Q \quad (5)$$

where

$$a = \frac{2.3}{4\pi T} \log \frac{2.25Tt}{r_w^2 S} \quad (6)$$

and

$$b = \frac{2.3}{4\pi T} \quad (7)$$

The drawdown after n steps is given by (employing law of superposition)

$$s_{w(n)} = \sum_{i=1}^{n} (\Delta Q_i)\, \{a + b \log (t - t_i)\} \quad (8)$$

where

Q_i = constant discharge during the i-th step

$\Delta Q_i = Q_i - Q_{i-1}$ = discharge increment beginning at time t_i

t_i = time at which the i-th step begins

t= time since the step drawdown test started

This can be rewritten as

$$s_{w(n)} = aQ_n + b \sum_{i=1}^{n} (\Delta Q_i) \log (t - t_i) \quad (9)$$

where

Q_n = constant discharge during the n-th step.

Including Jacob's well loss term, this becomes

$$s_{w(n)} = aQ_n + bH_n + CQ_n^2 \quad (10)$$

$$H_n = \sum_{i=1}^{n} (\Delta Q_i) \log (t - t_i) \quad (11)$$

A plot of H against $s_{w(n)}$ will therefore be linear with different intercepts for each step. The intercepts are $aQ_n + CQ_n^2$ and if these are divided by Q_n and plotted against Q_n the slope will be C and the intercept a. This latter plot is much like the s/Q v. Q plot of Bierschenk & Wilson method. The difference is that all the data are used rather than just one number per step, one consistent slope being forced through all the plots for individual steps. This can lead to greater sensitivity and more recognition of data that do not fit the Jacob theory.

This method was applied using the Aquifer Win32 software (Rumbaugh&Rumbaugh 1999-2013). This method is only valid for confined aquifers of infinite areal extent and homogeneous. Those wells that are leaky or delayed-yield unconfined or have boundaries or have heterogeneous hydraulic properties or where well diameter or partial penetration occurs or have K varying with depth may be difficult to interpret.

5.2.4 Constant Yield Tests

The unsteady-state pumping test analysis was firstly developed by Theis (1935) with one basic assumption being that the confined aquifer is a homogeneous medium. In reality, the aquifer condition is often heterogeneous as highlighted by Vandenberg (1977). The drawdown curves can deviate from the Theis curves relating to specific aquifer conditions such as leaky (Hantush 1956, 1965), bounded, and unconfined (Neuman 1975) and due to issues like partial penetration, well-bore storage and interference from other abstraction wells (Mar Gonzalez & Rushton 1981, Rushton 1985, Weber & Chapuis 2013, Weber et al. 2014).

For equivalent porous media, the water flows radially into the well while water flows non radially (linearly) in a single fractured rock aquifer (Jenkins&Prentice 1982, Barker 1988, Lloyd 1999. For the study area, the aquifer will of necessity be treated as homogeneous in the sense that the equivalent continuum approach is adopted.

All the pumping test data are analysed using Cooper-Jacob's straight line method. This method is chosen because it can provide indications of aquifer boundaries, is suitable for property estimation in confined and leaky aquifers (provided $t < cS/20$ where c is the aquitard hydraulic resistance and also does not require well loss correction (Kruseman & De Ridder 1994). It is a reliable method even in heterogeneous media (Barker &Herbert 1982, Meier et al.1998, Sánchez-Vila et al. 1999). The effect of partial penetration and vertical anisotropy on the calculated transmissivity value in confined aquifers is minimal

according to Halford et al. (2006). The Cooper-Jacob method is analysed manually and by using Aquifer Win32 software. Though this is an approximate approach other possible processes are considered using numerical modelling in later sections.

The Cooper-Jacob method assuming the following:

a) the aquifer is confined
b) the aquifer is infinite
c) the aquifer is homogeneous and with uniform thickness
d) recharge is zero
e) the piezometric surface is horizontal before the pumping starts
f) the pumping rate is constant
g) the well is fully penetrating the aquifer
h) the flow to well is in unsteady state
i) u <0.01

The Jacob method is based on the Theis (1935) formula

$$s = \frac{Q}{4\pi KD} W(u) = \frac{Q}{4\pi KD} (-0.5772 - In\, u + u - \frac{u^2}{2.2!} + \frac{u^3}{3.3!} - \cdots)$$

where,

s = the drawdown (m) measured r distance (m) from pumping well

Q = pumping rate (m^3/day)

KD = the transmissivity of the aquifer (m^2/day)

t = the time since pumping start (in day)

u = $r^2S/(4Tt)$.

u decreases with increasing pumping time and with decreasing distance from well. For drawdown near the pumping well, the u is usually very small (<0.01). For example, in a well or radius 0.1m, at 1day of pumping in an aquifer with a T and S of 10 m^2/d and 10^{-4} is 2.5 x 10^{-8}. For any realistic T and S and r for the Shah Alam aquifer u will always be < 0.01 within the times of the data collection. For u <0.01,

$$s = \frac{Q}{4\pi KD}(-0.5772 - In\ \frac{r^2S}{4KDt})$$

$$s = \frac{2.30Q}{4\pi KD} log \frac{2.25KDt}{r^2S}$$

or

$$s = \frac{2.30Q}{4\pi KD}\log(t) + \frac{2.30Q}{4\pi KD} log \frac{2.25KD}{r^2S}$$

Thus a plot of s against log(t) will be a straight line with slope of 2.3Q/4πKD and an intercept of 2.3Q/4πKDlog(2.25KD/r^2S). If the slope of this plot is Δ, then KD can be calculated from:

$$KD = \frac{2.30Q}{4\pi\Delta s}$$

S can only be estimated if it is assumed that there is no well loss. In this case, if t_o is the time intercept for s = 0, then

$$0 = \frac{2.30Q}{4\pi KD} log \frac{2.25KDt_0}{r^2S}$$

$$\frac{2.30Q}{4\pi KD} \neq 0 \text{ so } \frac{2.25KDt_0}{r^2S} = 1$$

$$S = \frac{2.25KDt_0}{r^2}$$

S can then be calculated. However, S values cannot be calculated in single well test often as the assumption of no well loss is unrealistic. This inaccuracy for S is expected for single well tests (Misstear et al., 2006). Any well losses will have a strong effect on S (Kruseman & De Ridder, 1994)

K can be estimated using the length of well screen in place of aquifer thickness, but only when T< 10m^2/day according to Halford et al. (2006).

5.2.5 Recovery Analysis

Recovery data analysis is useful in a way to check the reliability of pumping test data. The data also more reliable since the data obtained when pump shuts down (Driscoll 1986, Kruseman & De Ridder, 1994). The recovery method of Theis (1935) has been applied here. This method can be applied for confined, leaky and unconfined aquifers. The water level recovery data only from constant discharge tests were used.

There are two ways to analyse the recovery data. The first method is using a residual drawdown plot against the ratio t/t' (t' is the time since pumping stopped) to get the T value as shown in Figure 5.2. This analysis is carried out using Aquifer Win32. The recovery data also can be analysed by assuming the well is at same discharge rate before the pump is switched off but that also another well starts pumping at the same rate but into the borehole starting from the time the actual pump is switched off. In this case the time-drawdown curve is extended and T and S can be calculated as shown in Figure 5.3.The drawdown data are obtained using the principle of superposition. This is carried out

manually. The recovery data analysis for wells in the study area were calculated using the first method for better T estimation value.

T and S is calculated using the Cooper-Jacob semi-log approach using following equation:

$$T = \frac{0.183Q}{\Delta s}$$

$$S = \frac{2.25Tt_o}{r^2}$$

The same u validity criterion applies as was discussed in the section of interpretation of the pumping phase.

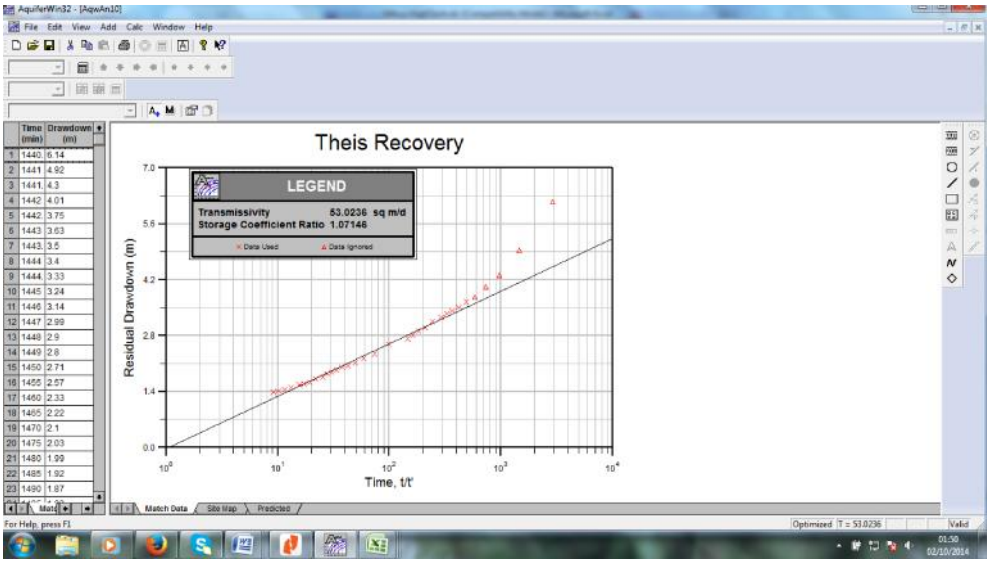

Figure 5.2. The residual drawdown plot against ratio t/t' for one of the wells in the study area

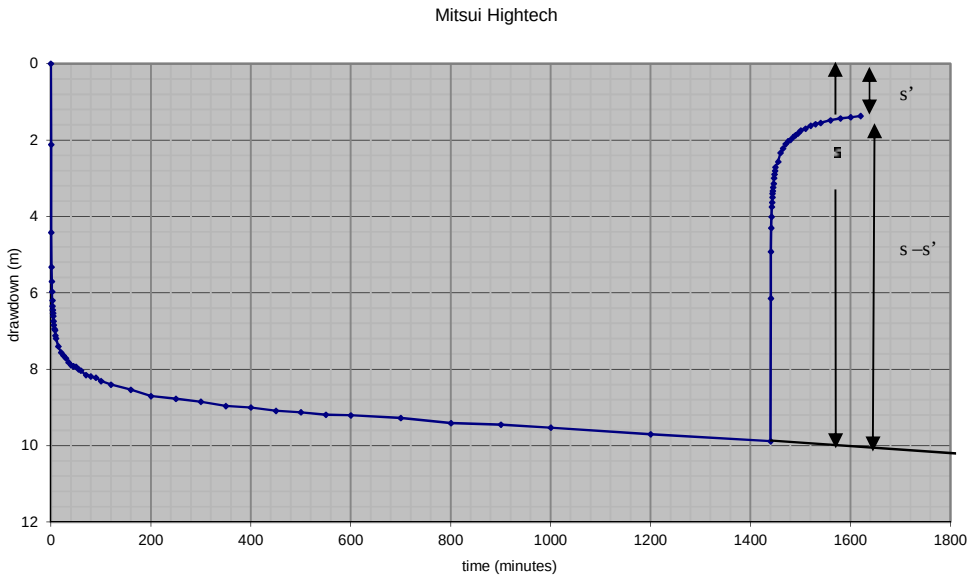

Figure 5.3. The residual drawdown is s'. The drawdown curve, s is extended to obtain the calculated recovery value (s –s'). The calculated recovery then is plotted against time after pumping stopped.

5.3 Results and interpretation -Preliminary Aquifer Characterization Using Diagnostic Plots

5.3.1 Introduction

In this first pass analysis in this section the wells have been grouped into groups that show similar pumping test behaviour and the patterns on the plots examined to deduce likely classes for each of the patterns of response identified. Both semi-log and log-log drawdown-time plots have been constructed for all the constant yield pumping tests available in Shah Alam. Both types of plot should indicate the same things, but in practice it is often useful to see both together. From diagnostic plots, the wells in the study area can be divided into 5 classes (Classes A to E). All the plots are shown in Appendix A. Wells in Class A suggest that there is only a finite source of water for some wells. Class B responses suggest that a source of water becomes continuously available part

way through the pumping test. Wells in Class C show ‘patchy aquifer’ response. Wells in Class D show there is a major source of water recharging the aquifer that is encountered part way through the test (an extreme version of Case B). Wells in Class E are consistent with the presence of an infinite confined aquifer system.

Table 5.1 summarises the classification. In some cases the class which a well belongs to is not completely clear as the plot has features of more than one class. These cases are indicated in Table 5.1 by fractions that indicate very approximately the proportions of features from each class. These classes are discussed in the following sub-sections. Figure 5.4 shows the tubewell locations with their diagnostic classes.

Table 5.1 Well response classes

Multi-well sites	Site	T (m^2/d)			Approximate proportions of each response				
		Jacob's Straight method	Logan	Class (% wells)	A (8)	B (44)	C (5)	D (13)	E (31)
X	Aquatics Int TW3	133	51	A	1.0				
X	Aquarium Express	215	158	A	1.0				
X	Aquatics Int TW2	3	95	A	0.5				0.5
X	Ansell TW1	10	7	B		1.0			
X	Ansell TW5	63		B		1.0			
	Good Year	2	16	B	0.5	0.5			
	Suzuki Latex	9	2	B		0.5	0.5		
X	Proton Well A	4	6	B		1.0			
	Scientex Polymer*	133	15	B		1'			
	Anshin Steel*	2	12	B		1'			
X	Panasonic 2	4	6	B		1.0			
X	MT Pictures TW1	4	6	B		1.0			
X	CCM Fertilizer 3	9	10	B		1.0			
X	CCM Fertilizer 2	1	4	B		0.5		0.5	
X	Ansell TW7	7	5	B		1.0			
X	Canon Opto TW4	31	30	B		1.0			
X	Canon Opto TW2	33	8	B		1.0			
X	MT Pictures TW3	7	5	B		1.0			
X	MT Pictures TW2	7	10	B		1.0			
X	MT Pictures TW4	10	11	B		1.0			
X	Canon Opto TW1	10	37	C			1.0		
X	Ansell TW6	8	50	C			1.0		
X	Carlsberg 1	5		D				1.0	
X	Proton B	14	11	D				1.0	
	AESBI		5	D				1.0	
X	Carlsberg 2		23	D				1.0	
	Gaya Color Labs		7	D				1.0	
X	Ansell TW4	6	13	E					1.0
	Mitsui High Tech	18	47	E			0.25		0.75
X	Ansell TW3	9	8	E					1.0
	Universal Nutri	3	3	E					1.0
X	MT Pictures TW5	7	9	E					1.0
X	UEDA Pl 1	18	27	E		0.5			0.5
X	UEDA Pl 2	17	1	E					1.0
	Pokka Ace**	46	16	E					1.0
X	Panasonic 1***	42		E					1.0
X	CCM Fertilizer 1	0	16	E			0.2		0.8
X	CCM Fertilizer 4	0	38	E					1.0
X	Ansell TW2	0	4	E					1.0
X	Ansell TW5A	5.4	8.74	E					

**Gentle flattening of slope of semi-log plot, unlike rest of Class B where change is sudden*

***Assumed that Q changes during test*

****Assumed that Q changes during test; if not, C*

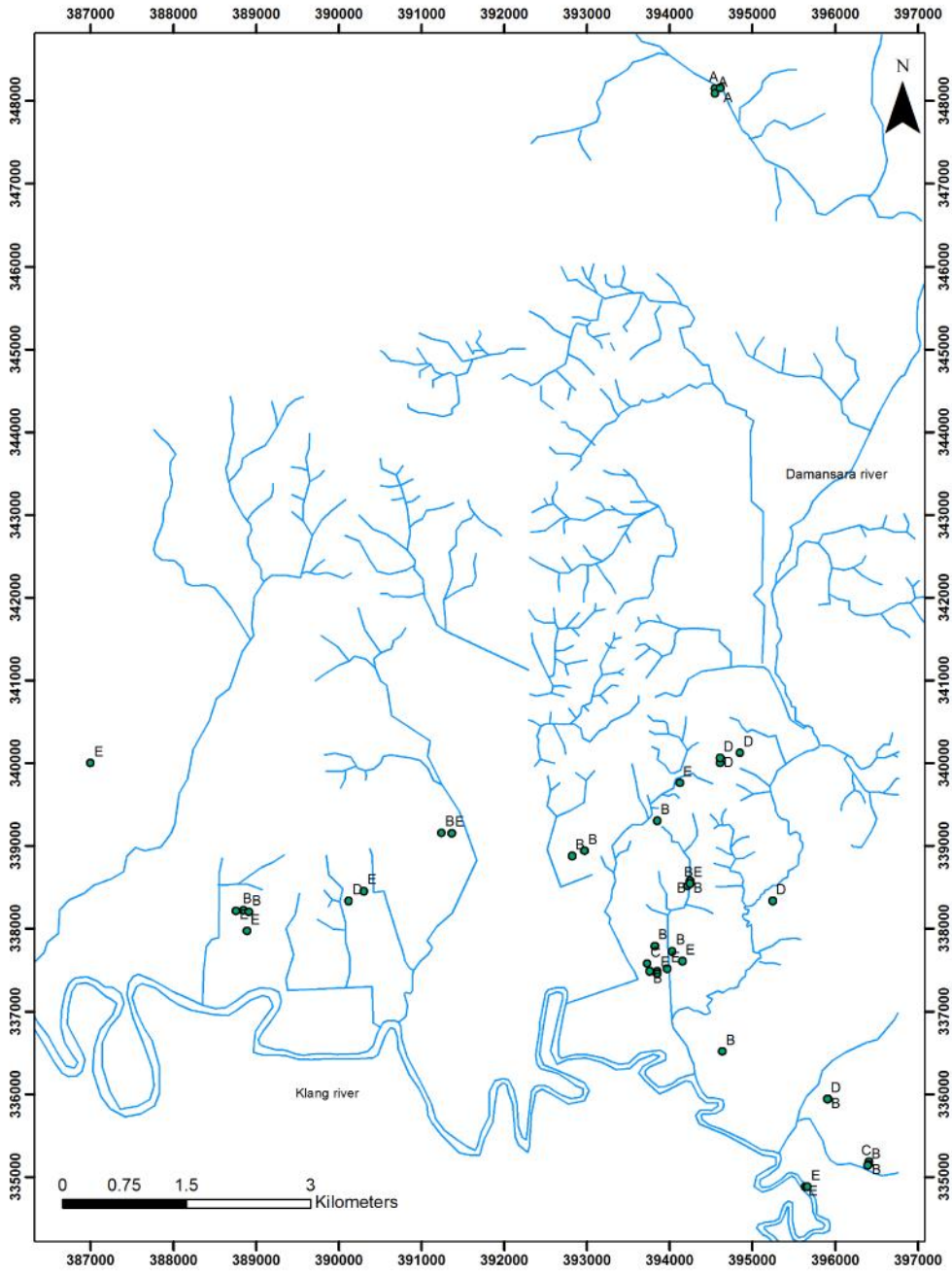

Figure 5.4 The wells in study area is grouped into 5 classes (A to E) based on diagnostic plots.

In the following sections, the red boxes on the semi log plots indicate the times when well bore storage effects should be negligible (i.e. when $t > 25r_c^2/T$). Using Logan's approximation (Logan 1964, Misstear 2001) to get T from specific capacity would have resulted in estimated well bore storage times being about 50% greater. It is known that this method is not ideal but it does result in a simpler interpretation of the well responses that later seems to work. K is calculated by dividing T with length of well screen.On the log(s)-log(t) plots a line has been plotted to indicate a slope of 1 ($\Delta s_w/\Delta t=1$), again indicative of well bore storage effects.

5.3.2 Class A pumping test responses

The wells in the first group have a drawdown-time plot with a shape characterised by a steeper initial section, a flatter middle section, and a steeper end section seen in both the semi-log and log-log plots (Figure 4.5). There are only three wells in this class. Aquatics International TW3 shows the effect best. The lesser effect in Aquarium Express and Aquatics International TW2 might even be because of changes in pumping rate. Hence this class of responses is rather uncommon.

Table 5.2 shows the information for wells in this group. All three wells have very high Logan T values compared with any of the other wells for which data are available. K values for Aquatic International TW3 is lower than other two wells. The weathered zone thickness is moderate.

The most likely cause of this response is that there is release of finite amount of water in the middle of the pumping test. This could be from draining of the unsaturated zone as in an unconfined unconsolidated aquifer or from drainage from matrix (or small fractures) in a predominantly fractured aquifer. (e.g. Singhal & Gupta 2010). For example, the fractured schist in Aquatics International TW3 is overlain by 15m of sandy clay layer material. The source of the water could be drainage from the sandier bits of the overlying weathered layer or from less permeable sections of the rock fracture network. The fact that the specific capacities are high means that flow could be rapid then possibly setting up the head gradients that result in dewatering of less permeable bits of the aquifer (Lloyd, 1999). However, given that this class has only 3 wells in it (8% of all the wells), and these show differing characteristics, little more can be concluded.

These three wells are located near to river. The river is in northwest-southeast direction which is interpreted earlier as fault with lower permeable (see Figure 5.4).The final rise of the curve possibly due to boundary effect where the drawdown hits the lower permeable boundary such as fault. It also possibly due to well interference effect since the wells are locating very close to each other.

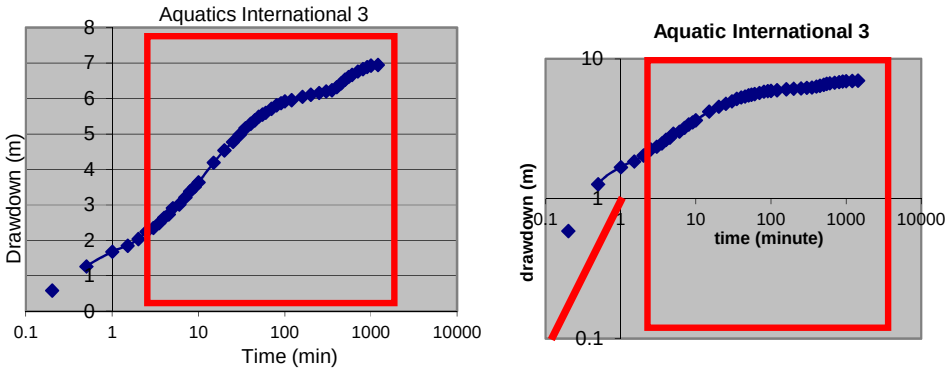

Figure 5.5 An example of a drawdown curve representing Class A. The red box on both plots represents the zone where well bore storage effects should be negligible. The red line on double log plot represents slope of 1, expected where well bore storage dominates the water level decline.

Table 5.2 The properties of wells in Class A

Class A	**Aquifer**	**No. of fractures**	**Interval of well screen (m)**	**Screen interval (m)**	**Depth of well (m)**	**Well design; gravel pack (m)**	**Pumping rate (Q, m^3/ day)**	**Draw-down (m)**	**Specific capacity (m^2/ day)**	**Thickness of weathered layer (m)**	**Logan T (m^2/d)**	**~ K (m/ d)**
Aquatic International TW3	Grey schist	1	32.6-50.9	18.3	50.9	25 -50.9	293.76	6.98	42.1	24	51	3
Aquarium Express	Limestone	1	29.5-41.75	12.25	41.75	29.5 – 41.75	316.32	2.45	129.1	26	158	13
Aquatic International TW2	Grey schist	1	36.5 – 45.7	9.2	45.7	30-45.7	130.8	1.68	77.86	15	95	10

5.3.3 Class B pumping test responses

Class B is the biggest class as it contains 44% of wells. For Class B, there are two patterns of time-drawdown plots as shown in Figure 5.6 and 5.7. The time-drawdown plots are characterised by a drawdown-time relationship that becomes shallower with time (Figure 5.6) while the change in slope on the semi-log plots is sudden for other type of time-drawdown plot as shown in Figure 5.7.

The form of the drawdown plots for Class B with sudden change in slope suggests a source of water that continues from part way through the pumping test until its end. It could be that if the test continued for longer that the shape of the plots might be similar to Class A in other words water supply rate was finite. Besides, it also possibly due to interference from other wells since this drawdown-time plots was observed in pumping wells in compound with more than 1 well.

For drawdown plots which show gradual changes with time, it is possibly a source of water comes from permeable weathered layer e.g sandstone origin (sandy silt). All wells which show the gradual changes with time are in sandstone or interbedded sandstone and shale except for Suzuki Latex. It also suggests that the quick response of weathered layer to the recharge (e.g rainfall).

Table 5.3 gives well details. Class B wells have lower transmissivities (and permeabilities) than Class A. The depth of wells in Class A is shallower (less than 100m) compared to wells in Class B (deeper than 100m). Though sandstone and granite and shale sequences are in this Class most are interbedded

arenaceous and argillaceous deposits. The weathered layer averages 38m thick and ranges from 18-60m.The weathered layer for Class A is thinner which is 15 to 24m thick.

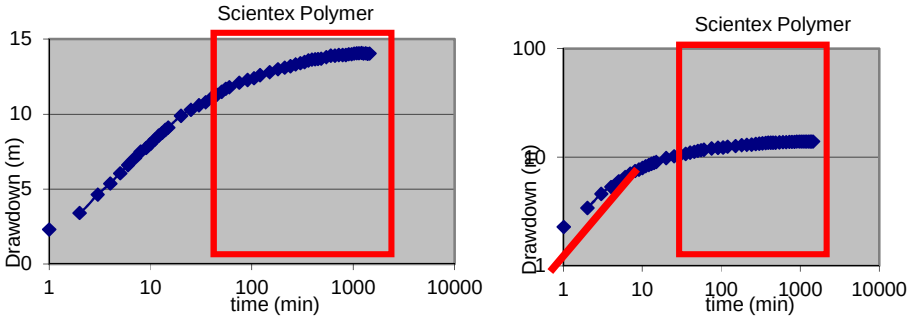

Figure 5.6 An example of a Class B where the drawdown increase becomes gradually shallower with time.

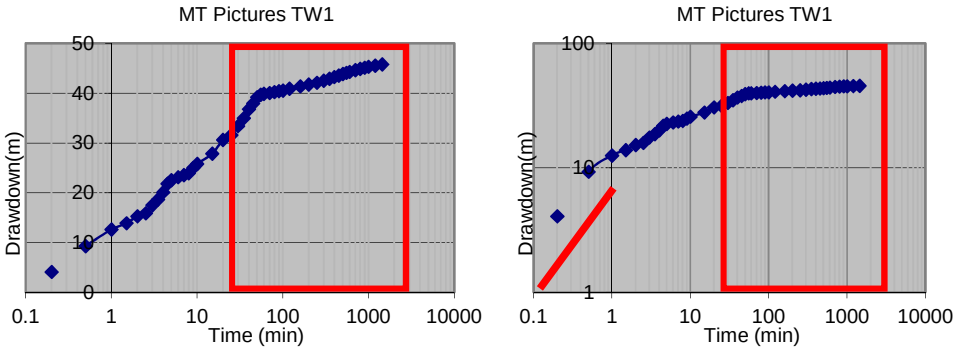

Figure 5.7 An example of a Class B well where there is a sudden shallowing of slope part way through the test.

Table 5.3 The properties of wells in Class B. The wells with (*) mark show the gradual changes of time-drawdown plots.

Site	Aquifer layer	No. of fract-ure	Interval of well screen (m)	Screen length (m)	Depth of well (m)	Well design; gravel pack (m)	Pumping rate (Q, m^3/day)	Draw-down (m)	Specific capacity (m^2/day)	Thickness of weathered layer (m)	Logan T (m^2/d)	K (m/d)
***Scientex Polymer**	Sandstone with thin layer of shale	0	40 - 70	30	70	5 - 70	167.83	14.04	11.95	35	14.6	0.5
***Anshin Steel**	NA (sandstone?)	NA	61 - 70	9	70		264	27	9.78	NA	11.9	1.3
***CCM Fertilizer TW3**	Quartzite with shale	5	42 – 141.8	99.8	141.8	Open hole	285.7	35.27	8.1	38	9.9	0.1
***Ansell TW1**	13.6m in interbedded quartzite-phyllite, 13.9m in shale	2	102– 129.5	27.5	129.5		228	40.35	5.65	79	6.9	0.3
Ansell TW 7	Weathered sst (14m) over interbedded quartzite/phyllite	3	42 - 99	57	104	30 - 99	180.96	43	4.21	34	5.1	0.1
Canon Opto TW2	grey granite	1	23 – 32	9	121.9	Open hole	246	40.04	6.14	23	7.5	0.8
Good Year 1	Shale	0	53..34-67.06	14	95	Granite chips	408	32.05	12.73	18	15.5	1.1
***Proton A**	grey carbonaceous schist	4	60-110	50	122	5 - 60	264	53.4	4.94	40.5	6.0	0.1

MT Pictures TW1	16m in grey shale with quartzite,49.55 in fractured shale	2	60-120	60	125.6	42-120	228	45.78	4.98	43	6.1	0.1
MT Pictures TW2	grey shale with quartzite	3	66-120	54	125	43-120	324	40.54	7.99	42	9.7	0.2
MT Pictures TW3	grey shale with quartzite	1	66-130	64	136.7	42-130	204	46	4.43	64	5.4	0.1
MT Pictures TW4	18m in grey shale with quartzite,20m in fractured shale	5	48-69	21	100.2	40-96	336	39	8.62	24	10.5	0.5
Panasonic TW2	*Shale?interbedded shale-sandstone	0	60-100	40	100	30-100	250.8	42.88	5.1	60	6.2	0.2
***Suzuki Latex**	NA (shale?)	NA	45-100	55	100		60	32.32	1.86	NA	2.26	0.04
***Ansell TW5**		1	24-87	63	92.35	42-92.35	144	49.1	2.9	42	3.57	0.067
CCM Fertilizers 2	Quartzite with shale	3	34 – 178.4	144.4	178.4	Open hole	143.99	48.55	2.97	30	3.62	0.02
***Canon Opto 4**	6m in weathered sandstone,21.34m in sandstone,9.14m in granite	1	18.3 – 27.43	9.13	121.9	Open hole	468.57	18.83	24.88	24	30.36	3.3

5.3.4 Class C pumping test responses

Class C responses only have two wells (5%) in the group (Figure 5.8). The response has a very low slope followed by a much steeper slope on both types of plot. This seems to suggest a barrier type effect or at least high permeability around the well extending to lower permeability further away. This latter case is what is sometimes referred to as a 'patchy' aquifer response (Herbert and Barker, 1981) with higher K in the vicinity of the well perhaps through fracture development. It is very interesting that so few wells have a recognisable barrier response especially when there is evidence of sealing of faults by quartz veining (Chapter 3). Table 5.4 gives the well details.

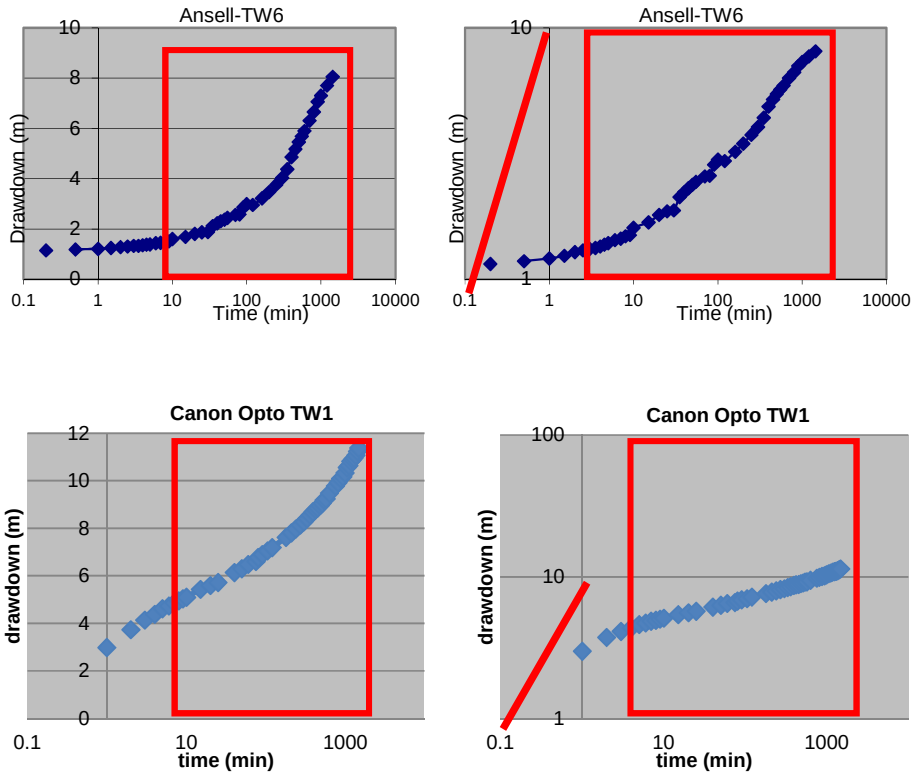

Figure 5.8 Example wells with Class C responses.

Table 5.4 The properties of well in Class C

Class C	**Aquifer layer**	**No. of fracture**	**Interval of well screen (m)**	**Screen length (m)**	**Depth of well (m)**	**Well design; gravel pack(m)**	**Pumping rate (Q, m^3/day)**	**Draw-down (m)**	**Specific capacity (m^2/day)**	**Thickness of weathered layer (m)**	**Logan T (m^2/d)**	**~ K m/d**
Ansell TW6	phyllite with quartzite-	3	36-66 70-114	74	122	30-114	327.36	8.05	40.67	14	49.6	0.7
Canon Opto TW1	Weathered granite over grey granite	1	9.14-16.8 19–21.3	12.16	71.63	3.15 (gravel packed) Open	350	11.39	30.73	17	37.5	3.08

5.3.5 Class D pumping test responses

Class D plots (Figure 5.9) show a sudden flattening off to a constant drawdown value. This is unlike Class B where the drawdown continues to increase with time after the change in slope. It indicates a significant supply of water to the well has been intercepted, perhaps a river. Figure 5.10 shows the wells in Class D which are located near to a river The wells in this class are in carbonaceous shale except Gaya Color Lab which lies in sandstone. With more permeable weathered layer (sandy silt) and an effectively infinite supply of water to weathered overlying layer ,this drawdown-time plot is possibly created.

Table 5.5 gives the details of the Class D wells. The inferred permeabilities are low (<0.2 m/d). The rock type tends to be 'shale' dominated. Weathered zone thickness averages 38m and ranges 22-59m thick. The distances to the nearest rivers, possible reasons for the boundary effect, are given and are usually about 300m or so.

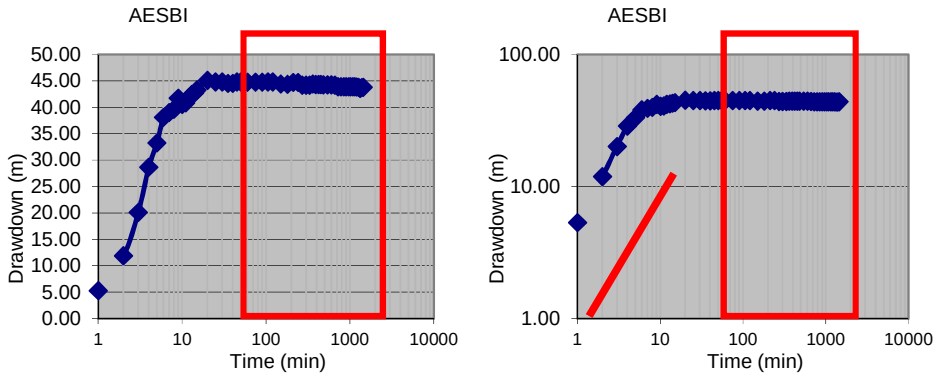

Figure 5.9 An example of a well in Class D where the flattening drawdown curve indicates strong, sudden recharge.

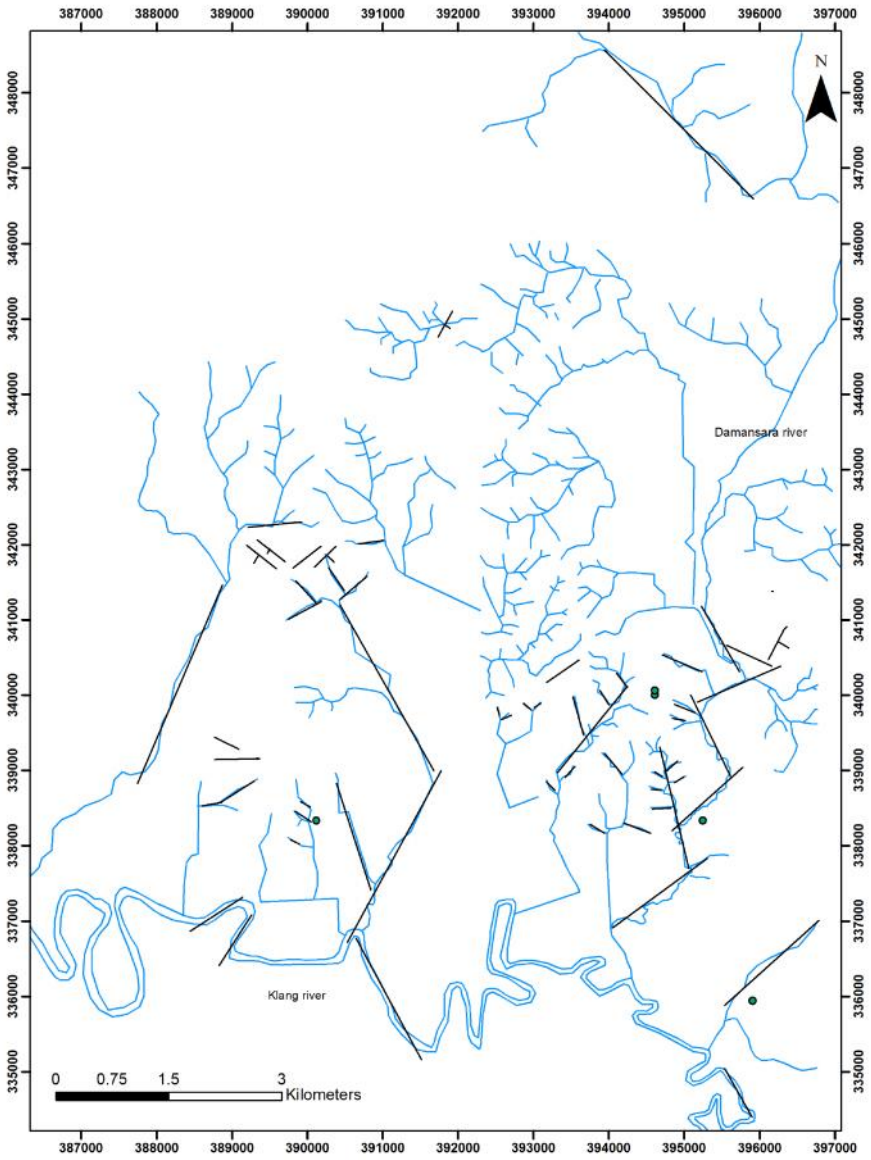

Figure 5.10 Wells in Class D which are near to the rivers.

Table 5.5 The properties of wells in Class D

Site	Aquifer	No of Fracture	Potential source of recharge	Interval of well screen (m)	Screen length (m)	Depth of well (m)	Well design; gravel pack	Pumping rate (Q, m^3/day)	Drawdown (m)	Specific capacity (m^2/ day)	Thickness of weathered layer (m)	Logan T (m^2/d)	K m/d
AESBI	Carbonaceous shale	2	Damansara river Distance: 350m	60-100	40	100	Gravel packed	180	44	4.09	59	5.0	0.1
Carlsberg Well No 2	Carbonaceous shale	2	Damansara river Distance: 320m	34-183	149	183	20-102 (gravel packed), 102-183 (Open hole)	600.87	32	18.74	33	22.9	0.2
Gaya Color Lab	Sandstone	0	Renggam river Distance: 1090m	60.97-91.46	30.5	137.19	5-60.97 (gravel packed) 91.46-137.19 (Open hole)	120	21.4	5.61	45	6.8	0.2
Proton B	grey carbonaceous schist	4	Klang river Distance: 1240m	70-142	72	155		454.21	51.7	8.79	22	10.7	0.1

Carlsberg No. 1	Shale	3	Damansara river Distance: 310m	94-102	6	100	20-102 (gravel packed),102-183 (open hole)	600	32.3	18.6	31	22.66	3.78

5.3.6 Class E pumping test responses

Class E wells have pumping test plots that appear to conform most closely to the Theis shape (Figure 5.11), i.e. they are consistent with an extensive approximately homogeneous confined aquifer.

Table 5.6 gives the characteristics of the wells in Class E. The wells are mainly in interbedded sandstone/quartzite – 'shale' with thicker weathered layer compared in sandstone. The weathered material is clay to silty clay. Average weathering depth is 34m and ranges from 17-60m. The average specific capacity estimated K is 0.2 m/d and ranges from 0.05 to 1.9 m/d.

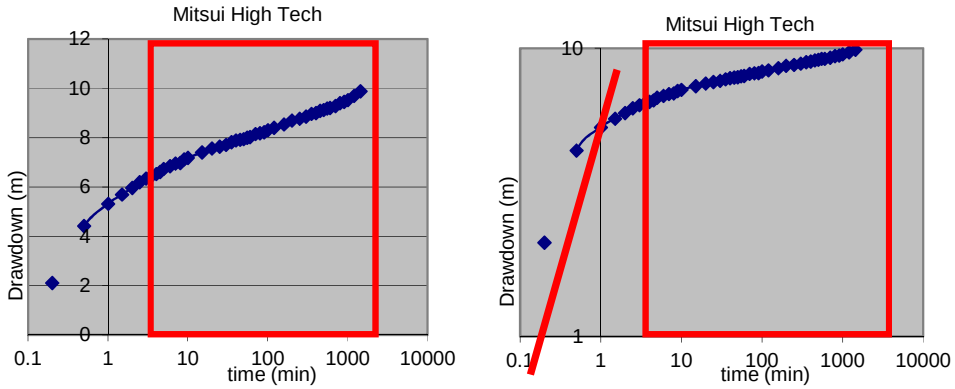

Figure 5.11. An example of a well in Class E, wells in homogeneous confined aquifer

Table 5.6 The Properties of wells in Class E

Site	Aquifer layer	No of fract-ure	Interval of well screen (m)	Screen length (m)	Depth of well (m)	Well design; gravel pack	Pumping rate (Q, m^3/day)	Draw-down (m)	Specific capacity (m^2/day)	Thickness of weathered layer (m)	Logan T (m^2/d)	~ K (m/d)
CCM Fertilizer TW4	Interbedded quartzite-shale	0	80 - 100	20	100		576	18.42	31.27	NA	38.1	1.9
Universal Nutri Beverages	shale	0	48.78 - 60.97	12	60.97	?	86.4	33.4	2.59	17	3.2	0.3
Panasonic 1	Shale-sandstone	0	60-100	40	100	70	250.8	28	8.9	60	10.93	0.27
Ueda Plating 1	NA		40-70	30	70		249.6	11.33	22.03	NA	26.9	0.9
Mitsui High Tech	grey slate with quartz vein	4	36-93.7	57.7	99.7	25-99.7	382.32	9.88	38.69	18	47	0.8
Pokka Ace	NA	NA	37.5	77.5	115		216	16.4	13.17	NA	16	0.2
CCM Fertilizers 1	54m in quartzite-shale, 35m in quartzite	4	54-143.3	89.3	143.3	Open hole	223.47	21.16	10.6	50	12.88	0.14

Ansell TW2	grey shale-phyllite with quartzite	1	42 - 122.5	80.5	122.5	36-122.5	164.4	52.18	3.15	36	3.8	0.05
Ansell TW3	grey shale-phyllite with quartzite	0	54 - 136.3	82.3	136.3	40-136.3	288	43.9	6.56	42	8.0	0.09
Ansell TW4	7m in weathered sandstone, 30m in fractured shale, 11m in interbedded quartzite-phyllite	1	20 - 67.55	47.55	67.55	36-67.55	294	26.83	10.96	27	13.4	0.28
MT Pictures 5	Interbedded sandstone-shale	1	52 - 72 78 - 108	59.3	111.3	28-111.3	300	43	6.98	24	8.5	0.14
Ueda Plating 2	NA	NA	43-61	18	61		57.6	51.48	1.12	NA	1.4	0.08
Ansell 5A	phyllite	2	65-106.8	41.7	106.7		216	30.16	6.1	17.98	8.74	0.21

5.3.7 Conclusions

Wells in Classes A, B and D seem to induce extra water during pumping. Class A wells' water source is a temporary finite source but the sources for Classes B and D are longer lived. In the case of Class D the water source is so significant that it stops drawdown increase. Possible temporary water sources are the dewatering of the weathering zone and discharge from the 'matrix' (either intergranular flow or small fractures). For example, wells in Class B which the weathering layer material is sandy silt shows the quick response to any recharge sources. This evidence observed from gradual changes of time-drawdown plots. For Class E, the weathered layer is clayey and thicker. Rivers are main likely major water sources but there could be very leaky conditions locally too. The connection between the wells and the rivers could be large fractures (see Figure 5.10).

Figure 5.12 shows the T values for Class A and Class B. T values for Class A are much higher than other classes. For Class B, T values are higher($>10m^2$/day) for wells which coincide with lineaments Figure 5.13 shows T values for Class C and D. The T values for these two classes are higher ($>10m^2$/day) except for AESBI and Gaya Color Lab. It can be concluded that the T values of the wells are related to the lineaments.

Figure 5.14 shows the K values for Class A and B. K values for Class A are also much higher than other classes. For Class B, K values are less than 1m/day except for wells at Anshin Steel, Good Year and Canon Opto 4. Both well at Anshin Steel and Canon Opto 4 lie in sandstone which possibly contributes to

higher K values. While well at Good Year coincides with lineaments and fractures (see Figure 5.14)

Figure 5.15 shows the K values for Class C and D. K values are less than 1m/day except at Canon Opto TW1 and Carlsberg No 1. Canon Opto TW1 lies in granite and Carlsberg No 1 coincides with lineaments.

The number of wells in Classes A, B and D (those that indicate an induced water source) are 64% of the wells available indicating that induced recharge sources are available to most wells. However, at least in Class A the source is temporary. If the wells are representative and Class D indicates connection with surface water bodies then about 13% of the area may be connected with rivers; Class B may also be connected with rivers and if so then around 57% of the area may be connected with surface water bodies.

Though classes have been defined, gradation in characteristics is seen in each class. And it could be viewed that Class D is the extreme of Class B and that Class B after longer pumping could show a pattern like Class A. Because Class D involves a lot of water it is possible that it may not eventually have a Class A shape.

Class C may represent higher K around the well due perhaps to development (flushing out) of fractures. But may also represent barrier boundaries (faults). The geological evidence (Chapter 3) suggested that faults with low K may be quite common but this is not confirmed by the pumping tests.

Class E is the simplest system and seems likely (though this needs testing) to be consistent with a homogeneous confined aquifer. This class represents 31% of the wells so this is a common condition.

The classes do not seem to correlate obviously to the aquifer property values listed in the tables, with the exception that Class A wells have by far the greatest (estimated) K values, and it is concluded in a preliminary way that the local characteristics of the wells (e.g. rock type, depth) are less important to their behaviour than other properties that are not recorded (e.g. the geometry of the weathering zone sand bodies or the geometry of the fracture network and how it might link to rivers).

These conclusions are all speculations until the fuller analysis has been undertaken and they relate to limited areas round the wells as the tests were only short length ones. But they do add to the conceptual model from Chapter 3. In particular the importance of induced recharge is considerable but the importance of barrier boundaries seems limited. This model will continue to be developed in the following Section.

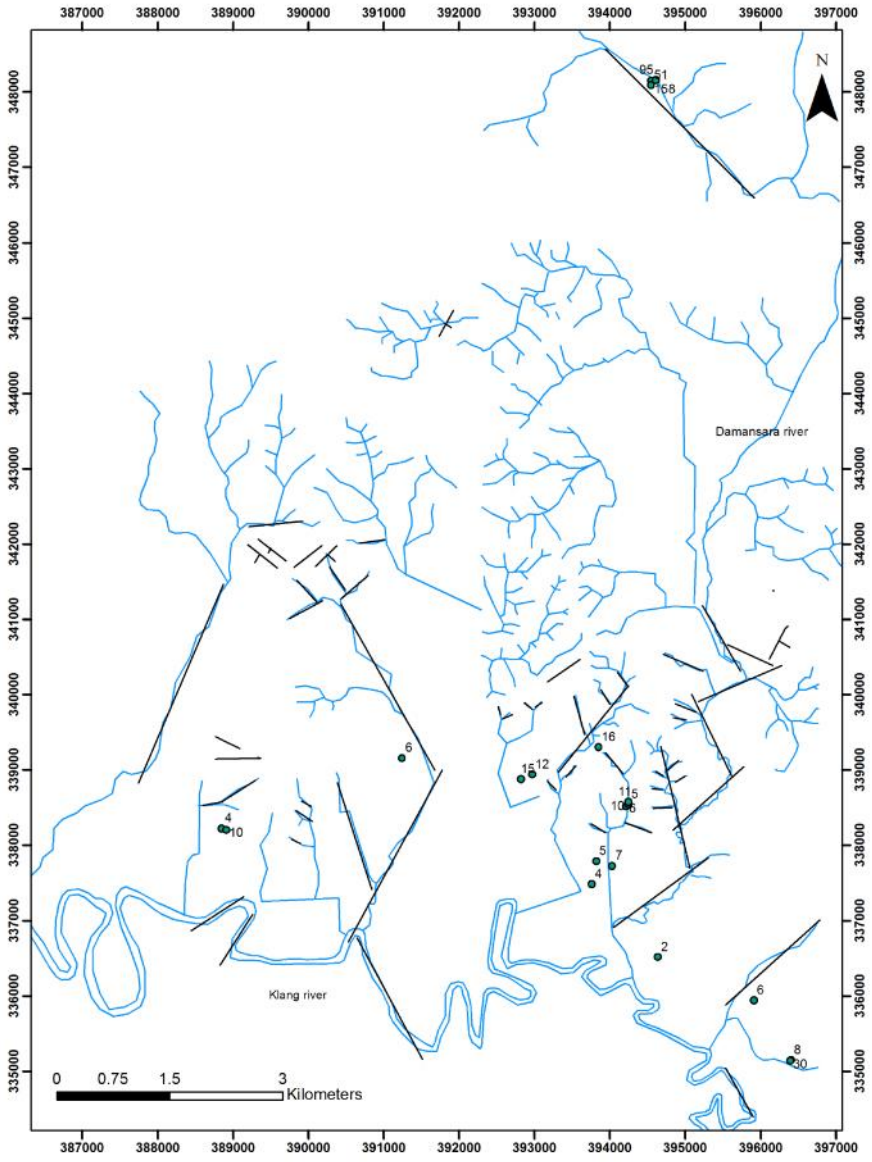

Figure 5.12 The transmissivity values for Class A and B. T values for Class B are higher (>10m^2/day) along the lineament.

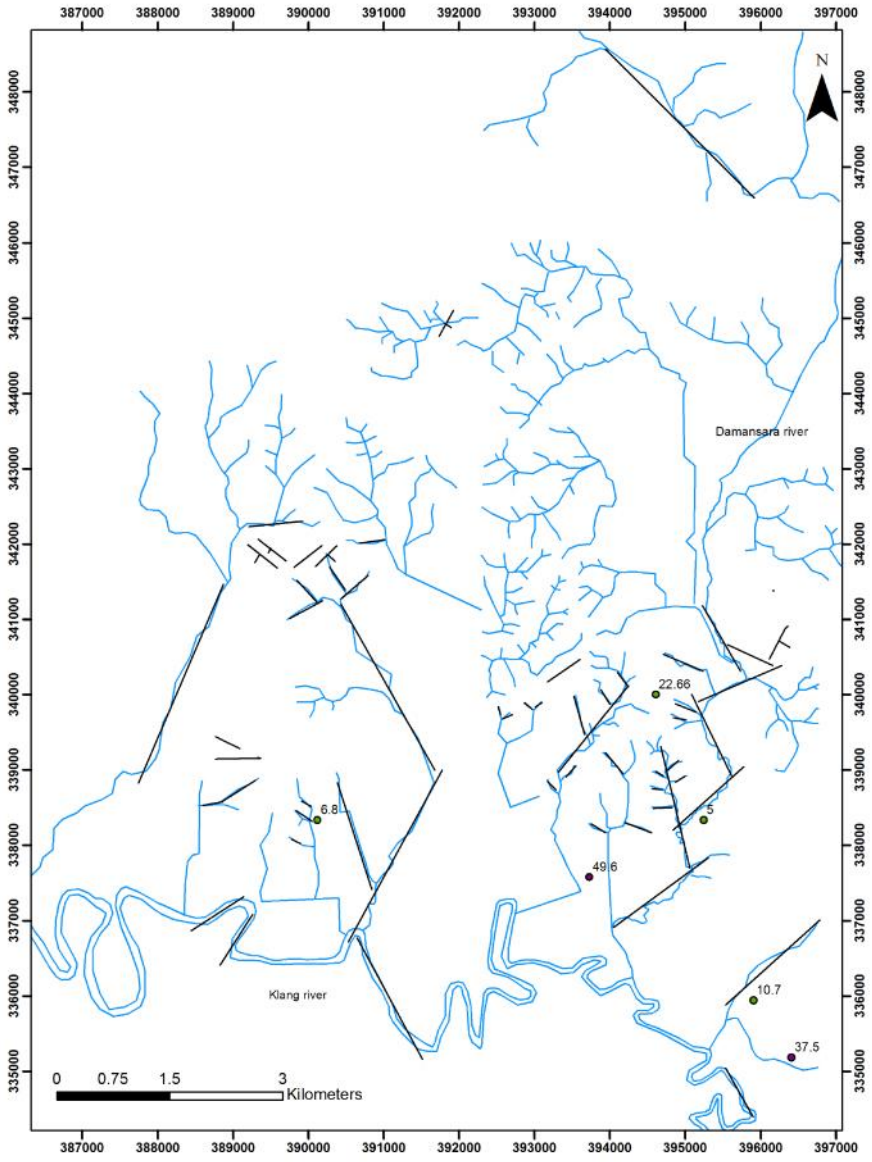

Figure 5.13 Transmissivity values for wells in Class C & D. T values in these two classes are higher than $10m^2$/day except for AESBI and Gaya Color Lab.

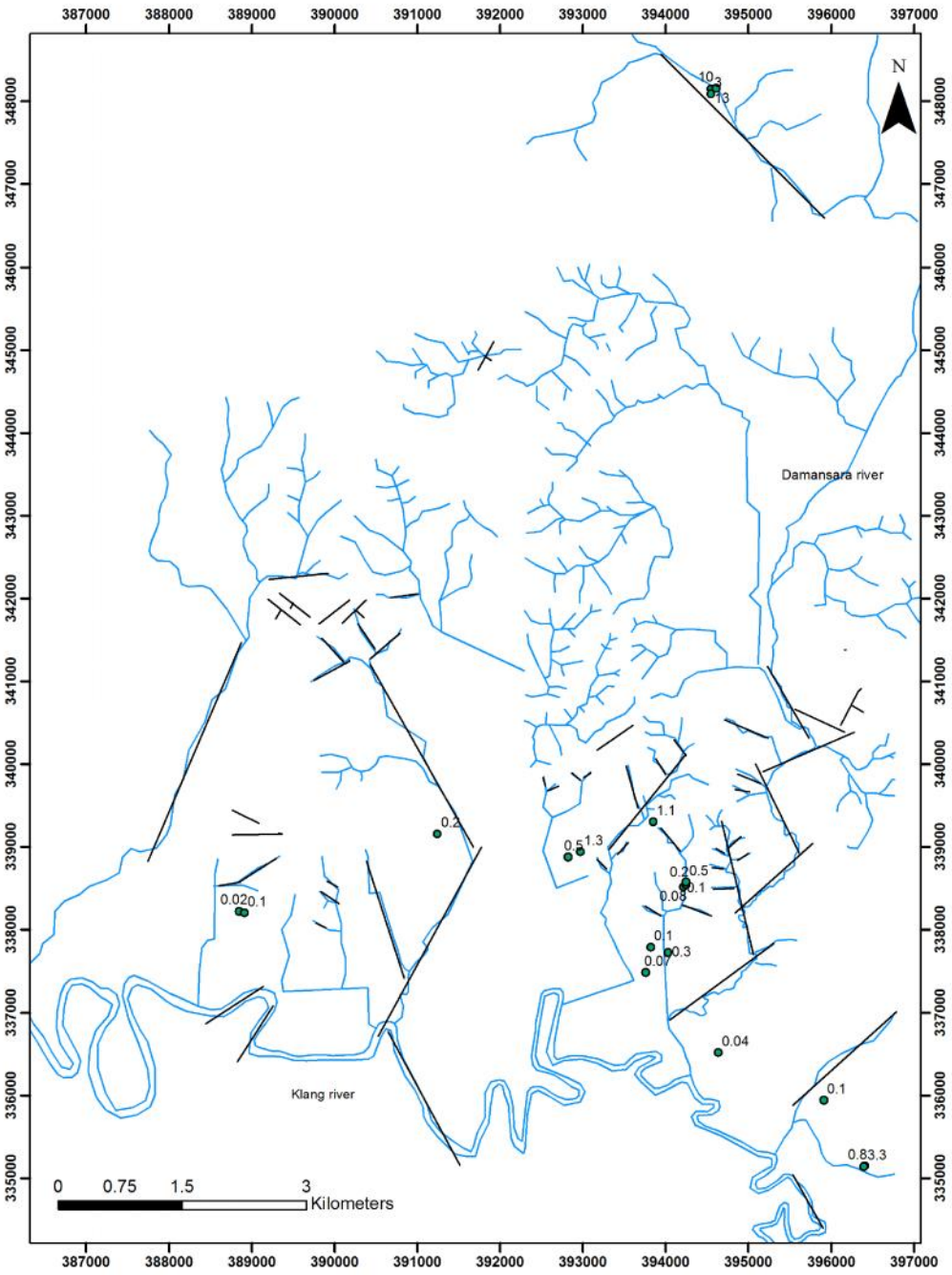

Figure 5.14 K values distribution for Class A and B.

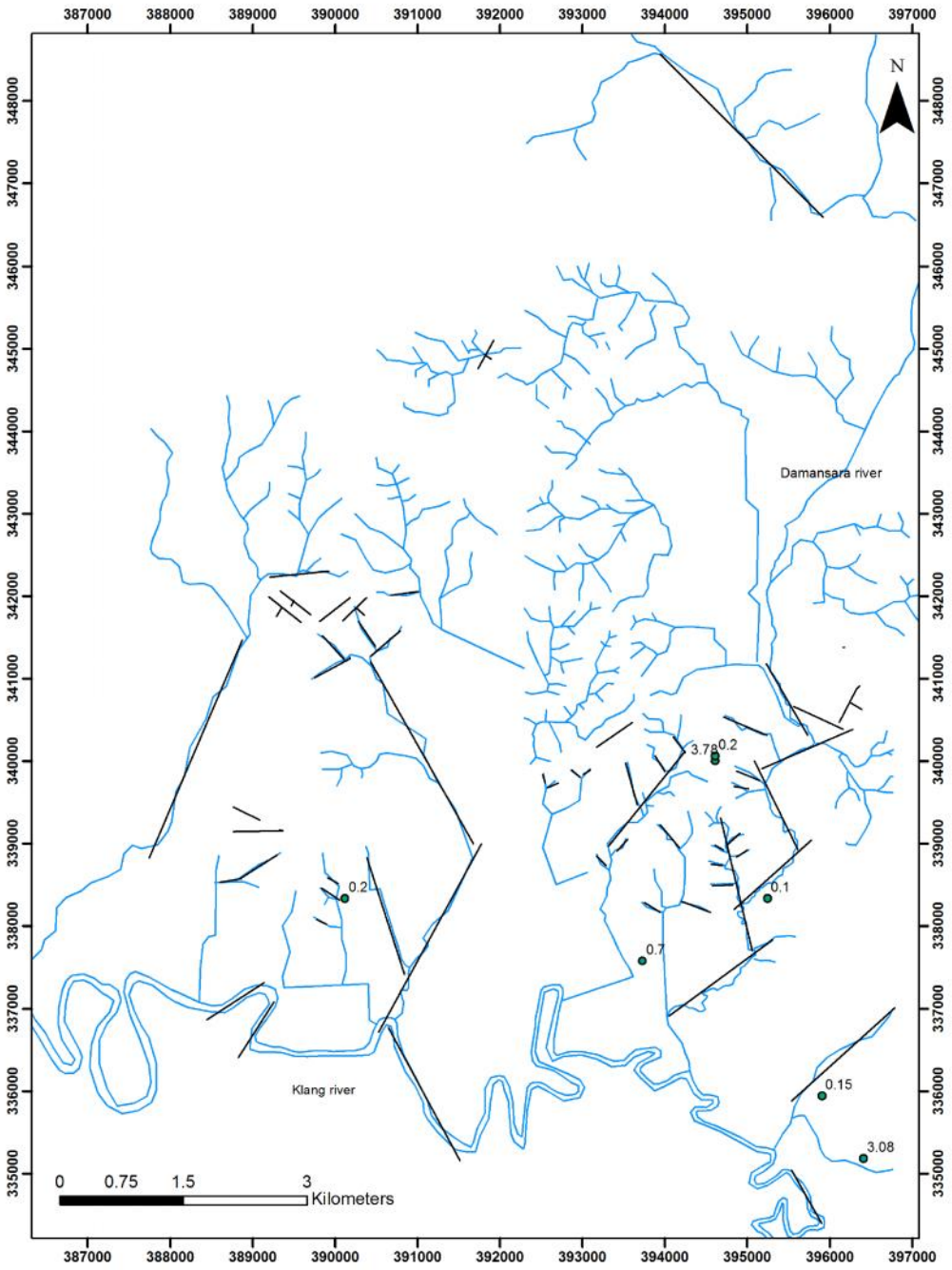

Figure 5.15 K values distribution for Class C and D.

5.4 Aquifer and Well Characterization Using Step Drawdown Test Analysis

5.4.1 Introduction

There are 14 tubewells with step drawdown test data in the study area. Each of the wells has been analyzed using the Bierschenk & Wilson method and the Eden & Hazel method which will be discussed in Section 5.4.2 and 5.4.3. The results obtained from two methods are compared in Section 5.4.4. Well loss calculation is discussed in Section 5.4.5. Perhaps the most potentially useful results are those that do not follow the theoretical models behind the analytical methods, as they can indicate where assumptions are not valid, thus suggesting possible new insights into the flow processes. In Section 5.4.6, the causes of non-linear and negative s_w/Q v. Q relationships will be discussed. The conclusions will be in Section 5.4.7

5.4.2 Bierschenk & Wilson method

The responses have been classified into three groups. Figure 5.16 shows the wells in Class 1 with a positive relationship between specific discharge and Q (C>0). Table 5.7 shows the step drawdown test results from Class 1. When the discharge rate increases, the specific drawdown value increases for wells in Class 1 as they should do according to the step test theory. The wells in this class therefore have positive C values. These values average 2 x 10^{-5} d^2/m^5 except for the wells at Pokka Ace and Anshin Steel which have rather higher values (10^{-4} d^2/m^5). The B values for wells in Class 1 are positive as required by the theory except for Ansell TW5A which has a B value of around -0.103d/m^2. This result must therefore be ignored for the purpose of determining hydraulic properties though it is interesting from the point of view of understanding the hydraulic processes and is discussed in the discussion section below. The T values obtained using the approximate Logan method range from 17 to 254 m^2/day with an average of less than 100m^2/day.

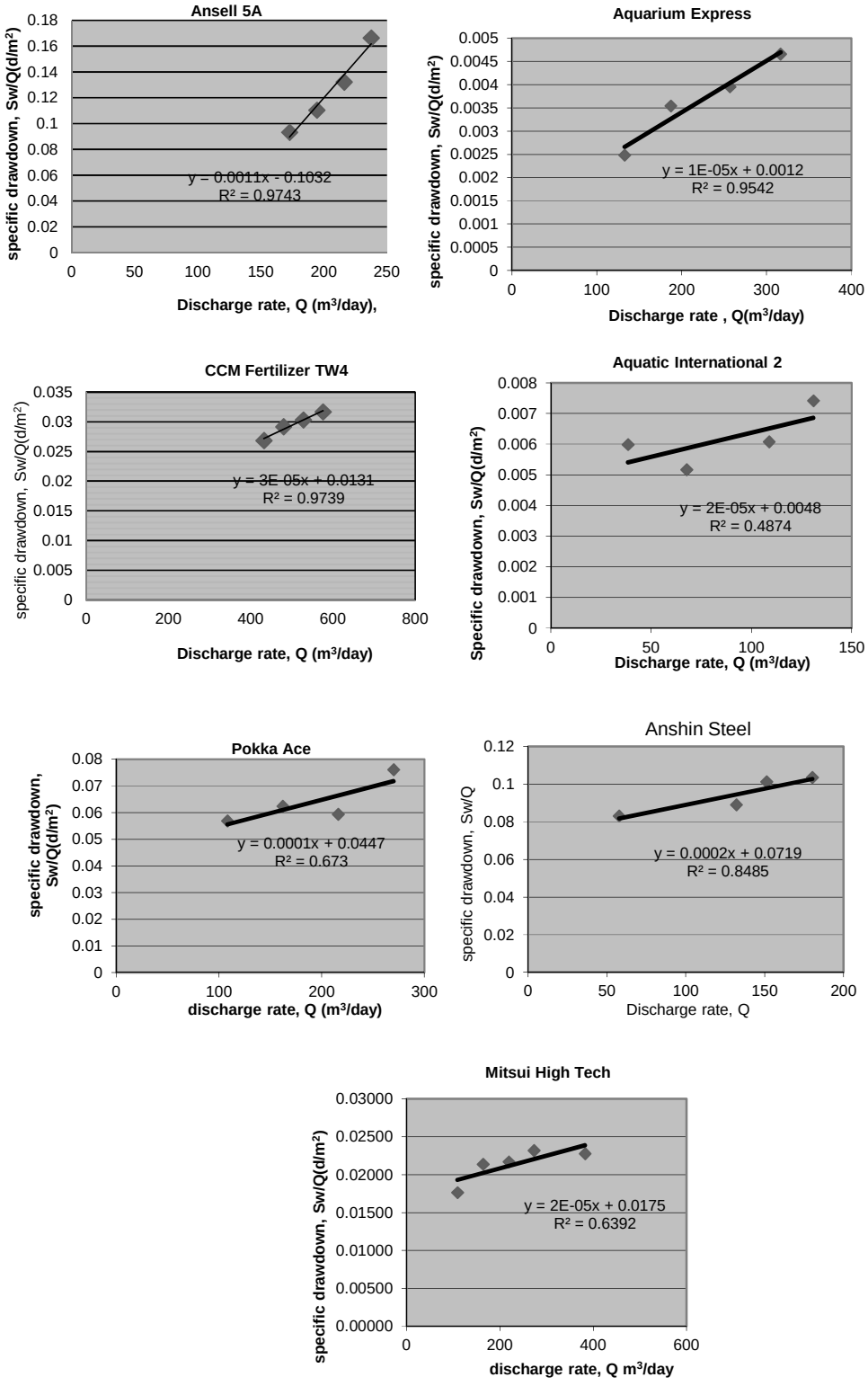

Figure 5.16 Wells in Class 1 with positive slopes

Table 5.7 The hydraulic properties interpreted using the Bierschenk & Wilson method for wells in Class 1

Class 1	B value (d/m^2)	C value (d^2/m^5)	T value (m^2/day) (Logan approx.)	Specific capacity (m2/d)	Group
Mitsui High Tech	0.017	2×10^{-5}	72	58.82	E
Pokka Ace	0.0447	1×10^{-4}	27	22.37	E
Anshin Steel	0.0719	2×10^{-4}	17	13.9	B
Aquarium Express	0.001	1×10^{-5}	1017	1000	A
Aquatic International 2	0.004	2×10^{-5}	254	250	A
Ansell TW5A	-0.103	1×10^{-3}	11.84	9.7	E
CCM Fertilizer TW4	0.013	3×10^{-5}	94	76.92	E

Figure 5.17 shows the plots for the wells in Class 2. The C values for wells in Class 2 are effectively 0 (Table 5.8). Though some are comparable with Class 1 wells, the plots show that the values are uncertain given the significant variation in slope from one step to another. Hence Class 2 wells are those whose well losses cannot be distinguished from 0 rather than those whose well losses are 0. The B values are close to $10^{-1} d/m^2$. The rough estimates of T range from 2 to 53 m^2/d.

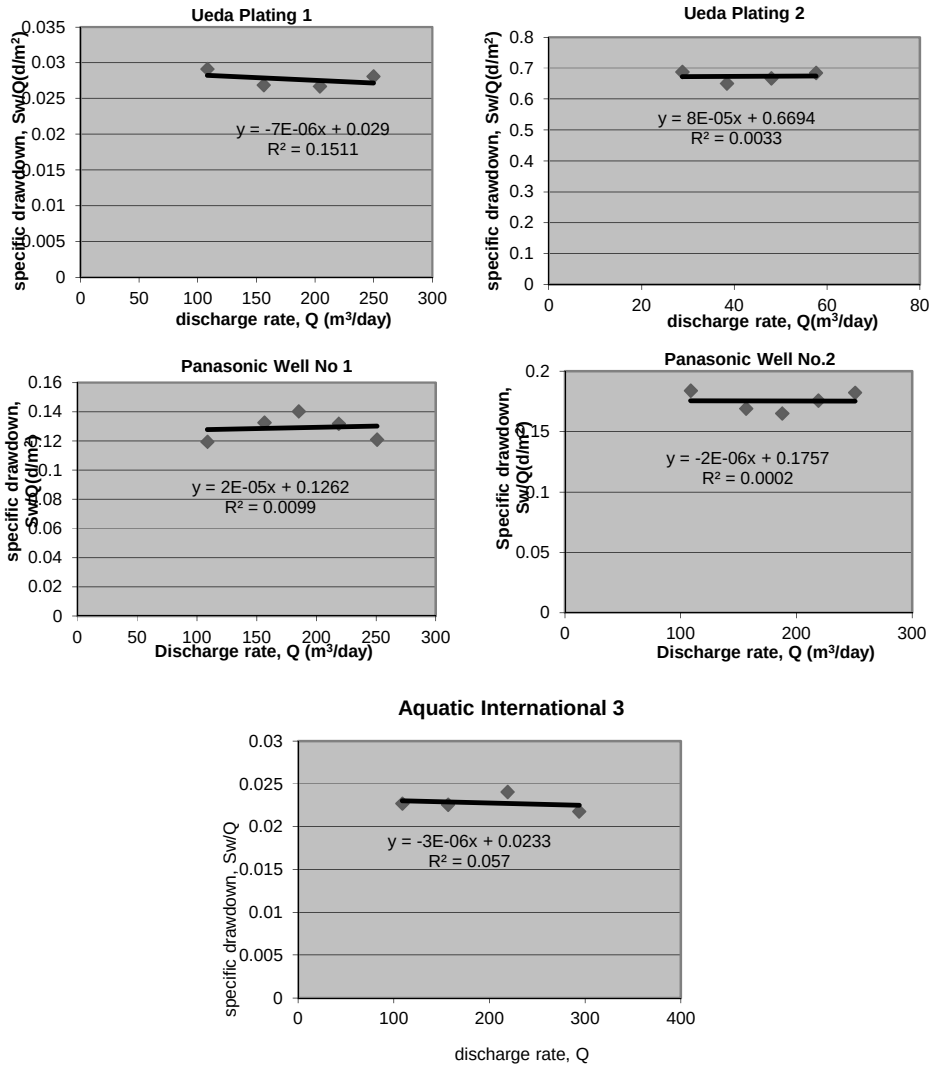

Figure 5.17 Wells in Class 2 with no variation of specific discharge (zero slopes)

Table 5.8 The hydraulic properties for wells in Class 2 interpreted using the Bierschenk & Wilson method

Class 2	B value (d/m^2)	C value (d^2/m^5)	T value (m^2/day)	Specific capacity(m2/d)	Group
Panasonic TW1	0.126	2×10^{-5}	10	7.93	E
Panasonic TW2	0.1757	-2×10^{-6}	7	5.69	B
Ueda Plating 1	0.029	-7×10^{-6}	42	34.48	E
Ueda Plating 2	0.669	8×10^{-5}	2	1.49	E
Aquatic International 3	0.023	-3×10^{-6}	53	43.47	A

Figure 5.18 shows the plots for wells in Class 3. For wells in Class 3, the C value is negative and therefore impossible without another process occurring. As a result no results are presented for Class 3. It is possible that whatever process that is affecting these wells may also affect the tests in the Class 1 and especially Class2.

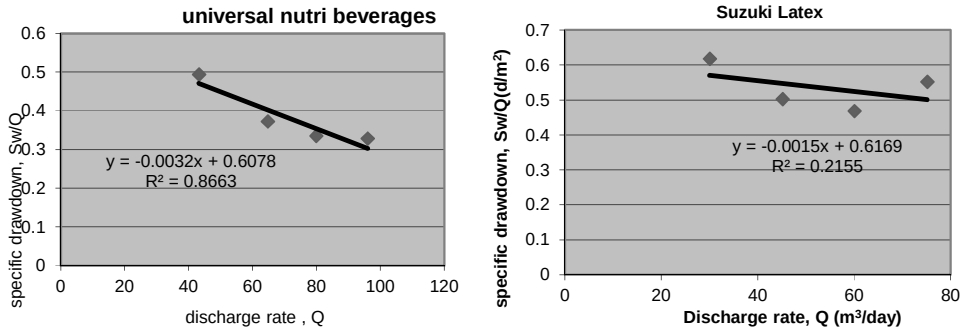

Figure 5.18 Wells in Class 3 with negative slopes. Group E and Group B respectively.

Figure 5.19 shows that the efficiency of the wells in Class 1 varies significantly with pumping rate. A wide range of efficiencies is indicated. Well efficiency is calculated to using formula:

$$\text{Efficiency (\%)} = \frac{\text{aquifer loss}}{\text{Aquifer loss + well loss}} \times 100$$

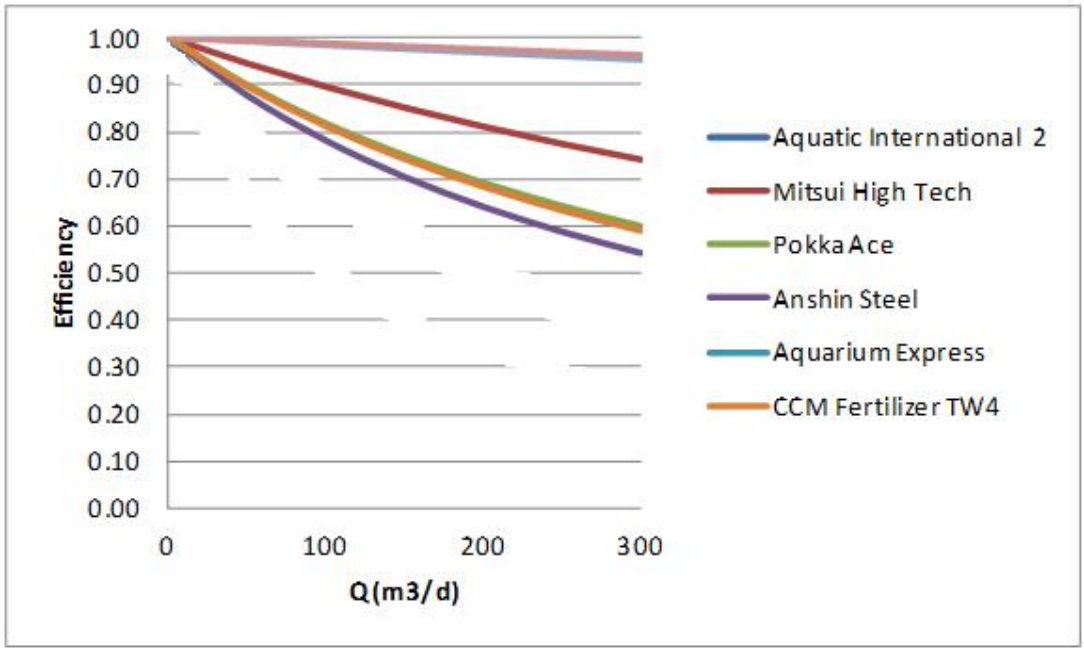

Figure 5.19 Efficiency of wells from Class 1 (C > 0).

5.4.3 Eden & Hazel method

Figure 5.20 shows the example of a well where the analysis was possible. The full results can be seen in Appendix B. The number of tests where the Eden and Hazel method was possible is much fewer than for the B&W method as expected (see theory description in Section 5.2.3). The wells where analysis was possible were limited to Class 1 wells except for Anshin Steel and Aquarium Express. Figure 5.21 includes the case of Universal Nutri Beverages to illustrate a typical case where analysis was not possible, from Class 3. The Bierschenk & Wilson analysis here indicated a negative and so impossible specific discharge – discharge relationship. Class 2 wells were not analysed because C is effectively zero and the Eden & Hazel analysis gives only a value for a which is better investigated using the constant yield test data.

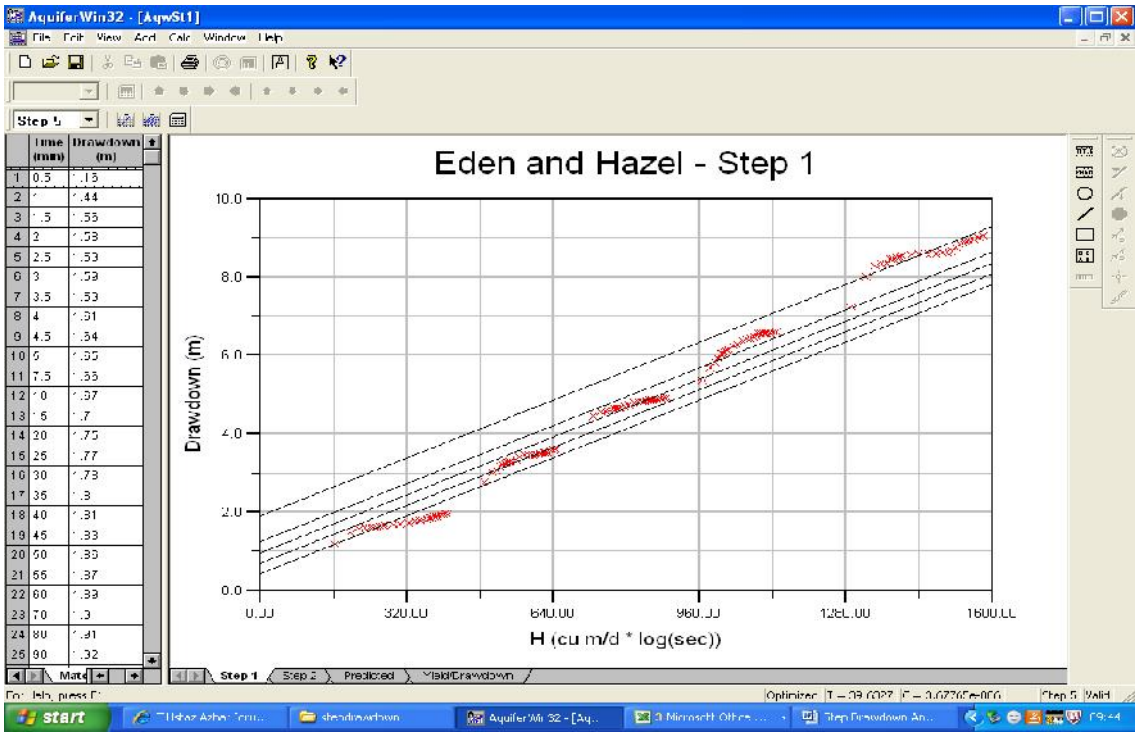

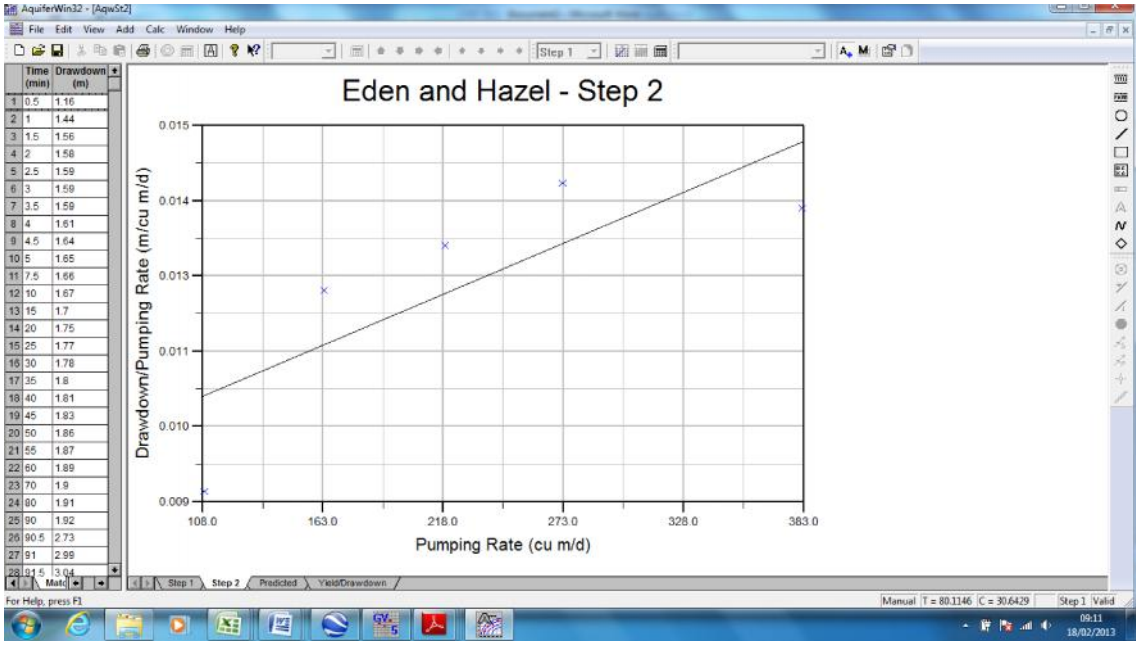

Figure 5.20 An example of well where the Eden & Hazel method was attempted (Mitsui High Tech)

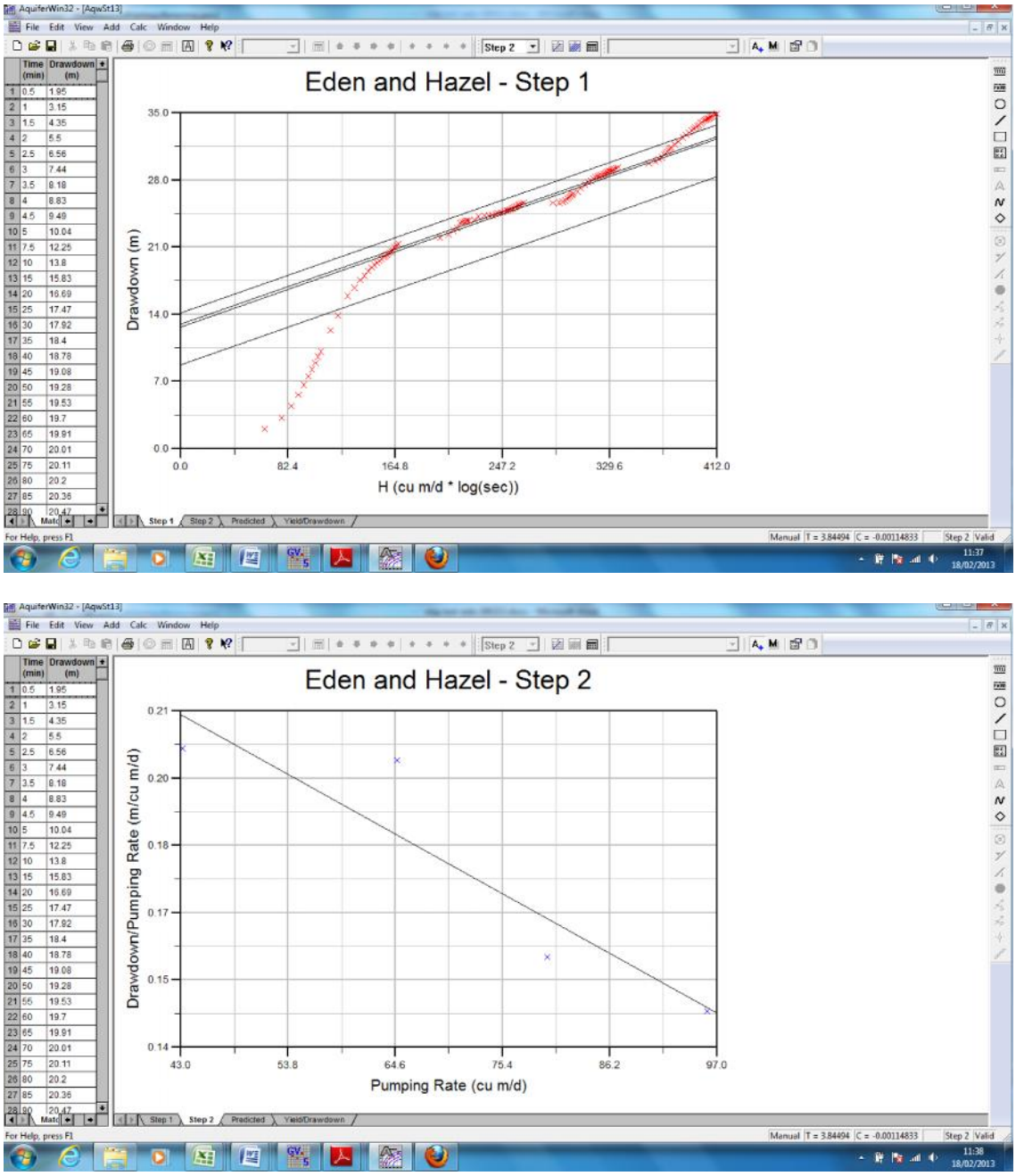

Figure 5.21 The example of well with negative C (Universal Nutri Beverages).

5.4.4 Comparison between two methods

The hydraulic properties obtained from the two methods are compared in Table 5.9. The transmissivity value calculated from the Biershenk & Wilson method is higher than that from

the Eden-Hazel method. Linear correlation forced through the origin of the T values has an r^2 value of 0.98 and a slope of 0.62. This is reasonable agreement given that the Logan approximation used in the Bierschenk & Wilson method is a crude estimation method. Logan's approximation assumes that ratio of radius of influence to radius of well is 2138 (log(re/rw) = 3.33) so most of the wells in Shah Alam would have a radius of influence predicted at 160m. If steady-state is not reached, drawdown will be too small and T will be over not under-estimated by Logan's method. If as in Class A, B and D wells there is probably a recharge boundary then the T value will be over estimated. In the case of Class C wells where barrier may be present then T will be underestimated but there are only 2 Class C wells. To get the T value obtained using Eden & Hazel method, the Logan constant would have to be 3.33 x 0.62 = 2.06 making the radius of influence for most of the wells approximately 10m. Using the Jacob linear approximation, a radius of influence for a first 100 minute step could be around 10-40 m depends on the choice of T and S, but presumably would be bigger if in later steps.

Eden and Hazel's method is for confined aquifer (Kruseman &de Ridder 1994). From aquifer characterization in Section 5.3, Anshin Steel is in Group B which shows recharge response upon pumping. This is possibly the reason why it is difficult to analyze Anshin Steel step drawdown test data using this method though it belongs to Class 1 using B&W method. And for Aquarium Express, the C value is negative when analyzed using Eden and Hazel's method. Most of the wells in Class 1 are from Group E (confined aquifer) except for Aquatic International 2 which is also from Group A. However, this idea will be investigated further in next section.

Various questions remain unanswered: (i) do the departures from theory seen in the step test analysis indicates anything about flow processes?; (ii) do the wells of Class 2 really have C = 0?; and (iii) can the Class 3 step tests (negative specific discharge – discharge slopes) indicate flow mechanisms? These and other questions will be looked at in next section.

Table 5.9 Comparison of hydraulic property values obtained from the Bierschenk & Wilson / Logan (B & W) and Eden & Hazel (E & H) methods

	B value (d/m^2)		C value (d^2/m^5)		Transmissivity, T, value (m^2/day)		Class	Group
	B & W	**E & H**	**B & W**	**E & H**	**B & W**	**E & H**		
Aquarium Express	0.001	3.2×10^{-3}	1×10^{-5}	-	1017	184.54	1	A
Aquatic International 2	0.004	-0.0008	2×10^{-5}	3×10^{-5}	305	196	1	A
Mitsui Hightech	0.017	0.0036	2×10^{-5}	3×10^{-6}	72	40	1	E
CCM Fertilizer TW4	0.013	0.0107	3×10^{-5}	7×10^{-6}	94	51	1	E
Pokka Ace	0.0447	-0.0025	1×10^{-4}	5.65×10^{-5}	27	13.5	1	E
Ansell 5A	-0.103	-0.189	1×10^{-3}	7.7×10^{-4}	-	4.58	1	E

5.4.5 The causes of non-linear and negative s_w/Q v. Q relationships

5.4.5.1 Introduction

In this section reasons for the step test results not following the Jacob theory are discussed. If the Jacob theory is not followed then the sw/Q v. Q relationship will not be linear and even when an approximate linear relationship exists in some cases, no sensible Eden & Hazel interpretation will be possible. Just because the plot is linear does not mean that the theory is followed but in this case it will not be possible to tell. By looking at the departures from theory it may be possible to tell something more about the aquifer behaviour.

Well losses are due to resistance of flow near and in the well due to turbulent conditions (non-linear head losses) and flow in and near the well due to laminar flow (linear head losses) (Clark 1975). According to Rushton & Rathod (1988), there are a few factors which cause non-linear s_w/Q v. Q relationships in step test data. Possibilities are: when the aquifer condition changes from confined to unconfined conditions; any change of hydraulic conductivity value in the vicinity of the well (development, clogging) during the testing; seepage face occurrence; and decreasing of well penetration due to drawdown increase especially in layered aquifers. In addition, the presence of barriers and recharge boundaries may in some cases have an effect on especially Eden & Hazel interpretability. Also well bore storage could be an issue. It is possible for the well to have one of these conditions or more than one together. Each of these situations have been investigated to try and determine the likely reasons for so many step tests not following the Jacob theory (Bierschenk & Wilson Class 3 and Class 2 (see below), and why Anshin Steel cannot be interpretable using Eden & Hazel method. The main issues are an apparent increase in efficiency with pumping rate (negative C) or at least a change in efficiency with pumping rate. A similar result might occur through a change in aquifer losses (B) with pumping rate.

5.4.5.2 Presence of hydraulic boundaries

Of the step tests done, 2 were from constant yield Group A wells, 3 from Group B, 0 from Group C and Group D wells, and 8 from Group E wells. Of the 5 interpretable step tests, 4 were Group E (consistent with extensive homogeneous system), 2 were Group A (delayed finite yield systems). It is expected that the more interpretable step tests would be from Class E. May be more important is that only 50% of Class A and Class E tests were interpretable and 0% of Class B (out of 3) were interpretable. Hence the aquifer having a boundary is not always enough to make the data uninterpretable and also that not having any obvious

boundary does not make all datasets interpretable. There must be other reasons for uninterpretability.

Having a recharge boundary (including a high permeability fracture?) will mean that the drawdown increment for a step will be less than expected and hence the s/Q v Q plot gradient will flatten a bit. Table 5.10 shows the drawdown in every step of wells. For wells in Group A (Aquatic International 3) and B (e.g Anshin Steel), the drawdown decreases when pumping rate increases. For wells (e.g Suzuki Latex, Panasonic 2, Ansell5A, Pokka Ace) which the drawdown shows the increment on the third step onwards with increasing pumping rate is possibly due to the barrier boundary. For Ansell5A and Panasonic 2, the barrier boundary possibly due to well interference since there are other 6 pumping wells in Ansell and another well in Panasonic.

For a barrier boundary (including a low permeability cemented fracture?) the slope would be expected to increase. Sometimes this will not be enough to cause a significant change in slope and sometime it will happen early enough in the step test so that the relationship over the steps is approximately linear. The Eden & Hazel interpretation especially when applied using a computerised optimisation will be more sensitive to these differences as explained in Section 5.4.3. In addition, for low pumping rate steps, the features of the constant yield higher pumping rate tests may not occur simply because the zone of influence of the well has not widened far enough, but as the test continues the features may be encountered and the step responses therefore appear inconsistent – the step test may in this sense be a good indicator of lateral heterogeneity.

Table 5.10 Drawdown of each steps in step drawdown test for wells in C;

Well	Class	Group	Step Test (drawdown,m)				
			S1	S2	S3	S4	S5
Mitsui High Tech	1	E	1.92	1.58	1.25	1.58	2.38
Aquarium Express	1	A	0.33	0.333	0.354	0.458	-
Aquatic Int 2	1	A	0.23	0.12	0.31	0.31	-
CCM Fertilizer TW4	1	E	11.6	2.4	2.2	2.24	-
Pokka Ace	1	E	6.15	3.96	2.71	7.71	-
Anshin Steel	1	B	5.0	7.08	3.96	3.33	-
Ansell 5A	1	E	16.13	5.32	7.1	10.97	-
Panasonic 2	2	B	20	6.5	4.5	7.5	7.25
Panasonic 1	2	E	12.57	7.71	3.43	3.71	1.43
Ueda Plating 1	2	E	3.15	1.04	1.26	1.56	-
Ueda Plating 2	2	E	19.81	5.19	7.04	7.41	-
Aquatic Int 3	2	A	2.47	1.07	1.73	1.13	-
Suzuki Latex	3	B	18.54	4.17	5.42	13.33	-
Universal Nutri Beverages	3	E	21.33	2.83	2.67	4.67	-

5.4.5.3 Well bore storage

As discussed in Section 5.2.1, the well bore storage time limit for lower T wells, can be quite long; sometimes more than the 100 minute steps (e.g. Universal Nutri Beverages and UEDA Plating 2). So the first step could be mainly controlled by dewatering the well bore rather than testing the aquifer. This could lead to first step with a s/Q value inconsistent with later steps (see Table 5.10). The drawdown recorded in first step for Ansell5A, Universal Nutri Beverages, UEDA Plating 2, Suzuki Latex, CCM Fertilizer TW4 and Panasonic 2 are much higher than drawdown recorded in following steps. Table 5.10 shows the drawdown every step for wells. These wells are from Class 2 and 3 except two of them are from Class 1.

5.4.5.4 Seepage face

Seepage condition occurs when the pumping water level falls below the bottom of the solid casing in the borehole. Discharge from the seepage face is less efficient than from the same length of saturated borehole wall. Table 5.11 shows the pumping water level in final step in

each well and the depth of the casing. It should be noted that a seepage face might also occur at the interface with the gravel pack if this rises above the base of the casing.

Table 5.11 The depth of the casing and the pumping water level of each of the wells.

	Class	Group	Depth of the solid casing (m)	Pumping water level (m bgl)	Seepage Face likely?	Weathered Zone Thickness (m)	Change to Unconfined Likely?
Mitsui High Tech	1	E	36	15.14	No	18	No
Pokka Ace	1	E	37.5	31.18	No	?	No
Aquarium Express	1	A	29.5	3.94	No	26	No
Aquatic Int2	1	A	36.5	2.62	No	15	No
CCM Fertilizer TW4	1	E	80	19.18	No	?	No
Anshin Steel	1	B	48.8	22.29	No	?	?
Ansell 5A	1	E	65	59.78	No	38	Yes
Aquatic Int 3	2	A	25	9.3	No	24	No
Ueda Plating 1	2	E	40	13.6	No	?	?
Ueda Plating 2	2	E	43	48.4	Yes	?	?
Panasonic TW1	2	E	30	38.9	Yes	60	No
Panasonic TW2	2	B	30	58.0	Yes	60	No
Suzuki Latex	3	B	45	50.0	Yes	?	?
Universal Nutri Beverages	3	E	48.78	36.4	No	17	Yes

From the information in Table 5.11, for Class 1 boreholes would not be likely to have a seepage face. Of the Class 2 boreholes (C indistinguishable from 0), two are unlikely to have seepage faces, and three probably have, at least on the higher step rates. Of the Class 3 boreholes (C apparently < 0) one is likely to have a seepage face and one is not. If seepage faces contribute to non-standard behaviour then it is not always the only reason.

However, if it is a reason then it would have to reduce the C value. As the drawdown increases the seepage face will develop as a larger fraction of the drawdown so to have the same inflow rate drawdown has to increase more than expected and hence C should increase rather than decrease. This is what Rushton & Rathod (1988) show. So seepage faces can only

result in steepening of the s/Q v. Q plot after the water has dropped below the casing. This could be the case for Ansell 5A and Pokka Ace where there is a negative s/Q intercept.

5.4.5.5 Low or high K layers

Lower or higher K layers can have a similar effect on s/Q v. Q plot according to Rushton & Rathod (1988) as water level falls below them. This would result in increasing slope with increasing Q. Again this is not clear from the plots.

5.4.5.6 Hydraulic conductivity changes near to the well

The flow of water into the well depends on the hydraulic conductivity of the area near the well. Non linear well losses can occur due to hydraulic conductivity changes near the well (Rushton & Rathod 1988, Rushton 2003). The hydraulic conductivity of this zone can be reduced by drilling fluid clogging the voids and fractures adjacent to the well (Walton 1962) or by developing during pumping. As Rushton & Rathod (1988) show this will result in increase in B and if the permeability changes during the test as more water is extracted this will mean also a change in slope (C) with clogging resulting in C increase and development in C decrease. This may be seen as non-linear s/Q v. Q plot or may be even if happening the plot is still linear but could be higher or lower slope than expected and even negative slope.

5.4.5.7 Turbulent conditions in fractures

Rushton & Rathod (1988) indicate that this may cause non-linear s/Q v. Q plot with slope decreasing with increasing Q. This might contribute to some of the cases. This is possibly due to fracture near the well as for Aquarium Express where the well is embedded in fractured limestone while Ansell 5A is in phyllite.

5.4.5.8 The change of aquifer condition

A non linear s/Q v Q relationship can occur when the aquifer changes the condition from confined to unconfined conditions (Rushton & Rathod 1988, Rushton 2003). This condition is denoted by negative C value, the specific drawdown decreasing with increasing pumping rate. There are two wells in study area with negative C values which are Universal Nutri Beverages and Suzuki Latex. Both wells lie in the shale.

5.4.6 Conclusion

From step test analysis, there are many possible reasons why the step test is not following Jacob theory. There appears to be no single process that explains all the non-theoretical results. Table 5.12 indicates the processes that could be responsible for non-theoretical step test behaviour in the tests where theory is not followed. It seems there much be combinations of reasons. Most likely are due to the hydraulic boundaries such as recharge boundary.Least likely are turbulence in the fracture. This indicates that step drawdown test is very useful for understanding processes occur in aquifer.

Table 5.12 Processes that could possibly have affected the step drawdown tests in particular wells where responses were not as expected from theory (CM is conceptual model; Rushton & Rathod ,1988)

CM = conceptual model; ? = no data and/or possibly;

Affects CM?	-	-	No	Yes	No	Yes	Yes	Yes (r)	No	
Well	**Class**	**ST Type**	**Seepage Face?**	**Con/ Uncon**	**Bore S**	**Rech Bound**	**Layers ?**	**K(t, r)**	**Turb**	**Concl**
Aq Int3	A	2	No	No		No	No	?	-	K(t,r)?
UEDA1	E?	2	No	?		No	No	?	-	
UEDA2	E?	2	Yes	?	?	No	No	?	-	Seepage face
Pan 1	E	2	Yes	No	?	No	No	?	-	Seepage face
Pan 2	B	2	Yes	No	?	Yes	No	?	-	Seepage face
Suzuki	B	3	Yes	?	?	Yes	No	?	-	Seepage face
UNB	E	3	No	Yes	?	No	No	?	-	Con/Uncon

5.5 Aquifer Characterization Using Constant Yield Test Analysis

5.5.1 Introduction

As was the case for the step tests, the aim of this section is to analyze the available constant yield pumping test data to obtain the hydraulic properties of the aquifer and to see if they indicate anything about aquifer behaviour.

The pumping tests for wells in study area have all been carried out in the pumping well itself. No observation wells or piezometers have been installed at the sites. The well is pumping for 24 hours, a short time, and the water level changes are recorded. The drawdown measurements in a single well test are influenced by well losses (as discussed in Section 5.2.4) and possibly by well bore storage. As discussed in Section 5.4, there are only six wells (Table 5.13) with well losses calculation.

There are various methods for analysing constant yield test data. Therefore, the method used for data analysis is based on the conceptual model developed earlier. For study area, Cooper Jacob method is used since this method would not be influenced by well losses (Lloyds 1999). Whereas the drawdown data which is deviated from Jacob straight method indicates other hydrogeologic condition such as recharge boundary and barrier boundary (Sterrett, 2007).

It is of interest to compare the consistency of the step test results and the constant yield test results, where this can be done. Using the pumping rate of the constant yield tests, the B and C values from the step test were used to calculate the total predicted drawdown for the constant yield test at t = length of each step in the step test. This was compared with observed constant yield drawdown at the same time. The difference between the observed

and predicted drawdowns is a measure of the lack of agreement between the methods. The results are shown in Table 5.13.

The ratio of predicted to observed drawdown is almost 1 for Class E wells. For Class B, the ratio is more than 1, where the predicted is higher than observed drawdown. The results for these two classes are as expected except for Class A which the ratio of predicted to observed drawdown is less than 1. This indicates how uncertain quantitative analysis is at least in some cases. However, since wells in Class A are located far from other wells in study area; it can be lots of uncertainties in between while Class E is in good agreement.

From the well loss calculation in Table 5.13, the well losses values for the wells are quite significant except for Mitsui High Tech and CCM Fertilizer TW4. The drawdown data for these two wells have been corrected due to well losses before the analysis.

Table 5.13Well losses (observed-calculated drawdown) for wells in Class 1 (C>0)

Class 1 (Group)	**B value (d/m^2) (B&W)**	**C value (d^2/m^5) (B&W)**	**B value (d/m^2) (E&H)**	**C value (d^2/m^5) (E&H)**	**Drawdown obtained from pumping test(m)**	**Drawdown calculated from step test(m) (B&W)**	**Well losses (observed-calculated drawdown) (m) (B&W)**	**Q m^3/d**	**Predicted/ Observed drawdown (B&W)**
Mitsui High Tech (E)	0.017	0.00002	0.0036	$3x10^{-6}$	9.88	9.62	0.26	382.3	0.97
Pokka Ace (E)	0.0447	0.0001	-0.0025	$5.7x10^{-5}$	16.4	14.32	2.08	216	0.87
Anshin Steel (B)	0.0719	0.0002	-0.015	$1.1x10^{-4}$	27	32.92	-5.92	264	1.22
Aquarium Express (A)	0.001	0.00001	$3.2x10^{-3}$	-	2.45	1.32	1.13	316.3	0.54
Aquatic Int2 (A)	0.004	0.00002	-0.0008	$3x10^{-5}$	1.68	0.87	0.82	130.8	0.52
CCM Fertilizer TW4 (E)	0.013	0.00003	0.0107	$7x10^{-6}$	18.42	17.44	0.98	576	0.95
Ansell 5A (E)	-0.103	$1x10^{-3}$	-0.189	$7.7x10^{-4}$	30.16	24.04	6.12	216	0.80

5.5.2 Results and interpretation

Figure 5.22 shows one of the well tests which comes close to fitting the Theis curve. Only 13 wells follow the Theis curve which is from Class E while majority of the drawdown plots for wells in study area were deviated from Theis curve. Figure 5.23 shows one of the Cooper-Jacob plots for constant yield test data from Shah Alam. The full results can be seen in Appendix C. The plots are approximately linear for all the Class E wells, by definition. In the other classes, the straight line fit was carried out manually as it requires some judgement not so easily incorporated in AquiferWin32, as shown in Figure 5.24.

As can be seen in Figure 5.24, the early data have been ignored in the fitting procedure, in effect assuming that they are due to well bore storage (the Cooper Jacob method can be applied when $t>25r^2/KD$ or using 1:1 slope on log-log plot). However, the flat late time data could be due to a recharge boundary, e.g. with a river, and this hypothesis, and the leakage mechanism, is further explored by monitoring work data analysis and numerical modelling in the next Section and by groundwater chemistry analysis in Chapter 6.

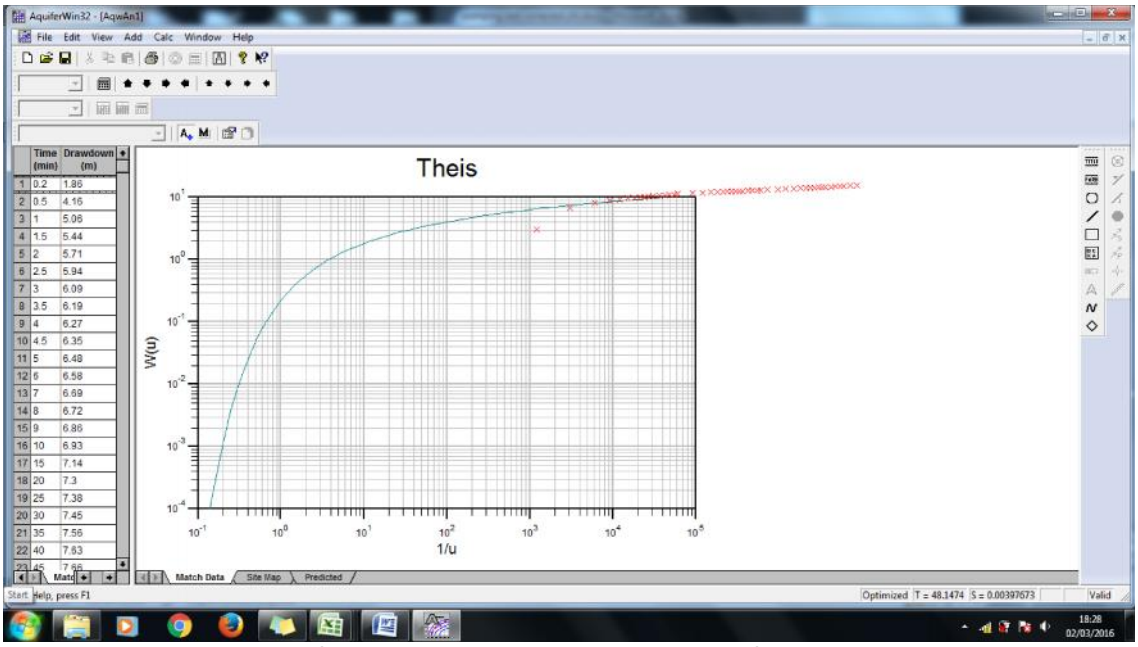

Figure 5.22 An example of a test which can be approximately fitted by the Theis curve Mitsui High Tech -Class E).

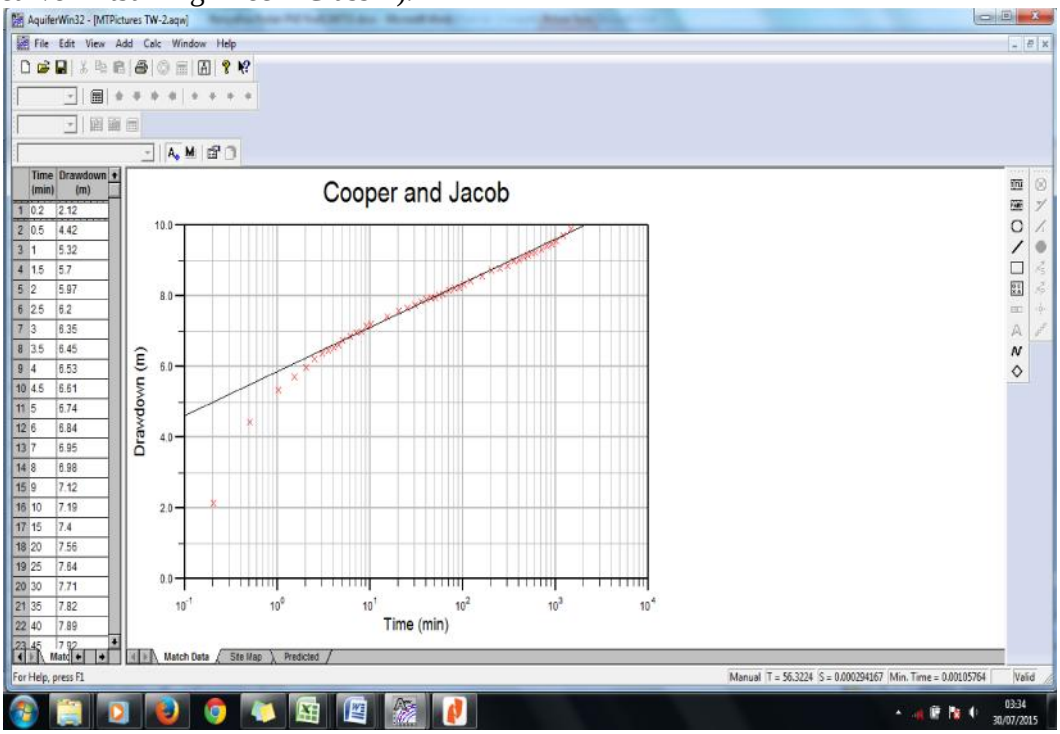

Figure 5.23. An example of a well in Class E (Mitsui Hightech) where the Cooper Jacob plot has been applied. Well bore storage effects are negligible when t > about 3.5 minutes.

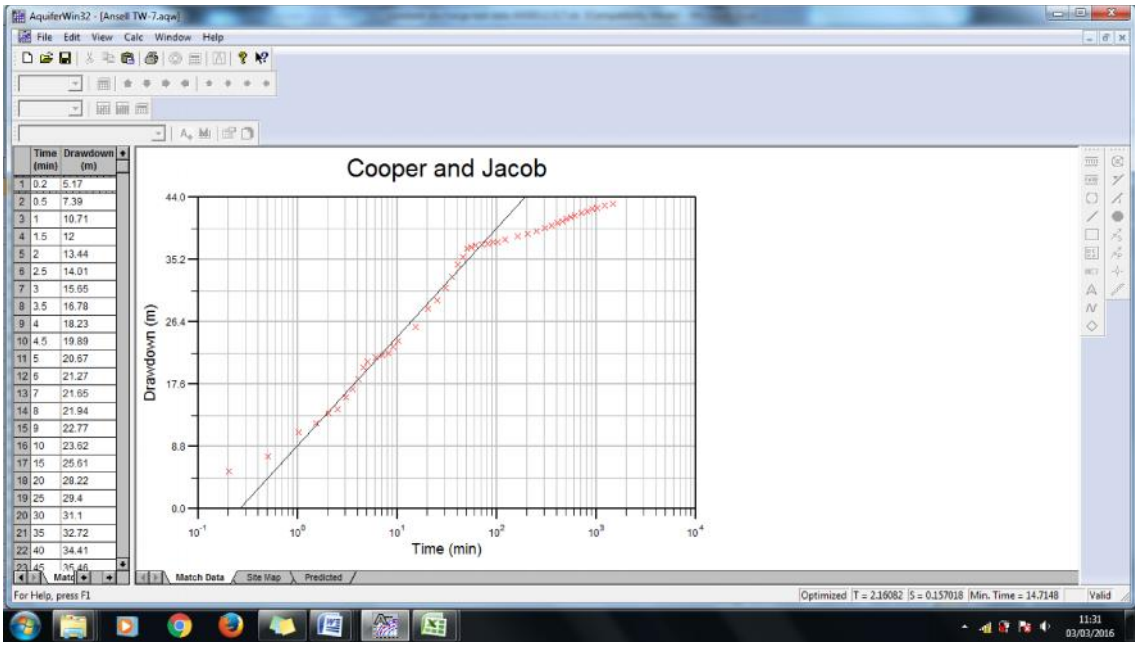

Figure 5.24 An example of a well in Group B (Ansell TW7) where the slope of straight line changes with time. The change of slope is interpreted as recharge where the drawdown encountered the water source at t=50min.

5.5.3 Discussion and Conclusion

From constant yield test analysis,T value for Class A is over 100m^2/d except Aquatic International 3. K value is also higher than 10m/day except for Aquatic International 3. The hydraulic properties obtained using Cooper Jacob is much lower values obtained from step test in Section 5.4.

T values for Class B are less than 10 m^2/d which range from 2 to 8 m^2/d except for Canon Opto 4. K values range from 0.01 to 0.6m/day except for Canon Opto 4. Wells in this class (Class C) with higher T and K values compared to other wells

T value for class D range from 2 to 9 m^2/d . K values is less than 0.1m/day except for Carlsberg No. 1. AESBI is not possible to analyse using Cooper Jacob

due to decreasing flatten drawdown . Therefore, the recovery data in next section will be inspect for further investigation.

45% of well in Class E with high T values (>10 m^2/d) are from this class while the T values for the rest of this class range from 0.5 to 9.1m^2/d. K values range from 0.05 to 0.98m/d except for CCM Fertilizer TW4.

The transmissivity values obtained are plotted against the specific capacities of the wells (Figure 5.25). The specific capacities increase with transmissivities. Most of the transmissivities in the study area range from 1 to 10m^2/day as shown in Figure 5.26.This makes the aquifer low to intermediate transmissivity in the classification of Sharp & Krásny (2003). There are 11 wells with T values higher than 10m^2/day. There are from Class A (3), Class B (1), Class C (2) and Class E (5). Those wells lie in limestone (1), carbonaceous schist (2), interbedded phyllite-quartzite (2), sandstone/quartzite (2), shale (2) and granite (2).Therefore do not relate very clearly to specific rock types again indicating that the interception of fractures is the main control on observed T. All these wells are located near lineaments as shown in Figure 5.27.

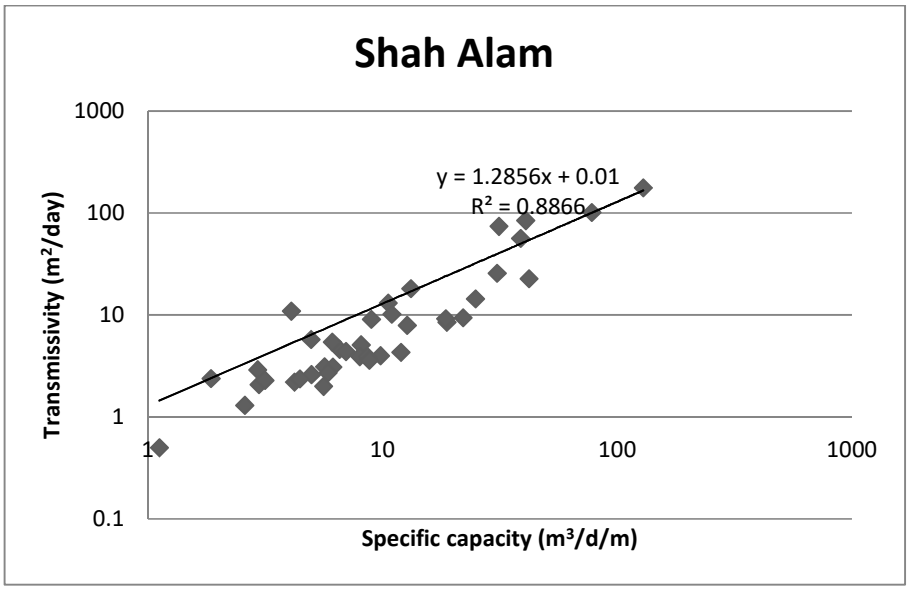

Figure 5.25. The linear relationship of specific capacity with transmissivity obtained by Cooper Jacob method.

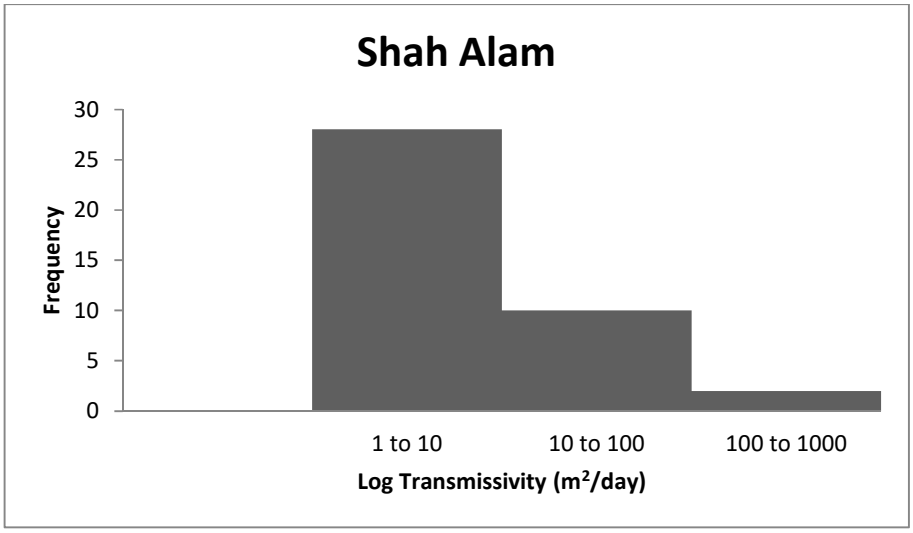

Figure 5.26. The frequency distribution plot of log transmissivity for wells in study area

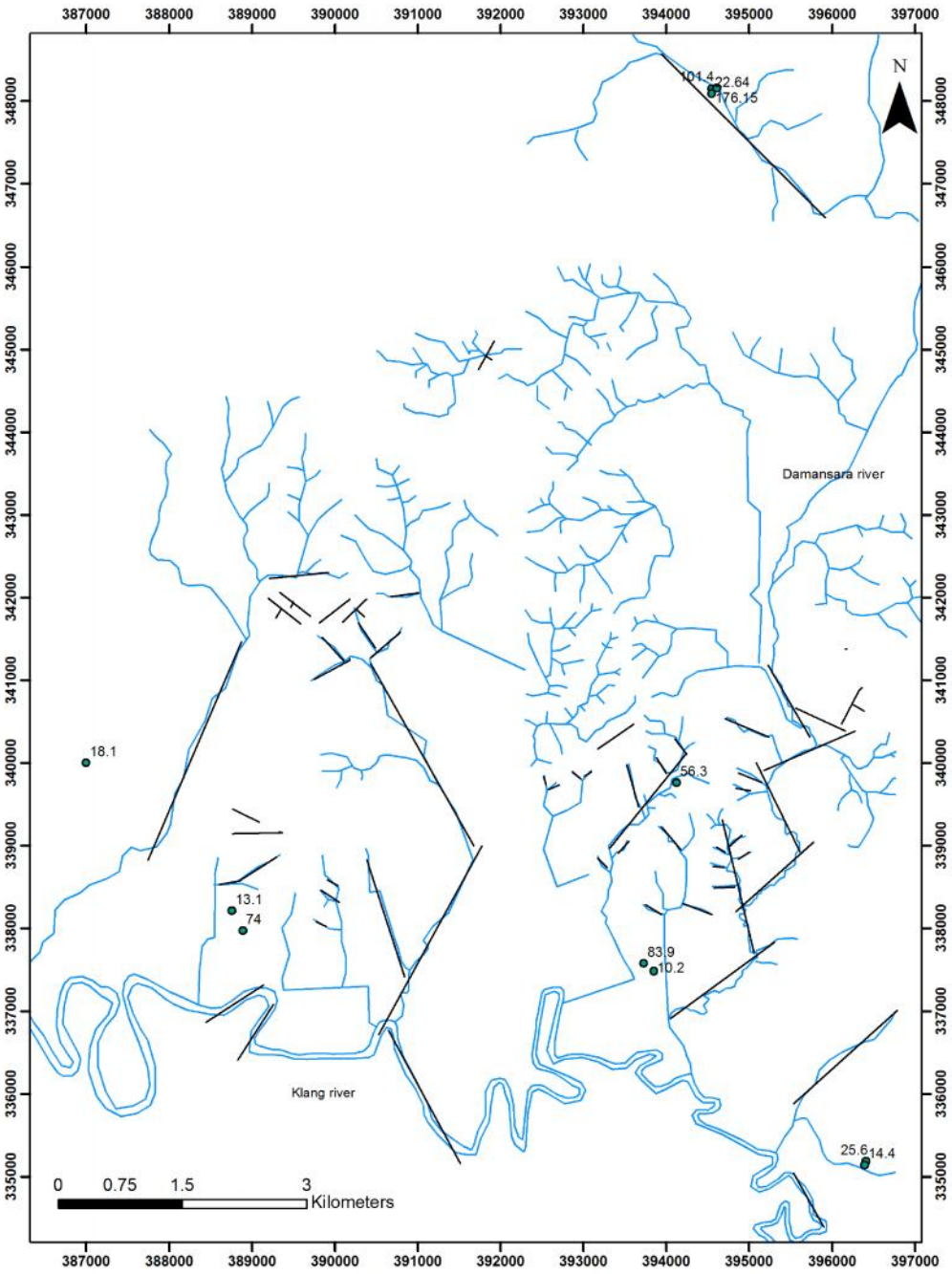

Figure 5.27 Wells with higher T values ($T>10m^2/day$)

Most of the K values estimated range from 0.01 to 1 m/day as shown in Figure 5.28. There are 8 wells with K values which are higher than 1m/d. Those wells lie in limestone (1), carbonaceous schist (2), interbedded phyllite-quartzite (1), sandstone/quartzite (1), shale (1) and granite (2). However, 3 of the 8 wells are in a restricted geographical area, well to the north of the other wells, and from Class A. Figure 5.29 shows the relationship between K values and depth of well. K values increase when the depth of the wells decrease.

The transmissivities value obtained from constant yield test is compared with T values obtained from step test using Bierschenk & Wilson method (Figure 5.30) and Eden & Hazel method (Figure 5.31). The T values obtained from constant yield test are in better agreement with T values obtained using Eden & Hazel method.

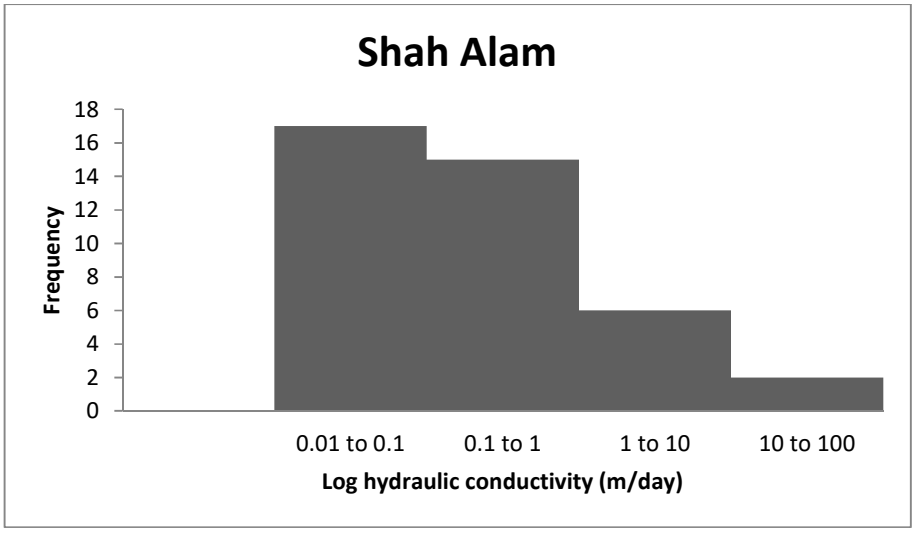

Figure 5.28 A plot of log hydraulic conductivity frequency for wells in study area

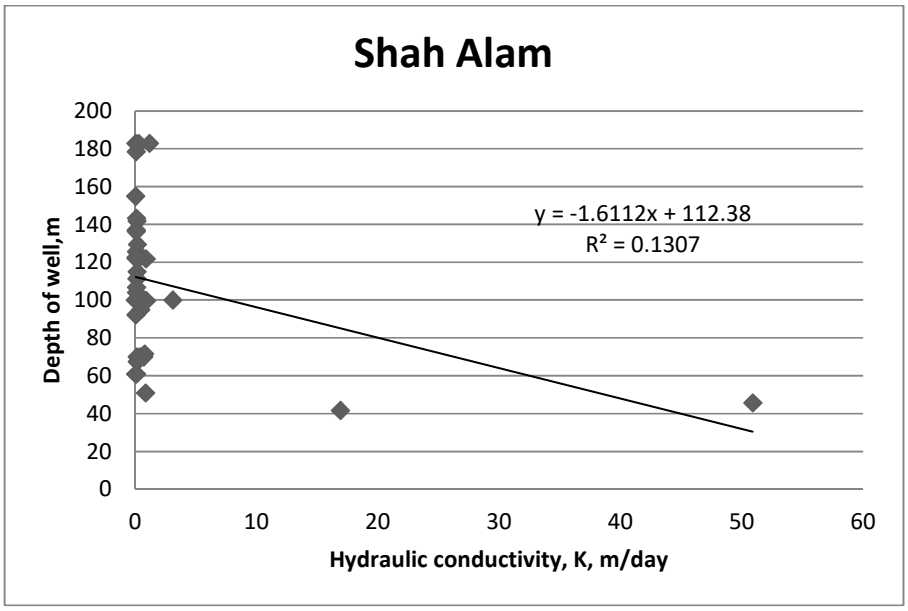

Figure 5.29. K value increases with decreasing depth of well.

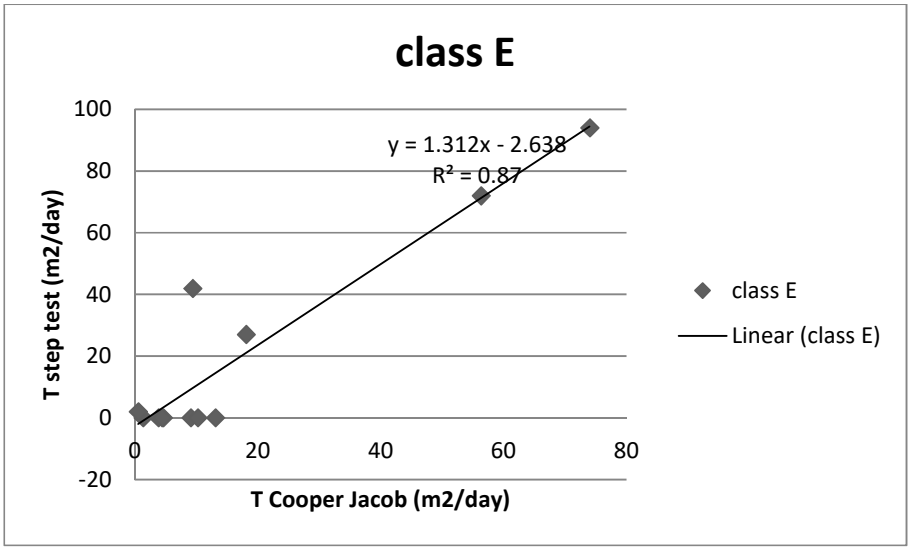

Figure 5.30.Step drawdown test analysis using Bierschenk & Wilson method

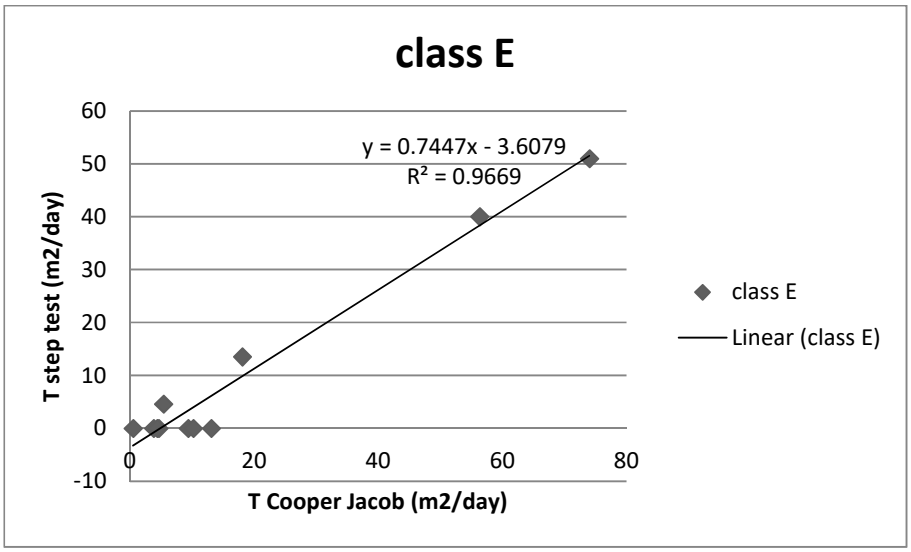

Figure 5.31. Step drawdown test analysis using Eden & Hazel method

5.6 Aquifer Characterization Using Analysis of Water- Level Recovery Data

5.6.1 Introduction

After the well is pumped for a day, the water level during recovery is recorded.The data are analysed by plotting the ratio t/t' (time/time since pumping stopped) against residual drawdown (drawdown after pumping stops). Recovery data for a single well test is more reliable than pumping test data since the data will not be influenced by well loss (Driscoll 1986, Kawecki 1993).

Table 5.14 shows the water level before the pumping test started and final water level after the recovery period. The duration of recovery period varies as shown in Figure 5.32. The shortest period of recovery is 30 minutes while the longest is 600 minutes. The minimum duration for recovery test for well with yield less than 500m^3/day like most of the wells in study area should be at least 1 day (Misstear et al.2006). With a short recovery period, barrier effects may be missed.

All three wells in Class A quickly recovered (almost fully recovery after 210minutes) suggesting that the aquifer system at Aquarium Express and International area has high hydraulic diffusivity (T/S). While in other areas, the water levels are almost recovered at CCM Fertilizer after 360 minutes (excluding CCM Fertilizer 4). The wells in Class D e.g. in the Carlsberg area which has been pumped at the highest rate ($600m^3$/day), the water level is recovered after 500 minutes as shown Figure 5.33. However, this effect cannot be seen for AESBI, Proton B and Gaya Color Lab due to shorter recovery period applied. For wells in Class E, it takes longer than 500minutes for water level to recover. Figure 5.34 shows the relationship between pumping rate and short of recovery for wells in study area.

Table 5.14 Water table information during the constant yield test recovery period

Class	Tubewell	Static Water Level (m.b.g.l)	Q,m^3/d	Recovery test duration (min)	Final water level (m.b.g.l)	short of recovery (m)
A	AQUARIUM EXPRESS	1.83	316.3	210	2	0.17
A	AQUATICS INT2	1.58	130.8	210	1.72	0.14
A	AQUATICS INT3	2.22	293.8	210	2.37	0.15
B	CANON OPTO TW2	0.92	246	30	9.46	8.54
B	CANON OPTO TW4	5.4	468.6	30	14.9	9.5
B	ANSHIN STEEL	2.5	264	600	3.52	1.02
B	PANASONIC TW2	7.84	250.8	300	10.76	2.92
B	PROTON (A)	5.4	264	240	21.2	15.8
B	SCIENTEX POLYMER	7.2	167.8	20	9.58	2.38
B	ANSELL TW1	6.45	228	360	15.78	9.33
B	ANSELL TW7	5.69	180.96	360	12.54	6.85
B	SUZUKI LATEX	2.97	60	60	15.89	12.92
B	CCM FERTILIZERS TW2	3.59	144	360	3.61	0.02
B	CCM FERTILIZERS TW3	2.91	285.7	360	3.77	0.86
B	GOODYEAR TW1	19	408	600	22	3
B	MT PICTURES TW1	6	228	360	11.1	5.1
B	MT PICTURES TW2	5.95	324	360	9.13	3.18
B	MT PICTURES TW4	3.55	336	360	5.17	1.62
B	ANSELL TW5	6	144	300	18.99	12.99
C	ANSELL TW6	6.45	327.4	360	8.86	2.41
C	CANON OPTO TW1	0.5	350	30	3.24	2.74
D	CARLSBERG TW2	7.32	600.9	480	7.62	0.3
D	CARLSBERG TW1	8.54	600	300	8.84	0.3
D	GAYA COLOR LAB	4.12	120	60	5.69	1.57
D	AESBI	3	180	120	11.55	8.55
D	PROTON (B)	2.8	54.5	240	20	17.2
D	CARLSBERG TW4	6.25	600	240	7.03	0.78
E	UNB	1.55	86.4	60	11.42	9.87
E	UEDA PLATING 1	5.48	249.6	90	11.75	6.27
E	UEDA PLATING 2	6.2	57.6	60	13.58	7.38
E	POKKA ACE	9.85	216	60	11.98	2.13
E	MT PICTURES TW5	4.6	300	360	8.2	3.6
E	ANSELL 5A	18.4	216	60	25.04	6.64
E	ANSELL TW2	7.2	164.4	360	26.1	18.9
E	ANSELL TW3	4.57	288	360	16.96	12.39

E	ANSELL TW4	2.55	294	300	3.27	0.72
E	CCM FERTILIZERS TW1	3.48	223.5	360	3.6	0.12
E	CCM FERTILIZERS TW4	1.4	576	60	3.35	1.95
E	MITSUI HIGH-TEC	6.57	382.3	180	7.94	1.37
E	PANASONIC TW1	7.25	250.8	210	8.28	1.03

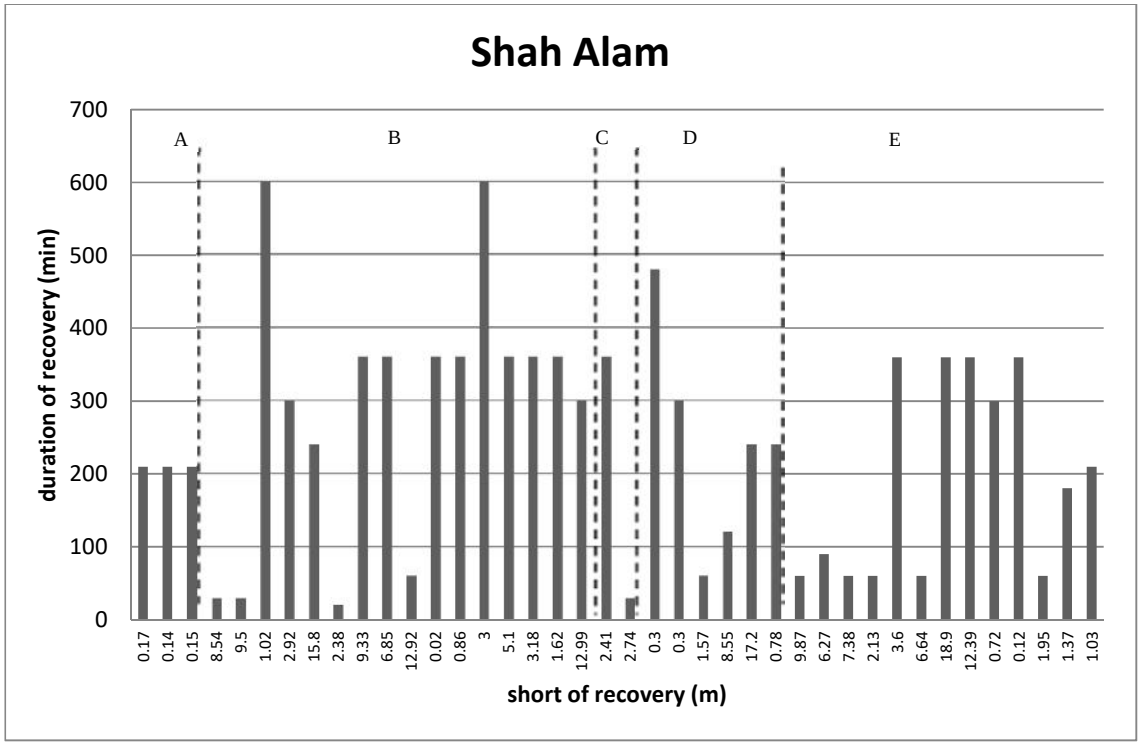

Figure 5.32.The duration of recovery for each well and by how much the water level at the end of the test is short of recovery.

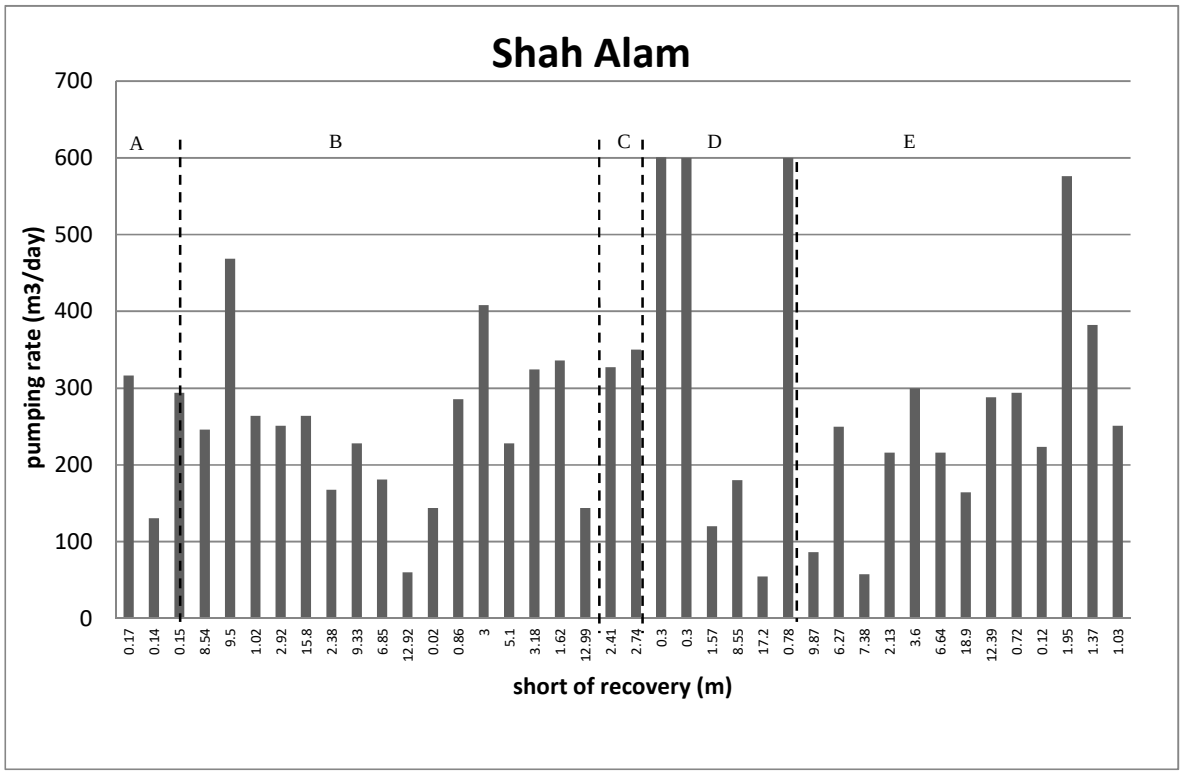

Figure 5.33. The pumping rate for each well and how much water level needs to be recovered

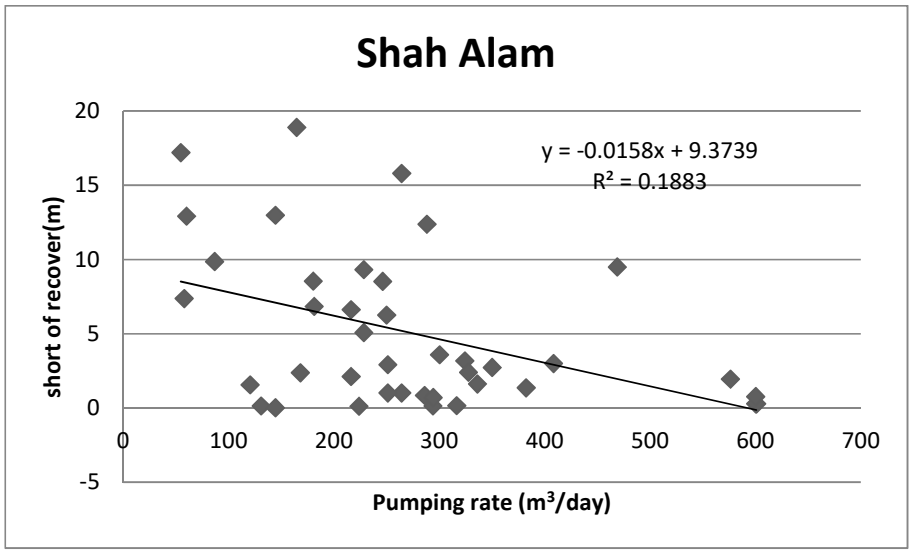

Figure 5.34 The relationship of pumping rate with short of recovery of water level

5.6.2 Results and interpretation

The water level recovery shows linear response with time for wells in Class A, C and E as shown in Figure 5.35. The rest of the plots are in Appendix D. For Class E, all wells can be analysed using Theis recovery method (when $t'>25r_c^2/T$) except for Universal Nutri Beverages and UEDA Plating 2.The t'value for these two wells in bigger than duration of recovery test. The recovery curves for wells in Classes B, C and D show a deviation from expected curve. Theis recovery method for these classes is applicable when $t'<L^2S/20KD$ or $t_p+t'<cS/20$ (Kruseman and de Ridder, 1994, p233). However, due to short duration of recovery test therefore Theis recovery method only applicable for Class E.

The high t/t' deviation is due to well bore storage, these points having $t'<25r_c^2/T$ (Kruseman and de Ridder, 1992, p233) as shown in Figure 5.36. The change of residual drawdown slope for all the wells in Classes B, C and D are possibly due to drawdown caused by well interference except AESBI, Suzuki Latex and Anshin Steel. This suggests that other processes happen in these wells such as recharge from river nearby e.g. AESBI which only located 350m away from the Damansara river. This hypothesis will be further investigated in next section (water level monitoring and numerical modelling).

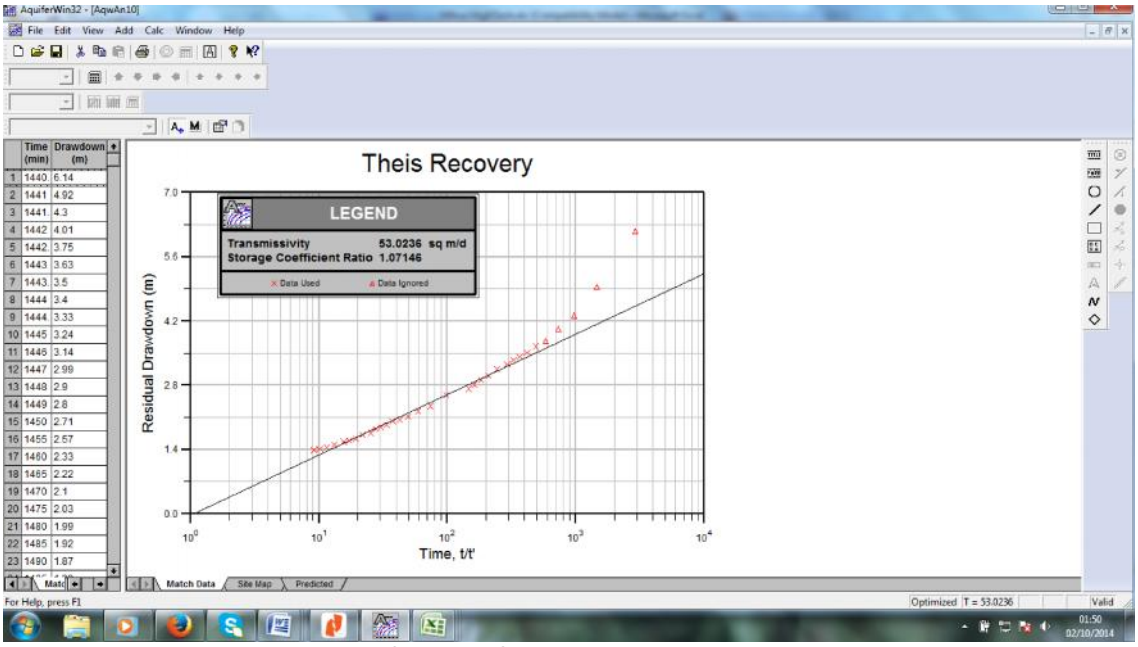

Figure 5.35 Theis recovery plot for one of the wells in Class E (Mitsui High Tech)

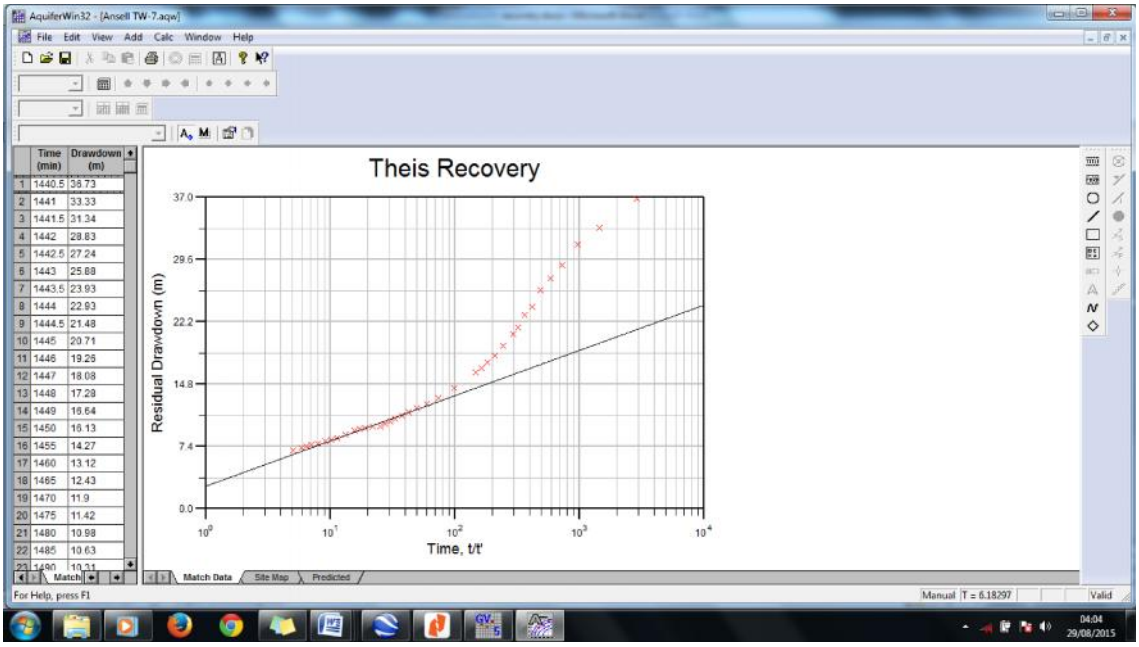

Figure 5.36. Theis recovery plot for one of the wells with high deviation t/t'.

5.6.3 Conclusion

From recovery test analysis, the wells Table 5.15 shows the T values obtained from Theis recovery method and Cooper Jacob method calculated drawdown. The T values from both methods are compared as shown in Figure 5.37. For Class E wells, the T values from both method almost the same with r^2 value is 0.9542 .

Table 5.15 Hydraulic properties obtained from Cooper Jacob and Theis recovery method.

Class	Well	Aquifer	Cooper Jacob T (m^2/d)	~ K (m/d)	Theis recovery T (m^2/d)	~ K (m/d)
A	Aquatic International TW3	Grey schist	22.6	1.2	15.5	0.85
	Aquarium Express	Limestone	176.2	14	207.3	16.9
	Aquatic International TW2	Grey schist	101.4	11	468.4	51
C	Ansell TW6	Phyllite with quartzite	83.9	1.1	20	0.27
	Canon Opto TW1	Granite	25.6	2.1	9.4	0.77
E	CCM Fertilizer TW4	Interbedded quartzite-shale	74	3.7	62.17	3.11
	Universal Nutri Beverages	shale	1.3	0.1	-	-
	Panasonic 1	Shale-sandstone	9.1	0.2	6.6	0.05
	Ueda Plating 1	NA	9.37	0.3	20.6	0.7
	Mitsui High Tech	grey slate with quartz vein	56.3	0.98	53	0.92
	Pokka Ace	NA	18.1	0.2	11.3	0.15
	CCM Fertilizers 1	quartzite-shale,	13.1	0.15	8.69	0.09

	Ansell TW2	grey shale-phyllite with quartzite	3.8	0.05	3.17	0.04
	Ansell TW3	grey shale-phyllite with quartzite	4.6	0.06	5.98	0.07
	Ansell TW4	sandstone-shale	10.2	0.2	7.36	0.16
	MT Pictures 5	Interbedded sandstone-shale	4.4	0.07	6.81	0.09
	Ueda Plating 2		0.5	0.03	-	-
	Ansell 5A	phyllite	5.4	0.1	4.62	0.1

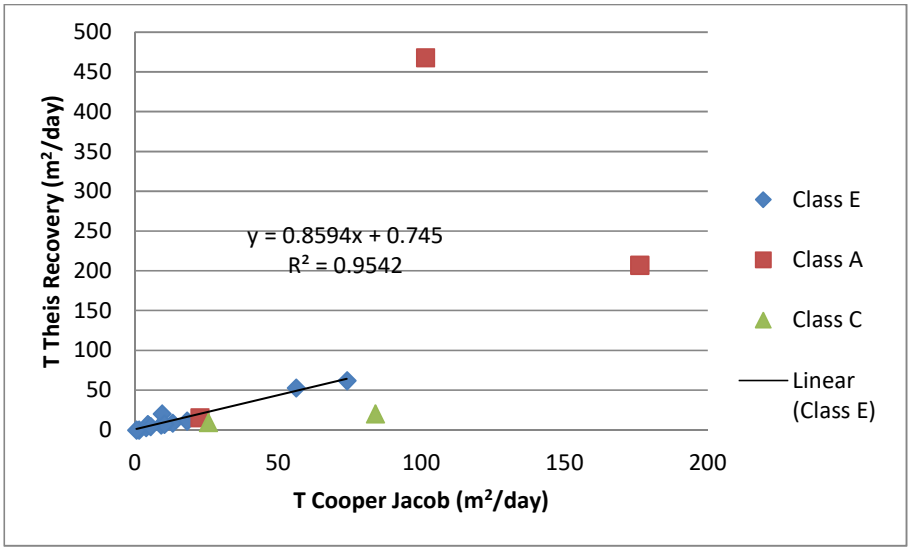

Figure 5.37. The T values obtained using Cooper Jacob and Theis Recovery shows good agreement.

5.7 Aquifer Characterization Using Water Level Measurement in Selected Areas

5.7.1 Introduction

In order to investigate the hydraulic behaviour in wells in the aquifer in more detail, water level and temperature monitoring was carried out at three sites using

a transducer/logger system suspended in the pumping borehole. In systems where the pumping is discontinuous, this approach effectively results in a series of repeats of a pumping test that could provide information on such issues as the effects of recharge and interference from other wells, all at limited cost. However, the pumping is designed for operational use not for testing, and recovery between pumping periods may not be complete. Though there were technical difficulties, including the loss of one of the devices (thus significantly increasing the cost) in one well and the trapping of the system at a level too often above the water table for useful results to be obtained, one set of good results was obtained from Ansell TW7.

The Ansell TW7 well has several features that make it typical of many of the wells in the study area. It is located in interbedded shale and quartzite, which showing 'recharge boundary' effects in their pumping responses. This well is an example of a Class B response, the class to which most wells belong. Its pumping response is one with a sudden change in drawdown slope part way through the test.The well also lies in a compound with several other wells, thus offering a chance to examine the effects of any changes in pumping in these.

5.7.2 Monitoring work in Ansell compound

The Ansell compound is situated in Section 19 beside Pesiaran Perusahaan. There are 8 pumping wells in the Ansell compound (Figure 5.38). The pump for each well is set ON and OFF automatically to refill the 10 ft high storage tank alternately for 24 hours. The pumping rate for each well varies as shown in Table 4.17. TW7 is the most remote of the 7 wells, being over 200m from the nearest.

The Ansell TW7 well was monitored for 12 days from 18th Feb 2011 until 2nd March 2011. From personal communication with the operator, the pump was switched off on 26th and 28th Feb and 1st March 2011.The 'static' water level was measured before the Micro Diver was installed in the well. The 'static' water level is 13.55m. The barometer is installed on top of the well for atmospheric pressure measurement. The atmospheric pressure will be deducted from the water pressure measured in the well to get the water pressure above the diver. The water pressure above the diver was converted to metres. The length of the cable used was 42.24m, and thus the groundwater level could be calculated. The depth of pump is at 85m below the ground. It is important to ensure the diver was not installed near the pump.

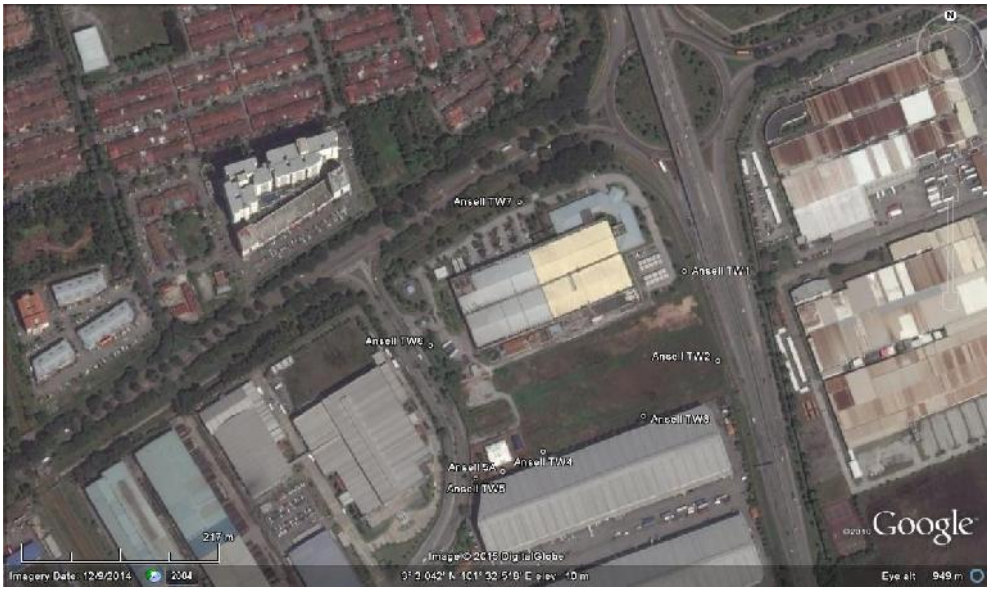

Figure 5.38. Tubewells in the Ansell compound.

Figure 5.39 shows the 'static' water level measured at Ansell TW7 from 2007 to the 2011.Before the static water level was recorded, the pump was switched off

for at least a day: this may not have been enough to get full recovery, but the consistency of the levels suggests it may be reasonable except in 2011.

Table 5.16 The pumping rate, Q for wells in Ansell area.

Tubewell	Pumping rate,Q (m^3/day)
Ansell TW1	228
Ansell TW2	164
Ansell TW3	288
Ansell TW4	294
Ansell TW5	144
Ansell TW6	327
Ansell TW7	181
Ansell 5A	182

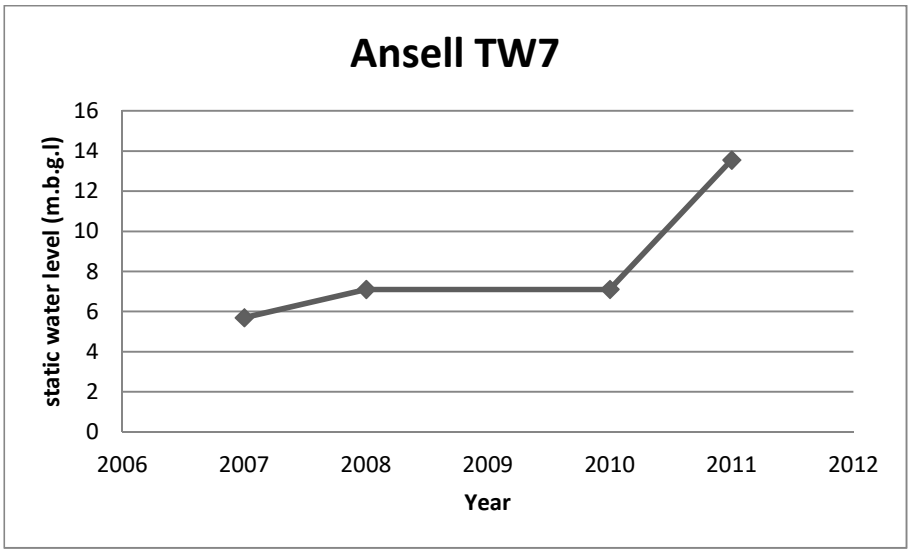

Figure 5.39.The static water level recorded in Ansell TW7

5.7.3 Results and interpretation

Figure 5.40 shows the changes of water level and temperature at Ansell TW7. The measurement was taken at one minute intervals. The pumping rate for Ansell TW7 (according to person incharge) is 4.5m^3/hr (108 m^3/d) which is lower than pumping rate recorded during pumping test. One cycle of measurement

comprises pumping and recovery periods. The data from the pumping and recovery data for each cycle were analysed individually.Table 5.17 shows the period for each cycle. The duration of pumping and recovery varies as shown in Figure 5.41. The wells will be pumping until the tank is full. The longest duration of pumping is 572 minutes which was recorded in Cycle 12. The average recovery period is 54 minutes. The longest period of recovery is 422 minutes which was recorded in Cycle 30.

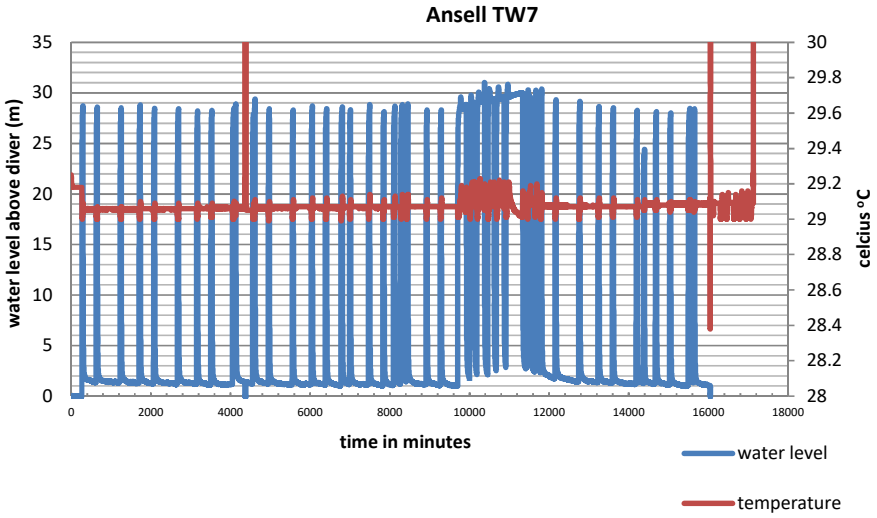

Figure 5.40. The water level measurement at Ansell TW7.

Table 5.17 The period of measurement for each cycle.

Date (2011)	Cycle Number
18th February	1 to 2
19th February	2 to 5
20th February	5 to 8
21st February	8 to 12
22th February	12 to 17
23rd February	17 to 19
24th February	19 to 24
25th February	24 to 29
26th February	29 to 36
27th February	36 to 39
28th February	39 to 43
1st March	43 to 48
2nd March	48 to 52

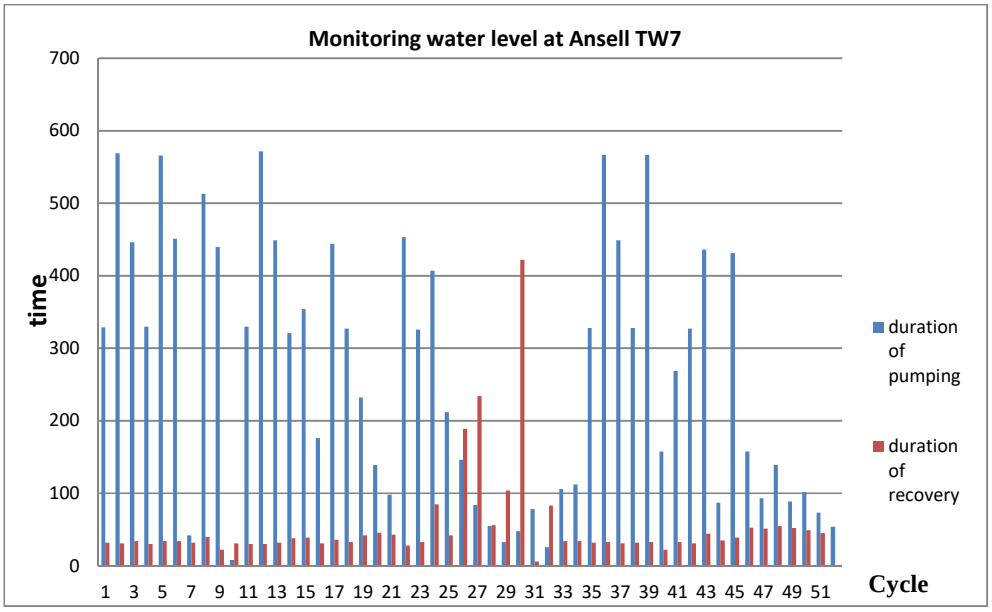

Figure 5.41. The duration of pumping and recovery in Ansell TW7.

From analysing water level patterns each cycle, there are variation of water level. When the pump was switched off, the water level above the Diver ranges from 25 to 28m except for Cycle 10, 34, 43 and 47 to 52 (see Figure 5.40). The water level dropped lower; to 22m in Cycle 10 and even lower in Cycle 34 and Cycle 43 (18m). From Cycle 47 to Cycle 52, the water level is 40m above the diver (36.91m for Cycle 49). When the pump is switched on, the water level above the diver is reduced to 1.5m except in Cycle 10 and Cycle 46 to 52. The water level in well changes rapidly from Cycle 27 to Cycle 33. The variation of water level shows how permeable the weathered layer on top of fractured aquifer as reacted to the rainfall events as been discussed in Section 3.4.2.

The temperature of water is around 18.5ºC. The temperature values fluctuate from 17 ºC to 19 ºC every time pumping activity is stopped (see Figure 5.40). The water temperature from 10000 to 12000 minutes (Cycle 19 and Cycle 29) fluctuates from 17 ºC to 21 ºC rapidly.

The water level above the Diver for each cycle is plotted against time in minutes (e.g. Figure 5.43). The full plots are in Appendix E. Water level dropped around 25 metres for the first 10 minutes of pumping and subsequently decreased much more gently with time, as expected. A similar pattern is also observed for the recovery as shown in Figure 5.44. The water recovers quickly for the first 10 minutes and subsequently there is a markedly slower increase with time.

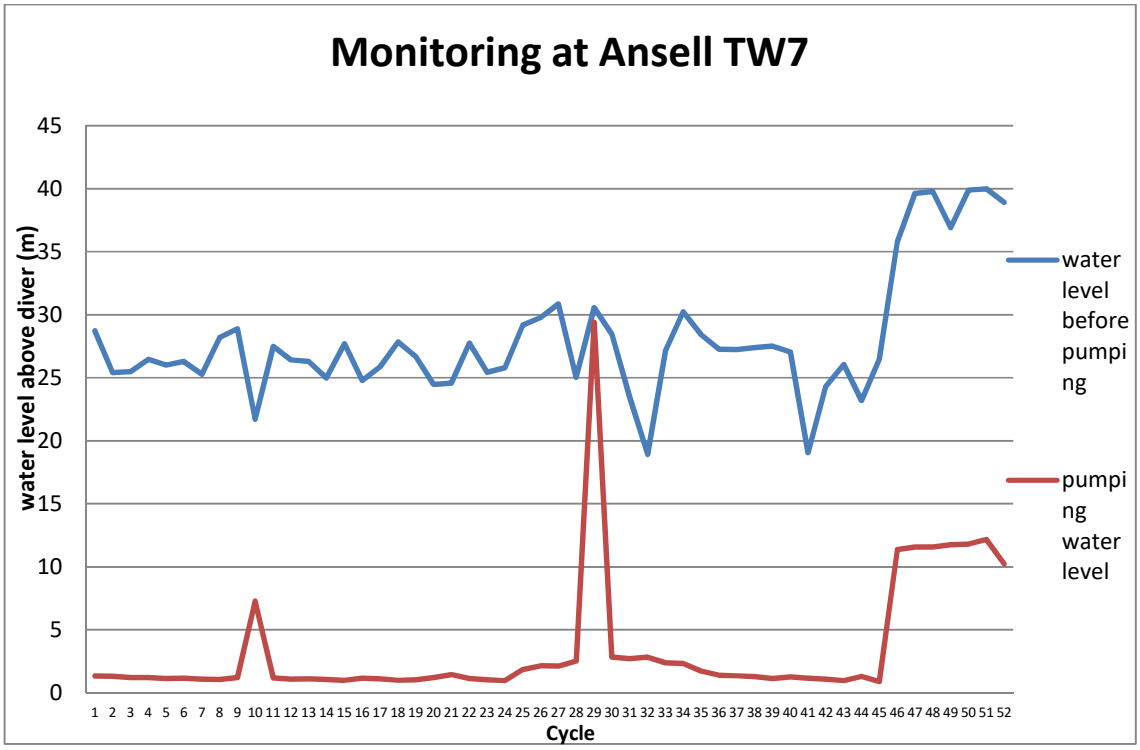

Figure 5.42. The response of water level at Ansell TW7 when pump was ON and OFF.

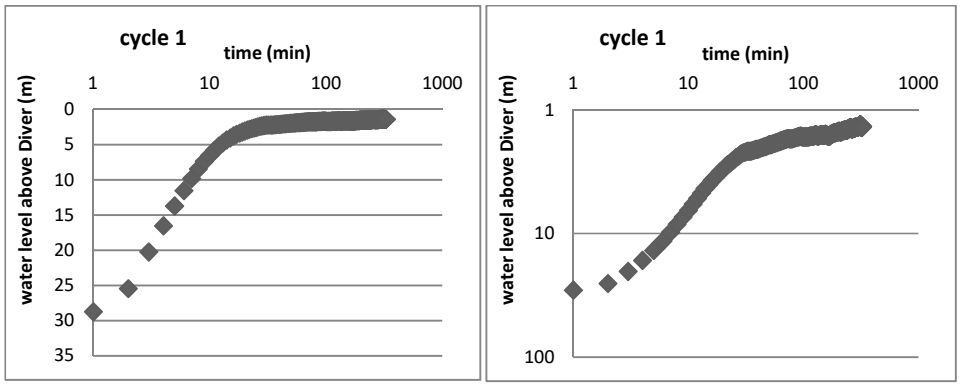

Figure 5.43. The example of semi log and double log plots for Ansell TW7 (Cycle 1)

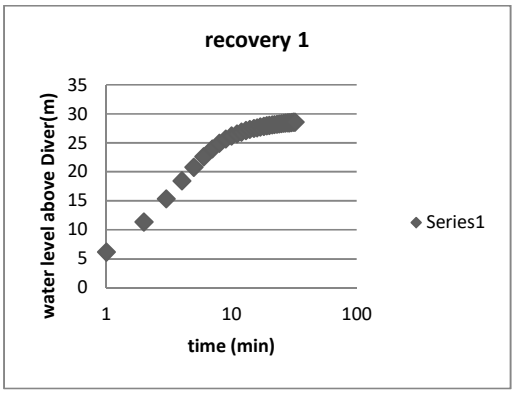

Figure 5.44. An example of a recovery plot for Ansell TW7 (Cycle 1)

The pattern is similar for all cycles except for 27 and 30 (recovery stage) as shown in Figure 5.45. In Cycle 27, the water level dropped for 20 minutes after 40 minutes of recovery. The water level decreased after 60 minutes in Cycle 30. The recovery period for these two cycles is longer compared to the others and may have seen effects of other wells pumping. The recovery period for Cycle 27 is 234 minutes and 422 minutes for Cycle 30.

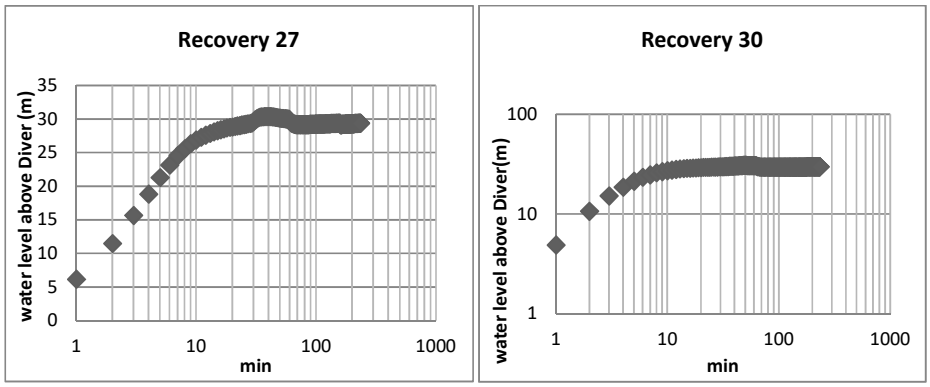

Figure 5.45. The water level dropped in Cycle 27 and 30 during recovery period before the water level becomes approximately static.

The measured drawdown pattern is similar to that seen in the pumping test data as shown in Figure 5.46. It is therefore concluded that the pumping test on this well was completed satisfactorily, and therefore it is also likely that Class B responses are a real indication of the well - aquifer system conditions. If the pumping test on Ansell TW7 has been carried out satisfactorily there is no reason to doubt that the other pumping tests have not also been carried out well too. This suggests that in other circumstances monitoring of abstraction wells might be an alternative way of obtaining pumping test type data.

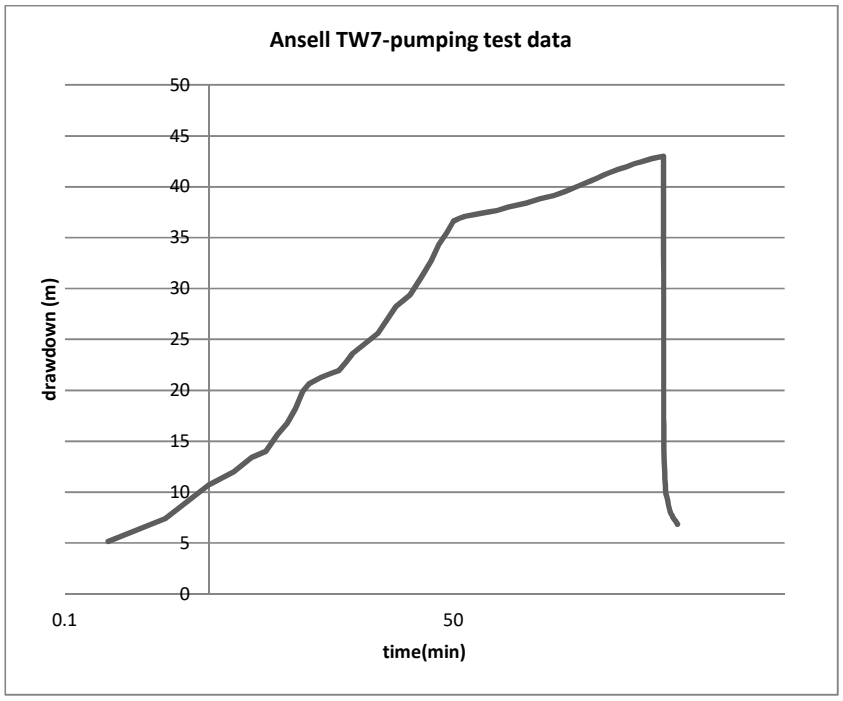

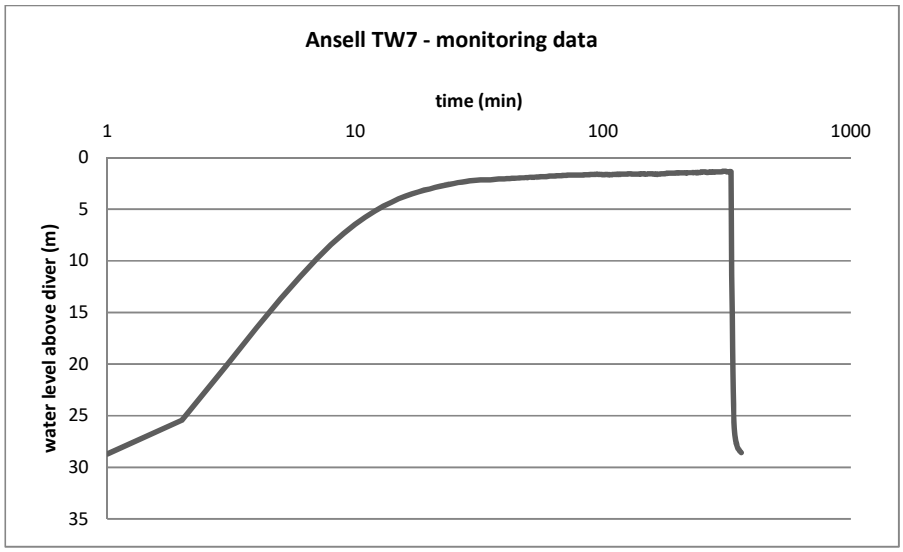

Figure 5.46. Drawdown curves for the constant yield pumping test and from a typical cycle. The monitoring data are obtained at minute intervals whereas the pumping test data are obtained at increasing minute intervals.

5.8 Aquifer Characterization Using Numerical Model

5.8.1 Introduction

The pumping tests results show that there are remaining unanswered question regarding aquifer behaviour. The aquifer behaviour is further explored using

numerical modelling. Though the standard analytical models used in the interpretation of the pumping tests provide a reasonable idea of how the wells respond to pumping, numerical modelling provides much more flexibility. The aims of the modelling are therefore to improve the interpretation of the hydraulic behaviour of the Shah Alam aquifer and to improve estimation of hydraulic aquifer properties obtained by the pumping tests which are discussed in previous sections.

The numerical modelling is used to see the response of the aquifer to the one day pumping tests. It is a near well simulation using the pumping test data to see the response of aquifer near pumping well. The pumping wells are assumed to have an effect on aquifer behaviour which is dominant over regional groundwater flow. There are 12 steps in modelling the groundwater/aquifer behaviour. Each of the steps is explained by Anderson & Woessner (1992). After the purpose of modelling is established, the models are designed based on the conceptual models produced from Chapter 3. The numerical modelling code used is MODFLOW with Groundwater Vista 5 as the interface (Rumbaugh & Rumbaugh 2000-2007) and hence each of the models is designed using a finite difference grid.

From Chapter 3, the aquifer in Shah Alam has been interpreted as usually:

- semiconfined or confined, and more likely to be semi confined in areas of quartzite and interbedded sequences;
- possibly compartmentalized especially near the rivers;

- aquifer is a hard-rock one with low storage capacity which relies on the network of fractures for its permeability;
- the precipitation rate is higher than the evapotranspiration rate, but runoff is significant and hence recharge may be limited;
- the water level shows a delayed response to the rainfall;
- the groundwater flows into the river in unpumped conditions;
- The thick weathered layer may enhance the storage capacity of the aquifer, as the material includes sandy deposits in the quartzite dominant region.
- The role of geological structure; fault controlling the aquifer

Some of these hypotheses will be investigated using the numerical modelling. Different scenarios will be set up and then pumping tests simulated. The plan is not to model specific tests as there are many local conditions (nearby pumping, aquifer heterogeneity, changes in pumping rate) for which there is little evidence but to investigate the style of the pumping test response under for example different weathered zone properties and to compare the predicted behaviour against the pumping test behaviour represented by the Classes of response defined earlier in this chapter.

5.8.2 The flow model

5.8.2.1 Model Representation

The following have been assumed for the modelling:

- flow near the pumping well is dominated by fractures, but there is a minimum representative volume that is small enough that a continuum equivalent porous

medium approach can be used (fractures do not need to be represented separately);

The equation for flow that will be solved by MODFLOW using the finite difference method is:

$$\frac{\partial}{\partial x}\left(Kxx\frac{\partial h}{\partial x}\right)+\frac{\partial}{\partial y}\left(Kyy\frac{\partial h}{\partial y}\right)+\frac{\partial}{\partial z}\left(Kzz\frac{\partial h}{\partial z}\right)-W=Ss\frac{\partial h}{\partial t}$$

Where Kxx, Kyy,Kzz are hydraulic conductivites along the x,y,z coordinates

h is hydraulic head

W – pumping /sink (flux term) Ss-specific storage t-time

5.8.2.2 Aquifer scenarios

Underlying the study area is a thick weathering layer on top of fractured metasedimentary rock. The confining layer material is sandy to silty clay and clay. The fractured rock comprises interbedded fine to medium grained quartzite with shale. The thickness of shale increases to the east of Damansara river while quartzite is dominant to the west.

To understand the aquifer behaviour, the most important (common) aquifer conditions will be investigated to see how the aquifer might be expected to respond to pumping and the results compared in a general way with the pumping test results.

In order to understand the aquifer behaviour in study area, the aquifer condition for each lithology will be investigated. using three wells: Mitsui High Tech (fractured shale, Class E), AESBI (compartmentalization or barriers, Class D) and Scientex Polymer (semi-confined or confined system, Class B).

5.8.2.3 Calibration procedure

The calibration of the model can be done automatically (automated calibration) or by trial and error (Anderson & Woessner1992). The models are calibrated using the trial and error method using pumping test data. The modelling error is quantified by assessing the mass water balance. The calibrated data later are tested using sensitivity analyses to determine the sensitivity of the model to each parameter.

5.8.3 Modelling the aquifer in the fractured shale (Mitsui High Tech, Class E)

Figure 5.47 shows the conceptual model representing the confined aquifer in the Mitsui High Tech area. It is a fractured carbonaceous shale overlain with a clay layer 18 metres thick. The distance to the river is 710m. From borehole logs, the shale in this area contains quartz veins. Quartz veins are interpreted as correlating with faulting in this area based on fieldwork observations.

To model this area, 44 layers are used. Layer 1 to Layer 9 represent clay layers and Layer 10 to Layer 44 represent fractured shale. The thickness of each layer is 2m. The well is located at the centre of the model. The well screen is entirely in the aquifer (shale) layer. The grid around the well is refined, becoming coarser away from well with an increment of not more than 1.058m. It is a transient model, with one day of pumping and 180 minutes of recovery. The far boundaries are assumed all to be no flow.

From the pumping test analysis, Mitsui High Tech belongs to Class E wells – wells that are interpreted as pumping from an extensive confined aquifer. The wells from this class are tapping the interbedded sequence and the 'shale' sequence. To simulate this condition, the size of the model must be big enough to avoid the radius of influence hitting the boundary. The size of model is 1420m x 1420m with the well in the middle (Figure 5.47). The pumping rate is 382.32m^3/day. The horizontal hydraulic conductivity is set higher than the vertical hydraulic conductivity. The hydraulic conductivity that is used for the modelling was obtained from the pumping test analysis. The T value used is 47m^2/day giving a hydraulic conductivity of 0.8 m/day and with an Ss of $3.79x10^{-6}m^{-1}$. After calibration, the Kh value is 0.7m/day, Kv is 0.6m/day and the Ss value is $7x10^{-6}m^{-1}$. Figure 5.48 shows the calibrated model results.

Most of the pumping wells in the study area are located near rivers. Therefore, the interaction between aquifer and river has been investigated using this model. The pattern of the rivers in the study area is interpreted as controlled by the geological structure. The Damansara river is set as a constant head with the water level the same as the static water level measured at Mitsui High Tech well.

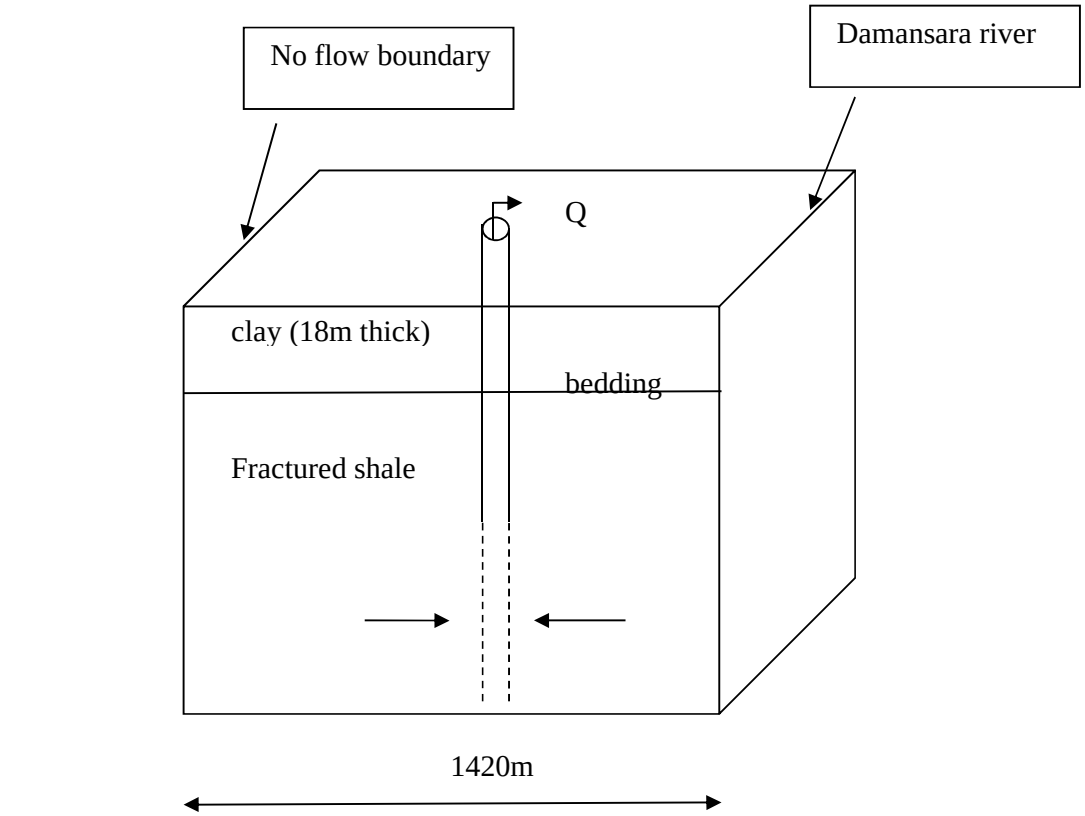

Figure 5.47 The conceptual model of Mitsui High Tech

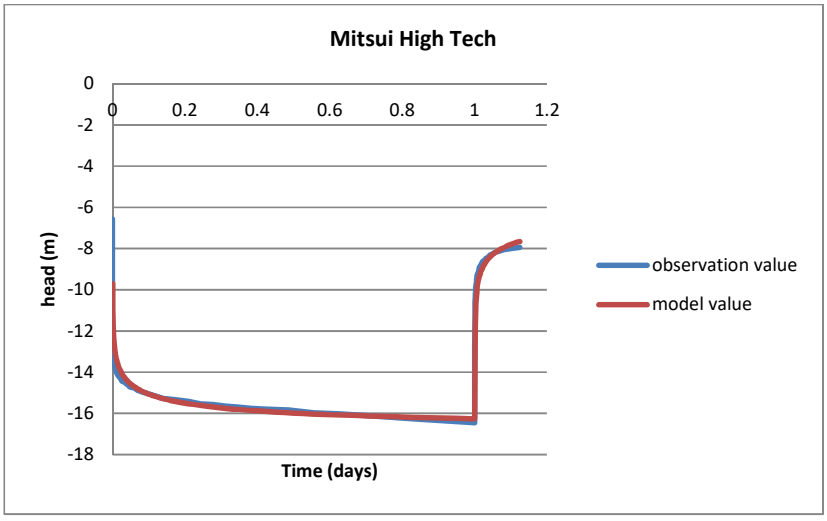

Figure 5.48 The modelled value fits the observed value with error -0.46 which is obtained from MODFLOW mass balance error.

5.8.4 Modelling a well in an individual compartment (AESBI, Class D)

The aquifer in Shah Alam is interpreted as possibly divided into individual compartments especially near the river. Therefore the aquifer condition for areas near the river has been simulated. The AESBI well lies in a fractured carbonaceous shale overlain with 45m of weathered shale with quartzite. The area is represented by a model with 49 layers; Layer 1 to Layer 21 is weathered shale with quartzite and Layer 22 to Layer 49 is fractured carbonaceous shale. The vertical thickness of each layer is 2m. The size of model is 640m x 640m. The well is located at the centre of the model (Figure 5.49). The well screen is entirely in the aquifer layer. The grid around the well is refined; the grid is coarser away from well with increment not more than 1.128m. It is a transient model: one day pumping and 115 minutes of recovery. The pumping rate is 180m^3/day. The aquifer is bounded by fault which is aligned with the Damansara river as shown in Figure 5.50. The river is set as a constant head boundary.

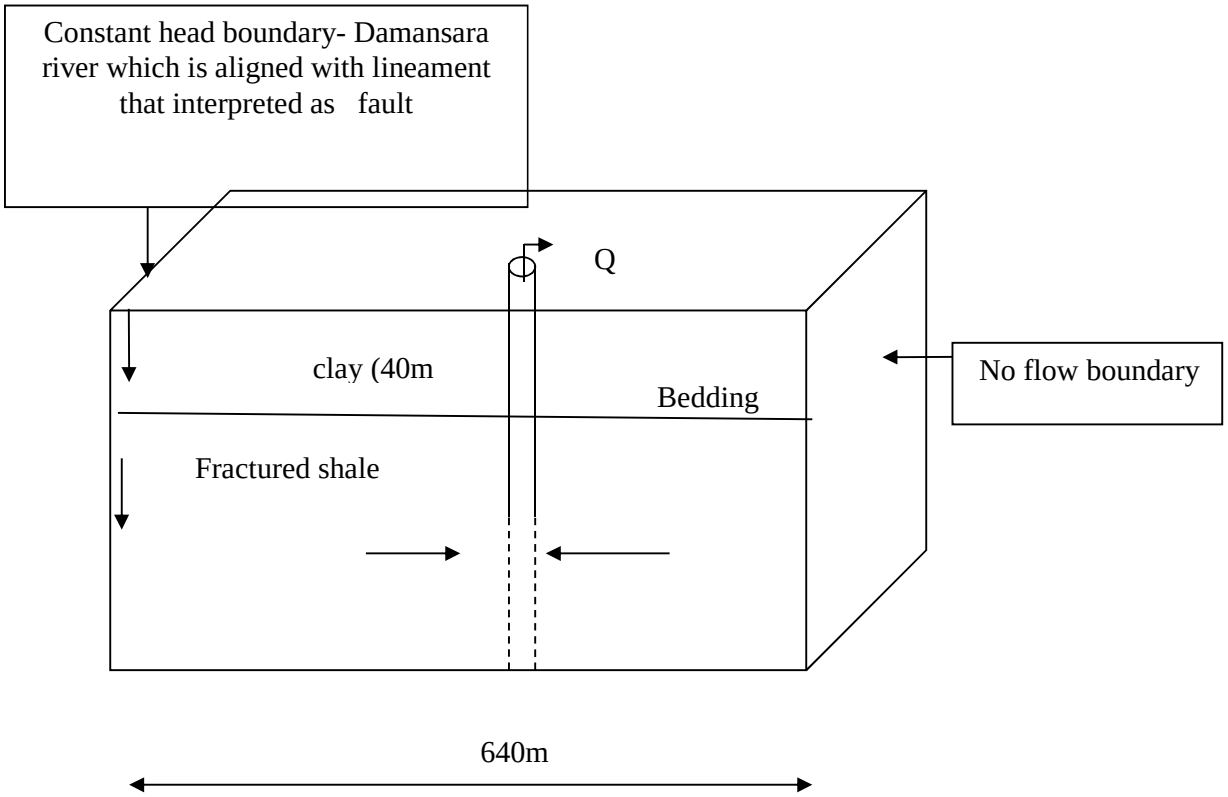

Figure 5.49 The conceptual model of AESBI

Figure 5.50. Location of well at AESBI and the river

The specific yield value for the weathered layer is 1%. The transmissivity and hydraulic conductivity values are from the pumping test analysis: T =5m^2/day from which K =0.1m/d. After calibration, the K value is 0.073m/day and Ss value is $10^{-7}m^{-1}$.

From the pumping test analyses, the wells that show a similar pattern as AESBI are classified as leaky aquifer/recharge boundary aquifer (Class D). There are two ways of recharge; either through the weathered layer or via river flows into aquifer. Both conditions are simulated. The recharge value that has been applied on the weathered layer in this area is 0.005m/day. The interaction between the river and the aquifer in this area is simulated by applying various K values for a fault running along one of the model boundaries. The K value for the fault is set at 10, 1, 0.01m/day. The river flows into the aquifer when the K of the fault equals 0.01m/day.

Figure 5.51 shows the model predictions for K of the fault = 1m/d. It is clear that the model has not been able to reproduce fully the drawdown response seen, and this was found to be the case whatever the properties used. Neither the recovery nor the shape of the drawdown is properly reproduced. It is suggested that the system may not be appropriately represented and that other more complex models need to be investigated. However, the main characteristic of the drawdown phase (the flattening of the drawdown curve) is reproduced, confirming that the Class D pumping tests are consistent with high inflows from nearby rivers.

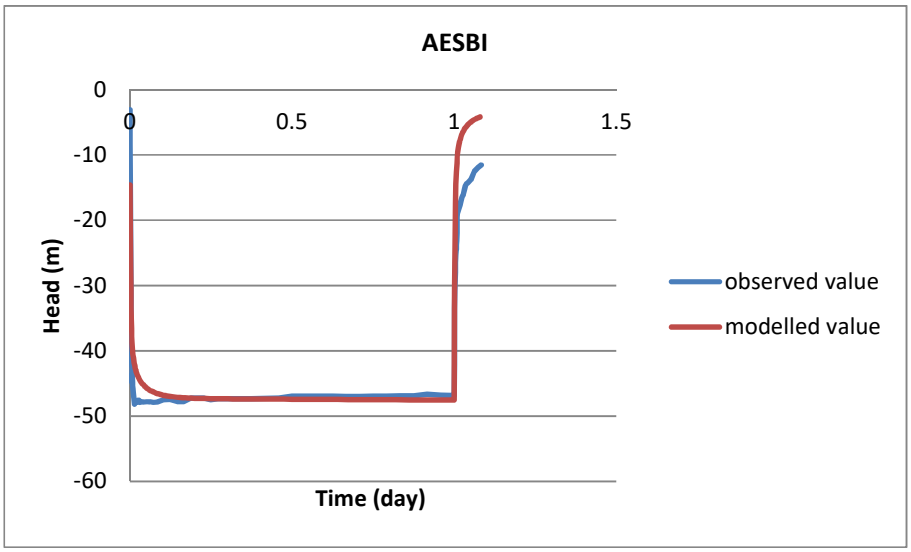

Figure 5.51. The modelled value fits the observed value except at the early of pumping and at recovery stage with error -0.13 which is obtained from MODFLOW mass balance error.

5.8.5 Modelling the confined-semi confined aquifer (Scientex Polymer, Class B)

The Scientex Polymer well in this area lies in fractured quartzite overlain with 36m of weathered quartzite. The area is represented by a model with 32 layers; Layer 1 to Layer 15 is weathered quartzite and Layer 16 to Layer 32 is fractured quartzite. The vertical thickness of each layer is 2m. The size of model is 1250m x 1250m. The well is located at the centre of the model (Figure 5.52). The well screen is entirely in the aquifer layer. The grid around the well is refined; the grid is coarser away from well with increment not more than 1.061m. It is a transient model; one day pumping and 20 minutes of recovery. The pumping rate is 167.83m^3/day. The aquifer is located 2km from Damansara river. Therefore the river is not included as a boundary.

The specific yield value is set at 5%. The transmissivity and hydraulic conductivity values are from pumping test analysis with T =14.6m^2/day and K =0.5m/d.

Most of the pumping test results show responses similar to Scientex Polymer (Class B) with a water supply continuously from part way through the test. The recharge source is assumed to be leakage from the upper weathered layer. When the well is pumping, the aquifer is changing condition from confined to unconfined (Rushton & Wedderburn 1972, Rushton 2003). This condition is simulated by allowing all layers to be in the unconfined condition. Figure 5.53 shows the observed curve and modelled curve. The fit is close indicating that the leakage conceptual model is possible.

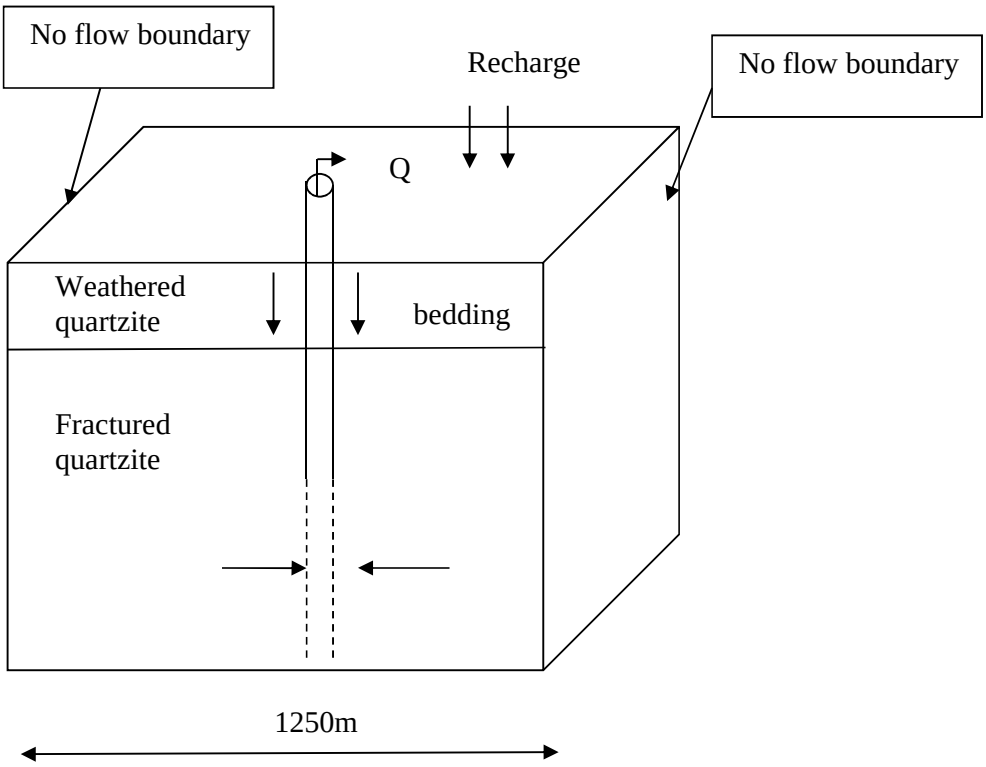

Figure 5.52. The conceptual model for Scientex Polymer

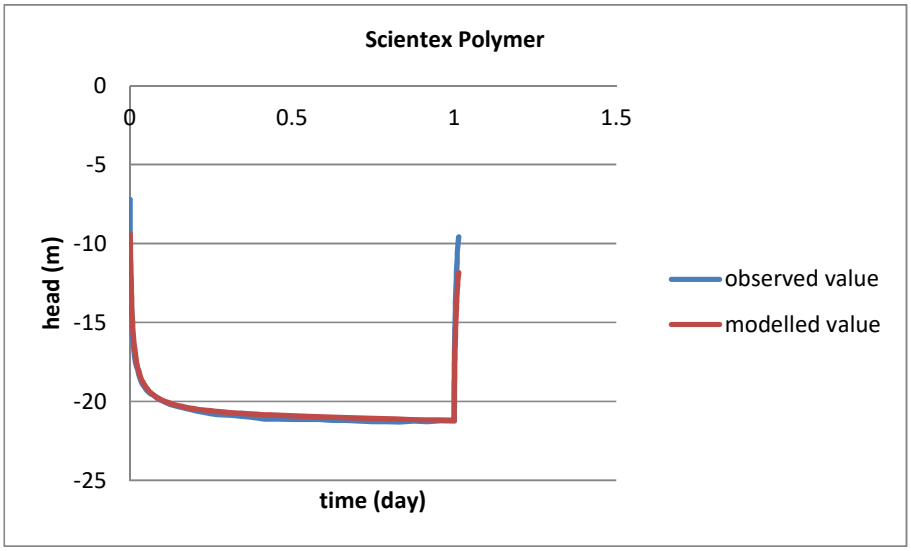

Figure 5.53. The modelled value fits the observed value with error -0.61 which is obtained from MODFLOW mass balance error.

5.8.6 Conclusion

Table 5.18 lists the hydraulic properties obtained from modelling. More importantly, the models have demonstrated that Class E well responses are consistent with infinite homogeneous aquifers as suggested in the previous sections. Also that Class B wells can be represented as leaky systems that become unconfined during pumping. However, the odd responses of Class D wells have been much more difficult to reproduce even with very permeable faults connected to rivers. This last class of responses therefore needs further investigation, possibly using non-radial flow or even non-Darcian flow models. Some trials with non-Darcian flow were attempted but without success. In Figure 5.51 it can be seen that the recovery does not manage to get back to the start water level, and this is another feature that needs looking at. However, the stabilization of the drawdown was modelled successfully and so it looks like Class D are in part explainable by inflow from nearby recharge boundaries, in this case mainly formed by rivers connected with permeable faults.

Table 5.18. Hydraulic properties obtained from numerical modelling

Layer type	Thickness,b (m)	Specific yield,Sy	Storage coefficient Ss, m^{-1}	Kx=Ky (m/d)	Kz (m/d)	T=Kb (m^2/d)
Weathered layer (sandy)	30	0.05		0.01 to 0.1	0.0025	0.3
Weathered layer (clay)	18	0.05		0.001	0.001 to 0.0001	0.018
Fractured	55		10^{-7}	0.06 to	0.05 to	6

shale (in compartment)				0.073	0.06	
Fractured Shale with quartz vein	82		7×10^{-6} to 9×10^{-6}	0.47 to 0.7	0.38 to 0.6	55
Fractured Sandstone	70-100		10^{-5}	0.3 to 0.33	0.066	23-33m^2/day
Fault				0.01 to 10		

5.9 A revised hydrogeological conceptual using pumping test data analysis

In this chapter, the hydrogeological conceptual model developed from geological information is further developed using the results of the pumping test analysis. Pumping test data for 42 wells were analysed beginning with diagnostic plots. In the diagnostic plots, the log drawdown against log time and drawdown against log time curves for each well were grouped together into different classes based on their shapes, and then compared with the theoretical plots expected from different hydrogeological conditions (Kruseman & De Ridder 1994). Using this approach, the wells in study area were grouped into 5 classes, A to E.

Wells in Class A are located to the north of Shah Alam (8% of the 42 well test locations). The wells in this area are located in limestone covered by a sandy clay layer. The wells show delayed yield type responses when pumping. Water from finite sources is possibly from the sandy clay layer on top of the limestone or

from less fractured aquifer. The T values are relatively high being over 100m^2/day. The wells in Class B (44% of wells tests) show a sudden change in slope suggesting a source of recharge whilst pumping. This is possibly from permeable weathered layer (sandy silt) since the wells in this class are in sandstone or interbedded sandstone and shale that weathers to a sandy clay that could provide the leaky conditions. Numerical modelling confirms quantitative validity of the interpretation. T values obtained ranged from 23 to 33 m^2/day.

Class C wells (5% of wells tests) are characterised by a steepening of the drawdown/time plot with time. These are interpreted as wells located in patchy aquifers, i.e. there is a nearby decrease in T value that is intercepted as the cone of depression expands. Class D are wells (13% of well tests) where the drawdown suddenly stabilises after a certain period of pumping. This is interpreted as representing the cone of depression encountering a major source of recharge such as river or river/fault system. Numerical modelling, though struggling to reproduce the sharpness of the change in drawdown slope, indicated that this conceptual model could explain the stabilising of the drawdown using physically reasonable parameter values. All other conceptual models including non-Darcian flow failed to produce better fits to the data. This is the Class of tests where boundaries were least ambiguously recognised. However, because the tests were relatively short (< 300 minutes usually), it is possible that boundaries might be relatively frequent.

Class E are wells (31% of wells tested) that display a standard Theis response and are interpreted t as being in confined and effectively infinite aquifers, and this was confirmed by numerical modelling. The wells in this class are mainly in

interbedded sandstone and shale. The weathered layer material is clay to silty clay with average thickness 34m (range from 17-60m).T values obtained from pumping and recover phase interpretation ranged from X to X.

The well classification is further developed with step drawdown test analysis. However, step drawdown test data are only available for 14 wells. From step drawdown test analysis, the wells are grouped into 3 classes based on their interpreted C values. 8 of the 14 well responses show reasonable Jacob-theory responses, but 6 have apparent C values ≤ 0. The behaviour showed no correlation to the Class from constant yield test (wells were from A, B and E classes). Detailed examination of possible causes for non-theoretical responses indicated that no single cause explained all the well responses. The most frequent possible causes were the presence of a seepage face, boundaries, the well turned from confined to unconfined during the test and radial changes in T.

In conclusion, the pumping test data have shown that several conditions are present within the aquifer, namely: delayed yield conditions (Class A); leaky conditions, interpreted as water being supplied from the weathered zone (Class B);wells located close to T changes (patchy aquifers)(Class C, 5%); wells with major effectively infinite recharge boundaries (Class D); and wells that are consistent with being in an infinite homogeneous aquifer area (Class E). So boundaries were seen in 18% of cases, 13% major recharge boundaries and 5% barrier boundaries. Given the short time of pumping it suggests that there are frequent boundaries in this aquifer. The connection with rivers in the case of Class D suggest rapid route to groundwater from rivers. River / groundwater

connection is further investigated in Chapter 6. Leaky conditions occurred in 52% of cases suggesting that the weathered zone is an important source of water for pumping wells though in 8% of these cases the source of water was finite even within limited pumping times. There was no obvious correlation between leakiness and weathered zone grain size, or between rock type and T, except that the highest T wells were those in limestone.

6.0 WELLWATER CHEMISTRY ANALYSIS

6.1 Introduction

Groundwater chemistry analysis is carried out for various purposes and in Malaysia, the studies are focused on shallow aquifer systems. For example, the effects of landfill on groundwater quality (Abdelatif & Wan Norazmin 2001, Ahmad Fariz et al. 2009, Bahaa-eldin et al. (2010), Nasiman et al. 2011, Siti Nur Syahirah et al.2013, Fauziah et al.2014, Khaki et al. 2014) and the impact of agricultural activity also (Ahmad et al.1996). The groundwater quality issues for shallow aquifers include bacteria such as coliforms, *E.coli and Salmonella* (Idrus et al.2014), salt water intrusion (Umar et al.2007, Abdul Rahim et al.2008), heavy metals (Kamaruddin et al.2009), nitrate (Mohamed Azwan et al.2010, Noraziah et al.2013) and iron and manganese. This study aims to characterize the groundwater chemistry perhaps in a similar way, but unlike the previous studies in Malaysia, examining a deeper and fractured aquifer.

In the previous chapter, the aquifer was characterized using pumping test results and numerical modelling. Since the lithology of study area has a low matrix hydraulic conductivity, the fractures play the dominant role in controlling the groundwater flow. The fractures act as water conduits (bedding plane and other joints) and also can act as flow barriers (faults with low hydraulic conductivity) though the pumping test results suggest that this is not too common. These ideas are supported by the pumping test and numerical modelling analysis. For example, 65% of wells in the study area appear to have a recognizable recharge response. This recharge is thought to be from the overlying weathered layer or from a river. There are some pumping wells (Class D) which encountered a

significant water source (e.g. river) which has flattened the drawdown curve. From numerical modelling, the weathered layer of quartzite (sandy material) has higher hydraulic conductivity than weathered shale (clay material) and is therefore more likely to deliver recharge. The weathered layer can also increase the hard rock storage capacity which is low itself being a fractured hard-rock.

In this chapter the groundwater chemistry will be used to develop the hydrogeological model of the Shah Alam aquifer further.

In Section 6.2, general information about the chemistry data available, e.g. sampling method and the determinands that have been analysed, will be presented. Then, in Section 6.3, the wellwater chemistry will be analysed. In Section 6.4, pollution will be discussed. Section 6.5 draws together the conclusions and implications for the hydrogeological conceptual model and susceptibility to contamination.

6.2 Water Sampling Method and Sample Analysis

6.2.1 Introduction

Groundwater abstraction in Shah Alam is mainly for industrial purposes, so sampling is biased towards industrial land use areas. There are 19 factories with different types of industries who use groundwater in their operation as shown in Table 6.1. Groundwater chemistry data from 35 tubewells in Shah Alam have been collected. The period of sampling is from 2001 until 2011. It is unknown when the pumping activity started in some cases. These data have been supplied by LUAS. Starting in 2005, each company must carry out groundwater chemistry analysis at the time of abstraction licence application and renewal.

Table 6.1 The type of industries in Shah Alam which are using groundwater

Name of the companies	No of wells	Type of industry
Ansell Shah Alam Sdn Bhd	8	Manufactures examination medical glove and surgical glove
MT Picture Display (M) Sdn Bhd	5	Manufactures cathode ray tubes and colour monitor tubes
AESBI Power System Sdn Bhd.	1	Manufactures bodies for motor vehicles (bus)
Panasonic Manufacturing Malaysia Berhad	2	Manufactures electrical appliances such as refrigerator, washing machine and others
Carlsberg Brewery Malaysia Berhad	3	Manufactures beer, stout and other beverages
Perusahaan Otomobil Nasional Berhad (PROTON).	2	Manufactures cars
CCM Fertilizers	4	Manufactures fertilizers
Gaya Color Laboratory	1	Film laboratory
Universal Nutri Beverages	1	Manufactures drinks
Good Year Malaysia Berhad.	2	Manufactures rubber tyre
Anshin Steel Industries Sdn Bhd	1	Manufactures engineering steel bars
Suzuki Latex Industry Malaysia Sdn Bhd	1	Manufactures finger cots and finger stalls
Aquatic International Sdn Bhd.	2	Export fish business
Aquarium Express Sdn Bhd.	1	Import fish business
Ueda Plating (M) Sdn Bhd	2	Metal plating with gold, silver, copper, tin, nickel
Canon Opto (M) Sdn Bhd	5	Manufactures camera lenses
Pokka Ace (M) Sdn Bhd	1	Manufactures drinks (non carbonated Tetra Pak and canned drinks) and soft drink.
Scientex Polymer	1	Manufactures stretch film, consumer and industrial packaging,solar encapsulant film, automotive interior and PP strap-ping belt
Mitsui Hightech	1	manufactures IC leadframes, motor cores and stamping dies

6.2.2 Sampling method

The sampling of groundwater using wells should be carried out with caution (Shapiro 2002) and it is safest to consider samples as wellwaters rather than groundwaters when starting interpretation. There are various methods of sampling including purging to remove the “stagnant” water in the well and low flow sampling (e.g Puls & Barcelona (1996), Lerner & Teutsch (1995), and McMillan et al. (2014)).

For the study area, the water sampling is carried out at least once a year as a requirement for abstraction licence renewal. The sampling is carried out in the

production wells and was undertaken by the companies owning the well. The well pump was switched off for a day before the measurement. After the static water level was measured, the pump will be switched on and a water sample was taken from a sampling tap as shown in Figure 6.1. Therefore, the water sample is a non filtered sample and not taken from after the treatment plant.

There is no information on whether the samples were acidified except for Ansell wells starting in 2010. The water samples from Ansell wells after 2010 were treated by addition of sulphuric acid, nitric acid, sodium hydroxide and ascorbic acid in separate plastic bottles and sterilized amber glass bottles for sodium thiosulphate. Acidification will stop the bacteria from growing and keep metals especially in solution (Appelo & Postma 2005); sulphuric acid is used to preserve ammonium; sodium hydroxide will preserve cyanides and sulphides; ascorbic acid can be used to neutralize oxidants when the sample is effectively a mix of oxidized and reduced waters (e.g. Johnson et al. 2012).

Figure 6.1 Water sample is taken directly from the well through sampling tap.

6.2.3 Sample analysis

There are six different laboratories that have been assigned individually by the companies to analyse the water samples, causing variety of determinand suites to been analysed. Samples are analysed using atomic absorption spectrometry mostly, but not all methods have been recorded. For all the tubewells the following have been measured: the total dissolved solids (TDS), pH, turbidity, colour, hardness, conductivity, Mg, Cl, SO_4, NO_3, Fe and Mn. The majority of the tubewell samples have been measured for alkalinity, ammoniacal nitrogen, Zn, NO_2, As, Cd, Cu, Hg, Pb, Se, CN and phenol. Some of the tubewell samples

have been tested for EC, Na, K, Ca, Al, P, F, SiO_2, organic matter, 'oil and grease' and 'detergent'. The majority of the tubewell samples have not been analysed for bacteria (coliforms) except for Ansell Shah Alam Sdn Bhd, MT Picture Display (M) Sdn Bhd, Universal Nutri Beverage, UEDA Plating (M) Sdn. Bhd and Pokka Ace Sdn Bhd. Some well samples have been tested for radioactivity and these are Ansell Shah Alam Sdn Bhd, CCM Fertilizers, Panasonic Manufacturing Malaysia Berhad, and Suzuki Latex Industry Malaysia Sdn Bhd.

6.2.4 Checking the analyses

The reliability of data can be checked by calculating ionic balances and total dissolved solids (TDS) values (Lloyd & Heathcote 1985). The ion balance error should be less than 5%. The ionic balance error formula is shown below:

$$\text{Ion balance error} = \frac{\Sigma\text{cations} - \Sigma\text{anions}}{\Sigma\text{cations} + \Sigma\text{anions}} \times 100\%$$

where for example Σcations means the sum of all the measured cation concentrations in equivalents.

Most samples have incomplete major ion analyses (see Table 6.4). Out of 106 samples, only 37 samples have complete major ion analyses as shown in Table 6.2. Of the latter, the ionic balance errors average 1.58%, which is reasonable, but the errors range from 82% to -100%, i.e. are very big in some cases. Some of the high error samples are those with unusual concentrations which will be discussed later. The ionic balance calculations were undertaken using major ion, Fe, Mn, and NH_4 concentrations. H^+ and OH^- concentrations are negligible.

Total Dissolved Solids (TDS) also can be estimated using Electrical conductivity value by using the following equation (Misstear et al. 2006):

TDS (mgl^{-1}) = EC x F; F is 0.64 (average value between water dominated by sodium chloride and calcium carbonate). Plotting the data from cases where TDS has been measured indicates that this result is very closely true for the samples from Shah Alam (Figure 6.2) despite any volatilisation of CO_2 (Lloyd and Heathcote, 1985). However, plotting up TDS as calculated by summing up the major ion concentrations produces a much less good correlation (Figure 6.2 bottom), i.e. measured TDS and summed TDS do not agree too well (note only those samples in the upper plot that had all major ions analysed were plotted up). Figure 6.2 (bottom) includes the best fit line from the upper plot, and the samples which lie on the line are also those with the best ion balance errors, as might be expected, and all those with poor balances lie below the line. These results fit in with the sample analyses with bad ion balances. It seems as if there are problems with the standard analyses made by the chemical laboratories used. However, almost all the samples have low or very low TDS. This means that in many cases analysis may be at the low end of the ranges for the instrumentation used, and that also small absolute errors (e.g. a mg/l or two) may result in significant ionic balance errors. As major ion concentrations in these waters are not much above the concentrations that would be present for minor ions it is suggested that in effect the analyses are incomplete and that if all the minor ion data were available better balances might be obtained (e.g. Fe, Mn, Sr, Ba, P). 60% of samples have balances within ±25%.

Table 6.2 The ionic balance error for each of the tubewell (with major ion analysis)

Wells	Year of sampling	Ionic balance error(%)
Ansell TW1	2010	-67.62
Ansell TW2	2010	-80.58
Ansell TW6	2010	-95.90
Ansell TW7	2010	44.66
Pokka Ace 2010	2010	14.35
Canon Opto TW1	2010	-23.96
Canon Opto TW2	2010	2.19
Canon Opto TW3	2010	36.66
Canon Opto TW4	2010	-4.69
Canon Opto TW5	2010	4.68
Ansell TW1	2008	-13.64
Ansell TW2	2008	20.35
Ansell TW3	2008	6.76
Ansell TW7	2008	36.93
Gaya Color Lab	2008	15.26
Suzuki Latex 2008	2008	-29.70
Pokka Ace 2008	2008	5.41
Carlsberg 3	2006	25.20
CCM Fertilizer 1	2006	81.19
CCM Fertilizer 2	2006	13.15
CCM Fertilizer 3	2006	78.82
Suzuki Latex (April) 2006	2006	21.27
Suzuki Latex (October) 2006	2006	45.24
MTPictures 2	2005	-0.62
MTPictures 3	2005	10.31
MTPictures 4	2005	26.24
MTPictures 5	2005	1.95
Scientex Polymer	2007	-15.57
Gaya Color Lab	2009	13.30
Ansell TW4	2008	-0.32
Ansell TW6	2008	60.32
Carlsberg 1	2010	7.64
Carlsberg 2	2010	6.17
Ansell TW3	2010	-65.61
Ansell TW4	2010	-99.51
Ansell TW5	2008	-14.90
CCM Fertilizer 4	2006	-7.00

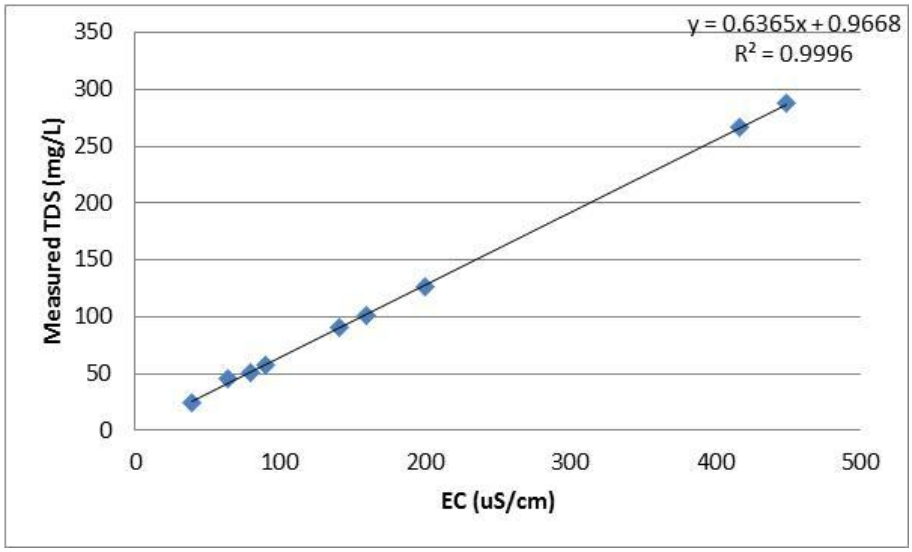

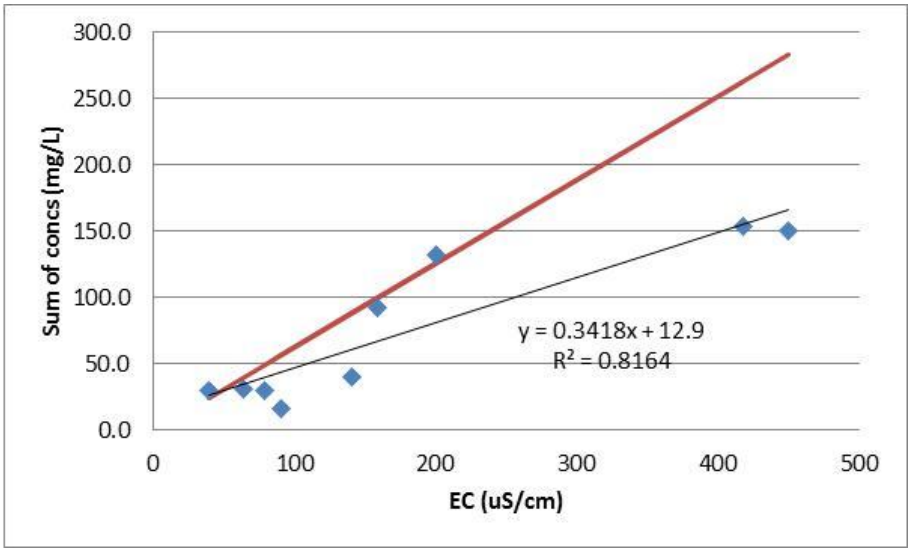

Figure 6.2. Plot of measured TDS against EC (top) and a plot of TDS calculated by summing the analysed major ions plotted against EC (bottom). Also included in the latter plot is the best fit straight line from the upper plot (in red). Only samples with full major ion analysis are included.

The data set is not ideal given the uncertain ionic balance errors and the differences in the TDS estimates. However, this is the only data set available. It

will be assumed that if the data from different wells are in agreement with each other then the data will be taken as reasonable. Where data are unusual or do not fit in with each other, error in analysis will always be one possible explanation. For example, the measured TDS value for Ansell TW2 in 2010 is 6mg/l which is too low compared to calculated TDS (142.3mg/l). In general though it is thought that one explanation for the poor ionic balances is that the major ion concentrations are similar to what might be expected for some minor ion concentrations, so the errors may not be because of bad analysis but because not all minor ion concentrations are available, but in some cases the very low concentrations present will mean that small absolute error values will be large % errors. This is especially the case for major ions but also could be case for Fe for example where using for example flame AAS could mean big % errors for concentrations < 2 mg/l.

6.2.5 Phreeqc

The ion activities and saturation states are calculated using the Phreeqc code which was developed by Parkhurst and Appelo (1999).

Table 6.3 The calculated TDS values (TDS_c) obtained from Electrical conductivity values with measured TDS (TDS_m).

Tubewell	Date of measurement	EC(μScm^{-1})	TDS_c	TDS_m
Carlsberg 1	2010	1304	834.56	977
Carlsberg 2	2010	1280	819.2	1152
MTPictures 2	2005	200	128	126
MTPictures 3	2005	141	90.24	89
Ansell TW1	2010	55	35.2	34
	2011	58.4	37.376	55
Ansell TW2	2011	60.4	38.656	68
Ansell TW3	2010	132	84.48	67
	2011	212	135.68	137
AESBI	2009	36.5	23.36	200
Ansell TW4	2010	269	172.16	176
	2011	414	264.96	247
Ansell TW6	2010	105	67.2	54
	2011	100	64	84
Ansell TW7	2010	24	15.36	22
	2011	26.8	17.152	40
MTPictures 4	2005	90	57.6	57
MTPictures 5	2005	79	50.56	50
CCM Fertilizer 1	2006	417	266.88	228
CCM Fertilizer 2	2006	39	24.96	22
CCM Fertilizer 3	2006	449	287.36	246
CCM Fertilizer 4	2006	159	101.76	87
Gaya Color Lab	2008	58	37.12	27
Suzuki Latex	2006	64	40.96	46
Canon Opto TW5	2010	335	214.4	256
Ansell 5A	2010	266	170.24	172

6.3 The Wellwater Chemistry of the Shah Alam Aquifer

6.3.1 Introduction

The chemistry of the samples collected from wells in study area is suggested to represent wellwaters rather than groundwater. Water samples which are drawn from wells with long screens are often called depth integrated water samples. The wellwaters represent mixtures of groundwater with different compositions (Cherry 1983, Church & Granato 1996, Reilly & Le Blanc 1998, Shapiro 2002, McDonald & Smith 2009, Mayo 2010, McMillan et al. 2014) and this must be considered when examining the data. The length of well screens in the study area ranges from 9 to 90 m.

Information from previous studies in nearby areas is limited. The hydrochemistry of Klang Valley area (Klang) is influenced by the sea according to Ismail (1981). This area is located to the southwest of the study area. Saim (1991) suggested that the hydrochemistry 'facies' of the Kenny Hill Formation are mixed which not dominated by any major cation and anion while Nasiman et al. (2011) suggested that the groundwater facies for Selangor area is sodium bicarbonate type.

Shah Alam's aquifer is a confined or semi confined system (Chapter 4). In confined areas (more likely to be fractured shale areas), the aquifer is capped with the lowest hydraulic conductivity weathered layer. The pumping test evidence indicated that the aquifer is recharged from induced leakage through the more permeable parts of the weathered layer but flow could also come from river infiltration. Therefore, the wellwater chemistry compositions are expected to be influenced by the chemical composition of rainfall and by river water.

Groundwater in urban aquifers experiences a few issues such as organic and inorganic pollution (e.g Rivett et al. 1990, Ford et al. 1992, Ford & Tellam 1994, Lerner & Barrett

1996, Trauth & Xanthopoulos 1997). Since the wells in Shah Alam are in an industrial area, the well water chemistry is possibly influenced by type of industry and other landuse activity which will be investigated further in next section. In this context the list of industrial activities given in Table 6.1 is important.

6.3.2 Classification into Water Types

Wellwater classification will give an idea of the general character of the groundwater system and help in determining the processes involved from recharge onwards. It is important to understand the chemical processes if the susceptibility of the aquifer to pollution is to be determined. Table 6.4 shows the major ion analyses of the wellwater samples from Shah Alam.

The major ions are plotted against ion Cl^-. The wellwater samples which show similarity of the chemical composition and relationship will be put in same Water Types. Cl- is chosen as the ion with which the others are compared because it is less reactive compared to the other ions. All the major ions plots are shown in Figures 6.3 to 6.10.

Examination of the Cl/Na plot indicates three possible groupings, and further looking at the data indicates that these groupings also occurring in the concentrations of other determinands. Most wellwater samples are of Type 1 water, i.e. very low TDS. Type 2 water consists of wellwaters with much higher TDS and an approximately 1:1 molar Na:Cl ratio. Type 3 waters have much higher Na/Cl ratios than Type 2 waters, and much higher Na concentrations generally than Type 1 waters. The water chemistry of each type is considered in the following sections. There are no clear correlations between water type and type of industry and there are cases of different water types at the same compound..

Table 6.4 Major ion analyses (mg/l) of wells in Shah Alam.

Wells	pH	Na	K	Ca	Mg	Cl	SO_4	HCO_3	NO_3
Carlsberg 1 2010	6.83	159.0	2.8	48.0	19.2	277.0	7.6	78.1	9.7
Carlsberg 2 2003	5.7			3.3	4.8	20.0	2.0	17.1	4.4
Carlsberg 2 2010	6.6	170.0	2.6	42.9	18.2	289.0	12.5	76.9	8.6
Carlsberg 3 1998	7.3	143.0			12.1	242.0	15.0		2.6
Carlsberg 3 2006	5.38	3.8		3.5	2.3	8.0	4.7		8.4
Carlsberg 4 1998	7.11					246.0		2.4	3.4
MTPictures 1 2005	7.66			2.3	6.8	0.8	1.6		8.9
MTPictures 1 2005		1.6	0.9			0.4		59.8	
MTPictures 2 2005	7.36	12.5	1.5	4.1	8.1	0.4	0.3	102.5	2.76
MTPictures 3 2005	6.54	5.2	2.3	2.7	1.4	1.1	0.6	25.6	0.80
Ansell TW1 2005	6.85			3.4	3.7	0.4	2.5		2.0
Ansell TW1 2006	5.93			4.3	2.3	0.4	0.7		3.3
Ansell TW1 2008	5.94	0.9	1.8	0.7	4.3	6.5	3.4	31.7	0.75
Ansell TW1 2010	6.01	0.0	0.1	0.1	0.1	4.3	3.7	26.8	5.1
Ansell TW1 2011	6.09	1.0	0.6	4.5	4.5	2.7	7.7	32.9	0.58
Ansell TW2 2005	5.8			8.8	3.5	0.4	0.4		0.99
Ansell TW2 2006	6.03			4.1	2.3	0.4	0.8		3.8
Ansell TW2 2008	6.02	2.9	1.2	0.6	4.6	6.3	0.3	39.0	0.35
Ansell TW2 2010	5.74	0.0	0.1	0.1	0.1	9.8	6.5	26.8	61.6
Ansell TW2 2011	5.94	2.2	0.1	4.1	4.8	3.0	4.6	32.9	0.13
Ansell TW3 2005	5.4			1.2	2.3	0.4	2.5		1.0
Ansell TW3 2006	5.99			2.8	1.4	0.4	2.5		2.9
Ansell TW3 2008	6.09	11.0	0.7	1.0	2.9	2.7	1.1	46.4	0.62
Ansell TW3 2010	5.75	8.8	2.4	0.1	0.1	27.2	11.3	29.3	43.1
Ansell TW3 2011	5.81	18.7	0.3	4.2	6.1	43.4	11.3	29.3	0.13
AESBI 2004	5.5					4.0			
AESBI 2006	7.1			18.0	12.0	20.0		19.5	
AESBI 2008	7.1			20.0	15.0	12.0			
AESBI 2009	5.8	4.8	7.3	4.9	2.9	2.9	0.3	31.4	2.8
Ansell TW4 2005	6.6			2.5	5.3	0.4	3.6		24.7
Ansell TW4 2006	7.13			1.3	0.7	0.4	0.3		11.2
Ansell TW4 2008	5.98	57.2	5.3	1.2	1.9	5.7	17.0	144.0	5.5
Ansell TW4 2010	6.69	0.0	0.1	0.1	0.1	25.1	6.8	144.0	15.01
Ansell TW4 2011	6.14	88.1	5.3	4.2	1.1	50.6	5.6	146.4	0.13
Ansell TW5 2005	5.77			1.4	1.4	10.4	2.7		7.99
Ansell TW5 2006	6.33			2.9	1.4	2.8	2.8		4.69
Ansell TW5 2008	6.11	37.1	2.0	1.6	4.7	66.0	3.4	54.9	2.44
Ansell TW6 2007	6.46			3.4	1.7	0.6	0.3		38.50
Ansell TW6 2008	6.3	74.5	1.4	0.9	4.3	2.3	0.3	52.5	0.97
Ansell TW6 2010	5.95	0.0	0.1	0.1	0.1	1.3	4.4	54.9	0.75
Ansell TW6 2011	6.09	11.3	1.0	4.4	3.8	2.7	6.0	51.2	0.13
Ansell TW7 2007	5.48			1.8	1.3	0.9	0.8		2.84
Ansell TW7 2008	4.61	0.9	0.0	0.8	0.5	0.4	2.7	0.31	0.35
Ansell TW7 2010	4.73	8.3	2.3	0.1	0.1	2.1	0.7	5.12	10.01
Ansell TW7 2011	4.84	0.3	0.1	3.6	0.8	2.1	0.9	7.44	2.13
MTPictures 4 2005	5.31	1.8	0.3	0.8	0.6	3.0	0.3	8.54	0.81
MTPictures 5 2005	5.53	1.4	0.6	0.8	0.4	1.1	0.3	12.2	13.00
Proton 1 2006	5.8			7.8	3.1	6.0	16.0	47.6	0.01
Proton 1 2010	5.86			0.1	0.5	49.8	15.4		1.37
Proton 2 2006	6.2			2.0	0.0	58.0	6.0	87.8	0.01
Proton 2 2010	5.58			2.6	1.9	5.4	6.7		6.03
Aquarium Express 2005	7.31				2.3	3.9	0.7		16.96
Aquatic International 2 2003	6.97				2.4	4.4	0.8		12.31
Aquatic International 3 2003	6.86				2.8	2.5	0.3		19.44
Ueda Plating 1 2006	5.5			0.1	4.4	7.1	7.0	11.0	3.10
Ueda Plating 1 2007	6.71				15.2	188.0	4.5	328.2	19.93
Ueda Plating 1 2009	6.55								
Ueda Plating 2 2007	6.54						12.6		
CCM Fertilizer 1 2004	5.8			0.1	1.3	1.0	2.1	15.1	1.24
CCM Fertilizer 1 2006	3.8	2.0	2.0	1.5	2.0	0.5	0.8	0.61	144.37
CCM Fertilizer 2 2004	5			0.1	0.2	0.7	0.3	10.2	5.58
CCM Fertilizer 2 2006	5.3	4.7	1.6	1.1	1.5	0.5	1.6	17.1	2.30
CCM Fertilizer 3 2004	4.4			0.2	0.6	0.6	0.3	0.31	0.71
CCM Fertilizer 3 2006	3.6	1.1	1.9	1.1	1.2	0.5	0.3	0.61	143.93
CCM Fertilizer 4 2006	4.3	29.3	1.2	0.4	1.1	54.0	1.2	0.61	4.34
Universal Nutri Beverages 2006	6.61			2.2	1.6	0.9	5.1	70.8	4.30
Universal Nutri Beverages 2008	6.44							69.5	
Panasonic TW1 2005	7.5	72.9	2.5	1.5		2.3	46.0	258.6	0.89
Panasonic TW1 2010	7.3	61.8			0.7	9.6	25.0		0.89
Panasonic TW2 2005	6.9	123.0	2.5	1.5		2.3	46.0	314.8	0.89
Panasonic TW2 2010	7.2	126.0			10.5	38.5	23.0		1.33
Panasonic Compressor 2004	7			1.0	4.0	0.9	6.2	33.4	2.39
Gaya Color Lab 2001	5.2				1.2	8.7		8.5	9.74
Gaya Color Lab 2006	5.5			0.5	0.9	5.0	3.0	3.7	12.40
Gaya Color Lab 2008	5.8	5.2	0.9	1.1	1.0	7.0	3.0	1.22	11.07
Gaya Color Lab 2009	5.6	6.2	1.1	1.3	1.0	8.0	4.0	7.3	1.30
Gaya Color Lab 2010	5.6	3.4			0.7	8.0	4.0		

Good Year 1 2007	4.63				0.3	1.1	0.3	4.9	1.68
Good Year 1 2008	4.86				0.4	3.7		3.7	0.02
Good Year 2 2007	4.97				0.7	1.9	2.1	11.0	3.14
Good Year 2 2008	4.46				0.4	5.3		1.22	0.02
Anshin Steel 2007	4.81				0.3	0.8	0.3	1.22	11.07
Anshin Steel 2009	3.57			1.3	0.3	0.4	0.4	2.44	0.40
Suzuki Latex (April) 2006	5.4	2.6	1.3	0.7	0.7	7.1	8.0	11.0	0.30
Suzuki Latex (October) 2006	5.4	1.9	0.9	0.2	0.3	2.0		0.31	0.01
Suzuki Latex 2008	6.8	0.4	1.2	0.1	0.1	3.2		3.90	0.29
Suzuki Latex 2010	4.9	0.5	0.1	0.0	0.4	1.2		5.4	0.77
Lafarge	5.77			0.74	0.35	0.8	0.25	7.3	0.3
Pokka Ace 2006	6.5	2.9				5.4	1.1		1.03
Pokka Ace 2008	5	2.3	0.2	0.2	0.5	4.4	1.1	0.31	2.83
Pokka Ace 2010	4.13	2.6	0.7	0.9	0.6	3.1	1.6	3.2	3.19
Scientex Polymer 2007	6.2	6.0	2.1	19.5	2.9	0.5	7.0	133.0	7.97
Scientex Polymer 2008	6.1			18.6	2.8	10.0	9.0	25.6	6.64
Scientex Polymer 2009	6.5			16.5	2.6	9.0	2.0	75.6	4.43
Scientex Polymer 2010	6.2			15.0	2.3	10.0	0.5	89.1	4.43
Mitsui High Tech 2006	7.2			0.6	2.4	1.3	2.9	12.6	0.66
Canon Opto TW1 2006	5.77			3.9	0.6	2.2	0.3	18.3	5.80
Canon Opto TW1 2010	5.67	0.0	0.7	4.6	0.9	3.1	2.6	28.1	0.02
Canon Opto TW2 2006	7.21			18.6	2.1	1.4	2.9	111.0	14.22
Canon Opto TW2 2010	6.08	0.0	0.6	11.2	1.6	1.0	5.1	48.8	0.49
Canon Opto TW3 2006	7.15			12.1	2.0	0.4	3.4	84.2	13.29
Canon Opto TW3 2010	5.74	0.0	0.4	6.1	1.4	0.4	3.1	19.5	0.02
Canon Opto TW4 2006	6.8			7.9	1.6	1.7	6.0	61	15.85
Canon Opto TW4 2010	5.99	0.0	2.2	7.9	2.8	1.7	8.0	61	0.02
Canon Opto TW5 2010	6.9	10.1	3.0	53.9	3.0	4.5	0.3	184.2	10.14
Ansell 5A	6.58	32.4	1.09	3.94	2.05	17.8	3.15	124.44	8.19

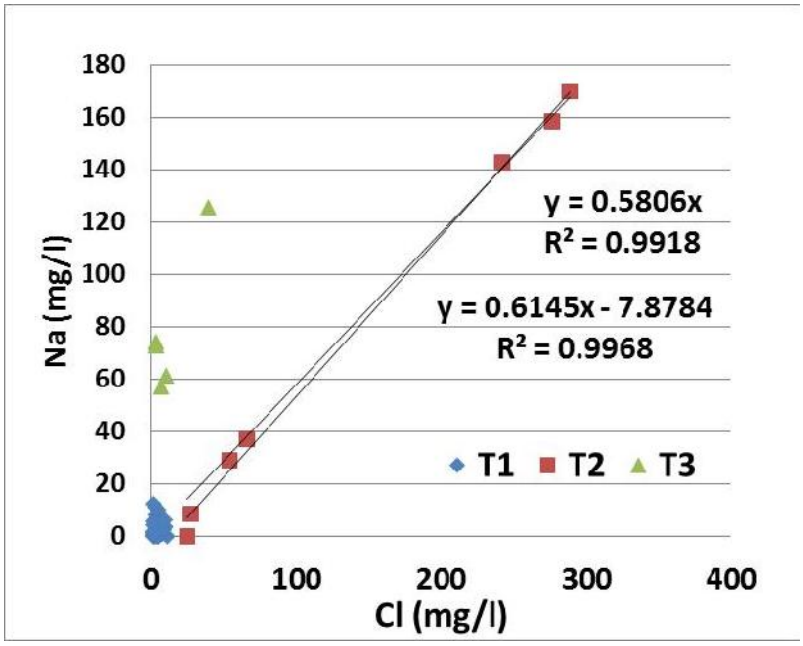

Figure 6.3. Plot of Na concentrations against Cl concentrations.

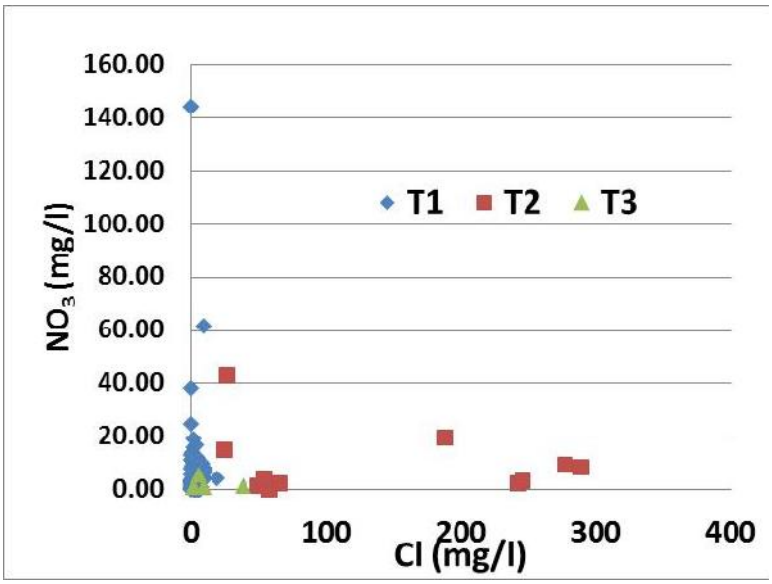

Figure 6.4. Plot of NO_3 concentrations against Cl concentrations.

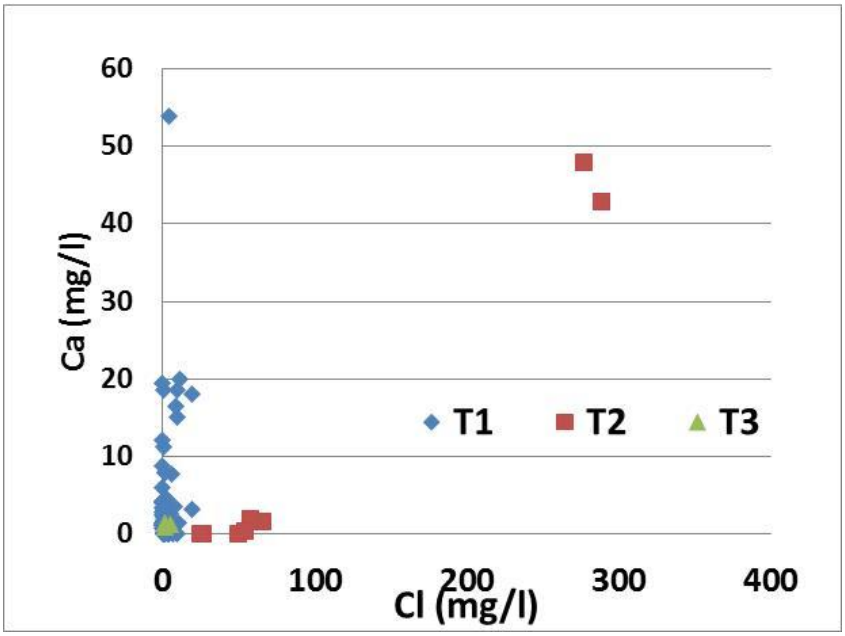

Figure 6.5. Plot of Ca concentrations against Cl concentrations.

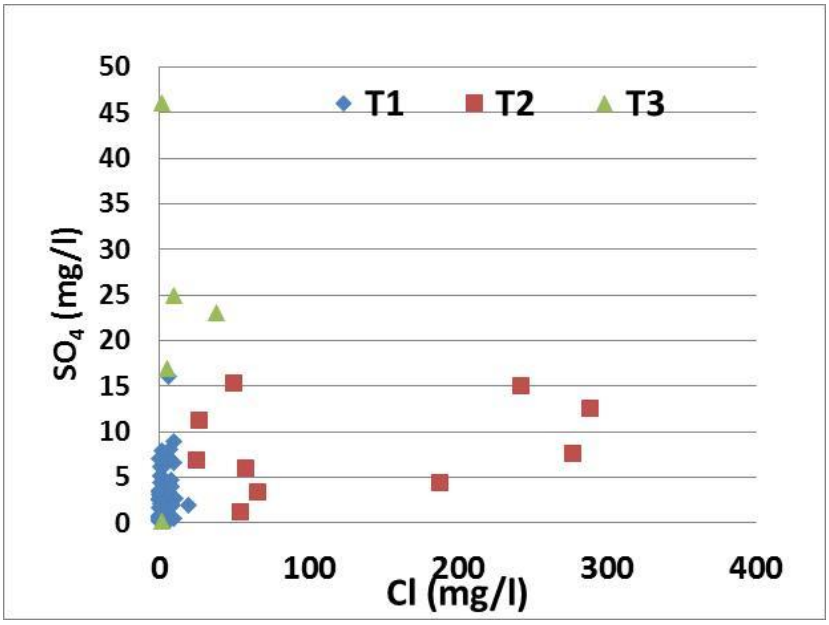

Figure 6.6. Plot of SO_4 concentrations against Cl concentrations.

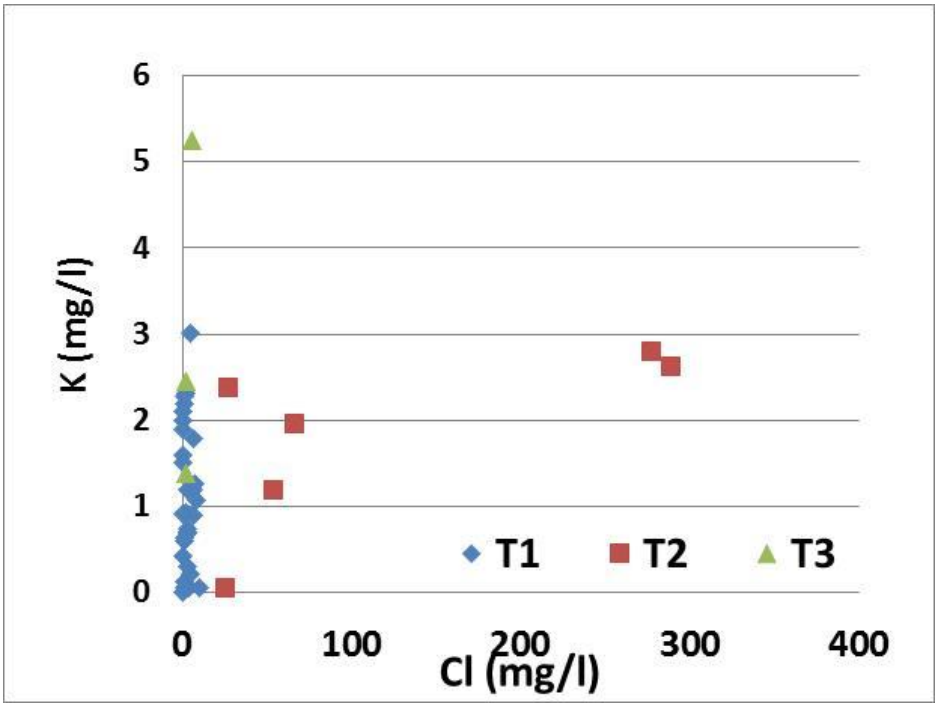

Figure 6.7. Plot of K concentrations against Cl concentrations.

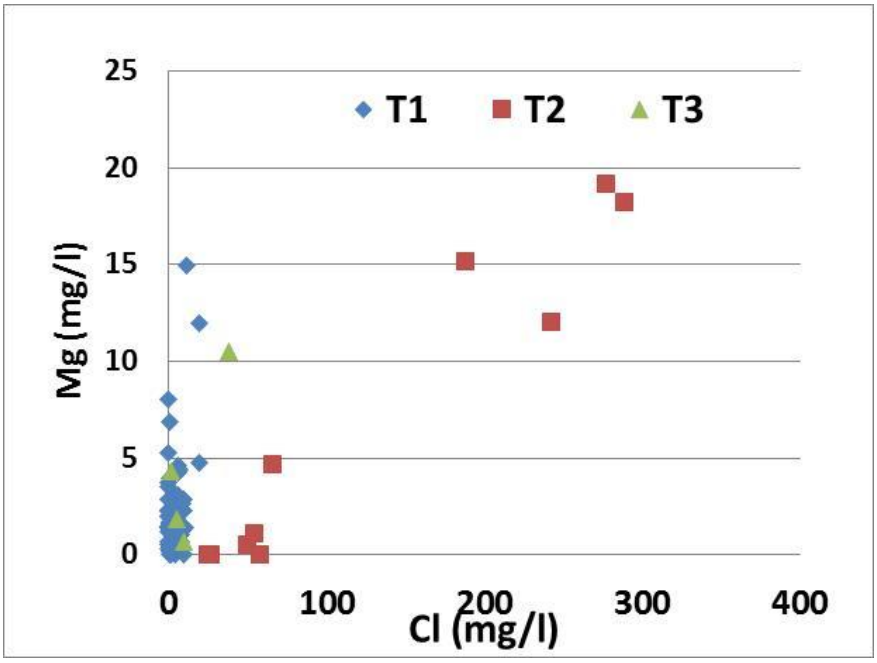

Figure 6.8. Plot of Mg concentrations against Cl concentrations.

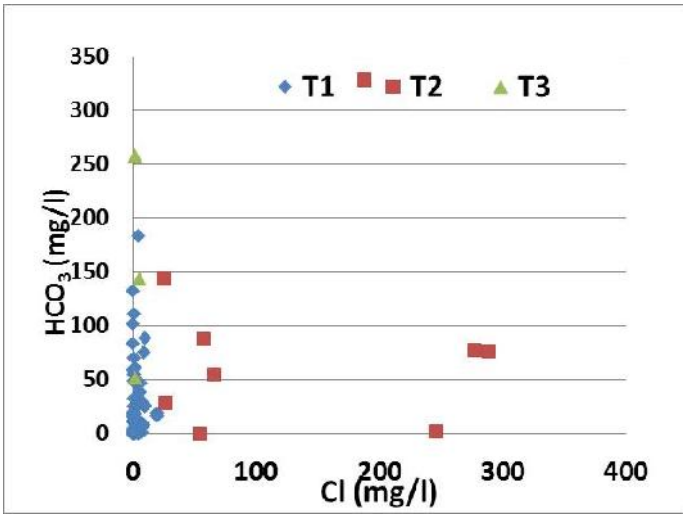

Figure 6.9. Plot of HCO_3 concentrations against Cl concentrations.

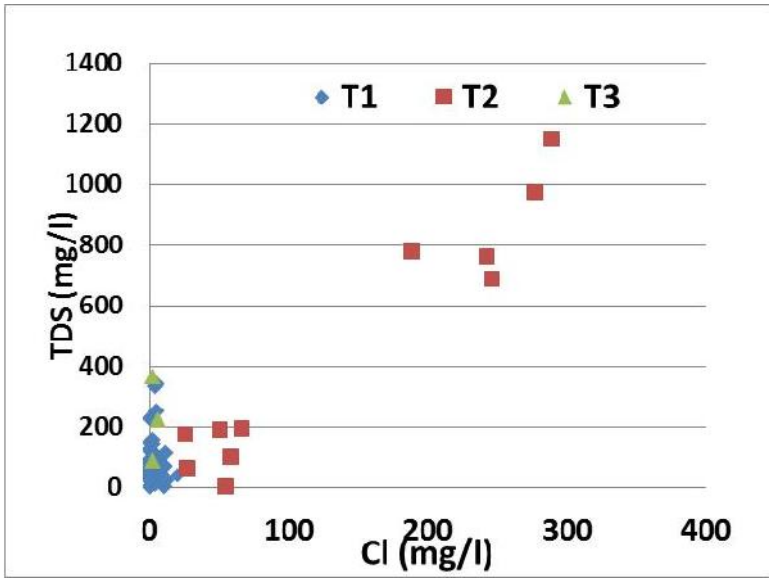

Figure 6.10. Plot of TDS against Cl concentrations.

6.3.3 Water Type 1

6.3.3.1 Introduction

Wellwater samples with low TDS (see Figure 6.10) are classified as Water Type 1. Other major ions also show low concentration as shown in Figure 6.3 to 6.9. There is no obvious relationship between the major ions and Cl^-. Water Type 1 is interpreted to represent the natural chemistry of study area since low ions concentration is common in hard rock aquifer system, though this does not mean that they are entirely unpolluted just that their main chemical characteristics are dominated by the natural signature. This is discussed further below. Figure 6.11 shows the distribution of wellwater samples Type 1. They are spread throughout the area with no obvious spatial grouping.

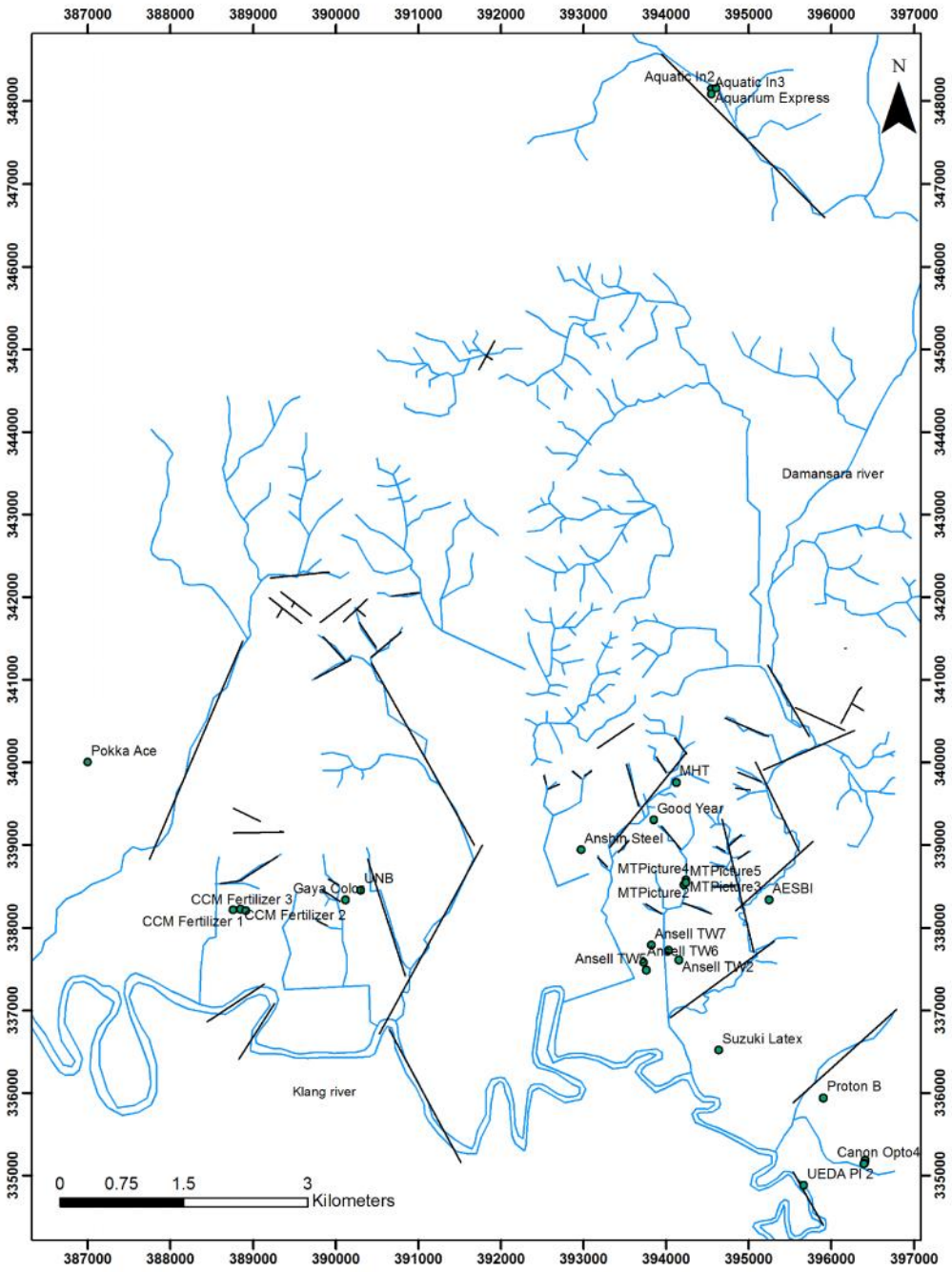

Figure 6.11. The distribution of Type 1 wellwaters.

6.3.3.2 The chemistry of Type 1 wellwaters

Table 6.5 shows example water chemistries for Type 1 wellwaters with no or only one determinand indicative of pollution (see Table 6.11). The major ion concentrations are all very low, usually in the single mg/L range, with low pH values (3.8 to 6.6). Such low concentrations suggest little interaction with rock, as often is the case with mature weathering profiles and acid hard rock systems (Lloyd 1999; Lloyd & Heathcote 1985). There is no general relationship between Cl and the other ions plotted in Figures 6.3 to 6.10, just all concentrations are small suggesting variable degrees but similar processes or lack of processes being dominant.

These concentrations are close to what might be expected for precipitation. Table 6.5 includes annual weighted precipitation concentrations for a forest area in Peninsular Malaysia given by Zulkifli et al. (1989). Comparing with the median values for the wells indicates that Ca, Mg and Cl concentrations are greater in the rainfall than in the wellwaters. Using a mass balance relationship for the other major ions (recharge = (precipitation-runoff) x precipitation concentration / wellwater concentration with runoff calculated by the equation developed in Chapter 3) gives even for one precipitation value (2200 mm/y, about average) a wide range of recharge values (129-502 mm/y) with actual ET of 793-1165 mm/y. If solutes are dissolved during recharge then recharge will be underestimated, but on other hand this does not mean that the recharge estimates will always be underestimated because in the cases of Ca, Mg and Cl, the precipitation has higher concentrations than the wellwaters. It seems that these data are not good enough to obtain the recharge estimates.

Table 6.5. Wellwaters with no indication of pollution or have only one of the possible determinands indicative of pollution listed in Table 6.11. Concentrations in mg/L. Bold is for outlier concentrations including local pollutants.

Name	pH	Na	K	Ca	Mg	Cl	SO_4	Alk	NO_3	Fe	Mn	Si
AESBI 210704	5.5					4		1		0.05		
CCM Fertilizer 1	3.8	2	2	1.5	2	0.5	0.8	0.5	**144.4**	0.24	0.18	3.01
CCM Fertilizer 3	3.6	1.1	1.9	1.1	1.2	0.5	0.3	0.5	**143.9**	0.04	0.13	2.83
Universal Nutri Bev.	6.61			2.21	1.62	0.9	**5.13**	58	4.3	2.35	0.19	0.06
Gaya Color Lab	5.2				1.24	**8.7**		7	9.7			
Anshin Steel	4.81				0.25	0.8	0.25	1	11.1	0.15	0.005	4.23
Suzuki Latex 1a	5.4	2.59	1.26	0.67	0.66	**7.1**	**8**	9	0.3	17.3	0.05	
Suzuki Latex 1b	5.4	1.94	0.93	0.24	0.32	2		0.25		0.16	0.3	
Lafarge	5.77			0.74	0.35	0.8	0.25	6	0.3	0.61	0.005	2.73
Pokka Ace	6.5	2.92				5.4	1.1	1	1.03	0.69	0.04	1.48
Median	5.4	2.0	1.58	1.10	0.66	1.45	0.80					
Mean Ann Weighted Precip*	5.98	0.20	0.34	2.64	0.94	1.64	0.31	9.11	0.35	-	-	-
Precip from Petaling Jaya	4.35	0.54	0.07	0.30	0.04	0.32	2.87					

**Zulkifli et al. (1989), forest site in Peninsular Malaysia*

Table 6.5 also contains some annually averaged wet fallout from Petaling Jaya. Repeating the calculations using these data results in recharge (mm/y) for precipitation =2200 mm/y of 350 (Na), 57 (K), 353 (Ca), 78 (Mg) and 286 (Cl) with ET varying between 942 and 1237 mm/y. Low recharge estimates can come from dissolution which is assumed zero in the calculations so the inference is that perhaps recharge is about 300 mm/y. If so it would be double that estimated by the meteorological data. However, SO_4 concentrations are greater in rainfall than in the wellwaters so this indicates that we cannot be sure that the values calculated are underestimates of recharge. The actual recharge figure is then uncertain. However, it is concluded that the range of concentrations seen in the

wellwaters might be largely explained by precipitation inputs with nearly no major ion inputs from the aquifer. This will be investigated further later in this section.

If the recharge passes through the soil zone as opposed to entering direct from a surface water body or from piped water leaking from below the water table, then it would be expected that P_{CO2} was higher than in equilibrium with atmosphere above ground level as it got CO_2 from the soil zone. Looking at the pP_{CO2} values calculated by Phreeqc (Table 6.6) it seems that many of the wellwaters contain much higher CO_2 concentrations than in equilibrium with the atmosphere (where pP_{CO2} = 3.5). Most waters contain 100 times more CO_2. However, the data are not all reasonable in that a few concentrations are above atmospheric pressure which is unlikely. Nevertheless the consistency of most of the values and values from the other more polluted wellwaters suggests that there is a source of acidity and the most likely is CO_2 from the soil zone. It is therefore likely that most recharge has passed through soil zone.

Table 6.6 Saturation indices for carbonate minerals

Name	**pH**	**pPCO2**	**Calcite saturation index**	**Dolomite saturation index**
Proton 2	6.2	1.24	-2.90	-7.76
AESBI 21 July 2004	5.5	2.32		
CCM Fertilizer 1	3.8	-0.23	-6.41	-12.35
CCM Fertilizer 3	3.6	-0.63	-6.54	-12.70
Universal Nutri Beverages	6.61	0.75	-6.91	-13.03
Gaya Color Lab	5.2	1.75	-2.53	-4.85
Anshin Steel	4.81	1.41	-1.88	
Suzuki Latex 1a	5.4	1.23		
Suzuki Latex 1b	5.4	1.45		
Lafarge	5.77	1.34	-5.06	-9.78
Pokka Ace	6.5	2.63	-6.75	-13.02

Table 6.6 also shows that most waters are carbonate mineral very undersaturated and that therefore very little carbonate is likely to be present as the study of the geology (Chapter 2) indicated.

Figure 6.12 shows a plot of pH against log(HCO_3^-). It is clear that there is some acid-base reactions occurring causing the pH to rise in possibly an open system (or at least pP_{CO2} is not changing much as many points are approximately lying on pP_{CO2} ~ 1.2 contour). If carbonates are not available this change must be due to silicate weathering reactions.

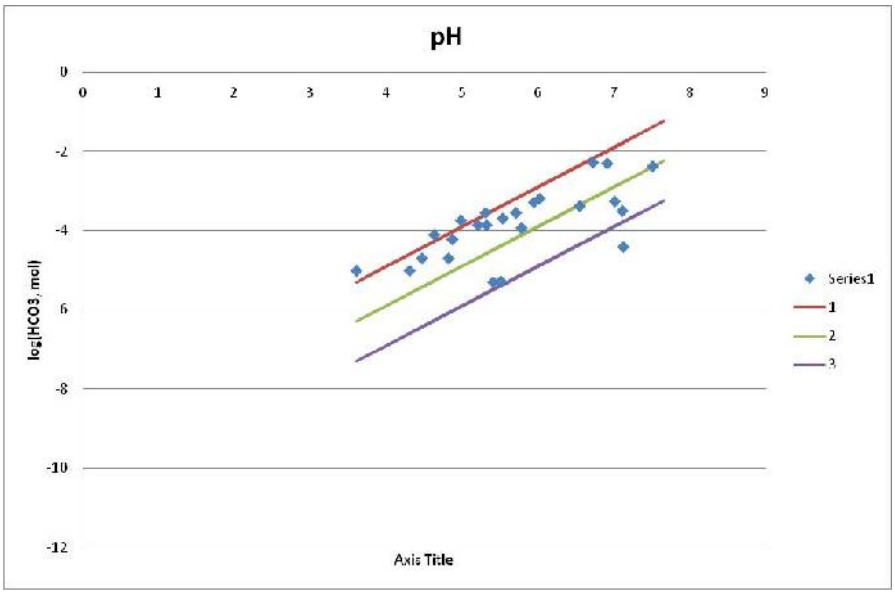

Figure 6.12. A plot of pH against log[HCO3-] for all samples where data are available. Lines are for pPCO2 ~ 1, 2 and 3.

In general weathering reactions have the form:

Silicate mineral + CO_2 + H_2O → Clay mineral + ions + HCO_3^- + (H_4SiO_4)

Stumm & Morgan (1996) give the following examples:

$CaAl_2Si_2O_8 + CO_2 + 3H_2O \rightarrow Al_2Si_2O_5(OH)_4 + Ca^{2+} + 2HCO_3^-$

Anorthite Kaolinite

$NaAlSi_3O_8 + 2CO_2 + 6H_2O \rightarrow Al_2Si_4O_{10}(OH)_2 + 2Na^+ + 2HCO_3^- + 2H_4SiO_4$

Albite Montmorillonite

$2NaAlSi_3O_8 + 2CO_2 + 11H_2O \rightarrow Al_2Si_2O_5(OH)_4 + 2Na^+ + 2HCO_3 + 2H_4SiO_4$

Albite Kaolinite

$[CaMg_{0.7}Al_{0.3}Si_{1.7}]O_6 + 3.4CO_2 + 4.5H_2O \rightarrow 0.3Al_2Si_2O_5(OH)_4 + Ca^{2+} + 0.7Mg^{2+} + 3.4HCO_3^-$

Pyroxene Kaolinite

$2KAlSi_3O_8 + 2CO_2 + 11H_2O \rightarrow Al_2Si_2O_5(OH)_4 + 2K^+ + 2HCO_3^- + 4H_4SiO_4$

K-feldspar Kaolinite

Montmorillonite usually is in drier climates but kaolinite might occur in Malaysia. Table 6.7 gives saturation indices for feldspars and clays for the 'unpolluted' Type 1 waters. It indicates that feldspars are very undersaturated and that though kaolinite is only oversaturated in a couple of the cases it is much closer to saturation than feldspars. This is similar in the other waters. Taking the albite-kaolinite reaction above it has the stoichiometry that is consistent with the pH-log(HCO_3^-) plot – one mole of CO_2 used per mol of HCO_3 produced – same as calcite dissolution and hence plots in the same path on the pH-log(HCO_3^-) plot. Na/Cl ratios are in general quite high (in the unpolluted waters average molar ratio is 2.5, with values from 0.6 to 6.6) and this would be happen if the Na feldspars (like albite) are the main minerals dissolving.

If clays are being precipitated, then this will increase the cation exchange / sorption capacity of the aquifer and hence increase natural attenuation for pollutants. But it will

also reduce the permeability. Clay cation exchange capacity varies in the order: smectites (e.g. montmorillonites)(~80-120 meq/100g) illite & chlorite (~ 10-50 meq/100g) > kaolinite (~3-15 meq/100g) (Lloyd & Heathcote 1985). If kaolinite is being produced then the increase in cation exchange capacity will be smaller than for montmorillonite.

Table 6.7. Saturation indices for feldspars and clays for the 'unpolluted' waters.

Name	Albite	Anorth-ite	K Felds	Illite	Ca-Mont	Chlor-ite	Kaol-inite	K-mica
AESBI 21 July 2004								
CCM Fertilizer 1	**-9.8**	**-16.3**	**-7.5**	**-8.9**	**-5.3**	**-49.2**	**-1.11**	**-3.75**
CCM Fertilizer 3	**-11.1**	**-18.2**	**-8.5**	**-10.9**	**-7.1**	**-53.8**	**-2.56**	**-6.14**
Universal Nutri	**-12.3**	**-17.1**	**-11.3**	**-12.1**	**-9.1**	**-48.3**	**-2.45**	**-5.46**
Gaya Color Lab								
Anshin Steel	**-1.8**	**-4.3**	**-1.1**		**2.6**		**4.65**	**8.09**
Suzuki Latex 1a								
Suzuki Latex 1b								
Lafarge	**-7.5**	**-12.0**	**-5.5**	**-5.8**	**-3.3**	**-33.9**	**0.26**	**-0.27**
Pokka Ace	**-9.3**	**-14.6**	**-7.3**	**-8.8**	**-6.3**	**-37.8**	**-1.97**	**-3.74**

Table 6.8 shows the saturation indices for silica and simple aluminium minerals. Most Type 1 waters are at saturation with quartz though appear to be undersaturated with respect to amorphous silica. Gobbett & Hutchison (1973) (p88) mention quartz overgrowths and recrystallization of chert but these could have taken place at any time in past.

Though the redox state of the waters is uncertain Fe oxides and hydoxides are mostly oversaturated (Table 6.9) even at pe = 4 (E_H ~ 240 mV). This is consistent with Figure 6.13 that shows a weak positive correlation between Fe concentrations and turbidity. Fe seems to be precipitating on contact with air after sampling. Oxides are seen in the field on fracture surfaces (Chapter 2) and could provide some reaction surface for interacting with pollutants. Mn minerals are generally undersaturated may be because Mn is not very

much in the rock and hence there is little source of Mn. Fe/Mn correlation is very weak, but positive. The generally high Fe concentrations suggest that there is reduction and we know that some of the rocks contain organic matter (carbonaceous shales) and Gobbett & Hutchison (1973) (p88) mention pyrite. High Fe and Mn concentrations and often present NH_4 and NO_2 suggest O_2 may have been removed in many waters.

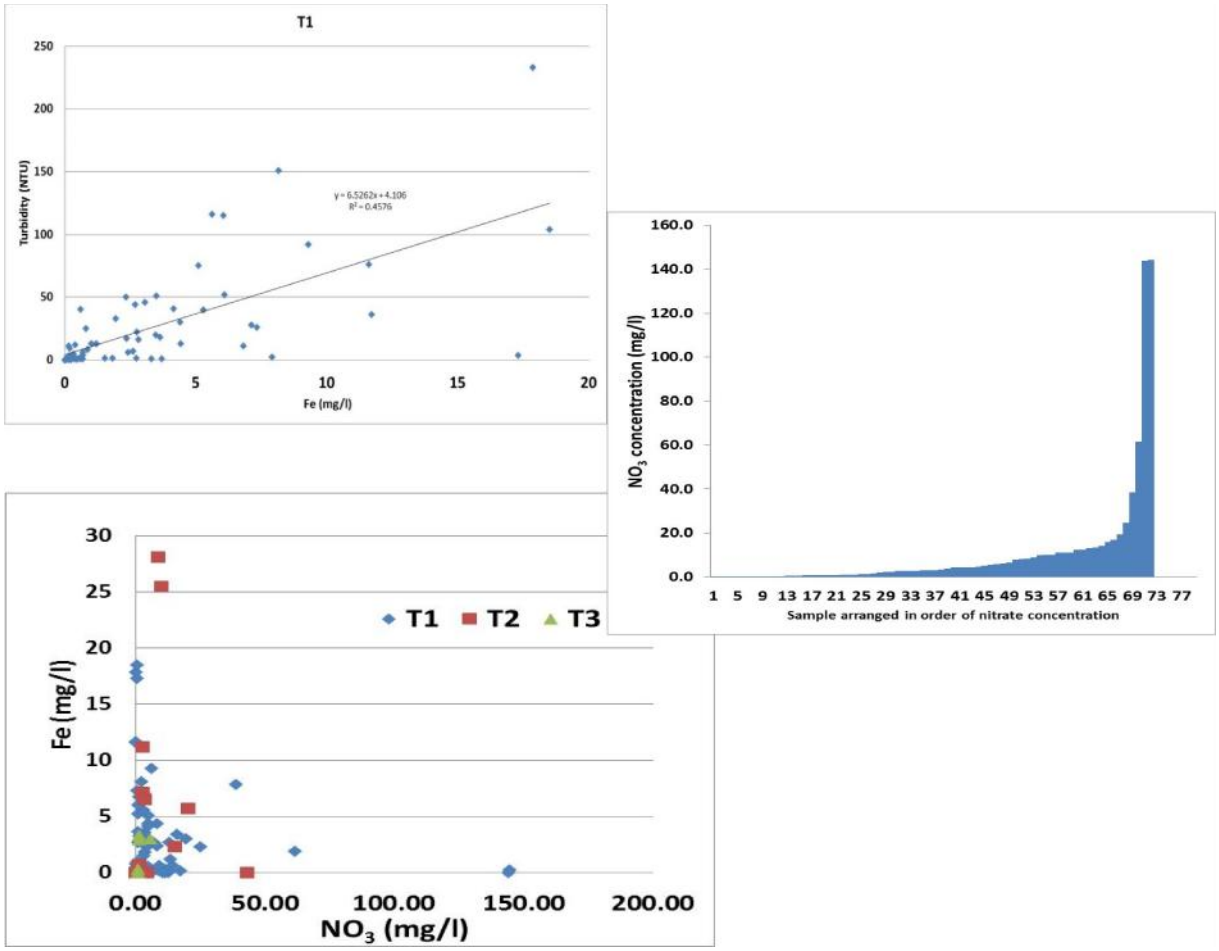

Figure 6.13. Fe relationships. Upper plot: a plot of turbidity against Fe concentrations for Type 1 waters. Middle plot: a plot of NO_3 concentrations for Type 1 waters. Lower plot: a plot of Fe against NO_3 concentrations for all water types.

Table 6.8. Saturation indices for silica and simple aluminium minerals for the 'unpolluted' wellwaters. Calculated using Phreeqc.

Name	SiO_2(a)	Quartz	Chalcedony	$Al(OH)_3$(a)	Alunite	Gibb-site
AESBI 21 July 2004						
CCM Fertilizer 1	-1.31	-0.07	-0.47	-3.61	-3.36	-0.92
CCM Fertilizer 3	-1.34	-0.09	-0.50	-4.31	-5.70	-1.62
Universal Nutri	-3.04	-1.79	-2.20	-2.56	-1.35	0.13
Gaya Color Lab						
Anshin Steel	-1.17	0.08	-0.33	-0.88	-0.72	1.81
Suzuki Latex 1a						
Suzuki Latex 1b						
Lafarge	-1.36	-0.11	-0.52	-2.89	-3.90	-0.20
Pokka Ace	-1.62	-0.38	-0.78	-3.73		-1.04

Table 6.9. Saturation indices for Fe and Mn minerals assuming pe = 4. Using Phreeqc

Name	Hematite Fe_2O_3	Goethite FeOOH	Pyrolusite MnO_2	Rhodo-chrosite $MnCO_3$
AESBI 21 July 2004	6.84	2.41		
CCM Fertilizer 1	-2.26	-2.13	-23.81	-4.82
CCM Fertilizer 3	-5.02	-3.51	-24.76	-4.96
Universal Nutri Beverages	-2.50	-2.26	-22.40	-5.40
Gaya Color Lab	19.43	8.71	-1.23	-1.12
Anshin Steel	12.56	5.27	-11.63	-0.47
Suzuki Latex 1a	0.00	0.00		
Suzuki Latex 1b	13.75	5.87	-5.93	-5.93
Lafarge	11.20	4.60	-17.90	-3.68
Pokka Ace	7.23	2.61	-17.07	-4.14

Though the Fe and Mn concentrations are in general high, NO_3 is present in many wellwaters and at concentrations above perhaps natural concentrations in about half the samples (Figure 6.13). This suggests that pollution, probably from sewers, is very common. Nitrate is present in many samples with high Fe concentrations suggesting mixing in the wellwaters with presumably nitrate containing water overlying deeper anoxic Fe containing groundwater.

In conclusion it is suggested that evaporation of rainwater dissolving CO_2 in the unsaturated zone and silicate weathering are the main controls on the concentrations in the 'unpolluted' wellwaters. Fe^{2+} minerals are oversaturated in wellwater samples which lie in carbonaceous shale (e.g. AESBI); also for wellwater samples in fractured sandstone (e.g. Anshin Steel, Gaya Color Lab).

6.3.4 Water Type 2

The wellwaters of Type 2 are the following samples:

Carlsberg 1 (2010), 2 (2010), 3 (1998), 4 (1998)

Ansell TW3 (2010), TW4 (2010), TW5 (2008)

Proton 1 (2010), 2 (2006)

CCM Fertilizer 4 (2006)

Ueda Plating 1 (2007)

All but CCM Fertilizer 4 and Carlsberg 1 and 4, have had samples that have also been in Type 1 (before or after date at which they were Type 2). In the case of CCM Fertilizer 4, other wells in the compound are water Type 1. So the Type 2 signature seems to be the result of intermittent processes.

Figure 6.14 shows the distribution of wells in Water Type 2 with high TDS (>100mg/l) values, high Cl (>25mg/l), high Ca (>10mg/l), high Mg (5mg/l), high HCO_3(60mg/l), high Fe (>5mg/l) and high Mn(>0.4mg/l). The wellwater samples in Water Type 2 are from various type of industry which are brewery (Carlsberg 1 and 2), Ansell TW3, TW4 and Ansell 5A (manufactures gloves), PROTON 1 (automotive) and Scientex Polymer.

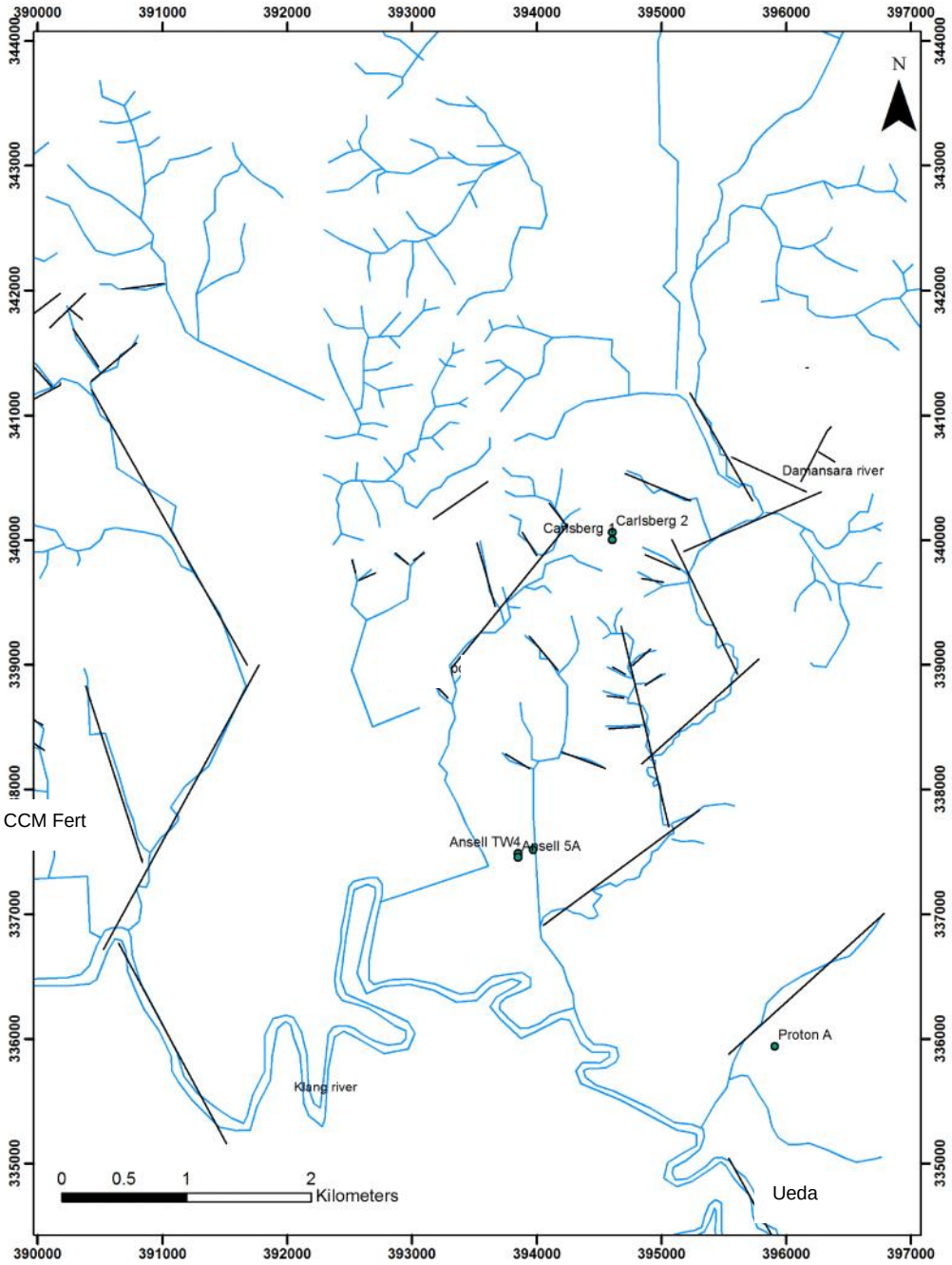

Figure 6.14. Wellwater samples (Type 2) in study area.

Wellwater samples in this group are dominated by Na and Cl (see Figure 6.3) which is different from Water Type 1. The Na/Cl molar ratio is close to but below 1, and the

concentrations of both ions are high. . The Na:Cl molar ratio is 0.89 if a best fit line is forced through the origin (r^2 = 0.99), and 0.95 otherwise with an intercept of -7.9 mgNa /l (r^2 = 1.00). This suggests that there is a sink for Na (as it is less than Cl), but what dominates is that there is a common source for the two ions. Possible sources for the NaCl are sewers leakage and industrial discharges.

Three of the Ca concentrations in Type 2 waters (Figure 6.5) are very unusually low with very negative ionic balances suggesting that there is a problem with the analysis (mistakenly entered as the detection limit of 0.05 mg/l?). Other Ca concentrations are similar to Type 1 but in two cases are very high with reasonable ionic balances. Mg similarly includes some very high concentrations (Figure 6.8). The samples with the highest Ca also have the highest Mg, and the highest Cl. It seems likely that the NaCl pollution has resulted in some ion exchange releasing Ca and Mg but it cannot explain all of the increase in Ca and Mg concentrations for the two highest concentrations of Ca and Mg. So there is a high Ca and Mg source of pollution as well as the NaCl, and it is not obviously associated with either HCO_3 or SO_4.

Again $pPco_2$~1, and pH/log[HCO_3] relationship is compatible with open system dissolution. So the waters have been through the soil zone. As discussed in Section 6.3.3, carbonate minerals are very undersaturated.

Wellwater samples in Type 2 have SO_4 concentrations up to 15mg/l (see Figure 6.6), slightly higher than the average in Water Type 1 and not closely related to the NaCl source. NO_3 concentrations are very variable (see Figure 6.4) and not really part of what characterises Type 2 waters. They are close to the range of Type 1 waters and are not closely related to the

NaCl source and this may suggest that the NaCl source is not sewage but on the other hand Type 2 waters are not correlated with particular industries or areas. Therefore the main characteristic of Type 2 (high NaCl and a Ca/Mg source, possibly with ion exchange increasing Ca and Mg further) seems to be an addition to the natural background concentrations rather than a completely different water, i.e. pollution of the natural water. This is consistent with the fact that wells with Type 2 water sometimes have samples with water Type 1 too (see above).

The relationship between Fe and turbidity is similar to Water Type 1 (see Figure 6.15) in that both are weakly positively correlated. Without the two highest Fe concentrations, the slope for the two water types is similar (5.6 NTU/mg/l for Type 2). Mn looks to have a similar source to Fe as shown in Figure 6. 16. Correlation is much stronger than for Type 1 (r^2 = 0.22). The source of Fe and Mn is probably from water and rock interaction. Again the high Fe concentrations suggest a reducing environment despite the presence of NO_3 (Figure 6.13) and again mixing in the well seems to be likely.

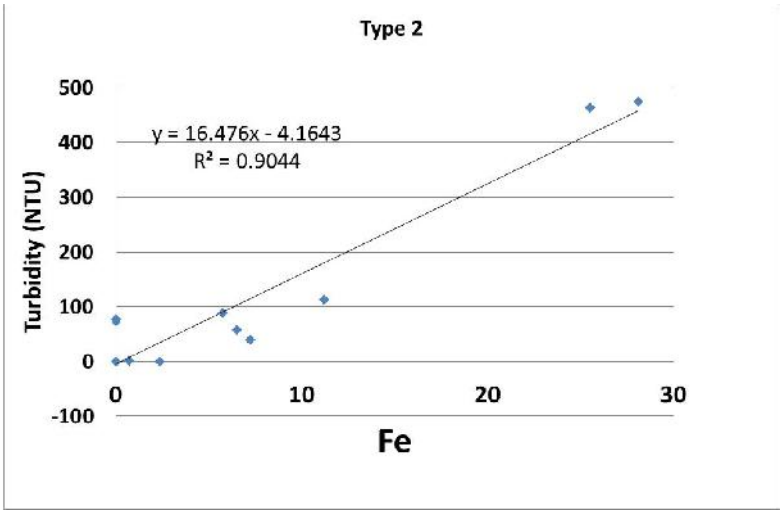

Figure 6.15. A plot of turbidity against Fe concentrations for Type 2 waters.

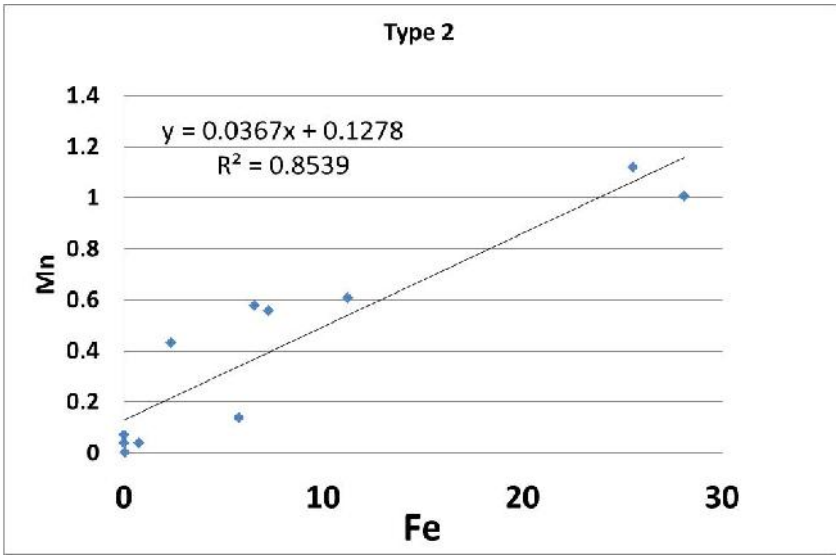

Figure 6.16. Plot of Fe against Mn concentrations (mg/l) for Type 2.

6.3.5Water Type 3

Figure 6.17 shows the distribution of wells for Water Type 3 with high TDS (>100mg/l) values and low Cl- (<25mg/l). The wellwater samples in this type are Ansell TW4 (2008) and TW6 (2008) (manufactures gloves), and Panasonic TW1 (2005, 2010) and TW2 (2010).

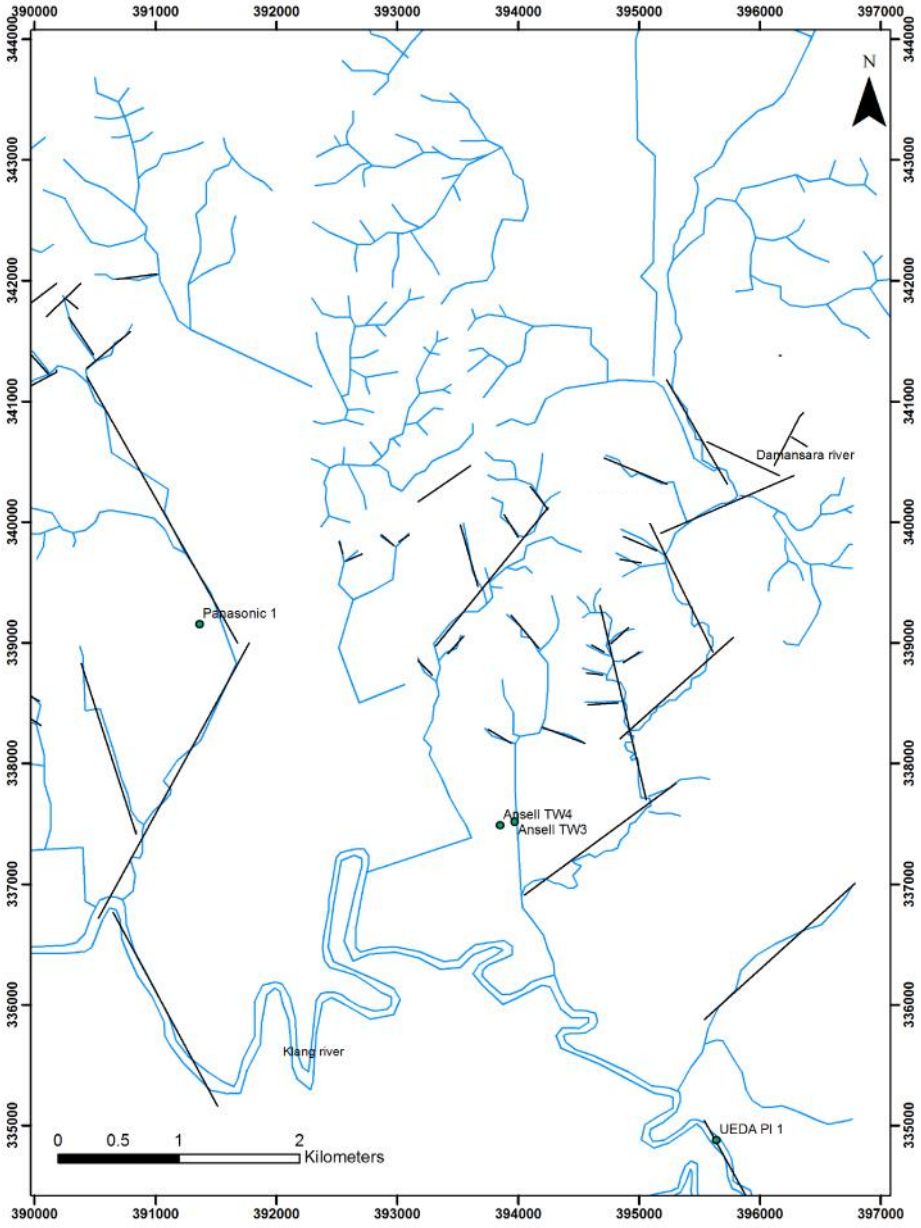

Figure 6.17. Type 3 waters are at Ansell and Panasonic only.

The features that characterise Type 3 waters are: (i) the very high Na/Cl ratios (Figure 6.3);(ii) the high HCO_3/Ca ratios as shown in Figure 6.18; and (ii) the generally higher SO_4 concentrations (Figure 6.6).

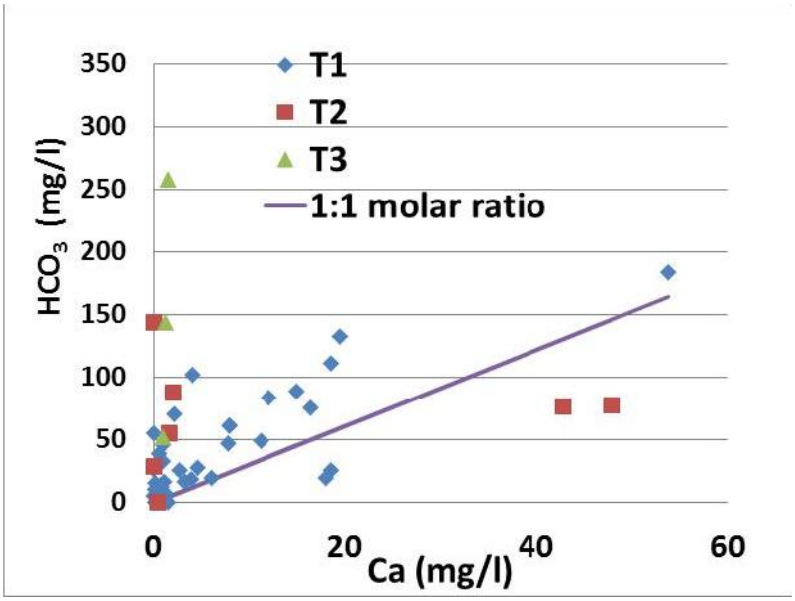

Figure 6.18. Relationship between Ca and HCO_3. The almost zero Ca concentrations in Type 2 water may be in error.

The features (i) and (ii) may be partly explained by ion exchange. Na is higher than expected from Cl concentration (Figure 6.3) and Ca is low (Figures 6.5 and 6.18). Though the latter is also true of some of the Type 2 waters (but see Figure 6.18 caption), the very high Na/Cl ratios for Type 3 waters suggest ion exchange may be important this time in removing Ca and adding Na to solution, the opposite to Type 2 waters. This would happen if a Na-rich groundwater was being flushed by a Ca-rich groundwater. It is not possible to determine what these waters may be, but it is unlikely that they come from flushing out of Type 2 waters as the latter have lower SO_4 concentrations.

HCO_3 has a large range (Figure 6.9), suggesting that Water Type 3 does not have a characteristic HCO_3 concentration, and pP_{CO2} ranges from 1 to ~2. So water has been through the soil zone. NO_3 is low enough mainly to be consistent with natural concentrations. Fe and Mn are similar to Water Type 1 and Type 2.

It is concluded that ion exchange is occurring here. The source of water for Water Type 3 is different, possibly as a result of made ground (e.g. plaster) leaching locally recharging. It looks like there may be other sites where similar process is occurring but to a less important degree (high Na/Ca group of Water Type 1 samples). The distribution of Type 3 waters (Figure 6.17) indicates little. It has only been seen at 2 sites.

6.4 Pollution

6.4.1 Introduction

Common major ion contaminants in urban aquifers include SO_4, NO_3, and Cl (e.g. Ford and Tellam, 1994; Grischek et al.1996; Anderson & Eisen 1979; Barrett et al.,1999; Bottrell et al., 2008). High nitrate, sulphate and chloride can be linked with leaky sewers (Eiswirth & Hötzl 1997). The presence of potassium in wellwater is also associated with leaking sewers sometimes. The concentration of potassium in domestic waste water ranges from 7 to 15mg/l. Excessive nitrate in rural aquifers is often from the use of fertilizers (Flipse et al. 1984, Spalding & Exner 1993, Bijay-Singh et al.1995, Zhang et al.1996) while nitrate in urban groundwater is linked with leakage from sewers and water mains, leachate from landfill and industrial spills (Lerner et al. 1999, Wakida & Lerner 2005).

In the previous sections, the waters have been divided into three types. Type 1 is mainly natural. Type 2 has a NaCl source and is also partly reverse ion exchanged. The NaCl has been assumed to be from pollution. Type 3 waters are also ion exchanged with very high Na concentrations but low Cl concentrations. It is unsure if these waters come from pollution but could represent flushing out of higher NaCl water by natural groundwater though with a higher SO_4 concentration than usual for the latter.

In this section pollution is looked at in more detail using not just the determinands discussed in Section 6.3.4 but also determinands that are definitely pollutants (e.g. grease, coliforms). This should give a fuller picture of the groundwater chemistry and also the groundwater susceptibility to pollution.

6.4.2 Rivers as sources of pollution

Since the tubewells in study area are located near rivers, and some pumping tests indicate recharge boundaries, it is possible that rivers are one of the pollution sources. There are two main rivers running through Shah Alam's area; Klang river and Damansara river. There are 10 measurement stations along the Klang river (from upper to lower stream) and 3 stations along the Damansara river which are located in study area. Malaysia uses a Water Quality Index (WQI) in monitoring river water quality. The WQI is calculated based on six major parameters which are Biochemical Oxygen Demand (BOD), Chemical Oxygen Demand (COD), suspended Solids, pH, dissolved oxygen and ammoniacal nitrogen NH_3-N as shown in Table 6.11. Waters are classed as: clean with WQI from 81-100; slightly polluted (60-80); and polluted (0-59).

The WQI for the Klang River Basin is in Class IV with Class III (Table 6.11) in the upper stream from 1997 to 2007 (Faridah et al. 2012). Klang river has third place among rivers in Malaysia, with low DO levels; with high ammonium levels and the highest turbidity level (DOE 2008). The parameters such as dissolved oxygen, temperature, colour and turbidity measured at Klang river and Renggam river, Shah Alam are influenced by the weather (dry or wet day) during the sampling (Mazlin et al 2001).

Comparing wellwater samples with river water data is difficult as the only parameter that is measured in both river and groundwater samples is ammoniacal nitrogen. The wellwater

samples have a low background of Cl^- and NH_3-N as shown in Figure 6.19. The samples with higher NH_3-N (> 0.1mg/l) are Carlsberg 3 and 4, MT Pictures 1 and 5, Ansell TW1, Ansell TW2, Ansell TW3, Ansell TW4 and Ansell TW5 in 2005, Ansell TW4 in 2006, Ansell TW4 and Ansell TW6 in 2011, Ansell TW7 from 2008 to 2011, Aquarium Express, Aquatic International 3, Suzuki Latex, Panasonic Compressor, Proton 1 and Proton 2 and Panasonic TW2. These wells are located near the Klang river, Damansara river and Renggam River. Unfortunately, NH_3-N is not measured in all water samples including AESBI. However, from chemical analysis, the concentrations of calcium, magnesium and potassium of the wellwater sample at AESBI are higher which is possibly influenced by Damansara river nearby, but this cannot be confirmed.

Table 6.10. The parameters evaluated Water Quality Index. Source : LUAS (2008) and Zaki (2010)

		Classes				
Parameters	**Unit**	**I**	**II**	**III**	**IV**	**V**
BOD		<1	1-3	3-6	6-12	>12
COD		<10	10-25	25-50	50-100	>100
DO		>7	5 - 7	3 - 5	1 - 3	<1
TSS		<25	50	50- 150	150-300	>300
pH		>7	6 - 7	5 - 6	<5	>5
Ammoniacal nitrogen	mg/l	<0.1	0.1-0.3	0.3-0.9	0.9-2.7	>2.7
Turbidity	NTU	5	50	-	-	-
Faecal Coliform		10	100	5000	5000	-
Total Coliform	counts/100ml	100	5000	50000	50000	>50000
WQI	mg/l	>92.7	76.5 – 92.7	51.9-76.5	31.0-51.9	<31.0

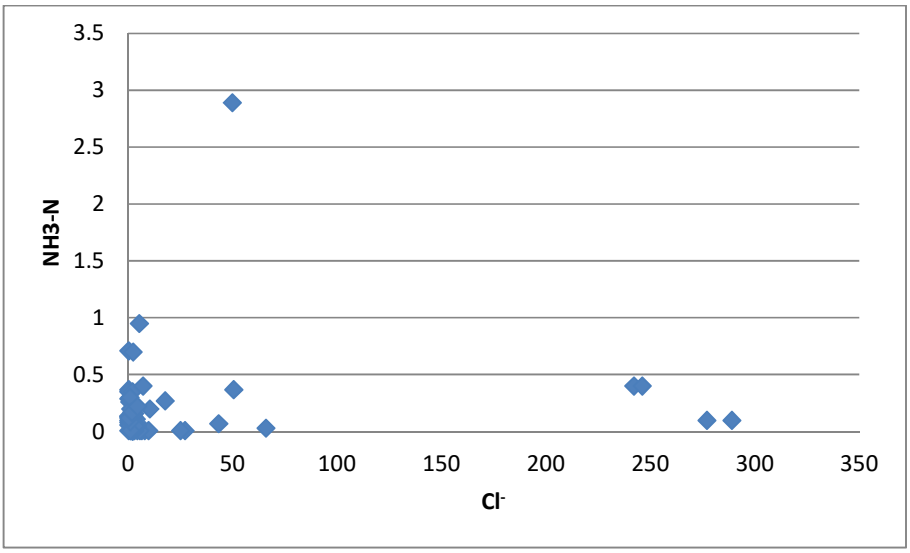

Figure 6.19. The wellwater samples have a low background of NH_3-N and Cl^-. The sample with highest values of NH_3-N is Proton 1.

6.4.3 Correlation between wellwater chemistry and industrial landuse

The tubewells in the study area are all located at industrial sites. There is no clear correlation between landuse and groundwater quality as shown in Figure 6.20 which shows the wellwater samples with TDS > 100 mg/l. Higher concentrations of major ions which probably means pollution are restricted to the following wells: Ansell (gloves), Carlsberg (brewery industry); UEDA Plating (metal plating industry); Panasonic (electrical appliances industry); and PROTON (automotive industry). The total dissolved solids values of other wellwaters are low (50 - 200 mg/l), typical of groundwater in many hard rock areas (Krasny & Sharp 2003). Industries that have wellwaters with lower TDS are manufacturers of: bus bodies; films; drinks; rubber tyres; steel bars; finger cots and finger stalls; lead products; and fish products. This could mean that these industries are less polluting or simply that the pollution has not yet reached the wells.

In general, it would be expected that particularly in a recently set up city that the pollution would show a good correlation with its source location (Tellam and Thomas, 2002), particularly as the wells abstract below the possible sources, but in this case industrial types are too varied to obtain a clear indication of correlation from just TDS.

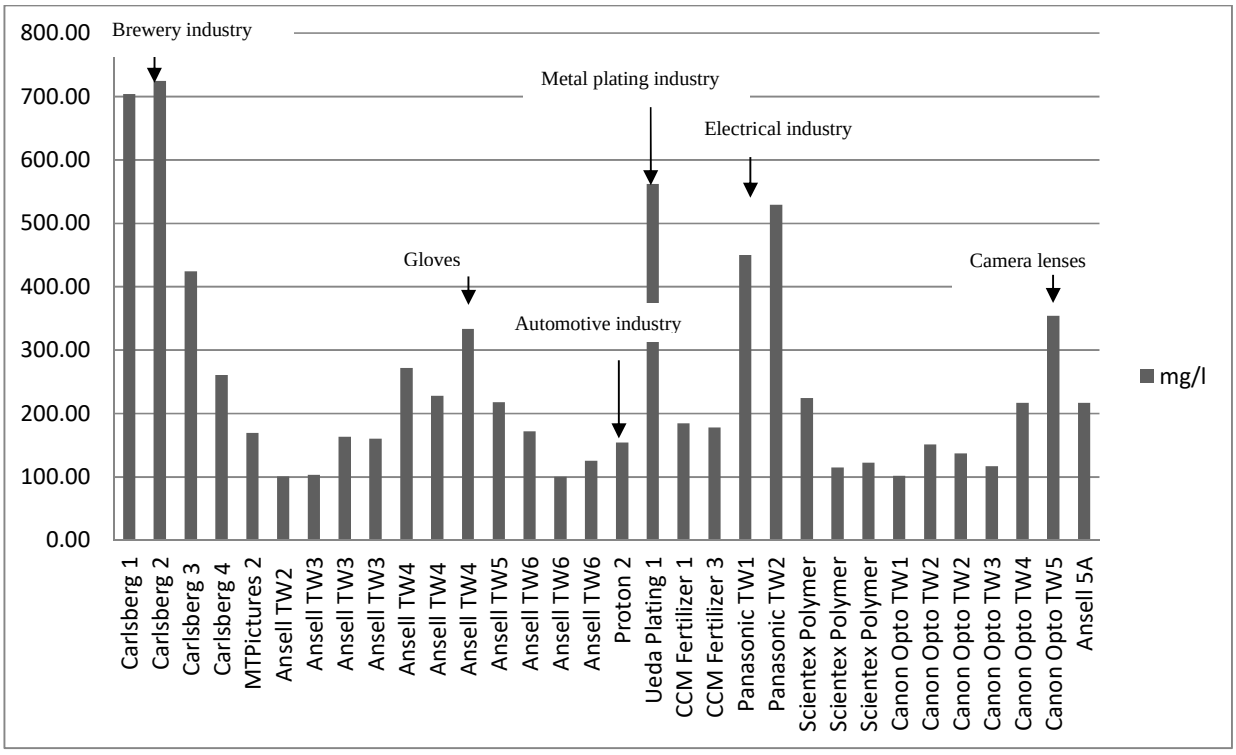

Figure 6.20 Wells with higher total dissolved solids (>100mg/l) and the industries with which they are associated.

6.4.4 Determinands of anthropogenic origin

Table 6.11 shows the list of analytes that can be used as a pollution indicator in that they are all of anthropogenic origin. Examination of the data (e.g. Table 6.11) suggests that only 30% of the total number of samples available (56) show any major ion pollution. This very different to the case of older cities, e.g. Birmingham (e.g. Ford and Tellam, 1994), and suggests that either sewer leakage is much less important, or that it has not happened to a

great extent so far. However, 21% of the total samples show NO_3 concentrations > 5 mg/L, so even in the short time since the city developed some pollution has occurred almost certainly from sewers. Sewer pollution is also indicated by the detection of E.coli, coliforms and detergents in some of the samples (Table 6.10), though not all of the cases have all the sewage indicating species present though this is also what Barrett et al (1999) also found.

Table 6.11 includes an indicator of the diversity of pollution, a pollution indicating ratio (PIR). This is the number of the determinands listed with a positive recorded concentration as a fraction of the total number of determinands listed expressed as a %. Cl and NO3 have been included when greater than 10 and 5 mg/l respectively. 50% of sites only have one identified pollutant. Most (66%) of the rest have 2 or 3 out of the 8 examined. Though PIR is affected by what species were analysed in each sample, it suggests that in most cases pollution is limited to a few species at most.

Figure 6.21 shows the plots of TDS against NO_3 and PIR, and it appears that there is little relationship. One reason for this is that HCO_3 has an effect on TDS (Figure 6.22), and HCO_3 may be from natural sources. It is clear that pollution is not related to TDS in a simple way and this may help explain why the link between TDS and landuse in Figure 6.22 is unclear.

From Table 6.11, it is clear that the pollution locations are in all water types, and not particularly associated with one in particular. 29 out of 47 sites have shown some indication of pollution and therefore pollution can get through from ground level quite rapidly.

Since the pollution occurs in all three water types, it will be discussed in the following sections together rather than type by type. It has been suggested in previous sections that the

major ion concentrations of types 2 and 3 are affected by pollution, but this is NaCl and possibly SO_4 -related pollution, and other pollution seems to be additional to this.

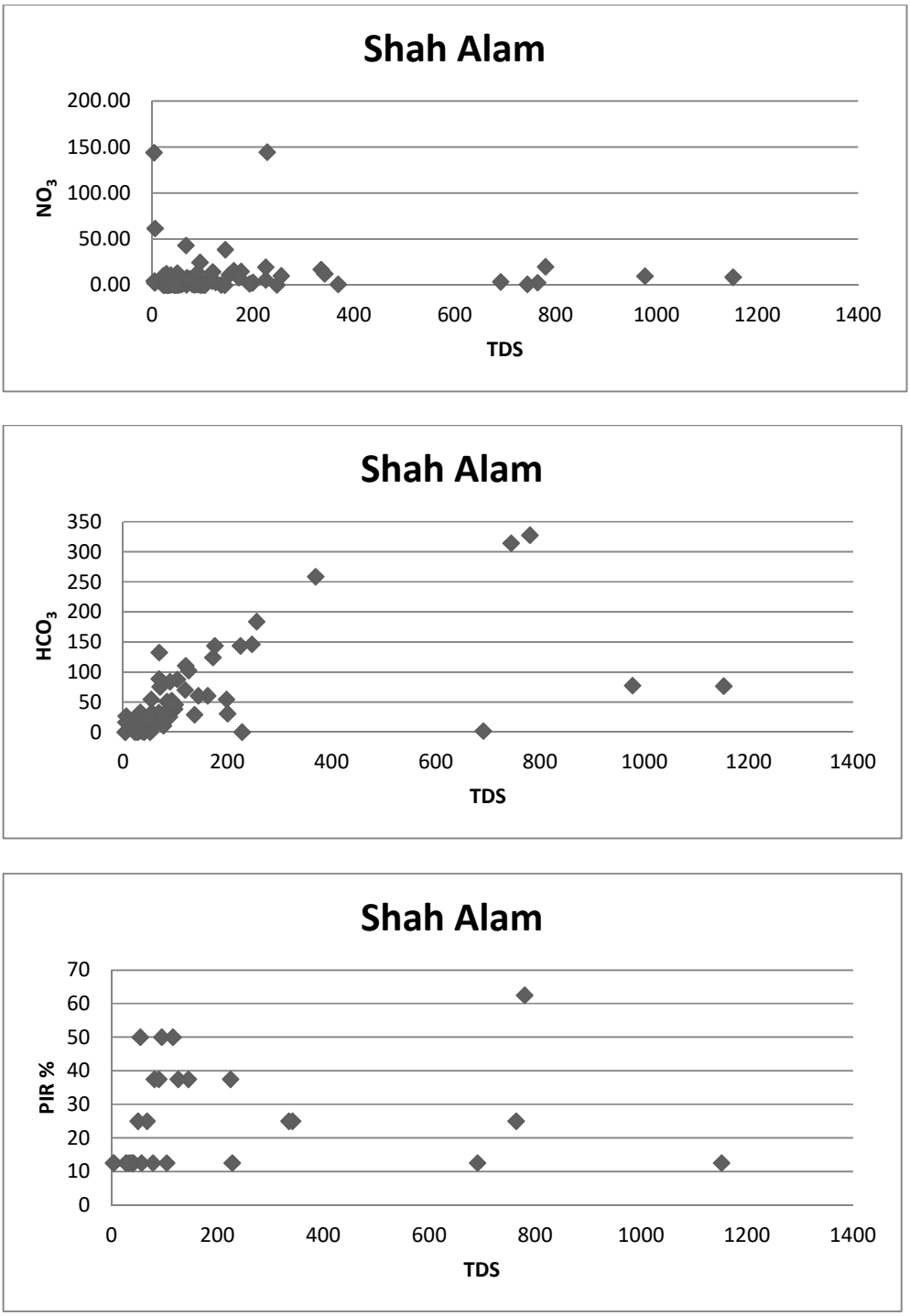

Figure 6.21. TDS is used as a pollutant indicator.

Table 6.11. Pollution indicating determinands (PIR – a pollution indicating ratio, that is number of the determinands listed with positive recorded concentrations as a fraction of the total number of determinands listed expressed as a %)

Site	Date of sampling	Water type	PIR (%) *	Detergent	Coliforms	E. coli	Oil/ grease	Phenol	CN	NO3> 5ppm	Cl> 10ppm
Ansell TW2	2005	1	50	X	X	X				X	
Ansell TW3	2010	2	37.5	X			X		X		
Ansell TW4	2005	1	50	X			X		X	X	
Ansell TW5	2005	1	50	X			X			X	X
Ansell TW6	2007	1	37.5		X	X				X	
Ansell TW7	2007	1	12.5	X							
MTPictures 1	2005	1	50	X	X	X				X	
MTPictures 2	2005	1	37.5	X	X		X				
MTPictures 3	2005	1	37.5	X	X		X				
MTPictures 4	2005	1	12.5	X							
MTPictures 5	2005	1	25	X						X	
Aquatic Int 2	2003	1	25						X	X	
Aquatic Int 3	2003	1	37.5	X					X	X	
Good Year 1	2007	1	12.5	X							
Ueda Plating 1	2007	3	62.5				X	X	X	X	X
Carlsberg 2	2010	3	12.5								X
Carlsberg 3	1998	3	25					X			X
Carlsberg 4	1998	2	12.5								X
Panasonic comp.	2004	1	12.5					X			
Panasonic 2	2010	3	12.5								X
Aquarium Express	2005	1	25						X	X	
Pokka Ace	2006	1	12.5						X		
Anshin Steel	2007	1	12.5							X	
Gaya Color Lab	2006	1	12.5							X	
Proton 2	2006	1	12.5								X
CCM Fertilizer 1	2006	1	12.5							X	
CCM Fertilizer 3	2006	1	12.5							X	
CCM Fertilizer 4	2006	1	12.5								X

6.4.5 Nitrogen Species

NO_3 in wellwater samples are very variable (see Figure 6.21), but often higher than would be expected from natural systems (perhaps a few mg/l at most). The wellwater samples with high NO_3 are therefore almost certainly polluted, probably from sewers mainly as has been seen in many urban aquifers. NH_4 is seen too (Figure 6.19), and this could be associated with sewer leakage, but it also could be from industrial sources and in some cases from the surface waters (see above).

NO_2 is high sometimes (Figure 6.22) suggesting that either reduction of NO_3 or oxidation of NH_4 is locally occurring. There are 45 samples which have been analysed for NO_2. NO_2 is quite reactive therefore appropriate care must been taken to do the NO_2 analysis. Most waters have high Fe suggesting limited O_2. This would normally mean that NO_3 would also be at low concentration through denitrification. Though overall, high Fe is associated with low NO_3 concentrations in Type 1 waters (Figure 6.23), there are many samples that contain significant amounts of both. This suggests one of the following: (i) Fe is particulate in groundwater in study area; (ii) high NO_3/low Fe and low NO_3/high Fe waters are mixing in the well during sampling; (iii) the reductant that has removed O_2 and allowed Fe minerals to become soluble is now depleted and there is insufficient left to completely remove all the NO_3.

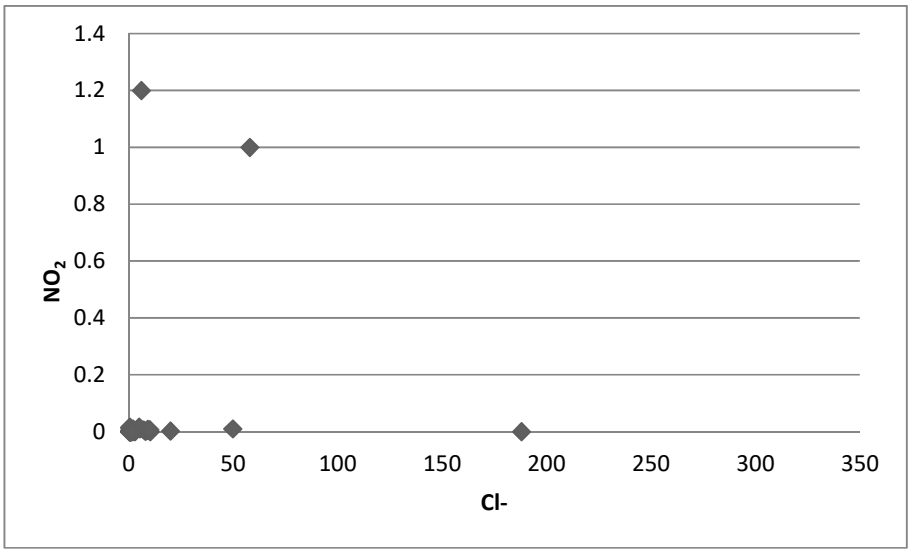

Figure 6.22 The wellwater samples have a low background of $NO_2^-$and Cl^-. The sample with highest values of NO_2^- is Proton 1 and Proton 2.

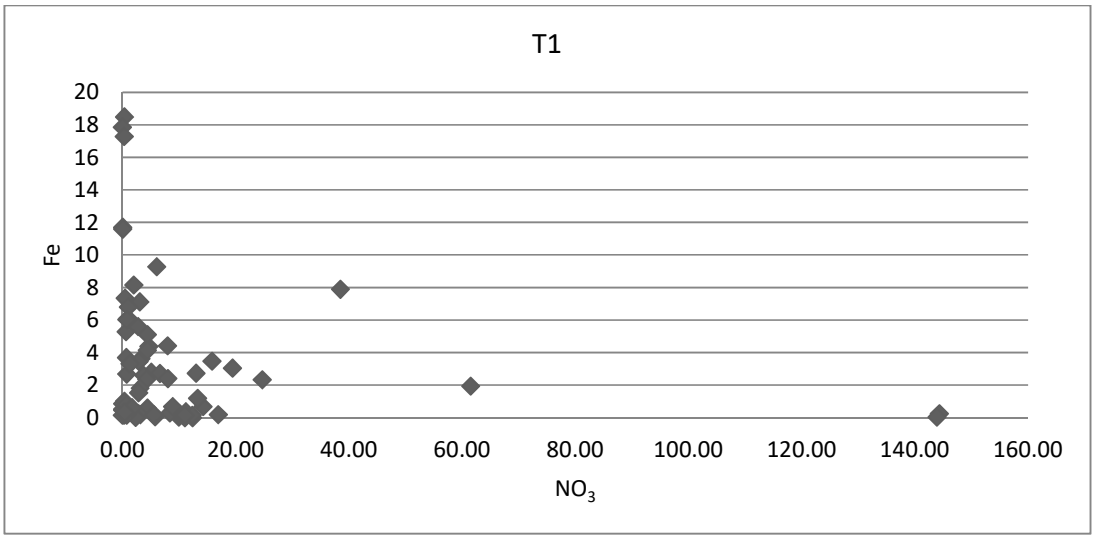

Figure 6.23. The relationship of Fe with NO_3 for Wellwater Type 1

A plot of turbidity with Fe shows a good linear relationship (see Figure 6.13) and suggests that Fe in the sample is particulate at the point of turbidity analysis. However, it is unclear if this relationship exists in the groundwater itself.

Reductant for denitrification could be organic matter. The organic matter in water samples is very variable but the maximum value is less than 1ppm (Figure 6.24). The denitrification is spatially variable and limited in extent; i.e. is reductant-limited, presumably most of the limited organics being used in reductive dissolution of Fe and Mn oxides.

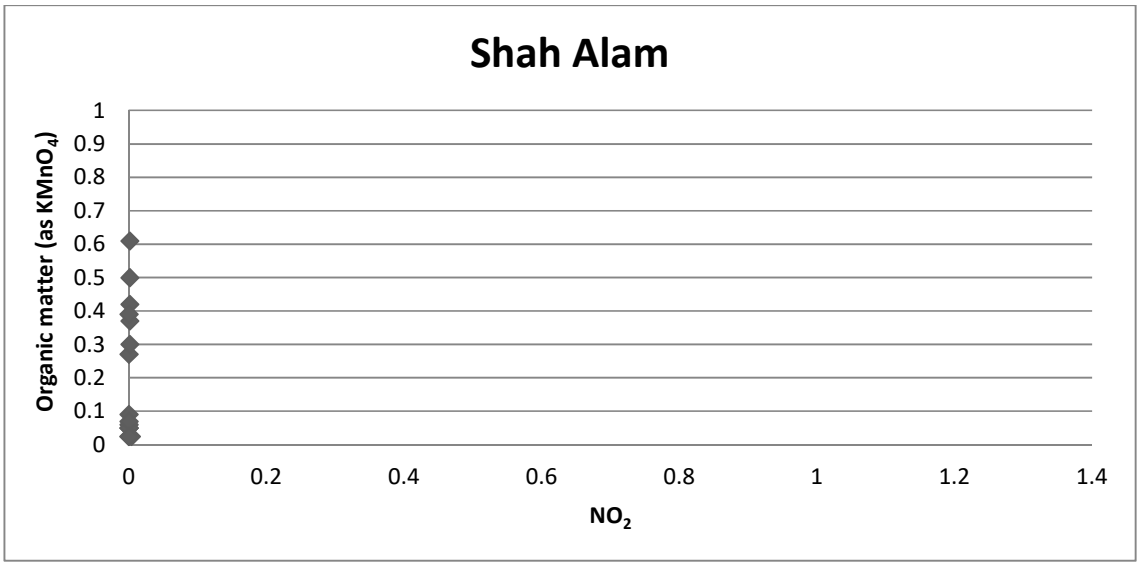

Figure 6.24 The organic matter in water samples (mg/l).

It can be concluded that the presence of NO_2 with NO_3 probably demonstrates that reduction can occur and the persistence of NO_3 in the presence of Fe suggests that locally the denitrification is reductant-limited. The presence of NO_3 suggests there is sewer leakage which possibly associated with combined sewer overflow during heavy storms as well as leakages.

6.4.6 Synthetic Organics

The sources of organic compounds can be naturally derived or anthropogenic (Boving 2005). Organic contaminants in urban aquifers vary depending on landuse activity; for example hydrocarbons (Clark & Kenrick 1986), chlorinated solvents (Rivett et al.1990), pharmaceutical compounds (Holm et al.1995, Barnes et al.2008) and other volatile organic compounds (Vroblesky et al.1996, Squillace et al. 1999). The organic compounds which are screened in water samples collected in study area are phenols, detergents, oil/grease and organic matter (permanganate). Phosphate, often organic-related, is also sometimes monitored.

Phenols occur in groundwater naturally normally at not more than 1µg/L (Thurman 1985). Phenols are linked with waste from industries and biocides e.g. pesticides and antimicrobial products (Domenico & Schwartz 1998) and also in septic waste (Rudel et al.1998). Phenols were detected (above the detection limit-0.002mg/L)) at Carlsberg Well 3 (0.006mg/L) and Well 4 in 1998 (0.001mg/L), and in Panasonic Compressor (0.001mg/L). The highest concentration of phenol was 0.01mg/L which was detected at Ueda Plating 1 in 2006.

There are three components of anionic detergent which are alkyl aryl sulfonates (AAS), linear alkyl aryl sulfonates (LAS) and sodium dodecyl sulphates (NaLS). LAS and NaLS are classified as soft detergents because they are more biodegradable than ABS (Thurman et al. 1986). It is unknown which type of detergent has been used in Shah Alam, or what the expected half-lives of detergents in this aquifer would be. Detergents in water samples of the study area are reported as methylene blue active substance (MBAS) except for three wells where anionic detergents were determined. Figure 6.25 shows the wells where detergent was detected Detergent was detected in 24 out of 39 wellwater samples which suggests that contamination from sewage discharges is very common. Concentrations range from 0.01 to

0.17ppm. Coughlin (1965) reports that in groundwater (deep wells) detergent concentrations are usually less than 0.1ppm and less than 0.5ppm in river waters; however, this work was undertaken nearly 50 years ago.

Phosphate in groundwater is possibly linked with sewage (Gschwend & Reynolds 1987). Figure 6.26 shows the relationship of P with Cl. There is no obvious relationship between P and Cl. The samples with higher values of P (>2mg/l) are AESBI, Ansell TW7 in 2011, Gaya Color Lab in 2008 and Canon Opto TW2 in 2010.

It can be concluded that the presence of synthetic organics indicates that the sources are from sewer leakage (also indicated by N data). The anthropogenic activity has affected groundwater concentrations widely, and that pathways from sewers / discharges are rapid and frequent (Figure 6.21).

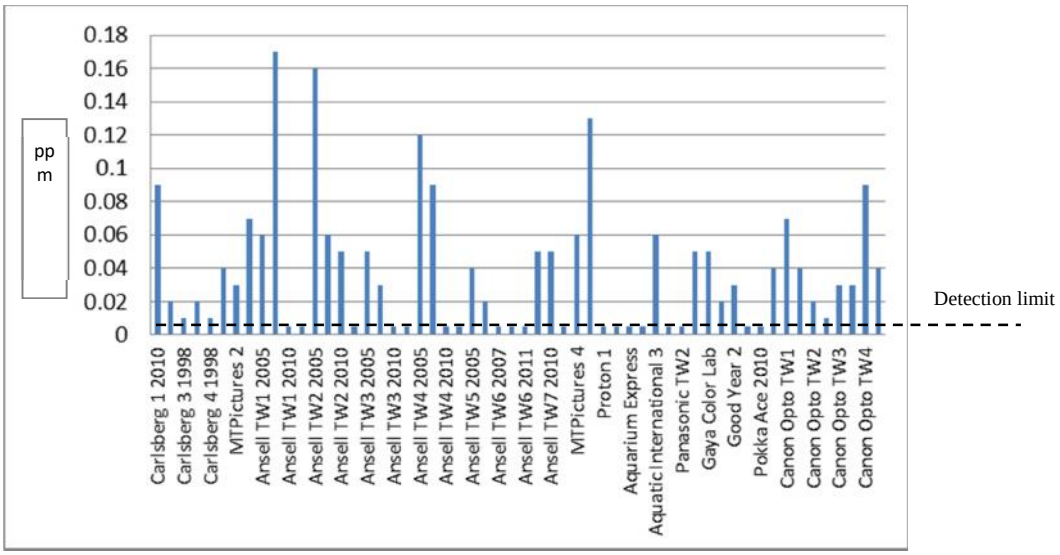

Figure 6.25. Detergent as MBAS in the wellwaters. The anionic detergent at three other wells are 0.05ppm (Proton 1 and 2 in 2006)) and 0.001ppm (Ueda Plating 1 also in 2006).

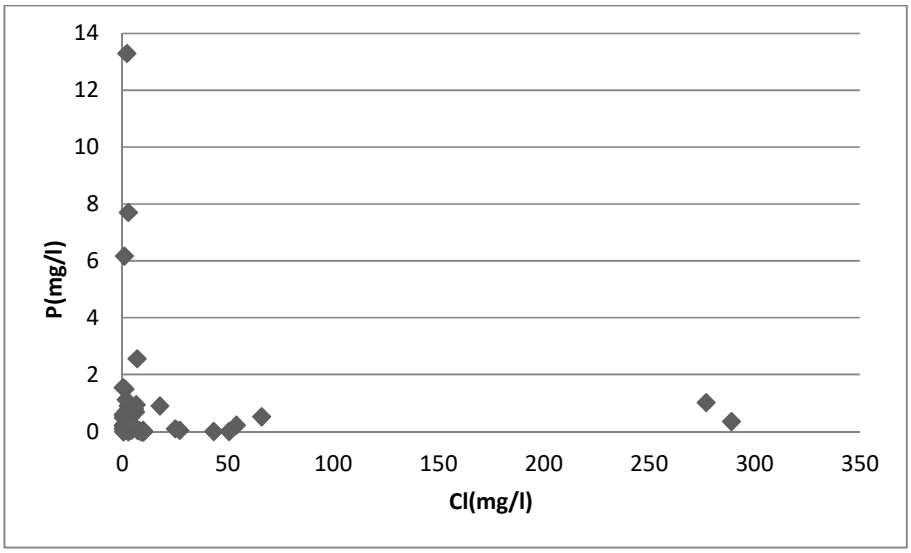

Figure 6.26. The relationship between P and Cl concentrations.

6.4.7 Bacteria

E.coli and coliform are 'markers' for sewer recharge (Barrett et al. 1999). Their occurrence in groundwater systems is due to leaking sewers (Lerner et al., 1994, Lerner 2002), which also can be indicated by high nitrate, ammonium and chloride concentrations (e.g. Whitehead et al.1999; Reynold et al., 2003), though these determinands can also come from many other sources (e.g. Ford & Tellam, 1994).

Table 6.12 shows the wells where either *E.coli* or coliforms have been detected along with concentrations of the other possible sewage pollution indicators. The analysis records viable bacteria. The bacteria were detected in wellwater samples only in 2005 and in 2007. The water sample at Ansell TW6 also shows a high nitrate concentration (> 10 mg/l). There was no coliform detected in Ansell wells in the following year. However, the nitrate concentration measured at Ansell TW2 and TW3 in 2010 was high which led to conclusion that the pollution had not completely flowed away but that the bacteria were no longer viable. These wells are in an interbedded sandstone-shale sequence. The main sewers in Shah Alam are

located along the main roads. Ansell and MT Pictures are located beside main roads, perhaps suggesting leakage from main sewers rather than from connections to buildings as is often the case. Many of sewers in Shah Alam are combined so high flows in main sewers may cause leakage.

Where leakage from sewers occurs, recharge will start from below ground surface unlike rainfall recharge where water infiltrates from the surface. It is possible that times from surface to aquifer may be significantly slower than from sewer to aquifer.

The presence of bacteria in groundwater can be without high concentration of Cl, NH_4, NO_3, or the other way around (Table 6.12), suggesting that there is no easy proxy for indicating sewer leakage. The signature of sewer pollution varies from condition to condition, and probably through time.

Table 6.12. The wells with E.coli and coliform (N.M-not measured; N.D-not detected; MPN – most probable number)

Tubewells	Year of measurement	Amount of E.coli (MPN/100ml)	Amount of coliform (org/100ml)	NO_3 (mg/l)	NH_4 (mg/l)	Cl (mg/l)
MT Pictures 1	2005	200	800	8.86	0.33	0.80
MT Pictures 2	2005	-	13	2.76	0.01	0.35
MT Pictures 3	2005	-	4	0.80	0.06	0.35
MT Pictures 4	2005	-	1	0.81	0.01	3.00
Ansell TW1	2005	13	50	2.00	0.48	1.10
Ansell TW2	2005	2	23	0.99	0.17	0.35
Ansell TW6	2007	14	220	38.50	0.13	0.60
Ansell TW2	2010	N.M	N.D	61.56	0.01	9.8
Ansell TW3	2010	N.M	N.D	43.05	0.01	27.2
Ansell TW5A	2010	N.M	96	8.19	0.35	17.8

6.4.8 Aluminium

There is no obvious relationship between Al^{3+} and Cl^- (Figure 6.27).The samples with higher values of Al^{3+} are all wells at CCM Fertilizer and Canon Opto TW2.

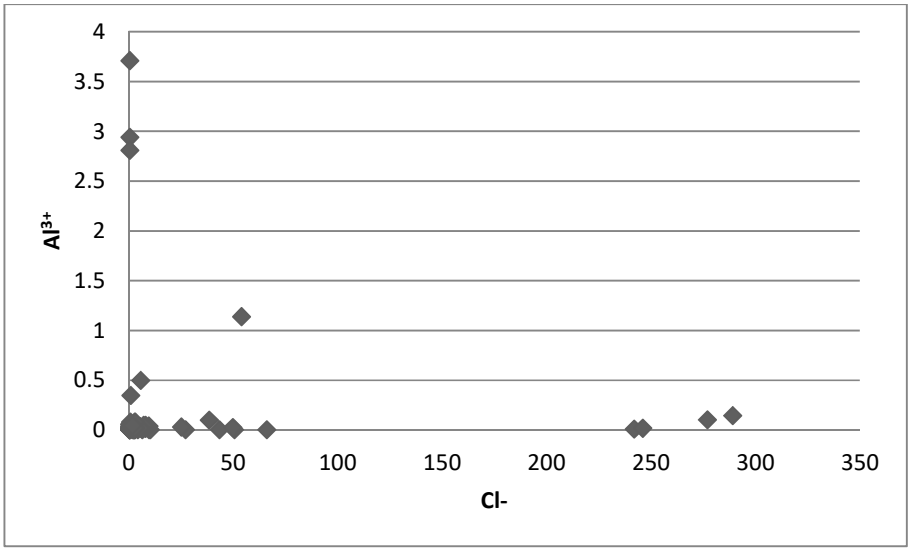

Figure 6.27. The wellwater samples have a low background of $Al^{3+}$and Cl^-.

Al mineral solubility is very low at middle pH values. pH needs to be <4.5 or >10 to get high Al concentrations. Figure 6.28 indicates that the highest concentrations of Al are for pH values ≤5. There are no samples with significant Al and turbidity, and therefore there is no evidence that Al is associated with the particulate phase.

There is no obvious relationship with Si either as shown in Figure 6.29, and this supports the non-particulate conclusion.

There is no obvious relationship with organic matter concentrations, so organic matter complexation is not important. Also there is no obvious relationship with F, a major ligand for ion pairs with Al.

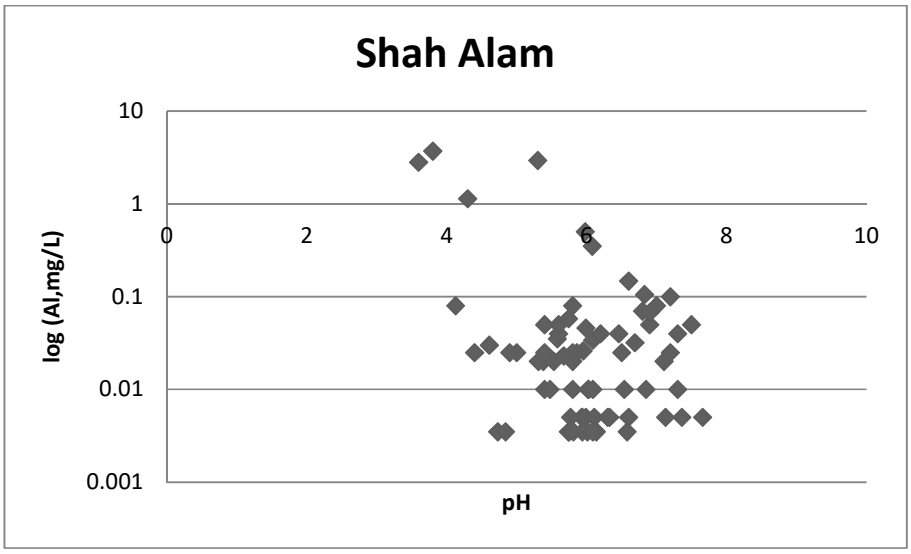

Figure 6.28 The relationship between Al and pH.

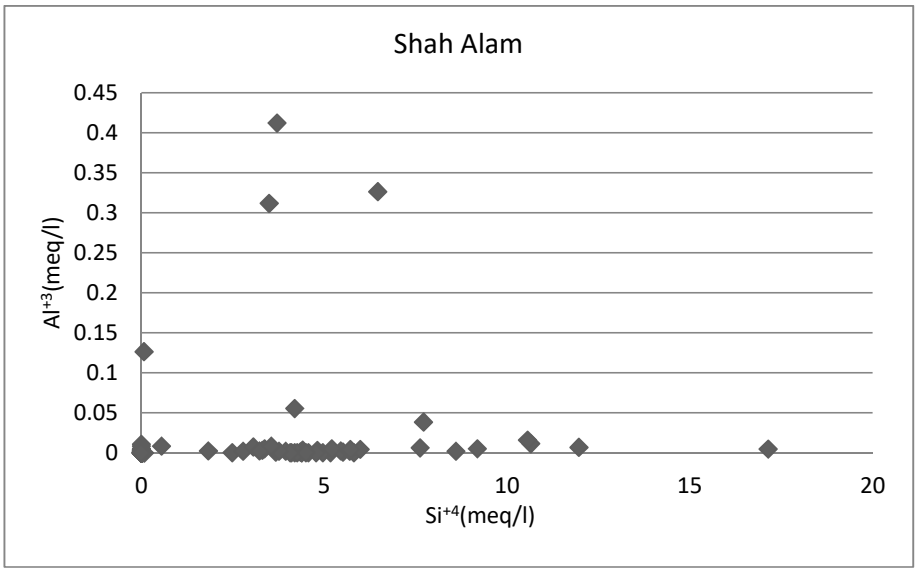

Figure 6.29. The relationship between Al^{3+} and Si^{4+}.

The three highest Al concentrations recorded (ppm range) are all from CCM Fertilizers in 2006, and high concentrations were not found here in 2004. So possibly the values represent analytical or unit error or alternatively the relatively low pH of these samples explains the concentrations.

6.4.9 Heavy Metals, Metalloids and CN and F

Trace metals in groundwater can be derived from natural sources, from weathering of the parent rock (Edmunds & Smedley,1996) or can be from landuse activity e.g. landfill (Adriano 1986, Misstear et al.2006) and atmospheric particles (Förstner& Wittmann 1981).Heavy metals concentration as measured in 5 sampling area/streets in Shah Alam by Norain et al. (2008) has shown that the presence of Fe (the highest), Zn, Pb, Cu, Ni, and Cd (the lowest).

The heavy metals which are detected in water samples in study area are Cd, Zn, Cu, Cr, Hg and Pb. Metalloids which have been detected in wellwater samples in study area are As and Se, and CN and F have also been detected. All samples have been analysed for all determinands except for fluoride which only been analyzed for some of the wells .The concentrations of each determinand are low in water samples (Zn < 1mg/L, Pb<0.01mg/L, Cd< 0.04mg/L, F<0.2mg/L),with a few samples exceed the limits as shown in Figure 6.30 to 6.34. Arsenic, cadmium, chromium, copper, mercury, selenium and silver are all below detection limit.

Metals and other trace elements were plotted against Cl to see if there is any relationship. There is no obvious relationship with Cl. There is also no obvious correlations between Fe and Mn with other metals as might have been expected if release of sorbed species following reductive dissolution was the main source of metals. There is no obvious relationship between Zn and Cu (Figure 6.34) or between Pb and Cd (Figure 6.35). However, the samples with high Cd and Pb are Ansell TW4 and Carlsberg 3 which belong to Water Type Types 2 and3. There is little obvious relationship with pH or organic matter (Figure 6.36).

Fe is the highest concentration metal found in soil especially in Kenny Hill Formation area (Khairiah et al. 2009) which is not surprising since it is common to find the iron coated on the surface of rocks of the Kenny Hill Formation (see Section 2.6.3).Often high Fe and Mn concentrations (see Figure 6.13) suggests that O_2 has been removed as Fe and Mn minerals have low solubility at all but moderate redox state, unless pH is very low.

Cyanide (CN) is observed in wellwater samples in Shah Alam. Figure 6.32 shows the relationship of CN with Cl. The samples with high CN are Canon Opto 4 and UEDA Plating 1. The presence of CN must be from industrial processes and this is very strong evidence for pollution either from industrial discharges or from sewers. CN is very reactive which means either the occurrence of CN was high or the pollution travels fast.

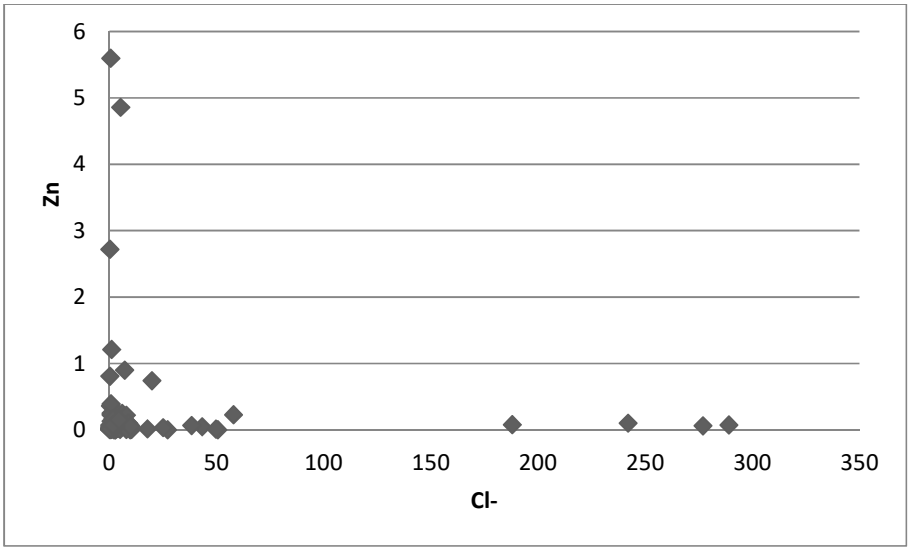

Figure 6.30. The wellwater samples have a low background of $Zn^{2+}$and Cl^{-}.

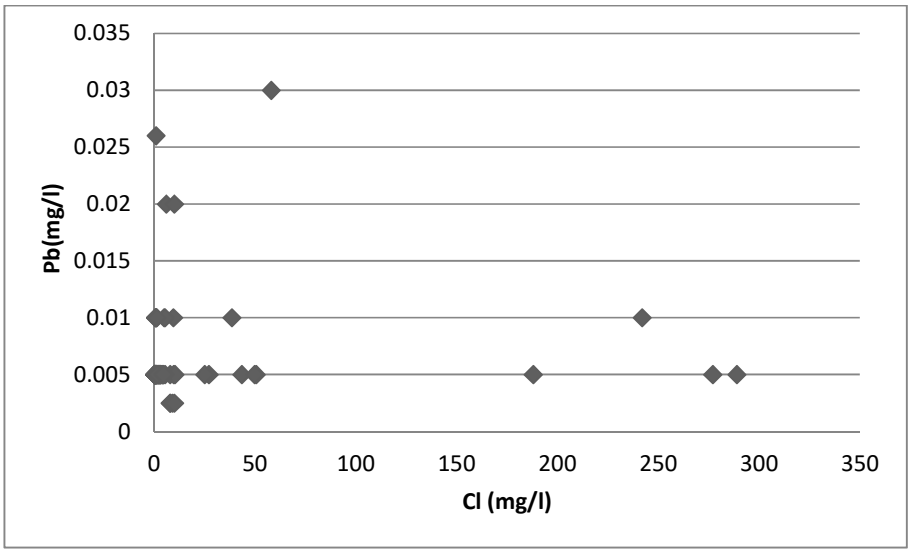

Figure 6.31. The wellwater samples have a low background of $Pb^{2+}$and Cl^{-}.

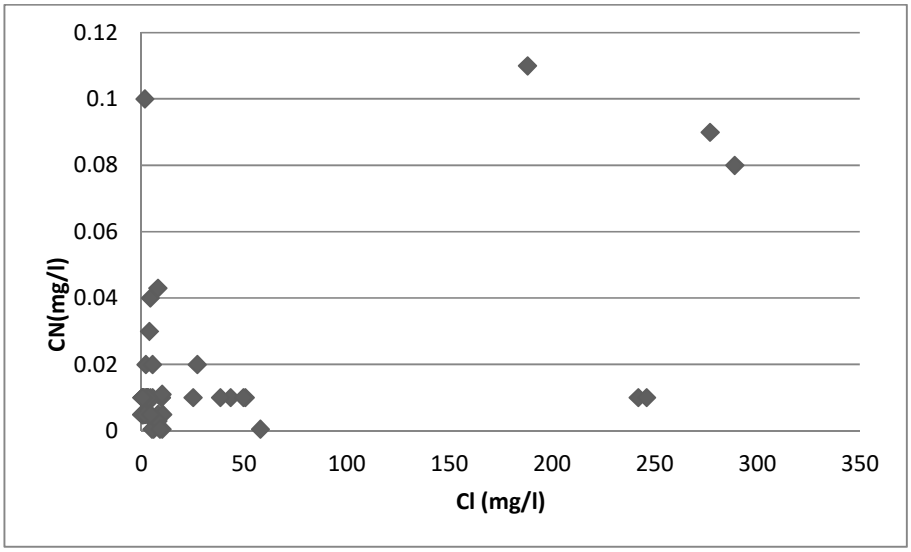

Figure 6.32. The wellwater samples have a low background of $CN^{-}$and Cl^{-}.

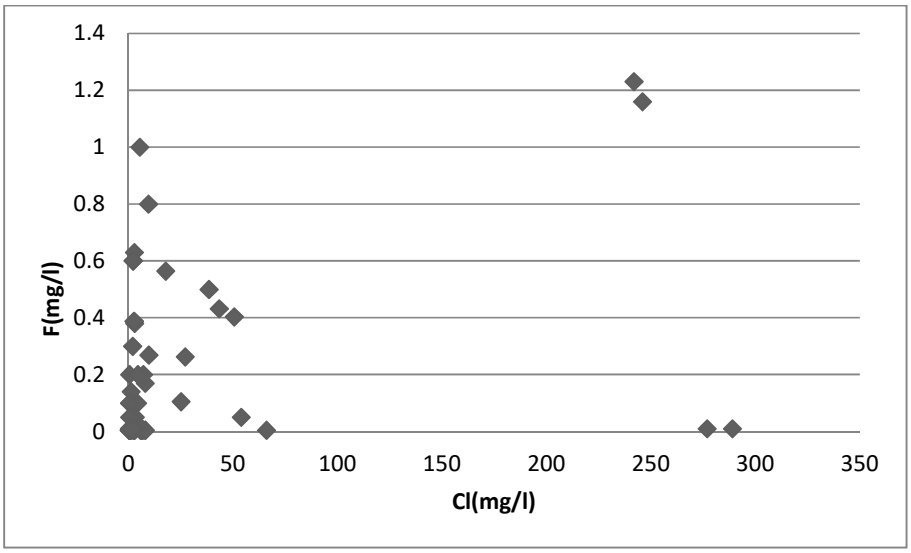

Figure 6.33. The wellwater samples have a low background of Cl^- and F^-.

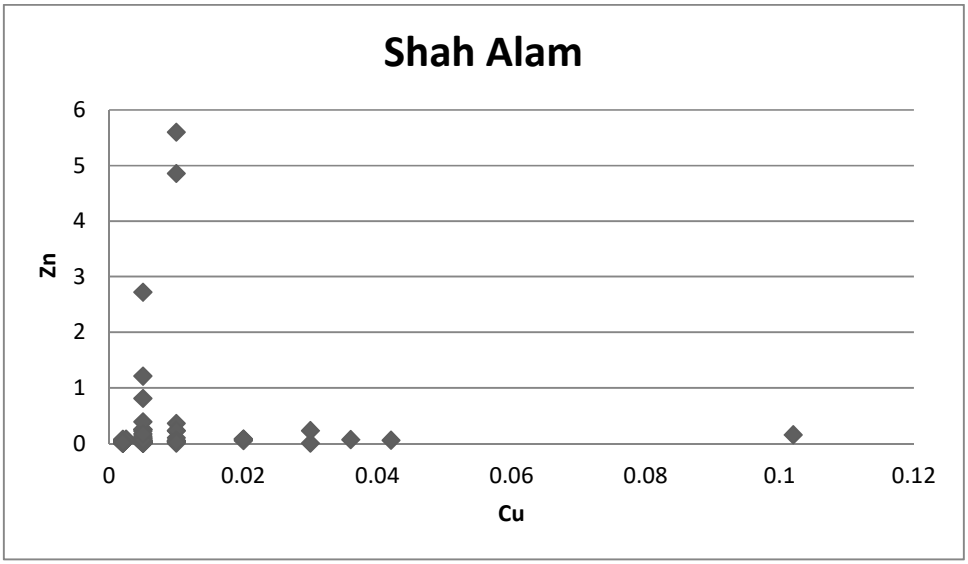

Figure 6.34 The relationship between Cu and Zn.

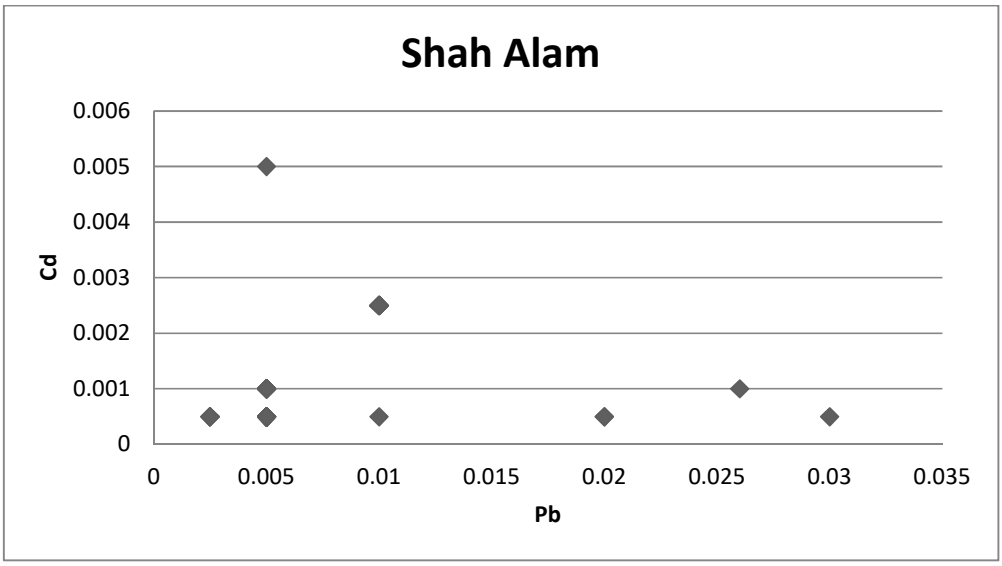

Figure 6.35. The relationship between Pb and Cd.

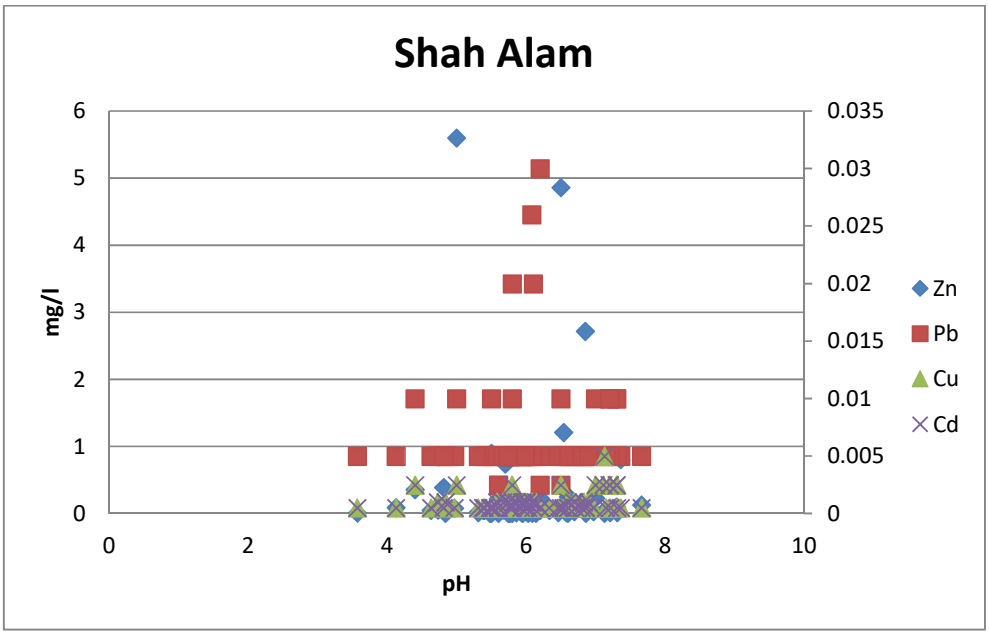

Figure 6.36. The relationship of heavy metals with pH (all but Zn on secondary axis).

In conclusion, even though concentrations are low, heavy metal and CN pollution can be seen to be occurring at various sites (e.g UEDA Plating 1).

Pollution is likely to be locally worse than it seems because of dilution in wells during pumping as found for example in Birmingham (Ford and Tellam, 1994; Tellam and Thomas, 2004). The natural attenuation of these pollutants cannot be determined in the absence of knowledge of source concentrations. However, it is certainly not complete attenuation. In some cases low pH could encourage mobility of cationic pollutants at least, both through less sorption to oxide surfaces and through less precipitation as hydroxides or carbonates. Ion exchange could also reduce mobility at least temporarily for cationic pollutants (e.g. Zn, Cu, Cd, Ni).

6.5 Discussion of Wellwater Chemistry Findings

From the wellwater chemistry analysis, there are significant findings which help to support or improve the hydrogeological conceptual model proposed in the previous chapter:

1. Most groundwaters have significant amounts of CO_2 (low pP_{CO2}) suggesting that the main source of recharge has passed through the soil zone. This suggests that 'direct recharge' is the dominant mechanism for recharge and that recharge from rivers and water pipes is limited. In addition, the wellwater Type 2 and Type 3 are from Class B and D (pumping test classification) which shows recharge response.
2. This also shows that the weathering zone must be significantly permeable.
3. The presence of bacteria, detergents, phosphate and NO_3 indicates that the sewage pollution occurs despite of the modern sewers.
4. Other pollution has come from industrial sites, including CN, and this may be through sewers or through surface disposal.
5. The travel times from sewer recharge to well is rapid (viable bacteria, CN).

6. The low TDS of the wellwaters, similar to the rainfall, show that the amount of ET during recharge is very small, suggesting large potential recharge rates with runoff being the main process limiting recharge.
7. Natural reactions are probably dominated by silicate weathering reactions.
8. There is almost certainly an O_2 sink, but the availability of reductants are limiting reactions (denitrification).
9. Ion exchange can occur, as might be expected from weathered profiles containing clays.
10. Contamination has occurred in the aquifer from industrial processes and hence is proved possible in relatively short time frames; the concentrations in general are low, though with a few 'hot spots' (e.g. for NO_3); there will be some dilution in wells during pumping, and this may obscure local contamination.
11. Little more can be deduced about natural attenuation. However, attenuation of metals and organics is not complete as they are seen in many samples. Low pH could encourage mobility in many cases.
12. The spatial distribution of water chemistry is largely dictated by pollution.
13. It is expected that the water quality away from the industrial areas will be much like the water quality in the least polluted industrial areas, i.e. like Water Type 1.

So in conclusion, the aquifer is susceptible to pollution. The weathering zone does not protect the groundwaters completely. Once in the aquifer, rapid flow occurs because of significant recharge and short flow path lengths and fractured, short response time nature of the aquifer, so there is not much time, for example, for decay or bacterial die-off. There is likely to be little natural attenuation capacity because of limited reductants, at least in the upper part of the aquifer, but there should be some ion exchange attenuation potential for metals.

7.0 SUMMARY, CONCLUSIONS AND RECOMMENDATIONS.

7.1 Introduction

The principal aim of the research undertaken was described in Chapter 1 is to develop a conceptual understanding of the hydrogeology of an urban metasedimentary hardrock aquifer in an equatorial climate and to use the understanding gained to determine the susceptibility of the aquifer to hydraulic and chemical impacts. This aim is achieved by using only information available from regulatory authorities and simple cheap additional observations (e.g. basic geological observations on outcrops and water level data logging of abstraction wells) as discussed in Chapter 2, 3, 4, 5 and 6. Therefore, in this chapter, the main finding of the research will be put together, the significance of this study will be discussed and the recommendations for future research will be made.

7.2 The Development of A Conceptual Understanding of The Hydrogeology Of An Urban Hardrock Aquifer In An Equatorial Climate by using Shah Alam as a study case.

Shah Alam in Peninsular Malaysia was chosen as the study area. Shah Alam is a newly urbanised area whose underlying geology is typical of much of Peninsular Malaysia. The greenschist facies sedimentary sequence is used by local industry for water abstraction, and as such data are available gathered by the well owners as part of the conditions for obtaining a licence. The data include geological borehole logs, water level measurements, pumping tests and water quality measurement. Again, these are typical of what is required elsewhere in Malaysia by the regulatory authorities.

Basic understanding of aquifer system is built first by producing a geological understanding. This has been done for the new city of Shah Alam in Peninsular Malaysia based on limited previous work and the geological logs supplied to the regulatory authorities by the well owners when they applied for licence to water abstract.

From the borehole logs, Shah Alam was found to be underlain by interbedded sandstone /quartzite with shale/phyllite which is overlain with a thick weathered layer. The hard-rock aquifer has usable permeability to depths of at least 100m with a weathered aquitard up to 80m thick overlying it but usually only 20-30m thick. The thickness of weathered layer in Shah Alam varies; thicker in interbedded sandstone and shale and thinner in sandstone. The material is clayey in shale area and silty sand in the sandstone-dominated area. The aquifer with a thick clay weathered layer is likely to allow less recharge and be less susceptible to pollution compared with aquifer with thinner, silty sand weathered layer. Most rock types whether fine or coarse grained are fractured and permeabilities across the region are not strongly lithology related. The permeability is possibly anisotropic and in places. Because of observed associated quartz veining for faulting in northwest-southeast, there are likely to be low permeability faults in these directions. Faults appear to have controlled the orientation of several of the major rivers and some of these faults may be of higher permeability being perpendicular to the regional direction of interpreted tension.

The main features of the system as indicated by the pumping tests is that there is plenty of water from weathered zone leakage and rivers with few obvious barriers. However, radii of influence in the short-term pumping tests are small and barriers may be common.

The aquifer properties determined suggest a low permeability aquifer with low storage coefficients. The aquifer has many water courses, and if these are in contact with the groundwater, representative flow paths for shallow flow may be as small as 250m, though perhaps closer to 10,000m for deeper flow. Taking some common values for T (10 m^2/d) and S (1 x 10^{-5}), an aquifer response time ($\alpha = Sx^2/T$) of 0.06 d for a representative distance of 250m and 100d. In both cases, this is a small response time comparable with UK Chalk (with S~10^{-4}, T~1000 m^2/d, x~10 km, α = 10d). The aquifer is therefore expected to be quite flashy when stressed, though under unstressed, 'Full' conditions it may appear less flashy.

As pumping occurs more recharge is expected to be released because of increase in heads across the weathering zone. Most recharge appears to have passed through the unsaturated zone as indicated by water CO_2 contents. The background water is of very low TDS suggesting little reaction and therefore probably little attenuation capacity. A significant proportion of the wellwaters are polluted with industrial contaminants and sewer leakage supporting the conclusion that little natural attenuation either through sorption or through oxidation or reduction. However, some ion exchange capacity is indicated by the wellwater chemistry and this may be due to the presence of kaolinite from the weathering profiles. The bacteria occurrence is suggesting from leaking sewers despite their newness and therefore expected good repair, and also that the aquifer does not filter out the bacteria. The existence of viable bacteria and also of the reactive CN is consistent with the rapid response times. The common occurrence of pollution suggests that the weathering zone is not a very good protection to the aquifer and is consistent with recharge getting through it. Pollution is likely to be severe locally as though most wellwaters are not heavily polluted wells are deep and there is a significant dilution potential.

Rainfall is high (about average 2200mm/y) and potential evapotranspiration is also high (about average 1060 mm/y) as is runoff; potential precipitation (not leakage) recharge is estimated at 100 to a few hundred mm/y but recharge will be controlled usually by the weathering zone.

7.3 Potential Susceptibility Of Shah Alam Urban Hardrock Aquifer To Hydraulic And Contaminant Stresses

The aquifer appears to be able to draw in recharge from the weathered zone and rivers when pumped and this means that it is relatively resilient though also dependent on surface sources with possibly limited storage capacity. Under unpumped conditions (e.g. if pumping were stopped for quality reasons) the aquifer will be close to full and added leakage from water supply or through 'sustainable urban drainage' would add to drainage problems, and discharges to sewers may be an important issue in the future.

The aquifer has little attenuation capacity (sorption, pH buffering capacity, filtering capacity especially) and thus pollutants are relatively mobile. Interestingly it appears that the groundwaters are often anoxic which may be useful for the attenuation of some pollutants (e.g. some synthetic organics and hexavalent Cr) and if the reductant is organic matter (carbonaceous shales) sorption of organics may be possible. However, the presence of waters with high Fe and NO_3 suggest that there are both anoxic and oxic zones in the aquifer and this needs more investigation: may be this relates to the presence of the carbonaceous shales. However, in general the frequency of occurrence of polluted wellwaters and the change in concentration with time is consistent with the model of a flashy system that is very susceptible to contamination. But it also means that the system may recover quickly from pollution though this needs to be confirmed.

7.4 Research approach and its limitations

The approach employed used only existing data with a minor amount of additional, specially collected data. The former consisted of: (i) a relatively small amount of existing published research, most dealing with regional scale geology, but some relating to very local issues; (ii) some data resulting from local engineering investigations; (iii) data collected by well owners specifically to satisfy Malaysian regulatory authority requirements. The latter consisted of monitoring of water levels in pumped wells and examination of rock outcrop. Importantly there were no observation borehole data.

The main problem of dealing with the data available was that there was an inadequate spatial and temporal coverage of a system. The wells were cited often in clusters at locations control by commercial factors. Boundaries of the aquifer were not identifiable and the relationship between surface waters and groundwaters was impossible to map out given the numerous streams and the close distances between them and few boreholes. The geology is so heterogeneous at the small scale but some similar at the large scale, and so affected by potentially complex structures that it could not be mapped by a small number of clustered observation points. As a result, there is no possibility of producing an accurate geological map or even a reliable water level map. Reliance therefore has to be placed on point observations and generalities that can be drawn from them.

On the positive side, a great deal of general information has been obtained about the aquifer and processes occurring in it, as summarised above. On the negative side there can be little said confidently about the distributions of aquifer properties, the flow directions, the locations of internal or outside boundaries of the aquifer, or the distributions of water quality. If the

aquifer can be regarded as many localised sections isolated from the next pumping compound, then the information obtained is probably quite reliable and useful for management. We could know therefore that there is a leaky system, connected to any nearby large river, with flow to perhaps at least 100 m, with recharge and quick groundwater flow, with little attenuation or protection capacity. These features could be the basis of a qualitative management policy.

This case where all wells or well clusters are isolated might be the case in current Shah Alam as indicated in Figure 1.2 (represents Morris et al (1997) model). But as the aquifer becomes more develop, further along the progression of Morris model, then the system may act more as a whole and regional flows may become separate from local surface water systems and some better representation of flow may be needed that takes spatial issues into account. In this case management questions need the whole flow system understanding.

7.5 Research contribution and its wider implications.

As explained in Chapter 1, this study has been of a type of aquifer rarely investigated: a sequence of sediments metamorphosed to greenschist facies and significantly deformed. For example, in his international review of hydraulic conductivity available in hard rock areas, Sam (2014) cites only two studies involving low grade regional metamorphosed sedimentary rocks, and one of these was investigated only using slug tests and the other was a quarry site, and neither in an equatorial climate. No hydrogeological studies of comparable scale as attempted here have been found on similar rocks types in urban areas.

Low grade metasediments however, are found in many parts of the world. For example, they found in much of the Malaysian Peninsula, in North America (e.g. the Rocky, Cascade and

Appalachian mountains regions) and in Europe (e.g. southwestern England, Wales, southern Scotland, parts of the Alps). Though it is not possible to extend the findings with any certainty to other locations internationally, especially in other climate and tectonic zones, without further evidence, the Shah Alam area appears to be typical geologically of much of the Malaysian Peninsula (Figure 2.19) and neighbouring regions. Though we cannot say this aquifer works in same way as other metasedimentary equatorial urban aquifers, there is no reason to think that this system is particular special.

7.6 Recommendations for future research

An important feature of the system studied is the role of the weathered zone. In the Malaysian context, much more could be learnt about the hydraulic behaviour of the weathered zone through longer scale pumping of wells in the fractured rock, ideally with observation borehole data, to obtain conductances for the leaky layer. This would be ideally undertaken with observation wells in the weathered layer itself. In Universiti Kebangsaan Malaysia, there are seven wells in the weathered layer (also in Kenny Hill Formation) which can be used for this purpose, if a deeper well were drilled. These 7 wells could also be used to undertake pumping tests within the weathered layer.

The question of whether the weathering layer properties are dependent on climate and hydrogeology is important in terms of extrapolation of results to other systems, and comparative studies of the weathering regime could help determine this.

If the water chemistry of the deep wells is to be understood, more evidence of the water chemistry in the weathered layer should be obtained and interpreted. This could be done along with study of the weathering processes. The study should include looking at natural

determinands, especially carbonate system, possibly using isotopes, as this can indicate processes in the unsaturated zone relevant to recharge. It also should look at pollutants, e.g. nitrate, to determine potential attenuation properties.

As country in equatorial climate region (with >2500mm of rainfall), further research on relationship of rainfall with groundwater level is needed. It is also crucial to carry out study on recharge processes starting at smaller scale (at selected industrial compound) and then regional scale (Klang river basin).

Since rivers in study area are fault controlled, and with most of pumping wells near to rivers, further data collection (such as well and river water level and quality) is required for further understanding the groundwater and river relationship. Besides that, the data also can be used to further develop the ideas on aquifer compartmentalization. In both of these cases, observation well data are needed and pumping tests need to be carried out for significantly longer than the current regulations required. Observation wells during pumping tests would allow investigation of anisotropy. If piezometers were possible, a much more detailed insight into the flow to wells in the environment could be obtained. If neither observation wells and piezometers were too expensive to have then monitoring of pumping wells would be potentially very useful particularly if all wells in a compound were monitored. The Class D wells in particular need investigating with more numerical modelling and longer pumping tests as their responses indicate that there may be connections with lineaments that in turn connect to rivers. This is potentially fast pathways for pollutants.

Bacteria are found in some wells suggesting very rapid pathways exist despite the presence of the weathered zone. This could be because in part the lineaments (see previous paragraph).

To investigate this further there could be a study on emerging contaminants like personal care products to determine if these might indicate water sources and residence times.

7.7 Recommendations for local authority to improve the quality of pumping test data

By analysing the data obtained from the regulatory, there a few recommendations for further improvements of current practice in Malaysia to improve the quality of pumping test data for future research. Since a large percentage of pumping wells in Shah Alam have shown hydrogeological boundaries effects, the duration of pumping test must be designed accordingly to the nature of the well (e.g. geology, well interference). Longer tests would enable boundaries and recharge effects to be determined with greater confidence. The period of recovery analysis must be longer which depends again on the nature of the well. The current standard practice in Malaysia is the aquifer must be recovered at least 80%, but it would be much better if this was increased.

The step drawdown analysis is very useful for understanding the aquifer behaviour. Therefore it must be compulsory to be carried out before constant yield test. It also must be carried out accordingly to the nature of the well.

One of the boundary effects is well interference. Most of the factories have more than one pumping wells such as at Ansell, Carlsberg, MT Pictures, PROTON and Panasonic. For example, Ansell has 8 pumping wells. The wells are located within 200 m of each other. Therefore, in the future, the interference effects of pumping wells nearby should be calculated, and all boreholes monitored during tests.

For aquifer protection, since the sewer leakage seems very common, regular inspection on the underground pipes should be done. In addition, controls on spills and discharges should be made much tighter. The safety measures like double lined and monitored tanks, bunds, liners can be installed and a tighter control over sewers or making them separate may be appropriate. The system may be close to full in the absence of pumping, therefore it may need tight controls on piped water leakage and do avoid ‘sustainable urban drainage’ as normally designed.

Besides that, the following also can be done by the regulatory authorities before the system becomes more pumped:

1. More observation wells be installed especially in urban area and monitored for water level and EC using transducer-logger systems with at least daily recoding;
2. water level and abstraction records are kept for all wells on at least a monthly basis;
3. a scheme of analysing the data collected on a yearly basis be implemented also to update the hydrogeological understanding of the system;
4. standardised geological terminology is instigated for well drillers;
5. implement standardised reporting and storage of all site investigation civil engineering data;
6. well abstraction licences be periodically reviewed based on the records examined;
7. water quality sampling on an annual basis for a set of standard determinands that is consistent across all sites together with additional species specific to the local site.

REFERENCES

Abdelatif, M.A, & Sulaiman, Wan Norazmin,S. (2001). Evaluation of groundwater and soil pollution in a landfill area using electrical resistivity imaging survey. *Environmental management, 28*(5), 655-663.

Abdul Rahim,S., Haryono, A., Umar,H., & Abdul Ghani,R. (2008). Salinity mapping of coastal groundwater aquifers using hydrogeochemical and geophysical methods: a case study from north Kelantan, Malaysia. *Environmental Geology*, *55*(8), 1737-1743.

Abdullah, A.M.K. (1982). Rural-urban migration and urbanization in Bangladesh. *Geographical Review*, 379-394.

Abdullah Sani, Hashim. (1985). Discovery of an ammonite in the Kenny Hill Formation and its significance. *Warta Geologi, 11*, 205-211.

Abustan, I., Sulaiman,A.H.,Wahid,N.A. (2008). *Urban rainfall-runoff study to validate the design chart in the Malaysian Urban Stormwater Management Manual (MSMA).* Paper presented at the 11th International Conference on Urban Drainage Edinburgh, Scotland, UK.

Acworth, R. I. (1987). The development of crystalline basement aquifers in a tropical environment. *Quarterly Journal of Engineering Geology and Hydrogeology*, *20*(4), 265-272.

Adams, B., & Foster, S. S. D. (1992). Land-Surface Zoning for Groundwater Protection. *Water and Environment Journal*, *6*(4), 312-319.

Adriano, D. C. (1986) Trace elements in the terrestrial environment. Springer Verlag New York.

Ahmad, A. R., Zulkefli, M., Ahmed, M., Aminuddin, B. Y., Sharma, M. L., & Mohd Zain, M. (1996). Environmental impact of agricultural inorganic pollution on groundwater resources of the Kelantan Plain, Malaysia. In *ACIAR proceedings* (pp. 8-21). Australian Centre for International Agricultural Research.

Ahmad Fariz,M.,Wan Zuhairi,W.Y., Mohd Raihan,T., & Abdul Rahim, S. (2009).Groundwater and soil vulnerability in the Langat Basin Malaysia. *European Journal of Scientific Research* 27, no. 4, 628-635.

Ahmed, K. M., Hasan, M. K., Burgess, W. G., Dottridge, J., Ravenscroft, P., & van Wonderen, J. (1999). The Dupi Tila aquifer of Dhaka, Bangladesh: hydraulic and hydrochemical response to intensive exploitation. In Chilton (Ed.), *Groundwater in the urban environment: Selected city profiles* (pp 19-30).Netherland: Balkema.

Aini, M. S., Fakhru'l-Razi, A., & Siew Suan, K. (2001). Water crisis management: satisfaction level, effect and coping of the consumers. *Water resources management*, *15*(1), 31-39

Alexander, J.B. (Cartographer). (1956). Geological map of Genting Sempah area, Kuala Lumpur.

Allen, R.G., Pereira,L.S.,Raes,D. & Smith,M. (1998). *Crop evapotranspiration; guidelines for computing crop water requirements*.

Anderson, M.P.&Eisen, C.(1979).The Effects of Urbanization on Ground-Water Quality - a Case Study. *Ground Water* 17 (5) .

Anderson, M.P.&Woessner, W.M. (1992). *Applied groundwater modeling: Simulation of flow and advective transport*: Academic Press.

Anonymous (2014,December 20).Syabas: Water disruption in Klang Valley for upgrading works on Tuesday.The Star. Retrieved from http://www.thestar.com.my/News/Nation/2014/12/20/water-supply-disruption-klang-valley/

Anonymous (2015,March 10). Syabas: Parts of Klang Valley to experience water supply disruption March 16.The Star. Retrieved from ***http://www.thestar.com.my/News/Nation/2015/03/10/water-disruption-klang-vly-Mar-16/***

Appelo, C.A.J. & Postma, D.(2005). *Geochemistry, Groundwater and Pollution*. 2nd edition ed.: CRC Press.

Archie, G.E. (1950). Introduction to petrophysics of reservoir rocks. *bulletin of The American Association of Petroleum Geologists, 34*(5).

Ayraud, V., Aquilina,L.,Labasque,T.,Pauwels,H.,Molenat,J.,Pierson-Wickmann, A.,Durand,V.,Bour,O.Tarits,C.,Le Corre,P.,Fourre,E.,Merot,P & Davy,P. (2008). Compartmentalization of physical and chemical properties in hard-rock aquifers deduced from chemical and groundwater age analyses. *Applied Geochemistry, 23*, 2686-2707.

Aydin, A. (2000). Fractures, faults and hydrocarbon entrapment, migration and flow. *Marine and Petroleum Geology, 17*, 797-814.

Bahaa-eldin, E.A.R., Ismail, Y., Abdul Rahim, S., Wan Zuhairi,W. Y., & Abdul Ghani, M. R. (2010).Deterioration of groundwater quality in the vicinity of an active open-tipping site in West Malaysia. *Hydrogeology journal* 18, no. 4 , 997-1006.

Banks, D., Solbjorg,M.L. & Rohr-Torp,E. (1992). Permeability of fracture zones in a Precambrian granite. *Quarterly Journal of Engineering Geology and Hydrogeology, 25*.

Barker, J. (1988). A generalized radial flow model for hydraulic tests in fractured rock. *Water Resources Research, 24*(10), 1796-1804.

Barker, J. A., & Herbert, R. (1982). Pumping tests in patchy aquifers. *Groundwater, 20*(2), 150-155.

Barnes, K. K., Kolpin, D. W., Furlong, E. T., Zaugg, S. D., Meyer, M. T., & Barber, L. B. (2008). A national reconnaissance of pharmaceuticals and other organic wastewater

Barrett, M.H., Hiscock,K.M., Pedley,S.,Lerner,D.N.,Tellam,J.H. and French,M.J.(1999).Marker Species for Identifying Urban Groundwater Recharge Sources: A Review and Case Study in Nottingham,Uk. *Water Research* 33 (14).

Bense, V.F. & Balen, R.V. (2004). The effect of fault relay and clay smearing on groundwater flow patterns in the Lower Rhine Embayment. *Basin Research, 16*.

Bernama (2014a, June 20). Water disruption hits 17,500 consumers in Klang Valley.*The Rakyat Post*.Retrieved from http://www.therakyatpost.com/news/2014/06/20/water-disruption-hits-17500-consumers-klang-valley/

Bernama (2014b, June 29).Seven areas in Klang/Shah Alam still experiencing water supply disruptions. *Astro Awani.*Retrieved from http://english.astroawani.com/malaysia-news/seven-areas-klang-shah-alam-still-experiencing-water-supply-disruptions-38709

Bernama (2014c, July 5). Water supply disruption in Klang Valley tonight.*New Straits Time Online*.Retrieved from http://dev.nst.com.my/news/water-supply-disruption-klang-valley-tonight

Bernama (2015a, July 14).Syabas: Water disruption in Klang Valley on July 28-29. *Astro Awani*.Retrieved from http://english.astroawani.com/malaysia-news/syabas-water-disruption-klang-valley-july-28-29-65886

Bernama (2015b, September 29). 30 areas in Klang,Shah Alam, Petaling experiencing water disruption – Syabas.*Astro Awani*.Retrieved from http://english.astroawani.com/malaysia-news/30-areas-klang-shah-alam-petaling-experiencing-water-disruption-syabas-74813

Bijay- Singh, Yadvinder-Singh & Sekhon, G. S. (1995). Fertilizer-N use efficiency and nitrate pollution of groundwater in developing countries. *Journal of Contaminant Hydrology*, *20*(3), 167-184.

Black, J. H. (1987). Flow and flow mechanisms in crystalline rock. *Geological Society, London, Special Publications*, *34*(1), 185-200.

Bottrell, S., Tellam, J., Bartlett, R., & Hughes, A. (2008). Isotopic composition of sulfate as a tracer of natural and anthropogenic influences on groundwater geochemistry in an urban sandstone aquifer, Birmingham, UK. *Applied Geochemistry*, *23*(8), 2382-2394.

Boving, T. B.(2005). Organic Compounds in Groundwater. *Water Encyclopedia*.

Brace, W.F. (1980). Permeability of crystalline and argillaceous rocks. *Int. J.Rock Mech.Min.Sci & Geomech.Abstr, 17*, 241-251.

Bujang, B.K. H., Faisal,A., Low, T.H.& Saravanan,M. (2005). Infiltration characteristics of unsaturated residual soils of various weathering grades. *Jurnal Teknologi, 42*(B), 45-46.

Burston, M. W., Nazari, M. M., Bishop, P. K., & Lerner, D. N. (1993). Pollution of groundwater in the Coventry region (UK) by chlorinated hydrocarbon solvents. *Journal of Hydrology*, *149*(1), 137-161.

Burton, C.K. (1973). Mesozoic. In C. S. H. D.J.Gobbett (Ed.), *Geology of the Malay Peninsula (West Malaysia and Singapore)* (pp. 97-141). New York: Wiley-Interscience.

Butler, D., Davies,J.W. (2000). *Urban Drainage*. London: Spon Press.

Caine, J.S., Evans,J.P. & Forster,C.B. (1996). Fault zone architechure and permeability structure. *Geology, 24*, 1025-1028.

Clark, L. (1977). The analysis and planning of step drawdown tests. *Quarterly Journal of Engineering Geology 10*, 125-143.

Clark, L. (1985). Groundwater abstraction from Basement Complex areas of Africa. *Quarterly Journal of Engineering Geology, 18*, 25-34.

Clark, L., & Kenrick, M. A. P. (1986). Trace organic compounds in groundwater: a survey of unpolluted groundwater from three major British aquifer systems. *Geological Society, London, Engineering Geology Special Publications*, *3*(1), 159-167.

Chen, B., Mustafa, K.S. & Khoo,T.T. (2002). Dating the Kenny Hill Formation:spores to the fore. *Warta Geologi, 28*(5), 189 - 191.

Cherry, J.A. (1983). *Piezometers and other permanently-installed devices for groundwater quality monitoring.* Paper presented at the Proceeding Conference on groundwater and petroleum.

Chilton, J. (Ed.). (1999). *Groundwater in the Urban Environment: Selected city profiles*.

Choy, K.W. (1970). *Geology of the western Kuala Lumpur area, West Malaysia.* (B.Sc.Honours), University of Malaya.

Chu, L.H.(2004).Groundwater Utilisation and Management in Malaysia." Paper presented at the 41st CCOP Annual Session, Tsukuba, Japan.

Church, P. and Granato, G. (1996).Bias in Ground-Water Data Caused by Well-Bore Flow in Long-Screen Wells. *Ground Water*, 34(2), 262-273

Clausen, J.A.&Gabrielsen, R.H. (2002). Parameters that control the development of clay smear at low stress:an experimental study using ring-shear apparatus. *Journal of Structural Geology, 24*, 1569-1586.

Coughlin, F.J. (1965). Detergents and Water Pollution Abatement. *American Journal of Public Health and the Nations Health, 55*(5), 760-771.

Courtois, N., Lachassagne, P., Wyns, R., Blanchin, R., Bougaïré, F. D., Somé, S., & Tapsoba, A. (2010). Large-Scale Mapping of Hard-Rock Aquifer Properties Applied to Burkina Faso. *Groundwater*, *48*(2), 269-283.

Cronin, A., Pedley, S., Hoadley, A., Haldin, L., Gibson, J., & Breslin, N. (2007). Urbanisation effects on groundwater chemical quality: findings focusing on the nitrate problem from 2 African cities reliant on on-site sanitation. *Journal of water and health*, *5*(3), 441-454.

Dale, W.L. (1960). The rainfall of Malaya,Part II. *Journal of Tropical Geography, 14*, 11-28.

Davis, S. N. (1969). Porosity and permeability of natural materials. *Flow through porous media*, 53-89.

Department, Mineral & Geosciences (1985). Geological Map of Peninsular Malaysia.

Dewandel, B., Lachassagne, P., Wyns, R., Maréchal, J.C. and Krishnamurthy, N.S., 2006. A generalized 3-D geological and hydrogeological conceptual model of granite aquifers controlled by single or multiphase weathering. *Journal of hydrology*, *330*(1), pp.260-284.

De Vries, J.J. & Simmers, I. (2002). Groundwater recharge:an overview of processes and challenges. *Hydrogeology Journal*, *10*, 5-17.

Director General, Geological Survey Malaysia (1976). Sheet 94- Kuala Lumpur.

Director of National Mapping Malaysia (1966). Sheet 93- Port Swettenhem&Kelang.

Director of National Mapping Malaysia(1970). Sheet 94- Kuala Lumpur.

DOE (2008). Department of Environment Malaysia, Ministry of Science, Technology and The Environment. http://www.doe.gov.my/en/content/river-water-quality-monitoring

DOE (2008). Department of Environment Malaysia, Ministry of Science, Technology and The Environment. http://www.doe.gov.my/en/content/groundwater-quality-monitoring

Dominico, P.A. & Schwartz, F.W. (1998).*Physical and Chemical Hydrogeology*. second edition ed.: John Wiley & Sons, Inc.

Driscoll, F.G. (1986). *Groundwater and wells*: Johnson Division.

Eaton, T.T., Anderson,M.P. & Bradbury,K.R. (2007). Fracture control of ground water flow and water chemistry in rock aquitard. *Ground Water, 45*(5).

Edmunds, W. M., & Smedley, P. L. (1996). Groundwater geochemistry and health: an overview. *Geological Society, London, Special Publications*, *113*(1), 91-105.

Eiswirth, M., & Hötzl, H. (1997). The impact of leaking sewers on urban groundwater. *Groundwater in the urban environment, 1*, 399-404.

Evans, J.P., Forster,C.B. &Goddard,J.V. (1997). Permeability of fault-related rocks, and implications for hydraulic structure of fault zones. *Journal of Structural Geology, 19*(11).

Ezdiani, S.F. (2005). *Sifat fiziko-kimia dan mineralogi lempung tanah baki di sekitar Bandaraya Shah Alam, Selangor Darul Ehsan.* (BSc.), Universiti Kebangsaan Malaysia, Bangi.

Faridah, O., Alaa Eldin, M.E., & Ibrahim, M. (2012).Trend analysis of a tropical urban river water quality in Malaysia. *Journal of Environmental Monitoring* 14 (12), 3164-3173.

Fauziah,M.N., Idrus A.S., Hani, M. H., & Wan Rohaila, W. A.(2014).Status of Groundwater Contamination in Rural Area, Kelantan. *Journal of Environmental Science, Toxicology and Food Technology, 8(1), 72-80*

Fauzie, M. J., Azwan, M. M. Z., Hasfalina, C. M., & Mohammed, T. A. (2014). Performance Evaluation and Characteristics of Selected Tube Wells in the Coastal Alluvium Aquifer, Selangor. *Pertanika Journal of Science & Technology*, *22*(1).

Fisher, Q. J., & Knipe, R. (1998). Fault sealing processes in siliciclastic sediments. *Geological Society, London, Special Publications*, *147*(1), 117-134.

Fisher, Q. J., & Knipe, R. J. (2001). The permeability of faults within siliciclastic petroleum reservoirs of the North Sea and Norwegian Continental Shelf. *Marine and Petroleum Geology*, *18*(10), 1063-1081.

Flipse, W. J., Katz, B. G., Lindner, J. B., & Markel, R. (1984). Sources of nitrate in ground water in a sewered housing development, Central Long Island, New York. *Groundwater*, *22*(4), 418-426.

Ford, M., & Tellam, J. H. (1994). Source, type and extent of inorganic contamination within the Birmingham urban aquifer system, UK. *Journal of Hydrology*, *156*(1), 101-135.

Ford, M., Tellam, J. H., & Hughes, M. (1992). Pollution-related acidification in the urban aquifer, Birmingham, UK. *Journal of Hydrology*, *140*(1), 297-312.

Förstner, U., & Wittmann, G. T. (1981). *Metal pollution in the aquatic environment*. Springer Science & Business Media.

Foster, S.S.D. (1988). *Impacts of urbanization on groundwater.* Paper presented at the Proceedings of the Duisberg Symposium.

Foster, S.S.D., Morris,B.L. & Lawrence,A.R. (1994). Effects of urbanization on groundwater recharge *Groundwater problems in urban areas*.

Foster, S.S., 1998. Groundwater recharge and pollution vulnerability of British aquifers: a critical overview. *Geological Society, London, Special Publications*, *130*(1), pp.7-22.

Foster, S.S.D., Morris,B.L. & Chilton,P.J. (1999). *Groundwater in urban development-a review of linkages and concerns.* Paper presented at the Proceedings of IUGG 99 Symposium HS5, Birmingham.

Foster, S. S. D., & Chilton, P. J. (2004). Downstream of downtown: urban wastewater as groundwater recharge. *Hydrogeology Journal*, *12*(1), 115-120.

Foster, S. D., Hirata, R., & Howard, K. W. (2011). Groundwater use in developing cities: policy issues arising from current trends. *Hydrogeology journal*, *19*(2), 271-274.

Fretwell, B., Burgess, W. and Barker, J., 2000. Contaminant retardation within the seasonally unsaturated zone of the Chalk aquifer: the SUZ process. *IAHS Publication (International Association of Hydrological Sciences)*, (262), pp.385-390.

Gale, J.E. (1982). Assessing the permeability characteristics of fractured rock. *Geological Society of America Special Paper, 189*.

Gill, C. E., Shepherd, M., & Millington, J. J. (2010). Compartmentalization of the Nelson field, Central North Sea: evidence from produced water chemistry analysis. *Geological Society, London, Special Publications*, *347*(1), 71-87.

Gobbett, D.J. (1973). Introduction. In C. S. H. D.J.Gobbett (Ed.), *Geology of the Malay Peninsula (West Malaysia and Singapore)* (pp. 1-12). New York: Wiley-Interscience.

Gobbett ,D.J. & Tjia,H.D. (1973). Tectonic history. In C. S. H. D.J.Gobbett (Ed.), *Geology of the Malay Peninsula (West Malaysia and Singapore)* (pp. 305 - 334). New York: Wiley-Interscience.

Goodman, Richard E. (1989). *Introduction to Rock Mechanics* (second edition ed.): John Wiley & Sons.

Greenbaum, D. (1992). Structural influences on the occurence of groundwater in SE Zimbabwe. *Geological Society Special Publication, 66*.

Grindley, J. (1967). Estimation of soil moisture deficits. *Meteorological Magazine*, *96*(1137), 97.

.

Grindley, J. (1969). *The calculation of actual evaporation and soil moisture deficit over specified catchment areas*. Meteorological Office, Hydrological Services.

Gschwend, P. M., & Reynolds, M. D. (1987). Monodisperse ferrous phosphate colloids in an anoxic groundwater plume. *Journal of Contaminant Hydrology*, *1*(3), 309-327.

Halford, K.J., Weight,W.D. & Schreiber,R.P. (2006). Interpretation of transmissivity estimates from single-well pumping aquifer tests. *Ground Water, 44*(3), 467-471.

Hamzah Mohamad, Mohd Faizal Abdullah, Rashidah Abd. Karim, Mohd. Johari Yaakob. (1986). Perbandingan fasies metamorf Formasi Bukit Kenny dan Skis Dinding. *Sains Malaysiana, 15*(1), 13 - 24.

Hantush, M. S. (1956). Analysis of data from pumping tests in leaky aquifers. *Eos, Transactions American Geophysical Union*, *37*(6), 702-714.

Hantush, M. S. (1965). Wells near streams with semipervious beds. *Journal of Geophysical Research*, *70*(12), 2829-2838.

Hara, Y., Takeuchi, K., & Okubo, S. (2005). Urbanization linked with past agricultural landuse patterns in the urban fringe of a deltaic Asian mega-city: a case study in Bangkok. *Landscape and Urban Planning*, *73*(1), 16-28.

Harbury, N.A., Jones,M.E.,Charles,M.G.A,Metcalfe,I.,Mohamed,K.R. (1990). Structural evolution of Mesozoic Peninsular Malaysia. *Geological Society of London, 147*, 11-26.

Hayashi, T., Tokunaga, T., Aichi, M., Shimada, J., & Taniguchi, M. (2009). Effects of human activities and urbanization on groundwater environments: an example from the aquifer system of Tokyo and the surrounding area. *Science of the total environment*, *407*(9), 3165-3172.

Hayes, J.B. (1979). *Sandstone diagenesis-the hole truth*.

Healy, R.W. & Cook, P.G. (2002). Using groundwater levels to estimate recharge. *Hydrogeology Journal, 10*, 91-109.

Hellström, D., Jeppsson, U., & Kärrman, E. (2000). A framework for systems analysis of sustainable urban water management. *Environmental Impact Assessment Review*, *20*(3), 311-321.

Hitchmough, A.M., Riley,M.S.,Herbert,A.W.&Tellam,J.H. (2007). Estimating the hydraulic properties of the fracture network in a sandstone aquifer. *Journal of Contaminant Hydrology, 93*, 38-57.

Holm, J. V., Ruegge, K., Bjerg, P. L., & Christensen, T. H. (1995). Occurrence and distribution of pharmaceutical organic compounds in the groundwater downgradient of a landfill (Grindsted, Denmark). *Environmental science & technology*, *29*(5), 1415-1420.

Holmes, A. (1965). *Principles of physical geology*. London: Nelson.

Howard, K.W.F. & Lloyd, J.W. (1979). The sensitivity of parameters in the Penman Evaporation equations and direct recharge balance. *Journal of Hydrology, 41*, 329-344.

Howard, K.W.F. & Israfilov,R.G.(2002).Current problems of hydrogeology in urban areas, urban agglomerates and industrial centres. *NATO Science Series IV. Earth and Environmental Sciences 8*

Huong, H. T. L., & Pathirana, A. (2013). Urbanization and climate change impacts on future urban flooding in Can Tho city, Vietnam. *Hydrology and Earth System Sciences*, *17*(1), 379-394.

Hurst, A. & Rosvoll, K.J. (1991). *Permeability variations in sandstones and their relationship to sedimentary structures.* Paper presented at the Proceedings of the Second International Reservoir Characterization Technical Conference.

Hutchison, C.S. (1973). Metamorphism. In D. J. Gobbett, Hutchison, C.S. (Ed.), *Geology of the Malay Peninsula (West Malaysia and Singapore)*: Wiley-Interscience.

Hutchison, C.S. (1977). Granite emplacement and tectonic subdivision of Peninsular Malaysia. *Geological Society Malaysia, 9*, 187-207.

Ibrahim,K. (1986). *Engineering geological aspects of clastic metasediments in the Kuala Lumpur area, Peninsular Malaysia*. Paper presented at the GEOSEA V Proceedings Vol I Geological Society Malaysia.

Ibrahim,K.& Mogana, S.N.(1988). Physical characterization of weathering profile of clastic metasediments in Peninsular Malaysia. In *Proceedings 2nd Conference on Geomechanics in Tropical Soils. Singapore* (Vol. 1, pp. 37-42).

Ibrahim,K.&Jasni,Y. (1990). *Engineering properties of weathered metamorphic rocks in Peninsular Malaysia.* Paper presented at the 6th International IAEG Congress.

Ibrahim, M.S. & Fakhru'l-Razi, A. (2006).Disaster types in Malaysia: an overview.*Disaster Prevention and Management: An International Journal*, Vol. 15 (2), 286 - 298

Ismail,M.N.(1979).Prefeasibility Study of Potential Groundwater Development in Kelantan, Malaysia. PhD Thesis,University of Birmingham.

Ismail, C.M.Z. (1981). *Hidrogeologi kawasan kelang, Selangor.* (BSc.Thesis), Universiti Kebangsaan Malaysia.

Jacob, C. E. (1947). Drawdown test to determine effective radius of artesian well. *Transactions of the American Society of Civil Engineers*, *112*(1), 1047-1064.

Jasni,Y. (1989). *Teknik penentuan sifat kejuruteraan bahan metasedimen klastik terluluhawa dan pengelasan.* (MSc), Universiti Kebangsaan Malaysia.

Jenkins, D. N., & Prentice, J. K. (1982). Theory for aquifer test analysis in fractured rocks under linear (nonradial) flow conditions. *Groundwater*, *20*(1), 12-21.

JICA, Japan International Cooperation Agency. (1984). National Water Resources Study, Malaysia : main report. *vol.1-2.*

Johnson, K. T., Germain, M. W.-St., Ko, S. and Huling, S. G. (2012). Binary Mixtures of Permanganate and Chlorinated Volatile Organic Compounds in Groundwater Samples: Sample Preservation and Analysis. *Groundwater Monitoring & Remediation, 32*(3), 84-92.

Jolley, S. J. (Ed.). (2010). Reservoir compartmentalization. Geological Society of London.

Jones, C.R. (1973). Lower Paleozoic. In C. S. H. D.J.Gobbett (Ed.), *Geology of the Malay Peninsula (West Malaysia and Singapore)*: Wiley-Interscience.

Jones, M. J. (1985). The weathered zone aquifers of the basement complex areas of Africa. *Quarterly Journal of Engineering Geology and Hydrogeology,18*(1), 35-46.

Jones, H. K., & Cooper, J. D. (1998). Water transport through the unsaturated zone of the Middle Chalk: a case study from Fleam Dyke lysimeter. *Geological Society, London, Special Publications, 130*(1), 117-128.

Kale, S. S., Kadam, A. K., Kumar, S., & Pawar, N. J. (2010). Evaluating pollution potential of leachate from landfill site, from the Pune metropolitan city and its impact on shallow basaltic aquifers. *Environmental monitoring and assessment, 162*(1-4), 327-346.

Kamarudin,S., Ismail A., Mohd Tadza, A.R., & Mohamed Hasnain, I.(2009).Distribution of heavy metals profile in groundwater system at solid waste disposal site. *Eur J Sci Res* 1 ,58-66.

Kamaruzaman, J. (1989). Physical soil properties associated with recreational use of of a forested reserve area in Malaysia. *Environmental Conservation, 16*(4).

Karami, G.H. & Younger, P.L. (2002). Analysing step-drawdown tests in heterogeneous aquifers. *Quarterly Journal of Engineering Geology and Hydrogeology, 35*, 295-303.

Kawecki, M.W. (1993). Recovery analysis from pumping tests with stepped discharge. *Ground Water, 31*(4).

Kawecki, M.W. (1995). Meaningful interpretation of step-drawdown tests. *Ground Water, 33*(1).

Khairiah, J., Habibah, J., Ahmad Mahir, R., Maimon, A., Aminah, A., & Ismail, B. S. (2009). Studies on heavy metal deposits in soils from selected agricultural areas of Malaysia. *Adv Environ Biol, 3*(3), 329-336.

Khaki, K., Yusoff, Y., & Islami, I. (2014). Integrated Geoelectrical Resistivity and Geochemical Survey to Study Groundwater-a Case Study from Selangor, Malaysia. In *76th EAGE Conference and Exhibition 2014*.

Koledoye, B. A., Aydin, A., & May, E. (2003). A new process-based methodology for analysis of shale smear along normal faults in the Niger Delta. *AAPG bulletin, 87*(3), 445-463.

Krasny, J.&Sharp, J.M.Jr. (2003). *Hydrogeology of fractured rocks from particular fractures to regional approaches: State-of-the-art and future challenges*. Paper presented at the Groundwater in fractured rocks International Conference, Prague.

Kruseman, G.P.& de Ridder, N.A. (1994). *Analysis and evaluation of pumping test data* (Second Edition (completely revised) ed.): International Institute for Land Reclamation and Improvement.

Larsson, Ingemar (1984). *Ground water in hard rocks : Project 8.6 of the International Hydrological Programme*: UNESCO.

Lerner, D.N., Issar,A.S. & Simmers,I. (1990). Groundwater recharge; a guide to understanding and estimating natural recharge. *International Association of Hydrogeologists, 8*.

Lerner, D. N., & Teutsch, G. (1995). Recommendations for level-determined sampling in wells. *Journal of Hydrology, 171*(3), 355-377.

Lerner, D. N., & Barrett, M. H. (1996). Urban groundwater issues in the United Kingdom. *Hydrogeology Journal, 4*(1), 80-89.

Lerner, D. N., Yuesuo, Y., Barrett, M. H., & Tellam, J. H. (1999). Loadings of non-agricultural nitrogen in urban groundwater. *IAHS PUBLICATION*, 117-124.

Lerner, D.N. (2002). Identifying and quantifying urban recharge: a review. *Hydrogeology Journal, 10*, 143-152.

Levadowski, D.W., Kaley,M.E.,Silverman,S.R. & Smalley,R.G. (1973). Cementation in Lyons Sandstone and its role in oil accumulation, Denver Basin,Colorado. *The American Association of Petroleum Geologist Bulletin, 57*(11), 2217-2244.

Lim, T.H. (1995). Some engineering geology characteristics of the Kenny Hill Formation, Kuala Lumpur. *Warta Geologi, 21*(1), 9-11.

Lloyd, J.W., Drennan,D.S.H.&Bennell,B.M.U.(1966). A groundwater recharge study in north east Jordan. *Proceeding Institute Civil of Engineer, 35*, 615-631.

Lloyd, J.W.&Heathcote, J.A. (1985). *Natural inorganic hydrochemistry in relation to groundwater*. Oxford: Clarendon Press.

Lloyd, J.W. (1999). *Water resources of hard rock aquifers in arid and semi-arid zones*: UNESCO.

Logan. (1964). Estimating transmissibility from routine production tests of water wells. *Ground Water, 2*, 35-37.

LUAS (2008). State of River Report (2008)-Sungai Klang.

Magara, K. (1976). Water expulsion from clastic sediments during compaction-directions and volumes. *The American Association of Petroleum Geologist Bulletin*.

Magara, K. (1980). Comparison of porosity-depth relationships of shale and sandstone. *Journal of Petroleum Geology, 3(2)*, 175-185.

Manap, M. A., Sulaiman, W. N. A., Ramli, M. F., Pradhan, B., & Surip, N. (2013). A knowledge-driven GIS modeling technique for groundwater potential mapping at the Upper Langat Basin, Malaysia. *Arabian Journal of Geosciences*, *6*(5), 1621-1637.

Mar Gonzalez, M., & Rushton, K. R. (1981). Deviations from classical behaviour in pumping test analysis. *Groundwater*, *19*(5), 510-516.

Maréchal, J. C., Dewandel, B., & Subrahmanyam, K. (2004). Use of hydraulic tests at different scales to characterize fracture network properties in the weathered-fractured layer of a hard rock aquifer. *Water Resources Research*, *40*(11).

Mast, R.F. & Potter, P.E. (1963). Sedimentary structures,sand shape fabrics and permeability. *The Journal of Geology*, *71*(5).

Mayo, A. (2010). Ambient well-bore mixing, aquifer cross-contamination, pumping stress, and water quality from long-screened wells: What is sampled and what is not?.*Hydrogeology Journal*,18, 823-837

Mazlin, M., Ismail, B., Yap,C.H & Agnes,P. (2001)Kajian kualiti air di sekitar kawasan perindustrian Subang Jaya dan Shah Alam, Lembah Kelang. *Malaysian Journal of Analytical Sciences*. 7(1): 139-149

McBride, E.F. (1989). Quartz cement in sandstones: A review. *Earth-Science Reviews*, *26*, 69-112.

McDonald, J. P., & Smith, R. M. (2009). Concentration profiles in screened wells under static and pumped conditions. *Groundwater Monitoring & Remediation*, *29*(2), 78-86.

McMillan, L. A., Rivett, M. O., Tellam, J. H., Dumble, P., & Sharp, H. (2014). Influence of vertical flows in wells on groundwater sampling. *Journal of contaminant hydrology*, *169*, 50-61.

Megahan, W. F., & Clayton, J. L. (1986). Saturated hydraulic conductivities of granitic materials of the Idaho Batholith. *Journal of Hydrology*, *84*(1-2), 167-180.

Meier, P. M., Carrera, J., & Sánchez-Vila, X. (1998). An evaluation of Jacob's method for the interpretation of pumping tests in heterogeneous formations.*Water Resources Research*, *34*(5), 1011-1025.

Metcalfe,I. (1991). Late Paleozoic and Mesozoic paleogeography of Southeast Asia. *Paleogeography, Paleoclimatology, Paleoecology, 87*, 211-221.

Michalski, A. (1990). Hydrogeology of the Brunswick (Passaic) Formation and implications for ground water monitoring practice. *Ground Water Monitoring & Remediation*, *10*(4).

Michalski, A. & Britton, R. (1997). The role of bedding fractures in the hydrogeology of sedimentary bedrock-evidence from the Newark basin, New Jersey. *Ground Water*, *35*(2).

Misstear, B. D. (2001). The value of simple equilibrium approximations for analysing pumping test data. *Hydrogeology Journal*, *9*(2), 125-126

Misstear, B., Banks,D.&Clark,L. (2006). *Water wells and boreholes*: John Wiley & Sons Ltd.

Mogana,S. (1991). *Sifat geologi kejuruteraan profil luluhawa batuan metasedimen klastik di Negeri Selangor dan Wilayah Persekutuan.* (MSc), Universiti Kebangsaan Malaysia, Bangi.

Mohammed Thamer,A. & Abdul Halim,G. (2009).Evaluation of yield and groundwater quality for selected wells in Malaysia. *Pertanika Journal of Science & Technology* 17 (1),33-42.

Mohamed, E.A. & Worden, R.H. (2006).Groundwater Compartmentalisation : A Water Table Height and Geochemical Analysis of the Structural Controls on the Subdivision of a Major Aquifer, the Sherwood Sandstone,Merseyside,UK. *Hydrology and Earth System Sciences* 10 : 49-64.

Morgan, R.P.C. (1970). An Analysis of basin asymmetry in the Klang Basin, Selangor. *Geological Society Malaysia, 3*, 17-26.

Morin, R.H., Carleton,G.B. & Poirier,S. (1997). Fractured -aquifer hydrogeology from geophysical logs; The Passaic Formation, New Jersey. *Ground Water, 35*(2).

Mohamed Azwan, M. Z., Mohd Kamil, Y., Hazilia, H., & Suhani, N. (2010). Nitrate-nitrogen concentration variation in groundwater flow in a paddy field.*Journal-The Institution of Engineers Malaysia 71(4), 2-10*

Murakami, A., Zain, A. M., Takeuchi, K., Tsunekawa, A., & Yokota, S. (2005). Trends in urbanization and patterns of land use in the Asian mega cities Jakarta, Bangkok, and Metro Manila. *Landscape and Urban Planning*, *70*(3), 251-259.

Musbah, A.W. (1980). Keratan stratigrafi Formasi Bukit Kenny di Bukit Pantai, Kuala Lumpur. *Sains Malaysiana, 9*(1), 1-10.

Naik, P. K., Tambe, J. A., Dehury, B. N., & Tiwari, A. N. (2008). Impact of urbanization on the groundwater regime in a fast growing city in central India. *Environmental monitoring and assessment*, *146*(1-3), 339-373.

Nasiman, S., Raja Zainariah, R.A., & Hisyam,J. (2011). Quantity and Quality of Groundwater in Fractured Metasedimentary Rocks of the West Coast of Peninsular Malaysia. *Sains Malaysiana*, *40*(6), 537-542.

Nasiman S, Raja Zainariah,R.A, & Hisyam,J. (2012). Groundwater from fractured Granite and Metasedimentary Rocks in the West Coast of Peninsular Malaysia.*Editorial Board*, 371.

Neuman, S. P. (1975). Analysis of pumping test data from anisotropic unconfined aquifers considering delayed gravity response. *Water Resources Research, 11*(2), 329-342.

Neuzil, C.E. (1994). How permeable are clays and shale. *Water Resources Research, 30*(2), 145-150.

Nickson, R. T., McArthur, J. M., Ravenscroft, P., Burgess, W. G., & Ahmed, K. M. (2000). Mechanism of arsenic release to groundwater, Bangladesh and West Bengal. *Applied Geochemistry*, *15*(4), 403-413.

Noguchi,S., Abdul Rahim, N., Baharuddin, K., Tani,M., Sammori,T. & Morisada,K.. (1997). Soil physical properties and preferential flow pathways in tropical rain forest, Bukit Tarek, Peninsular Malaysia. *Journal Forest Research, 2*, 115 -120.

Norain, I., Fairus,M.D., Wirda, A. & Rusdin,L. (2008). Heavy metal concentration in street dust of Shah Alam City, Selangor. In: Jamaluddin Md Jahi, Kadaruddin Aiyub, Muhammad Rizal Razman, Kadir Ariffin & Azahan Awang. Human Habitat and Environmental Change. Bangi: UKM Press.

Noraziah,J.,Shaharuddin,M.S., Sharifah,N.S.I. (2013). Health risk assessment of nitrate exposure in well water of residents in intensive agriculture area. *American Journal of Applied Sciences*, *10*(5), 442-448.

Noorazuan,M.H., Ruslan, R., Hafizan,J., Sharifuddin,M.Z & Nazari,J. 2003.GIS Application in evaluating land use-land cover change and its impact on hydrological regime in Langat River Basin, Malaysia. 2nd Annual Asian Conference of Map Asia 2003.

Nur Hayati, H., Ismail,Y.,Yatimah,A.,Sharifah,M.,Nurul Yani,R., & Muhammad Aqeel,A. (2014). Ionic liquid as a medium to remove iron and other metal ions: a case study of the North Kelantan Aquifer, Malaysia. *Environmental earth sciences,71*(5), 2105-2113.

Palmer,R.C.,Holman, I. P., Robins, N. S., & Lewis, M. A. (1995). *Guide to groundwater vulnerability mapping in England and Wales*. National Rivers Authority.

Papadopulos, I. S., & Cooper, H. H. (1967). Drawdown in a well of large diameter. *Water Resources Research*, *3*(1), 241-244.

Parkhurst, D. L., & Appelo, C. A. J. (1999). User's guide to PHREEQC (Version 2): A computer program for speciation, batch-reaction, one-dimensional transport, and inverse geochemical calculations.

Pauwels, H., Ayraud-Vergnaud, V., Aquilina, L., & Molénat, J. (2010). The fate of nitrogen and sulfur in hard-rock aquifers as shown by sulfate-isotope tracing. *Applied Geochemistry*, *25*(1), 105-115.

Pettijohn, F.J., Potter,P.E. & Siever,R. (1987). *Sand and sandstone* (second edition ed.): Springer-Verlag.

Prasad, R. K., Singh, V. S., Krishnamacharyulu, S. K. G., & Banerjee, P. (2011). Application of drastic model and GIS: for assessing vulnerability in hard rock granitic aquifer. *Environmental monitoring and assessment*, *176*(1-4), 143-155.

Price, N. J. (1966). *Fault and joint development: in brittle and semi-brittle rock*. Elsevier.

Puls, R. W., & Barcelona, M. J. (1996). *Low-flow (minimal drawdown) ground-water sampling procedures*. US Environmental Protection Agency, Office of Research and Development, Office of Solid Waste and Emergency Response

Quinn, P. M., Parker, B. L., & Cherry, J. A. (2011). Using constant head step tests to determine hydraulic apertures in fractured rock. *Journal of contaminant hydrology*, *126*(1), 85-99.

Raja Zainariah,R.A..(1997). *Characteristics of Groundwater from Fractured Hardrocks in West Coast of Peninsular Malaysia*. MSc. Universiti Putra Malaysia.

Ramnarong,V.(1999). Evaluation of groundwater management in Bangkok: positive and negative. In Chilton (Ed.), *Groundwater in the urban environment: Selected city profiles* (pp 51-62).Netherland: Balkema.

Rancangan Tempatan Majlis Bandaraya Shah Alam (MBSA) 2020 (2003).

Reilly, T. and LeBlanc, D. (1998). Experimental Evaluation of Factors Affecting Temporal Variability of Water Samples Obtained from Long-Screened Wells. *Ground Water*,36(4),566-576

Reynolds, J.H. & Barrett, M.H. (2003). A review of the effects of sewer leakage on groundwater quality. *Water and Environment Journal, 17*(1).

Rivett, M. O., Lerner, D. N., Lloyd, J. W., & Clark, L. (1990). Organic contamination of the Birmingham aquifer, UK. *Journal of Hydrology*, *113*(1), 307-323.

Rivett, M. O., Ellis, P. A., & Mackay, R. (2011). Urban groundwater baseflow influence upon inorganic river-water quality: The River Tame headwaters catchment in the City of Birmingham, UK. *Journal of Hydrology*, *400*(1), 206-222.

Robins, N. S. (1998). Recharge: the key to groundwater pollution and aquifer vulnerability. *Geological Society, London, Special Publications*, *130*(1), 1-5.

Roe, F.W. (1951). The geology and mineral resources of the Fraser's Hill area Selangor, Perak and Pahang, Federation of Malaya, with an account of the mineral resources. *Memoir Geological Survey Department, Federation of Malaya,5*.

Roe, F.W. (1953). The geology and mineral resources of the neighbourhood of Kuala Selangor and Rasa, Selangor, Federation of Malaya with an account of the Batu Arang Coal-field. *Memoir Geological Survey Dept. Fed. Malaya, 7*, 163.

Rosly, M.N. (1979). *Geology of Kenny Hill Formation,Peninsular Malaysia.* (BSc.), University of Malaya.

Rudel, R.A., Melly,S.J.,Geno,P.W.,Sun,G. & Brody,J.G. (1998). Identification of alkylphenols and other estrogenic phenolic compounds in wastewater, septage and groundwater on Cape Cod, Massachussetts. *Environmental Science Technology, 32*, 861-869.

Rumbaugh, D.B.& Rumbaugh, J.O. 1999-2013.Guide to using Aquifer Win32 Version 5.

Rumbaugh, J.O..& Rumbaugh, D.B.. 2000-2007. Guide to using Groundwater Vistas Version 5.

Rushton, K. R. (1985). Interference due to neighboring wells during pumping tests. *Groundwater, 23*(3), 361-366.

Rushton, K.R. (2003). *Groundwater Hydrology :Conceptual and Computional Models*: John Wiley & Sons Ltd.

Rushton, K.R.& Rathod, K.S. (1988). Causes of non-linear step pumping test responses. *Quarterly Journal of Engineering Geology, 21*, 147-158.

Sam, Frederick. (2014). *The assessment of potential impacts of open cast gold mining on the regional groundwater flow system in hard rock environments: with special reference to Ghana.* (PhD), University of Birmingham.

Saim,S. (1991). *Hidrogeologi kawasan Lembah Klang dengan penekanan terhadap akuifer batukapur.* (MSc.), Universiti Kebangsaan Malaysia.

Sánchez-Vila, X., Meier, P. M., & Carrera, J. (1999). Pumping tests in heterogeneous aquifers: An analytical study of what can be obtained from their interpretation using Jacob's method. *Water Resources Research, 35*(4), 943-952.

Scanlon, B.R., Healy,R.W. & Cook,P.G. (2002). Choosing appropriate techniques for quantifying groundwater recharge. *Hydrogeology Journal, 10*, 18-39.

Schirmer, M., Leschik,S.& Musolff,A.(2013).Current Research in Urban Hydrogeology-a Review. *Advances in Water Resources* 51 , 280-91.

Schmidt, V. & McDonald, D.A. (1979). *The role of secondary porosity in the course of sandstone diagenesis*.

Seymour, K. J., Ingram, J. A., & Gebbett, S. J. (2006). Structural controls on groundwater flow in the Permo-Triassic sandstones of NW England. *Geological Society, London, Special Publications, 263*(1), 169-185

Sham, S. (1973). The urban heat-island-its concept and application to Kuala Lumpur. *Sains Malaysiana, 2*(1), 53-64.

Sham, S. (1980). *The climate of Kuala Lumpur-Petaling Jaya area Malaysia. A study of the impact of urbanization on local climate within the humid tropics*. Bangi: Universiti Kebangsaan Malaysia.

Sham, S. (1990). Urban Climatology in Malaysia: an Overview. *Energy and Buildings, 15 - 16*, 105-117.

Shepherd, K. A., Ellis, P. A., & Rivett, M. O. (2006). Integrated understanding of urban land, groundwater, baseflow and surface-water quality—The City of Birmingham, UK. *Science of the Total Environment, 360*(1), 180-195.

Sim, L. K., & Balamurugan, G. (1991). Urbanization and urban water problems in Southeast Asia a case of unsustainable development. *Journal of Environmental Management*, *32*(3), 195-209.

Singhal, B.B.S., Gupta,R.P. (1999). *Applied hydrogeology of fractured rocks*. Netherland: Kluwer Academic Publishers.

Siti Nur Syahirah,M.A., Sumiani,Y., and Yan P. C.(2013).Soil chemistry and pollution study of a closed landfill site at Ampar Tenang, Selangor, Malaysia. *Waste Management & Research.*

Smith, D.A. (1980). Sealing and nonsealing faults in Louisiana Gulf Coast Salt Basin. *The American Association of Petroleum Geologist Bulletin, 64*.

Somasundaram, M. V., Ravindran, G., & Tellam, J. H. (1993). Ground-Water Pollution of the Madras Urban Aquifer, India. *Groundwater*, *31*(1), 4-11.

Spalding, R. F., & Exner, M. E. (1993). Occurrence of nitrate in groundwater—a review. *Journal of environmental quality*, *22*(3), 392-402.

Sperrevik, S., Faerseth,R.B. & Gabrielsen,R.H. (2000). Experiments on clay smear formation along faults. *Petroleum Geoscience*, *6*, 113-123.

Squillace, P. J., Moran, M. J., Lapham, W. W., Price, C. V., Clawges, R. M., & Zogorski, J. S. (1999). Volatile organic compounds in untreated ambient groundwater of the United States, 1985-1995. *Environmental Science & Technology*, *33*(23), 4176-4187.

Stauffer, P.H. (1968). The Kuala Lumpur fault zone: a proposed major strike-slip fault across Malaya. *Geological Society Malaysia Newsletter, 15*, 2-4.

Stauffer, P.H. (1973). Kenny Hill Formation. In D. J. Gobbett (Ed.), *Geology of Malay Peninsula (West Malaysia and Singapore)* (pp. 87-95): Wiley-Interscience.

Sterrett, R. J. (Ed.). (2007). *Groundwater and wells*. Johnson Screens.

Swartz, M., Misstear, B. D. R., Daly, D., & Farrell, E. R. (2003). Assessing subsoil permeability for groundwater vulnerability. *Quarterly Journal of Engineering Geology and Hydrogeology*, *36*(2), 173-184.

Takahashi, M. (2003).Permeability Change During Experimental Fault Smearing. *Journal of Geophysical Research* 108, no. B5.

Tan, B. K., & Tai, T. O. (1999). Physico-chemical properties of graphitic schist soils from Malacca, Peninsular Malaysia. In *Proc. 2nd Asian symp. on engineering geology & environment, Bangi* (pp. 2-8).

Tan, B. K., & Yew, C. K. (2002). Physico-chemical properties of andesitic soils in the Kg. Awah area, Pahang. In *Bulletin no. 45, Geological Society of Malaysia annual geological conf, Kota Bharu* (pp. 31-35).

Tan, B.K., Yeap,E.B. (1977). Structure of the Kenny Hill Formation, Kuala Lumpur and Selangor. *Geological Society Malaysia, 8*, 127-129.

Tan, B.K.,& Ezdiani,S.F. (2005). Physico-chemical properties of residual soils of the Kenny Hill Formation in the Shah Alam area, Selangor. *Geological Society of Malaysia, 51*, 13-17.

Taylor, R., & Howard, K. (2000). A tectono-geomorphic model of the hydrogeology of deeply weathered crystalline rock: evidence from Uganda. *Hydrogeology Journal*, *8*(3), 279-294.

Tellam, J. H., & Thomas, A. (2002). Well water quality and pollutant source distributions in an urban aquifer. In *Current Problems of Hydrogeology in Urban Areas, Urban Agglomerates and Industrial Centres* (pp. 139-158). Springer Netherlands.

Thomas, A. & Tellam, J. (2006). Modelling of recharge and pollutant fluxes to urban groundwaters. *Science of the Total Environment, 360*(1-3), 158-179.

Thurman, E.M. (1985).*Organic Geochemistry of Natural Waters*. Dordrecht,The Netherlands: Martinus Nijhoff/Dr. W.Junk Publishers.

Tjia, H.D. (1974). inverted facing of Kenny Hill Formation at Bukit Pantai, Kuala Lumpur. *Sains Malaysiana, 3*(2), 163-176.

Tjia, H.D. (1976). Isoclinal to recumbent folds and thrust in Selangor. *Sains Malaysiana, 5*(1), 49 - 65.

Tjia, H.D. (1977). Western extension of the Kuala Lumpur fault zone. *Geological Society Malaysia, 8*, 123-125.

Tjia, H.D. (1979). Westward tectonic transport of Kenny Hill rocks at Bukit Pantai, Kuala Lumpur. *Sains Malaysiana, 8*(2), 153 - 161.

Tjia, H.D. (1984). A case of cross folding in Kenny Hill beds of Kuala Lumpur. *Sains Malaysiana, 13*(1), 131 - 136.

Tjia, H.D. (1984). A case of cross folding in Kenny Hill Beds of Kuala Lumpur. *Sains Malaysiana, 13*(1), 131-136.

Tjia, H.D., Zaiton,H. (1985). Regional structures of Peninsular Malaysia. *Sains Malaysiana, 14*(1), 95 - 107.

Tjia, H.D. . (1989). Major faults of Peninsular Malaysia on remotely-sensed images. *Sains Malaysiana, 18*(1), 101-114.

Trauth, R., & Xanthopoulos, C. (1997). Non-point pollution of groundwater in urban areas. *Water research*, *31*(11), 2711-2718.

Umar,H., Rahman,Y., Abdul Rahim,S., & Mohd Syahid,A. (2006). Electrical imaging of the groundwater aquifer at Banting, Selangor, Malaysia.*Environmental Geology*, *49*(8), 1156-1162.

Umar,H., Abdul Rahim,S., & Edna, P.M. (2007). Groundwater investigation in Kuala Selangor using vertical electrical sounding (VES) surveys. *Environmental geology*, *51*(8), 1349-1359.

Umezawa, Y., Hosono, T., Onodera, S. I., Siringan, F., Buapeng, S., Delinom, R., Yoshimizu, C., Nagata, T.& Taniguchi, M. (2008).“Sources of nitrate and ammonium contamination in groundwater under developing Asian megacities”. *Science of the Total Environment*, *404*,361-376.

United Nations. Department of Economic, & United Nations. Department of Public Information. (2009). *The millennium development goals report 2009*. United Nations Publications.

Yeap, E.B. (1970). *Geology of the Petaling Jaya-Salak South area, Selangor, West Malaysia.* University of Malaya.

Yeap, E.B. (1986). Irregular topography of the subsurface carbonate bedrock in the Kuala Lumpur area, foundation problems in limestone areas of Peninsular Malaysia. In G. E. Division (Ed.): Institute Engineering Malaysia.

Van Der Zee, W. & Urai, J.L. (2005).Processes of Normal Fault Evolution in Siliciclastic Sequence: A Case Study from Miri, Sarawak, Malaysia. *Journal of Structural Geology* 27 .

Van Golf-Racht, T. D. (1982). *Fundamentals of fractured reservoir engineering* (Vol. 12). Elsevier.

Vroblesky, D. A., Rhodes, L. C., Robertson, J. F., & Harrigan, J. A. (1996). Locating VOC contamination in a fractured-rock aquifer at the ground-water/surface-water interface using passive vapor collectors. *Groundwater*, *34*(2), 223-230.

Wakida, F. T., & Lerner, D. N. (2005). Non-agricultural sources of groundwater nitrate: a review and case study. *Water research*, *39*(1), 3-16.

Walton, W.C.(1962).Selected Analytical Methods for Well and Aquifer Evaluation.Urbana: Department of Registration and Education.

Wang, J.-A. & Park, H.D. (2002). Fluid permeability of sedimentary rocks in a complete stress-strain process. *Engineering Geology, 63,* 291-300.

Weber, S., & Chapuis, R. P. (2013). Interpretation of a pumping test with interference from a neighboring well. *Groundwater*, *51*(6), 935-944.

Weber, S., Chapuis, R. P., & Duhaime, F. (2014). Interpreting a Pumping Test Influenced by Another Well in an Anisotropic Aquifer. *Groundwater*, *52*(5), 717-727.

West, G. & Dumbleton, M.J.(1970).The Mineralogy of Tropical Weathered Illustrated by Some Malaysian West Soils.*Quarterly Journal of Engineering Geology* 3, 25-40.

Whitehead, E., Hiscock,K.& Dennis,P. (1999). *Evidence for sewage contamination of the Sherwood Sandstone aquifer beneath Liverpool,UK*. Paper presented at the Proceedings of IUGG 99 Symposium HS5, Birmingham.

Wright, E.P.& Burgess, W.G. (1992). The hydrogeology of crystalline basement aquifers in Africa. *Geological Society Special Publication, 66*, 264p.

Wyns, R., Baltassat, J.M., Lachassagne, P., Legchenko, A., Vairon, J. and Mathieu, F., 2004. Application of proton magnetic resonance soundings to groundwater reserve mapping in weathered basement rocks (Brittany, France). *Bulletin de la société géologique de France*, *175*(1), pp.21-34.

Yang, Y., Lerner, D.N., Barrett, M.H., Tellam, J.H.T . (1999). Quantification of groundwater recharge in the city of Nottingham, UK. *Environmental Geology, 38*(3), 183-198.

Yin, E.H. (1986). The Geology and Mineral Resources of the Kuala Lumpur-Klang area: Jabatan Penyiasatan Kajibumi Malaysia.

Zainab, M, Rafek,A.G.,Komoo ,I. (2007). Characterisation and classification of the physical deterioration of tropically weathered Kenny Hill rock for civil works. *Electronic Journal of Electrical Engineering, 12*.

Zaki, Z. (2010).Benchmarking river water quality in Malaysia. *Jurutera* (2010): 12-15.

Zhang, W. L., Tian, Z. X., Zhang, N., & Li, X. Q. (1996). Nitrate pollution of groundwater in northern China. *Agriculture, Ecosystems & Environment*, *59*(3), 223-231.

Zulhaimi Abdul Rahman (2000). Sifat fiziko kimia dan mineralogy lempung tanah baki sekitar Rawang. (BSc.), Universiti Kebangsaan Malaysia

APPENDIXES A Semi log and Log-log plot for each Classes (Class A to Class E)

Class A

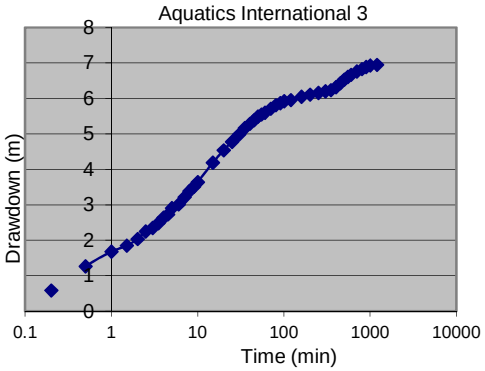

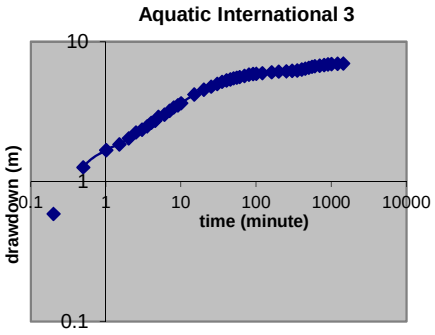

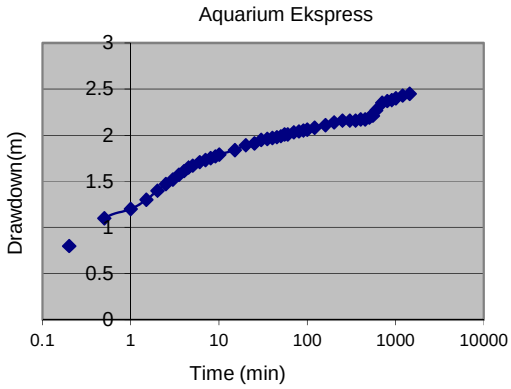

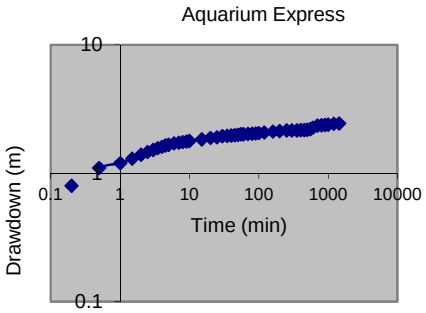

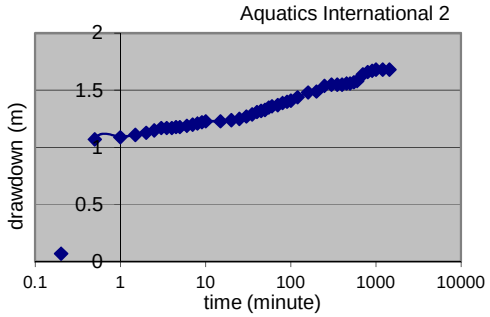

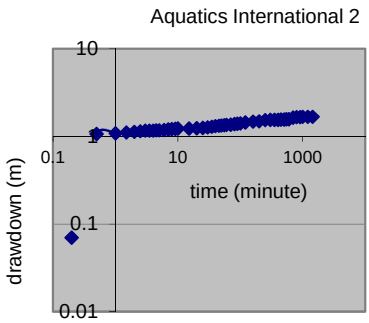

Class B

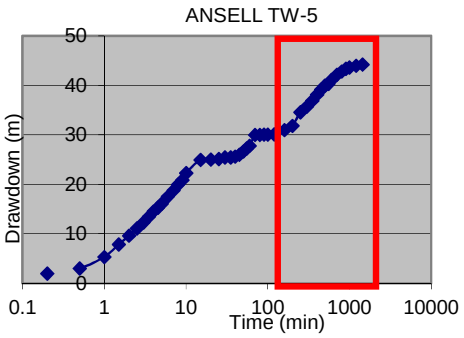
ANSELL TW-5
Drawdown (m)
50
40
30
20
10
0
0.1
1
10
100
1000
10000
Time (min)

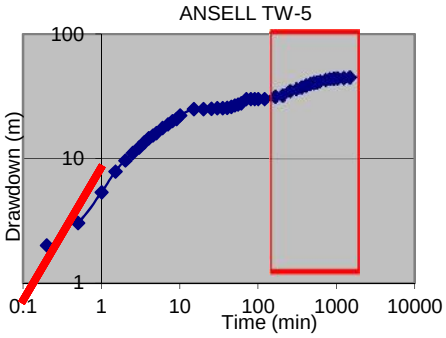
ANSELL TW-5
Drawdown (m)
100
10
1
0.1
1
10
100
1000
10000
Time (min)

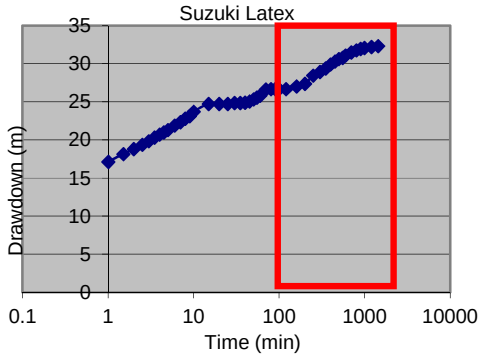
Suzuki Latex
Drawdown (m)
35
30
25
20
15
10
5
0
0.1
1
10
100
1000
10000
Time (min)

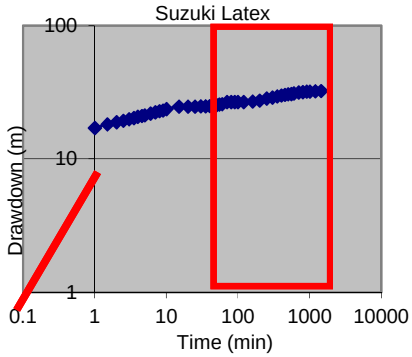
Suzuki Latex
Drawdown (m)
100
10
1
0.1
1
10
100
1000
10000
Time (min)

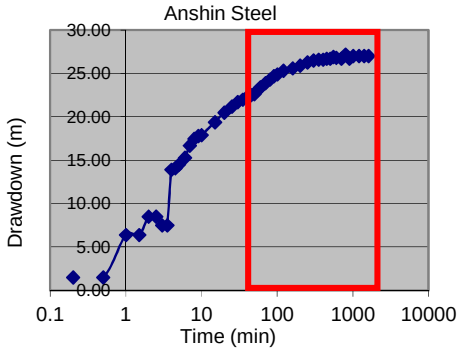
Anshin Steel
Drawdown (m)
30.00
25.00
20.00
15.00
10.00
5.00
0.00
0.1
1
10
100
1000
10000
Time (min)

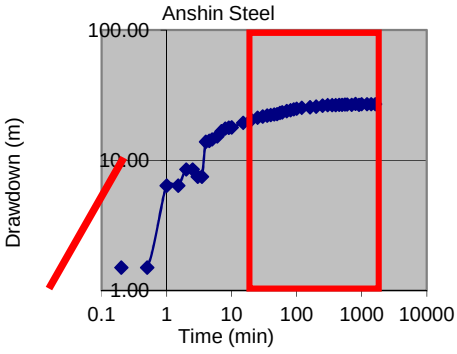
Anshin Steel
Drawdown (m)
100.00
10.00
1.00
0.1
1
10
100
1000
10000
Time (min)

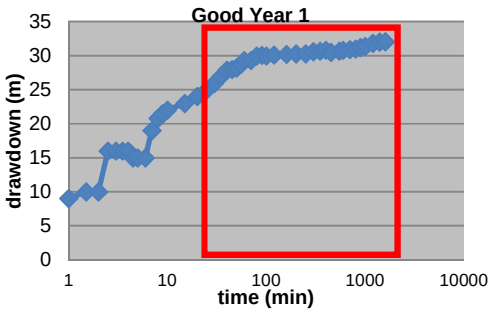
Good Year 1
drawdown (m)
35
30
25
20
15
10
5
0
1
10
100
1000
10000
time (min)

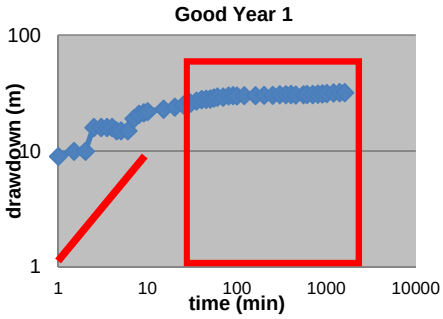
Good Year 1
drawdown (m)
100
10
1
1
10
100
1000
10000
time (min)

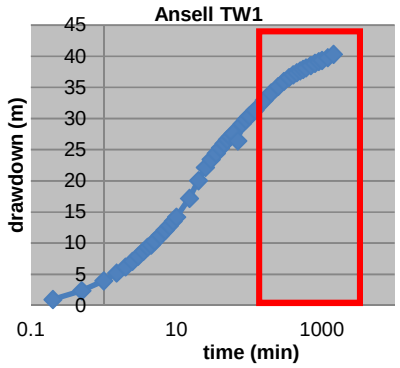
Ansell TW1
drawdown (m)
45
40
35
30
25
20
15
10
5
0
0.1
10
1000
time (min)

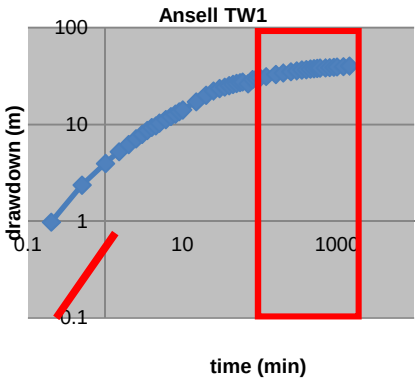
Ansell TW1
drawdown (m)
100
10
1
0.1
10
1000
0.1
time (min)

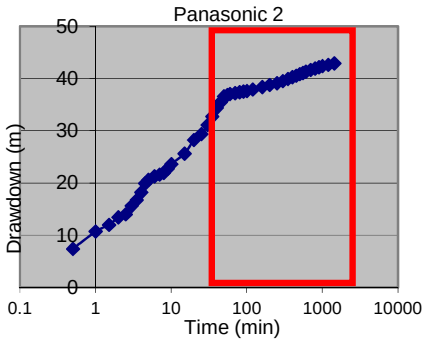
Panasonic 2
Drawdown (m)
50
40
30
20
10
0
0.1
1
10
100
1000
10000
Time (min)

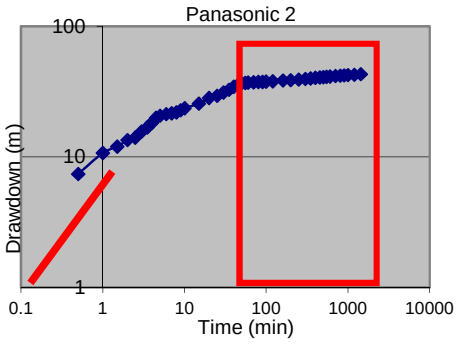
Panasonic 2
Drawdown (m)
100
10
1
0.1
1
10
100
1000
10000
Time (min)

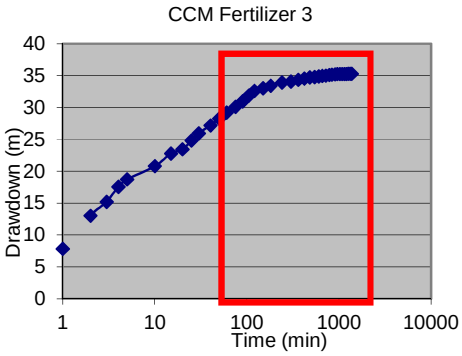
CCM Fertilizer 3
Drawdown (m)
40
35
30
25
20
15
10
5
0
1
10
100
1000
10000
Time (min)

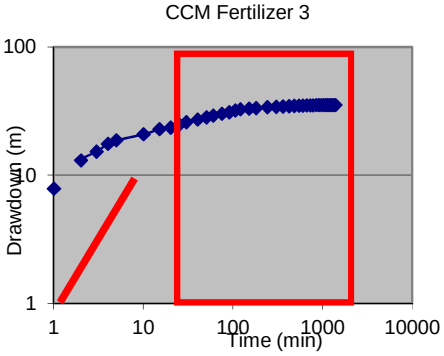
CCM Fertilizer 3
Drawdown (m)
100
10
1
1
10
100
1000
10000
Time (min)

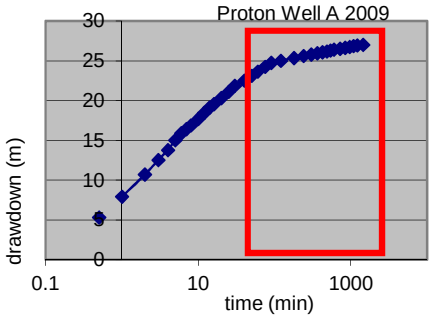
Proton Well A 2009
drawdown (m)
30
25
20
15
10
0
0.1
10
1000
time (min)

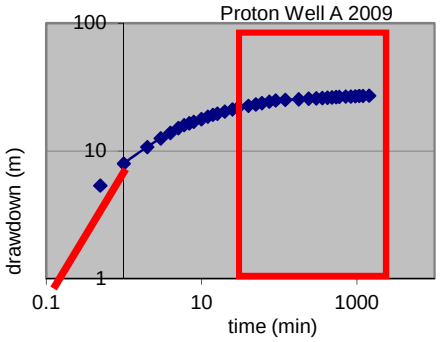
Proton Well A 2009
drawdown (m)
100
10
1
0.1
10
1000
time (min)

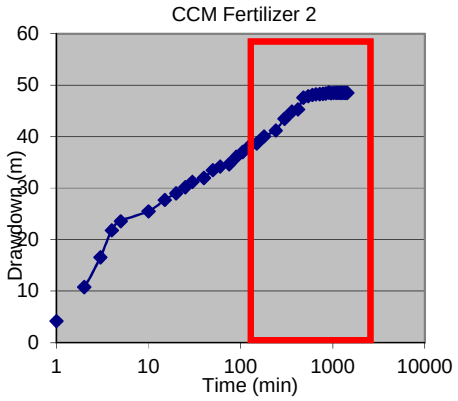
CCM Fertilizer 2
Drawdown (m)
Time (min)

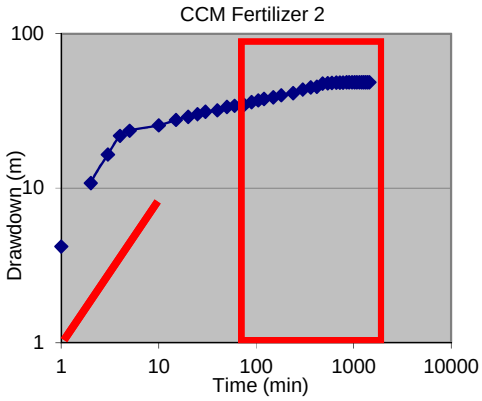
CCM Fertilizer 2
Drawdown (m)
Time (min)

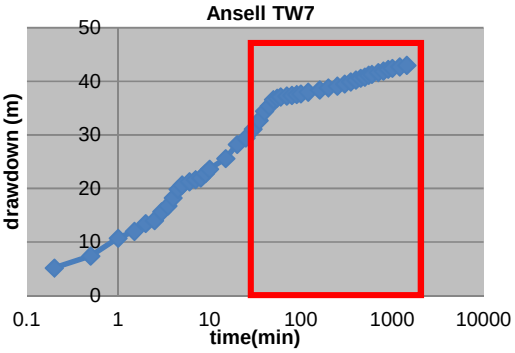
Ansell TW7
drawdown (m)
time(min)

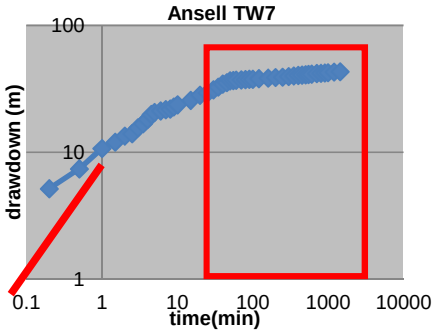
Ansell TW7
drawdown (m)
time(min)

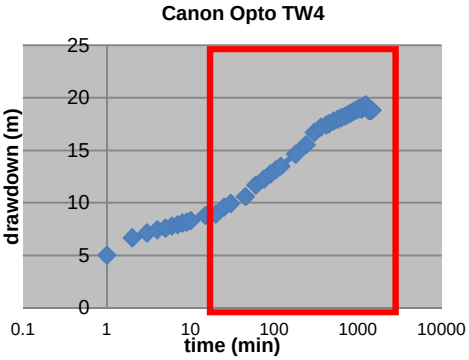
Canon Opto TW4
drawdown (m)
time (min)

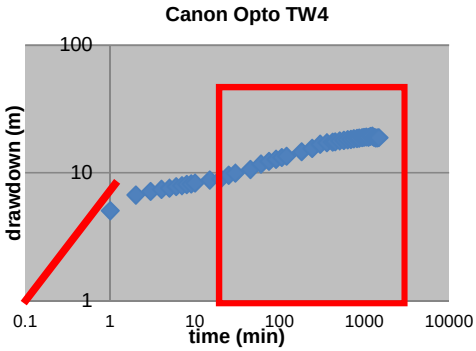
Canon Opto TW4
drawdown (m)
time (min)

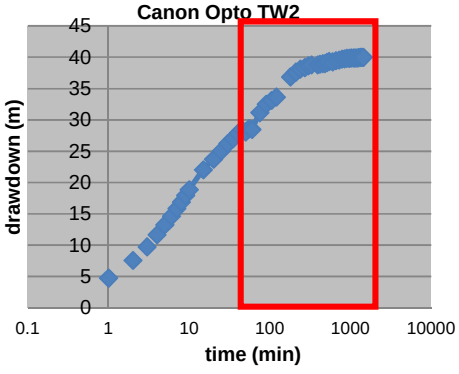
Canon Opto TW2
drawdown (m)
time (min)

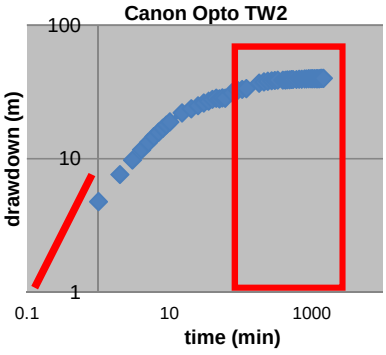
Canon Opto TW2
drawdown (m)
time (min)

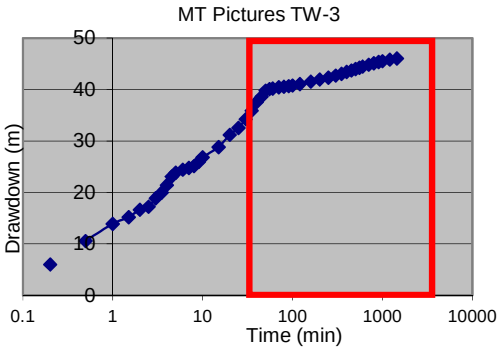
MT Pictures TW-3
Drawdown (m)
Time (min)

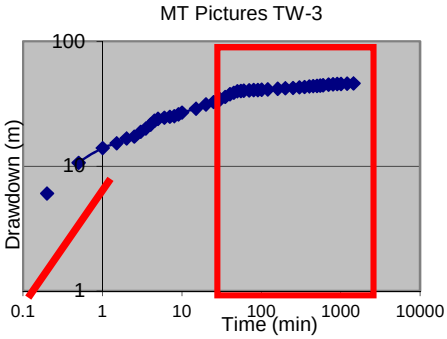
MT Pictures TW-3
Drawdown (m)
Time (min)

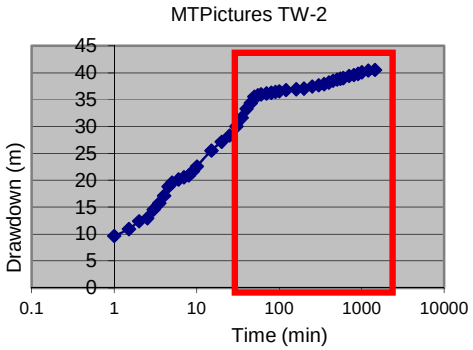
MTPictures TW-2
Drawdown (m)
Time (min)

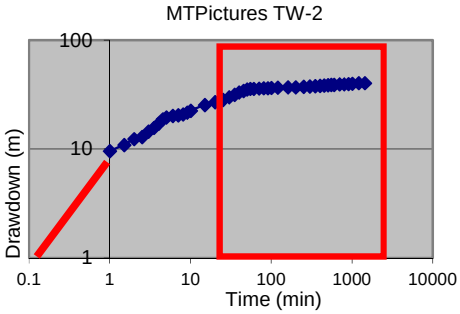
MTPictures TW-2
Drawdown (m)
Time (min)

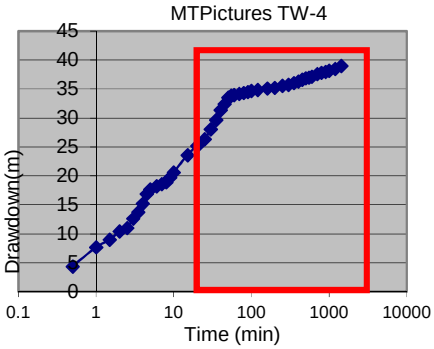
MTPictures TW-4
Drawdown(m)
Time (min)

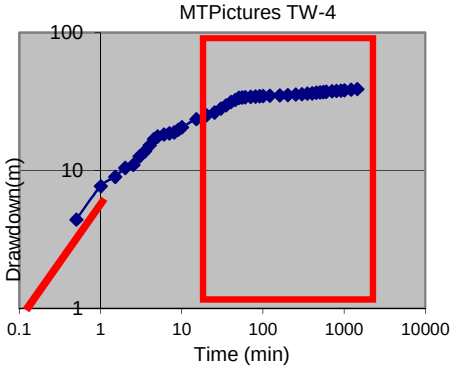
MTPictures TW-4
Drawdown(m)
Time (min)

Class D

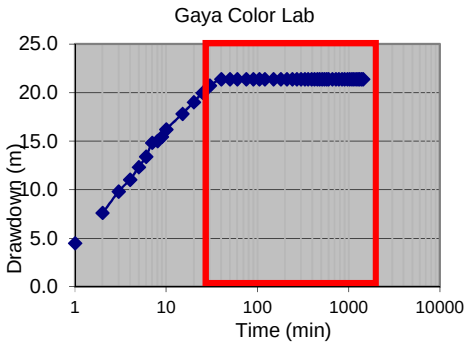
Gaya Color Lab
Drawdown (m)
Time (min)

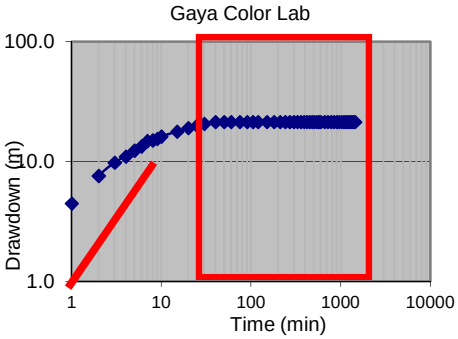
Gaya Color Lab
Drawdown (m)
Time (min)

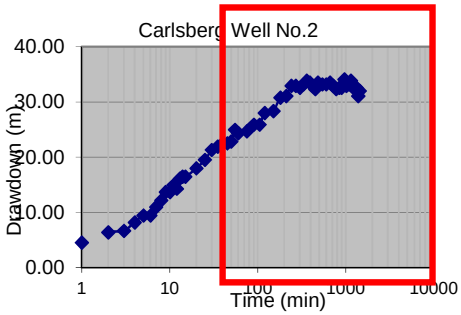
Carlsberg Well No.2
Drawdown (m)
40.00
30.00
20.00
10.00
0.00
1
10
100
1000
10000
Time (min)

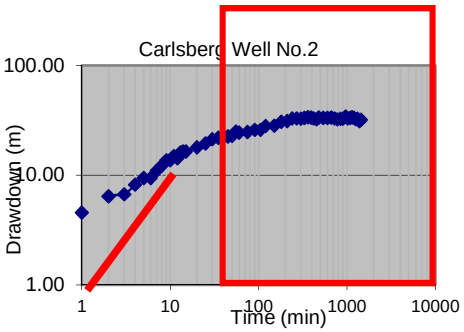
Carlsberg Well No.2
Drawdown (m)
100.00
10.00
1.00
1
10
100
1000
10000
Time (min)

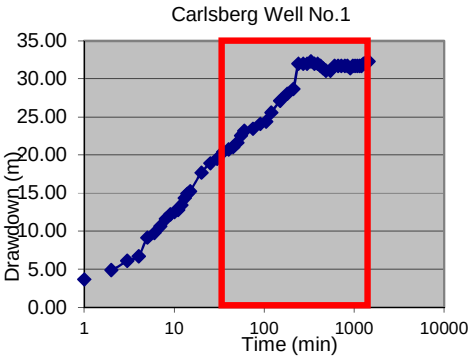
Carlsberg Well No.1
Drawdown (m)
35.00
30.00
25.00
20.00
15.00
10.00
5.00
0.00
1
10
100
1000
10000
Time (min)

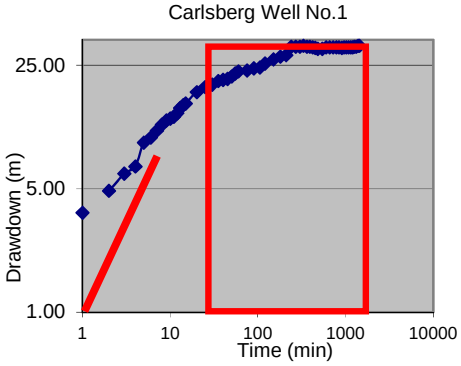
Carlsberg Well No.1
Drawdown (m)
25.00
5.00
1.00
1
10
100
1000
10000
Time (min)

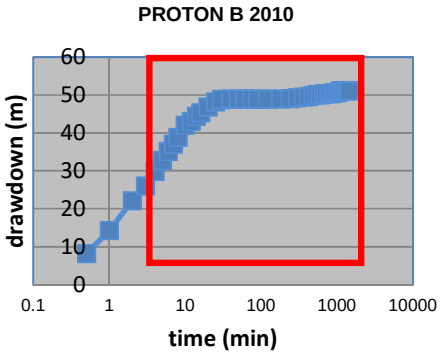
PROTON B 2010
drawdown (m)
60
50
40
30
20
10
0
0.1
1
10
100
1000
10000
time (min)

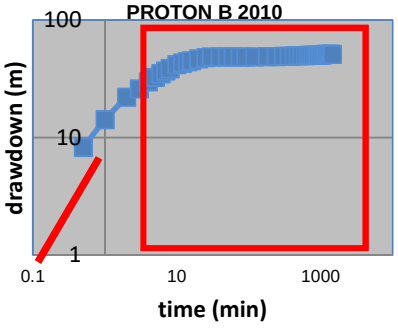
PROTON B 2010
drawdown (m)
100
10
1
0.1
10
1000
time (min)

Class E

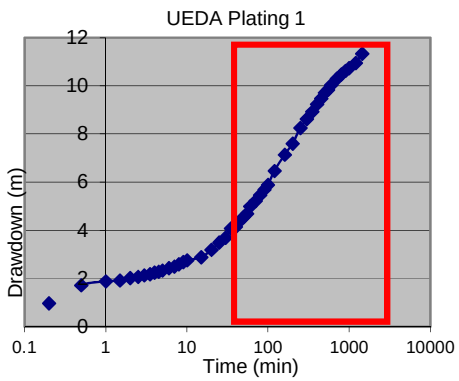
UEDA Plating 1
Drawdown (m)
Time (min)
0.1
1
10
100
1000
10000
0
2
4
6
8
10
12

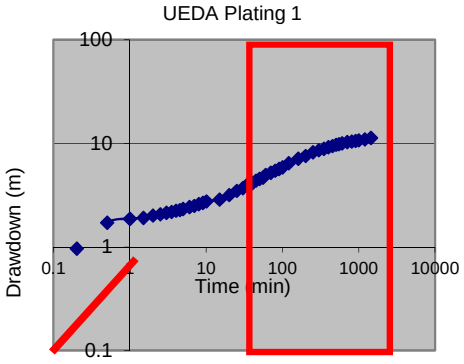
UEDA Plating 1
Drawdown (m)
Time (min)
0.1
1
10
100
1000
10000
0.1
1
10
100

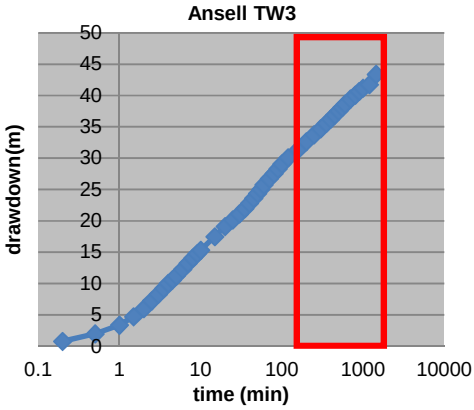
Ansell TW3
drawdown(m)
time (min)
0.1
1
10
100
1000
10000
0
5
10
15
20
25
30
35
40
45
50

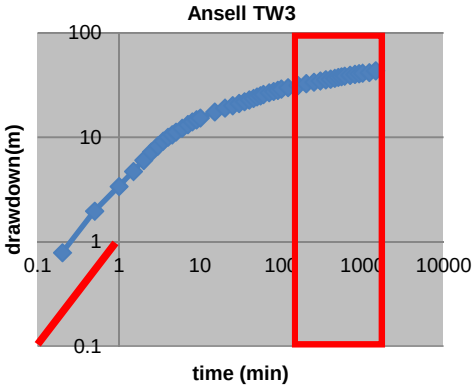
Ansell TW3
drawdown(m)
time (min)
0.1
1
10
100
1000
10000
0.1
1
10
100

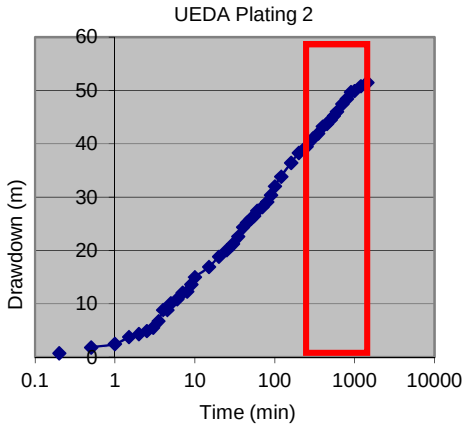
UEDA Plating 2
Drawdown (m)
Time (min)
0.1
1
10
100
1000
10000
0
10
20
30
40
50
60

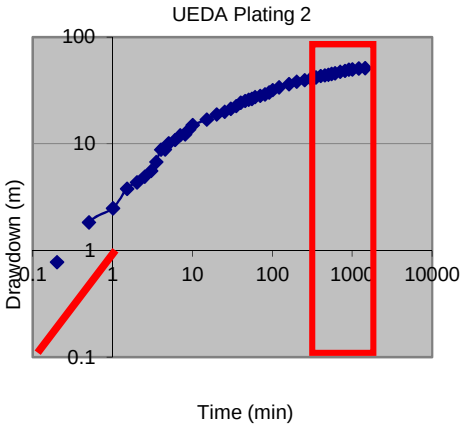
UEDA Plating 2
Drawdown (m)
Time (min)
0.1
1
10
100
1000
10000
0.1
1
10
100

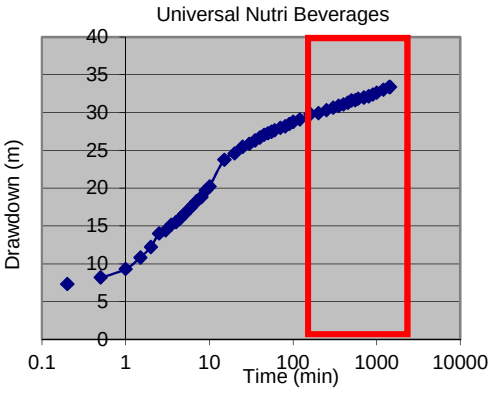
Universal Nutri Beverages
Drawdown (m)
Time (min)
0
5
10
15
20
25
30
35
40
0.1
1
10
100
1000
10000

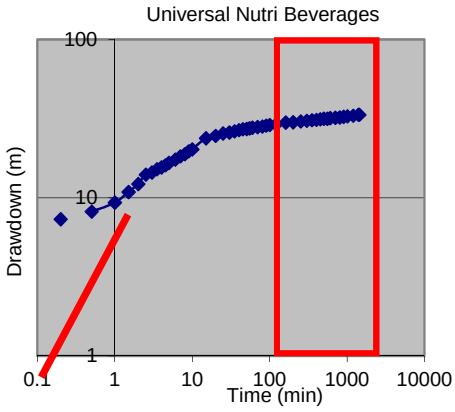
Universal Nutri Beverages
Drawdown (m)
Time (min)
1
10
100
0.1
1
10
100
1000
10000

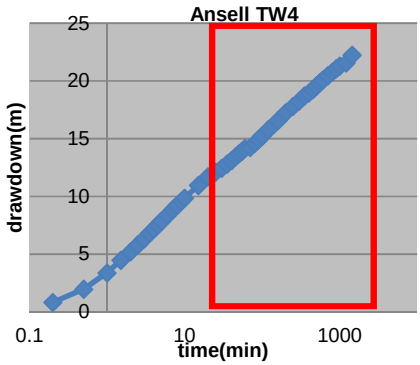
Ansell TW4
drawdown(m)
time(min)
0
5
10
15
20
25
0.1
10
1000

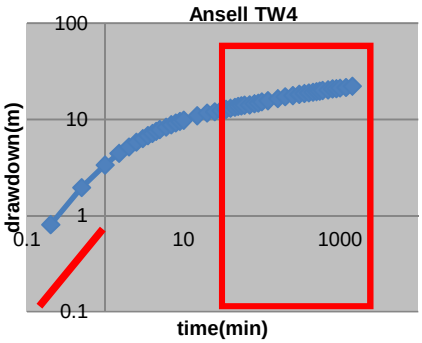
Ansell TW4
drawdown(m)
time(min)
0.1
1
10
100
0.1
10
1000

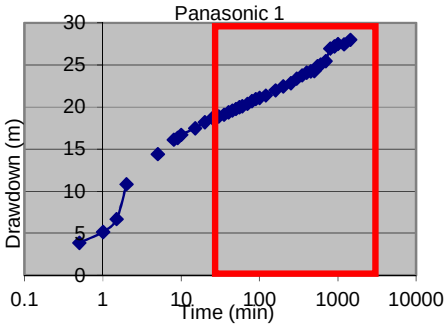
Panasonic 1
Drawdown (m)
Time (min)
0
5
10
15
20
25
30
0.1
1
10
100
1000
10000

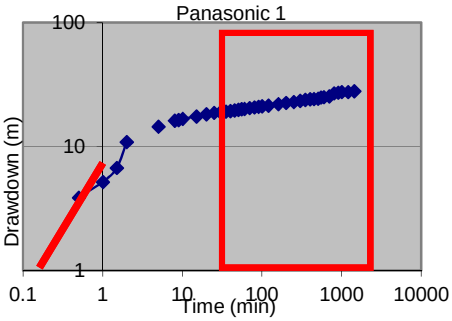
Panasonic 1
Drawdown (m)
Time (min)
1
10
100
0.1
1
10
100
1000
10000

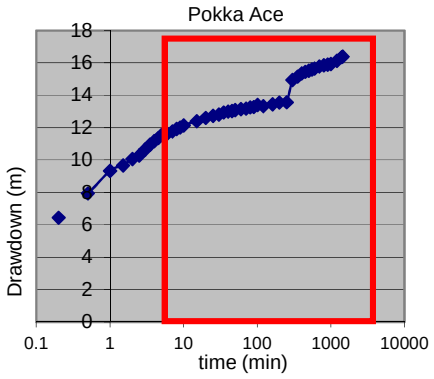
Pokka Ace
Drawdown (m)
time (min)

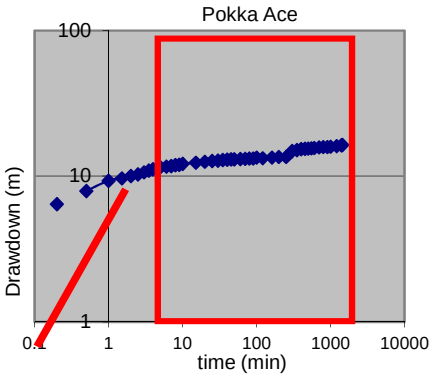
Pokka Ace
Drawdown (m)
time (min)

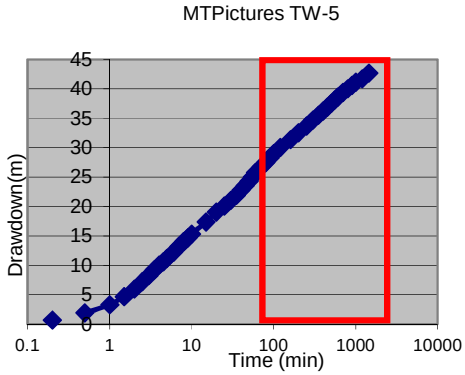
MTPictures TW-5
Drawdown(m)
Time (min)

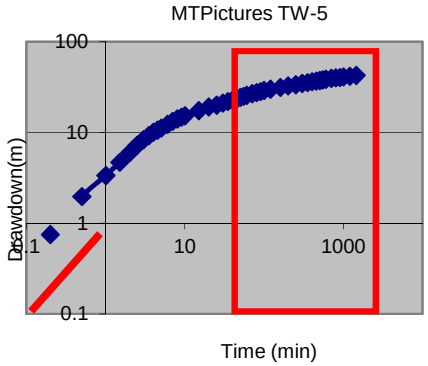
MTPictures TW-5
Drawdown(m)
Time (min)

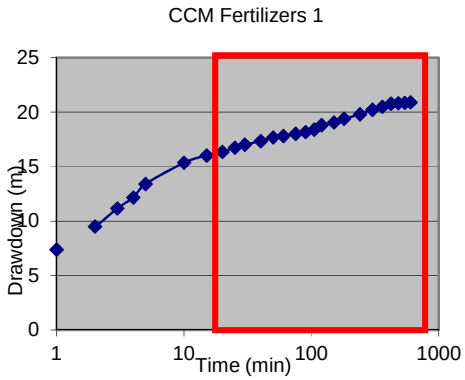
CCM Fertilizers 1
Drawdown (m)
Time (min)

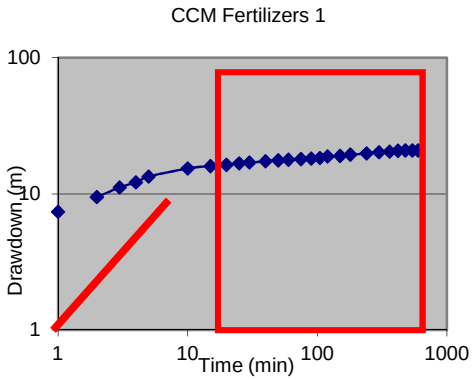
CCM Fertilizers 1
Drawdown (m)
Time (min)

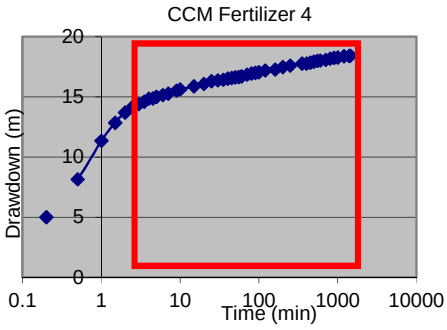
CCM Fertilizer 4
Drawdown (m)
Time (min)

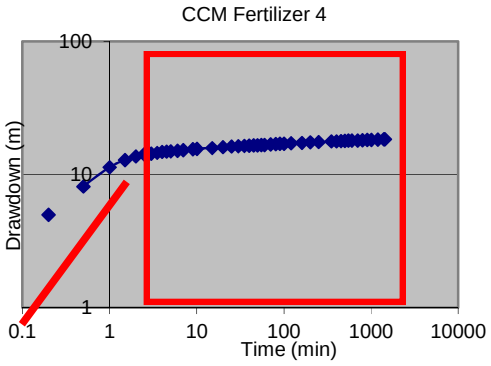
CCM Fertilizer 4
Drawdown (m)
Time (min)

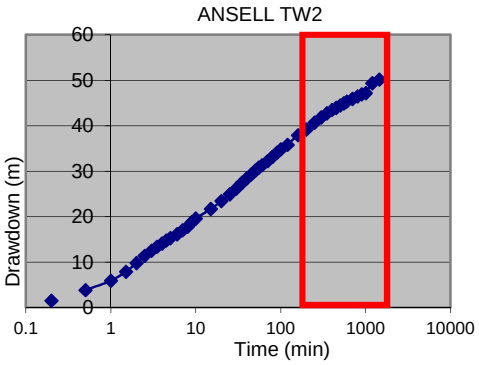
ANSELL TW2
Drawdown (m)
Time (min)
0
10
20
30
40
50
60
0.1
1
10
100
1000
10000

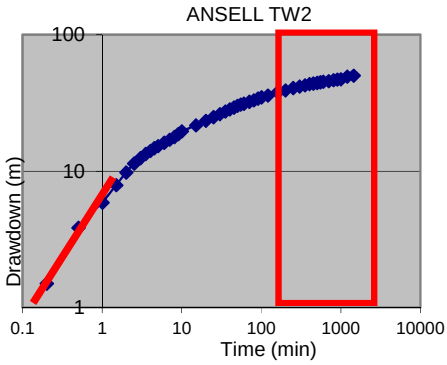
ANSELL TW2
Drawdown (m)
Time (min)
1
10
100
0.1
1
10
100
1000
10000

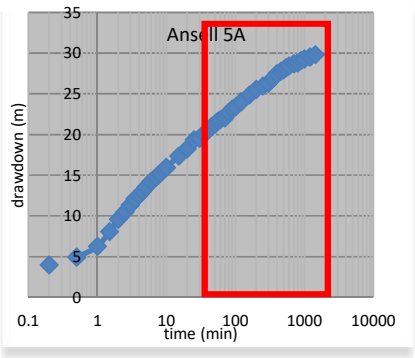
Ansell 5A
drawdown (m)
time (min)
0
5
10
15
20
25
30
35
0.1
1
10
100
1000
10000

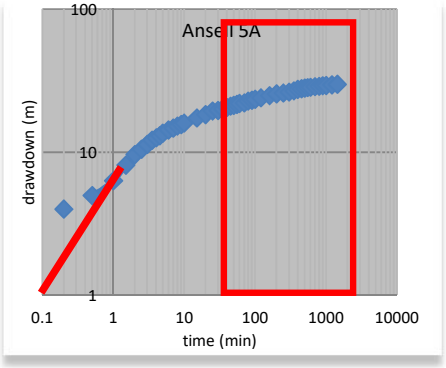
drawdown (m)
time (min)
1
10
100
0.1
1
10
100
1000
10000

APPENDIX B Wells that can be analysed using Eden & Hazel method

Aquatic International 2

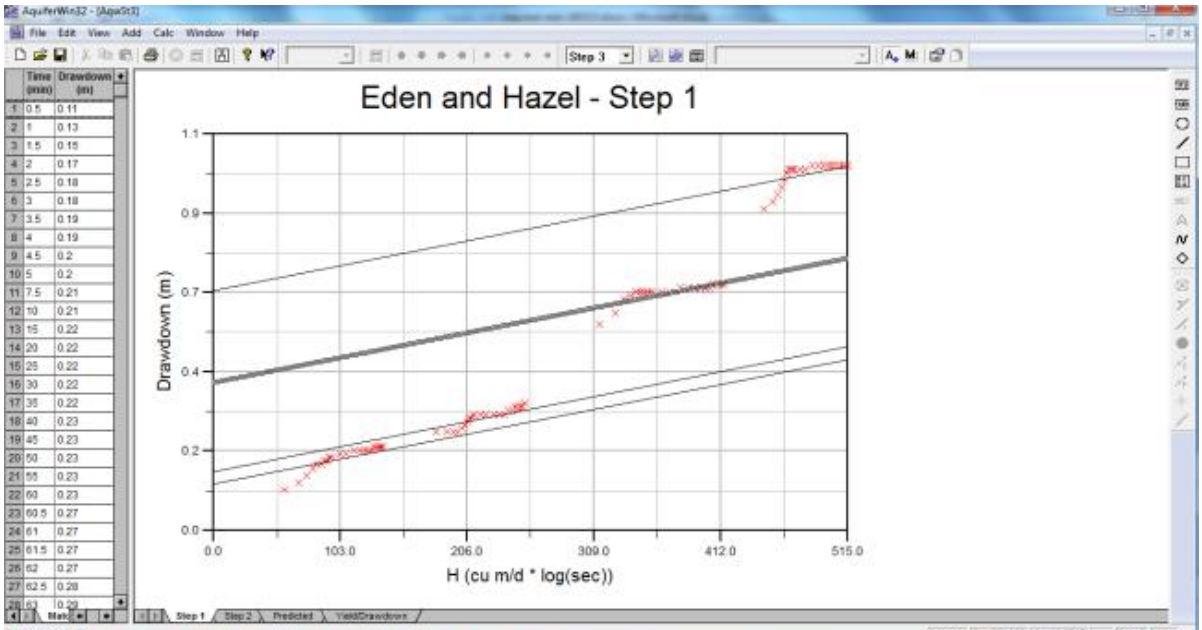

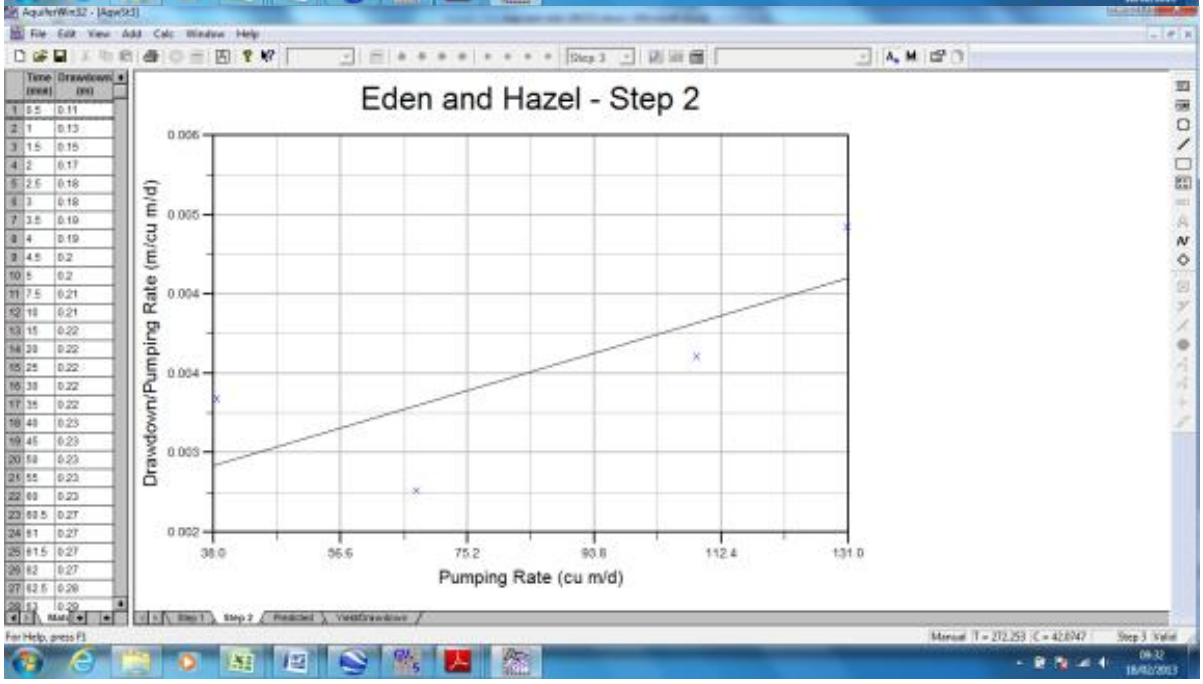

Aquarium Express

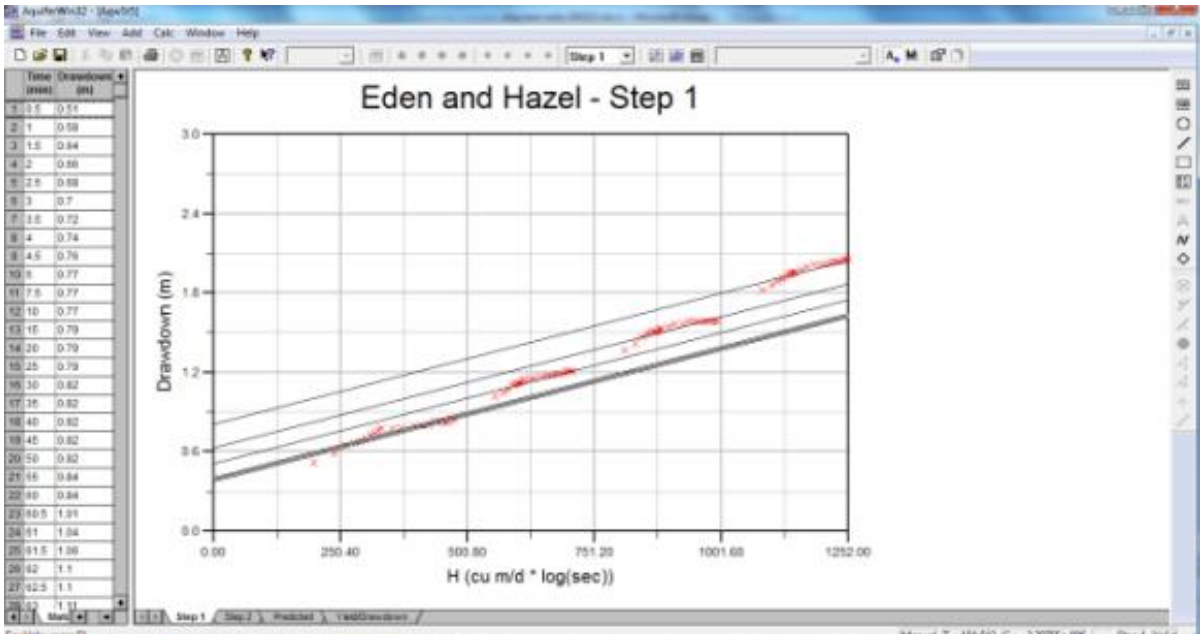

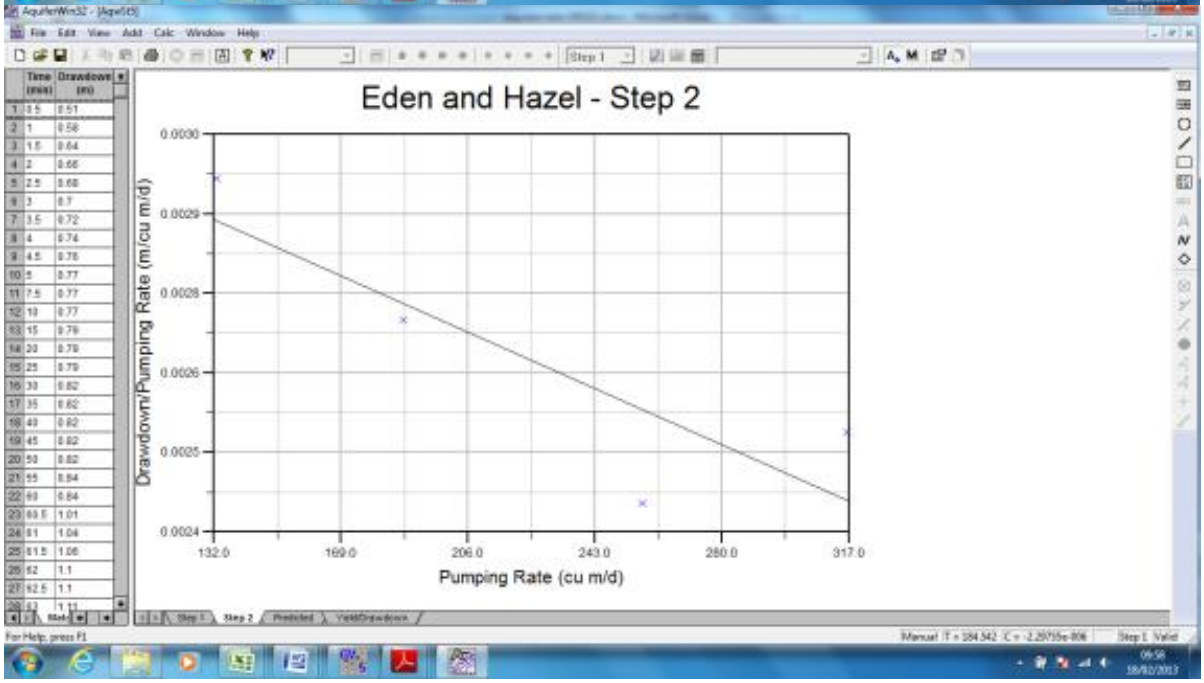

CCM Fertilizer TW4

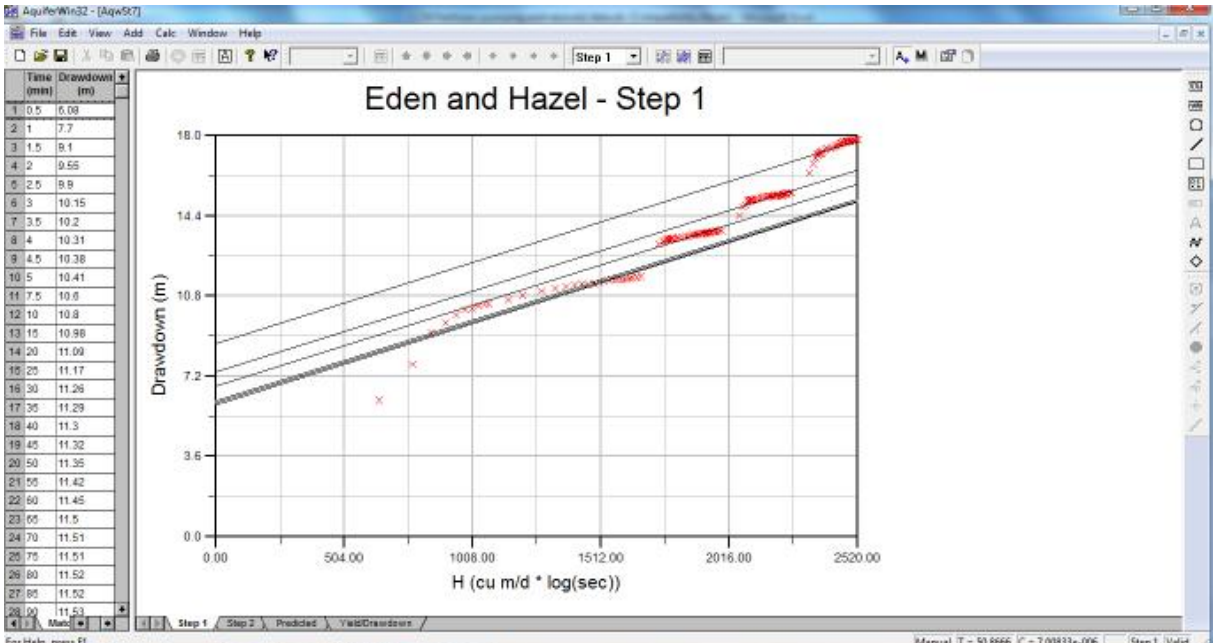

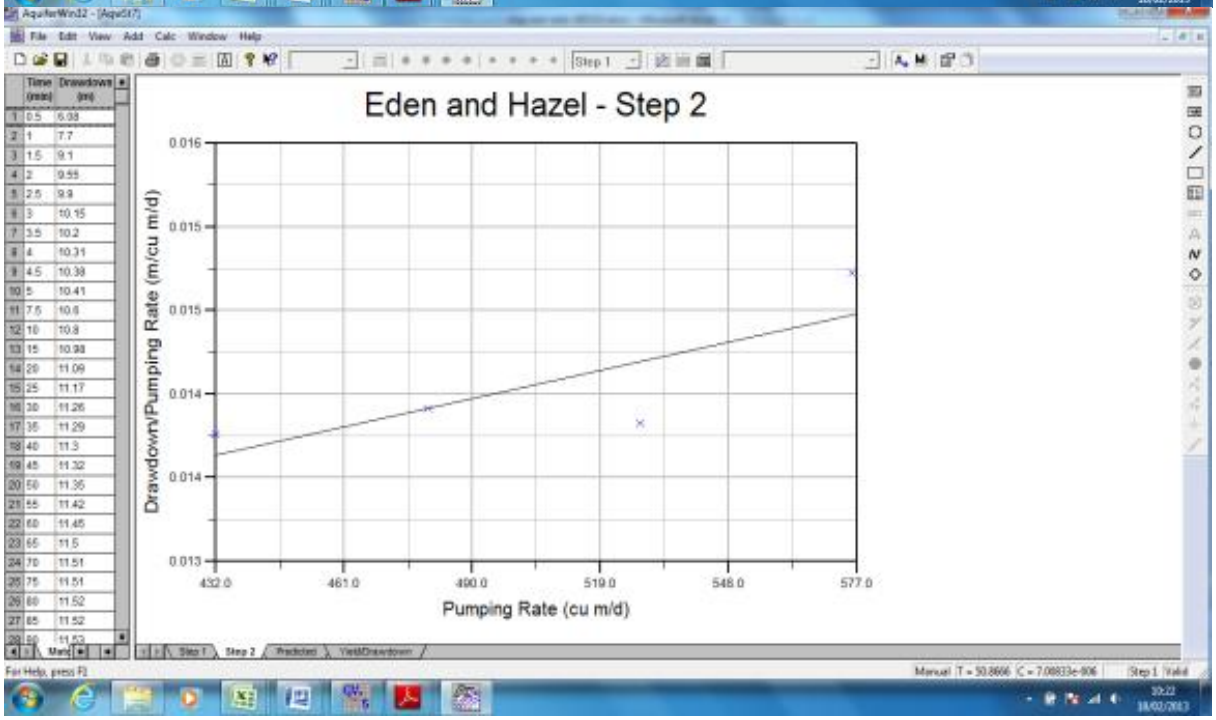

Pokka Ace

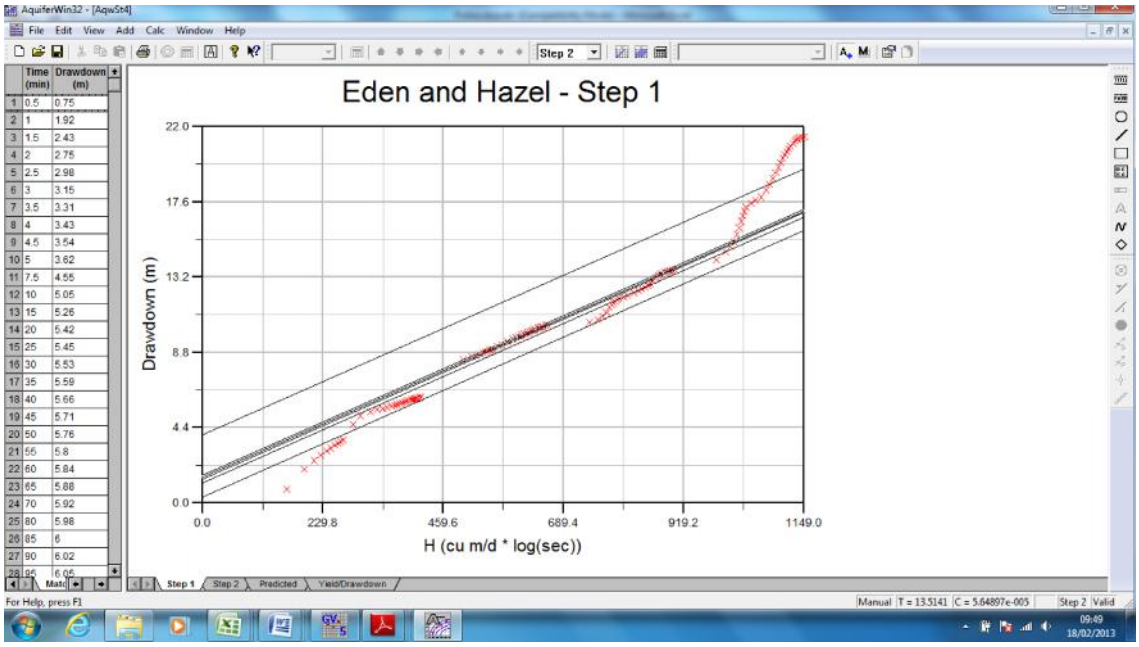
AquiferWin32 - [Aqw5t4]
File Edit View Add Calc Window Help
Step 2
Time (min) Drawdown (m)
1 0.5 0.75
2 1 1.92
3 1.5 2.43
4 2 2.75
5 2.5 2.98
6 3 3.15
7 3.5 3.31
8 4 3.43
9 4.5 3.54
10 5 3.62
11 7.5 4.55
12 10 5.05
13 15 5.26
14 20 5.42
15 25 5.45
16 30 5.53
17 35 5.59
18 40 5.66
19 45 5.71
20 50 5.76
21 55 5.8
22 60 5.84
23 65 5.88
24 70 5.92
25 80 5.98
26 85 6
27 90 6.02
Eden and Hazel - Step 1
Drawdown (m)
22.0
17.6
13.2
8.8
4.4
0.0
0.0
229.8
459.6
689.4
919.2
1149.0
H (cu m/d * log(sec))
Step 1 Step 2 Predicted Yield/Drawdown
For Help, press F1
Manual T = 13.5141 C = 5.64897e-005
Step 2 Valid
09:49
18/02/2013

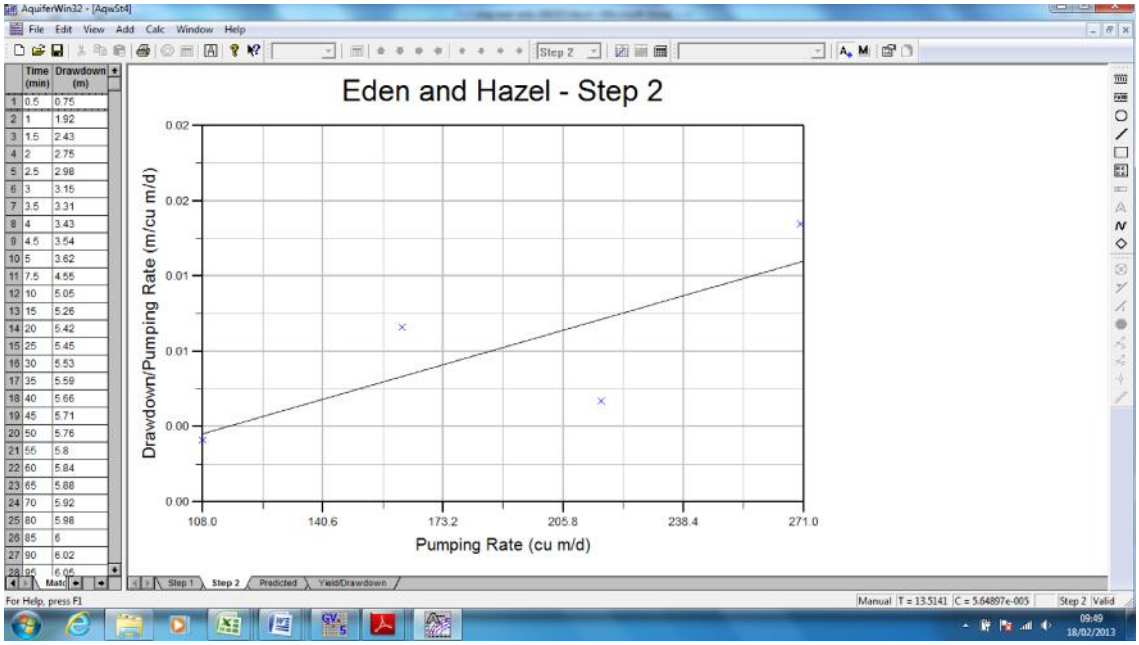
AquiferWin32 - [Aqw5t4]
File Edit View Add Calc Window Help
Step 2
Time (min) Drawdown (m)
1 0.5 0.75
2 1 1.92
3 1.5 2.43
4 2 2.75
5 2.5 2.98
6 3 3.15
7 3.5 3.31
8 4 3.43
9 4.5 3.54
10 5 3.62
11 7.5 4.55
12 10 5.05
13 15 5.26
14 20 5.42
15 25 5.45
16 30 5.53
17 35 5.59
18 40 5.66
19 45 5.71
20 50 5.76
21 55 5.8
22 60 5.84
23 65 5.88
24 70 5.92
25 80 5.98
26 85 6
27 90 6.02
Eden and Hazel - Step 2
Drawdown/Pumping Rate (m/cu m/d)
0.02
0.02
0.01
0.01
0.00
0.00
108.0
140.6
173.2
205.8
238.4
271.0
Pumping Rate (cu m/d)
Step 1 Step 2 Predicted Yield/Drawdown
For Help, press F1
Manual T = 13.5141 C = 5.64897e-005
Step 2 Valid
09:49
18/02/2013

Anshin Steel

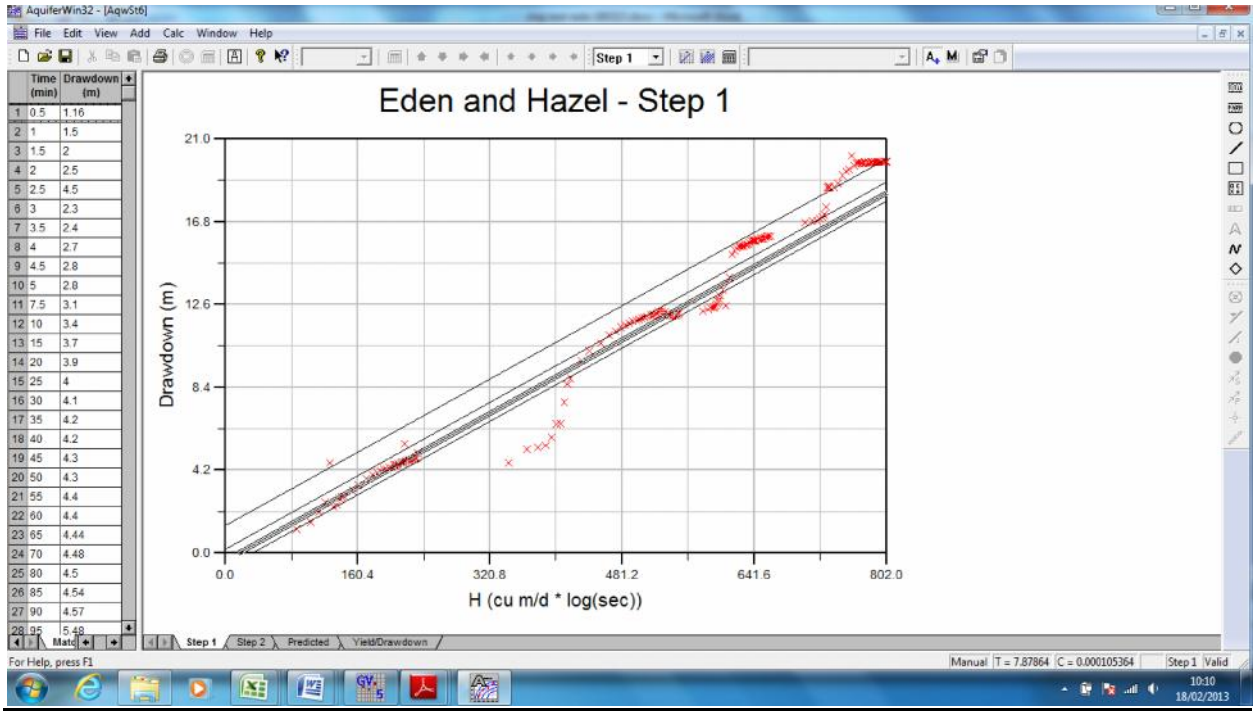

	Time (min)	Drawdown (m)
1	0.5	1.16
2	1	1.5
3	1.5	2
4	2	2.5
5	2.5	4.5
6	3	2.3
7	3.5	2.4
8	4	2.7
9	4.5	2.8
10	5	2.8
11	7.5	3.1
12	10	3.4
13	15	3.7
14	20	3.9
15	25	4
16	30	4.1
17	35	4.2
18	40	4.2
19	45	4.3
20	50	4.3
21	55	4.4
22	60	4.4
23	65	4.44
24	70	4.48
25	80	4.5
26	85	4.54
27	90	4.57
28	95	5.48

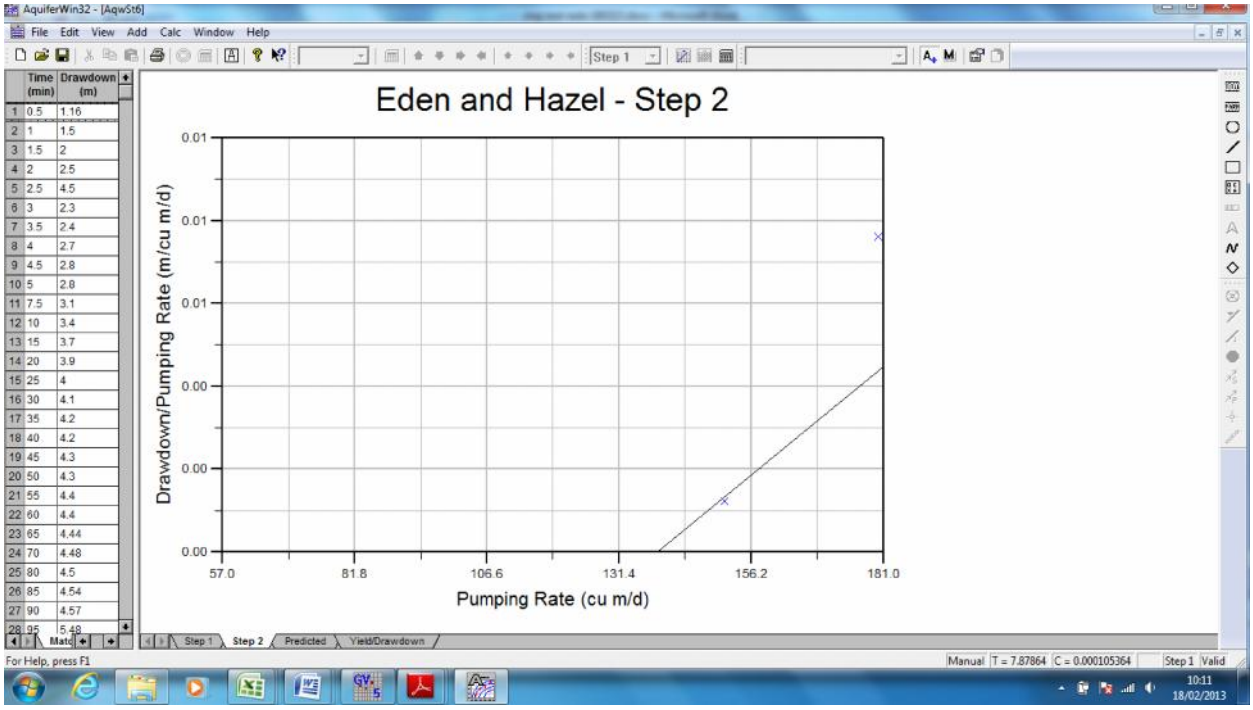

	Time (min)	Drawdown (m)
1	0.5	1.16
2	1	1.5
3	1.5	2
4	2	2.5
5	2.5	4.5
6	3	2.3
7	3.5	2.4
8	4	2.7
9	4.5	2.8
10	5	2.8
11	7.5	3.1
12	10	3.4
13	15	3.7
14	20	3.9
15	25	4
16	30	4.1
17	35	4.2
18	40	4.2
19	45	4.3
20	50	4.3
21	55	4.4
22	60	4.4
23	65	4.44
24	70	4.48
25	80	4.5
26	85	4.54
27	90	4.57
28	95	5.48

APPENDIX C Constant Yield Test Analysis using Cooper Jacob .

Class A

Aquatic International 3

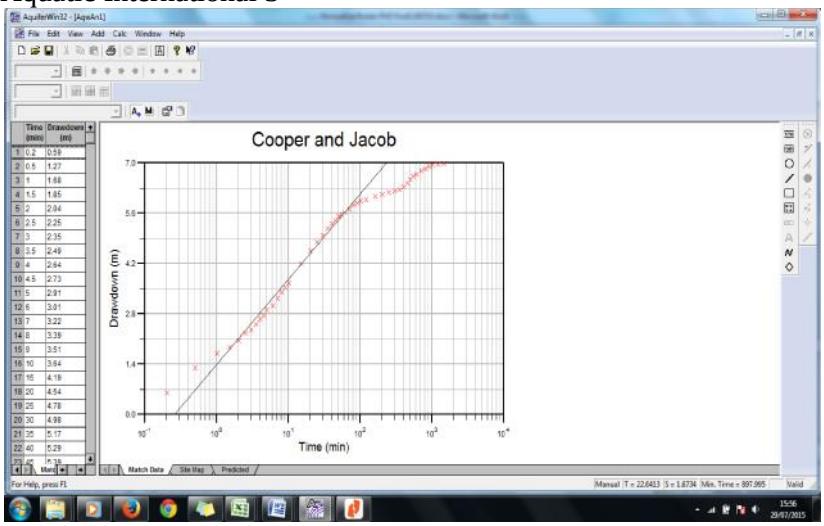

Well bore storage effect is negligible is when t > 1.52 min.

Aquarium Express

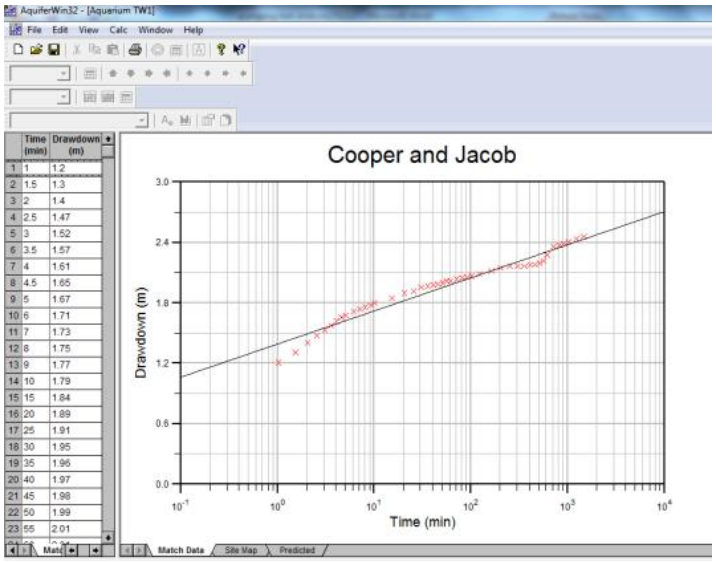

Well bore storage effect is negligible is when t > 0.94 min.

Aquatic International 2

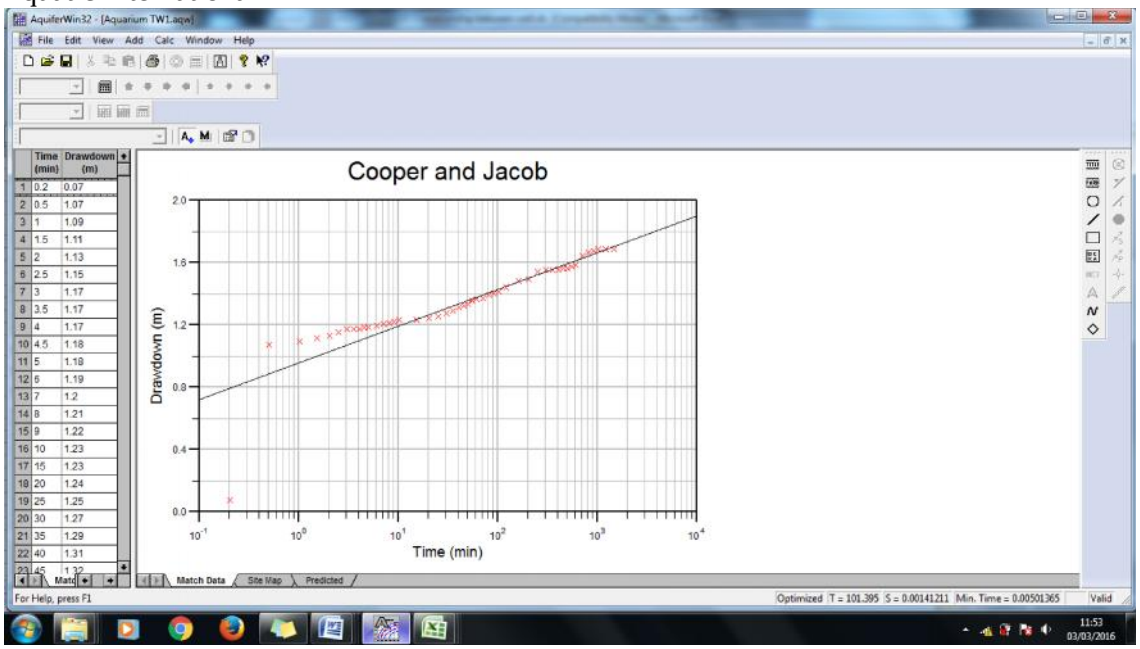

Well bore storage effect is negligible is when t > 1.52 min

Class B

Scientex Polymer

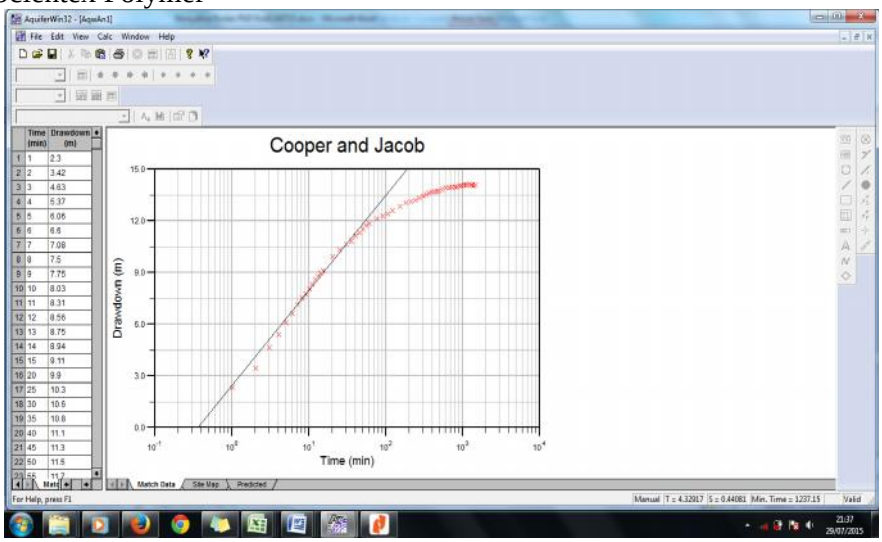

Well bore storage effect is negligible is when t > 28.48min

Anshin Steel

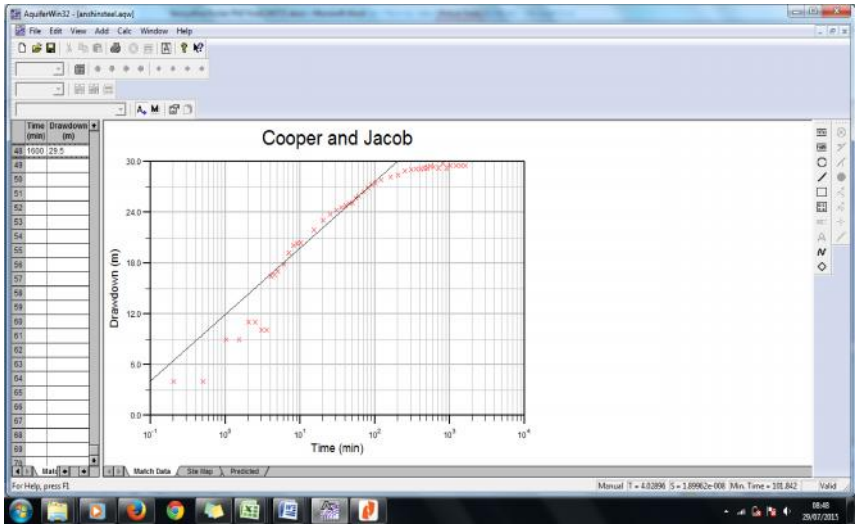

Well bore storage effect is negligible is when t > 29.35min

Panasonic 2

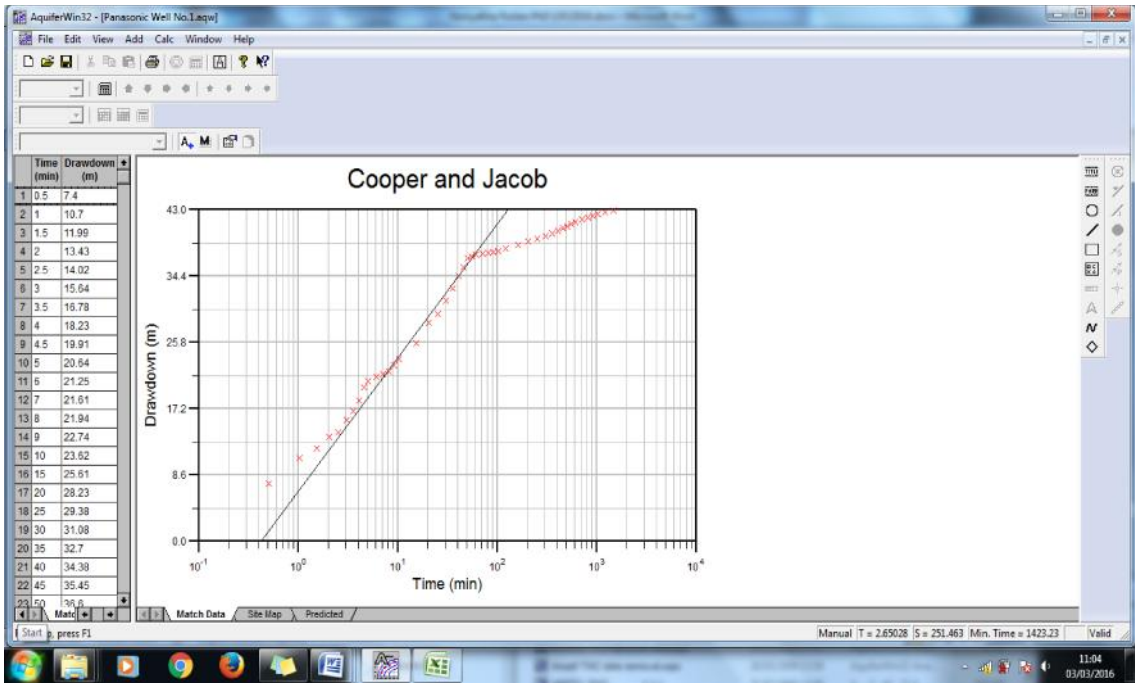

Well bore storage effect is negligible is when t > 37.44min

MT Picture 1

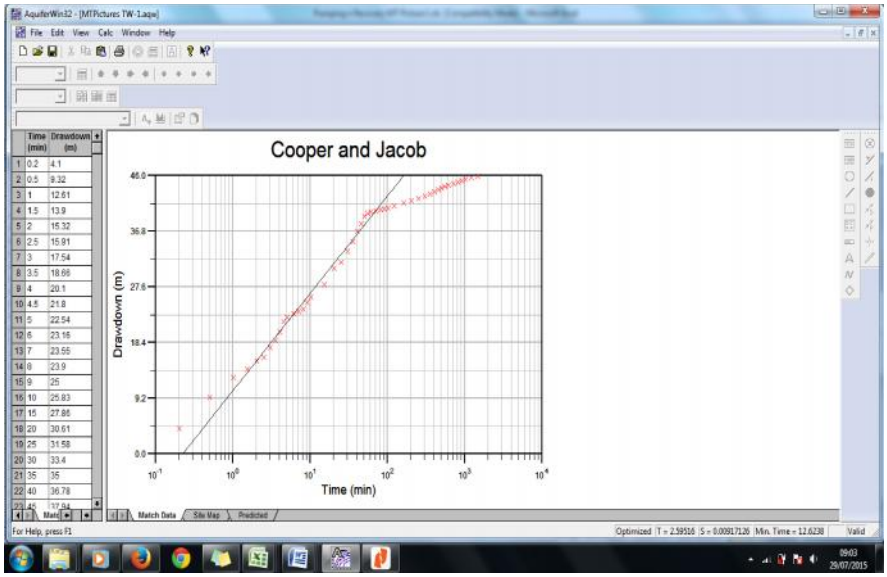

Well bore storage effect is negligible is when t > 24.26min

CCM Fertilizer 3

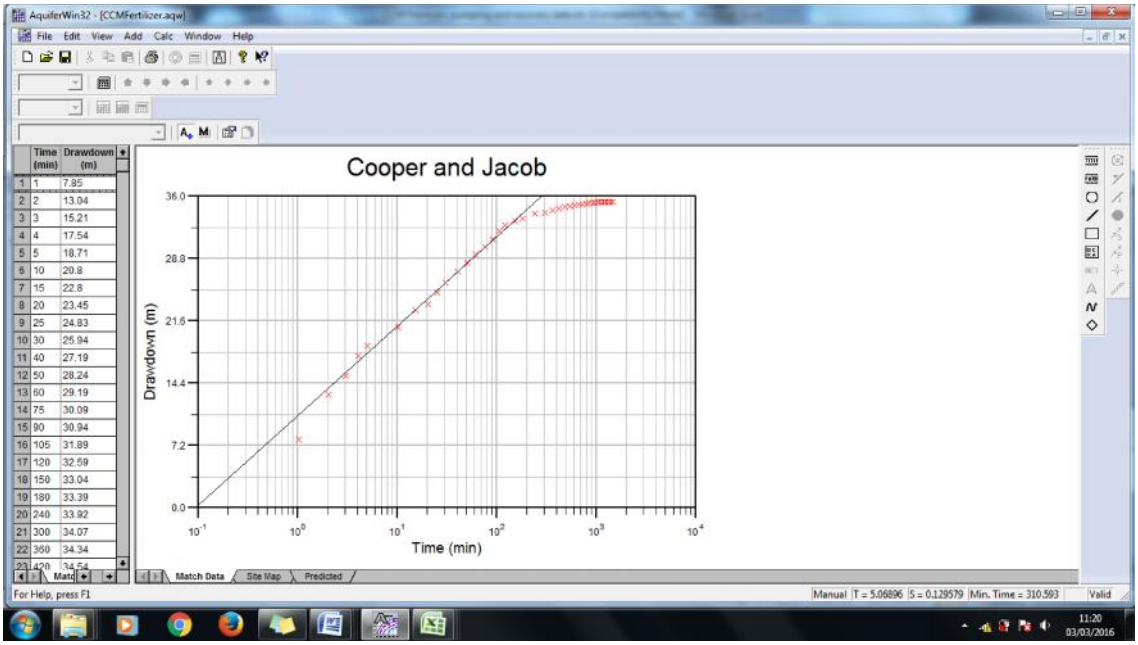

Well bore storage effect is negligible is when t > 41.75min

CCM Fertilizer 2

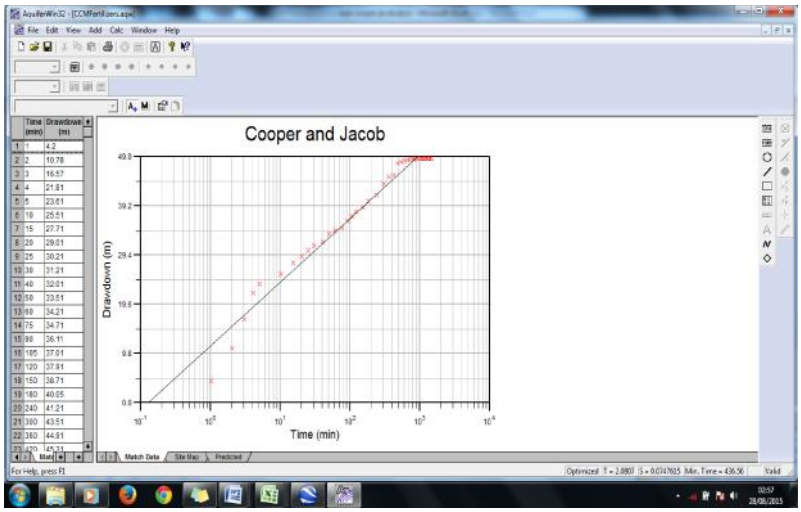

Well bore storage effect is negligible is when t > 84.73min

Ansell TW7

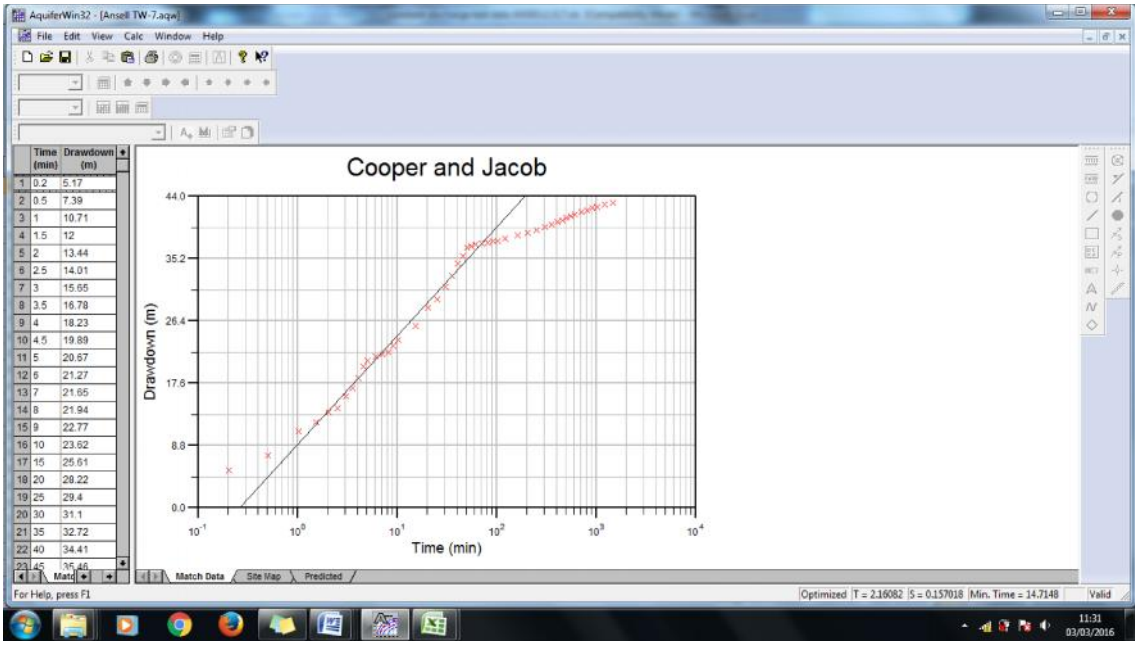

Well bore storage effect is negligible is when t > 31.39min

Canon Opto TW4

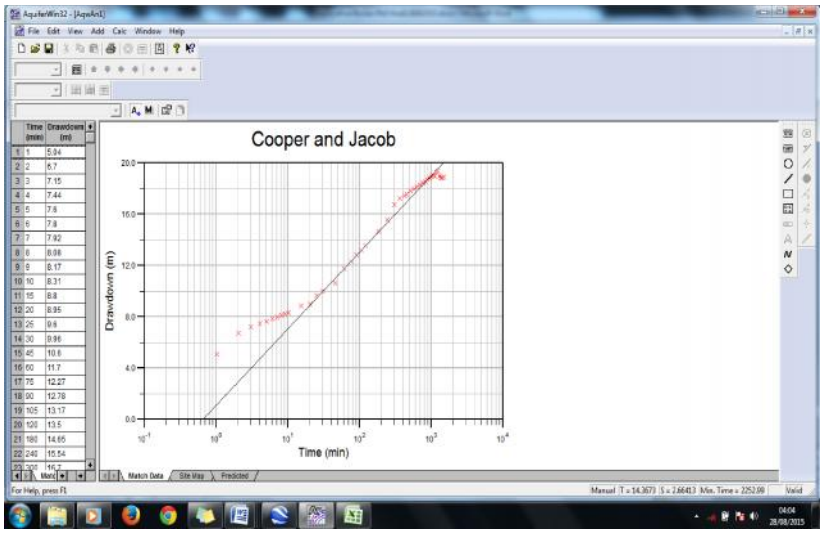

Well bore storage effect is negligible is when t > 10.98min

Canon Opto TW2

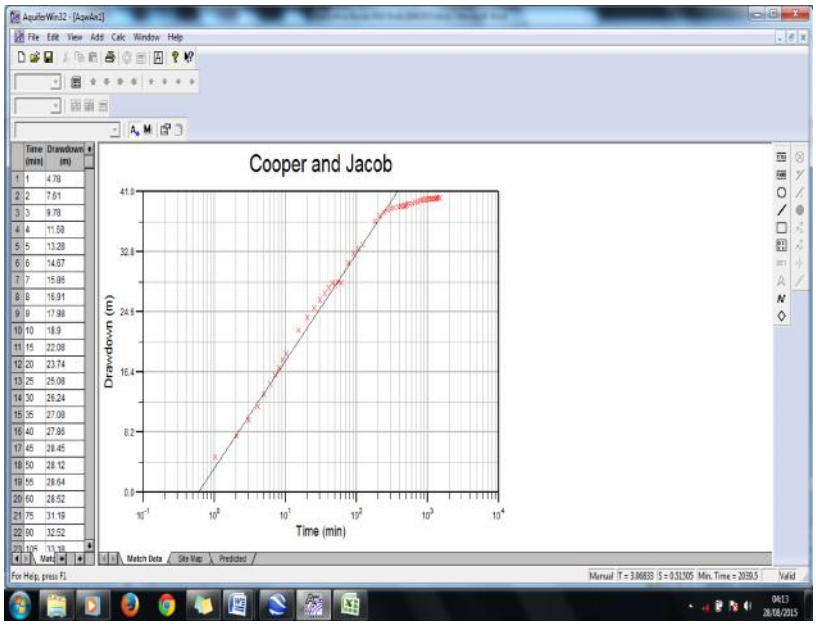

Well bore storage effect is negligible is when t > 63.48min

MT Picture TW3

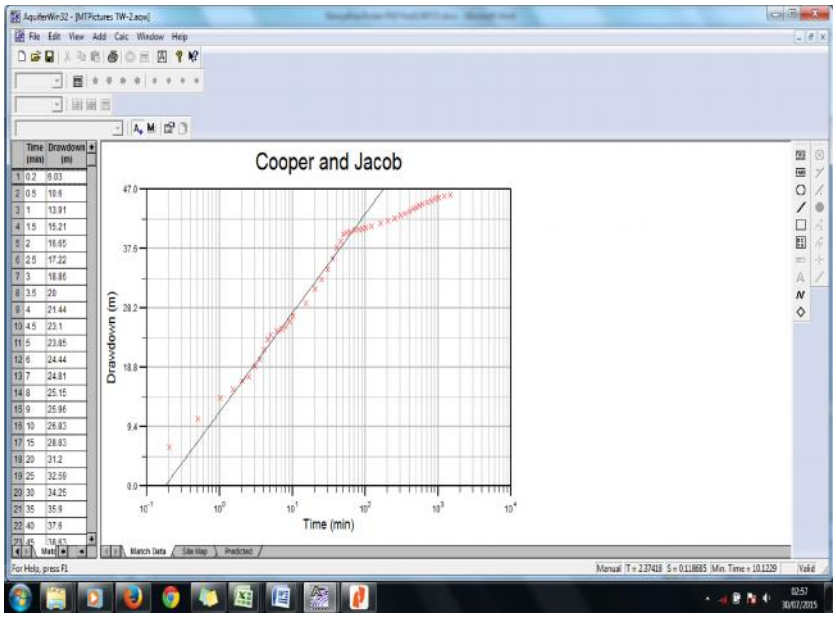

Well bore storage effect is negligible is when t > 27.12minMT Picture TW2

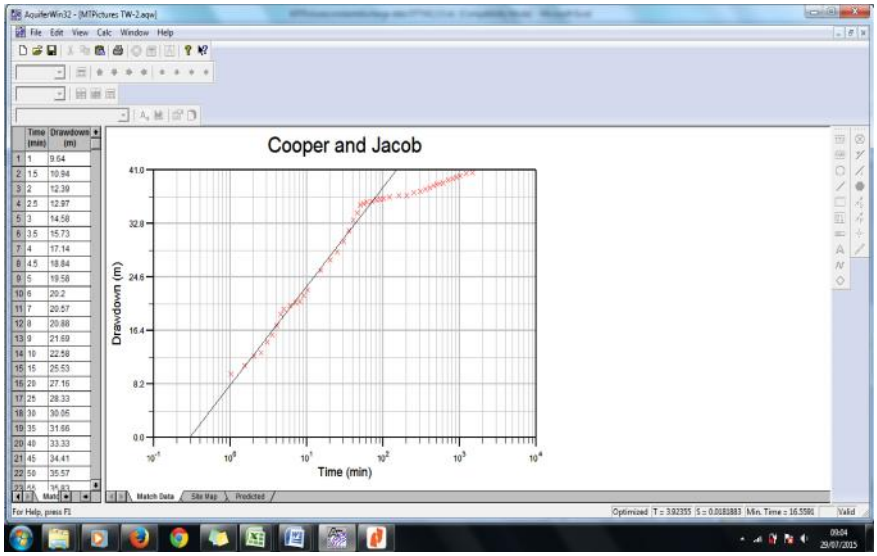

Well bore storage effect is negligible is when t > 11.37min

MT Picture TW4

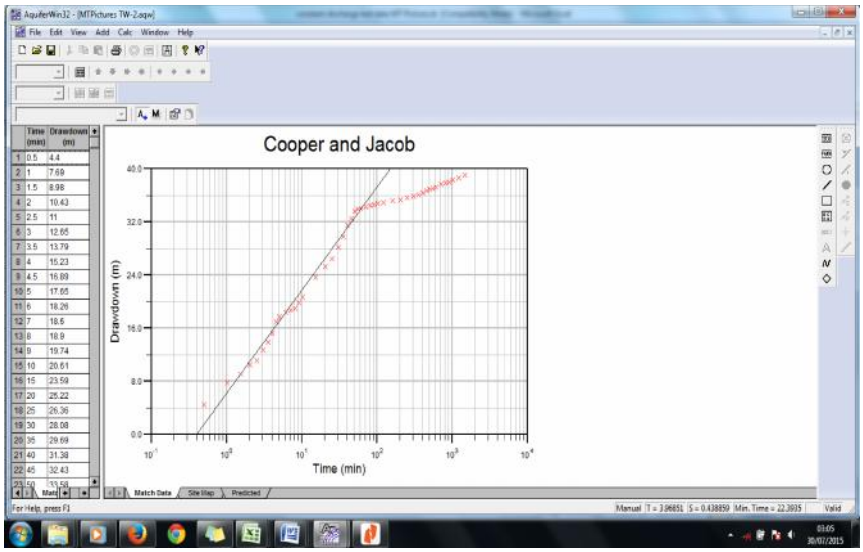

Well bore storage effect is negligible is when t > 11.95min

Ansell TW1

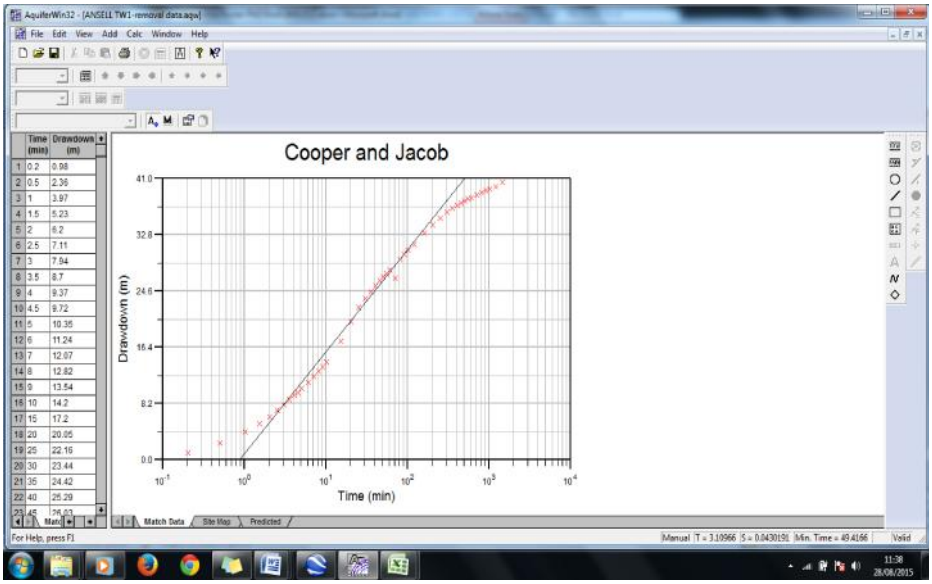

Well bore storage effect is negligible is when t > 79 min.

Ansell TW5

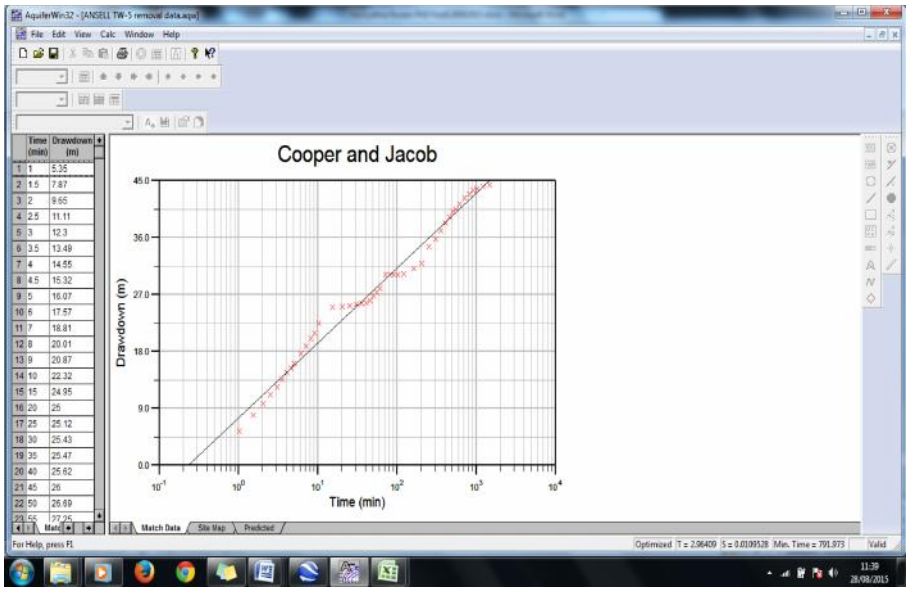

Well bore storage effect is negligible is when t > 106.79 min

Good Year

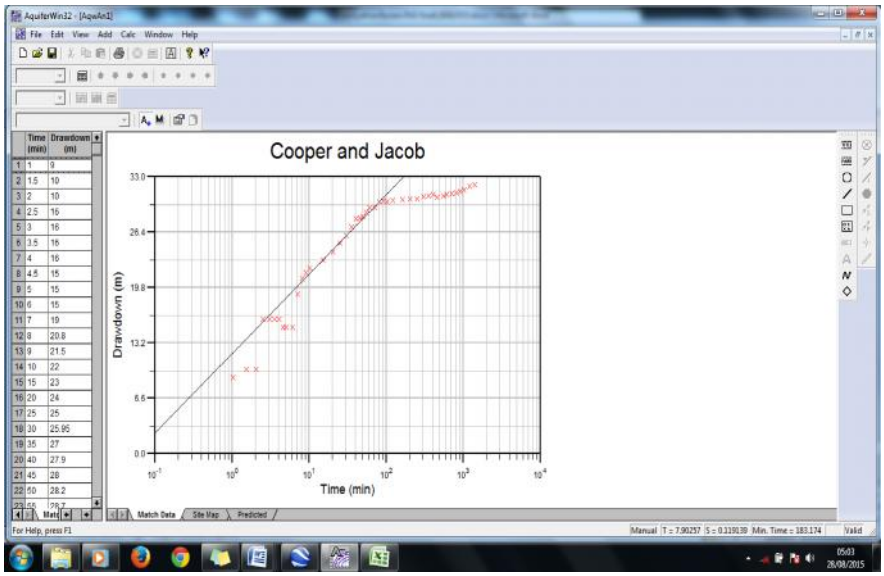

Well bore storage effect is negligible is when t > 21.7 min

Suzuki Latex

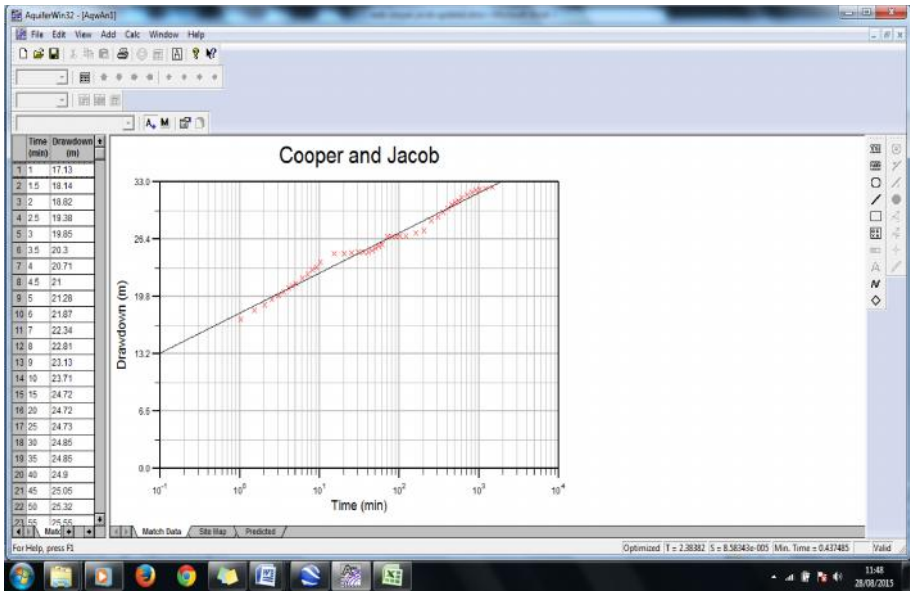

Well bore storage effect is negligible is when t > 54.58min

Proton A

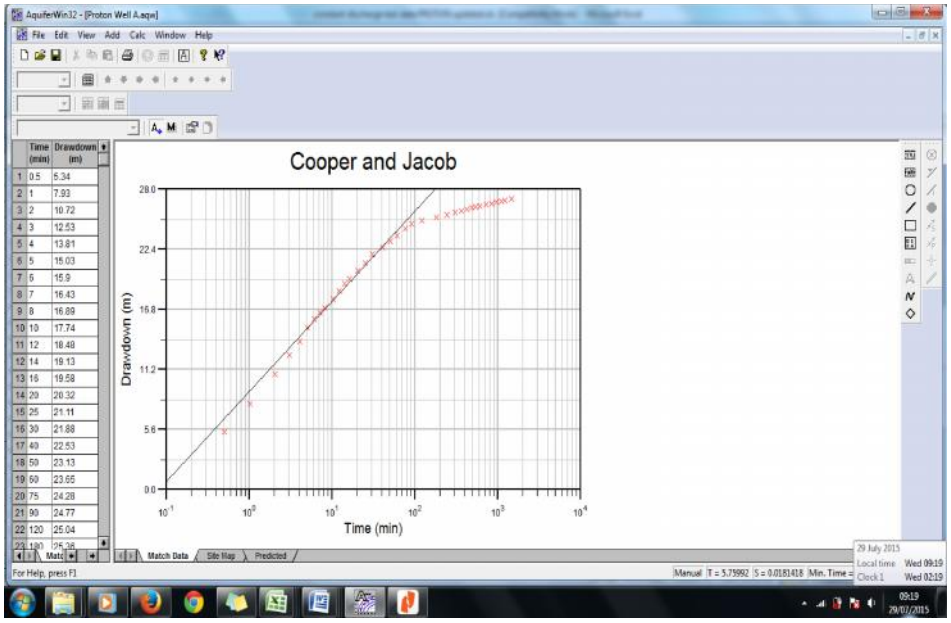

Well bore storage effect is negligible is when t > 29.91min

Class C

Ansell TW6

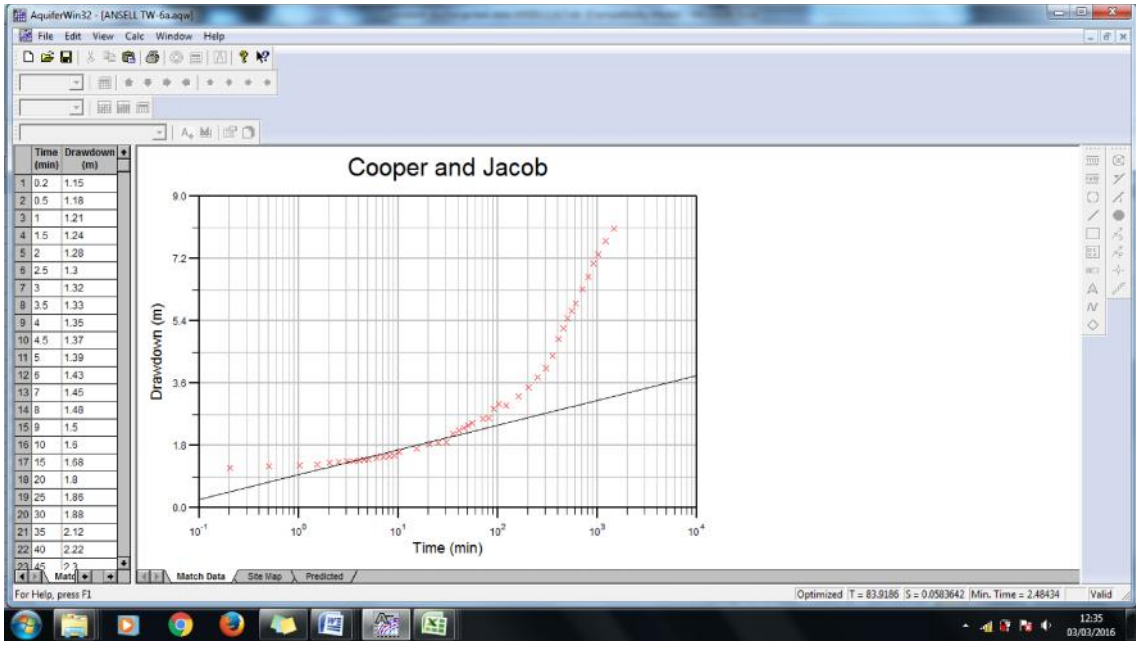

Well bore storage effect is negligible is when t > 4.82min

Canon Opto TW1

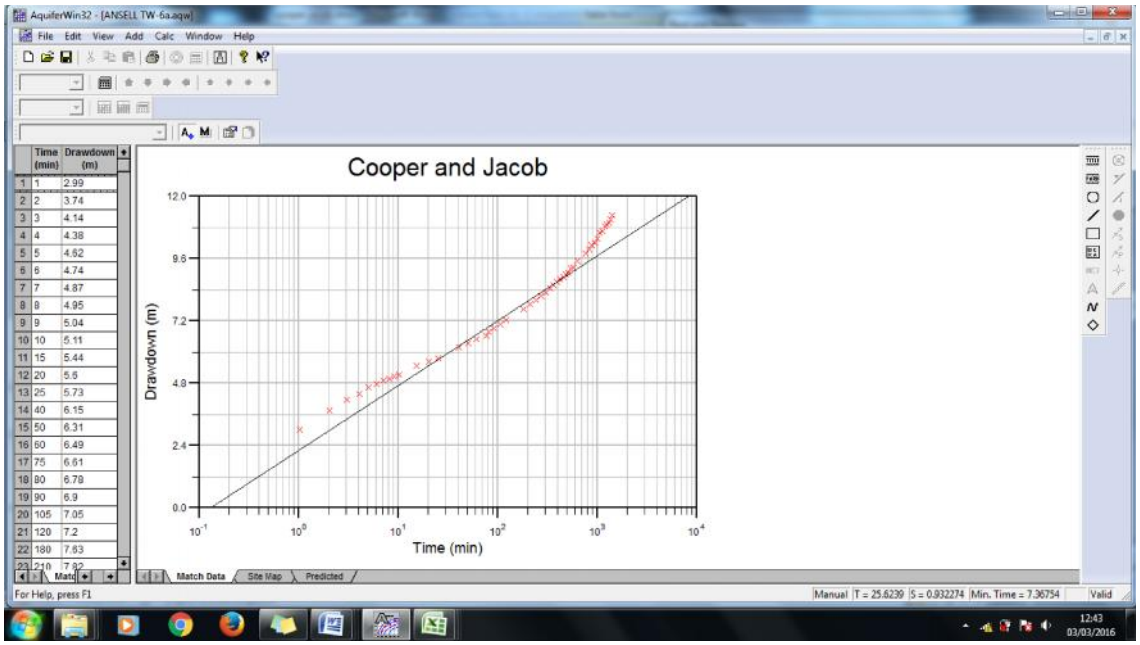

Well bore storage effect is negligible is when t > 6.06min

Class D

AESBI

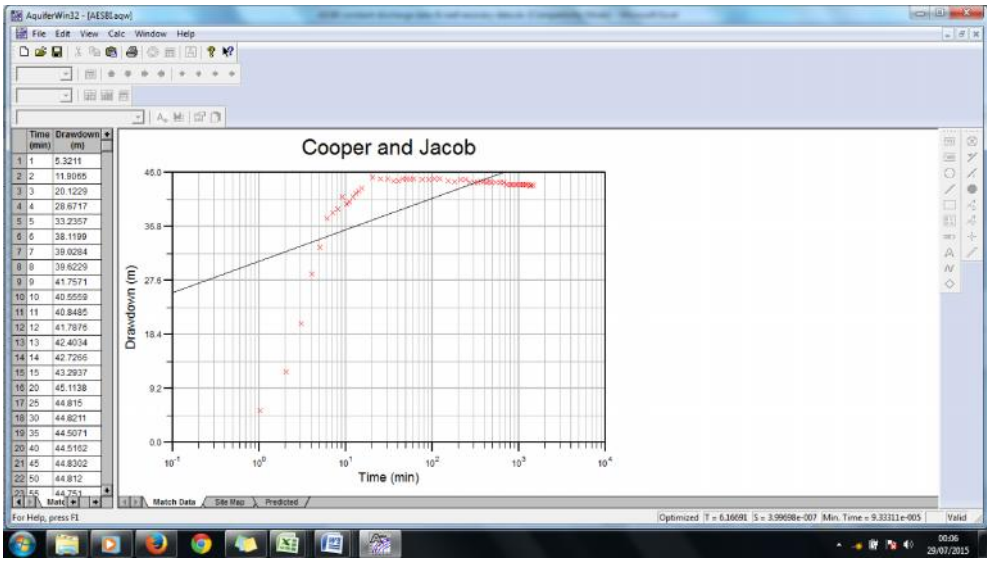

Carlsberg Well 2

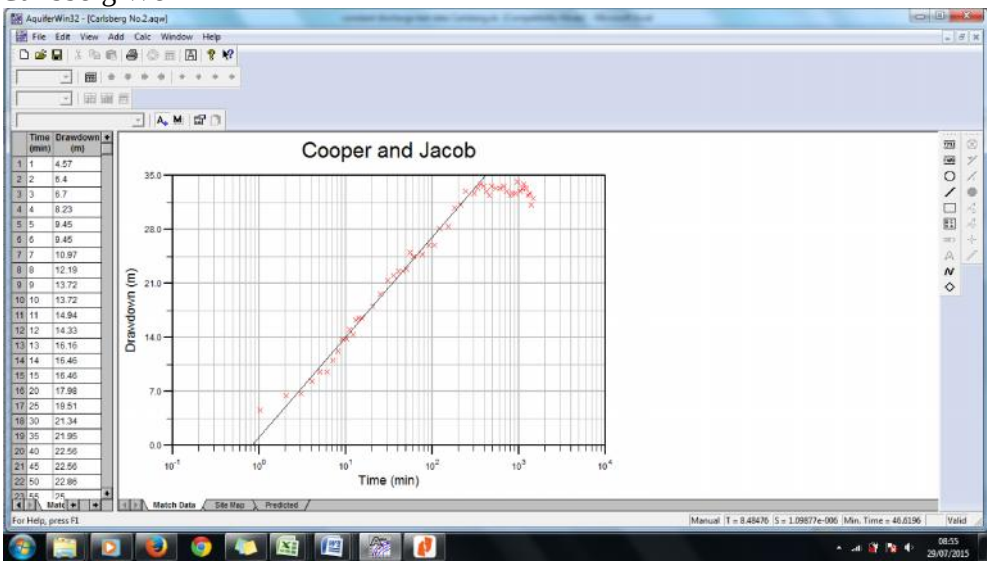

Gaya Color Lab

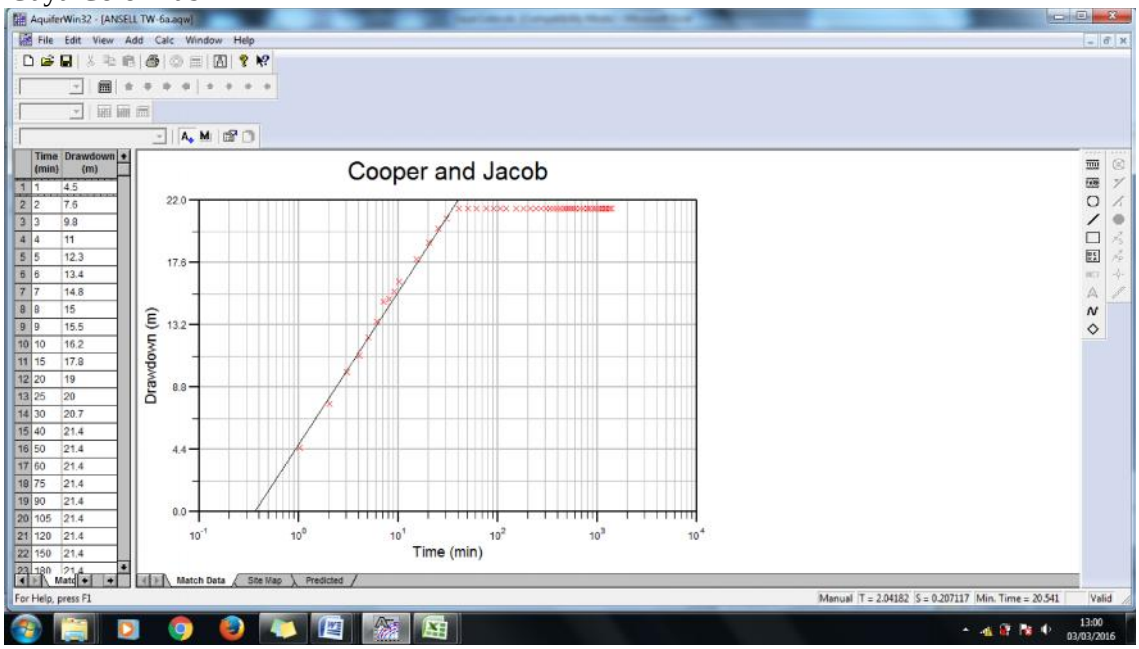

Carlsberg Well 1

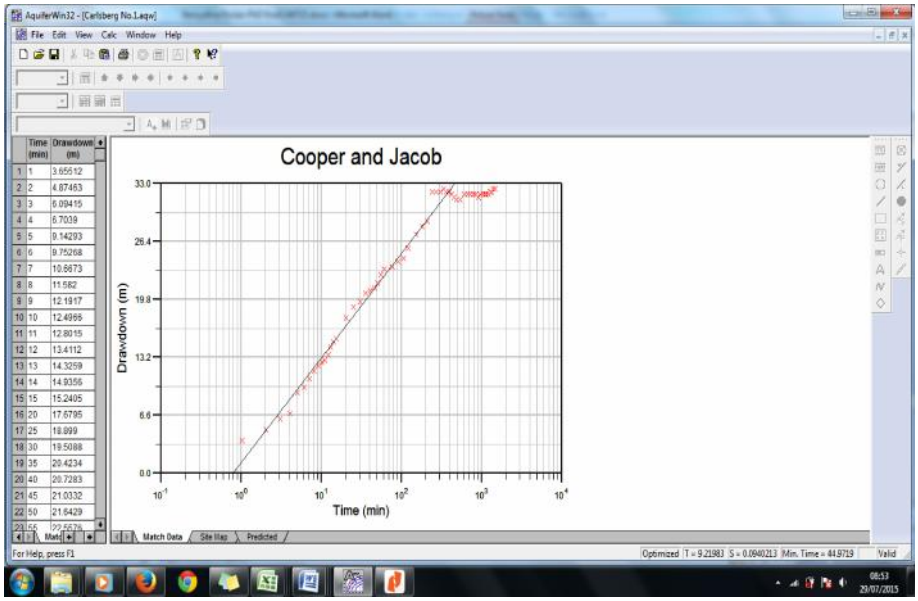

Proton B

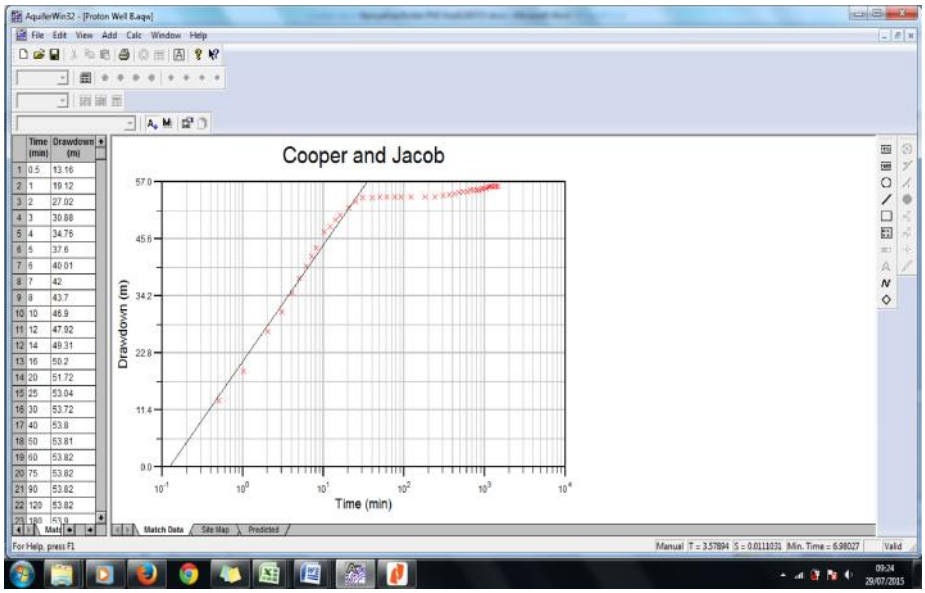

Class E

Ansell TW2

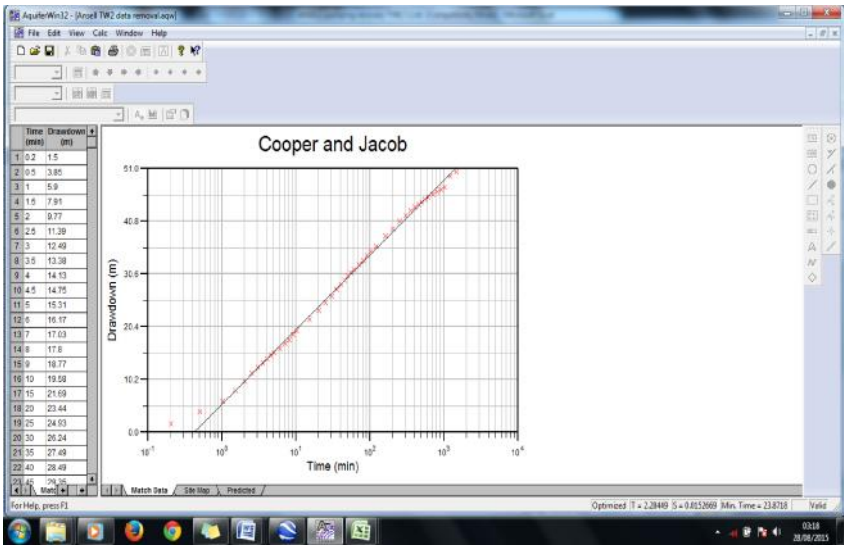

Well bore storage effect is negligible is when t > 105.55min

CCM Fertilizer 4

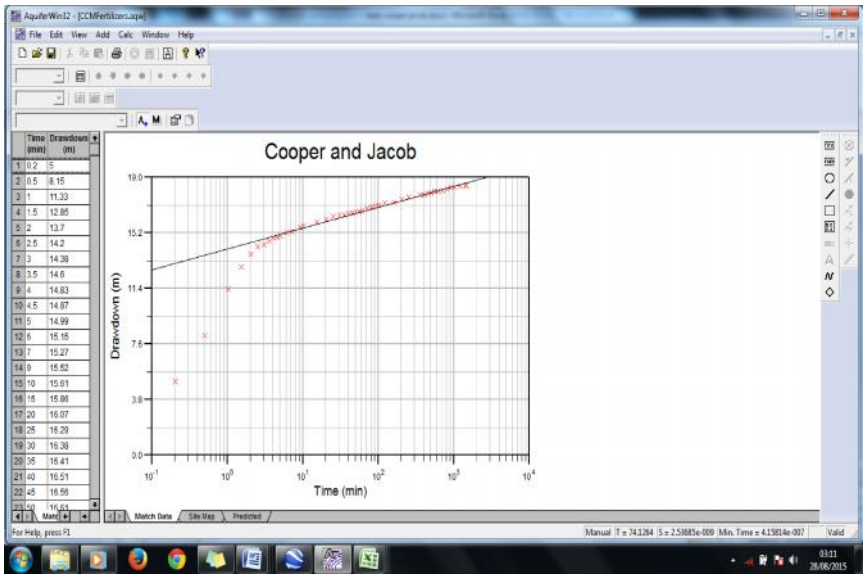

Well bore storage effect is negligible is when t > 2.77min

CCM Fertilizer 1

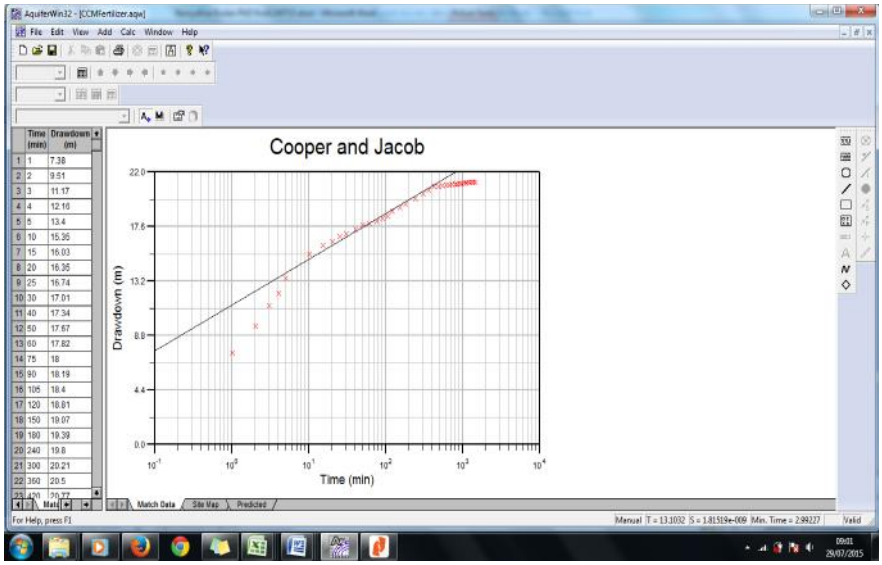

Well bore storage effect is negligible is when t > 14.56min

Panasonic 1

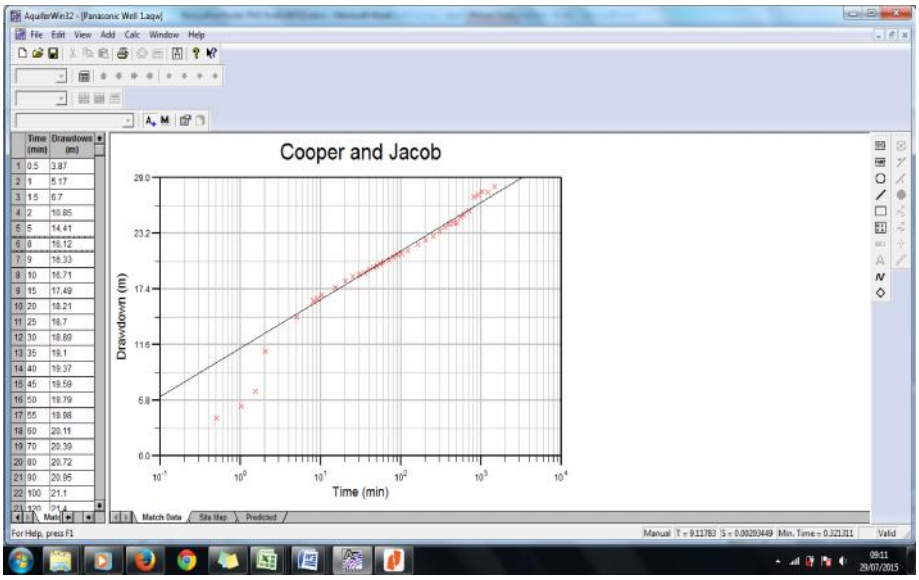

Well bore storage effect is negligible is when t > 34.45min

Pokka Ace

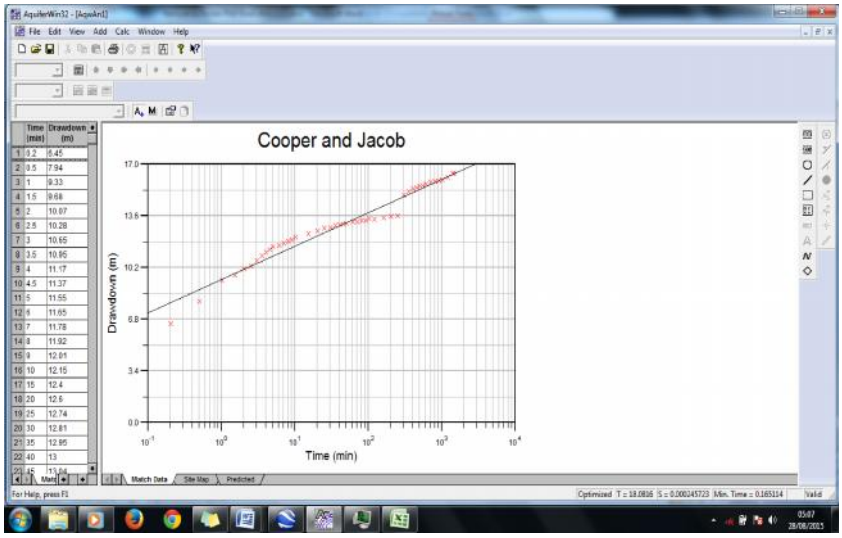

Well bore storage effect is negligible is when t > 6.5min

UEDA Plating 2

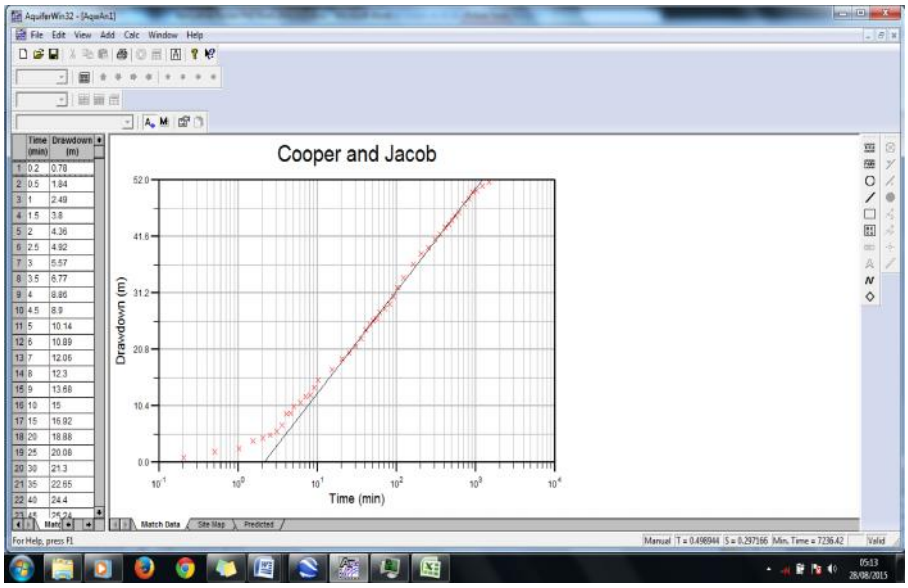

Well bore storage effect is negligible is when t > 343.22min

UEDA Plating 1

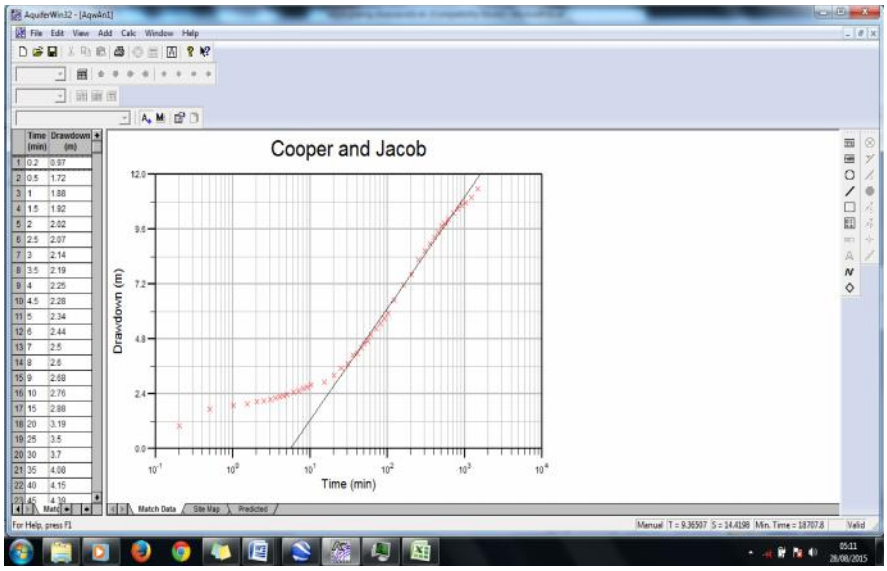

Well bore storage effect is negligible is when t > 21.5min

MT Pictures 5

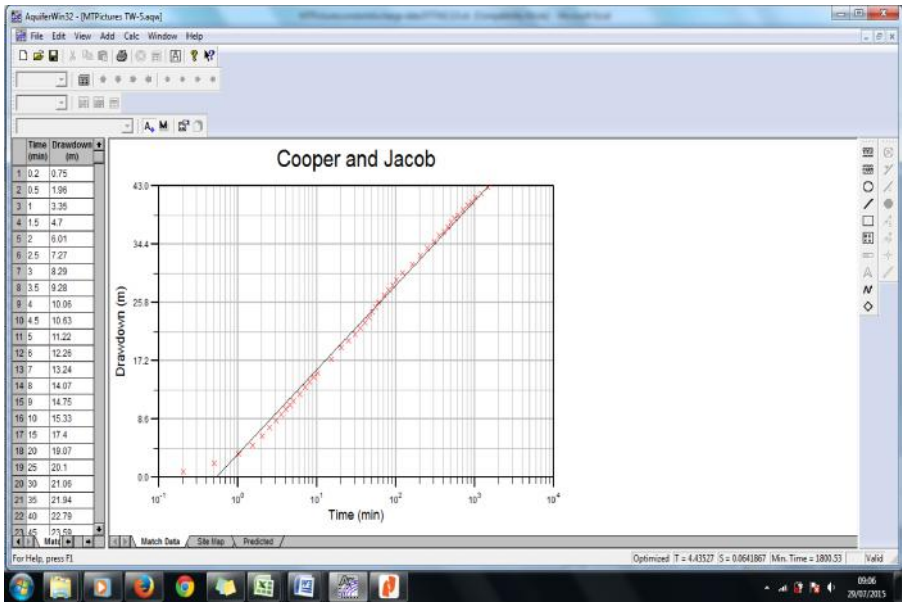

Well bore storage effect is negligible is when t > 50.63 min

Universal Nutri Beverages

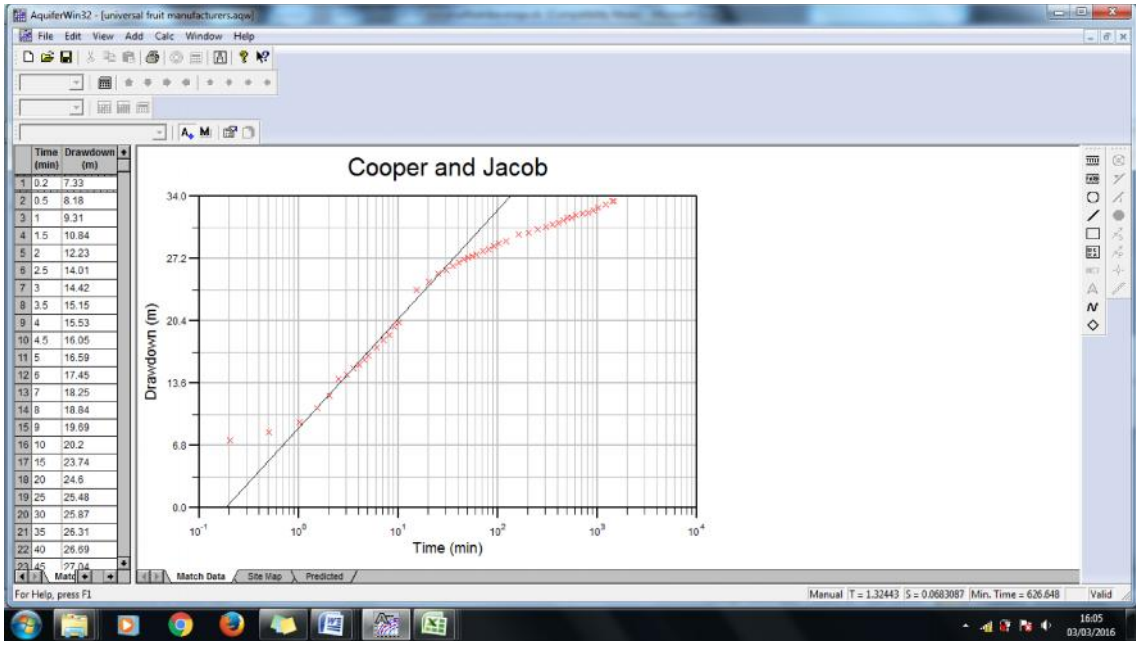

Well bore storage effect is negligible is when t > 110.1 min

Ansell TW3

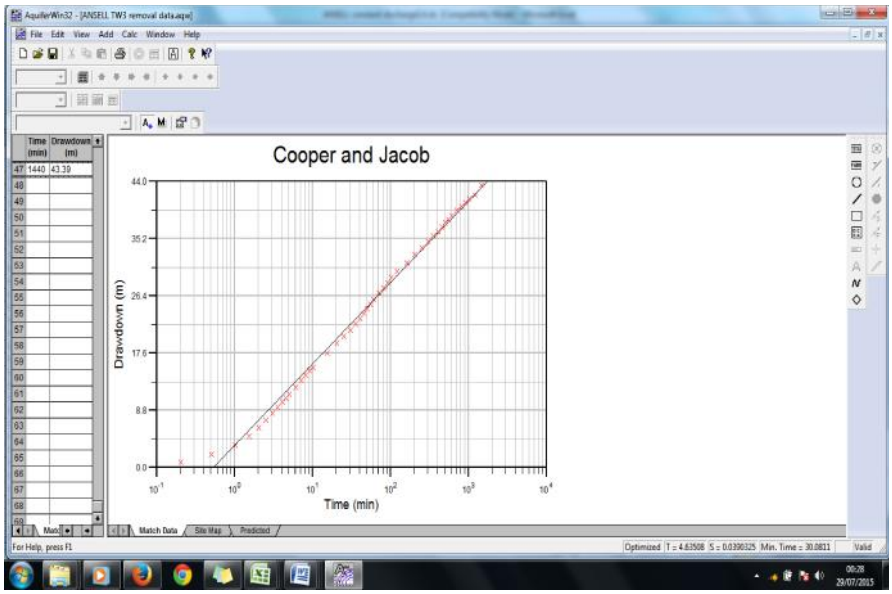

Well bore storage effect is negligible is when t > 54.29 min

Mitsui Hightech

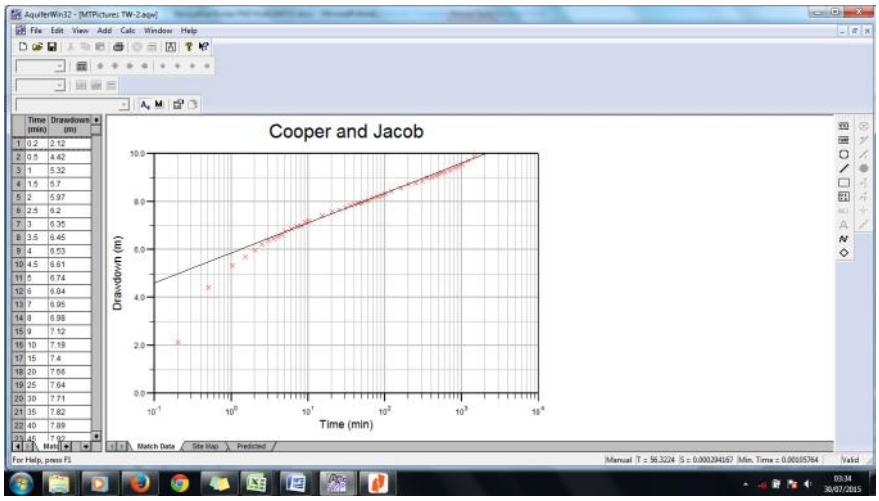

Well bore storage effect is negligible is when t > 3.24 min.

Ansell TW4

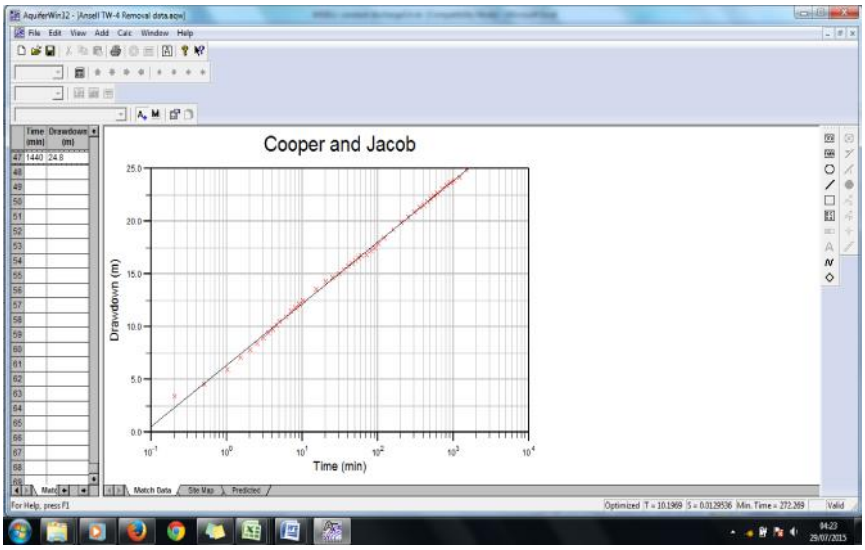

Well bore storage effect is negligible is when t > 20.33 min.

Ansell 5A

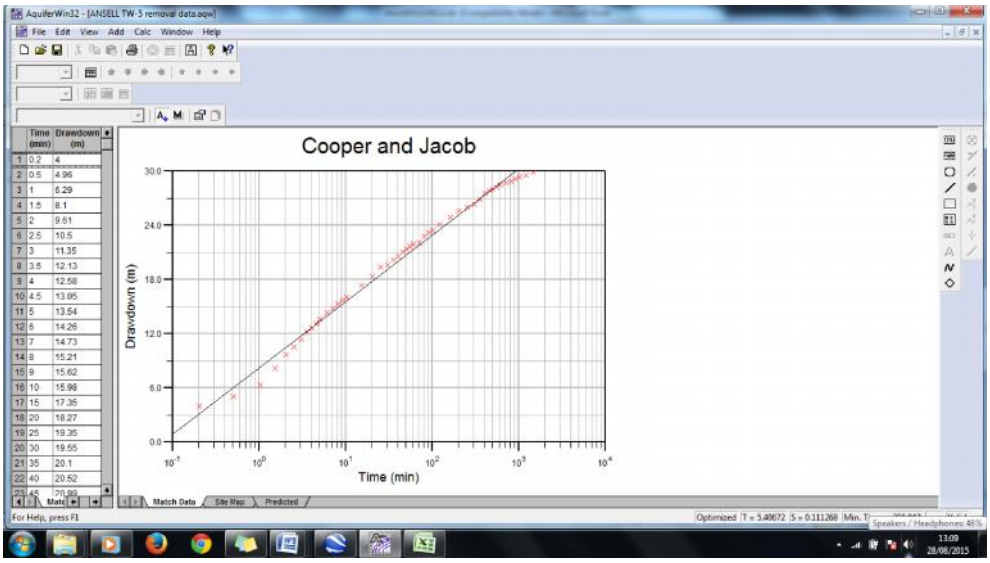

Well bore storage effect is negligible is when t > 35 min.

APPENDIXES D Theis Recovery plot

Class E

MT Pictures 5

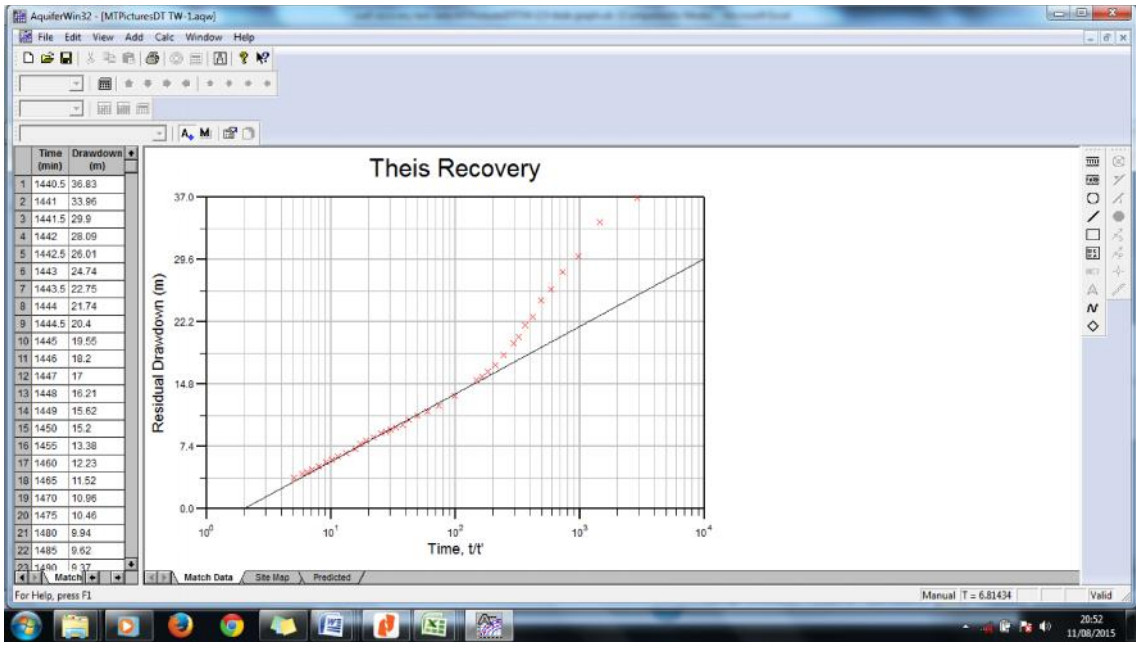

Ansell TW3

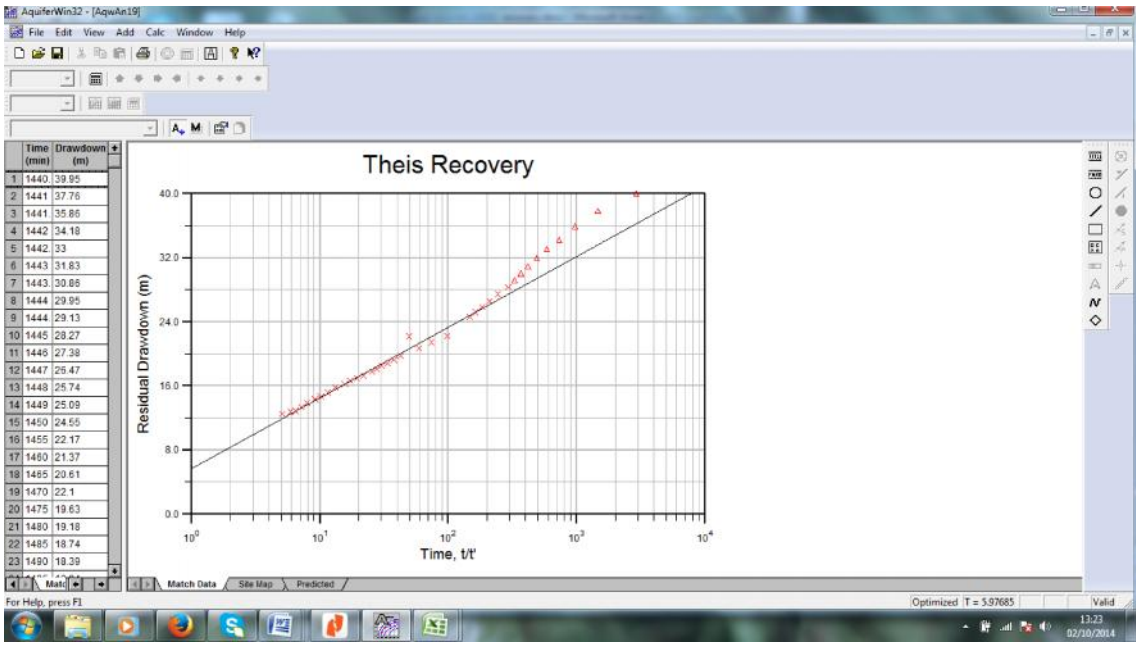

Ansell TW4

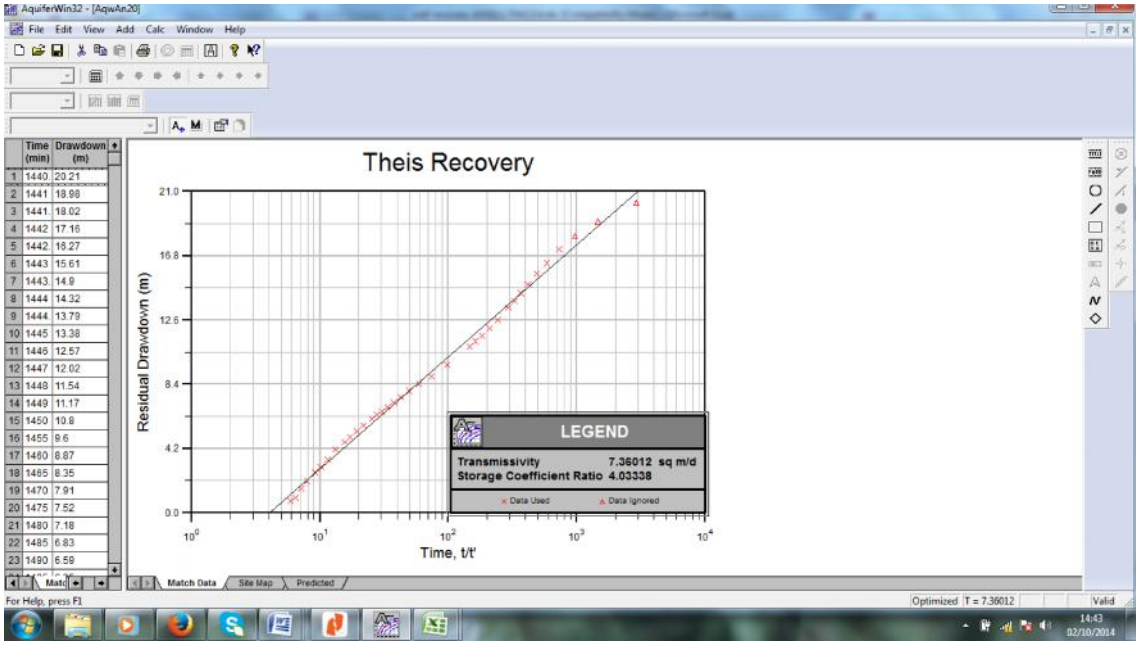

CCM Fertilizer 1

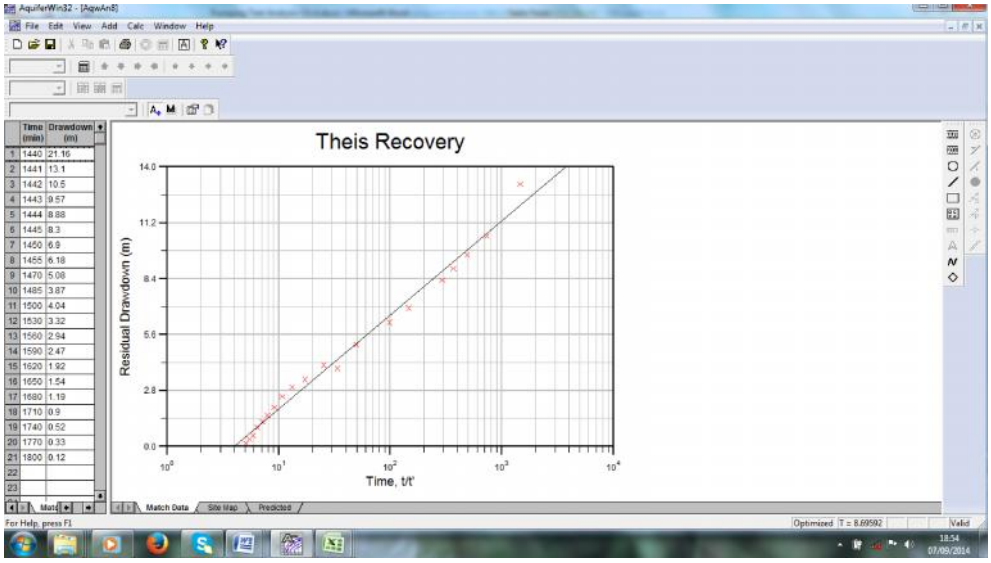

CCM Fertilizer 4

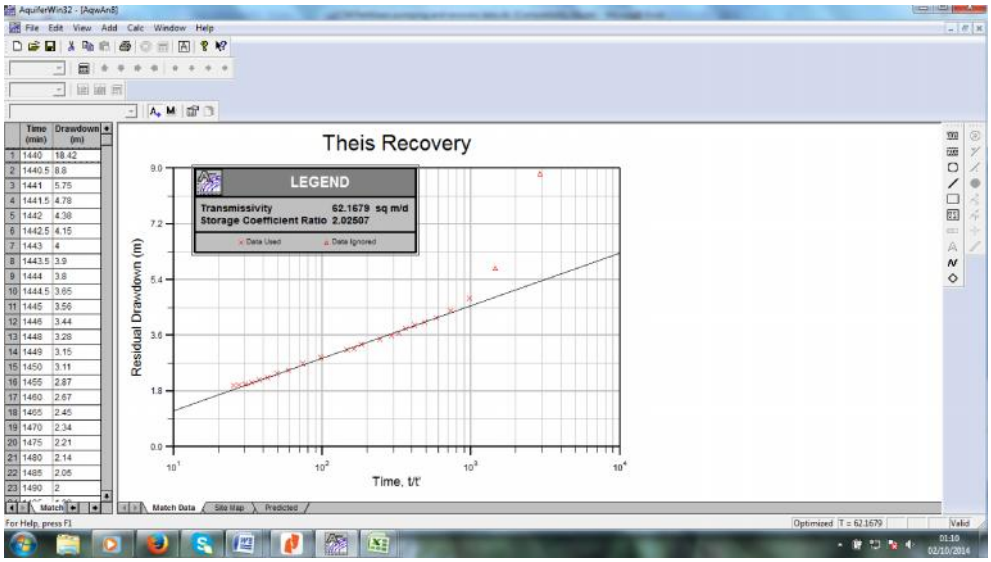

Mitsui High tech

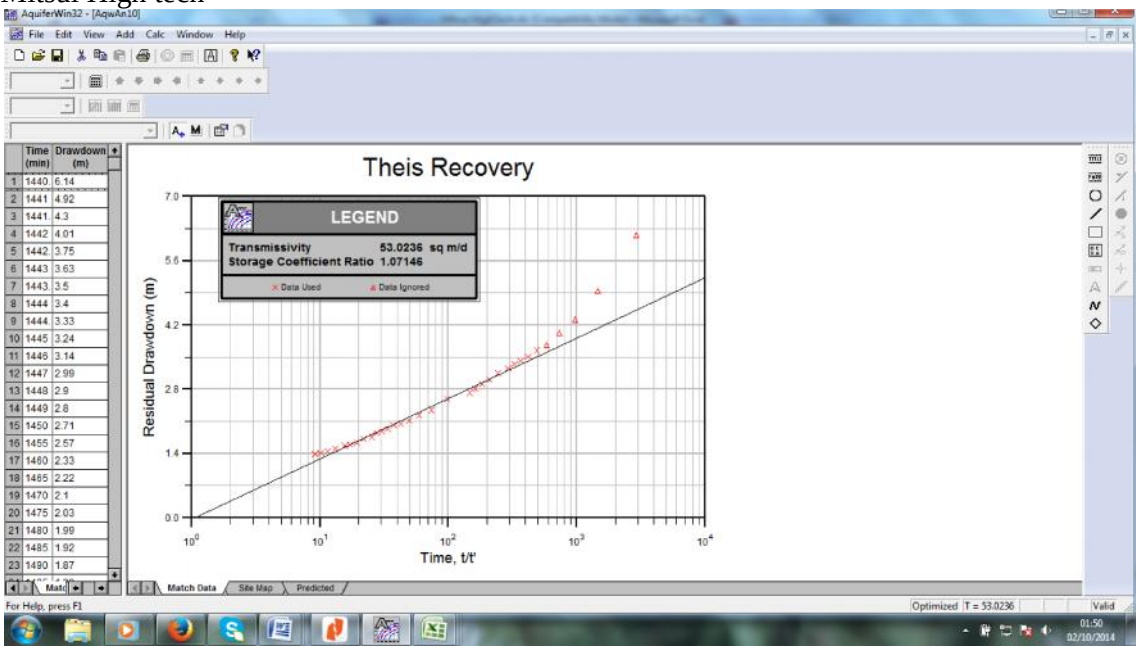

Universal Nutri Beverages

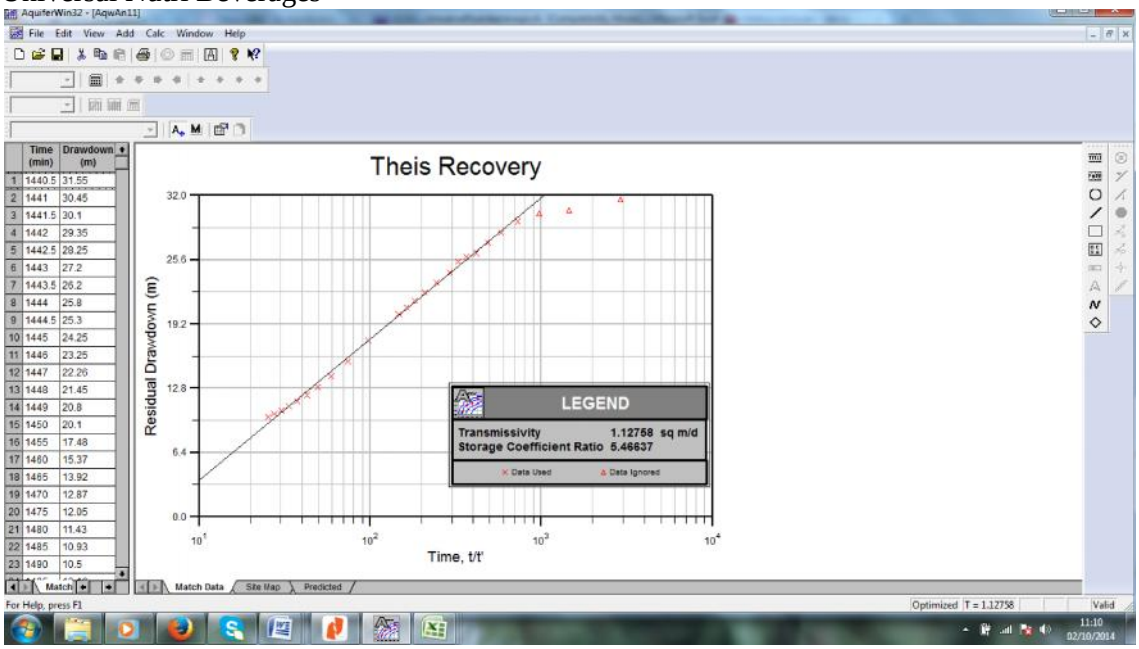

Panasonic 1

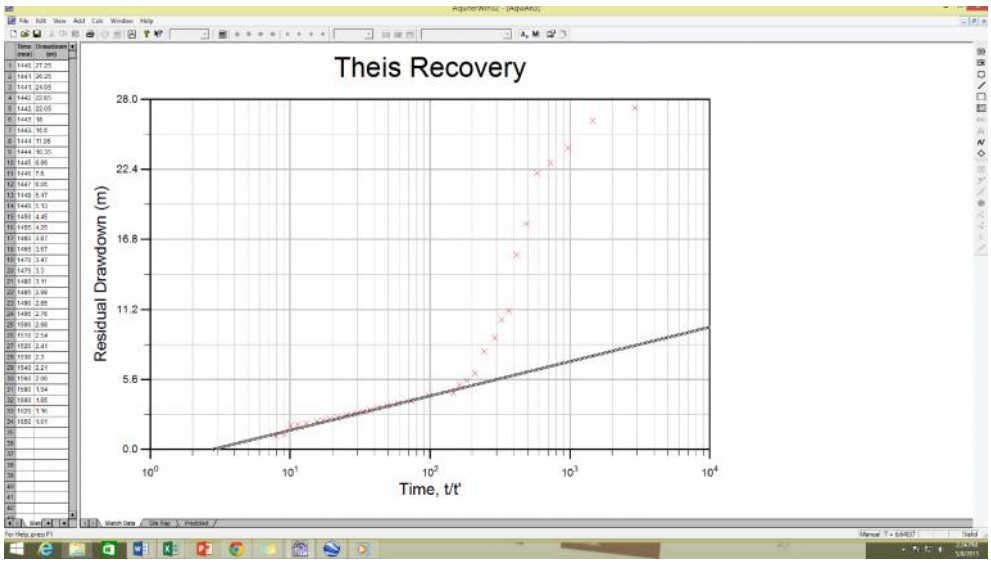

Ueda Plating 1

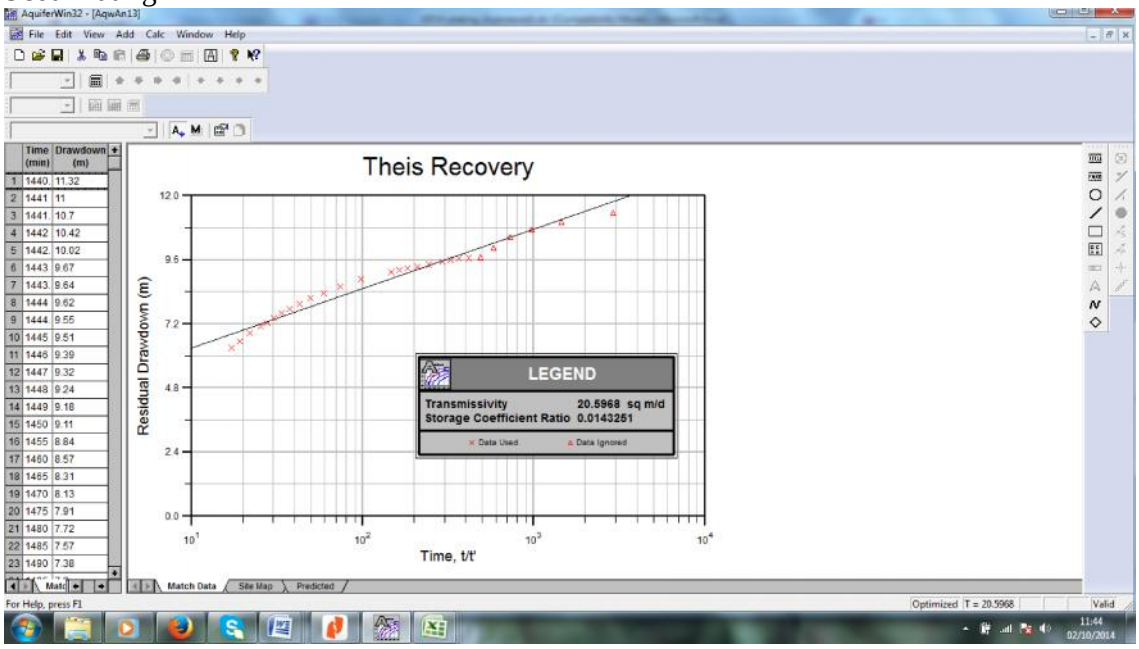

Ueda Plating 2

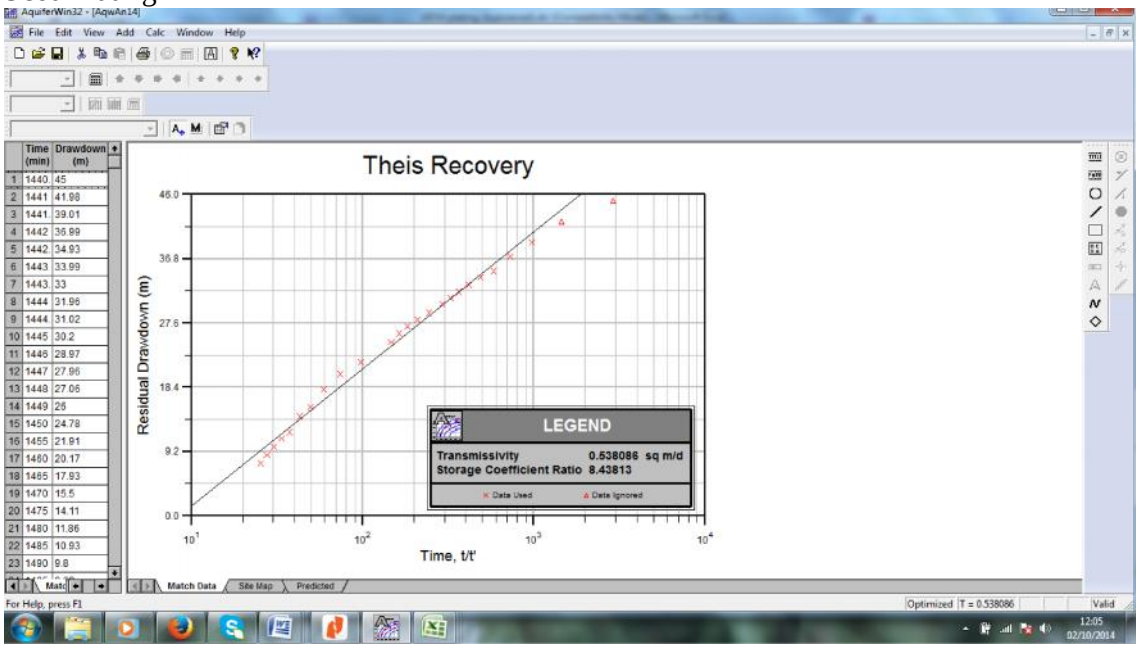

Pokka Ace

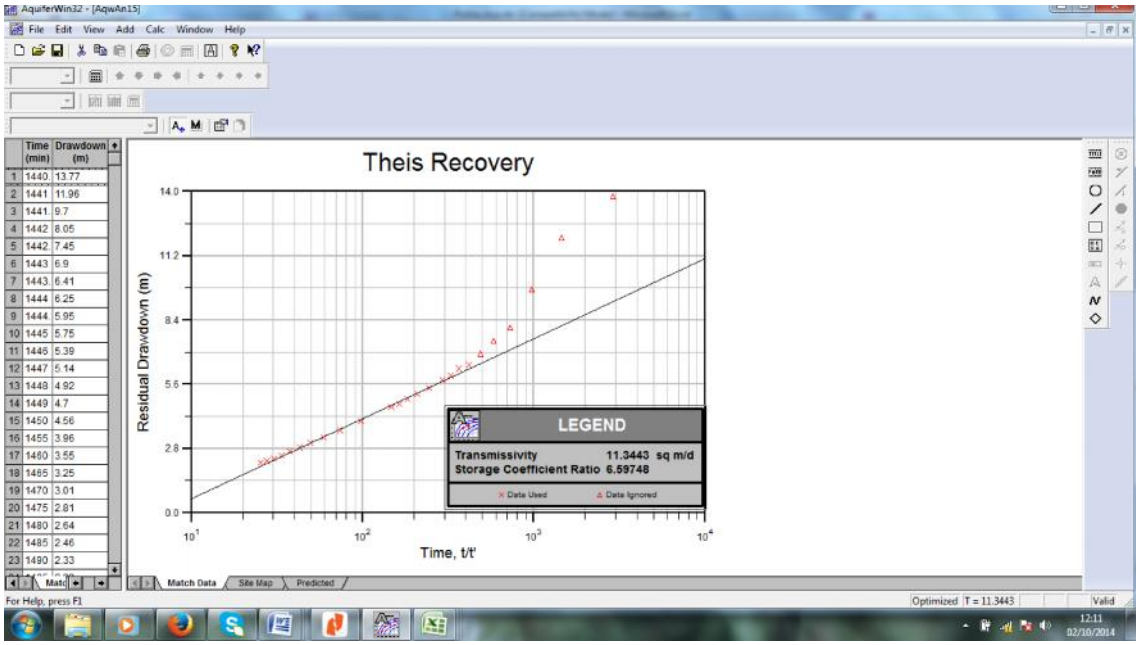

	Time (min)	Drawdown (m)
1	1440	13.77
2	1441	11.96
3	1441	9.7
4	1442	8.05
5	1442	7.45
6	1443	6.9
7	1443	6.41
8	1444	6.25
9	1444	5.95
10	1445	5.75
11	1446	5.39
12	1447	5.14
13	1448	4.92
14	1449	4.7
15	1450	4.56
16	1455	3.96
17	1460	3.55
18	1465	3.25
19	1470	3.01
20	1475	2.81
21	1480	2.64
22	1485	2.46
23	1490	2.33

Ansell TW2

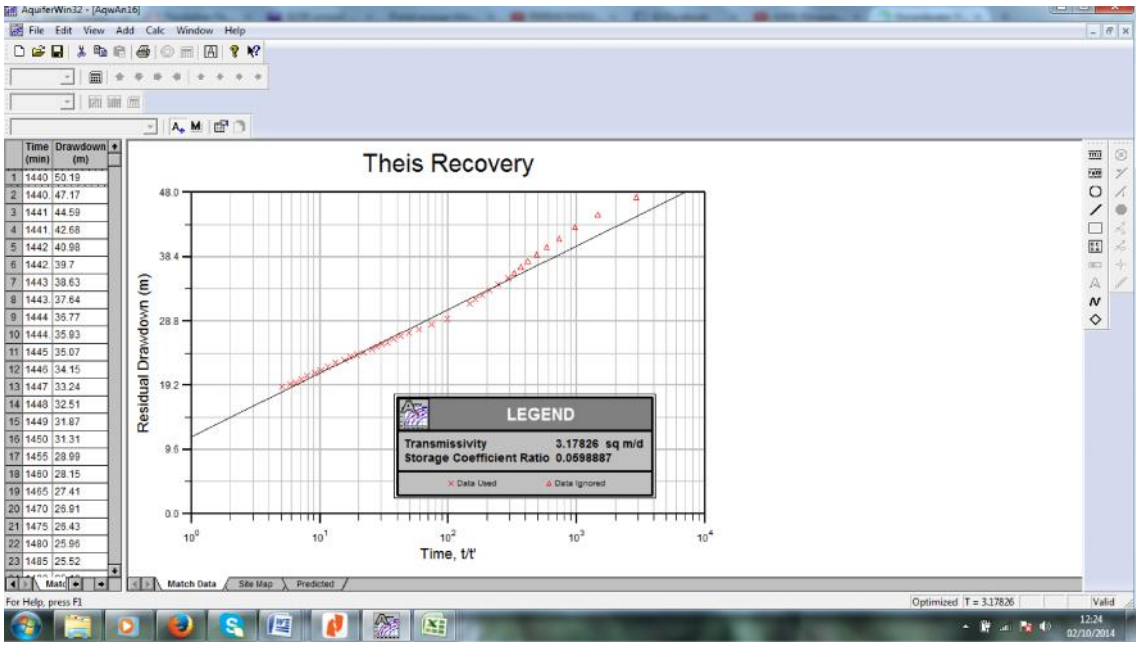

	Time (min)	Drawdown (m)
1	1440	50.19
2	1440	47.17
3	1441	44.59
4	1441	42.68
5	1442	40.98
6	1442	39.7
7	1443	38.63
8	1443	37.64
9	1444	36.77
10	1444	35.93
11	1445	35.07
12	1446	34.15
13	1447	33.24
14	1448	32.51
15	1449	31.87
16	1450	31.31
17	1455	28.99
18	1460	28.15
19	1465	27.41
20	1470	26.91
21	1475	26.43
22	1480	25.96
23	1485	25.52

Ansell 5A

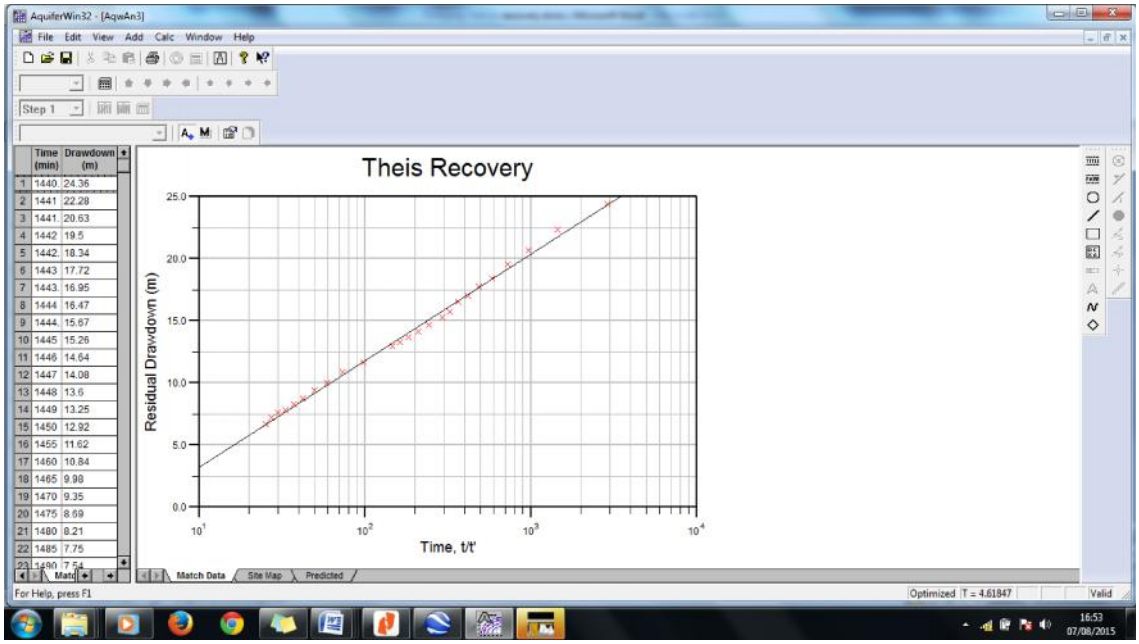

UEDA plating 1

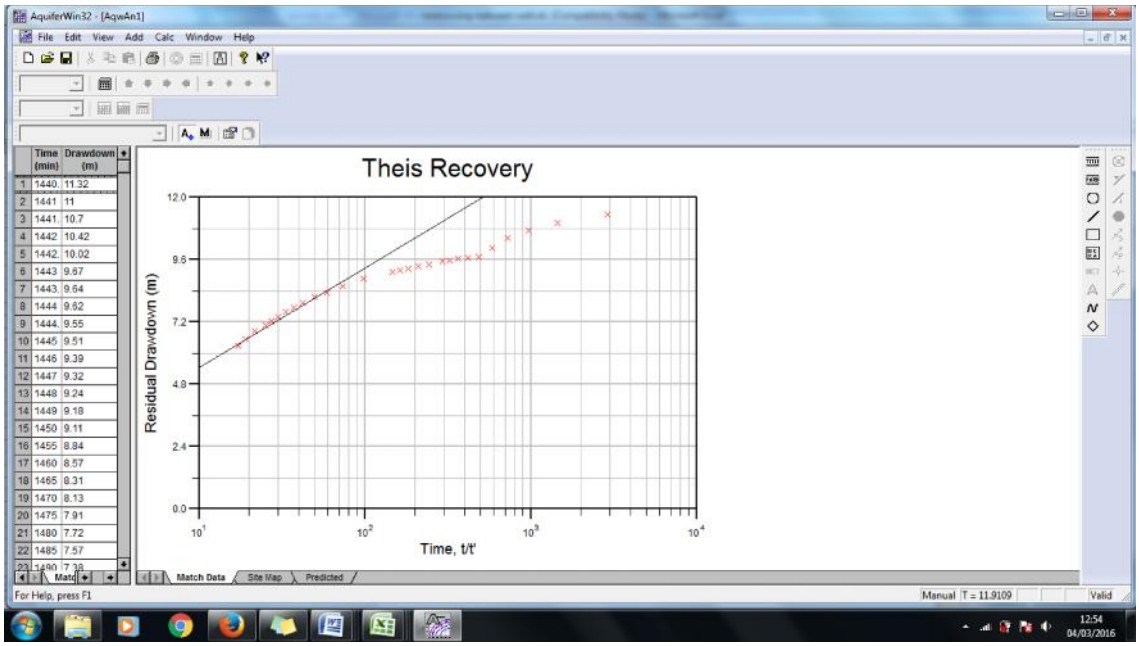

APPENDIX E Monitoring data

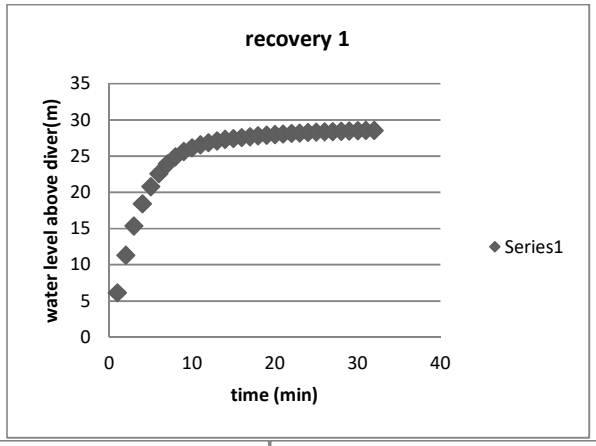

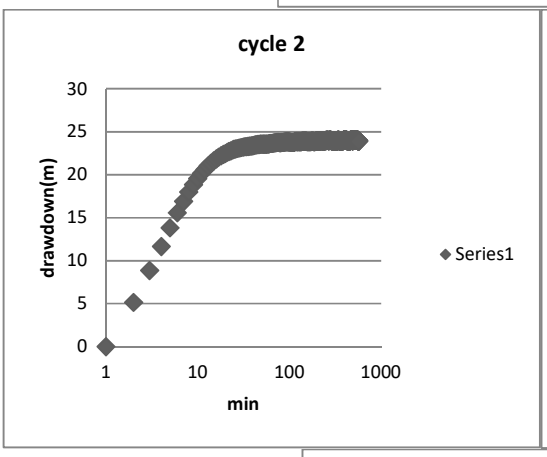

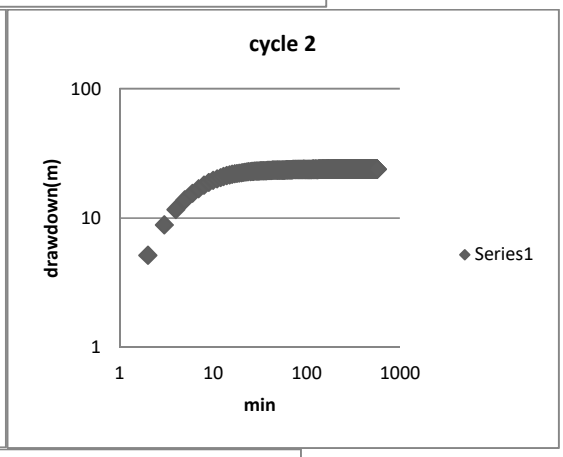

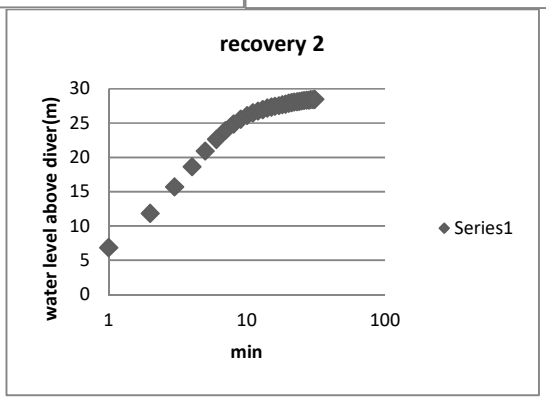

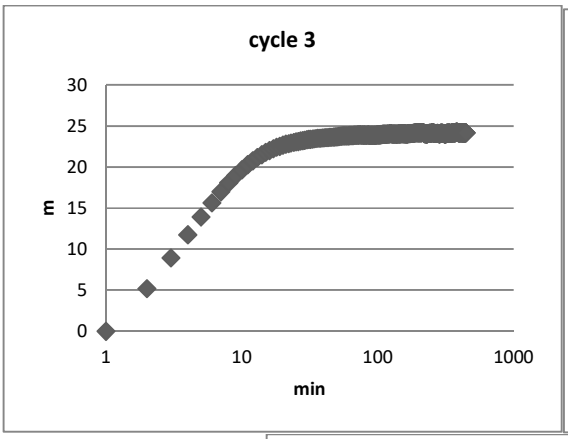
cycle 3
30
25
20
15
10
5
0
m
1
10
100
1000
min

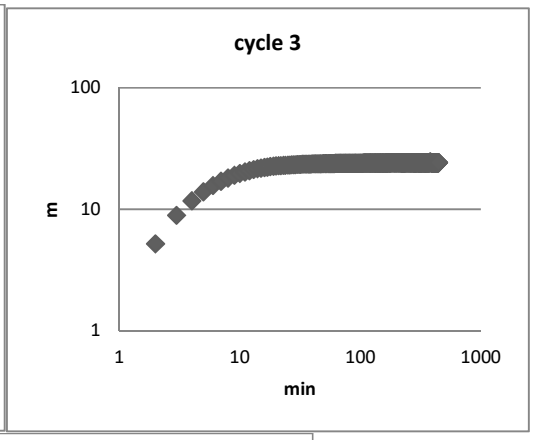
cycle 3
100
10
1
m
1
10
100
1000
min

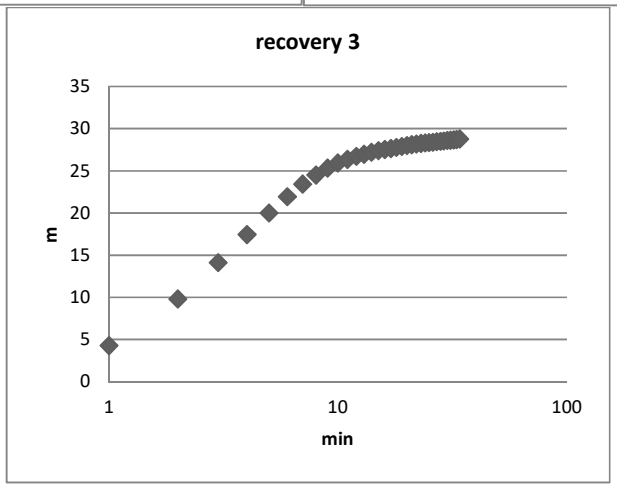
recovery 3
35
30
25
20
15
10
5
0
m
1
10
100
min

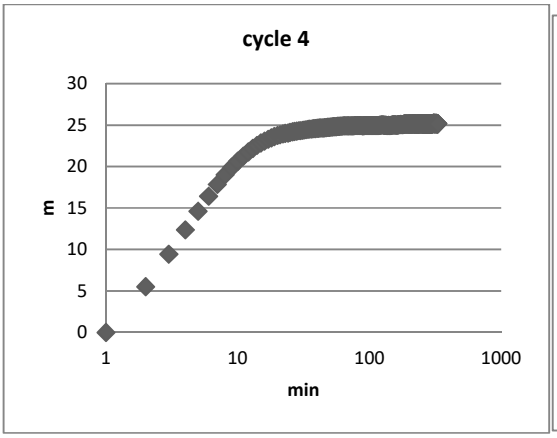
cycle 4
30
25
20
15
10
5
0
m
1
10
100
1000
min

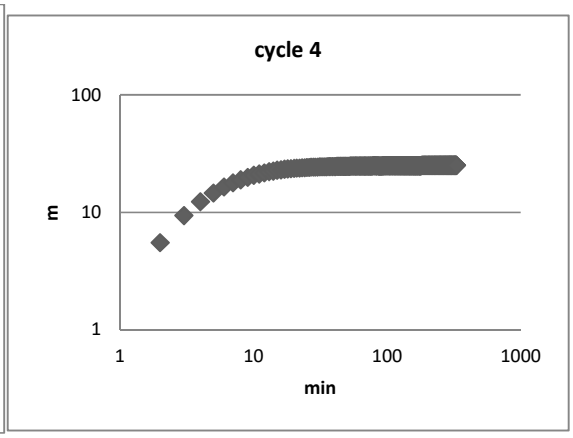
cycle 4
100
10
1
m
1
10
100
1000
min

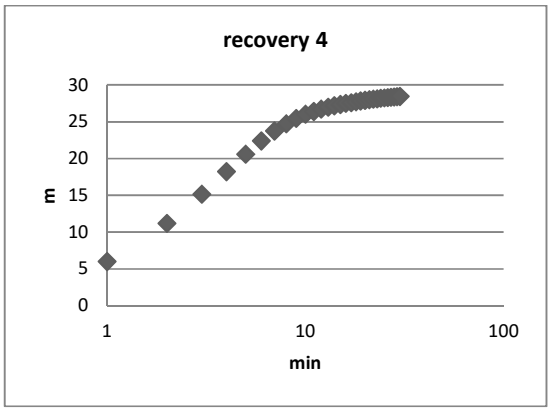
recovery 4
m
30
25
20
15
10
5
0
1
10
100
min

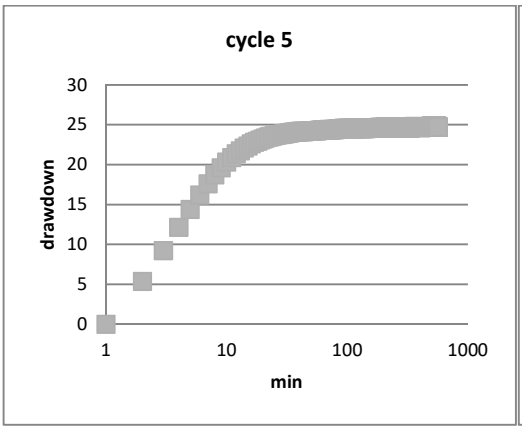
cycle 5
drawdown
30
25
20
15
10
5
0
1
10
100
1000
min

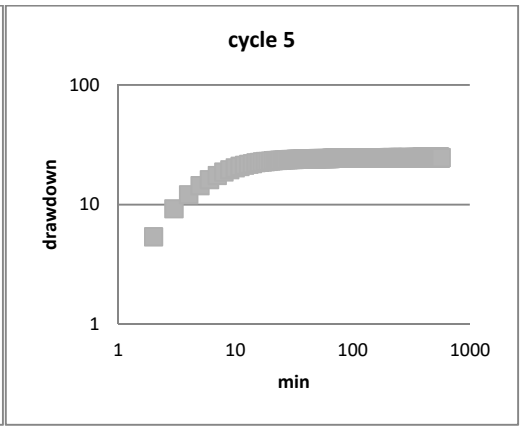
cycle 5
drawdown
100
10
1
1
10
100
1000
min

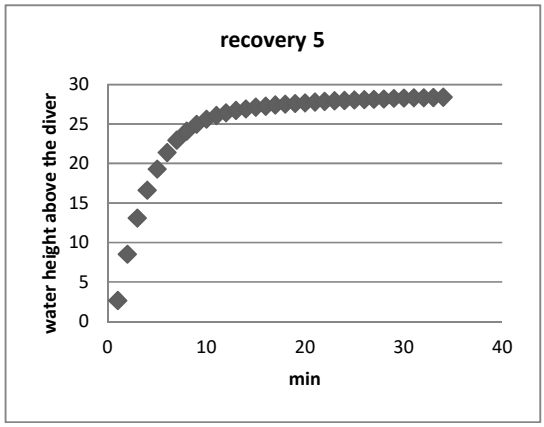
recovery 5
water height above the diver
30
25
20
15
10
5
0
0
10
20
30
40
min

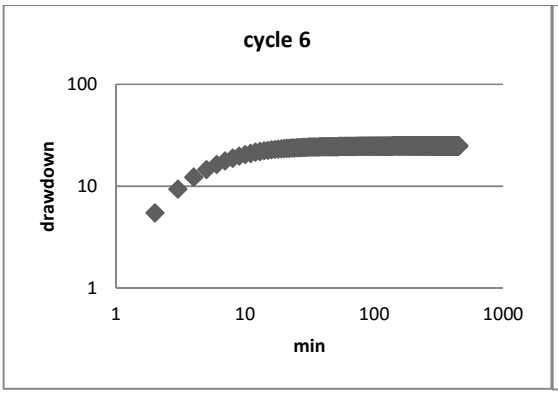
cycle 6
drawdown
100
10
1
1
10
100
1000
min

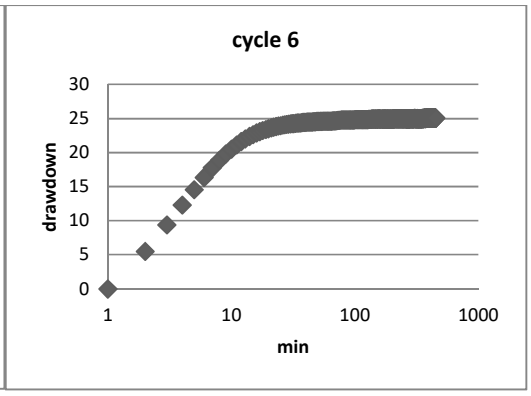
cycle 6
drawdown
30
25
20
15
10
5
0
1
10
100
1000
min

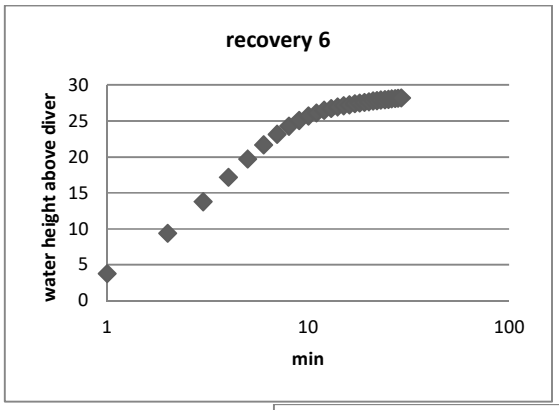
recovery 6
water height above diver
30
25
20
15
10
5
0
1
10
100
min

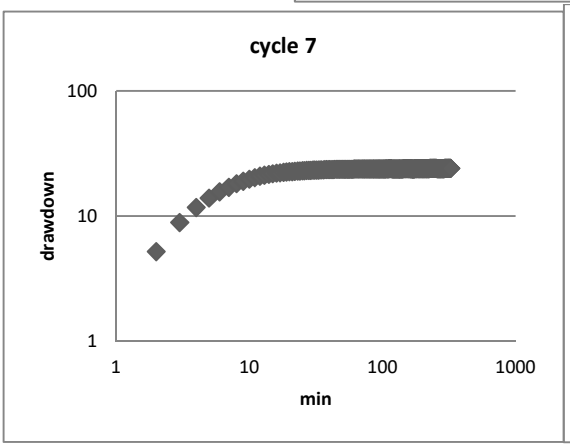
cycle 7
drawdown
100
10
1
1
10
100
1000
min

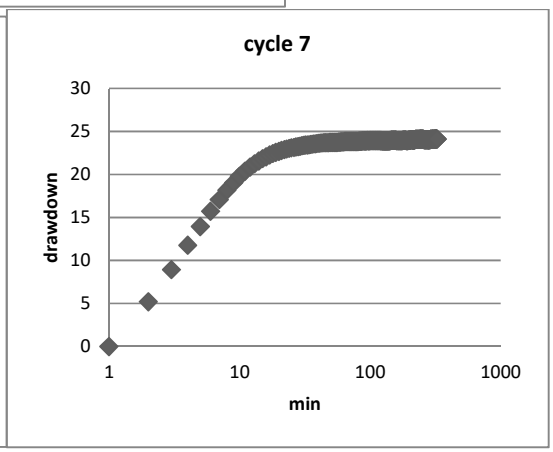
cycle 7
drawdown
30
25
20
15
10
5
0
1
10
100
1000
min

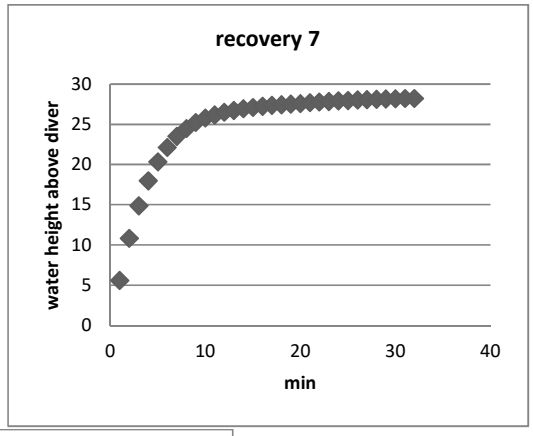
recovery 7
water height above diver
30
25
20
15
10
5
0
0
10
20
30
40
min

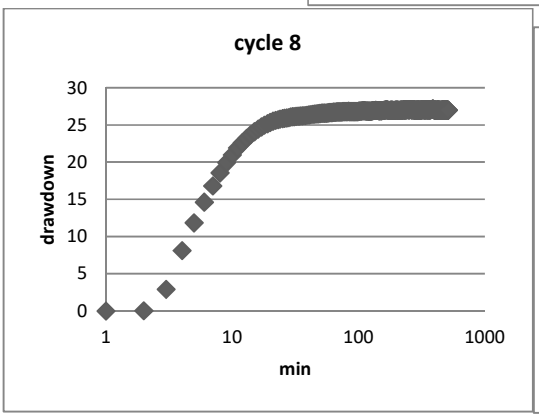
cycle 8
drawdown
30
25
20
15
10
5
0
1
10
100
1000
min

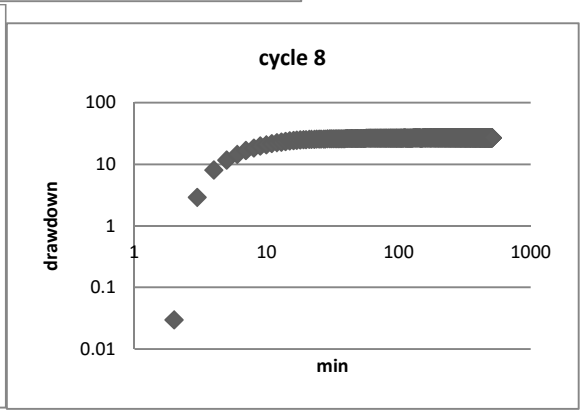
cycle 8
drawdown
100
10
1
0.1
0.01
1
10
100
1000
min

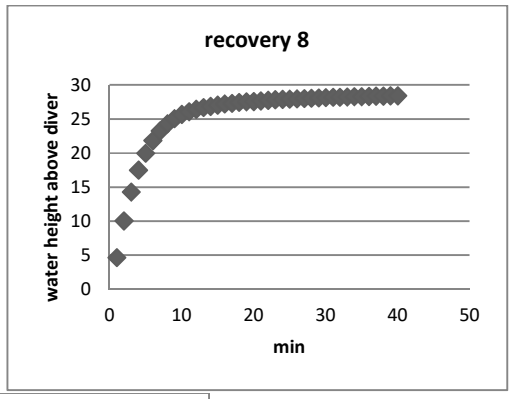
recovery 8
water height above diver
30
25
20
15
10
5
0
0
10
20
30
40
50
min

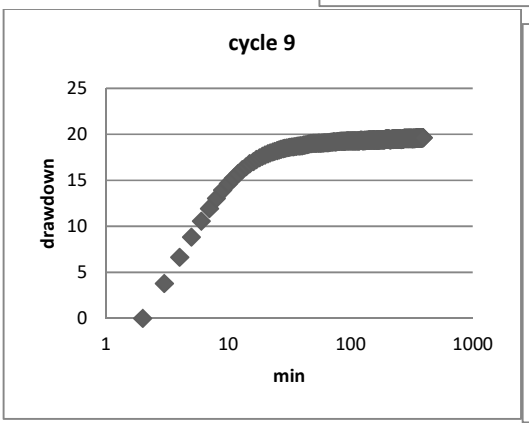
cycle 9
drawdown
25
20
15
10
5
0
1
10
100
1000
min

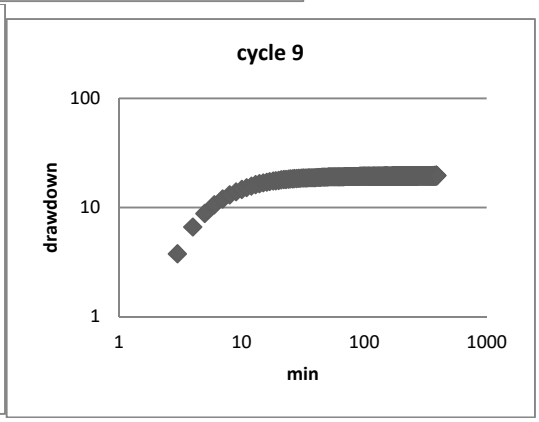
cycle 9
drawdown
100
10
1
1
10
100
1000
min

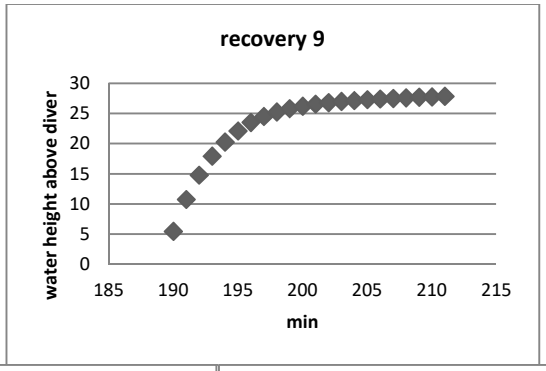
recovery 9
water height above diver
30
25
20
15
10
5
0
185
190
195
200
205
210
215
min

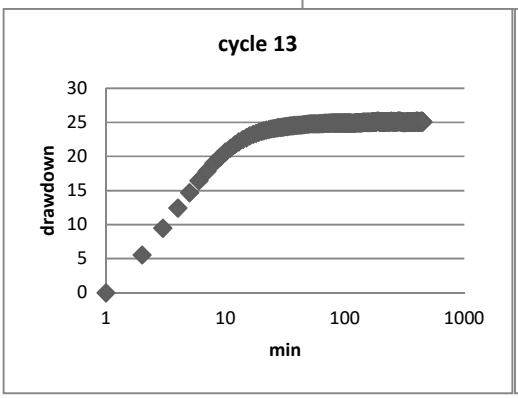
cycle 13
drawdown
30
25
20
15
10
5
0
1
10
100
1000
min

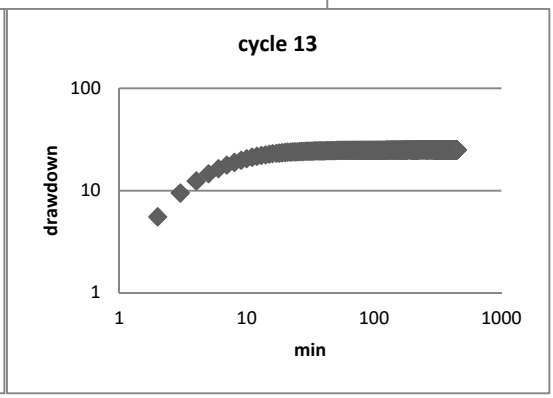
cycle 13
drawdown
100
10
1
1
10
100
1000
min

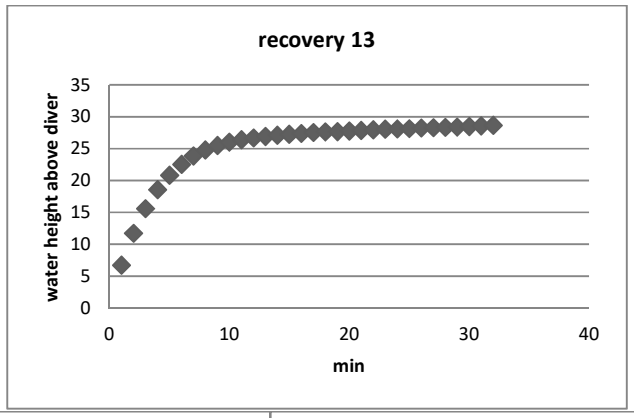
recovery 13
water height above diver
35
30
25
20
15
10
5
0
0
10
20
30
40
min

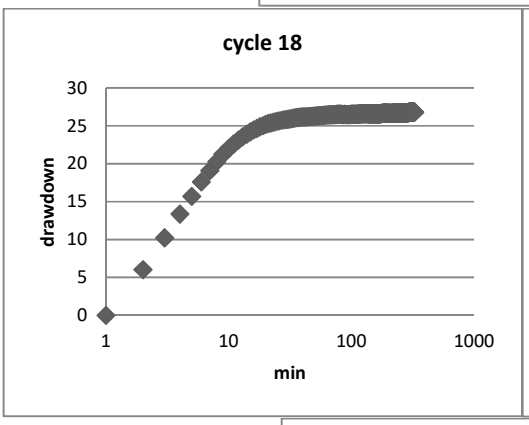
cycle 18
drawdown
30
25
20
15
10
5
0
1
10
100
1000
min

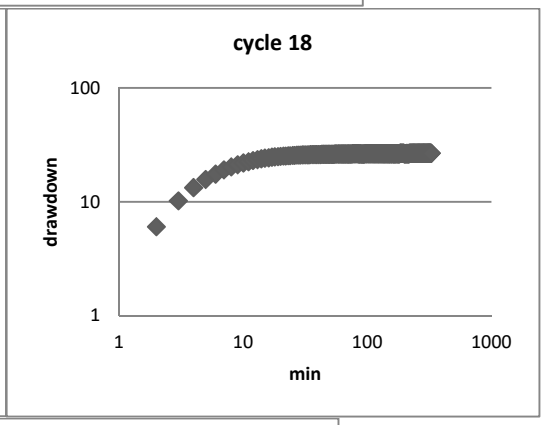
cycle 18
drawdown
100
10
1
1
10
100
1000
min

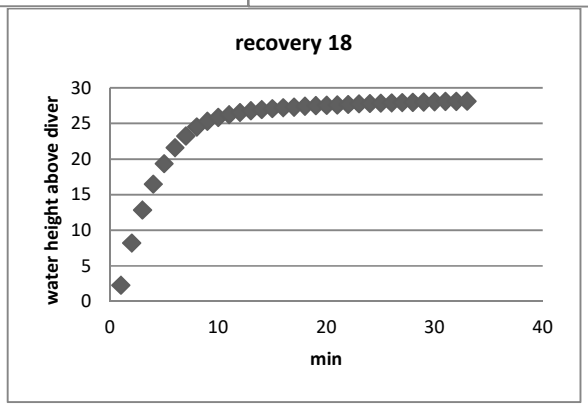
recovery 18
water height above diver
30
25
20
15
10
5
0
0
10
20
30
40
min

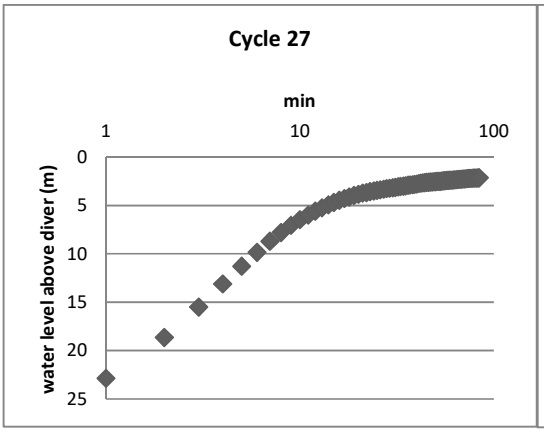
Cycle 27
min
1
10
100
water level above diver (m)
0
5
10
15
20
25

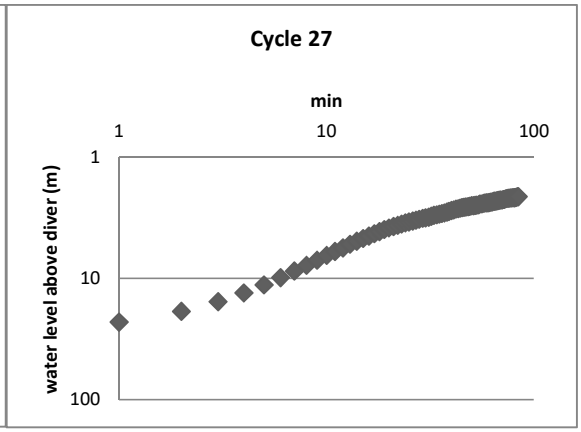
Cycle 27
min
1
10
100
water level above diver (m)
1
10
100

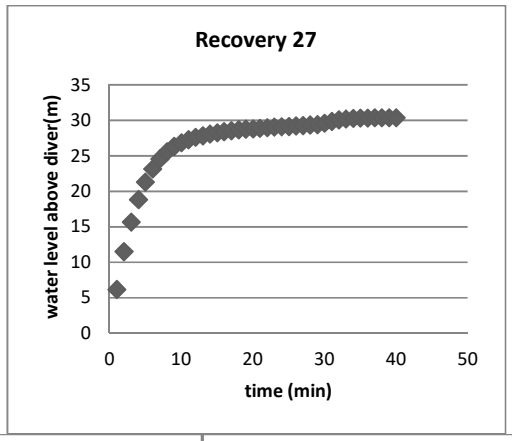
Recovery 27
water level above diver(m)
35
30
25
20
15
10
5
0
0
10
20
30
40
50
time (min)

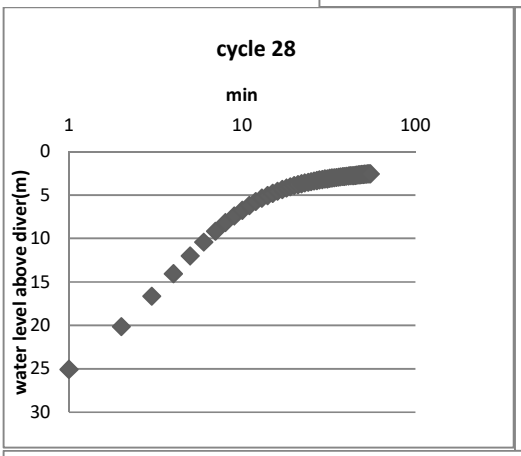
cycle 28
min
1
10
100
water level above diver(m)
0
5
10
15
20
25
30

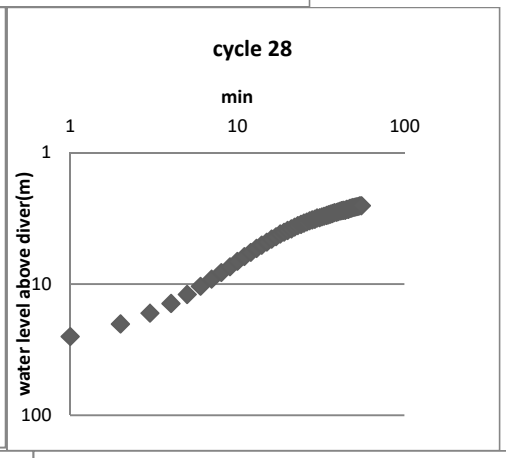
cycle 28
min
1
10
100
water level above diver(m)
1
10
100

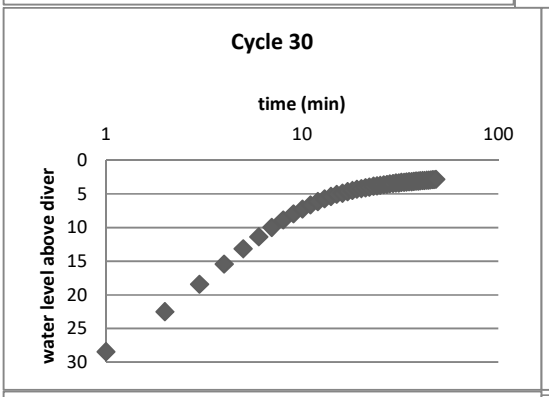
Cycle 30
time (min)
1
10
100
water level above diver
0
5
10
15
20
25
30

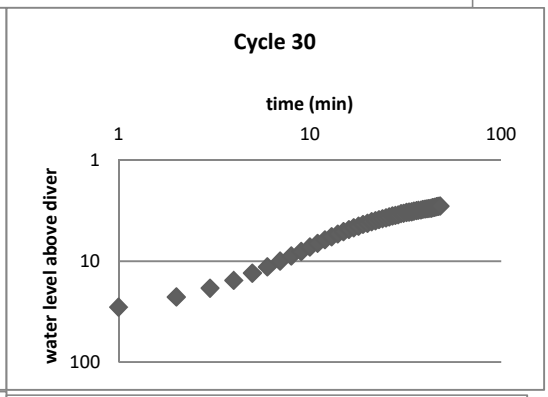
Cycle 30
time (min)
1
10
100
water level above diver
1
10
100

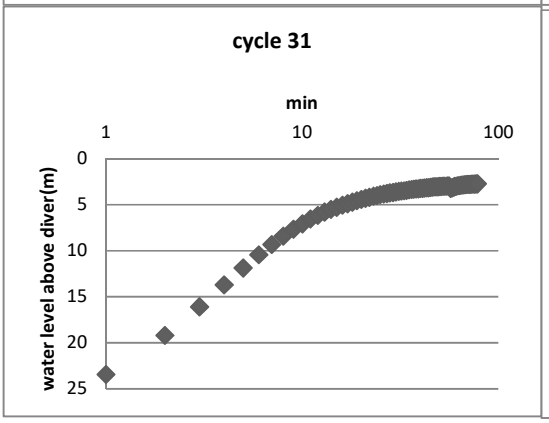
cycle 31
min
1
10
100
water level above diver(m)
0
5
10
15
20
25

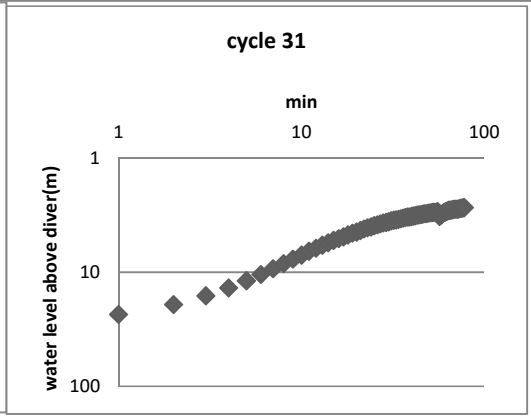
cycle 31
min
1
10
100
water level above diver(m)
1
10
100

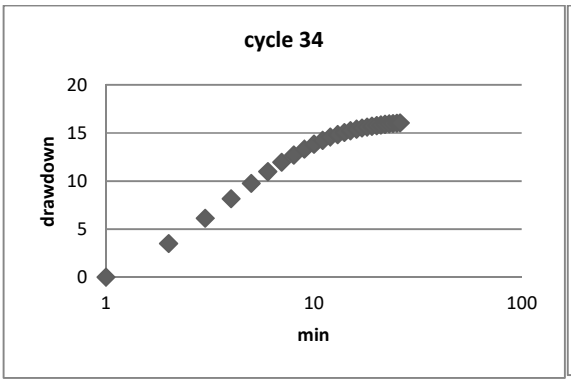
cycle 34
drawdown
20
15
10
5
0
1
10
100
min

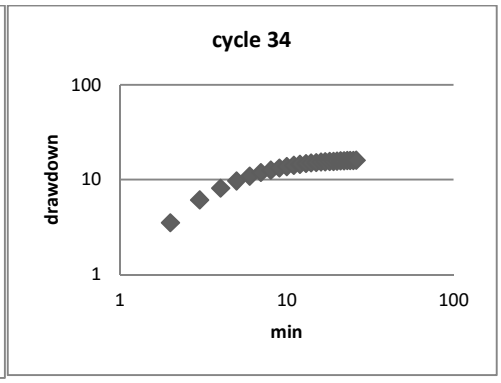
cycle 34
drawdown
100
10
1
1
10
100
min

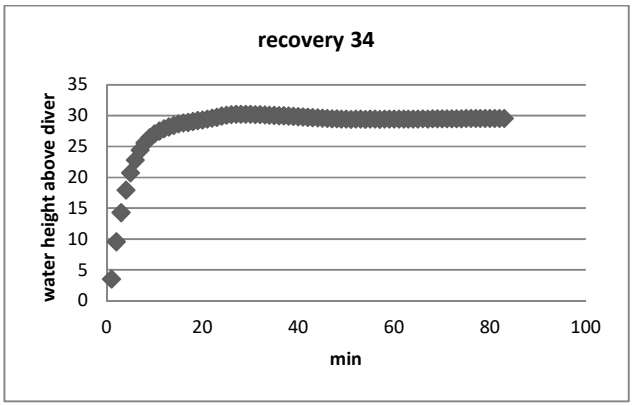
recovery 34
water height above diver
35
30
25
20
15
10
5
0
0
20
40
60
80
100
min

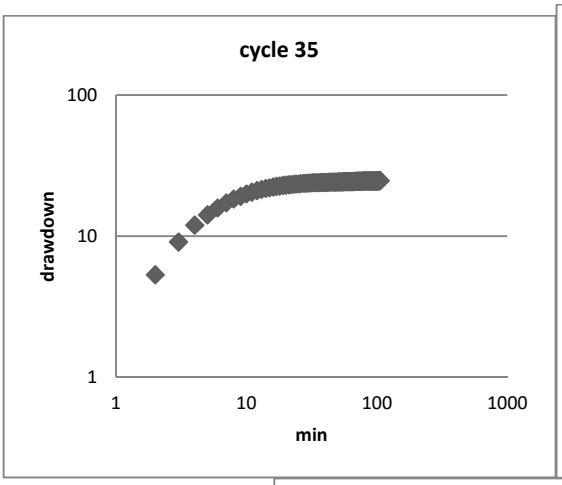
cycle 35
drawdown
100
10
1
1
10
100
1000
min

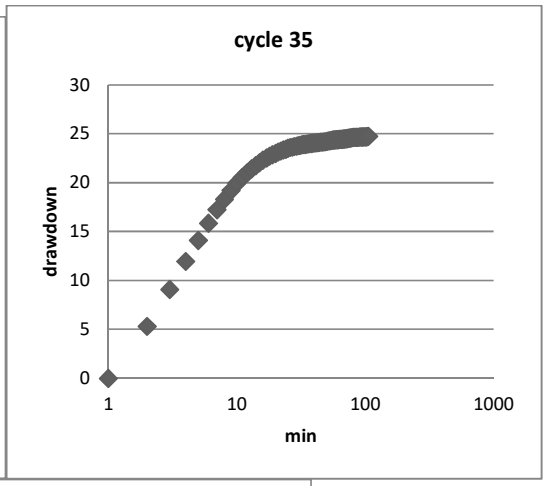
cycle 35
drawdown
30
25
20
15
10
5
0
1
10
100
1000
min

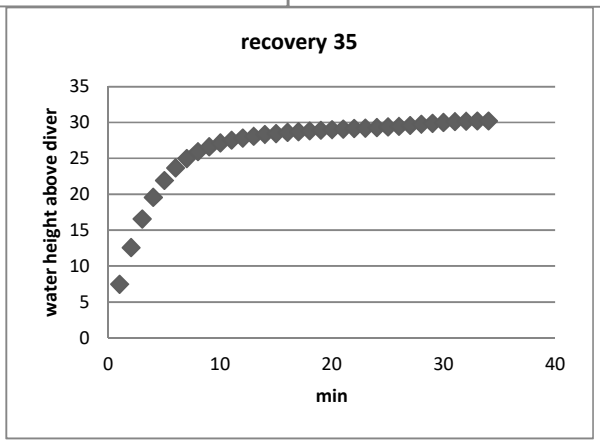
recovery 35
water height above diver
35
30
25
20
15
10
5
0
0
10
20
30
40
min

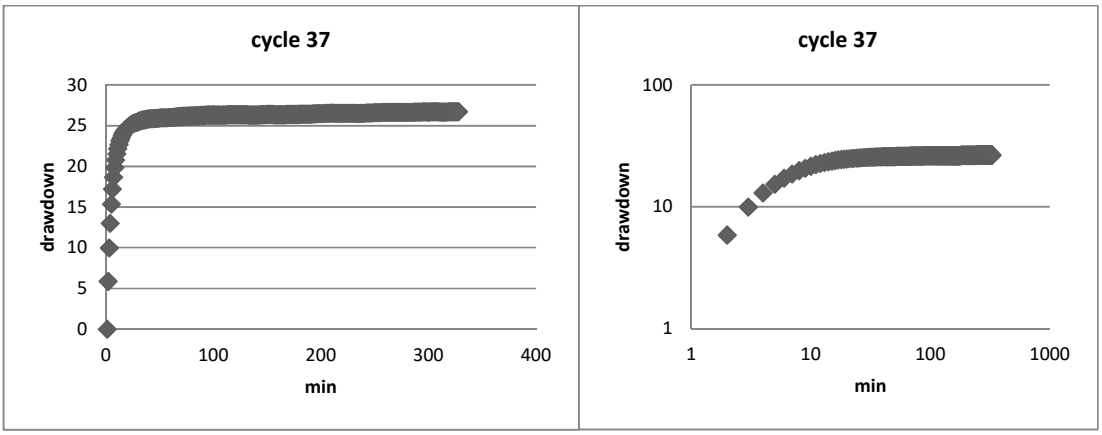
cycle 37
drawdown
30
25
20
15
10
5
0
0
100
200
300
400
min

cycle 37
drawdown
100
10
1
1
10
100
1000
min

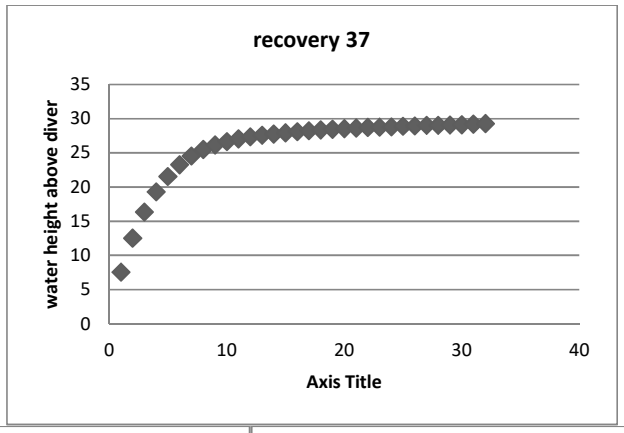
recovery 37
water height above diver
35
30
25
20
15
10
5
0
0
10
20
30
40
Axis Title

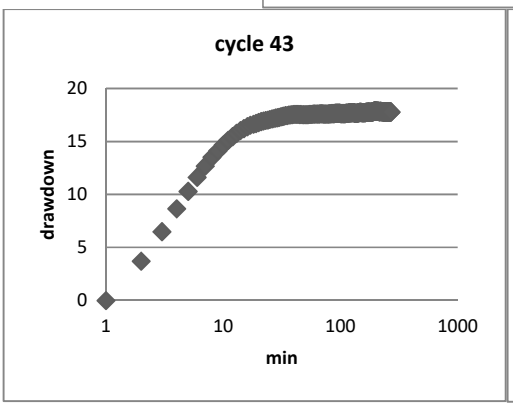
cycle 43
drawdown
20
15
10
5
0
1
10
100
1000
min

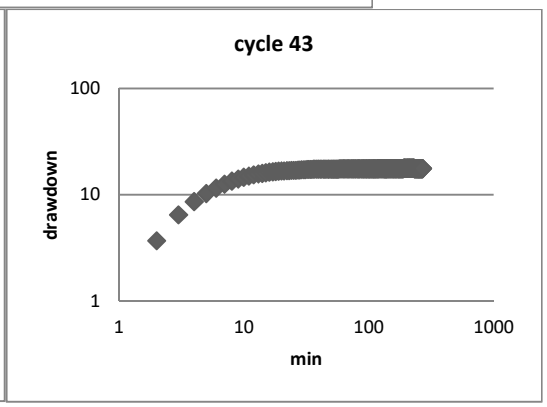
cycle 43
drawdown
100
10
1
1
10
100
1000
min

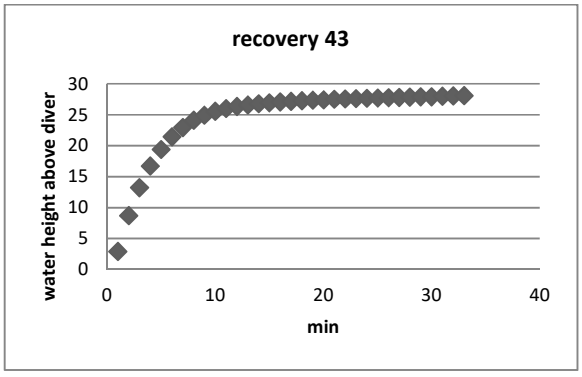
recovery 43
water height above diver
30
25
20
15
10
5
0
0
10
20
30
40
min

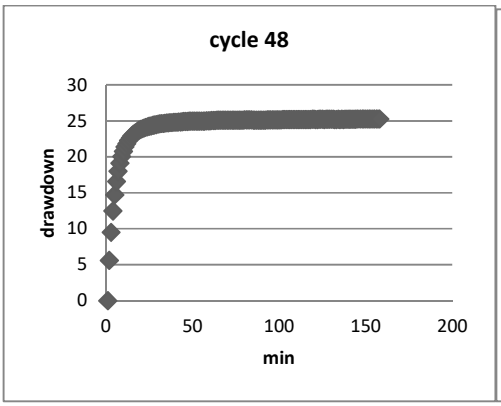
cycle 48
drawdown
30
25
20
15
10
5
0
0
50
100
150
200
min

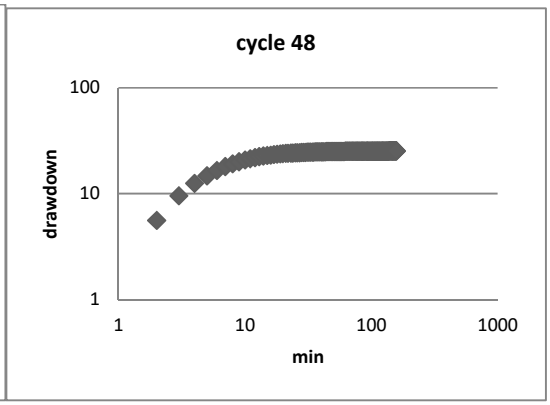
cycle 48
drawdown
100
10
1
1
10
100
1000
min

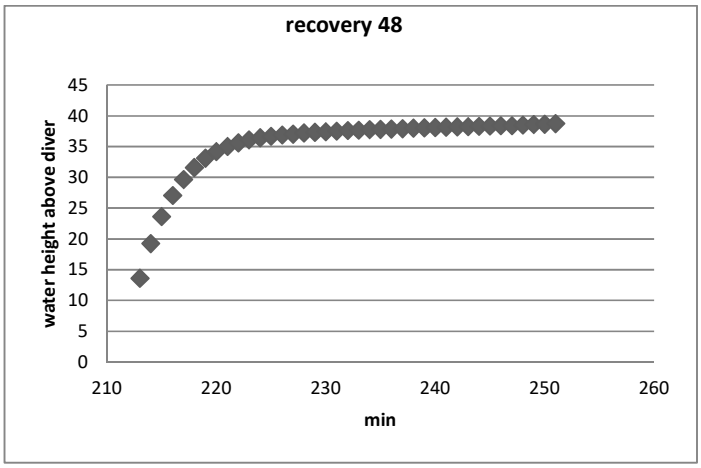
recovery 48
water height above diver
45
40
35
30
25
20
15
10
5
0
210
220
230
240
250
260
min